

D. Schulze

Powders and Bulk Solids

Behavior, Characterization, Storage and Flow



Springer

Dietmar Schulze

Powders and Bulk Solids

Dietmar Schulze

Powders and Bulk Solids

Behavior, Characterization, Storage and Flow

With 352 Figures



Springer

Professor Dr.-Ing. Dietmar Schulze
Institute for Recycling
University of Applied Sciences Braunschweig/Wolfenbüttel
Robert-Koch-Platz 8a
D-38440 Wolfsburg
Germany
e-mail: D.Schulze@fh-wolfenbuettel.de

Co-Translator:
em. Professor Dr.-Ing. Jörg Schwedes
Schwedes + Schulze Schüttguttechnik GmbH
Petzvalstr. 56
38104 Braunschweig
Germany

Review English text:
John W. Carson, Ph.D.
President
Jenike & Johanson, Inc.
400 Business Park Dr.
Tyngsboro MA 01879
USA

English translation based on German edition "Schulze: Pulver und Schüttgüter"

Library of Congress Control Number: 2007934525

ISBN 978-3-540-73767-4 Springer Berlin Heidelberg New York

This work is subject to copyright. All rights are reserved, whether the whole or part of the material is concerned, specifically the rights of translation, reprinting, reuse of illustrations, recitation, broadcasting, reproduction on microfilm or in any other way, and storage in data banks. Duplication of this publication or parts thereof is permitted only under the provisions of the German Copyright Law of September 9, 1965, in its current version, and permission for use must always be obtained from Springer. Violations are liable for prosecution under the German Copyright Law.

Springer is a part of Springer Science+Business Media

springer.com

© Springer-Verlag Berlin Heidelberg 2008

The use of general descriptive names, registered names, trademarks, etc. in this publication does not imply, even in the absence of a specific statement, that such names are exempt from the relevant protective laws and regulations and therefore free for general use.

Typesetting: Camera ready by authors

Production: LE-T_EX Jelonek, Schmidt & Vöckler GbR, Leipzig

Cover Design: eStudio Calamar S.L., F. Steinen-Broo, Girona, Spain

Printed on acid-free paper 7/3180/YL 543210

Preface

In the engineering community the handling of powders and bulk solids is called bulk solids technology being, at least in Germany, part of mechanical process engineering. Process engineering involves study of the change and transformation of material properties. If mechanical processes are used for this transformation, the engineering discipline is called mechanical process engineering. The best known unit operations of mechanical process engineering are grinding, agglomeration, mixing, and separation. Due to the mechanical treatment, the particles – either single particles or a collection of particles – increase in value. To profit from this value increase industry and academia perform research and development. When handling bulk solids, e.g. storing, dosing and conveying, no value increase can be achieved, because the material properties are not changed. What can be achieved is “at most” the elimination of problems which is less interesting research and development compared to the development of new products or processes with the chance to obtain a patent.

A silo for the intermediate storage of bulk solids often seems to be only a single, unimportant element for the realization of a larger process. Bulk solid is filled into the silo continuously or discontinuously and discharged later at predetermined points of time in desired quantities. That is not always unproblematic. The known problems of arching and ratholing can lead to irregular discharge or complete blockage. The hammer often found close to a silo is a known auxiliary means which often is subsequently resorted to due to incorrect silo design. Nearly forty years ago the author of this preface wrote a monograph on bulk solids storage, called this discipline as belonging to the “stepchildren” of technology, and summarised that it often happens that a problem is accepted as given due to its frequent appearance. Has that changed much up to today?

Today the characterization and handling of bulk solids is taught at many (in Germany, nearly all) universities and technical schools in faculties of mechanical and chemical engineering. For more than twenty years seminars and short courses have been offered which cover the basics and application potential of modern bulk solids technology. The most important theoretical fundamentals are known, from which reliable silo design is possible. The necessary information is available, but it is often not consid-

ered or understood. Avoidable failures, unnecessary overtime and production shortages or stoppages have to occur before those who have lived with the mentioned problems become willing to adopt the available design method in which the silo geometry is fitted to measurable bulk solid properties.

When designing silos for flow a procedure has to be followed that is similar to the one used when designing a heat exchanger. The material properties of the concerned fluids have to be known to design the heat exchanger. This procedure is state-of-the-art. The necessary data can be found in equivalent text books (e.g., “Heat Exchanger Design Handbook”, “VDI-Wärmeatlas”) or have to be measured following standardized test methods. The procedure to design a silo is similar. Unfortunately there are no equivalent text books (no “Silo Design Handbook” containing material parameters). So the experimental determination of relevant bulk solid properties is much more important. If these properties are known the silo geometry can be fitted to the measured values and trouble-free operation can be achieved. A prerequisite is that the bulk solid properties measured with laboratory equipment are representative. But this prerequisite also holds regarding a heat exchanger. If, for example, “fouling” takes place on the heat exchanger surfaces the material parameters have changed, and the heat exchanger can no longer fulfil the demanded requirements. In a similar way a silo might not provide trouble-free operation when bulk solids with different properties are stored.

A text book (“Silo Design Handbook”) containing reliable quantitative data concerning silo design for flow will never exist. A fluid for which the composition is known always has identical material properties. This only very seldom holds for bulk solids. Besides chemical composition, which is sufficient for characterizing a fluid, further parameters based on the disperse nature of bulk solids have an influence on their properties. Of influence are particle size, particle size distribution, particle shape, porosity, humidity and many more. If one would determine the influence of all these parameters on the relevant properties for silo design, many experiments would be necessary. Thus it is more practical to measure relevant bulk solid properties directly on representative samples. To obtain these properties shear testers are used. But only when those shear tests are performed correctly can data be obtained which enable reliable silo design for flow. Experience indicates that the prerequisite of correct performance of a shear test is often not realized, due to which it is often concluded – usually too quickly – that shear tests only have limited usefulness.

Today I would not judge bulk solid storage anymore as belonging to the “stepchildren” of technology. The most important theoretical fundamentals are known, and there are sufficiently many examples available which

prove that silos fulfil the demanded requirements when they have been designed according to the present state-of-the-art on the basis of properties measured in shear testers. What still can be called shabby and therefore could be improved is the broad application, confidence in the method and the necessity to apply it. This is all the more remarkable when considering that the percentage of bulk solids used in process industry is enormous. A few years ago the president of the EFCE (European Federation of Chemical Engineering) judged that about 60% of all products produced in the chemical industries in Europe are bulk solids. An additional 20% of products use bulk solids in the processes.

This book by Dietmar Schulze certainly will help to improve the understanding of bulk solids behavior, especially for people who only occasionally deal with bulk solids. After having obtained his diploma at the Technical University of Braunschweig he has been continuously concerned with all aspects of the characterization of bulk solids, application of measured bulk solids properties for silo design, and theoretical fundamentals of bulk solids technology. He has written important contributions to nearly all aspects of bulk solids technology which are documented in many publications. His effort in the determination of relevant bulk solid properties has been very intensive. He developed a special ring shear tester that is today known worldwide as the “Schulze Ring Shear Tester”. It is often erroneously asserted when mentioning shear testers that they are too complicated or too time consuming for many applications. Neither statement is correct. Depending on the task and on the problem, only a few experiments with a ring shear tester which has been adapted to the problem yield results that are more reliable than those which follow from empirical tests or from the application of so-called “simple testers”.

This book was published in German in autumn 2006. One of the main merits of the book is the fact that all chapters have been written by the same person who is an expert in all of the mentioned topics. The wording, nomenclature and mode of presenting graphs and sketches are identical throughout the book. This helps in understanding and searching for special questions. This has been missing in the English literature. Indeed there are some good books on bulk solids technology in English that are worth reading. But the single chapters of these books were mostly written by different authors using different nomenclature, etc. Thus, Dietmar Schulze was pressed by many of us to prepare an English version of his book, which is now available.

It is my hope this book will help to improve the understanding of bulk solids and the problems caused by them. This book treats nearly all problems which can arise in the technical application of storage and flow of bulk solids. The broad understanding and know how are based on the au-

thor's own experience in the measurement of bulk solids properties, planning and performing investigations of large silos and laboratory equipment, consulting with companies in solving problems or planning new silo facilities, and on a continuous and broad literature study.

Jörg Schwedes

Braunschweig, in July 2007

Foreword

This book provides an introduction into bulk solids technology starting from the flow properties of particulate solids to the flow of powders and bulk solids in hoppers, bins, and silos. Besides the basics some newer findings are also included. Furthermore, frequent questions that have been addressed to the author in the past are taken into account.

The level of the book should make it well-suited to a wide range of readers who are interested in an introduction into the topic. The major part of the contents is based on contributions to seminars and conferences, and on lectures at the University of Applied Sciences Braunschweig/Wolfenbüttel.

Regarding the topics “measurement of flow properties” and “silo design”, the book follows the great work of Andrew W. Jenike. About 45 years ago Jenike developed a theory on the flow of bulk solids in silos which is still applied today, and he presented a shear tester which can be regarded as the basis for the quantitative measurement of flow properties. Starting from these results, many research projects on bulk solids technology have been performed at many places around the world for several decades. Thus, a lot of knowledge is available today, but, unfortunately, sometimes it can be observed that the corresponding publications, some of which are older than twenty years, are not known, not found, or just ignored. Therefore, it is a further goal of this book to spread and to preserve at least a part of the existing knowledge.

Here as well as in the title of the present book the words “powder” and “bulk solid” are intentionally mentioned side-by-side since in some industries, e.g., the pharmaceutical industry, the word powder is common, whereas materials like cement, sand, and coal are known as bulk solids. For reasons of simplification, in the present book the term bulk solid is used to represent all materials consisting of particles, i.e., fine, cohesive powders, granulates, and coarse bulk materials.

The first chapters deal with the flow behavior and flow properties of bulk solids. Knowledge of flow properties is necessary to design hoppers, silos and other equipment to avoid flow problems (flow obstructions, segregation, ...). However, even when handling small amounts of bulk solids, e.g. when filling the dies of tabletting machines, or when operating dosage

equipment, sufficiently good flow behavior is important. Furthermore, to an increasing extent quantitative information on flowability is needed, e.g., for comparative tests, product development, and quality control.

In serious bulk solids technology shear testers are mostly used for the measurement of flow properties. Thus, shear testers can be regarded as the standard testers in bulk solids technology, especially if quantitatively applicable results with defined physical meaning are required. In this book their principle is explained in great detail, because their function and theoretical background are sometimes felt to be complicated by newcomers and non-experts.

In the second half of the book the flow of bulk solids in hoppers, bins, silos, etc. is considered. This includes, above all, the procedure to design bins in order to avoid problems such as flow obstructions and segregation. Additional topics like, for example, stresses in bulk solids, feeders, and flow promoting devices, are considered in order to support those who have to design or operate plants or equipment where bulk solids are stored or transported.

I would particularly like to thank all who helped me to gain experience in bulk solids technology, and, thus, to finally prepare this book. About twenty years ago I started as a research assistant at the Institute of Mechanical Process Engineering of the Technical University of Braunschweig, where I got my first insight into bulk solids technology with financial support of the German Research Foundation (Deutsche Forschungsgemeinschaft) and supervision of Professor Jörg Schwedes. After I obtained my Ph.D., the consultancy “Schwedes + Schulze Schüttgutechnik” was founded where I could make use of my experience from research work and also gain more experience. Also my work as a Professor at the University of Applied Sciences Braunschweig/Wolfenbüttel has allowed me to learn more about the behavior of bulk solids, supported, besides others, by the Deutsche Forschungsgemeinschaft, the Lower Saxony’s Federation of Innovative Projects (AGIP), and the university itself.

Special thanks are given to emeritus Prof. Dr. Jörg Schwedes for his kind assistance in the translation of this book into English, and to Dr. John Carson, President of Jenike & Johanson, Inc., for his highly appreciated assistance in the review of the English text and many helpful comments and discussions.

Finally, my sincere thank goes to Springer for the agreeable and uncomplicated cooperation.

Contents

Contents	XI
1. Introduction.....	1
1.1 Common problems with bulk solids	1
1.2 Milestones of bulk solids technology	4
2 Fundamentals.....	9
2.1 Particles or continuum?	9
2.2 Forces and stresses.....	10
2.3 Stresses in bulk solids.....	12
2.3.1 Introduction of the Mohr stress circle.....	12
2.3.2 Derivation of the Mohr stress circle	16
2.4 Bulk density	20
2.5 Elastic and plastic deformation.....	21
2.6 Adhesive forces	23
2.7 Influence of particle size on the behavior of a bulk solid	32
3 Flow properties of bulk solids.....	35
3.1 Uniaxial compression test.....	35
3.1.1 Consolidation of bulk solids	35
3.1.2 Time consolidation	38
3.1.3 Representation of stresses using Mohr stress circles	39
3.1.4 Numerical characterization of flowability	41
3.2 Principles of shear testing	47
3.2.1 Test procedure	47
3.2.3 Yield locus and flow properties.....	55
3.2.4 Time consolidation (caking)	66
3.3 Wall friction.....	69
3.3.1 Test procedure for wall yield loci	69
3.3.2 Wall yield locus and wall friction angle	70
3.3.3 Time wall yield locus, static wall friction	72

4 Practical determination of flow properties.....	75
4.1 Measurement with shear testers.....	75
4.1.1 Measurement of yield loci with the Jenike shear tester	76
4.1.2 Measurement of yield loci with the ring shear tester.....	84
4.1.3 Measurement of time consolidation	88
4.1.4 Measurement of kinematic wall friction.....	91
4.1.5 Measurement of static wall friction	94
4.1.6 Attrition test.....	94
4.1.6 Compressibility test.....	97
4.2 Selection of stresses.....	99
4.2.1 Yield locus (flowability).....	99
4.2.2 Time yield locus (flowability after time consolidation)	107
4.2.3 Wall yield locus (wall friction).....	109
4.3 Application-related measurement of flow properties	110
4.3.1 Comparative tests	110
4.3.2 Silo design for flow	110
5 A more detailed look at properties of bulk solids	113
5.1 Anisotropy and influence of deformation on stresses.....	113
5.1.1 Stresses	115
5.1.2 Bulk density	125
5.1.3 Unconfined yield strength (compressive strength)	126
5.2 Shear deformation, shear zones, localization	129
5.2.1 Idealization: simple shear and pure shear.....	129
5.2.2 Shear zones and shear bands	132
5.2.3 Dilatancy.....	139
5.2.4 Steady-state flow and dilation during flow property testing	144
5.3 Yield locus	147
5.3.1 Preshear point, shear points and Mohr stress circles	148
5.3.2 Tensile strength and cohesion.....	151
5.3.3 Flow properties at very small stresses	156
5.4 Influence of velocity	160
6 Discussion of testers and test procedures	163
6.1 Influences on test results.....	163
6.1.1 Procedure and principal stresses	163
6.1.2 Stresses in the measuring plane	166
6.2 Requirements for testers to measure flow properties.....	168
6.3 Measuring techniques and equipment (overview)	169
6.3.1 Funnel	171
6.3.2 Angle of repose.....	172
6.3.3 Avalanching.....	174

6.3.4 Imse test.....	175
6.3.5 Carr flowability index.....	176
6.3.6 Stirrer.....	177
6.3.7 Compressibility test	178
6.3.8 Cohesion tester, flowability test	179
6.3.9 Penetration test	180
6.3.10 Uniaxial compression test.....	181
6.3.11 Monoaxial shear test.....	182
6.3.12 Powder bed tester with tensile strength test.....	183
6.3.13 Uniaxial tensile strength test.....	184
6.3.14 Tensile strength test with gas flow	185
6.3.15 Johanson Hang-up Indicizer™, similar techniques	186
6.3.16 Quality control tester	188
6.3.17 Biaxial compression test.....	189
6.3.18 Jenike shear tester.....	190
6.3.19 Torsional shear tester.....	191
6.3.20 Ring shear tester	192
6.4 Remarks on reliability and accuracy.....	193
6.5 Measurement of adhesive forces	196
6.6 Summary.....	198
7 Properties exhibited by some bulk solids.....	199
7.1 Effects in flowing bulk solids	199
7.1.1 Slip-stick behavior.....	199
7.1.2 Variation of wall friction with displacement	209
7.2 Parameters and conditions influencing flow behavior.....	210
7.2.1 Particle size distribution	210
7.2.2 Flow agents.....	211
7.2.3 Liquids, moisture	215
7.2.4 Gas flow.....	219
7.2.5 Particle shape.....	223
8 Examples of measured flow properties.....	231
8.1 Flow agent	231
8.2 Moisture content	233
8.3 Temperature	235
8.4 Time consolidation	236
8.5 Particle size	237
8.6 Attrition	240
8.7 Bulk density	241
8.8 Stress dependency of wall friction.....	243
8.9 Influence of wall material on wall friction angle.....	245

9 Stresses.....	249
9.1 Stress states in silos	249
9.1.1 Ratio of horizontal to vertical stress	249
9.1.2 Stresses in silos.....	252
9.2 Assessment of stresses.....	258
9.2.1 Stresses in vertical channels (Janssen's approach).....	259
9.2.2 Further application of Janssen's equation.....	262
9.2.3 Bulk solid properties for calculation of stresses	266
9.2.4 Estimation of stresses at an outlet opening.....	270
9.2.5 Assessment of the stress distribution in a silo	271
9.3 Loads on feeders.....	272
9.3.1 Vertical stress at an outlet opening.....	272
9.3.2 Estimation of driving forces	274
9.4 Disturbances to the stress distribution	278
9.4.1 Local variations of the cross-section	278
9.4.2 Eccentric flow.....	285
10 Silo design for flow.....	291
10.1 Flow profiles: mass flow and funnel flow	291
10.2 Flow problems in silos.....	293
10.3 Jenike's procedure for silo design	295
10.3.1 Design of mass flow silos.....	296
10.3.2 Design of funnel flow silos.....	307
10.4 Application of results.....	312
10.5 Design diagrams	313
11 Silo configurations	319
11.1 Influence of flow properties on silo configuration	319
11.2 Hopper configurations	320
11.2.1 Hopper shape	320
11.2.2 Transitions and inclined walls	323
11.2.3 Multiple outlets.....	325
11.2.4 Special cases: hoppers with varying steepness	326
11.3 Inserts	328
11.3.1 Inverted cones and wedges	329
11.3.2 Cone-in-cone insert	332
11.3.3 Discharge tubes	333
12 Discharge of bulk solids.....	339
12.1 Maximum discharge rate	339
12.1.1 Discharge rate of coarse-grained bulk solids.....	341
12.1.2 Discharge rate of fine-grained bulk solids.....	342

12.2 Discharge aids.....	347
12.2.1 Pneumatic discharge aids.....	347
12.2.2 Mechanical discharge aids.....	350
12.2.3 Application of discharge aids	352
12.3 Feeders and other discharge devices.....	353
12.3.1 Rules for design regarding mass flow	353
12.3.2 Types of discharge devices (selection)	357
12.4 Feeder dimensions and placement of discharge aids	377
13 Segregation	381
13.1 Segregation mechanisms	381
13.1.1 Sifting and other segregation mechanisms on inclined surfaces	382
13.1.2 Percolation in particle beds.....	384
13.1.3 Effect of air resistance	386
13.2 Techniques to reduce segregation.....	390
13.2.1 Modification of the bulk solid	391
13.2.2 Optimization of the filling process	392
13.2.3 Remixing	396
13.3 Sampling.....	403
13.4 Final remarks	404
14 Silo quaking and silo honking.....	405
14.1 Phenomenon	405
14.2 Shocks as a result of sudden flow	406
14.3 Sudden flow and pulsating flow caused by slip-stick friction ..	408
14.4 Shear zones in silos.....	409
14.5 Silo shocks due to slip-stick friction	413
14.5.1 Shear zones in flowing bulk solid.....	413
14.5.2 Unstable stagnant zones (funnel flow)	419
14.5.3 Flow at the silo wall.....	422
14.5.4 Combinations of different mechanisms	429
14.6 Shocks and vibrations due to other reasons	429
14.6.1 Large discharge rate with respect to outlet size	429
14.6.2 Cyclic excitation by a feeder	430
14.6.3 Collapsing arches and ratholes	430
14.7 Means for reducing silo quaking and silo honking	431
14.7.1 Reduction of the accelerated mass.....	432
14.7.2 Regular initiation of small shocks	434
14.7.3 Increasing roughness of the vertical section	435
14.7.4 Reduction of velocity gradients.....	436
14.7.5 Transforming funnel flow into mass flow	437

15 Sample problems and solutions	439
15.1 General remarks.....	439
15.2 Sample problems	439
Sample problem 1: Stresses in the vertical section of a silo.....	439
Sample problem 2: Maximum stress in a mass flow silo	441
Sample problem 3: Discharge tube.....	442
Sample problem 4: Driving force of a feeder	444
Sample problem 5: Press	445
Sample problem 6: Stresses in combined bins	447
Sample problem 7: Stresses in FIBCs and sacks on pallets.....	449
Sample problem 8: Discharge rate.....	450
Sample problem 9: Selection of a wall material for mass flow	451
Sample problem 10: Design of a mass flow silo	452
Sample problem 11: Design of a funnel flow silo	456
Sample problem 12: Design of a silo under consideration of time consolidation.....	461
Symbols.....	467
References.....	473
Index	503

1. Introduction

Powders and bulk solids have to be handled or stored in nearly all industries, from powder coating to food, from nano-scale powders and pharmaceutical substances to products like cement, coal, and ore, from dry materials like fly ash to moist bulk solids like filter cake and clay. All these materials have to be transported, conveyed, or handled otherwise. Thus the characterization of powders and bulk solids regarding their flow properties plays an important role, e.g., for product development and optimization, customer support and the response to customer complaints.

Especially the discharge of powders and bulk solids from silos, hoppers, transport containers etc. may result in severe problems, e.g., due to flow obstructions, segregation, shocks and vibrations, or unsteady flow. To avoid such complications, solutions have to be found considering the flow properties of the bulk solid.

1.1 Common problems with bulk solids

When a plant is designed, silos, hoppers, and bins are usually not the main objective of the design work, because they do not contribute much to the processing and refinement of bulk materials like, for example, a mill or a mixer. On the other hand, poorly designed silos can reduce throughput and product quality. Nevertheless many silos and bins are built without considering the flow behavior of the bulk solid to be stored. This results in well-known problems, e.g., the occurrence of flow obstructions. Typical indications for the latter are hammering traces on hopper walls (Fig. 1.1).

Even if bulk solids are handled on a smaller scale (e.g., dosage), the problems are similar to those in silos, because the basic processes are the same and independent of the scale.

Figure 1.2 shows several problems which can emerge during the operation of a silo. If the outlet opening is too small, a stable arch can form above the outlet and the flow stops (Fig. 1.2.a). If particles are large with respect to the opening, the reason for arch formation is the interlocking of particles. Materials of very fine particle size can form cohesive arches as a

result of the compressive strength caused by consolidation and interparticle adhesive forces.

Another possible source of problems is funnel flow (Fig. 1.2.b). One reason for funnel flow is a hopper wall which is too shallow or too rough. In this case in a filled silo the bulk solid cannot slide downwards along the hopper walls. Thus, so-called stagnant zones build up and the material flow is limited to a flow zone above the outlet opening. In a silo used as a buffer and never discharged completely, bulk material can remain in the stagnant zones over long periods of time and change its properties (e.g., decomposition of food products). Furthermore, the bulk solid in the stagnant zones can consolidate with time to such an extent that it will not be able to flow out after the flow zone has emptied out. The latter results in a “pipe” or “rathole” reaching from the outlet opening to the top of the filling (Fig. 1.2.c).



Fig. 1.1. Traces of hammering at a hopper wall indicating flow problems

The residence time of the bulk solid in the flow zone of a funnel flow silo can be extremely short (Fig. 1.2.d), so that the material, which has just been fed into the silo, is immediately discharged. Within this short time an easily fluidized bulk solid (e.g., flour, fine chalk) cannot sufficiently deaer-

ate. Hence, it will flood out of the outlet opening like a fluid, resulting in increased dust generation and flooding of the feeder.

Funnel flow can also result in reduced product quality due to segregation (Fig. 1.2.e). When filling a silo, one has to take into account that the product can segregate across the cross-section of the silo. When the silo is filled centrally, one often will observe an increased amount of fines close to the silo axis, and more coarse particles close to the silo wall. If funnel flow takes place at discharge, at first the material from the center (the fines) flows out, followed by the coarser material from the silo periphery. The time-dependent composition of the discharged bulk solid can be, for example, a quality problem during the filling of small packages, or when steady-state downstream processes have to be charged.

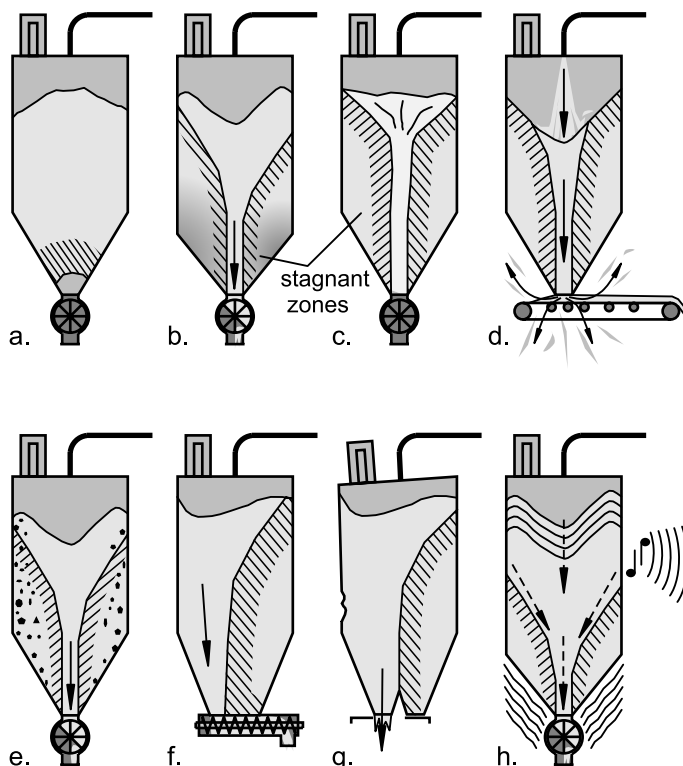


Fig. 1.2. Possible problems during the operation of silos; a. arching; b. funnel flow with wide residence time distribution and deterioration in product quality; c. rat-holing; d. flooding; e. segregation; f. non-uniform discharge with screw feeder; g. buckling caused by eccentric flow; h. vibrations (silo quaking and silo noise)

Less well-designed feeders can result in a non-uniform withdrawal of the bulk solid and, thus, in funnel flow. The screw feeder shown in Fig. 1.2.f discharges the bulk solid at its rear end and then conveys it horizontally to its outlet, i.e., the screw is filled already at the rear end of the feeder so that along the rest of the outlet length no further bulk solid can enter the screw. Another reason for eccentric flow is, for example, the discharge from only one of multiple outlets (Fig. 1.2.g). Eccentric flow results in unfavorable non-symmetrical loads on the silo structure thus increasing the danger of buckling of thin-walled metal silos and cracking of reinforced concrete silos that have only a single layer of reinforcing steel.

For different reasons the flow of a bulk solid in a silo can result in vibrations and shocks (Fig. 1.2.h). Depending on the frequency, the effect is called silo noise (audible) or silo quaking (low frequency, individual shocks).

The problems described above result on the one hand from the given equipment (e.g., design of the feeder), on the other hand from the properties of the bulk solid (e.g., strength, friction). When designing silos, hoppers, bins etc., at first the properties of the bulk solid have to be determined. This data in combination with proven design procedures yields the appropriate geometry (e.g., hopper slope, outlet size). Therefore in the present book the flow properties of bulk solids and their measurement as well as design procedures (e.g., stresses, avoidance of flow problems) and design considerations (e.g., hopper shape, feeder) are described.

1.2 Milestones of bulk solids technology

As much as Bernoulli's equation can be regarded as a milestone in fluid dynamics, the work of two persons, variously referred to in the present book, need to be mentioned with respect to their impact on bulk solids technology: H.A. Janssen and A.W. Jenike.

Janssen was an engineer living in Bremen, Germany, at the end of the 19th century, when increasing amounts of corn were imported from overseas and, thus, needed to be stored. In the United States corn was stored in silos (corn being the first bulk solid stored in large silos; cement and flour followed around 1900 [1.1]). Engineering books at the time did not list design procedures for silos, but from the literature [1.2,1.3] Janssen knew that stress at the bottom of a silo does not increase linearly with filling height as in the case of fluids, but becomes constant from a certain filling height.

In order to investigate the dependence of the stress on the filling height, Janssen used the experimental set-up shown in Fig. 1.3 [1.4]. Model silos with square cross-section of different size made from wood were placed above a balance. At different filling levels the force acting on the balance, and thus the vertical stress, was measured. This way Janssen could confirm that the vertical stress is not proportional to the filling level (Fig. 1.4). The bulk solid did not show the linear increase of stress with filling height typical for fluids.

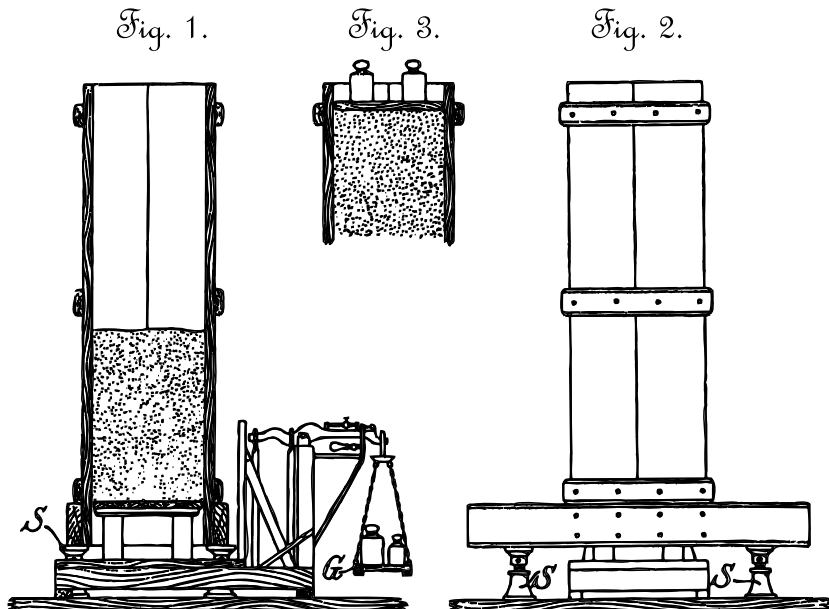


Fig. 1.3. Janssen's test set-up for the measurement of vertical stress (figure copied from [1.4])

Janssen recognized that the bulk solid in the silo is supported by friction at the silo wall. For the measurement of the coefficient of friction between the wall material and the bulk solid he employed the set-up shown in Fig. 1.5, where a platen made from the wall material (wood) was loaded vertically with weights and moved horizontally across the surface of the bulk solid whereby the force F was measured. Furthermore, Janssen derived an equation from the equilibrium of forces on a differential slice of bulk solid in the silo. This equation, which allows the calculation of stresses in the vertical section of a silo, is still applied today and known as the “Janssen equation”. It is part of the silo design codes in several countries and can be

found, for example, in the old German code DIN 1055 part 6 [1.5] and the new Eurocode EN 1991-4:2006-12 [1.6].

Fig. 4.
Versuch 1.

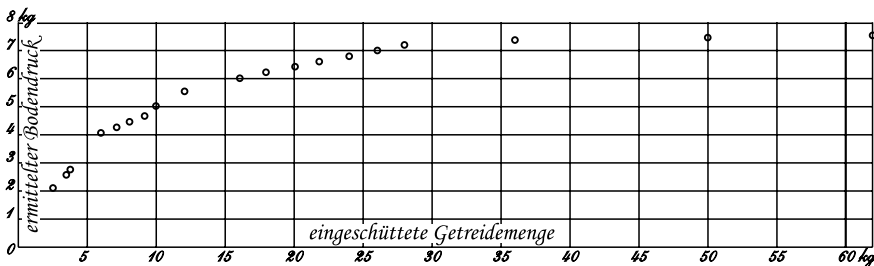


Fig. 1.4. Janssen's test results: Measured vertical stress ("ermittelter Bodendruck") in dependence on the amount of corn ("eingeschüttete Getreidemenge") filled into the silo (figure copied from [1.4])

Fig. 4.

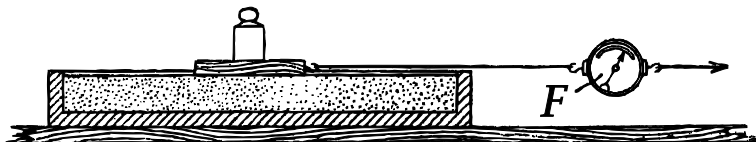


Fig. 1.5. Set-up for the measurement of the friction coefficient between bulk solid and wall material (figure copied from [1.4])

Dr. Andrew W. Jenike graduated in Mechanical Engineering from Warsaw Polytechnic Institute in 1939. After World War II he obtained his Ph.D. in Structural Engineering in England, immigrated to Canada and later to the United States. In the Fifties, when he was approaching the age of 40, he looked for a field in which he could make a unique and significant engineering and scientific contribution. Within one year he studied about 40 different fields of technology. Finally Jenike chose bulk solids technology, because in this field he identified a very low level of technology. With financial support from different sources, Jenike set up the "Bulk Solids Flow Laboratory" at the University of Utah [1.7].

On the basis of principles known from soil mechanics, Jenike described the behavior of bulk solids by introducing the yield locus. Furthermore, he derived a theory describing the stresses in silos, especially in the hopper section [1.8,1.9]. Jenike defined the terms *mass flow* and *funnel flow* [1.10], which are the most important criteria for the assessment of the flow

regime in a silo. In case of funnel flow, only a portion of the bulk solid in the silo moves downwards during discharge whereby the rest of the bulk solid is at rest in the stagnant zones (Fig. 1.6.a). In case of mass flow the whole silo contents, i.e., every particle, move during discharge (Fig. 1.6.b).

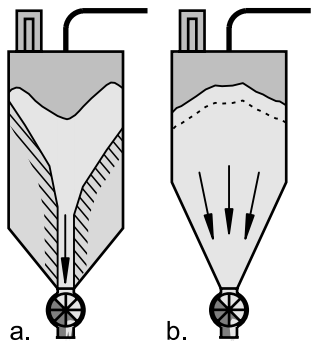


Fig. 1.6. a. Funnel flow; b. mass flow

On the basis of his theoretical considerations, Jenike derived a procedure for designing silos for unobstructed flow. From this point on it was possible to calculate the slope of the hopper walls to ensure mass flow (Fig. 1.6.b), and to predict the minimum outlet dimensions required to avoid stable arches (Fig. 1.2.a) or ratholes (Fig. 1.2.c). Furthermore, Jenike worked on the practical design of silos, e.g., regarding the influence of the feeder on the flow in the silo (e.g. Fig. 1.2.f). For the determination of the flow properties, which have to be known for the application of Jenike's design procedure, he developed a tester, which is widely known as the Jenike shear tester. Still today the Jenike design procedure is the most widely applied method, although in the meantime other (similar) procedures have been published. Jenike's work, especially his most important publication for practical application, Bulletin 123 "Storage and flow of solids" [1.9], is still cited as fundamental literature for bulk solid and silo technology.

With the introduction of the yield locus for the representation of flow properties and the presentation of a suitable tester, Jenike laid the foundation for the quantitative measurement of flow properties (e.g., flowability), which goes far beyond archaic, relatively inaccurate methods like, for example, the measurement of the angle of repose.

2 Fundamentals

2.1 Particles or continuum?

A bulk solid consists of individual particles. In principle it is possible to describe the behavior of a bulk solid by regarding the particle-particle interactions. But, as is easily understandable, this would be a difficult procedure, because the number of particles in a powder-handling system is usually very large (e.g., 10^9 particles of a diameter of $10 \mu\text{m}$ are contained in one cm^3), each particle has a different shape, and the adhesive forces between particles can hardly be accurately calculated. Although in the last few years more and more calculations based on particle-particle interactions (DEM - discrete element method) have been presented, the output with respect to the number of particles and the complexity of particle shapes is limited by the available processing power.

Another approach is to regard the bulk solid as a continuum. Therefore, instead of forces between individual particles, one regards forces or stresses, respectively, on boundary areas of volume elements and the resulting deformations, similar to procedures in fluid mechanics and strength theory. The volume elements have to be sufficiently large with respect to the particle size so that local interactions between individual particles do not need to be considered.

The last mentioned procedure, i.e., the application of the methods of continuum mechanics, is the classic way of proceeding in bulk solids technology and will be outlined in the present book. This is true for the measurement of flow properties, where usually stresses and deformations on a defined volume of bulk solid are investigated, as well as for calculation procedures.

2.2 Forces and stresses

The state of load on a bulk solid is described using the methods of continuum mechanics: One does not consider the forces at the individual particles of the bulk solid, but the forces on the boundary areas of individual volume elements. Resolution of force F acting on an area A (Fig. 2.1) in an arbitrary direction leads to:

- the normal force, F_N : force acting perpendicular (“normal”) to area A .
- the shear force, F_S : force acting parallel to area A .

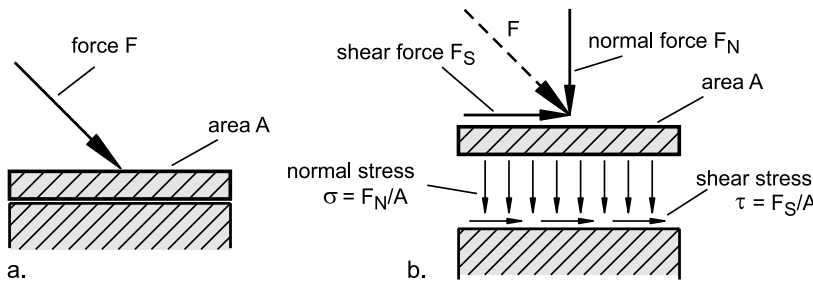


Fig. 2.1. a. applied force, F ; b. resolution of force, F ; stresses

To be able to describe the load on the bulk solid independently of the dimensions of the area considered above, stresses are calculated from the forces. A stress is defined through the relationship of force to area. If one divides the above-described forces, F_S and F_N , by area A , one obtains:

- the normal stress $\sigma = F_N/A$: stress acting perpendicularly (“normally”) on area A ;
- the shear stress $\tau = F_S/A$: stress parallel to area A .

If a force of any direction is acting on the plane, a resolution of this force in a component perpendicular to the plane and another component parallel to the plane yields the normal and shear component of this force and thus normal and shear stresses acting on the plane can be calculated as described above.

In bulk solids technology, shear stresses always emerge due to frictional effects: If, for example, a bulk solid is located on a horizontal plane (Fig. 2.2.a) and is subjected only to gravity acting perpendicularly to the plane, (in the mean) no shear stress is acting between plane and bulk solid. The bulk solid remains at rest.

If the plane becomes inclined to the horizontal by a sufficiently large angle α , the bulk solid will slide downwards (Fig. 2.2.c). In contrast to this,

the bulk solid will remain at rest at a smaller inclination (Fig. 2.2.b). In both cases a shear stress, τ , is acting between bulk solid and plane. The directions of the stresses acting on the bulk solid are shown by the arrows in Fig. 2.2. If the force transferred through the shear stress is not less than the force that pulls the bulk solid downwards, the bulk solid will remain at rest. If the transferable shear stress is too small, the bulk solid will slip downwards.

The magnitude of the transferable shear stress is dependent on the friction between the bulk solid and the plane surface: A rough surface will be able to transfer larger shear stresses than a smooth surface, i.e., on an inclined plane with a rough surface the bulk solid will slip downwards only at a larger angle α than on a plane with a smooth surface. If the surface were frictionless (ideally smooth), the bulk solid would slip downwards at any inclination $\alpha > 0^\circ$, because there would be no shear stress for the plane to transfer.

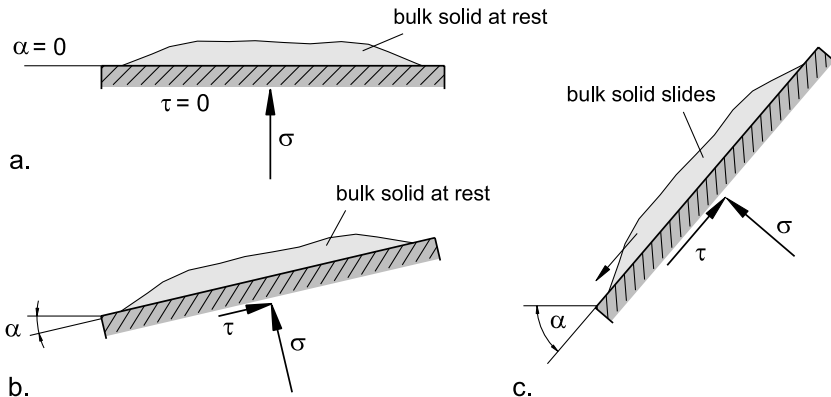


Fig. 2.2. Shear stresses (example)

In bulk solids technology, e.g., storage of a bulk solid in a container, normal stresses are mainly compressive stresses. This means that compressive normal stresses are acting on arbitrary volume elements within the bulk solid (similar to Fig. 2.1). Tensile forces are found rarely in bulk solids technology. In contrast to classic engineering mechanics, but similar to the pressure in fluid dynamics, compressive forces are defined as positive forces, and compressive stresses as positive normal stresses. Tensile forces and tensile stresses are characterized by negative values ($\sigma < 0$). There are also rules for the direction of positive and negative shear stresses, but these are not important for the purpose of this book (for more about this see [2.1,2.2,2.3]).

The unit used for stress is Pa (Pascal) according to the International System of Units (SI). 1 Pa is equal to 1 Newton per square meter (1 N/m^2). 1 bar is equal to 100 000 Pa, 1 psi is 6 894.76 Pa.

2.3 Stresses in bulk solids

Figure 2.3 shows a bulk solid element in a container (assumptions: infinite filling height, frictionless internal walls). In the vertical direction, positive normal stress ($\sigma_v > 0$, compressive stress) is exerted on the bulk solid.

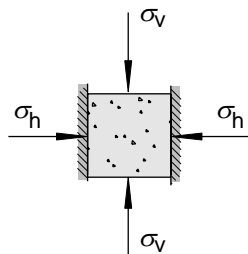


Fig. 2.3. Bulk solid element

If the bulk solid were to behave like a Newtonian fluid, the stresses in the horizontal and vertical direction (and in all other directions) would be of equal magnitude. In reality the behavior of a bulk solid is quite different from that of a fluid, so the assumption of analogies is often misleading.

Within the bulk solid (Fig. 2.3) the horizontal stress, σ_h , is a result of the vertical stress, σ_v , where the resulting horizontal stress is less than the vertical stress exerted on the bulk solid from the top. The ratio of horizontal stress, σ_h , to vertical stress, σ_v , is the lateral stress ratio, K (alternative designation: λ):

$$K = \lambda = \frac{\sigma_h}{\sigma_v} \quad (2.1)$$

Typical values of K are between 0.3 and 0.6 [2.4].

2.3.1 Introduction of the Mohr stress circle

It follows from Fig. 2.3, that – in analogy to solids – in a bulk solid different stresses can be found in different cutting planes – even if the bulk solid

is at rest. Stresses in cutting planes other than vertical and horizontal can be analyzed using a simple equilibrium of forces.

No shear stresses are exerted on the top or bottom surface of the bulk solid element in Fig. 2.3, i.e., the shear stresses, τ , in these planes are equal to zero. No shear stresses are acting at the lateral walls, since the lateral walls were assumed to be frictionless. Thus only the normal stresses shown are acting on the bulk solid from outside. Using a simple equilibrium of forces on a volume element with triangular cross-section cut from the bulk solid element shown in Fig. 2.3 (Fig. 2.4), the normal stress, σ_α , and the shear stress, τ_α , acting on a plane inclined by an arbitrary angle α , can be calculated. After some mathematical transformations (e.g. [2.1]), which are considered in the following section, it follows that:

$$\sigma_\alpha = \frac{\sigma_v + \sigma_h}{2} + \frac{\sigma_v - \sigma_h}{2} \cos(2\alpha) \quad (2.2)$$

$$\tau_\alpha = \frac{\sigma_v - \sigma_h}{2} \sin(2\alpha) \quad (2.3)$$

The pairs of values $(\sigma_\alpha, \tau_\alpha)$, which are to be calculated according to Eqs. (2.2) and (2.3) for all possible angles α , can be plotted in a σ, τ diagram (normal stress - shear stress diagram); see Fig. 2.4. If one joins all plotted pairs of values, a circle emerges, i.e., all calculated pairs of values form a circle in the σ, τ diagram.

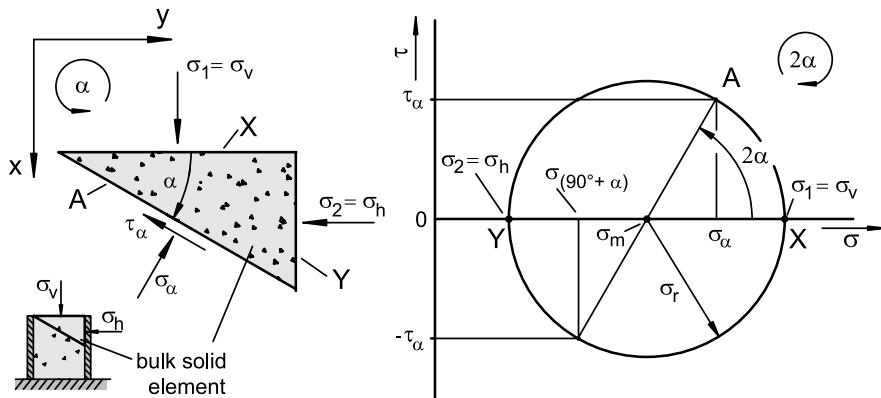


Fig. 2.4. Equilibrium of forces on a bulk solid element; Mohr stress circle

This circle is called the “Mohr stress circle”. Its center is located at $\sigma = \sigma_m = (\sigma_v + \sigma_h)/2$ and $\tau = 0$. The radius of the circle is $\sigma_r = (\sigma_v - \sigma_h)/2$. The Mohr

stress circle represents the stresses in all cutting planes at arbitrary inclination angles α , i.e., in all possible cutting planes within a bulk solid element. Since the center of the Mohr stress circle is always located on the σ axis, each Mohr stress circle has two points of intersection with the σ axis. The normal stresses defined through these points of intersection are called the principal stresses, whereby the larger principal stress – the major principal stress – is designated as σ_1 and the smaller principal stress – the minor principal stress – is designated as σ_2 (Please note that, in contrast to bulk solids technology, in continuum mechanics the minor principal stress is usually designated as σ_3). If both principal stresses are given, the Mohr stress circle is defined.

In the example of Fig. 2.4 both horizontal and vertical planes are free from shear stresses ($\tau = 0$) and are thus principal stress planes. In this case the vertical stress, σ_v , which is greater than the horizontal stress, σ_h , is the major principal stress, σ_1 , and the horizontal stress, σ_h , is the minor principal stress, σ_2 .

The angle α also can be found with the Mohr stress circle. The stresses acting in a cutting plane that is rotated at an angle α to the first cutting plane are found at a point on the Mohr circle rotated by an angle 2α relative to the point representing the stresses in the first cutting plane, where the angle 2α on the Mohr stress circle is measured in the opposite direction from the angle α between the cutting planes in the bulk solid. For example, the horizontal and vertical cutting planes in Fig. 2.4 are perpendicular to each other, i.e., the angle inclined by these planes is $\alpha = 90^\circ$. In the stress circle one finds the points that represent the stresses in the cutting planes at two positions inclined by $\alpha = 180^\circ$.

From the explanation above it follows that the state of stress in a bulk solid cannot be completely described by only a single numerical value. Depending on the actual load acting on a bulk solid element, the corresponding Mohr stress circle can have a smaller or a larger radius, a center at a lesser or greater normal stress, and hence also different principal stresses σ_1 and σ_2 . Generally, at a given major principal stress, σ_1 , there are an infinite number of stress circles with different values for the lowest principal stress, σ_2 . Therefore, a stress circle is defined clearly only if at least two numerical values are given, i.e., σ_1 and σ_2 .

The relationships are actually more complicated because in reality a three-dimensional state of stress exists, which cannot be represented by only one stress circle in one plane as shown in Fig. 2.4. The Mohr stress circles in the two planes which are perpendicular to this plane and perpendicular to each other also are required for representation of the three-dimensional stress state [2.1,2.3,2.5,2.6]. Thus, altogether there are three principal stresses, which are perpendicular to each other (Fig. 2.5).

The volume element in Fig. 2.5 is cut along the principal stress planes, i.e., the surfaces of the volume element are parallel to the principal stress planes. For each principal stress plane the Mohr stress circle is plotted in the σ, τ diagram. The largest Mohr stress circle represents the stresses in the cutting plane perpendicular to the mean principal stress, σ_3 , because in this plane the smallest minor and largest major principal stresses, σ_2 and σ_1 , are acting. For many applications in bulk solids technology it is sufficient to consider only one plane. In those cases one refers to a “two-dimensional” state of stress. As a rule the plane considered is the one in which the smallest minor and largest major principal stresses, and, thus, the greatest shear stress, are acting [2.1, 2.5, 2.6]. Shear stress is especially important because it is responsible for the movement of particles relative to each other, i.e., the flow of a bulk solid.

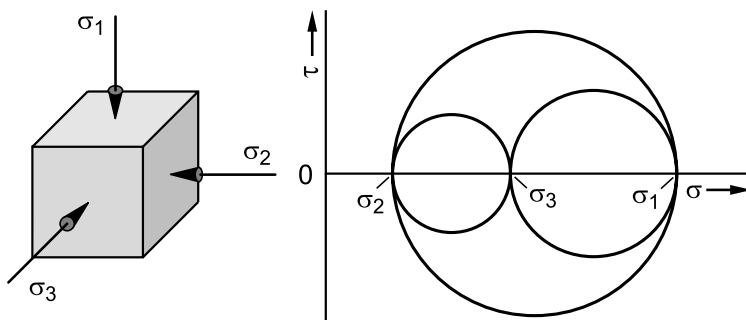


Fig. 2.5. Volume element with the three principal stresses being perpendicular to each other; stress circles for the three principal stress planes

For simple practical applications (e.g., flowability tests) it is often too complicated to characterize a two-dimensional stress state by two principal stresses (i.e., the minor and the major principal stresses), so that usually only the major principal stress, σ_1 , is mentioned. Accordingly, one would mark the state of stress presented in Fig. 2.4 through the major principal stress, σ_1 , which in this case is equal to the vertical stress, σ_v , exerted on the bulk solid. Therewith one assumes that the greatest of all normal stresses acting in different directions within a bulk solid element is responsible for the actual condition of the bulk solid.

This simplification or approximation is used, e.g., when loading a bulk solid sample with a certain vertical stress, for example, through weights of mass m (Fig. 2.6). Thereby, as a rule, one characterizes the stress state by the major principal stress, σ_1 , which in this case is equal to the force of gravity, $m \cdot g$, of the weights divided by the area, A , and denotes this stress as the consolidation stress, σ_1 .

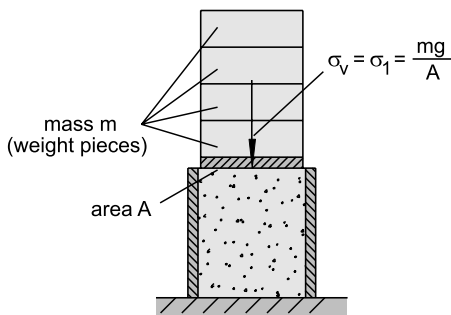


Fig. 2.6. Consolidation stress, σ_l , at uniaxial consolidation of a bulk solid in a hollow cylinder with frictionless walls

2.3.2 Derivation of the Mohr stress circle

In the following the mathematical derivation of the Mohr stress circle and Eqs.(2.2) and (2.3) is outlined starting from the equilibrium of forces on the volume element. Furthermore, the existence of two principal stress planes which are perpendicular to each other is shown.

The equilibrium of forces on the triangular bulk solid element in Fig. 2.4 in x and y direction yields (dimension of the bulk solid element perpendicular to the x,y plane is equal to 1):

$$\sum F_x = \sigma_v l \cos \alpha - \sigma_\alpha l \cos \alpha - \tau_\alpha l \sin \alpha = 0 \quad (2.4)$$

$$\sum F_y = \sigma_\alpha l \sin \alpha - \tau_\alpha l \cos \alpha - \sigma_h l \sin \alpha = 0 \quad (2.5)$$

It follows:

$$\tau_\alpha = \frac{\sigma_v \cos \alpha - \sigma_\alpha \cos \alpha}{\sin \alpha} \quad (2.6)$$

$$\sigma_\alpha = \frac{\tau_\alpha \cos \alpha + \sigma_h \sin \alpha}{\sin \alpha} \quad (2.7)$$

Substitution of τ_α in Eq.(2.7) by Eq.(2.6):

$$\sigma_\alpha = \frac{\sigma_v (\cos \alpha)^2 - \sigma_\alpha (\cos \alpha)^2}{(\sin \alpha)^2} + \sigma_h .$$

$$\Rightarrow \sigma_\alpha \left(1 + \frac{(\cos \alpha)^2}{(\sin \alpha)^2} \right) = \sigma_v \frac{(\cos \alpha)^2}{(\sin \alpha)^2} + \sigma_h$$

$$\Rightarrow \sigma_\alpha ((\sin \alpha)^2 + (\cos \alpha)^2) = \sigma_v (\cos \alpha)^2 + \sigma_h (\sin \alpha)^2 \quad (2.8)$$

The well-known equation

$$(\sin \alpha)^2 + (\cos \alpha)^2 = 1 \quad (2.9)$$

yields:

$$\sigma_\alpha = \sigma_v (\cos \alpha)^2 + \sigma_h (\sin \alpha)^2. \quad (2.10)$$

With the known mathematical equations

$$(\sin \alpha)^2 = \frac{1}{2}(1 - \cos 2\alpha) \quad (2.11)$$

$$(\cos \alpha)^2 = \frac{1}{2}(1 + \cos 2\alpha) \quad (2.12)$$

follows from Eq.(2.10) in analogy to Eq.(2.2):

$$\sigma_\alpha = \frac{1}{2}\sigma_v(1 + \cos 2\alpha) + \frac{1}{2}\sigma_h(1 - \cos 2\alpha)$$

$$\Rightarrow \sigma_\alpha = \frac{\sigma_v + \sigma_h}{2} + \frac{\sigma_v - \sigma_h}{2} \cos 2\alpha \quad (2.13)$$

Substitution of σ_α in Eq.(2.6) by Eq.(2.10) results in:

$$\tau_\alpha = \frac{\sigma_v \cos \alpha - \sigma_v (\cos \alpha)^3 - \sigma_h (\sin \alpha)^2 \cos \alpha}{\sin \alpha}$$

$$\Rightarrow \tau_\alpha = \frac{\sigma_v \cos \alpha (1 - (\cos \alpha)^2) - \sigma_h (\sin \alpha)^2 \cos \alpha}{\sin \alpha}$$

$$\Rightarrow \tau_\alpha = \frac{\sigma_v \cos \alpha (\sin \alpha)^2 - \sigma_h (\sin \alpha)^2 \cos \alpha}{\sin \alpha}$$

$$\Rightarrow \tau_\alpha = (\sigma_v - \sigma_h) \cos \alpha \sin \alpha \quad (2.14)$$

With the well-known equation

$$\cos \alpha \sin \alpha = \frac{1}{2} \sin 2\alpha \quad (2.15)$$

it finally follows from Eq.(2.14) according to Eq.(2.3):

$$\tau_\alpha = \frac{\sigma_v - \sigma_h}{2} \sin 2\alpha . \quad (2.16)$$

The state of stress shown in Fig. 2.4 already assumes that the shear stress is zero in two directions perpendicular to each other. One can derive the equations for the Mohr stress circle also without this assumption. In a general state of stress, the infinitesimal volume element in Fig. 2.7 is subjected to (positive) compressive stresses, σ_x and σ_y , as well as to shear stresses, τ_{xy} and τ_{yx} . The directions of the shear stresses are chosen under consideration of the condition, that one obtains the positive direction of a shear stress by rotating the face normal (directed away from the volume element) clockwise by 90°.

The equilibrium of moments around the center of the bulk solid element yields that the shear stresses, τ_{xy} and τ_{yx} , have the same amount, but reverse sign:

$$\tau_{xy} = -\tau_{yx} \quad (2.17)$$

With Eq.(2.17) the shear stresses can be drawn as shown in Fig. 2.7.b. In an arbitrary cutting plane A different normal and shear stresses will act, depending on the inclination, α , of the cutting plane. The unknown stresses, σ_α and τ_α , acting on the cutting plane A, are drawn in Fig. 2.8 in positive direction according to the assumptions outlined in the last paragraph. The length of the bulk solid element perpendicular to the x,y plane is assumed to be equal to 1, the length of the cutting plane A in the x,y plane is also assumed to be equal to 1. The calculation of these stresses in a general way is possible based on an equilibrium of forces in x and y direction:

$$\sigma_\alpha = \sigma_y (\cos \alpha)^2 + \sigma_x (\sin \alpha)^2 + 2\tau_{xy} \cos \alpha \sin \alpha \quad (2.18)$$

$$\tau_\alpha = \sigma_y \sin \alpha \cos \alpha - \sigma_x \sin \alpha \cos \alpha - \tau_{xy} (\cos \alpha)^2 + \tau_{xy} (\sin \alpha)^2 \quad (2.19)$$

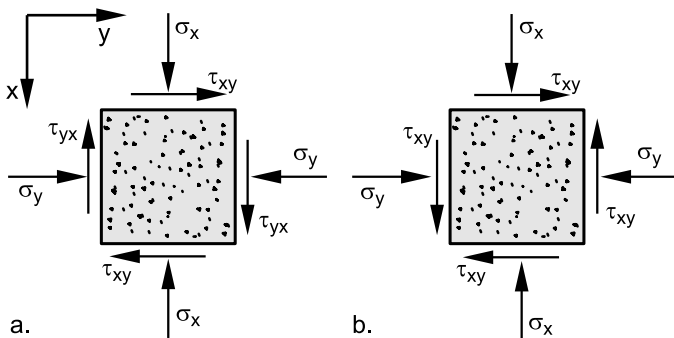


Fig. 2.7. Volume element (two-dimensional stress state)

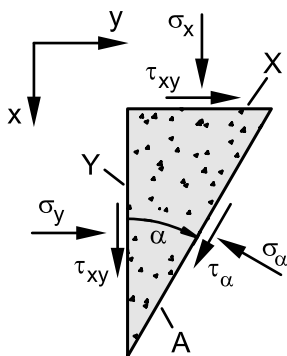


Fig. 2.8. Equilibrium of forces at a triangular bulk solid element

After some conversions similar to Eqs.(2.4) to (2.16) it follows:

$$\sigma_\alpha = \frac{\sigma_y + \sigma_x}{2} + \frac{\sigma_y - \sigma_x}{2} \cos 2\alpha + \tau_{xy} \sin 2\alpha \quad (2.20)$$

$$\tau_\alpha = \frac{\sigma_y - \sigma_x}{2} \sin 2\alpha - \tau_{xy} \cos 2\alpha \quad (2.21)$$

It can be shown that a cutting plane exists, which is inclined by the angle $\alpha = \alpha'$ to plane Y (Fig. 2.8), where the shear stress $\tau_{\alpha'}$ is equal to zero. Angle α' follows from Eq.(2.21) for $\tau_\alpha = 0$:

$$\tan 2\alpha' = \frac{2\tau_{xy}}{\sigma_y - \sigma_x} \quad (2.22)$$

Since the tangent function is π -periodical, $\tan(2\alpha' + \pi)$ is also a valid solution. Thus, two cutting planes exist which are perpendicular to each other

and free from shear stresses. These planes are the principal stress planes on which the principal stresses, σ_1 and σ_2 , are acting. A similar derivation is also possible for the three-dimensional state of stress (see e.g. [2.1]).

2.4 Bulk density

The bulk density is designated as ρ_b . Its unit is kg/m³. Bulk density is defined by the ratio of the mass, m , of an amount of bulk solid to its volume, V . If a bulk solid is in a container of known volume, V , one can calculate the bulk density, ρ_b , after having weighed the contents.

Bulk density, ρ_b , must be distinguished from solid density, ρ_s . Solid density is the density of the material of the individual particles. Bulk density is always less than solid density, since voids exist between the individual particles of a bulk solid, which are taken into consideration in the calculation of bulk density. Voids can also exist within particles. The relationship between bulk density, ρ_b , and solid density, ρ_s , depends on porosity, ε , which is the ratio of the void volume (voids between particles and voids within particles), V_{Voids} , to the total volume, V , of the bulk solid (including all voids):

$$\varepsilon = \frac{V_{Voids}}{V} \quad (2.23)$$

The bulk density, ρ_b , follows from the solid density, ρ_s , and the density of the fluid within the voids, ρ_f :

$$\rho_b = (1 - \varepsilon) \cdot \rho_s + \varepsilon \cdot \rho_f \quad (2.24)$$

If the fluid in the voids is a gas, the second term in Eq. (2.24) usually can be neglected. If the voids are partially filled with liquid, the degree of saturation, S , is used to describe the ratio of the liquid volume, V_{Liquid} , to the void volume:

$$S = \frac{V_{Liquid}}{\varepsilon \cdot V} \quad (2.25)$$

If the density of the gas is neglected, the bulk density of a moist bulk solid can be derived:

$$\rho_b = (1 - \varepsilon) \cdot \rho_s + S \cdot \varepsilon \cdot \rho_f \quad (2.26)$$

When a powder is tested, for example with a shear tester, often the bulk density, ρ_b , is determined by measuring mass and volume of the bulk solid specimen. The bulk density depends on the state of “compaction” or “compression” of the bulk solid, i.e., the magnitude of the consolidation stress acting on the bulk solid. With increasing consolidation stress porosity, ε , decreases and bulk density, ρ_b , increases, since with compaction of a bulk solid the volumes of the voids between the particles, but usually not the particle volumes, decrease.

With fine-grained bulk solids, bulk density can depend strongly on consolidation stress. There are bulk solids with porosities far greater than 0.9 (more than 90% of the total volume consists of voids); at sufficient consolidation (e.g. tabletting, briquetting) one can find porosities less than 0.1 [2.7]. A typical value for the porosity of a not too-finely grained ($> 1 \text{ mm}$) dry bulk solid whose particle shape does not deviate too much from that of a sphere (e.g. quartz sand) is $\varepsilon = 0.4$.

The porosity ε of a bulk solid can be calculated by Eq.(2.24), if the solid density is known and the bulk density has been measured, for example, with a shear tester.

Example: Limestone has a solid density, ρ_s , of around 2700 kg/m^3 . With a shear tester a bulk density of 1050 kg/m^3 has been determined for a fine-grained limestone powder at a certain stress level. For this stress level the porosity then can be calculated using Eq.(2.24): $\varepsilon = 1 - \rho_b/\rho_s = 0.61$. Thus the voids between the particles fill 61% of the volume of this bulk solid at the stress level considered.

Regarding moist bulk solids it has to be considered that compaction or dilation changes the bulk density and, thus, the degree of saturation, S , if the moisture content remains constant. The reason for this is that the void volume $\varepsilon \cdot V$ in the denominator of Eq.(2.25) is changed. Particularly when saturation is attained ($S = 1$), the bulk solid becomes a suspension and, thus, changes its properties dramatically (see Chap. 7). An example for this is moist sand on the beach. By compaction, for example tapping with a foot, the sand can be converted to a saturated state where it shows the properties of a sludge (suspension).

2.5 Elastic and plastic deformation

Elastic deformation occurs when a load (e.g. normal stress) is applied and the deformation disappears completely after the load is removed. Typical examples of elastic deformation are springs (e.g. helical spring, leaf-

spring). Here, the magnitude of the deformation is proportional to the load causing the deformation (Fig. 2.9.a).

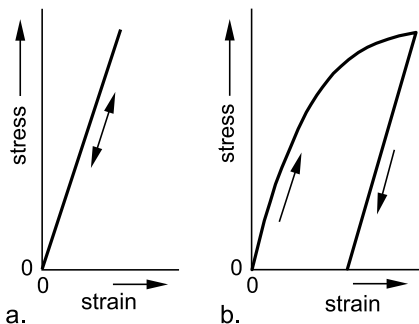


Fig. 2.9. Stress-strain relationships for elastic (a) and plastic (b) deformation of solids

Elastic deformation does not play an important role for most applications in bulk solids technology. In contrast, plastic deformation is of major importance. Plastic deformation occurs when the stress is sufficient to permanently deform the material, whereby the stress-strain relationship is not linear (Fig. 2.9.b). Since the total strain results from elastic and plastic deformation, at removal of the load the strain is reduced according to the elastic deformation whereby the plastic deformation remains.

Plastic deformation of bulk solids generally refers to the deformation of a bulk solid element by moving particles against each other rather than the deformation of individual particles since the deformation at the contacts of individual particles does not contribute much to the total deformation of the bulk solid. To describe this effect, the word “flowing” is often used instead of “deformation”. When a bulk solid element is flowing (= plastic deformation), the volume can increase, decrease, or remain constant, so that bulk density also can increase, decrease, or remain unchanged. As clarification of each of these processes, consider the following examples:

- Compaction of a bulk solid (e.g. tabletting):

Loose powder is compressed in a mold and thereby undergoes plastic deformation (Fig. 2.10). Hence, the bulk solid flows with an increase in bulk density. Thereby its stiffness increases which is indicated by the increasing steepness of the course of the vertical stress, σ_v , plotted versus the deformation, Δh . Upon removal of the compressive stress, only a relatively small elastic deformation will take place and the form of the tablet will remain. Therefore, the bulk solid was deformed plastically by a large force, whereby its volume was reduced and its bulk density was

increased. It has to be mentioned that even at unloading the stress-strain relationship is not linear, because the stiffness of the bulk solid (not the stiffness of the particle material itself) decreases with decreasing stress [2.1].

- Loosening of soil:

Compacted soil (soil is also a bulk solid) is loosened through mechanical influences (e.g. plowing); i.e., the soil is forced to flow plastically and thereby undergoes plastic deformation. The volume of the loosened soil is larger than before and thus its bulk density is less.

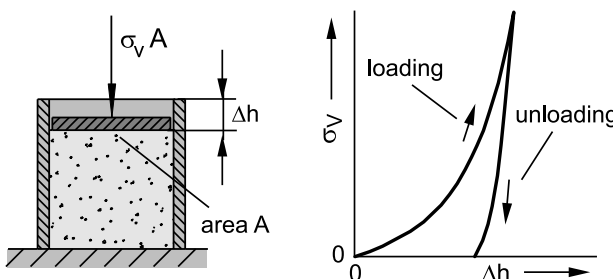


Fig. 2.10. Compaction of a bulk solid and corresponding course of the vertical stress, σ_v , vs. deformation, Δh , at loading and unloading

Whether bulk density increases, decreases, or remains constant depends on the state of compaction (consolidation) of the bulk solid before plastic deformation and on the load exerted on the bulk solid during plastic deformation. A slightly compacted bulk solid will consolidate under a large load (see the above example for tabletting). On the contrary, a strongly compacted bulk solid becomes loosened when it is forced into plastic deformation at relatively small loads, i.e., a load smaller than the consolidation load which created the actual compaction (see the above example of soil loosened by plowing).

2.6 Adhesive forces

The flowability of a fine-grained bulk solid depends largely on the adhesive forces between individual particles. Although adhesive forces are the source of such problems as poor flowability or caking, they are a useful property, e.g., for agglomeration processes, for powder coating, for blackboard chalk, or for the application of cosmetic powders.

Adhesive forces are caused by different mechanisms. With fine-grained, dry bulk solids, major adhesive forces are due to van der Waals interac-

tions and electrostatic forces. The van der Waals forces are based on electric dipoles of atoms and molecules. Their intensity depends on particle size and distance as well as on the materials of the interacting surfaces. The latter is taken into account with the Lifschitz-van der Waals constant.

Electrostatic forces are based on different electric potentials of particle surfaces. One needs to distinguish between conductors and insulators showing a different distribution of electrostatic charges.

With moist bulk solids, liquid bridges between the particles usually are most important. Liquid bridges are formed by small regions of liquid with sufficiently low viscosity in the contact zone of particles (if the viscosity is too high, the mobility of the liquid is limited and it cannot collect at the particle contacts). Due to surface tension the particles are attracted to each other. Furthermore, in the liquid a capillary pressure prevails. If this pressure is lower than the ambient pressure, it provides an additional adhesive force. Extensive derivations on capillary forces have been published by Schubert [2.8].

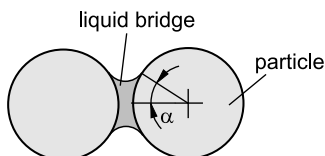


Fig. 2.11. Principle of a liquid bridge with low-viscosity fluid (α : bridge angle)

All types of adhesive forces described above are dependent on the distance. This is demonstrated by calculated adhesive forces, F_H , acting between a spherical particle and a wall (Fig. 2.12). The van der Waals force (curve 4) is very large at small distances, a , but decreases strongly with increasing distance already in the range of distances below 1 μm (10^{-3} mm). This shows that van der Waals forces are of large influence if the surfaces are in contact. The more the surfaces are pressed against each other (e.g. during tabletting), which goes along with particle rearrangement and plastic deformation at contact points, the larger the adhesive forces will be.

Adhesive forces due to liquid bridges (curve 1) are also large at small distances, but decrease only slightly with increasing distance. If the distance becomes too large, the liquid separates and, thus, the adhesive force diminishes. Compared to van der Waals forces and liquid bridges, electrostatic forces (curves 2 and 3) are clearly smaller at small distances, a , but do not decrease as much with increasing distance. Thus, at larger distances, adhesive forces due to electrostatic forces are larger than the other forces discussed here.

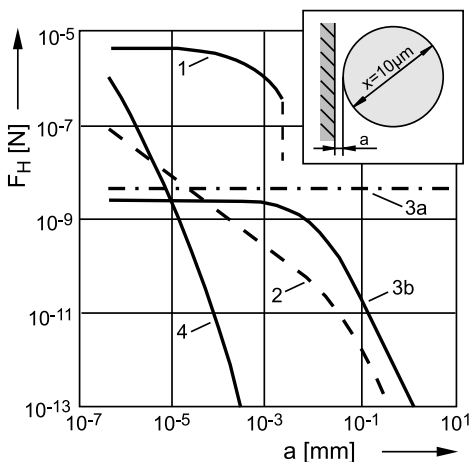


Fig. 2.12. Calculated adhesive forces, F_H , between a spherical particle (diameter $x = 10 \mu\text{m}$) and a wall as a function of the distance a [2.10,2.11]; (1) liquid bridge (bridge angle $\alpha = 20^\circ$, surface tension of the liquid $\gamma = 7.2 \cdot 10^{-2} \text{ N/m}$, contact angle $\delta = 0^\circ$); (2) electrostatic force for a conductor (contact potential $U = 0.5 \text{ V}$); (3) electrostatic force for an insulator (electric charge density $\sigma = 10^2 \text{ e}/\mu\text{m}^2 = 1.6 \cdot 10^{17} \text{ As}/\mu\text{m}^2$; 3a. sphere-semispace; 3b. sphere-point charge); (4) van der Waals force (Lifschitz-van der Waals constant $\hbar\bar{\omega} = 8 \cdot 10^{-19} \text{ J}$)

The above examination of adhesive force mechanisms shows that the flow of fine-grained bulk solids, where the particles are in contact with each other, is influenced above all by van der Waals forces and liquid bridges, whereby liquid bridges can only play a role in the presence of a low-viscosity liquid. Thus, for the flow of dry, fine-grained bulk solids, van der Waals forces are dominant. In contrast, electrostatic forces often can be neglected regarding powder flow because at small distances their influence is small compared to the other adhesive forces discussed here.

The adhesive force of a liquid bridge is strongly dependent on the amount of liquid. Figure 2.13 shows the adhesive force, F_H , related to the product of surface tension, γ , and particle diameter, x , as a function of the dimensionless distance, (a/x) , which is the ratio of the distance to the particle diameter. If only a small amount of liquid is present (small values of the fluid portion, φ , see Fig. 2.13), the variation of the distance has a strong influence on the shape of the liquid bridge, and, thus, on the adhesive force. Furthermore, due to the limited amount of liquid, stable liquid bridges are possible only at small values of the dimensionless distance, (a/x) . In contrast to this, for higher values of the fluid portion, φ , the influence of the distance is smaller (as discussed above, Fig. 2.12).

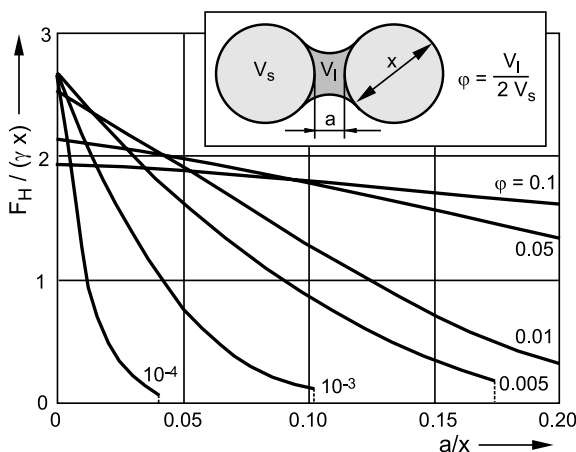


Fig. 2.13. Dimensionless adhesive force, $F_H/(\gamma \cdot x)$, of a liquid bridge between two spherical particles (diameter x) as a function of the dimensionless distance, a/x (contact angle $\delta = 0^\circ$) [2.9,2.12]

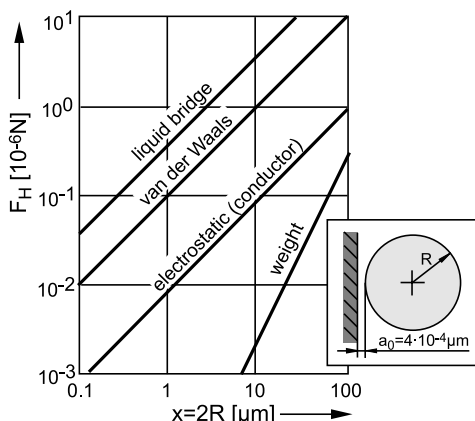


Fig. 2.14. Influence of particle size, x , on the adhesive force, F_H , between a spherical particle and a wall (taken from [2.10,2.11], where the conditions for the calculations are reported)

The influence of particle size on adhesive forces is shown in Fig. 2.14 for ideal conditions (ideally smooth surfaces of sphere and wall) [2.10,2.11]. As already shown in Fig. 2.12, at small distances (here: $a_0 = 4 \cdot 10^{-4} \mu\text{m}$) the adhesive forces due to liquid bridges are the largest, followed by van der Waals forces. The electrostatic force is clearly smaller. Also plotted in Fig. 2.14 is the particle weight, which is proportional to the third power of the diameter and increases steeper with increasing particle size than the adhesive forces. Therefore, the weight force becomes the dominant force above

a certain particle size. This is the reason for small particles (e.g. dust) being able to adhere to a vertical wall, whereby larger particles (e.g. sand grains) cannot.

It has to be recognized that the forces in Fig. 2.14 have been calculated for ideal conditions and are larger than the forces which can be expected in reality. One important reason for this is that real particles and walls have rough surfaces leading to an increase in distance and therefore a reduction of adhesive forces (see Fig. 2.12). The influence of roughness is shown in Fig. 2.15. The diagrams plot adhesive forces, F_H , acting between a spherical particle (radius R) and a wall, whereby the particle is provided with a hemisphere (radius r) acting as an artificial roughness.

Since the distance between the wall and the tip of the roughness, simulated by the hemisphere, is kept constant in Fig. 2.15, the distance between the spherical particle and the wall increases with the hemisphere radius, r . According to the influence of the distance on van der Waals forces (see Fig. 2.12), the increase of the hemisphere radius, r , leads to a decrease of the adhesive force, F_H , as long as the hemisphere radius is sufficiently small (see left diagram in Fig. 2.15). The adhesive force is plotted for three different particle diameters between 0.5 μm and 50 μm . In the left part of the diagram the proportionality between adhesive force and particle diameter as shown in Fig. 2.14 can be recognized. In the right part of the diagram, i.e., at larger values of the hemisphere radius, r , the calculated adhesive force increases with r . Here the adhesive force between the hemisphere itself and the wall becomes dominant relative to the adhesive force between the spherical particle and the wall.

The right diagram in Fig. 2.15 shows the influence of roughness on liquid bridges and electrostatic forces for several conditions. Forces of liquid bridges are plotted for two different values of the bridge angle ($\alpha = 2.5^\circ$ and $\alpha = 20^\circ$) in order to demonstrate the influence of the amount of liquid. Compared to the van der Waals forces, the influence of the roughness is in both cases smaller. Particularly for the larger amount of liquid ($\alpha = 20^\circ$), the influence of roughness is very small, since the variation of radius r has less influence on the shape of the liquid bridge. If a sufficient amount of liquid is present, the roughness (hemisphere) is surrounded by the liquid (as in the sketch in the right diagram). If the amount of liquid is too small, the liquid bridge forms between the hemisphere and the wall. Thereby an increasing radius, r , of the hemisphere acts similar as an increasing particle size (see Fig. 2.14): The adhesive force, F_h , increases proportional to r .

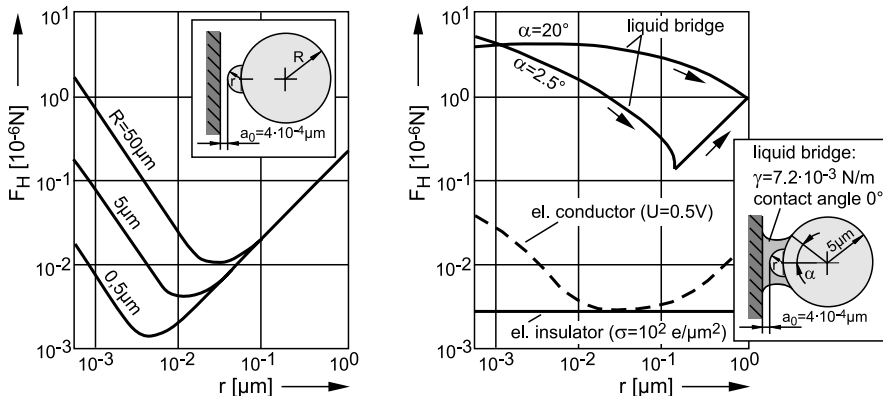


Fig. 2.15. Adhesive force, F_h , between a spherical particle and a wall in dependence on the radius, r , of a hemisphere simulating the roughness. Distance a_0 between tip of the roughness and wall is constant (taken from [2.10,2.11] where the conditions for the calculations can be found)

The electrostatic force between a spherical particle, which is an insulator, and a wall (Fig. 2.15, right diagram) is nearly independent of the roughness (as known from the distance, a , see curve 3a in Fig. 2.12).

The adhesive force of a particle made from conducting material at first decreases with increasing roughness (left part of the diagram: influence of increasing distance between particle and wall in analogy to Fig. 2.12), then, at larger values of hemisphere radius, r , the adhesive force increases (influence of adhesive force between the hemisphere and the wall in analogy to the influence of particle size as shown in Fig. 2.14).

The considerations above did not take into account the influence of adsorption layers, which form on the particle surface depending on ambient conditions. If the ambient atmosphere contains humidity, adsorption layers can build up on hydrophilic surfaces already at a relative humidity far below 60%. If the relative humidity is very small, mono-molecular adsorption layers form (Fig. 2.16). At higher values of relative humidity, multi-layer adsorption can be observed (in multilayer adsorption not all adsorbed molecules are in contact with the surface layer of the adsorbent; it is a special property of water to form hydrogen bonds). If the relative humidity exceeds approx. 60 – 85% (material depending), capillary condensation starts. Capillary condensation is said to occur when multilayer adsorption proceeds to the point at which pore spaces (2 to 100 nm [2.13]) including pores formed at particle contacts are filled with liquid separated from the gas phase by menisci [2.14]. Above the concave menisci moisture condensation is supported by the reduced saturation vapor pressure [2.13].

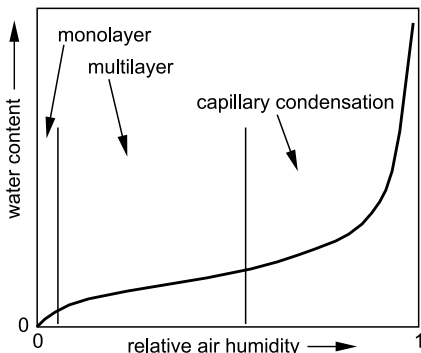


Fig. 2.16. Water adsorption isotherm (in principle) [2.14]

The influence of adsorption layers on adhesive forces is complex and cannot be described generally [2.11]. If particles with adsorption layers are in contact, there is no direct contact of the particles, but rather of the particles with the adsorbed liquid [2.15]. Therefore, the adsorption layers can lead to larger or smaller van der Waals forces, which are dependent on material-dependent parameters (e.g., Lifschitz-van der Waals constant). In the case of overlapping water-based adsorption layers one will obtain larger adhesive forces compared to the same particle contact without adsorption layers “with high probability” [2.11]. If the relative humidity leads to capillary condensation, one can expect the formation of liquid bridges at the particle contacts, which will result in adhesive forces due to liquid bridges. Thereby the liquid portions attained through capillary condensation are usually small compared to those resulting from typical technical processes (e.g., dewatering process with a filter press) [2.15].

Some bulk solids continue to gain strength if stored at rest under compressive stress for a long time period. This effect is called time consolidation. The reasons for time consolidation are also to be found in the effects of adhesive forces. Possible mechanisms are:

- Visco-plastic or plastic deformation at particle contacts, which leads to an increase in adhesive forces through approach of the particles (distance is reduced) and enlargement of contact areas.
- Solid bridges due to solid crystallizing when drying moist bulk solids, where the moisture is a solution of a solid and a solvent [2.1] (e.g., sand and salt water).
- Solid bridges from the particle material itself, e.g., after some material at the contact points has been dissolved by moisture (e.g., adsorbed moisture from the ambient atmosphere), and later the moisture has been removed [2.1,2.15] (e.g., crystal sugars with slight dampness).

- Bridges due to sintering during storage of the bulk solid at temperatures not much lower than the melting temperature [2.1,2.11]. This can appear, for example, at ambient temperature during the storage of plastics with low melting points.
- Chemical processes (chemical reactions at particle contacts).
- Biological processes (e.g., due to fungal growth on biologically active ingredients)

Whether a bulk solid flows well or poorly depends on the relationship of adhesive forces to other forces acting on the bulk solid. It can be shown that the influence of adhesive forces on flow behavior increases with decreasing particle size (see Sect. 2.7). Thus, as a rule, a bulk solid flows more poorly with decreasing particle size. Fine-grained bulk solids with moderate or poor flow behavior due to adhesive forces are called cohesive bulk solids.

If particles are pressed against each other by external forces, the compressive force acting between the particles increases. As a result large stresses prevail (locally) at the particles' contact points, because the contact points are small. This leads to plastic deformation of the particles in the contact area, so that the contact areas increase and the particles approach each other. Thereby the adhesive forces increase. Thus a compressive force acting from outside on a bulk solid element can increase the adhesive forces. This mechanism is used, for example, in the production of tablets or briquettes.

The dependence of adhesive forces between particles on external forces exerted on a bulk solid is characteristic of bulk solids, especially for cohesive bulk solids. Therefore an evaluation of bulk solids behavior must always take into consideration the forces or stresses previously acting on the bulk solid, i.e., its stress history. The stress history includes, for example, the consolidation stress exerted on a bulk solid, leading to certain adhesive forces and hence to a certain strength of the bulk solid (e.g., the strength of a tablet is dependent on the maximum consolidation stress at tabletting).

The short survey on adhesive forces presented above may be sufficient to give a basic understanding of the influence of the most important parameters such as particle size and distance. In reality various other (chemical and physical) quantities and effects have to be considered (for further reading please refer to [2.1,2.8,2.11,2.16,2.17]). Direct measurements of adhesive forces with centrifuges or atomic force microscopes (AFM) show that even particles of identical size exhibit a wide range of adhesive forces up to one or two orders of magnitude depending on the surface structure. Measurement principles and some results are presented in Sect. 6.5.

Regarding this subject matter, the topic of adhesive forces matches well to the so-called “Lotus effect”, which has been extensively discussed in recent years [2.18]. The name is taken from the sacred Lotus flower, which is provided with self-cleaning leaves. One reason for the self-cleaning effect is that the surface of the leaves is hydrophobic due to its chemical composition. The other reason is the microstructure of the surface, which increases the hydrophobic properties further. A water droplet located on such a surface touches the leaf only at a few points (the tips of the rough surface), whereby air can remain below the droplet (Fig. 2.17). The adhesive force between droplet and leaf is extremely small due to the small contact area. Thus the surface tension of the droplet dominates the adhesive forces, and the droplet has nearly the shape of a sphere. The Lotus effect can be regarded as the increase of hydrophobic properties of a hydrophobic surface by roughness due to a microstructure.

If dirt particles are deposited on such a surface, the roughness of the surface acts as a spacer and thus reduces the van der Waals forces which are dominant on dry surfaces (see Fig. 2.15: van der Waals forces decrease with increasing roughness, if the roughness radius is not too large). If water is added to this system, nearly spherical droplets form on the hydrophobic surface (Fig. 2.18). Even a small inclination of the surface will cause the droplets to roll downwards. If a droplet rolls over a dirt particle, the particle is wetted and adheres to the droplet. Hydrophilic particles move into the droplet, hydrophobic particles remain at the surface of the droplet, i.e., they adhere stronger to the surface of the droplet than to the leaf [2.18]. The technical application of the Lotus effect (in the meantime registered as *Lotus-Effect[®]*) focuses on dirt-repellent, self-cleaning surfaces, e.g., for facade paints and sanitary ware.

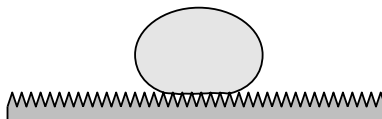


Fig. 2.17. Water droplet on a rough hydrophobic surface [2.18]

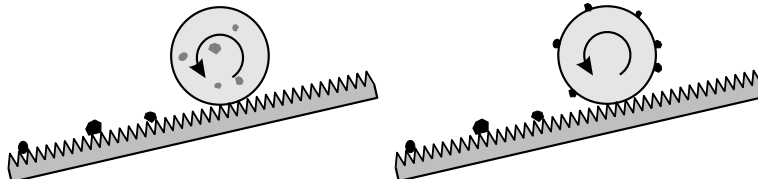


Fig. 2.18. Principle of self-cleaning (Lotus effect): particles (e.g. dirt) are caught by the droplets; left: hydrophilic particle, right: hydrophobic particle [2.18]

2.7 Influence of particle size on the behavior of a bulk solid

Adhesive, interparticle forces have a major influence on the flow behavior of a powder or bulk solid. In Sect. 2.6 the increase of the adhesive force between a sphere and a wall with increasing particle size was outlined (Fig. 2.14). The flow properties of a fine-grained bulk solid are mainly influenced by adhesive forces due to liquid bridges (if moisture is present) and van der Waals forces (dominating force for dry, fine-grained bulk solids). Both forces are proportional to particle size, x (Fig. 2.14). Similar dependencies can be found for adhesive forces between particles.

The general experience with bulk solids is that flowability increases with increasing particle size. The reason for this is to be found in the adhesive forces, even if according to Fig. 2.14 one would expect smaller adhesive forces with smaller particles. To outline the influence of particle size, in the following the tensile strength of a bulk solid is examined. Although tensile strength does not play an important role in practice where bulk solids have to be handled and usually are subjected to compressive stresses rather than tensile stresses (e.g., in a silo or a container), it is easy to understand the link between tensile strength and adhesive forces. To measure tensile strength, a platen is coated with a thin layer of glue on its underside and then vertically pressed into a powder sample with force F_V (Fig. 2.19). Afterwards the platen is carefully pulled upwards until the bulk solid fails. From the maximum force arising at failure the tensile strength, σ_t , is determined. The portion of the force related to the strength of the bulk solid (F_Z) is divided by the area A of the platen (for more information about the measurement principle refer to Sect. 6.3.13, further remarks can be found in Sect. 5.3.2).

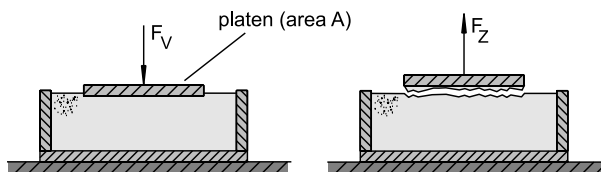


Fig. 2.19. Measurement of the tensile strength

The tensile strength, σ_t , can be regarded as the sum of the adhesive forces at a large number of particle contacts. In the following this is regarded on the basis of the van der Waals force. Then the adhesive force, F_H , between two spherical particles with diameter d of constant distance is proportional to the particle diameter:

$$F_H \propto d \quad (2.27)$$

The tensile strength, σ_t , can be calculated from the tensile force at failure, F_Z , divided by the area of the platen, A (see Fig. 2.19):

$$\sigma_t = \frac{F_Z}{A} \quad (2.28)$$

Now it is assumed that the force F_Z is the sum of the adhesive forces at the individual particle contacts in the failure plane. The number of contacts is n :

$$F_Z = n \cdot F_H \quad (2.29)$$

The number of particle contacts, n , is proportional to area A and inversely proportional to the square of the particle diameter, d , since the smaller the particles, the more particles can be found on a certain area (Fig. 2.20):

$$n \propto \frac{A}{d^2} \quad (2.30)$$

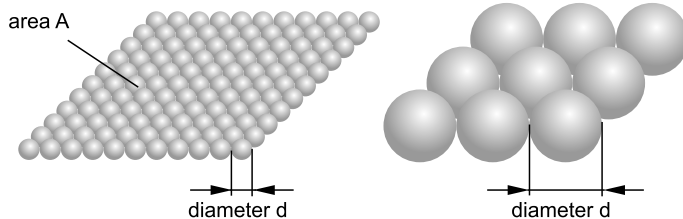


Fig. 2.20. Particles per area

With Eqs. (2.27), (2.29) and (2.30) it follows from Eq. (2.28):

$$\sigma_t = \frac{F_Z}{A} \propto \frac{n \cdot F_H}{A} \propto \frac{\frac{A}{d^2} \cdot F_H}{A} \propto \frac{F_H}{d^2} \propto \frac{1}{d} \quad (2.31)$$

Thus it is demonstrated that the tensile strength of a powder is inversely proportional to particle diameter. A similar relationship can be found for compressive strength, σ_c , which is described in the next section. Generally, it can be stated that with decreasing particle size the strength of a bulk solid becomes greater and, thus, its flowability is reduced. For the sake of completeness it has to be mentioned that there exist exceptions to this rule, e.g., when a fine-grained bulk solid is mixed with a small portion of an even more fine powder working as a flow agent. This leads to a smaller

mean particle size, but reduces the strength and increases the flowability (see Sect. 7.2.2).

An example taken from nature is the gecko, whose feet are provided with millions of thin hairs (so-called spatulae). Instead of a small number of contacts with a large diameter, the gecko can adhere to a wall with a large number of contacts of very small diameter due to the hairs at its feet. As outlined above, the tensile strength or transferable tensile force per area, respectively, can be increased by a reduction of the particle size (corresponding to the small diameter of the hairs). Due to this effect, in theory the feet of a gecko can transfer several times the gecko's weight, which allows the gecko to climb vertical walls [2.19].

3 Flow properties of bulk solids

The flow properties of bulk solids depend on many parameters, e.g.:

- particle size distribution,
- particle shape,
- chemical composition of the particles,
- moisture,
- temperature.

It is not possible to determine theoretically the flow behavior of bulk solids as a function of all of these parameters. Even if this were possible, the expense for the determination of all parameters of influence would be very high. Thus it is necessary, and also simpler, to determine the flow properties in appropriate testing devices.

To approach the subject of this section, at first a simple test procedure, the uniaxial compression test, will be considered. Following this the measurement of flow properties with shear testers based on Jenike's contributions [3.1] will be explained.

3.1 Uniaxial compression test

3.1.1 Consolidation of bulk solids

The phrase "good flow behavior" usually means that a bulk solid flows easily, i.e., it does not consolidate much and flows out of a silo or a hopper due to the force of gravity alone and no flow promoting devices are required. Products are "poorly flowing" if they experience flow obstructions or consolidate during storage or transport. In contrast to these qualitative statements, a quantitative statement on flowability is possible only if one uses an objective characteristic value that takes into account those physical characteristics of the bulk solid that are responsible for its flow behavior.

"Flowing" means that a bulk solid is deformed plastically due to the loads acting on it (e.g. failure of a previously consolidated bulk solid sam-

ple). The magnitude of the load necessary for flow is a measure of flowability. This will be demonstrated first with the uniaxial compression test.

In Fig. 3.1 a hollow cylinder filled with a fine-grained bulk solid is shown (cross-sectional area A ; internal wall of the hollow cylinder assumed as frictionless). The bulk solid is loaded by the stress σ_1 – the consolidation stress or major principal stress – in the vertical direction and, thus, compressed. The more the volume of the bulk solid is reduced, the more compressible the bulk solid.

With an easy-flowing, dry bulk solid with large, hard particles (e.g., wheat grains or glass beads), bulk density will increase very little. With a fine and/or moist bulk solid (e.g. flour, moist sand), one will observe a clear increase in bulk density.

In addition to the increase in bulk density from consolidation stress, one will observe also an increase in strength of the bulk solid specimen. Hence, the bulk solid is both consolidated and compressed through the effect of the consolidation stress.

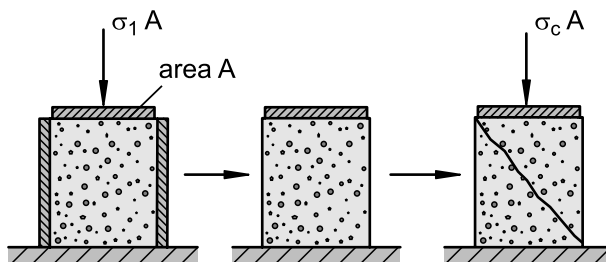


Fig. 3.1. Uniaxial compression test

After consolidation, the bulk solid specimen is relieved of the consolidation stress and the hollow cylinder is removed. If subsequently the consolidated cylindrical bulk solid specimen is loaded with an increasing vertical compressive stress, the specimen will break (fail) at a certain stress. The stress causing failure is called compressive strength, cohesive strength, or unconfined yield strength, σ_c (another common designation is f_c as introduced by Jenike [3.1]).

In bulk solids technology one calls the failure “incipient flow”, because at failure the consolidated bulk solid specimen starts to flow. Thereby the bulk solid dilates somewhat in the region of the surface of the fracture, since the distances between individual particles increase. Therefore incipient flow is plastic deformation with decrease of bulk density (see Sect. 2.5). Since the bulk solid fails only at a sufficiently large vertical stress, which is equal to its compressive strength, there must exist a material-

specific yield limit for the bulk solid. Only when this yield limit is reached does the bulk solid start to flow.

The yield limits of many solid materials (e.g. metals) are listed in tables. However, the yield limit of a bulk solid is dependent also on its stress history, i.e., previous consolidation: The greater the consolidation stress, σ_l , the greater are bulk density, ρ_b , and unconfined yield strength, σ_c .

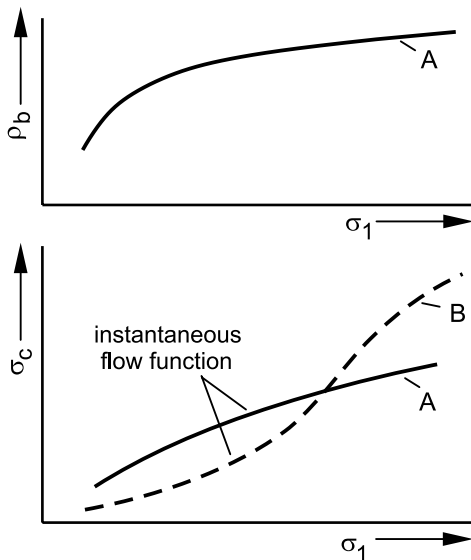


Fig. 3.2. Bulk density, ρ_b , and unconfined yield strength, σ_c , in dependence on consolidation stress, σ_l

Uniaxial compression tests (Fig. 3.1) conducted at different consolidation stresses, σ_l , yield different pairs of values (σ_c , σ_l) and (ρ_b , σ_l). Plotting these pairs of values as points in a σ_c, σ_l diagram and a ρ_b, σ_l diagram, respectively, and drawing in each diagram a curve through these points, usually results in curves like those for product A in Fig. 3.2, where bulk density, ρ_b , and unconfined yield strength, σ_c , typically increase with consolidation stress, σ_l . Very rarely a curve $\sigma_c(\sigma_l)$ like curve B is obtained where within a limited range of the consolidation stress a progressive slope is observed. The curve $\sigma_c(\sigma_l)$ is called the flow function, or instantaneous flow function to emphasize that the strength is measured directly after consolidation.

3.1.2 Time consolidation

Some bulk solids increase in strength if they are stored for a period of time at rest under a compressive stress (e.g. in a silo or an IBC). This effect is called *time consolidation* or *caking*. Time consolidation is the result of the increase of interparticle adhesive forces with time based on different mechanisms (see Sect. 2.6). If particles are moved relative to each other, these adhesive forces diminish and can build up again during further storage at rest.

Time consolidation can be determined with the test shown in Fig. 3.1, in order, for example, to simulate long-term storage in a silo. To conduct this test one loads the specimen with consolidation stress, σ_I , not just for a short moment, but for a defined period of time, t . Then the unconfined yield strength is determined following the principle explained above (right part of Fig. 3.1).

In Fig. 3.3 the instantaneous flow function $\sigma_c(\sigma_I)$ of product A (see Fig. 3.2) is shown. The instantaneous flow function represents the unconfined yield strength without influence of time consolidation, i.e., for a storage period $t = 0$. Additionally, examples of curves $\sigma_c(\sigma_I)$ for storage periods $t > 0$ (curves A_1 , A_2) are drawn. The curves $\sigma_c(\sigma_I)$ for the storage periods $t > 0$ are called time flow functions. Here each curve results from the connection of several pairs of values (σ_c, σ_I) , which were measured at identical storage periods, t , but at different consolidation stresses, σ_I .

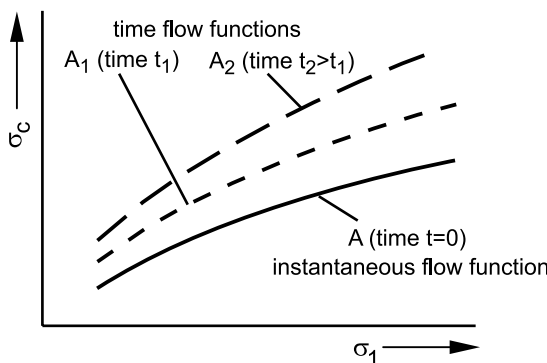


Fig. 3.3. Instantaneous flow function and time flow functions

For the example of bulk solid A, its unconfined yield strength, σ_c , increases with increasing storage time. This result is true for many bulk solids, but not for all. There are bulk solids which undergo no or only very slight consolidation over time; i.e., σ_c do not increase or increase only very slightly with increasing storage period (e.g. dry quartz sand). Other bulk solids un-

dergo a large increase in unconfined yield strength after storage periods of only a few hours, whereas after longer storage periods their unconfined yield strength does not increase further. These differences are due to the different physical, chemical, or biological effects that are the causes of consolidation over time, e.g. chemical processes, crystallizations between the particles, enlargement of the contact areas through plastic deformation, capillary condensation, or biological processes such as fungal growth (see Sect. 2.6).

With measurement of time consolidation, a “time-lapse effect” is not realizable, i.e., one must store a bulk solid specimen at the consolidation stress, σ_1 , for exactly that period of time for which one would like to get data on time consolidation. Without such a test no quantitative statement can be made regarding time consolidation.

3.1.3 Representation of stresses using Mohr stress circles

The uniaxial compression test presented in Fig. 3.1 is shown below in a σ, τ diagram (Fig. 3.4). If one neglects the force of gravity acting on the bulk solid specimen and assumes that no friction is acting between the wall of the hollow cylinder and the bulk solid, both vertical stress as well as horizontal stress are constant within the entire bulk solid specimen. Therefore at each position within the bulk solid sample the state of stress, which can be represented by a Mohr stress circle, is identical.

During consolidation the normal stress, σ_1 , acts on the top of the bulk solid specimen. Perpendicular to the vertical stress the smaller horizontal stress, σ_2 , prevails according to the stress ratio, K (see Sect. 2.3). At neither the top nor bottom of the specimen, nor at the internal wall of the hollow cylinder, which is assumed to be frictionless, will shear stresses be found; i.e., $\tau = 0$. The pairs of values (σ , τ) for vertical and horizontal cutting planes within the bulk solid specimen are plotted in the σ, τ diagram (Fig. 3.4). Both points are located on the σ -axis because $\tau = 0$. The Mohr stress circle, which describes the stresses in the bulk solid sample at consolidation, is thus well defined (because each stress circle has exactly two intersections with the σ -axis defining the principal stresses). The stress circle representing the stresses at consolidation is shown in Fig. 3.4 (stress circle A).

In the second part of the test shown in Fig. 3.1, the specimen is loaded with increasing vertical stress after it has been relieved of the consolidation stress and the hollow cylinder has been removed. Here vertical stress and horizontal stress are principal stresses.

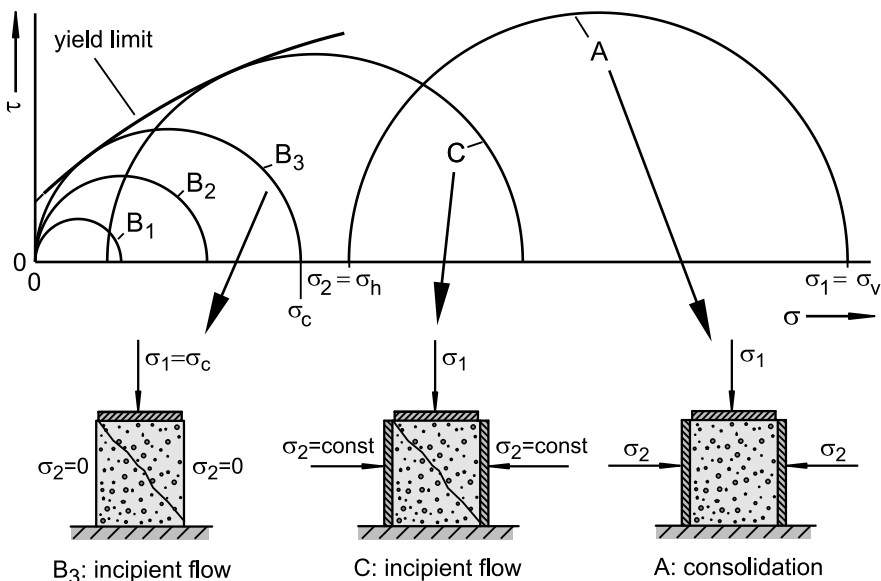


Fig. 3.4. Measurement of the unconfined yield strength in a σ, τ diagram

During the increasing vertical load in the second part of the test, the stress states at different load steps are represented by stress circles with increasing diameter (stress circles B_1 , B_2 , B_3 in Fig. 3.4). The minor principal stress, which is equal to the horizontal stress, is equal to zero at all stress circles, since the lateral surface of the specimen is unrestrained and not loaded.

At failure of the specimen the Mohr stress circle B_3 represents the stresses in the bulk solid sample. Since the load corresponding to this Mohr stress circle causes incipient flow of the specimen, the yield limit of the bulk solid must have been attained in one cutting plane of the specimen. Thus, Mohr stress circle B_3 must reach the yield limit in the τ, σ diagram. In Fig. 3.4 a possible yield limit is shown. A simplified interpretation of the yield limit is that it gives for every normal stress, σ , a shear stress, τ , which is necessary to initiate flow, i.e., to move particles relative to each other.

The Mohr stress circles B_1 and B_2 , which are completely below the yield limit, cause only an elastic deformation of the bulk solid specimen, but no failure and/or flow. Stress circles larger than stress circle B_3 , and thus partly above the yield limit, are not possible: The specimen would already be flowing when the Mohr stress circle reaches the yield limit (failure), so that no larger load could be exerted on the specimen.

In Fig. 3.5 the connection between the Mohr stress circle, the yield limit and the orientation of the failure plane is shown. The point where the Mohr stress circle B_3 touches the yield limit defines the pair of values of shear stress, τ , and normal stress, σ , that initiates flow. These stresses are attained only in cutting planes of two particular orientations. One orientation can be identified with the Mohr stress circle in Fig. 3.5. The angle from the point on the Mohr stress circle representing the horizontal plane, where the vertical stress, σ_v , is acting, to the point where it touches the yield limit is 2α . Thus, a failure plane in the bulk solid specimen is inclined by the angle α to the horizontal, whereby α is measured in the opposite direction as in the Mohr circle (see Sect. 2.2). The second orientation of the failure planes is defined by the point where the Mohr stress circle touches the yield limit mirrored along the σ -axis (not visible in Fig. 3.5).

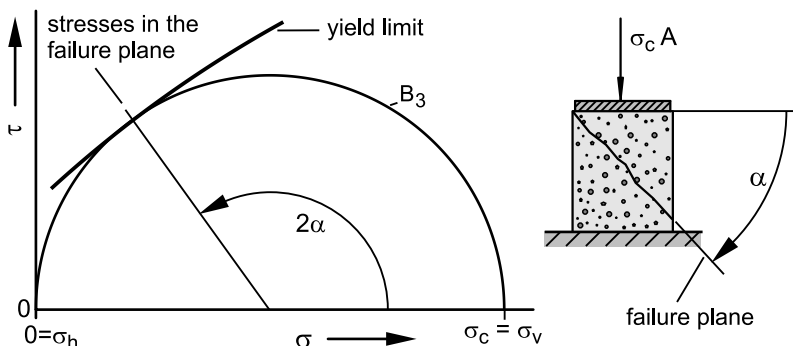


Fig. 3.5. Relationship between Mohr stress circle, yield limit and failure plane in the bulk solid specimen

If, during the second part of the experiment shown in Fig. 3.1 (measurement of compressive strength), one were to apply also a horizontal stress greater than zero ($\sigma_2 > 0$) on the specimen (in addition to the vertical stress, σ_v), one would likewise find stress circles that indicate failure of the specimen and reach the yield limit (e.g. stress circle C in Fig. 3.4). Thus the yield limit is the envelope of all stress circles that indicate failure of a bulk solid sample.

3.1.4 Numerical characterization of flowability

Flowability of a bulk solid is characterized mainly by its unconfined yield strength, σ_c , as a function of the consolidation stress, σ_I , and the storage period, t . Usually the ratio ff_c of consolidation stress, σ_I , to unconfined yield strength, σ_c , is used to characterize flowability numerically:

$$ff_c = \frac{\sigma_1}{\sigma_c} \quad (3.1)$$

The larger ff_c is, i.e., the smaller the ratio of the unconfined yield strength to the consolidation stress, the better a bulk solid flows. Similar to the classification used by Jenike [3.1], one can define flow behavior as follows:

- $ff_c < 1$ not flowing
- $1 < ff_c < 2$ very cohesive
- $2 < ff_c < 4$ cohesive
- $4 < ff_c < 10$ easy-flowing
- $10 < ff_c$ free-flowing

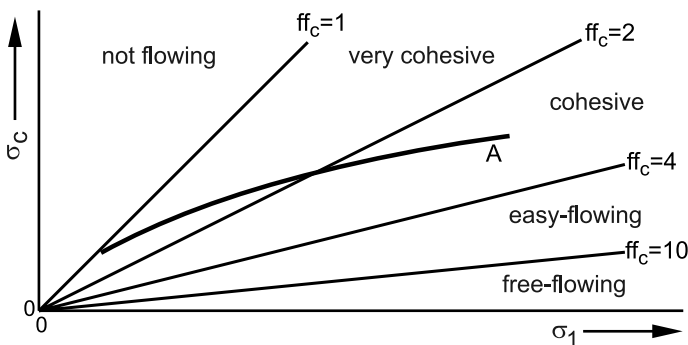


Fig. 3.6. Instantaneous flow function and lines of constant flowability

In Fig. 3.6 the instantaneous flow function A taken from the σ_c, σ_1 diagram in Fig. 3.2 is shown. Additionally, the boundaries of the ranges of the classifications listed above are shown as straight lines, each representing a constant value of flowability, ff_c . This diagram clearly shows that the ratio ff_c of a specific bulk solid is dependent on the consolidation stress, σ_1 (in most cases ff_c increases with σ_1 as with bulk solid A). Therefore, with each consolidation stress at which σ_c and thus ff_c were determined one obtains a different value of flowability: The flowability of a bulk solid depends on the stress level (= consolidation stress); thus for most bulk solids one will obtain a larger value of flowability (= better flowability) at a greater consolidation stress. For most bulk solids one will find a (possibly extremely low) consolidation stress at which the bulk solid flows poorly. Because of the dependence of flowability on consolidation stress, it is not possible (unfortunately) to describe the flowability of a bulk solid with only one numerical value.

The increase in flowability with increased consolidation stress at first glance may seem inconsistent, since unconfined yield strength, σ_c , increases with increasing consolidation stress, σ_I ; i.e., the bulk solid increasingly gains strength. How then can it flow better? The answer is to be found in the definition of flowability in Eq. (3.1): Flowability is the ratio of consolidation stress to unconfined yield strength, and this ratio becomes greater with increasing consolidation stress for most bulk solids (e.g. see curve A in Fig. 3.2).

The following will clarify that the definition of flowability is meaningful. In Fig. 3.7 the lower part of a hopper filled with bulk solid is shown. In a hopper the major principal stress (= consolidation stress, σ_I) decreases towards the hopper apex (see Sect. 9.1.2). The diagrams in Fig. 3.7 show the consolidation stress, σ_I , the unconfined yield strength, σ_c , resulting from the consolidation stress, and the flowability, ff_c , determined according to Eq.(3.1).

Poor flowability of the bulk solid in the hopper means that flow obstructions due to arching occur. From experience it is known that arching can be avoided if the outlet opening of the hopper is sufficiently large. This finding is supported by the hopper in Fig. 3.7: In the lower part of the hopper the flowability, ff_c , is close to 1, thus the bulk solid can be characterized as nearly not flowing. With increasing distance from the hopper apex the consolidation stress increases and the flowability becomes better, so that in the upper part of the hopper stable arches cannot form. Thus, if the outlet opening is sufficiently large, everywhere in the hopper the flowability of the bulk solid is high enough to avoid flow obstructions.

If a bulk solid is set to flow, its yield limit must be attained. Often only stresses of the same order of magnitude as at the previous consolidation can be applied (e.g. the force of gravity). In the above example (bulk solid in a hopper, Fig. 3.7) the bulk solid should flow after the outlet is opened. After opening of the outlet approximately the same stresses act on the bulk solid as previously (with the outlet closed). The bulk solid can flow out only if the stress acting on the bulk solid is greater than the strength of the bulk solid. A measure of this strength is the unconfined yield strength, σ_c . One can also say that the greater the ratio of the stress acting on the bulk solid to the unconfined yield strength, the more easily will the bulk solid flow. Precisely this relationship is indicated through the value of flowability, ff_c , according to Eq.(3.1). This value of flowability, being the ratio of the consolidation stress, σ_I , to the unconfined yield strength, σ_c , is therefore in many cases the criterion that determines whether a bulk solid flows in a certain situation or not.

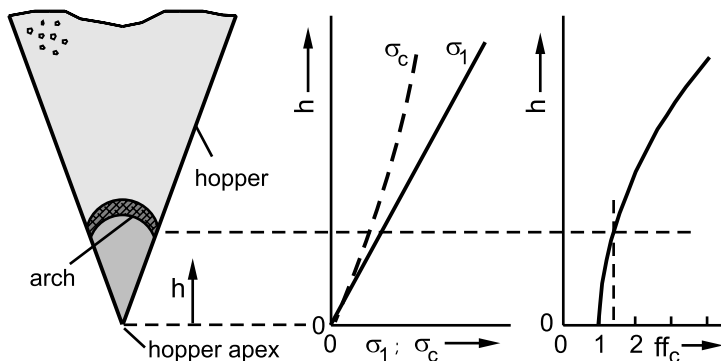


Fig. 3.7. Consolidation stress, σ_I , unconfined yield strength, σ_c , and flowability, ff_c , of the bulk solid in the hopper

With the results of time consolidation tests, flowability can be determined with Eq.(3.1), using the unconfined yield strength, σ_c , which was measured after the corresponding storage period. If the bulk solid shows a time consolidation effect, one will measure a larger unconfined yield strength with increasing storage period, so that from Eq.(3.1) lesser flowability will follow. This is logical: If a bulk solid gains strength with an increasing period of storage at rest at a certain consolidation stress, it will be more difficult to get this bulk solid to flow; i.e., its flowability decreases with increasing storage period.

In Fig. 3.3, Sect. 3.1.2, an instantaneous flow function and two time flow functions are shown. The instantaneous flow function represents unconfined yield strength, σ_c , as a function of consolidation stress, σ_I , without influence of a storage period, i.e., for the storage period $t = 0$. A time flow function represents the unconfined yield strength which emerges after storage at the consolidation stress over a period of time, t (see Sect. 3.1.2). The instantaneous flow function and time flow functions from Fig. 3.3 are shown in Fig. 3.8.a along with the boundaries of the ranges, which follow from the classification of flowability as outlined above. It can be seen that flowabilities, ff_c , measured at identical consolidation stress, but after different consolidation periods, decrease with increasing consolidation time. For the consolidation stress $\sigma_{Example}$ (Fig. 3.8.a) chosen as an example, one obtains measurement points in areas of decreasing flowability when increasing consolidation period t (see arrow in Fig. 3.8.a). The decrease of flowability with consolidation period is shown in Fig. 3.8.b.

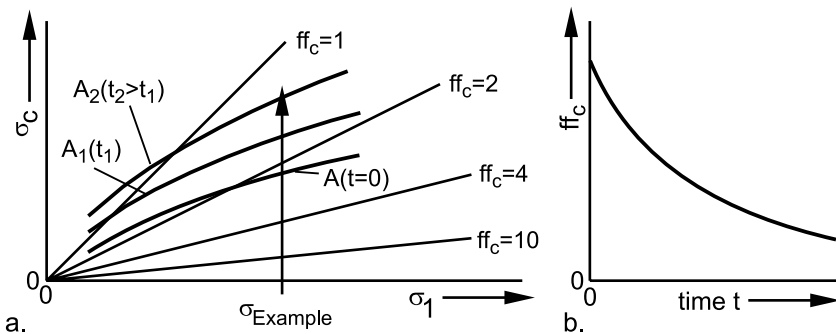


Fig. 3.8. Influence of storage period on flowability; a. instantaneous flow function A and time flow functions A_1 , A_2 ; b. flowability vs. time

From the dependence of flowability, ff_c , on consolidation stress, σ_1 , it follows that one can compare the flow behavior of several bulk solids quantitatively using ff_c only if all measurements have been performed at identical consolidation stresses. Otherwise, totally different (incorrect) statements might result. See the example in Fig. 3.9, where the instantaneous flow functions of two bulk solids, A and B, are shown. The flowability, ff_c , of the better flowing bulk solid A was measured at a very low consolidation stress, so that a relatively low flowability value emerged. The flowability of the more poorly flowing bulk solid B was measured at a clearly greater consolidation stress, where this bulk solid has a better flowability than the better flowing bulk solid A at the lower consolidation stress. Therefore, a comparison of ff_c values would result in an incorrect ranking of flowabilities. If one had measured flowability at identical consolidation stresses, one would have determined flowabilities that represent the true relationships.

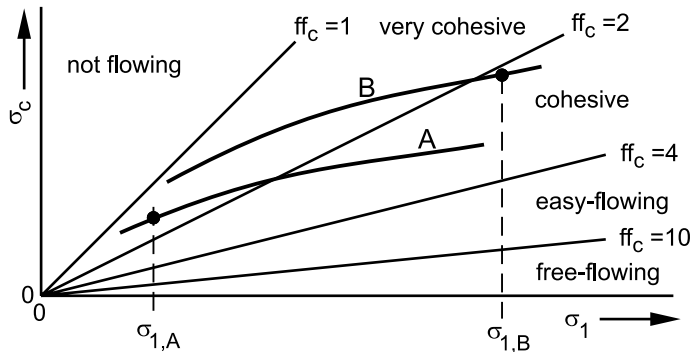


Fig. 3.9. Influence of consolidation stress on flowability

When providing the flowability value, ff_c , of a bulk solid, the consolidation stress at which flowability was measured must also be given. Otherwise the flowability value is meaningless because - as outlined above - depending on the consolidation stress selected one can measure very different values of flowability for any product.

In addition, the time consolidation of different bulk solids can be compared only at identical consolidation stress and identical consolidation time. Therefore, besides the ff_c value, one must provide the consolidation stress and the consolidation period values used.

The consolidation stress and the consolidation period selected for testing should reflect, as much as possible, the actual process conditions in which the problem occurs (e.g. stress and storage period for storage in bags on pallets, stress near the outlet opening of a silo, see Sect. 4.2). This is the most reliable way to achieve realistic data. Since the flowability ranking of several bulk solids is in many cases largely independent of stress level (example: Fig. 3.9: Product A flows better than product B throughout the consolidation stress range), it is often sufficient that the consolidation stresses measured roughly approximate the actual stresses. Very much more important than the absolute magnitude of the consolidation stress is that during comparative tests all products be tested at the same consolidation stress. This has already been discussed in detail above.

In exceptional cases a different ranking of the flowability of two products may result based on stress level (σ_l). This is shown by the flow functions of products A and B in Fig. 3.2. Due to the intersection of the flow functions there is a range of σ_l where the flow function of A is located above that of product B, so that product B flows better in this range of stresses. But there is also a range of σ_l , where product A flows better. In such a case it is very important to use a consolidation stress close to the stress acting in the practical application under consideration.

With many applications the bulk solid flows by gravity, e.g. when flowing out from a bin or silo. Two bulk solids with the same flowability value, ff_c , but a different bulk density, ρ_b , will flow differently because a larger gravitational force acts on the bulk solid with the larger bulk density. This means, for all applications utilizing gravity flow of bulk solids (e.g. flow out of a silo), that flow of a bulk solid with greater bulk density is supported by a greater force. Because of the greater force of gravity at equal flowability the strength of the bulk solid with the greater bulk density can be overcome more easily.

With comparative tests on similar samples of a product, often individual samples differ only slightly in their bulk density, so the influence of bulk density can be neglected. Then the flowability value, ff_c , is sufficiently accurate. Sometimes one finds very strong differences between the bulk den-

sities of samples to be compared, particularly with very fine-grained products. Here bulk density must be considered in order to reach conclusions about flowability under gravity flow. It might be useful then to consider the product of flowability, ff_c , and bulk density, ρ_b :

$$ff\rho = ff_c \cdot \frac{\rho_b}{\rho_w} \quad (3.2)$$

with $\rho_w = 1000 \text{ kg/m}^3$ (liquid water at 0°C , 1 bar).

In order to obtain a non-dimensional term, the bulk density, ρ_b , is divided by the density of liquid water ($\rho_w = 1000 \text{ kg/m}^3$ at 0°C and 1 bar, rounded). Of course, this is not physically meaningful, since the density of water plays no role in the gravity flow of a bulk solid, but in this way one obtains a non-dimensional term which is called the “density-weighed flowability”.

3.2 Principles of shear testing

The use of the uniaxial compression test with fine-grained, cohesive bulk solids is problematic, since one obtains unconfined yield strength values that are too low (Chap. 5) [3.2-3.6], and since preparation of the hollow cylinder to obtain frictionless walls is very time-consuming if not impossible to achieve (Sect. 6.3.10). In addition, further important parameters (e.g. internal friction and wall friction) cannot be determined with this test. Therefore shear testers are used in advanced bulk solids technology. The first shear tester designed for bulk solids is the translational shear tester developed by Jenike around 1960 (Jenike shear tester) [3.1]. Some years later the first ring shear testers designed for bulk solids followed [3.7]. In the following the test procedure (called “shear test”) is described in general, i.e., independent of a specific type of shear tester. The implementation of the procedure with different types of shear testers follows in Chap. 4.

3.2.1 Test procedure

The test procedure described in the following corresponds to the test procedure recommended by Jenike for the translational shear tester [3.1,3.8–3.12]. Similar to a uniaxial compression test, the test procedure is done in two steps: First the bulk solid specimen is consolidated, what is called “preshear”. Subsequently a point on the yield limit is measured. This step is called “shear” or “shear to failure”.

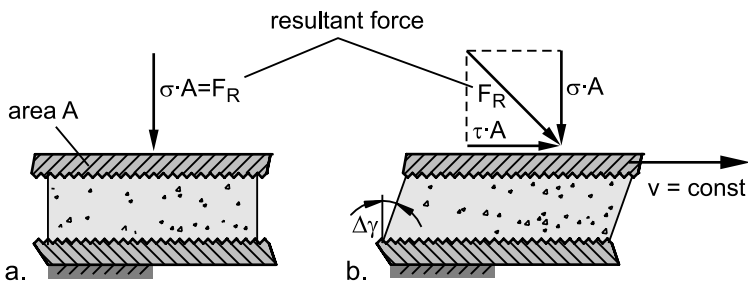


Fig. 3.10. a. Initial loading of the bulk solid specimen with a vertical normal stress, σ ; b. shear deformation (constant velocity, v)

Because the principle of a shear test is often regarded as difficult to understand, at first some simplified considerations are presented. Thus Fig. 3.10 shows the principle of shear deformation. The bulk solid specimen of cross-sectional area A (A seen from the top) is first subjected to a vertical normal stress, σ (Fig. 3.10.a). Afterwards the top is moved horizontally (velocity v) relative to the bottom (bottom is fixed) in order to shear the bulk solid specimen (Fig. 3.10.b). Due to friction between particles a shear stress, τ , is acting in the bulk solid which is transferred to the top and measured.

If a loose, uncompacted specimen of a fine-grained bulk solid is loaded with a normal stress, σ , as in Fig. 3.10.a, it is compressed and thus its bulk density, ρ_b , increases somewhat. During the following shear deformation the particles are moved against each other resulting in the shear stress, τ , indicated in Fig. 3.10.b. Shear stress and bulk density are plotted versus time in Fig. 3.11.a. Since the particles are relatively loosely packed at the beginning of shear, particles can move against each other and rotate. Inter-particle friction forces will be small and thus the shear stress will be small at the beginning (see Fig. 3.11.a). With increasing shear deformation the bulk solid becomes increasingly compacted, so that the particles are pressed against each other and thus the frictional forces increase. Shear stress and bulk density therefore increase as a result of further shear deformation. Thus the bulk solid is deformed plastically with increase of bulk density. Plastic deformation is a permanent deformation remaining even after removal of the load. A specimen that shows an increase in bulk density and strength when being sheared is called underconsolidated.

The increasing compaction and consolidation of the bulk solid specimen during shear can be explained by regarding the force, F_R , in Fig. 3.10.b, which results from normal stress and shear stress and, thus, increases with increasing shear stress. With time the curve of increase of shear stress vs. time becomes flatter (Fig. 3.11.a), and the same is true for the resultant

force, F_R . Finally the frictional forces between the particles are fully mobilized, so the maximum possible friction force – with respect to the applied normal load – is acting. The measured shear stress, τ , does not increase further after this state has been attained (see Fig. 3.11.a). Bulk density, ρ_b , also does not increase further. Thus flow, or plastic deformation (plastic deformation see Sect. 2.5), occurs at constant bulk density and constant stresses. This type of flow is called steady-state flow. The state of the bulk solid after steady-state flow is attained is called “critically consolidated with respect to the normal stress, σ ” [3.1,3.12]. The greater the normal stress, σ , the greater values of bulk density and shear stress will be attained during steady-state flow.

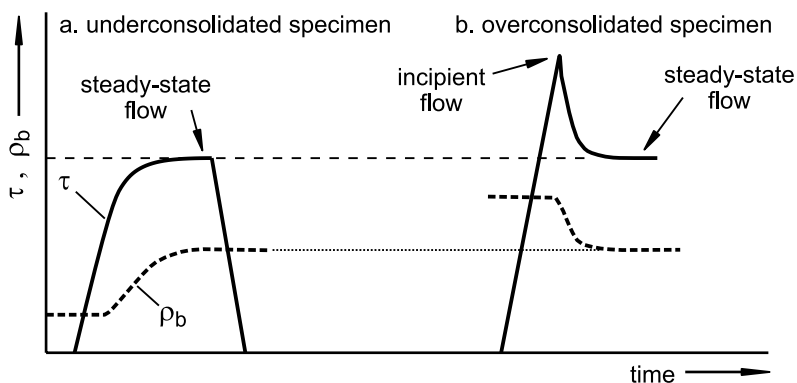


Fig. 3.11. Course of shear stress, τ , when shearing differently preconsolidated samples at identical normal stress, σ ; a. underconsolidated specimen, b. overconsolidated specimen

In the following the shear process shown in Fig. 3.10 is considered again, but instead of a loose, underconsolidated bulk solid specimen a highly consolidated (overconsolidated) specimen is sheared while the identical vertical normal stress, σ , is applied. Note that the bulk solid specimen is consolidated before shearing by a consolidation stress which is greater than the normal stress, σ , applied during shearing. Due to this previous consolidation, the particles have approached each other. Thus the bulk density and the adhesive forces have been increased. If this strongly consolidated bulk solid is sheared, flow will start only after the shear stress is sufficiently large to move the particles, which are adhering to each other due to the previous consolidation, against each other. In other words: The yield limit must be attained.

The latter is illustrated by the course of the shear stress, τ , in Fig. 3.11.b: At the beginning of shear the shear stress will increase, but it will cause

only elastic deformation - not (plastic) flow. The compacted bulk solid specimen will start to flow only after the shear stress acting on it is sufficiently large, i.e., only when the particles can move relative to each other (incipient flow) and the yield limit is attained. As a rule, failure will take place only in a thin planar area, the so-called shear zone.

After failure, the particles in the region of the shear zone move against each other, and the distances between the particles increase. Thus, bulk density in the shear zone decreases, and the material in the shear zone dilates. In accordance with increasing distances, adhesive forces decrease; i.e., the strength of the bulk solid and thus its shear resistance (the shear force required to shear the specimen) also decrease. Dilation of the bulk solid in the shear zone is plastic deformation with decreased density (Fig. 3.11.b).

If the specimen is further sheared after failure, the bulk solid in the shear zone will dilate increasingly until steady-state flow prevails, where shear stress and bulk density are constant. The values of shear stress and bulk density are the same as would have been attained in shearing a loose, uncompacted specimen (underconsolidated specimen, see above) under the same normal stress. Since shear deformation of the overconsolidated specimen occurs in a narrow shear zone, the above statement regarding bulk density is valid only for the shear zone. The mean bulk density at steady-state flow in the overall specimen is higher for an overconsolidated specimen.

Since steady-state flow is a process that transfers a bulk solid into a well-defined, reproducible state regarding bulk density and strength, shear to steady-state flow is commonly used as a procedure to attain a defined consolidation of a bulk solid specimen whose flow properties are to be measured. One starts with an underconsolidated specimen in order to get a largely homogenous specimen. If one were to start with an overconsolidated sample, steady-state flow would take place only in the narrow shear zone, and the rest of the sample would remain in the highly consolidated state with a high bulk density. Thus, the specimen would be less homogeneous.

After the initial considerations above, in the following the procedure of a shear tester is considered. As outlined above, it is started with an underconsolidated bulk solid specimen. For consolidation (preshear) the specimen is loaded in the vertical direction by the normal stress $\sigma = \sigma_{pre}$, called the normal stress at preshear, and then sheared (Fig. 3.12.a). The shear stress, τ , prevailing due to the deformation is measured.

At the beginning of preshear the shear stress, τ , increases with time (Fig. 3.12.c) as already discussed (Fig. 3.11.a). Often a linear increase in shear stress can be observed, indicating that the bulk solid has deformed elasti-

cally. With time the curve of increase of shear stress vs. time becomes flatter, and finally it remains constant even though the specimen is sheared further. The constant shear stress is called τ_{pre} . After constant shear stress has been attained, shear resistance (and strength) and bulk density do not increase further. Thus the bulk solid specimen is sheared at constant normal stress, σ , constant shear stress, τ , and constant bulk density, ρ_b . The state of the bulk solid after steady-state flow is attained is called “critically consolidated with respect to the normal stress, σ_{pre} ” [3.1,3.12].

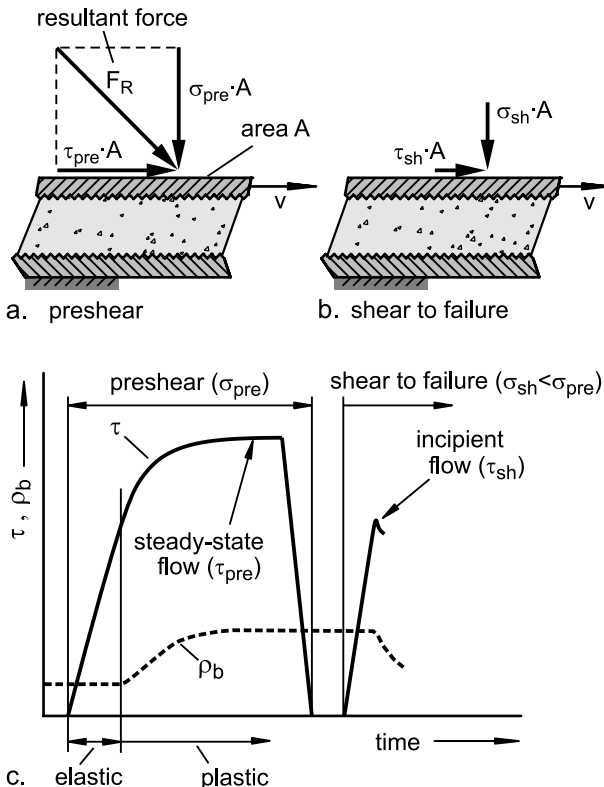


Fig. 3.12. Shear stress, τ , and bulk density, ρ_b , at preshear and shear to failure

The bulk density, ρ_b , and the shear stress, τ_{pre} , attained at steady-state flow are characteristic for the applied normal stress at preshear, σ_{pre} . In principle, an identical state of consolidation, characterized by the same bulk density, ρ_b , and the same shear stress, τ_{pre} , will be attained with other specimens of the same bulk solid presheared under the same normal stress, σ_{pre} .

From preshear until steady-state flow, the bulk solid specimen attains a well-defined and reproducible state of consolidation, known as critical

state. The preshear procedure corresponds to the consolidation step in the uniaxial compression test (Fig. 3.1), but has several advantages [3.2,3.5,3.6]. One advantage is that at preshear one can recognize when critical consolidation has been attained: One simply has to shear until steady-state flow prevails. If, for example, the specimen has been filled into the test device non-homogeneously (e.g. local voids or regions with low bulk density exist), one will not notice this with uniaxial compression. In contrast, one can expect that local inhomogeneities are compensated at sufficient shear deformation, and that the shear stress measured will be constant only after the specimen is sufficiently homogeneous.

After the bulk solid specimen has been consolidated by the preshear procedure, the direction of shear is reversed and thus the specimen is relieved from shear stress, i.e., the shear stress, τ , is reduced to zero (Fig. 3.12.c). The pair of values of normal stress and shear stress at steady-state flow (σ_{pre} , τ_{pre}) is plotted in a normal stress - shear stress diagram (σ, τ diagram, Fig. 3.13.a). The point (σ_{pre} , τ_{pre}) is called the preshear point.

After preshear the bulk solid specimen is defined as a critically consolidated specimen. The characteristic stress for this consolidation will be considered later. The second step of the test procedure – shear or shear to failure – is discussed next.

For shear to failure the normal stress acting on the specimen is decreased to a value $\sigma_{sh} < \sigma_{pre}$. Then the bulk solid specimen is sheared under the normal stress σ_{sh} , which is less than the normal stress at preshear, σ_{pre} . This corresponds to shearing of an overconsolidated specimen as shown in Fig. 3.11.b. Had the specimen been presheared under the lower normal stress, σ_{sh} , and not under σ_{pre} , its bulk density and strength would have been less. Since the specimen was presheared under the greater normal load, σ_{pre} , it was consolidated more than it would have been with the lower normal load, σ_{sh} . Therefore, the specimen is overconsolidated with respect to the normal stress at shear, σ_{sh} , and the course of shear stress as shown in Fig. 3.11.b is to be expected.

If the consolidated specimen is sheared under the normal stress $\sigma_{sh} < \sigma_{pre}$, it will start to flow (fail) when a sufficiently large shear stress is attained. Then the material will start to dilate (decrease in bulk density), and shear resistance and thus shear stress will decrease (Fig. 3.12.c). The maximum shear stress characterizes incipient flow. The corresponding pair of values (σ_{sh} , τ_{sh}) is a point on the yield limit of the consolidated specimen in the σ, τ diagram (Fig. 3.13.a). Such a point is called a “shear point” or a “point of incipient flow”.

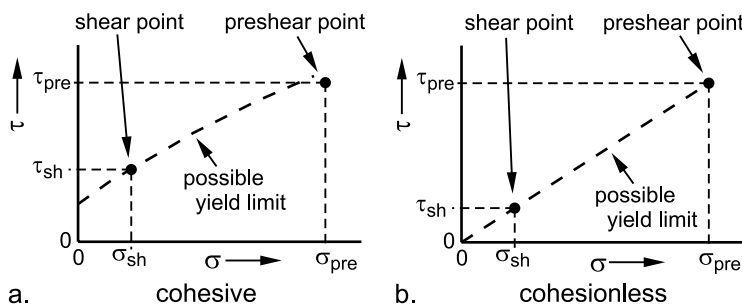


Fig. 3.13. Preshear point and shear point in a σ, τ diagram; a. cohesive bulk solid; b. cohesionless, free-flowing bulk solid

In the present section so far only bulk solids have been considered whose strength can be increased by applying a consolidation stress. Here the adhesive forces have a major influence on the location of the yield limit. The stronger the adhesive force, the more the shear point in Fig. 3.13.a is shifted towards higher shear stresses. If the influence of the adhesive forces can be neglected, a bulk solid is called cohesionless (free-flowing). A cohesionless bulk solid cannot be consolidated, so that at shear to failure no shear stress maximum is observed. In this case the yield limit is a straight line running through the origin with both the preshear point and the shear point being located on the yield limit. (Fig. 3.13.b).

In order to measure the yield limit, several of the tests described above must be performed, where the specimens must first be consolidated at identical normal stress, σ_{pre} (preshear). Then the specimens are sheared (to failure) under different normal stresses, $\sigma_{sh} < \sigma_{pre}$. As outlined above, by preshearing at identical normal stress, σ_{pre} , each specimen reaches the same state of consolidation. In Fig. 3.14 the courses of shear stress are plotted vs. time for several tests at the same normal stress at preshear, σ_{pre} . Each test yields the same preshear point (σ_{pre}, τ_{pre}), and one individual shear point (σ_{sh}, τ_{sh}) in accordance with the different normal stresses, σ_{sh} , applied at shear.

It would not be acceptable to preshear a bulk solid specimen only once and then measure several points of incipient flow one after the other, because already after the first shear to failure the state of the specimen is different from the state directly after preshear. The reason for this is that the specimen dilates at shear to failure (at least in the shear zone, see course of the bulk density in Fig. 3.12.c). Thus, shear to failure without directly preceding preshear would lead to too small shear stresses at shear to failure and thus to incorrect test results (for more about this refer to Sect. 6.1.1).

The yield limit follows from a curve in a σ, τ diagram plotted through all measured shear points (Fig. 3.14). The yield limit, extrapolated towards

higher normal stresses, is usually located above, i.e., at higher shear stresses, than the preshear point. When a bulk solid is free-flowing, the preshear point is located on the yield limit (Fig. 3.13.b).

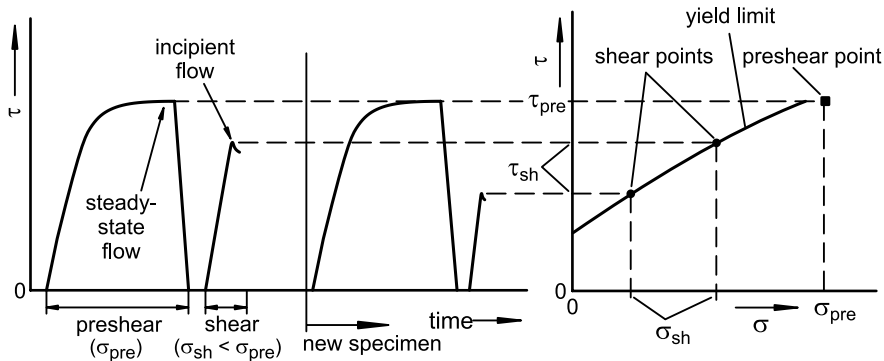


Fig. 3.14. Determination of the yield limit from the measured shear stresses

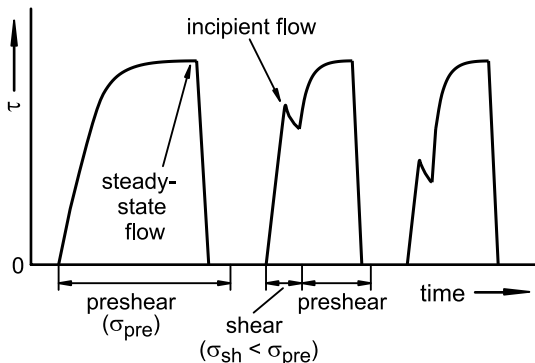


Fig. 3.15. Course of the shear stress when measuring several points of the yield limit with one bulk solid specimen

If the shear tester allows a sufficiently large shear deformation, in contrast to the procedure shown in Fig. 3.14, more than one point of the yield limit can be measured with one specimen. The course of shear stress with this procedure is shown in Fig. 3.15. The specimen is first presheared (consolidated) at the normal stress, σ_{pre} , and subsequently sheared the first time at a lower normal stress, $\sigma_{sh} < \sigma_{pre}$. Then the specimen is presheared again under the normal stress σ_{pre} , then sheared to failure, and so on.

3.2.3 Yield locus and flow properties

The yield limit of a consolidated bulk solid is called a *yield locus*, or instantaneous yield locus to emphasize that the strength is measured directly after consolidation [3.1].

A yield locus is valid for only one normal stress at preshear, σ_{pre} , i.e., for one well-defined state of consolidation (and one bulk density), which has been attained by preshearing until steady-state flow prevailed. If a different normal stress is applied at preshear, one will obtain a different yield locus. Since one can choose an infinite number of normal stresses at preshear, an infinite number of yield loci can be attained.

A yield locus is usually a slightly convex upward curve. The curvature increases towards smaller normal stresses. With free-flowing, cohesionless bulk solids one usually obtains a nearly straight-lined yield locus that goes through the origin. A yield locus is valid for one specific bulk density, namely that bulk density prevailing at the end of preshear when steady-state flow is attained. If the yield locus is known, various parameters called flow properties can be determined. These are the already mentioned parameters consolidation stress, unconfined yield strength, and flowability, but also include additional properties such as the internal angle of friction of the bulk solid.

3.2.3.1 Consolidation stress and unconfined yield strength

To determine consolidation stress and unconfined yield strength one applies the Mohr stress circle (see Sect. 2.3.1 and [3.1,3.8,3.9]). Each point on a Mohr stress circle represents the normal and shear stress on one particular cutting plane of a bulk solid specimen. As outlined at the derivation of the Mohr stress circle, the center of any Mohr stress circle is located on the σ -axis.

For each yield locus there is a Mohr stress circle that represents the stress state at the end of consolidation, i.e., at steady-state flow attained at the end of preshear.

From the shear test one knows one point on this Mohr stress circle: the preshear point (σ_{pre}, τ_{pre}). It represents the normal and shear stress acting in the horizontal cutting plane at steady-state flow.

Before the Mohr stress circle for steady-state flow can be drawn, one additional condition must be defined. Thus one assumes that the Mohr stress circle touches the yield locus at a normal stress $\sigma \leq \sigma_{pre}$ (usually the point of tangency is to the left of the preshear point; for free-flowing bulk solids the point of tangency is sometimes identical to the preshear point). This procedure for determining the Mohr stress circle for steady-state flow

is an approximation, but yields applicable results (see Sect. 5.3). The theoretical background is described, for example, in [3.1,3.8–3.10].

Therefore, under the conditions where

- the center of the Mohr stress circle is (per definition) on the σ -axis,
- the preshear point is a point on the Mohr stress circle, and
- the Mohr stress circle touches the yield locus at $\sigma \leq \sigma_{pre}$,

the Mohr stress circle representing steady-state flow can be determined uniquely (Fig. 3.16). For this, often the yield locus must be extrapolated somewhat toward greater normal stresses (broken line in Fig. 3.16), because the point of tangency of the yield locus and the Mohr stress circle representing steady-state flow is usually (but not always) to the right of the measured points of incipient flow. The point of tangency is by definition the end point of the yield locus (point e in Fig. 3.16). The major and minor principal stresses, σ_1 and σ_2 , are where the Mohr circle intersects the σ -axis.

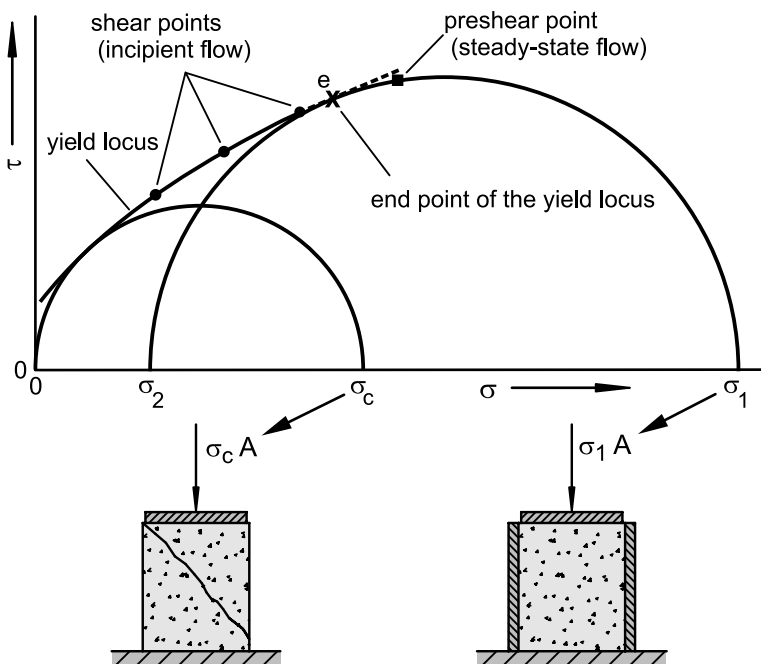


Fig. 3.16. Yield locus and Mohr stress circles defining the unconfined yield strength, σ_c , and the consolidation stress, σ_1 ; analogy to the uniaxial compression test

The major principal stress, σ_I , of a Mohr stress circle is the largest of all normal stresses acting during steady-state flow in all possible cutting planes of the specimen (see Sect. 2.3.1). This stress is regarded as the characteristic consolidation stress for the yield locus, and it is comparable to the consolidation stress, σ_I , of the uniaxial compression test (Sect. 3.1), where σ_I is also the largest normal stress. The other flow properties (e.g. bulk density, ρ_b) are usually presented as a function of consolidation stress, σ_I (and not as a function of normal stress at preshear, σ_{pre}).

The unconfined yield strength was described in Sect. 3.1 in the example of the uniaxial compression test: σ_c is the compressive strength of the bulk solid, measured at uniaxial compressive load. This kind of load cannot be realized in a shear test. Therefore, the unconfined yield strength cannot be measured directly with a shear test and must be determined from the yield locus. Here again the Mohr stress circle is applied. The Mohr stress circle represents the stresses acting in different cutting planes in the bulk solid specimen (Sect. 2.3.1). Consider first the stresses at the unconfined yield strength measured using the uniaxial compression test (Fig. 3.16, bottom). At incipient flow (failure) a normal stress, σ , and no shear stress ($\tau = 0$) act on the top of the specimen, and neither normal nor shear stresses act on the lateral surface of the specimen ($\sigma = 0, \tau = 0$).

The Mohr stress circle representing the stress state at failure runs through the origin of the σ, τ diagram ($\sigma = 0, \tau = 0$). The second point of intersection of the Mohr stress circle with the σ -axis is at the normal stress, $\sigma = \sigma_c$. A consolidated specimen will flow only if the Mohr stress circle of the actual stress state touches the yield locus and, thus, the yield limit is attained. Therefore the relation between the unconfined yield strength, σ_c , and the yield locus is given: The unconfined yield strength can be determined from a yield locus by drawing a Mohr stress circle which fulfills the following conditions:

- the center of the Mohr stress circle must be on the σ -axis,
- the origin of the diagram ($\sigma = 0, \tau = 0$) is a point on the Mohr stress circle, and
- the stress circle is tangent to the yield locus.

In Fig. 3.16 the Mohr stress circle for σ_c is drawn according to the above conditions. Once consolidation stress, σ_I , and unconfined yield strength, σ_c , are known, flowability, ff_c , can be calculated per Sect. 3.1.4.

Below the diagram in Fig. 3.16 the uniaxial compression test is shown to demonstrate the similarity of the shear test and the uniaxial compression test: in both tests a consolidation stress, σ_I , is acting on a bulk solid specimen, and in both tests the unconfined yield strength, σ_c , is determined. For

the sake of completeness it has to be mentioned that the two test procedures lead to different Mohr stress circles for the consolidation as well as for the unconfined yield strength even if the same consolidation stress is applied (see Sect. 5.1).

The difference between a flow function and a yield locus is summarized again below:

- A yield locus is the yield limit of a bulk solid in a σ, τ diagram. A yield locus is valid for only one consolidation stress, σ_1 ; i.e., for each consolidation stress there is a yield locus. The yield locus defines several parameters (flow properties), e.g. the unconfined yield strength, σ_c . The pair of values (σ_c, σ_1) of one yield locus defines one point on the flow function.
- The flow function represents unconfined yield strength, σ_c , as a function of consolidation stress, σ_1 . Several yield loci must be measured to determine a flow function.

3.2.3.2 Mohr stress circles for preshear and shear to failure

Now that the yield locus and the stress circles defining consolidation stress and unconfined yield strength have been discussed, preshear and shear to failure will be described by considering the Mohr stress circles. In Fig. 3.17 a σ, τ diagram with a yield locus and a Mohr stress circle representing steady-state flow is shown. The bulk solid specimen is first loaded by the normal stress, σ_{pre} , and then subjected to shear deformation.

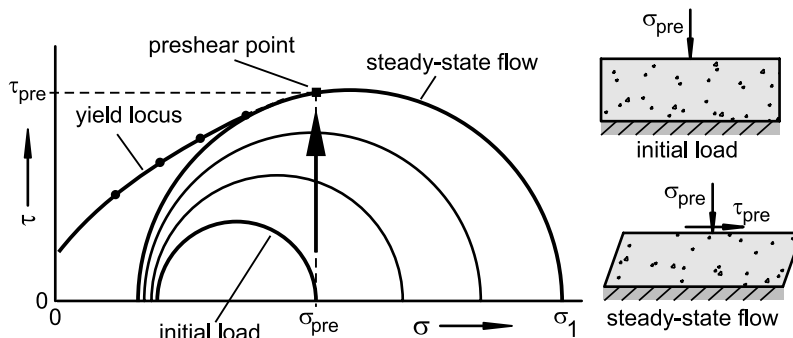


Fig. 3.17. Yield locus; Mohr stress circles during preshear

When the specimen is initially subjected to the vertical normal stress (initial load), σ_{pre} , it undergoes a uniaxial consolidation where the vertical stress is identical to the major principal stress. Perpendicular to this stress a smaller stress prevails which in most cases is about 40% to 50% of the ap-

plied normal stress, σ_{pre} (see Sect. 2.3). The stress circle representing this stress condition is drawn in Fig. 3.17 (initial load).

When the bulk solid specimen is sheared, the shear stress in the horizontal cutting planes increases. Thus the vertical stress, σ_{pre} , cannot be a principal stress, because in the horizontal cutting plane a shear stress is acting. Two Mohr stress circles, representing possible states of stress while the shear stress is increasing, are plotted in Fig. 3.17. The increasing shear stress, τ , inevitably results in an increase of the major principal stress (the major principal stress is to be found at the right point of intersection of the Mohr stress circle with the σ -axis). Finally steady-state flow is attained and the major principal stress, σ_1 , remains constant. This major principal stress is the characteristic consolidation stress of the yield locus. The construction of the Mohr stress circle according to Jenike's assumptions was outlined in the previous section.

Previously at the derivation of the Mohr stress circle in Sect. 2.3.1 and at the discussion of the stresses for the uniaxial compression test in Sect. 3.1.3, the relationship between the stress circle and the stresses in individual cutting planes of the bulk solid specimen was outlined. The same is done for steady-state flow in Fig. 3.18, where a Mohr stress circle and the corresponding bulk solid sample are shown.

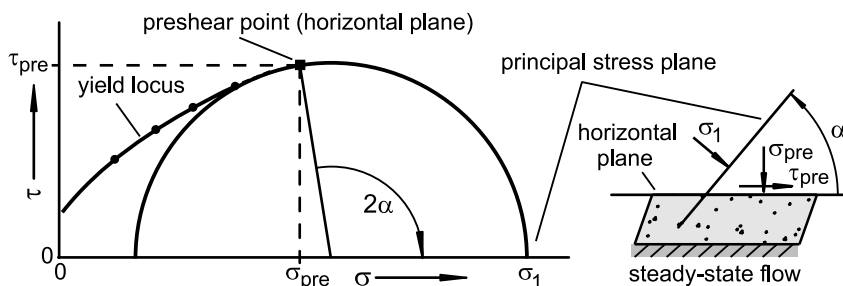


Fig. 3.18. Determination of the orientation of the principal stress plane at steady-state flow

In the horizontal plane the normal stress, σ_{pre} , and shear stress, τ_{pre} , are acting. These stresses represent the preshear point in the σ, τ diagram. In the Mohr stress circle the angle between the preshear point and the major principal stress is 2α measured in the clockwise direction. Thus in the bulk solid specimen the principal stress plane is inclined by the angle α to the horizontal plane measured in the counterclockwise direction. Since the preshear point (when the Mohr stress circle for steady-state flow is constructed as proposed by Jenike) is usually somewhat left to the zenith of the Mohr stress circle representing steady-state flow, it follows that the an-

gle (2α) is a bit greater than 90° . Thus, in the bulk solid sample the direction of the major principal stress at steady-state flow is inclined by an angle of little more than 45° to vertical (see bulk solid element in Fig. 3.18).

In Fig. 3.19 possible stress states emerging during shear to failure are shown. At the beginning of shear to failure, the previously consolidated bulk solid specimen (consolidation by preshear until steady-state flow, Fig. 3.18) is subjected to the vertical normal stress, σ_{sh} . The corresponding Mohr stress circle is plotted in Fig. 3.19. In this situation the applied normal stress, σ_{sh} , is identical to the major principal stress. When the bulk solid specimen is sheared, the shear stress on the horizontal cutting plane increases as shown by the arrow in Fig. 3.19. Due to the shear stress on the horizontal plane, the vertical normal stress, σ_{sh} , cannot be the major principal stress any longer. Two examples of Mohr stress circles passed during the increase of the shear stress are plotted in Fig. 3.19. They demonstrate the increase of the major principal stress with increasing shear stress, τ . Finally the Mohr stress circle touches the yield locus which causes the bulk solid specimen to flow (failure or incipient flow, respectively). Following this (not shown in Fig. 3.19) the bulk solid dilates and the shear stress decreases (see Fig. 3.12).

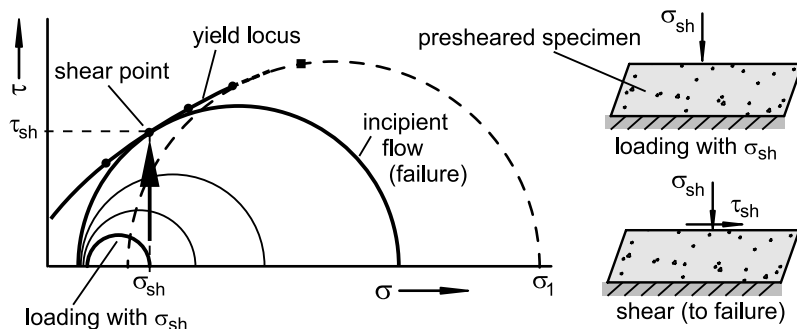


Fig. 3.19. Mohr stress circles at shear to failure

When a shear test is evaluated according to Jenike, one assumes that incipient flow happens in a horizontal plane, i.e., in a plane perpendicular to σ_{sh} and parallel to the shear velocity, v , and the measured shear stress, τ_{sh} . In this case the pair of values (σ_{sh}, τ_{sh}) measured at the shear stress maximum is a point on the yield locus and called a “shear point”. Thus the shear plane defined by the applied shear deformation is assumed to be a failure plane [3.11,3.13,3.14] (for more information see Sect. 5.3).

3.2.3.3 Further flow properties

For applications such as silo design, which go beyond merely determining flowability, further parameters (flow properties) can be determined from the yield locus:

- slope angle of the linearized yield locus, φ_{lin}
- effective angle of internal friction, φ_e (slope of the effective yield locus)
- angle of internal friction at steady-state flow, φ_{sf}
- bulk density, ρ_b

The angle of internal friction at incipient flow, φ_i , is defined as the local slope of the yield locus against the σ -axis (abscissa) of the σ, τ diagram. Since a yield locus is usually a convex upward curve, the angle of internal friction varies along the yield locus. For many applications it is sufficient to use a constant value for the angle of internal friction. Then the angle of internal friction is represented by the slope of the linearized yield locus, φ_{lin} , measured against the σ -axis (Fig. 3.20). The linearized yield locus is a straight line tangent to both Mohr stress circles, i.e., the Mohr stress circles defining σ_c and σ_l .

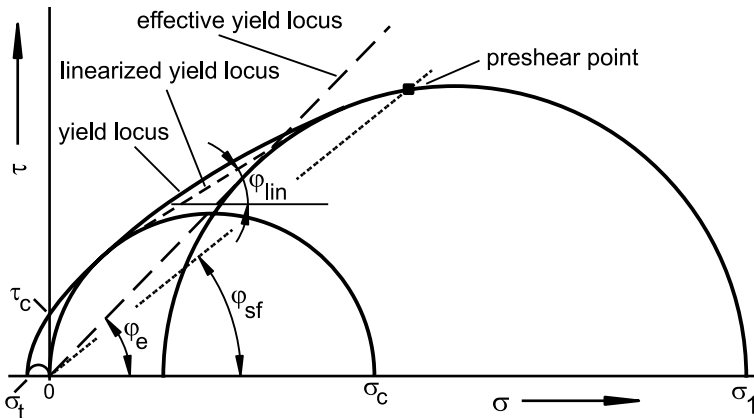


Fig. 3.20. Yield locus and flow properties

It must be mentioned here that neither the so-called angle of internal friction at incipient flow, φ_i , nor φ_{lin} are friction angles in the true sense. A friction angle is usually calculated from the arc tangent of the ratio of shear stress to normal stress; i.e., a friction angle is like a friction coefficient, a measure of the ratio of shear stress to normal stress (or shear force to normal force). As can be seen clearly in Fig. 3.20, a ratio of shear stress to normal stress is defined neither by φ_i nor by φ_{lin} .

In order to calculate the shear stress needed for a given normal stress to initiate flow in a consolidated bulk solid, one must proceed as follows: First draw the yield locus, then read the shear stress, τ , at the normal stress, σ , under consideration.

A straight line through the origin of the σ, τ diagram, tangent to the larger Mohr circle (steady-state flow), is the effective yield locus. The slope of the effective yield locus is called the effective angle of internal friction, φ_e (Fig. 3.20). Since the larger Mohr circle represents the stresses at steady-state flow, φ_e can be regarded as a measure of the internal friction at steady-state flow.

The effective angle of internal friction defines the ratio of the minor principal stress to the major principal stress at steady-state flow:

$$\sin \varphi_e = \frac{\sigma_1 - \sigma_2}{\sigma_1 + \sigma_2} \quad (3.3)$$

$$\frac{\sigma_2}{\sigma_1} = \frac{1 - \sin \varphi_e}{1 + \sin \varphi_e} \quad (3.4)$$

The angle of internal friction at steady-state flow, φ_{sf} , is calculated from the ratio of shear stress, τ_{pre} , and normal stress, σ_{pre} , at steady-state flow:

$$\varphi_{sf} = \arctan \left(\frac{\tau_{an}}{\sigma_{an}} \right) \quad (3.5)$$

φ_{sf} can be determined graphically by drawing a line through the origin and the preshear point $(\tau_{pre}, \sigma_{pre})$, see Fig. 3.20. The slope of this line against the σ -axis is equal to φ_{sf} . φ_{sf} characterizes the internal friction at steady-state flow in the cutting plane parallel to the shearing velocity, v , i.e., the horizontal cutting plane in Fig. 3.10. For information on the application of φ_{sf} see Sect. 9.3.2 and [3.15].

Bulk density, ρ_b , is calculated from the mass and the volume of the consolidated bulk solid specimen. Since the yield locus and the flow properties are related to the state of consolidation, which is characterized by the consolidation stress, σ_I , the bulk density also has to be determined for the consolidated bulk solid specimen.

Two more quantities can be determined from the yield locus at small and negative normal stresses:

- Cohesion, τ_c : Value of the shear stress where the yield locus intersects with the τ -axis, i.e., at the normal stress $\sigma = 0$.

- Uniaxial tensile strength, σ_t : Normal stress at the left end of the yield locus [3.9,3.11,3.16].

Although cohesion and tensile strength are well-defined quantities, it is difficult to measure the yield locus at small and negative stresses (see Sect. 5.3.2). Since in bulk solids handling more or less exclusively compressive stresses take place, the knowledge of cohesion or tensile strength is important only in very rare cases. Thus these quantities are not discussed further in the present section. Much more important is the unconfined yield strength, σ_c , which can be determined more easily and more accurately with the test procedures presented here.

3.2.3.4 Flow properties as a function of consolidation stress

When measuring yield loci with different normal stress loads at preshear, σ_{pre} , one obtains different yield loci, each with a different value of consolidation stress, σ_l . Figure 3.21 shows three yield loci with different consolidation stresses, σ_l . With increasing consolidation stress, σ_l , the yield locus is shifted towards greater shear stresses. This is to be expected: The more consolidated a bulk solid, the greater must be the shear stress, τ , necessary to initiate flow.

Each yield locus has one characteristic consolidation stress, σ_l (= major principal stress at consolidation). For each yield locus (and thus for each consolidation stress) corresponding values of the flow properties bulk density, ρ_b , unconfined yield strength, σ_c , and angles φ_{lin} , φ_e and φ_{sf} are found. In Fig. 3.21 the consolidation stress, σ_l , and the Mohr stress circle of σ_c are drawn for only one yield locus.

For every yield locus one effective yield locus can be found (see definitions in Sect. 3.2.3.3). The effective angle of internal friction, φ_e , usually decreases with increasing consolidation stress, σ_l . Sometimes the effective yield locus is confused with the steady-state yield locus introduced by Molerus [3.1]. The steady-state yield locus is the common tangent of all Mohr circles representing steady-state flow at different stress levels. It is approximately a straight line for free-flowing bulk solids. For cohesive materials this is true only at sufficiently high consolidation stresses, because close to the origin of the σ,τ diagram the steady-state yield locus is curved downwards (see Fig. 3.21) [3.17].

For free-flowing bulk solids, the effective angle of internal friction, φ_e , is not as a function of consolidation stress. In this case, all effective yield loci coincide with the steady-state yield locus and run through the origin. For bulk solids which are not free-flowing, φ_e increases with decreasing consolidation stress. Therefore, the steady-state yield locus (common tan-

gent to all Mohr circles representing steady-state flow) intersects with the τ -axis at $\tau > 0$ (Fig. 3.21). Recent measurements indicate that the steady-state yield locus is increasingly curved downwards as shown in Fig. 3.21 when approaching the τ -axis, and does not go far beyond the τ -axis towards negative normal stresses [3.17] (see Sect. 5.3.3).

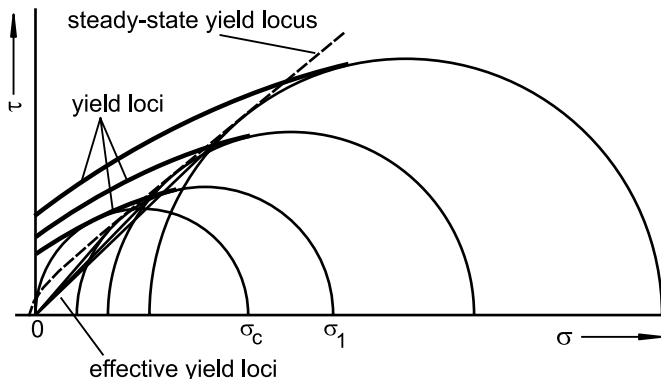


Fig. 3.21. Three yield loci and corresponding effective yield loci of a bulk solid; steady-state yield locus

Fig. 3.22 shows a typical graph of flow properties vs. consolidation stress, σ_I . Unconfined yield strength, σ_c , and bulk density, ρ_b , have been discussed already in Sect. 3.1 in connection with the uniaxial compression test.

Both bulk density and unconfined yield strength almost always increase with consolidation stress, whereas the graph of unconfined yield strength (the instantaneous flow function) usually shows a decreasing slope with increasing consolidation stress. In some cases a progressive increase occurs in parts of the flow function. Towards very small consolidation stresses the instantaneous flow function does not (or only very little, see Sect. 5.3.3) go above the line $\sigma_c = \sigma_I$ [3.17], i.e., the ratio $ff_c = \sigma_I/\sigma_c$ (flowability) approaches values close to 1 towards consolidation stresses $\sigma_I = 0$. With cohesive bulk solids this can be the case in the range of some 100 or 1000 Pa, as has been demonstrated by measurements at low stresses [3.17]. With free-flowing bulk solids this can be expected only for consolidation stresses close to zero.

The friction angles, φ_{sf} and φ_e , usually decrease with increasing consolidation stress, because they are dependent mainly on adhesive and frictional forces acting between the particles. The ratio of adhesive to frictional forces decreases with increasing stress (see Sect. 5.5), because adhesive forces do not increase as much with increasing stresses as frictional forces do.

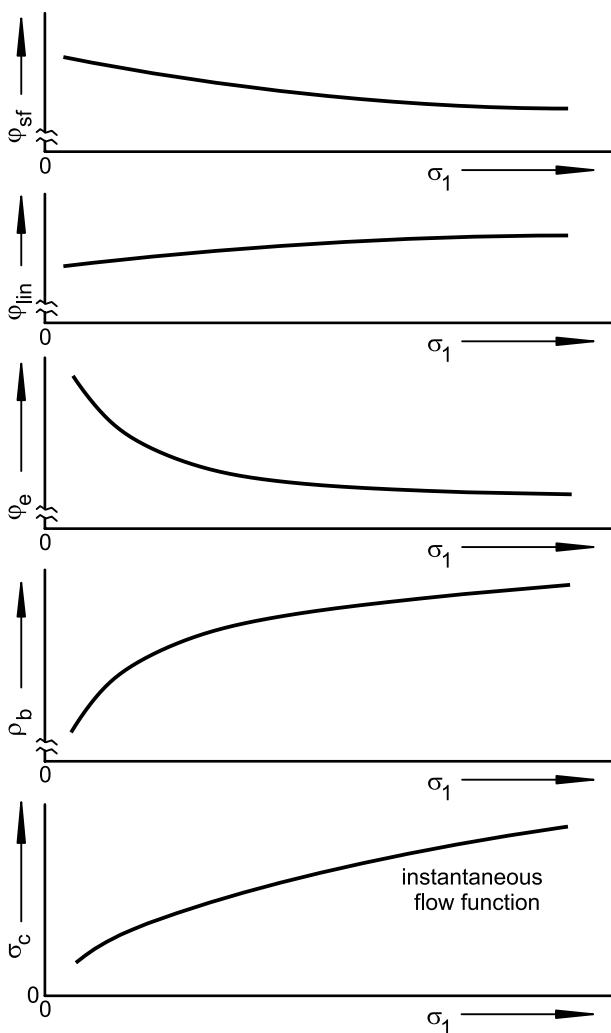


Fig. 3.22. Flow properties as a function of consolidation stress (cohesive bulk solid, qualitatively)

The slope angle of the linearized yield locus, φ_{lin} , often increases slightly with increasing consolidation stress. This is because, with increasing consolidation stress, σ_1 , the unconfined yield strength, σ_c , increases at a slower rate (usually). Thus the (smaller) Mohr stress circle representing the unconfined yield strength, σ_c , becomes smaller relative to the (larger) Mohr stress circle representing steady-state flow, and accordingly the slope of the yield locus against the σ -axis increases. However, sometimes a slight decrease of φ_{lin} can be observed.

3.2.4 Time consolidation (caking)

The effect of time consolidation has been outlined in Sect. 3.1. Before time consolidation can be measured, a yield locus must be determined at the same consolidation stress.

The time consolidation test is similar to the measurement of a yield locus. First a bulk solid specimen is presheared (consolidated). After pre-shear the specimen is stored for a period t under the vertically acting normal stress, σ , which is selected to be equal to the consolidation stress, σ_l , of the corresponding yield locus (Fig. 3.23). This ensures that during the consolidation period the same major principal stress (= consolidation stress, σ_l) acts on the specimen as during steady-state flow at preshear. The direction of σ_l during the consolidation time is inclined by about 45° to the direction of σ_l at steady-state flow (see Fig. 3.18).

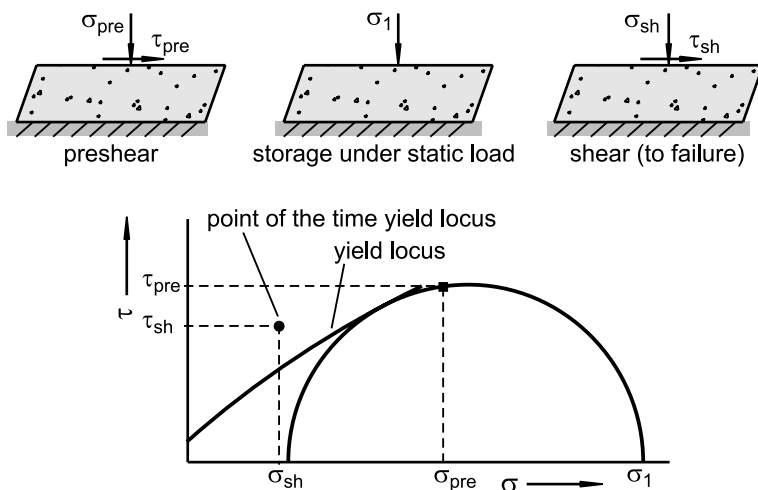


Fig. 3.23. The principle of a time consolidation performed with a shear tester

The reason for this procedure is that before the time consolidation period, the bulk solid specimen is consolidated by shearing it under a vertical normal load, σ_{pre} , until steady-state flow prevails (preshear) and shear stress, τ_{pre} , acts in the (horizontal) shear plane. The major principal stress at steady-state flow is the consolidation stress, σ_l (this follows from the Mohr stress circle representing steady-state flow, Fig. 3.23 and Sect. 3.2.3). This consolidation stress is clearly larger than the normal stress at preshear, σ_{pre} . During the time consolidation period t the specimen is subjected to a static (vertical) load; i.e., it is not sheared. Thus the major principal stress acting on the sample is equal to the applied vertical stress. If during the time con-

solidation period one were to exert a static vertical normal stress equal to the normal load at preshear, σ_{pre} , the major principal stress in the specimen would be much less than at steady-state flow, because the preshear normal stress, σ_{pre} , is less than the consolidation stress, σ_I , at steady-state flow. Therefore, during the consolidation period, a vertical normal stress equal to the consolidation stress, σ_I , acting at steady-state flow (preshear) must act on the specimen.

After the time consolidation period t the specimen is sheared (to failure). For this, a vertical normal load, $\sigma_{sh} < \sigma_I$, is selected (Fig. 3.23). As with shear without time consolidation (measurement of a point on a yield locus), so also after time consolidation one will observe a shear stress maximum (Fig. 3.24). If consolidation time affects the bulk solid under consideration, after the consolidation period t the shear stress maximum, τ_{sh} , will be larger than it would have been without a consolidation period between preshear and shear.

The maximum shear stress, τ_{sh} , is a point on a yield limit, which is valid for the applied storage period, t , and called a *time yield locus*. One can measure several points on a time yield locus by performing tests with the same consolidation stress and consolidation period, but different values of normal stress at shear (σ_{sh}). Figure 3.25 shows a (instantaneous) yield locus and two time yield loci obtained for different consolidation periods, t_1 and t_2 .

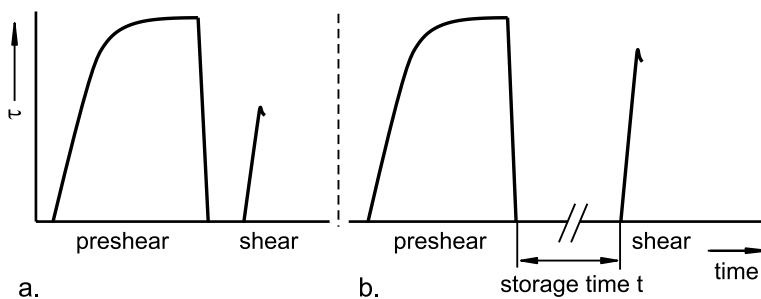


Fig. 3.24. Shear stress vs. time at shear without (a) and with (b) time consolidation

With the measured shear points a time yield locus can be approximated similarly to the approximation of a yield locus. Compared to the yield locus, the time yield locus is shifted towards greater shear stresses, τ (if the bulk solid shows an increase of strength with time, see Fig. 3.25, $t_2 > t_1$). Time yield loci can be determined for different storage periods (consolidation periods). Each time yield locus is valid for only one consolidation period and one consolidation stress. The unconfined yield strength, σ_c , is determined in the same way as for a yield locus by drawing a Mohr stress

circle through the origin and tangent to the time yield locus. In Fig. 3.25 the values of the unconfined yield strength for the consolidation periods, t_1 and t_2 , are designated as $\sigma_c(t_1)$ and $\sigma_c(t_2)$.

A value of flowability, ff_c , can be obtained also from a time yield locus, where ff_c is the ratio of the consolidation stress, σ_1 , to the unconfined yield strength, σ_c , of the time yield locus (e.g. $\sigma_c(t_1)$). Since unconfined yield strength usually increases with increasing consolidation period, flowability, ff_c , will decrease with increasing storage period (see Fig. 3.8).

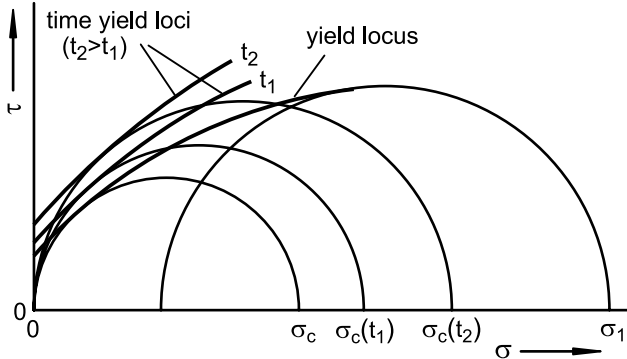


Fig. 3.25. Yield locus (instantaneous yield locus) and time yield loci

The angle of internal friction, φ_t , at incipient flow after a certain consolidation period is defined as the local slope of the time yield locus against the σ -axis. Since a time yield locus also can be a convex upward curve, the angle φ_t can vary along the time yield locus. For many applications it is sufficient to use a constant value for the angle of internal friction. Then the angle of internal friction is represented by the slope of the linearized time yield locus (time yield locus approximated as a straight line) measured against the σ -axis (Fig. 3.26). In accordance with [3.12], φ_t is determined by the slope of the time yield locus at the point of tangency with the Mohr circle for the unconfined yield strength, σ_c . If the time yield locus is approximated as a straight line, this value is identical to the slope of the time yield locus.

It must be mentioned here that the angle of internal friction of the time yield locus, φ_t , is not a true friction angle. The explanation of this is given in Sect. 3.2.3.3, where the angle of internal friction of the yield locus, φ_i , is discussed.

Since time consolidation tests are time-consuming, it is common practice to measure only one shear point of a time yield locus. The time yield locus is then approximated by a parallel to the linearized yield locus running through the measured shear point. When this procedure is applied, the

slope of the time yield locus is equal to the slope of the linearized yield locus. Thus, the internal angle of friction, φ_t , of the time yield locus is equal to the slope angle, φ_{lin} , of the linearized yield locus. If such a simplified test procedure is applied, it has to be ensured that the results are on the safe side regarding quantitative application (e.g. silo design).

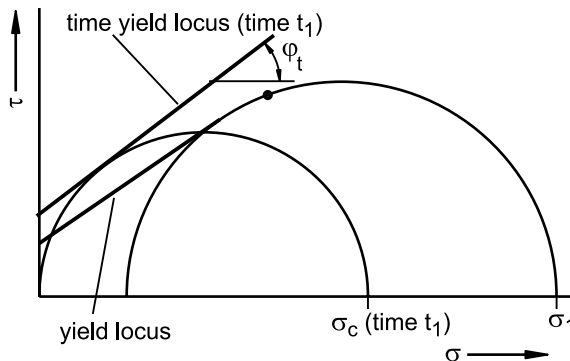


Fig. 3.26. Slope angle of the time yield locus (here: time yield locus approximated as a straight line)

3.3 Wall friction

Wall friction is the friction between a bulk solid and a solid surface, e.g. the wall of a silo or a bin. The wall friction angle is important for silo design for flow and for silo design for strength, but also for the design of chutes and other equipment, where the bulk solid will flow across a solid surface.

3.3.1 Test procedure for wall yield loci

A simplified description of the test procedure follows. The procedure corresponds to the procedure recommended for the Jenike Shear Tester [3.1.3.8–3.12].

The principle of the test setup for a wall friction test is shown in Fig. 3.27. The bulk solid specimen is subjected to a vertical normal stress. The normal stress acting between bulk solid specimen and wall material is called the wall normal stress, σ_w .

In order to measure the wall friction, a bulk solid specimen is moved across the surface of a wall material sample with constant velocity, v . This

process is called shear (similar to the yield locus test). At the beginning of the shear process the wall shear stress, τ_w , increases (Fig. 3.28). With time, the rate of increase of the wall shear stress becomes less until finally a constant wall shear stress is attained (steady-state shear stress). The constant wall shear stress, τ_w , is characteristic for the applied wall normal stress, σ_w .

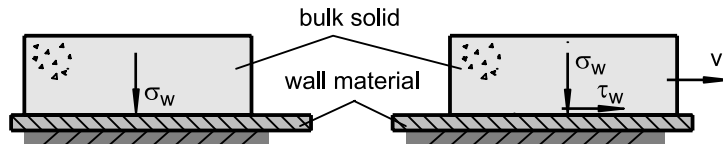


Fig. 3.27: Setup for measuring wall friction

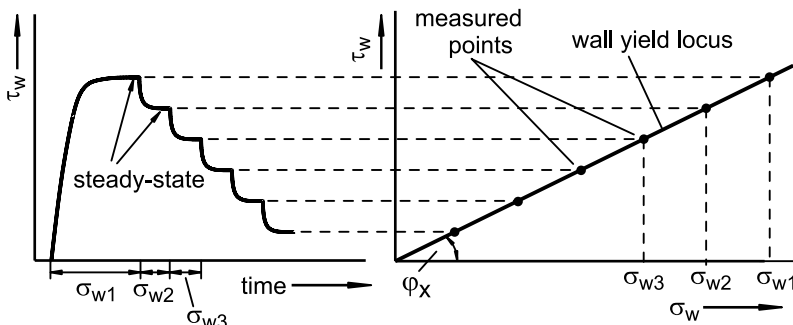


Fig. 3.28. Course of the wall shear stress in a wall friction test, wall yield locus in a σ_w, τ_w diagram

The pair of values of wall normal stress and constant wall shear stress (σ_w, τ_w) describes the kinematic wall friction at the wall normal stress, σ_w , and is used for the evaluation of the test. Since wall friction is often dependent on wall normal stress, wall normal stress is varied incrementally during the test. Thus the normal stress is adjusted to another value after steady-state flow has been observed. In this way values of steady-state wall friction at several wall normal stresses are measured.

The pairs of values of wall normal stress and steady-state wall shear stress are plotted in a σ_w, τ_w diagram (Fig. 3.28). The curve (or line) running through the measured points is called the *wall yield locus*.

3.3.2 Wall yield locus and wall friction angle

The wall yield locus is a yield limit like the yield locus. The wall yield locus describes the wall shear stress, τ_w , necessary to move a bulk solid continuously across a wall surface under a certain wall normal stress, σ_w . Since

the wall yield locus is based on the shear stresses measured at steady-state conditions, it describes the kinematic friction of the bulk solid. Thus the wall yield locus could more exactly be called a kinematic wall yield locus [3.12].

To quantify wall friction, the wall friction angle, φ_x , or the coefficient of wall friction, μ , are used. The larger the wall friction angle or coefficient of wall friction, the greater is wall friction. The coefficient of wall friction, μ , is defined as the ratio of wall shear stress, τ_w , to wall normal stress, σ_w , for a point on the wall yield locus:

$$\mu = \frac{\tau_w}{\sigma_w} \quad (3.6)$$

The wall friction angle, φ_x , is the slope of a line running from the origin of the σ_w, τ_w diagram to a point on the wall yield locus:

$$\varphi_x = \arctan\left(\frac{\tau_w}{\sigma_w}\right) \quad (3.7)$$

In Fig. 3.29 two wall yield loci are shown. If the wall yield locus is a straight line running through the origin (Fig. 3.29.a), the ratio of wall shear stress, τ_w , to wall normal stress, σ_w , has the same value for each point on the wall yield locus. Thus one obtains the identical wall friction coefficient, μ , and the identical wall friction angle, φ_x , for each point on the wall yield locus. In this case wall friction is independent of wall normal stress.

The wall yield locus shown in Fig. 3.29.b is curved and does not run through the origin. In this case one finds a different wall friction coefficient and wall friction angle for each point on the wall yield locus according to Eqs.(3.6) and (3.7). Thus the wall friction coefficient and the wall friction angle are dependent on wall normal stress, σ_w . This can be seen by the wall friction angles, φ_{x1} and φ_{x2} , which follow for the wall normal stresses, σ_{w1} and σ_{w2} (Fig. 3.29.b). In this case the wall friction angle is not equal to the slope of the wall yield locus.

When the wall friction angle is used for a certain application, e.g. for silo design for flow, it is important to take into account the stress dependence. The relevant wall normal stress must be assessed and then the wall friction angle for this stress can be determined from the wall yield locus.

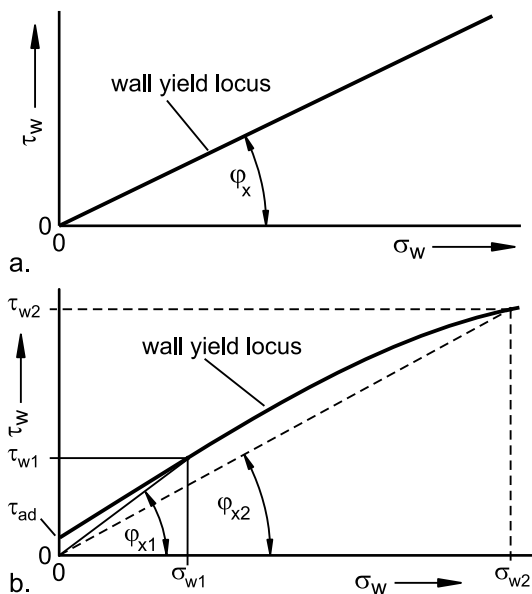


Fig. 3.29. Wall yield loci; a. constant wall friction angle, φ_x ; b. wall friction angle, φ_x , dependent on wall normal stress, σ_w

The shear stress at the point where the wall yield locus intersects with the τ -axis is called adhesion, τ_{ad} (Fig. 3.29.b). This value is equal to the shear stress which can be transferred if the normal stress, σ_w , is equal to zero. Values $\tau_{ad} > 0$ are found for bulk solid which can adhere at vertical walls due to large adhesive forces (e.g. moist clay, where the adhesive forces due to liquid bridges are dominant).

3.3.3 Time wall yield locus, static wall friction

An increase of adhesive forces with time, which is called time consolidation, can be observed not only within a bulk solid but also between a bulk solid and the surface of a rigid body. In analogy to the time yield locus the time consolidation at a surface is characterized by a time yield locus. In contrast to the wall yield locus, which describes kinematic wall friction, the time wall yield locus represents static wall friction(static wall yield locus) resulting from storage of a bulk solid on the surface of a rigid wall under a static normal stress over a given period of time [3.12].

The test setup is the same as for a wall friction test (Fig. 3.26). First the wall normal stress, σ_w , for the point on the time wall yield locus to be measured is selected. Then the wall normal stress for preparation, $\sigma_{w,prep}$,

which should be about 10% to 20% larger than σ_w used for the test, is chosen.

Measurement begins with preparation of the specimen, i.e., shearing the bulk solid specimen on the wall material under the wall normal stress for preparation, $\sigma_{w,prep}$. Thereby the wall shear stress, τ_w , increases and finally attains a constant value, $\tau_{w,prep}$ (Fig. 3.30).

Once steady-state wall friction is attained, the (lower) wall normal stress of the test point, σ_w , is adjusted, and the specimen is sheared further until steady-state wall friction prevails again (Fig. 3.30). The pair of values of wall normal stress, σ_w , and steady-state wall shear stress, $\tau_{w,pre}$, is a point of a (kinematic) wall yield locus. The described step is called preshear in analogy to a yield locus test.

After preshear, shear stress is reduced to zero. Then the specimen is stored at rest for the selected storage time. During storage, the same wall normal stress, σ_w , as during preshear is applied.

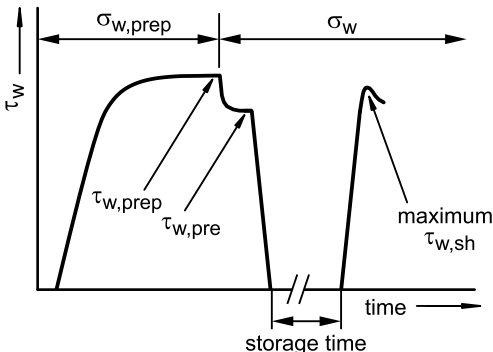


Fig. 3.30. Wall shear stress, τ_w , during measurement of a point of a time wall yield locus

At the end of the storage time, the specimen is sheared again under the same wall normal stress, σ_w , as applied at preshear and storage. This is called shear or shear to failure in analogy to a yield locus test. Often a shear stress maximum, $\tau_{w,sh}$, can be observed during shear. This maximum is interpreted as static wall friction. The pair of values of the wall normal stress, σ_w , and the maximum shear stress, $\tau_{w,sh}$, measured at shear, defines a point on a time wall yield locus in a σ_w, τ_w diagram (Fig. 3.31). To obtain several points on a time wall yield locus, the entire test procedure must be repeated several times at different wall normal stresses, σ_w , but with the same wall material sample and for the same storage time at rest, t . The time wall yield locus represents the static wall friction after a certain storage time at rest, t .

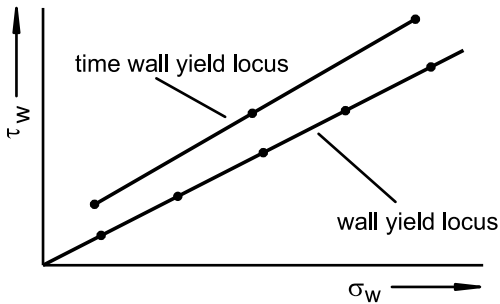


Fig. 3.31. Wall yield locus and time wall yield locus in a σ_w, τ_w diagram

The time wall yield locus defines the wall shear stress, τ_w , required to initiate flow of a bulk solid across the surface of a wall after the bulk solid has been stored at rest under the wall normal stress σ_w for a specific period of time on this surface. In analogy to a wall yield locus, wall friction angles can be determined from a time wall yield locus; these wall friction angles are static wall friction angles, $\phi_{x,st}$.

The procedure to determine the static wall friction angle, $\phi_{x,st}$, is the same as described for the wall yield locus (Fig. 3.29). In most cases the time wall yield locus is not a straight line running through the origin. Thus, the static wall friction angle is dependent on wall normal stress, σ_w .

4 Practical determination of flow properties

4.1 Measurement with shear testers

As outlined in Chap. 3, for a shear test a bulk solid specimen is subjected to a vertically acting normal stress, σ , and then sheared by shifting its upper and lower side relative to each other in the horizontal direction (Fig. 4.1). The shear stress, τ , in the horizontal plane prevailing due to the deformation is measured. If the relative displacement is translational, the shear tester is called a translational shear tester. The Jenike shear tester, which is described in Sect. 4.1.1, is the most common tester of this type.

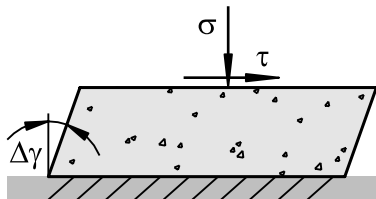


Fig. 4.1. Principle of the shear deformation in a translational shear tester

A shear tester, where the relative displacement is achieved by rotation of the top of the bulk solid specimen relative to the bottom, is called a rotational shear tester. The bulk solid specimen in Fig. 4.2.a is loaded vertically with a normal force, F_N , by a circular plate with a rough underside which results in a vertical stress, σ . Furthermore, by rotating the circular plate around its vertical axis the bulk solid specimen is subjected to shear deformation. The moment, M , resulting from the shear stress, τ , developing in the specimen is measured. Shear testers according to this principle are called torsional shear testers. Deformation of the bulk solid during shearing varies with the radius. It is zero in the center and increases linearly with the radius.

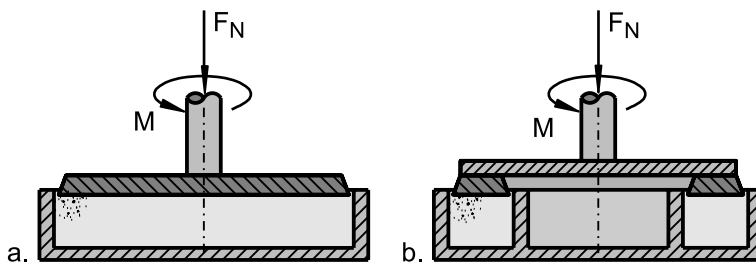


Fig. 4.2. Principle of rotational shear testers: a. torsional shear tester; b. ring shear tester

In contrast to a torsional shear tester, the shear cell of the ring shear tester is annular-shaped like a ring (Fig. 4.2.b). Thus the deformation of the bulk solid specimen is more homogeneous, but still dependent on the radius. Scientific investigations of ring shear testers with different ratios of inner to outer diameter of the annulus have shown that this influence can be neglected if the inner diameter is at least 50% of the outer diameter, and that with an appropriate test procedure results comparable to the Jenike shear tester are obtained [4.1–4.4].

In the following the test procedure is described regarding two common shear testers, the Jenike shear tester and the ring shear tester. These two types of shear testers have been investigated in science more than other testers. These testers have been built in a diversity of research institutes in many countries in order to investigate, for example, the stress distribution in a bulk solid specimen and the influence of the geometry of the shear cell. Thus quite a lot of information is available about the shear process in the bulk solid specimen. The torsional shear tester is used at several labs, but the test procedure and evaluation is somewhat different from Jenike's approach [4.5–4.7].

4.1.1 Measurement of yield loci with the Jenike shear tester

Jenike presented the major results of his work, the Jenike shear tester and an approach for silo design, around 1960 [4.8,4.9] (Sect. 1.2). At first the Jenike shear tester was mostly applied for silo design. It was developed on basis of direct shear testers known from soil mechanics (e.g., Casagrande shear box [4.10]), which could not be used for the stress range relevant for silo design.

The shear cell of the Jenike shear tester is shown in Fig. 4.3. The base of the shear cell is fixed to a stationary bearing plate. The shear ring is placed on the base. Base and shear ring contain the bulk solid specimen, which is

covered with the shear lid. The shear lid and thus the bulk solid specimen are loaded centrally by a normal force, F_N , by means of a weight hanger (the weight hanger is a device for carrying weights, which is set on the central tip of the shear lid) and weights.

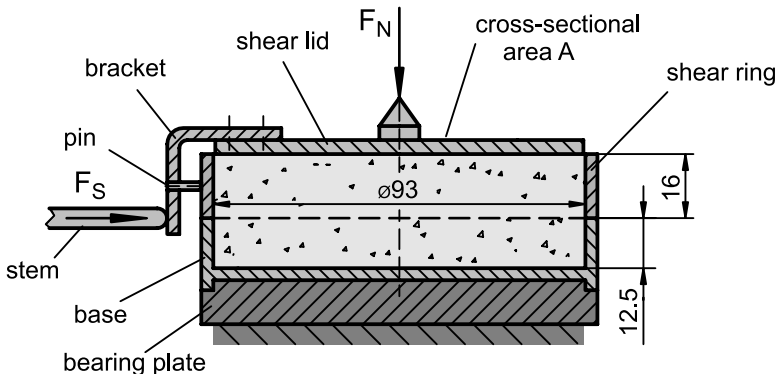


Fig. 4.3. Principle of the shear cell of the Jenike shear tester (dimensions in mm)

In Fig. 4.3 the standard dimensions of the shear cell are shown. In addition, shear cells with smaller or larger dimensions are possible, for example for the case that only a limited amount of bulk solid is available for testing, or if a bulk solid with large particles has to be tested. The latter follows from the condition that the specimen must contain a sufficient number of particles to ensure that it behaves like a continuum. If the number of particles is too small, the measured shear force fluctuates, since the stress is transferred through a small number of force chains which undergo a permanent change (force chains: see Sect. 5.1.1). Furthermore, the measured shear stresses are too large due to the restricted mobility of the particles [4.11,4.12]. With a shear cell as shown in Fig. 4.3 one can test bulk solids with a maximum particle size of about 2 mm in the case of a very narrow particle size distribution, and up to about 5 mm in case of a wide particle size distribution (e.g., 0 mm to 5 mm). If particles are hard and sharp-edged, the maximum particle size is somewhat smaller..

To shear the bulk solid specimen, the upper part of the shear cell, i.e., shear ring and shear lid, are moved horizontally (to the right in Fig. 4.3). This is caused by a stem that presses against the bracket attached to the shear lid. The stem is driven forward at a steady rate of approximately 1 to 3 mm/min. The stem is attached to the drive system through a force transducer which measures the shear force, F_s . The shear force is transferred to the bulk solid specimen through the bracket and the shear lid as well as through the small pin (attached at the bracket) and the shear ring.

The shear test procedure for the Jenike shear tester is outlined in the following according to the procedure described in the “Standard Shear Testing Technique” [4.13], which is an internationally agreed standard on the operation of the Jenike shear tester. The same procedure can be found in the ASTM standard D-6128 [4.14].

For the preparation of a test the base along with the shear ring is placed on the bearing plate (Fig. 4.4). A mould ring is then placed on the shear ring. Shear ring and mould ring are then pressed against locating screws (not shown in Fig. 4.4), which are adjusted so that shear ring and mould ring are in the offset position, i.e., a position where the shear ring has an offset against the shear direction. The offset is equal to the thickness of the wall of the shear ring. After the shear cell has been filled with the bulk solid, excess material is scraped off level with the top of the mould ring and, thus, a plane surface is attained.

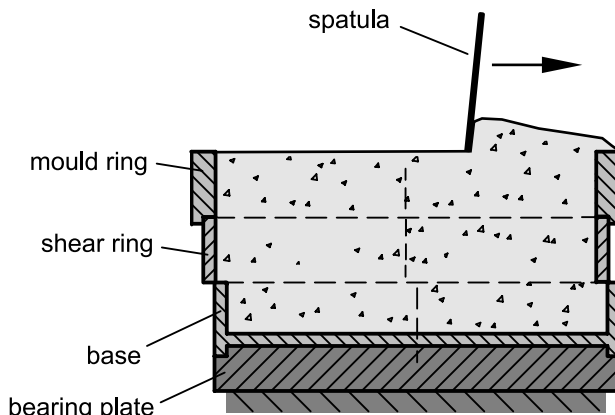


Fig. 4.4. Shear cell in initial position: The shear ring is in the offset-position, i.e., it is displaced against the shear direction by the shear ring wall thickness. After filling, excess material is removed by scraping off with a spatula.

The shear displacement of the Jenike shear cell is limited to twice the wall thickness of the shear ring, i.e., about 6 to 8 mm (depending on the shear cell dimensions). Therefore at preshear, steady-state flow has to be attained after a sufficiently small shear displacement. This is only possible when the bulk solid specimen is close to critical consolidation (consolidation attained at steady-state flow) prior to preshear, so that only a relatively small shear displacement is necessary until steady-state flow prevails. Thus the bulk solid specimen has to be preconsolidated prior to preshear. For this a procedure called “twisting” is used.

For twisting the twisting lid is placed on the bulk solid. With the hanger and appropriate weights the bulk solid specimen is loaded with the same normal force, F_N , which has been selected for preshear. For the case that the shear tester is provided with a twisting device as shown in Fig. 4.5, the twisting device is connected to vertical bolts on the top of the twisting lid. Then the twisting lid is twisted by means of the twisting device. Each twist consists of a 90° rotation of the twisting lid which is then reversed. Due to friction between the smooth underside of the twisting lid and the bulk solid, shear stresses develop in the circumferential direction. The shear stresses along with the normal stress created by the normal force, F_N , consolidate the bulk solid specimen. If the shear tester is not provided with a twisting device, the twisting lid is rotated with a wrench, whereby the procedure is in principle the same as described above.

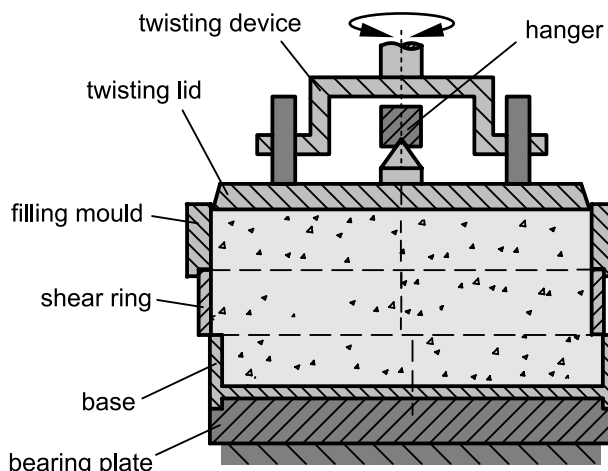


Fig. 4.5. Shear cell; setup for preconsolidation (twisting)

The required number of twists depends on the bulk solid and the stress level selected for the yield locus. It must be established with trial tests where it is varied until steady-state flow is attained within about 80% of the maximum shear displacement (some additional shear displacement is needed for shear to failure). If a very compressible bulk solid is tested, it may happen that as soon as the weight hanger has been placed on the twisting lid, the bulk density increases significantly and thus the twisting lid moves downwards well into the filling mould. In this case hanger and twisting lid have to be removed and the shear cell has to be filled further. This has to be repeated until a sufficient amount of bulk solid is in the shear cell, so that even after twisting the bulk solid surface is above the top

of the shear ring. If the latter is not the case, then it is necessary to prepare a new test specimen.

After twisting the twisting device and weight hanger are removed. Then the mould ring is carefully lifted and subsequently the twisting lid is slid off the bulk solid specimen in direction of the stem. Excess material is then scraped off in small quantities to be flush with the top of the shear ring (similar to Fig. 4.4, but without the mould ring). Care has to be taken that neither a downward force is exerted by the spatula nor the upper shear ring is moved relative to the base.

The last step of the preparation is to place the shear lid centered on the shear ring on the bulk solid specimen (Fig. 4.3 but with the shear ring in the offset position as shown in Fig. 4.4). In this position the width of the gap between the pin and the shear ring should be about 0.1 to 0.2 mm. Then the hanger with weights is placed on the central tip of the shear lid to apply the normal force, F_N . In order to ensure that the shear ring is not in contact with the base and thus shear and normal stresses are transferred between the rings, the shear ring is carefully rotated around its axis and simultaneously lifted until the distance between the base and the shear ring amounts to about 0.2 mm. Now the shear cell is ready for preshear. The normal stress at preshear, σ_{pre} , is the vertical stress in the horizontal plane between base and shear ring. This plane is called the shear plane, and for the stress calculation it is assumed that the shear deformation takes place in this plane. The normal stress at preshear is calculated from the normal force, F_N , resulting from the hanger and weights on the hanger, the weights of all other parts above the shear plane (shear lid, shear ring) and the bulk solid within the shear ring.

For preshear the stem is driven with constant velocity in direction towards the shear cell (Fig. 4.3). The position of the shear cell relative to the stem must be such that the stem acts on the bracket in the shear plane. Only in this way the shear force does not exert a moment on the shear plane which can be easily shown by equilibrium of forces and moments of the upper part of the shear cell (shear lid and shear ring with bulk solid) [4.15]. The measured shear force, F_S , is recorded during the test (chart recorder, data acquisition system). At preshear the shear force should at first increase with a steep slope, than become flatter and finally attain a constant value (Fig. 4.6). Thus steady-state flow is attained. The stem is then driven backwards until the shear force, F_S , is reduced to zero.

Prior to shear to failure, the normal stress, σ_{sh} , for the first point of incipient flow must be adjusted. For this the normal force, F_N , is reduced by removing weights from the hanger. The hanger must not be lifted because the bulk solid specimen should not be disturbed or unloaded completely. Subsequently the specimen is sheared by driving the stem in the forward

direction. In the case of a fine-grained, stiff bulk solid specimen the shear force increases quickly until it reaches a maximum. At the shear force maximum the specimen starts to flow (failure), subsequently the shear force, F_s , and the shear stress, τ , decrease (Fig. 4.6). After the shear stress maximum has been recognized, the stem is driven backwards to reduce the shear stress to zero. The filled shear cell is then removed from the tester and weighed in order to determine the overall bulk density under consideration of the known weight and volume of the shear cell. Since here the total internal volume of the shear cell is used, the calculated bulk density is the overall bulk density directly after twisting.

After measurement of the first point of the yield locus, more points have to be measured by repeating the procedure described above. For each individual test one should use a fresh bulk solid sample. If the material has not been changed by the shear test (e.g., by attrition), the same sample can be used repeatedly. In this case the material should be well loosened before each test. After several shear points have been measured at different normal stresses at shear, σ_{sh} , the yield locus and its parameters can be determined (Fig. 4.6).

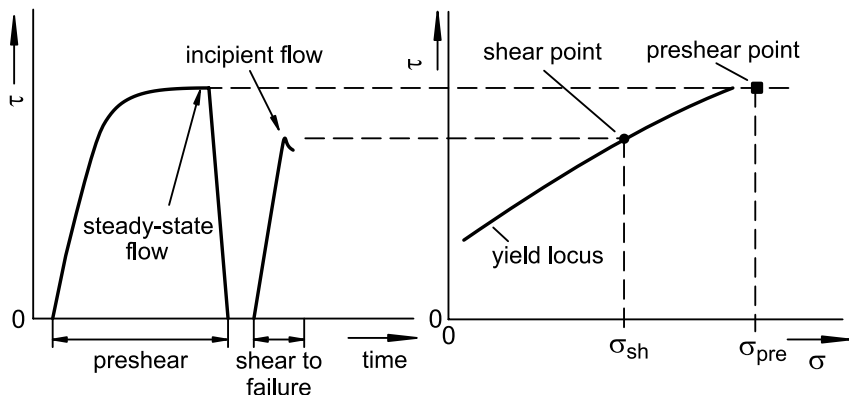


Fig. 4.6. Measurement of a point of the yield locus (shear point) by preshear and shear to failure

When running a shear test according to the procedure described here, the course of the shear force, F_s , and the shear stress, τ , respectively, has to be observed carefully in order to check whether the preconsolidation (twisting) of the specimen is appropriate. A course of the shear stress as shown in Fig. 4.7.a is typical for an initially underconsolidated specimen which is sheared until steady-state flow is attained: the bulk density increases during shear, and the maximum shear stress is the shear stress at steady-state flow. If, in contrast to this, an overconsolidated specimen is presheared,

the shear stress, τ , passes a maximum during preshear (Fig. 4.7.b) which is greater than the shear stress at steady-state flow. The maximum, which can be less pronounced than in Fig. 4.7.b, characterizes incipient flow or failure, respectively. Although at further shear steady-state flow prevails, the specimen is not in the same condition at the initially underconsolidated specimen described in Fig. 4.7.a, because steady-state flow is limited to the material in the region of the failure plane. Thus only the bulk solid close to the failure plane has properties corresponding to steady-state flow. The rest of the specimen remains in the state of overconsolidation. Thus, the specimen is nonhomogeneous, and the measured overall bulk density is too high compared to the bulk density corresponding to steady-state flow.

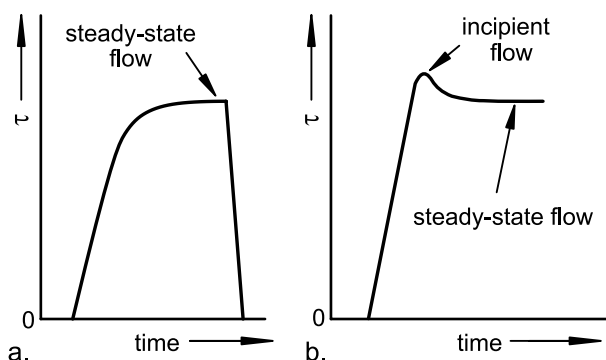


Fig. 4.7. Shear stress vs. time at preshear of an underconsolidated (a) and an overconsolidated (b) specimen

Because of the nonhomogeneity an overconsolidated specimen should not be used for measurement of a shear point [4.13]. Instead, for subsequent shear tests the number of twists has to be reduced. Thus it may be necessary to repeat preshear several times until the appropriate number of twists has been found out.

Sometimes a shear stress maximum at preshear can also be observed when shear is continued even after the shear stress has become constant for a certain time interval (shear stress plateau). This maximum, which is usually less pronounced than described above, is often caused by the height of the shear zone decreasing (shear localization, see Sect. 5.2.2) with ongoing shear deformation, and particles in the shear zone changing their orientation. These processes lead to a decrease of the shear stress. In addition, when coarse particles are presheared, dilation can be observed in the first part of preshear thus resulting in a shear stress maximum (see Sect. 5.2.3).

Sometimes the number of twists is not sufficient to attain steady-state flow within the available shear displacement, i.e., the shear stress is in-

creasing until the end of the available shear displacement. In this case the number of twists has to be increased. If after 50 twists steady-state flow still cannot be achieved, the normal load can be increased in steps of 50% of σ_{pre} . If this is done, care has to be taken in order to avoid the bulk solid specimen becoming overconsolidated, but the overconsolidation is not recognized because of the limited shear displacement. Especially when very fine-grained bulk solids (dry or moist) are tested, overconsolidation can lead to a shear stress maximum developing very slowly as shown in Fig. 4.8. If this specimen requires an extended shear displacement, the operator will be happy to have attained steady-state flow within the available shear displacement when seeing that the shear stress does not increase further with time (apparent steady-state flow). Thus the operator will stop preshear and proceed with shear to failure. But, as can be seen in Fig. 4.8, a larger shear displacement would lead to a decrease of the shear stress (broken curve in Fig. 4.8) since the shear stress at steady-state flow is smaller than assumed. Due to the limited shear displacement of the Jenike shear tester it is usually not possible to measure the broken curve in Fig. 4.8. This makes it sometimes difficult to identify an overconsolidated specimen.

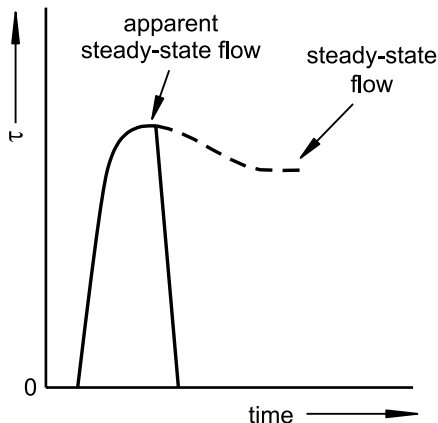


Fig. 4.8. Possible course of the shear stress when preshearing an overconsolidated specimen requiring a large shear displacement

It is not possible to quantify the time required to measure a yield locus since it depends on the bulk solid, the number of trials until the optimal number of twists has been found out, and the skill of the operator. Assuming that points of incipient flow (shear points) are measured at three different normal stresses, and each point is measured twice with respect to the accuracy of the test procedure (manual preconsolidation, operator's influ-

ence), a realistic time for the measurement of a yield locus lies between one and two hours.

4.1.2 Measurement of yield loci with the ring shear tester

The fundamental advantage of rotational shear testers over translational shear testers is that the shear displacement is not limited by the apparatus as demonstrated with the Jenike shear tester (see Sect. 4.1.1). The principle of the ring shear tester was developed by Hvorslev [4.16] in the 1930's for testing of soils. Since naturally in soil mechanics high stresses have to be applied, the tester was accordingly heavy and not suitable for the small stresses applied in bulk solids technology. The first ring shear tester especially designed for bulk solids was developed by Walker in the 1960's [4.17]. Other ring shear testers have been built in universities for research purposes [4.3,4.4,4.18–4.23] and rarely used for industrial applications. In this section a ring shear tester developed by the author in the early 1990's is described [4.15,4.24,4.25] (Fig. 4.9), which is employed in industry as well as in research. The main difference to earlier designs is the lighter construction, a shear cell which can be removed from the tester with lid and bulk solid specimen, the option of running wall friction tests, and the application of very small stresses. A computer-controlled version allows automatic measurement and evaluation.

In Fig. 4.9 the shear cell of a ring shear tester developed by the author is shown [4.15,4.24,4.25]. The ring-shaped (annular) bottom ring of the shear cell contains the bulk solid specimen. The annular lid is placed on top of the bulk solid specimen and attached to a crossbeam. Two parallel tie rods are connected to the crossbeam. Each of the tie rods is connected to a load beam (not visible in Fig. 4.9) so that the forces, F_1 and F_2 , which are acting in the tie rods, can be measured. To shear the bulk solid, the lid and the bottom ring of the shear cell must rotate relative to each other. This is accomplished by rotating the bottom ring in the direction of the arrow ω (ω is the angular velocity), while the lid and crossbeam are prevented from rotation by the tie-rods. The bottom of the shear cell and the lower side of the lid are rough in order to prevent the bulk solid from sliding relative to these surfaces. Therefore, rotation of the bottom ring relative to the lid creates a shear deformation within the bulk solid. The roughness of the bottom and the lid is realized, for example, by radially-oriented bars (vanes). During shear the shear force, which is the sum of the forces F_1 and F_2 , is recorded. The shear force is directly proportional to the shear stress acting in the bulk solid specimen in the circumferential direction.

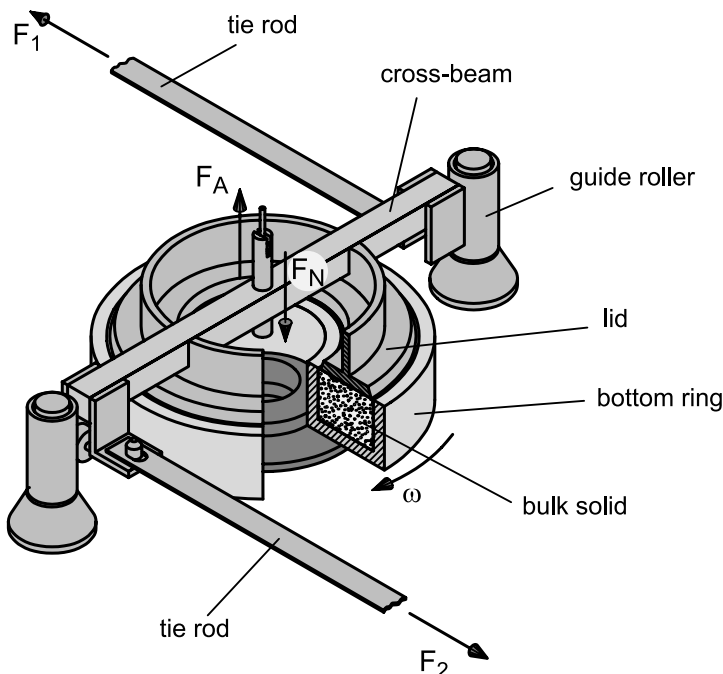


Fig. 4.9. Shear cell of the Schulze ring shear tester [4.15,4.24,4.25]

The horizontal position of the lid is adjusted by the tie rods and the two lateral guiding rollers. Thus a bearing for the lid, as used for earlier ring shear testers, is not necessary. The advantage of this construction is that the lid can tilt somewhat and thus can adjust to the bulk solid specimen (like the shear lid of the Jenike shear tester), which results in a more uniform stress distribution in the bulk solid specimen. Furthermore, similar to the Jenike shear tester this design allows one to remove the shear cell along with the lid and the bulk solid specimen, for example, for time consolidation tests with external storage.

The vertical normal force, F_N , is exerted on the crossbeam which is fixed at the lid. This can be accomplished with weights (as used with the Jenike shear tester) placed on a hanger which is attached to the crossbeam. Automatic ring shear testers are provided with a device for the computer-controlled adjustment of the normal force. The weights of the lid, hanger, crossbeam, and tie rods can be compensated by a counterbalance force, F_A , which is directed upward and acts at the crossbeam. The result of the counterbalance force which is created, for example, by a counterweight, is to make possible the application of normal stresses smaller than the stresses resulting from the weight forces of the lid and the parts connected to the

lid. In principle, this way normal stresses smaller than 100 Pa and even negative normal stresses can be applied on the bulk solid specimen [4.26,4.27].

The shear force is recorded versus time (chart recorder, data acquisition system, control system). If the lid of the shear cell is connected to a displacement transducer, the vertical position of the lid can also be measured. Thus the volume of the specimen and, if the mass of the bulk solid specimen is also determined by weighing, the overall bulk density, ρ_b , can be calculated. For evaluation of a yield locus and its parameters the bulk density prevailing at steady-state flow and thus corresponding to the consolidation stress, σ_I , is important.

Similar to the Jenike shear tester, the size of the shear cell is a limiting factor for the particle size of the bulk solid to be tested. Following the experience of the author, in a ring shear cell with 200 mm outer diameter and 900 cm³ specimen volume, bulk solids with particles up to a diameter of 5 mm in case of a very narrow particle size distribution, and up to 10 mm in case of a wide particle size distribution (e.g., coal with particles from 0 to 10 mm) can be tested. If very fine-grained bulk solids have to be tested (e.g., < 250 µm), also much smaller shear cells, and thus a smaller shear tester, can be used (e.g., specimen volumes in the range of 9 cm³ to 70 cm³ [4.28]). Accurate upper limits of the particle size cannot be given because, in addition to particle size, particle shape and hardness also play a role.

The test procedure of the ring shear tester is described in detail in ASTM standard D-6773 [4.29]. It is explained in the following regarding the manually-operated version of the ring shear tester discussed above.

For preparation of a test the bottom ring of the shear cell is filled with the test bulk solid. Excess material is removed by scraping off with a spatula until flush with the top of the bottom ring (similar as shown in Fig. 4.4 for the Jenike shear cell). Subsequently the filled bottom ring is weighed. The mass is required to calculate the bulk density when evaluating the test.

Since in principle the shear displacement of a rotational shear tester is unlimited, manual preconsolidation as with the Jenike shear tester (twisting) is not necessary. Thus, after filling, the bottom ring is set on the ring shear tester, and the lid is positioned concentrically to the bottom ring on the bulk solid specimen. Then hanger (force F_N , Fig. 4.9), counterweight system (counterbalance force, F_A) and tie rods (shear force, forces F_1 and F_2) are appended at the crossbeam. The hanger is loaded with weights to adjust the normal force, F_N , and thus the normal stress, σ_{pre} , required for preshear. Now preparation of the shear cell is finished and the shear test can begin.

For preshear the bottom ring is rotated clockwise (seen from the top), whereby the lid is prevented from rotation by the tie rods. At the beginning

of preshear the shear stress, which is calculated from the forces acting in the tie rods (forces F_1 and F_2 in Fig. 4.9), increases with time (Fig. 4.10), whereby the height of the specimen usually decreases according to the compaction of the bulk solid (a typical course of the bulk density at preshear is shown in Fig. 3.12). Only cohesionless, incompressible bulk solids can dilate at the beginning of preshear which results in the height of the specimen increasing somewhat (see Sect. 5.2.3).

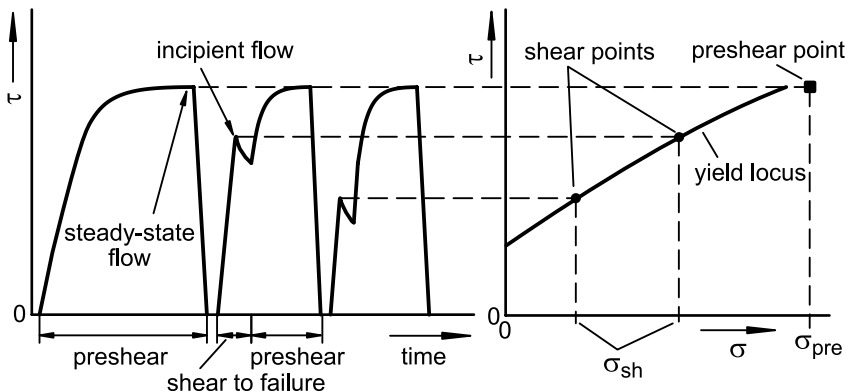


Fig. 4.10. Measurement of a yield locus by preshear and shear to failure with a ring shear tester where several points are measured with one bulk solid specimen

When the shear stress does not increase further and, thus, steady-state flow is attained, the direction of rotation of the bottom ring is reversed. After the shear stress is reduced to zero, the bottom ring is stopped, and the normal force, F_N , is reduced to adjust the normal stress, σ_{sh} , of the first point of incipient flow. Then the bulk solid specimen is sheared until the maximum value of shear stress can be identified. The shear stress maximum represents incipient flow (failure). It is interpreted as a point on the yield locus (same assumption as with the Jenike shear tester, see previous section).

After shear to failure, the specimen can usually be presheared again (σ_{pre}), then sheared to failure (σ_{sh}), and so on, until the desired shear points have been measured (Fig. 4.10). Thus with bulk solids which do not change their properties due to the shear deformation (true for nearly all bulk solids), a complete yield locus test can be performed with one specimen. This greatly reduces the time required for a shear test [4.30] and makes possible the automatic measurement of a yield locus [4.31].

For the automatic measurement the ring shear tester presented here is connected to a PC running the control and test software. The hanger and weights are replaced by a device for the computer-controlled adjustment of

the normal force, F_N . Furthermore, the computer controls the shear cell rotation and measures shear force and specimen height. The control software must be able to identify steady-state flow as well as incipient flow in order to terminate preshear or shear to failure when appropriate. Thus control, measurement and evaluation are done by the computer. This reduces the time that an operator is required to about five minutes per yield locus [4.31].

The ring shear tester is used increasingly as an alternative to the Jenike shear tester. Especially for bulk solids which cannot be accurately tested with the Jenike shear tester because of its limited shear displacement, the ring shear tester is advantageous, for example, for testing soft elastic (plastics powder, rubber granules) [4.10] or plastic materials (sewage sludge, filter cake, plastic clay). Furthermore, with the ring shear tester smaller stresses can be applied than with the Jenike shear tester [4.15]. Also better reproducibility [4.32], limited influence of the operator and clearly less time of operation [4.31] are arguments for the ring shear tester. The latter may be the reason for the growing number of users in other fields than silo design, for example, in quality control or product development, where the Jenike tester is rarely applied.

4.1.3 Measurement of time consolidation

The measurement of time consolidation with the Jenike shear tester and the ring shear tester is based on a similar procedure and thus described in the following for both testers.

The time consolidation test is similar to the measurement of a yield locus. First a bulk solid specimen is presheared. After preshear the specimen is not immediately sheared to failure (Fig. 4.11.a), but stored within the shear cell for a period t under static load. This can be done on the shear tester, whereby in this case the tester cannot be used for other tests during the storage period, or apart from the tester, for example, on a special device called a time consolidation bench (Fig. 4.12). In this device the shear cell with the bulk solid specimen is loaded vertically with weights. The weights are adjusted so that the stress state in the specimen is similar to the stress state at the end of consolidation, i.e., at steady-state flow. Thus, the vertical stress (= major principal stress) in the specimen applied during the consolidation period (which is the major principal stress in this situation) must be equal to the consolidation stress, σ_1 (the major principal stress at steady-state flow).

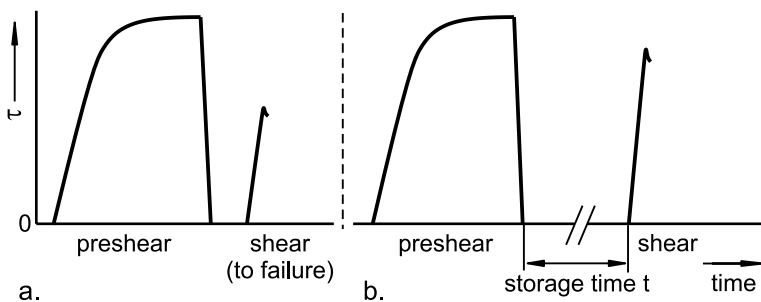


Fig. 4.11. Shear stress, τ , vs. time during preshear and shear to failure; a. measurement of a point on a yield locus; b. measurement of a point on a time yield locus

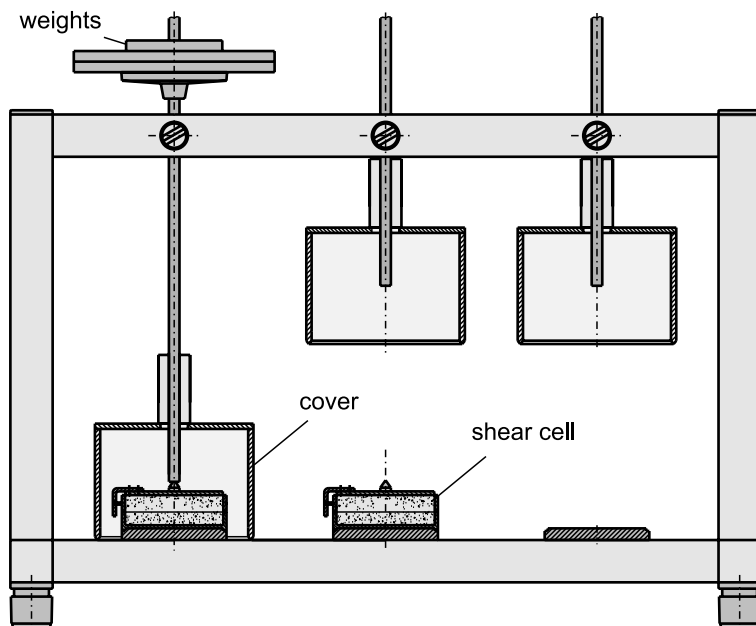


Fig. 4.12. Time consolidation bench with covers (version for Jenike shear tester)

The time consolidation bench in Fig. 4.12 is provided with covers to constrain the specimen and prevent or at least reduce influence from environmental effects such as evaporation or humidification during the consolidation period. Sometimes it is desired to store the specimen at defined conditions, e.g., in a climate chamber. In this case one would store the specimen without cover. However, under all circumstances it has to be ensured that the specimen is not subjected to vibration or unwanted temperature changes due to heating equipment or sunlight.

In the way described above several specimens are prepared, presheared, stored under the consolidation stress for the desired time, and finally sheared to failure. As with shear without time consolidation (measurement of a point on a yield locus, Fig. 4.11.a), so also after time consolidation one will observe a shear stress maximum (Fig. 4.11.b). If consolidation time affects the bulk solid under consideration, after the consolidation period the shear stress maximum will be larger than it would have been without a consolidation period between preshear and shear. If identically prepared specimens are sheared to failure after different consolidation times, t , one will obtain different shear points in the σ, τ diagram. It is common practice to measure only one shear point on a time yield locus, i.e., shear to failure at only one specific normal stress. The time yield locus is then approximated by a parallel to the linearized yield locus running through the measured shear point (Fig. 4.13). Each time yield locus is valid for only one consolidation period and one consolidation stress. The unconfined yield strength, σ_c , is determined in the same way as for a yield locus by drawing a Mohr stress circle through the origin and tangent to the time yield locus (minor principal stress $\sigma_2 = 0$). If only one point on a time yield locus is measured, the measured shear point should be close to the point where the Mohr stress circle representing σ_c touches the time yield locus. If this is not the case, the accuracy is reduced because the time yield locus has to be extrapolated to a larger extent to determine the unconfined yield strength, σ_c .

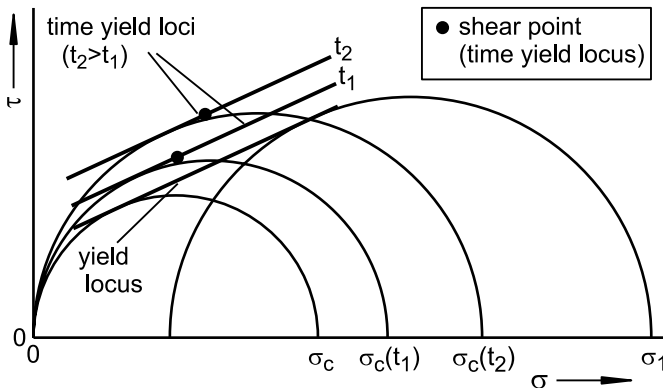


Fig. 4.13. Yield locus with time yield loci approximated as parallels to the yield locus

4.1.4 Measurement of kinematic wall friction

The test procedure for measuring wall friction is similar for the Jenike shear tester and the ring shear tester. Therefore it is described here for both testers in this section.

For measuring wall friction with the Jenike shear tester the base of the shear cell is replaced by a sample of the wall material (Fig. 4.14) which is fixed to the base plate of the shear tester.

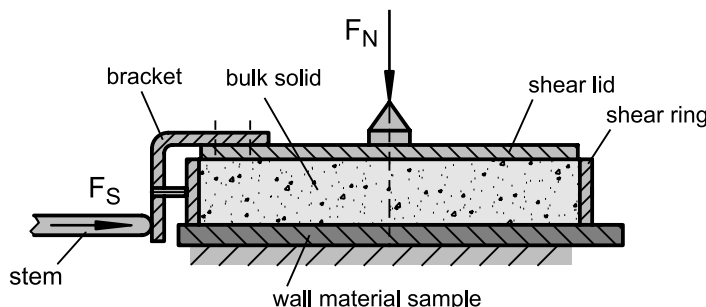


Fig. 4.14. Setup to measure wall friction with the Jenike shear tester

The shear cell is prepared similar to a yield locus test (Sect. 4.1.1). The mould ring is placed on the shear ring, and shear ring and mould ring are filled with the bulk solid. Excess material is scraped flush with the top of the shear ring. Then the twisting lid is placed on the bulk solid filling, the hanger is placed on the lid, and weights are placed on the hanger, corresponding to the largest normal stress of the intended wall friction test. Then the lid is twisted several times to homogenize the specimen and increase its bulk density thus ensuring that the shear lid will not move downwards too much when being loaded with hanger and weights. Since the dependence of wall friction angle on bulk density can usually be neglected, the time-consuming procedure for determination of the optimum number of twists, which is an important part of the preparation of a yield locus test, can be omitted.

During the test the bulk solid specimen is moved relative to the wall material surface. Since wall friction is usually smaller than the internal friction of the bulk solid, the complete bulk solid specimen moves relative to the wall material. Commonly wall friction is measured with one bulk solid specimen at different levels of wall normal stress, σ_w . This is possible because the influence of bulk density can be neglected and thus it is not necessary to prepare a new specimen for every stress level.

It is usual to start with the largest wall normal stress, σ_w , and then incrementally decrease the wall normal stresses once a constant wall shear stress has been attained (Fig. 4.15). Thus, the bulk solid specimen is first subjected to the largest wall normal stress, σ_w , and normal force, F_N , respectively. When using the Jenike shear tester, appropriate weights are placed on the hanger. Then the stem is driven forward in order to move the shear cell across the wall material sample. As shear starts, the shear force, F_s , and thus the wall shear stress, τ_w , increase (Fig. 4.15). When the shear stress reaches a constant value, weights are removed from the hanger until the normal stress is reduced to the next level. When the shear stress has again become constant, the normal load is again reduced and so on until the constant shear stress has been measured at all selected stress levels, σ_w . The pairs of values of wall normal stress, σ_w , and wall shear stress, τ_w , are plotted in a σ_w, τ_w diagram and a curve is drawn through the points. This is the wall yield locus of the tested bulk solid on the specific wall material. From the wall yield locus the wall friction angle can be determined according to Sect. 3.3.2.

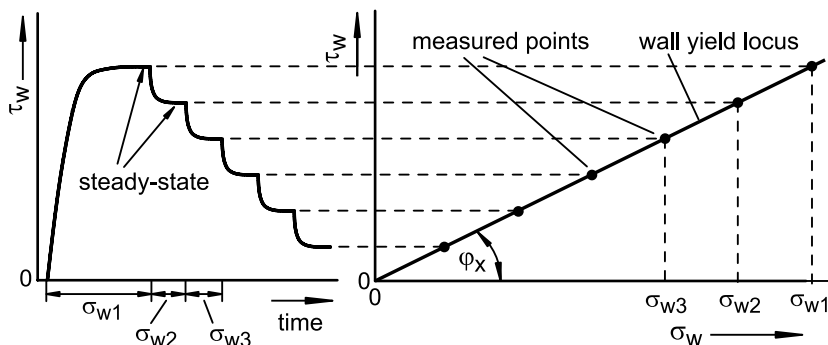


Fig. 4.15. Wall friction test: Shear stress vs. time and wall yield locus

In Fig. 4.16 the setup of the wall friction ring shear cell is shown. The annular bottom ring contains a sample of the wall material to be tested. On top of the wall material sample is the bulk solid specimen, which is covered with the annular lid of the shear cell. A normal force, F_N , is applied to the bulk material specimen with the lid of the shear cell (as with a yield locus test, Fig. 4.9). The normal force creates the vertical wall normal stress, σ_w , acting between the bulk solid specimen and the wall material sample. To measure wall friction the shear cell is rotated slowly in the direction of arrow ω , while the lid is prevented from rotating by the two tie rods. Since the layer of bulk solid located between the lid, which has a rough underside, and the surface of the wall material is also prevented from rotating,

the bulk solid is moved across the surface of the wall material sample while it is subjected to the normal stress, σ_w . The forces acting on the tie rods, F_1 and F_2 , are proportional to the wall shear stress, τ_w . Thus, from the measured forces, F_1 and F_2 , the wall shear stress, τ_w , can be calculated. The test procedure is the same as described above for the Jenike shear tester (Fig. 4.15).

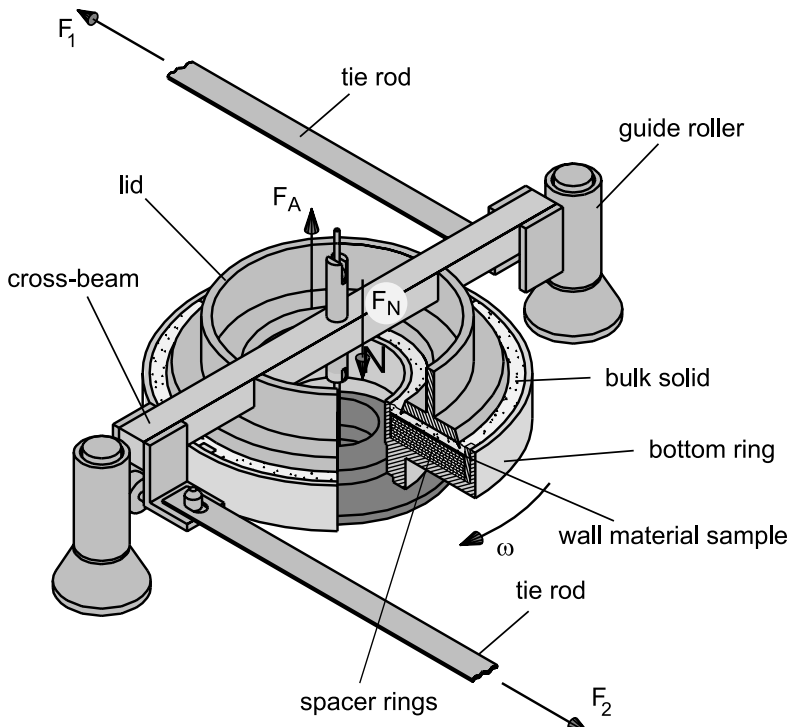


Fig. 4.16. Measurement of wall friction with a ring shear tester [4.33]

Comparing the ring shear tester and the Jenike shear tester regarding the wall friction test, one can say that the Jenike tester has the advantage that the required wall material sample is just a rectangular plate of sufficient dimensions, whereby the shear cell of the ring shear tester as shown in Fig. 4.16 requires an annular-shaped wall material sample. Therefore wall friction testing with many different wall materials, which are replaced by new samples very often, is less expensive with the Jenike shear tester. In addition, the dependence of wall friction angle on the shear direction, e.g., if the wall material surface has grooves in a certain orientation, can be measured with the Jenike shear tester due to the translational shear, whereby with a ring shear tester wall friction is measured in all directions simulta-

neously thus resulting in a mean wall friction angle for all directions. On the other hand the ring shear tester, which provides unlimited shear displacement, allows one to study the long-term behavior of the wall friction, e.g., with bulk solids changing the surface of the wall material by wear or by materials adhering at the surface (see Sect. 7.1.2). The unlimited shear displacement is also an advantage for combinations of bulk solid and wall material requiring large shear displacements. If such combinations are sheared with the Jenike tester, always after the maximum shear displacement is reached the stem has to be retracted and the shear cell pushed back to its initial position by hand [4.13,4.14].

4.1.5 Measurement of static wall friction

The time wall yield locus described in Sect. 3.3.3 gives information about the static angle of wall friction, which is dependent on the previous storage time at rest. From the author's experience wall friction time tests are required less often than measurements of kinematic wall friction. Therefore in the following only a short description of the test procedure is given.

The preparation and procedure of a wall friction time test are similar to a wall friction test. The main difference is that after steady-state wall friction has been attained the specimen is unloaded from shear stress and then stored at rest (consolidation time) on the wall material sample while the normal stress is kept constant (Fig. 3.30). For this the shear cell with the bulk solid specimen can remain on the shear tester, but the tester cannot be used for other tests during the consolidation time. Thus it is advantageous to store the specimen under static load on a time consolidation bench (Sect. 4.1.3, Fig. 4.12). After the storage time the shear cell with the bulk solid specimen is placed on the shear tester and sheared again under the same normal load as before the consolidation time. The maximum shear stress defines a point on the time yield locus (for more details refer to Sect. 3.3.3).

4.1.6 Attrition test

Attrition tests help to evaluate particle breakage and fines generation by abrasion (both are included here under the term attrition) from flow of a bulk solid (e.g., flow in a silo). With this kind of test products can be compared regarding their sensitivity to attrition, or the maximum stress for the storage of a specific product in order to minimize attrition can be determined [4.34,4.35]. It is important that the stress level of an attrition test

can be adjusted to the conditions that simulate where a product is stored or handled.

Fines are generated when particles are subjected to stresses, but a static load has to be distinguished from shear deformation (kinematic load). Commonly – and not unexpected – more fines are generated by kinematic load than by static load at the same stress level. For attrition testing at kinematic load a device is required where a bulk solid specimen can be subjected to an adjustable normal stress and a large shear deformation. This is fulfilled with a rotational tester like a ring shear tester [4.34–4.37] in contrast to a translational tester (Jenike shear tester) with its limited shear displacement allowing only limited deformation of the bulk solid specimen.

The procedure of an attrition test with a ring shear tester is as follows (with other testers the procedure has to be adjusted corresponding to their specific features): Particles smaller than a specific size are removed by sieving (e.g., if a granulate with particles from 2 mm to 5 mm must be tested for attrition, one could use a sieve with 1 mm mesh size to remove fines).

The prepared bulk solid sample is filled into the shear cell (Fig. 4.9). The shear cell is then placed on the tester, covered with the lid, and loaded with the selected normal stress, σ , or normal force, F_N , respectively. The specimen is sheared (similar to preshear during a yield locus test) to a certain shear displacement selected by the operator. Shear displacement is the relative rotational displacement of the bottom ring and lid, measured at the mean radius of the specimen. The relative displacement follows from the shear velocity times the duration of shearing.

After shearing the specimen is sieved with the same sieve used for preparation of the specimen, or with a sieve of a smaller mesh size. The amount of fines (material finer than the mesh size of the sieve) generated during the test is a measure of the bulk material's sensitivity to attrition. It can be useful to divide the mass of the fines by the total mass of the specimen.

Alternatively to the analytical procedure described in the previous paragraph, one can measure particle size distribution before and after shearing. A comparison of both particle size distributions may give more insight into the attrition processes.

Attrition tests provide only qualitative data. Among other reasons this is because during the shear process essentially only the bulk solid in the shear zone is subjected to a kinematic load, and the exact volume of the shear zone is unknown. The thickness of the shear zone for not too fine bulk solids is on the order of magnitude of five to twenty particle diameters (see Sect. 5.2.2). However, even if attrition could be measured quantitatively and independent of the test device, this would not be a significant

advantage, because the shear deformation in silos, hoppers etc. cannot be predicted quantitatively. One reason for this is that shear deformation is concentrated in shear zones (see Sect. 14.4).

In Fig. 4.17 it is shown qualitatively how the fines content evolves during an attrition test. The larger the normal stress, σ , the quicker the fines are generated. After a sufficient shear deformation the fines content attains a nearly constant level, since at the given test conditions no further attrition is possible. This state has been reached in Fig. 4.17 for the stresses σ_B and σ_C . The larger the normal stress, σ , the larger is the fines content to be expected, because the load on the individual particles increases with the stress level. If one selects a series of stresses for attrition tests, which are large relative to the strength of the particles, it can happen that all particles are destroyed independent of the applied stress.

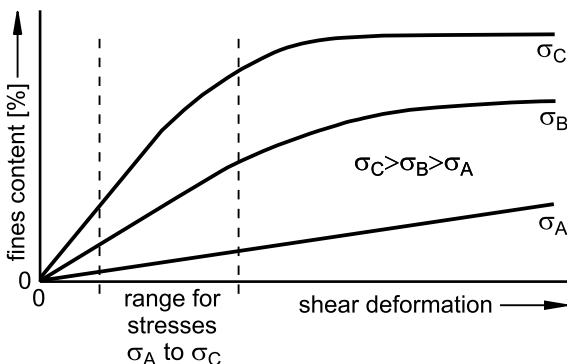


Fig. 4.17. Attrition test: fines content as a function of normal stress and shear displacement (qualitative)

Before attrition testing, preliminary tests to determine optimal shear deformation are recommended. If there is too little shear deformation, the quantity of fines generated might be too small to be precisely measured. If shear deformation is too large, all particles in the shear zone may be completely destroyed, so one cannot determine differences between various samples of a bulk solid or between different levels of the applied normal stress. During preliminary tests, therefore, several (identical) samples of a bulk solid should be subjected to different shear deformations. The results (amount of fines generated during the test) should show at least in a limited range of the applied shear deformation a measurable fines content and increased fines content with shear deformation. Such a range is indicated in Fig. 4.17. A shear deformation within this range should then be selected for the attrition tests. This ensures that a measurable amount of fines is produced and that shear deformation is not so large that all particles within

the shear zone are completely destroyed. Thus one can distinguish between the attrition sensitivity of individual samples.

4.1.6 Compressibility test

The term “compressibility” characterizes increasing bulk density with increasing consolidation stress (see example in Fig. 4.18). The more bulk density increases, the more compressible the bulk solid. For some applications it is of interest to know a characteristic value for the degree of compressibility. Other applications require knowledge of the dependence of bulk density on stress (e.g., the assessment of a silo’s mass capacity).

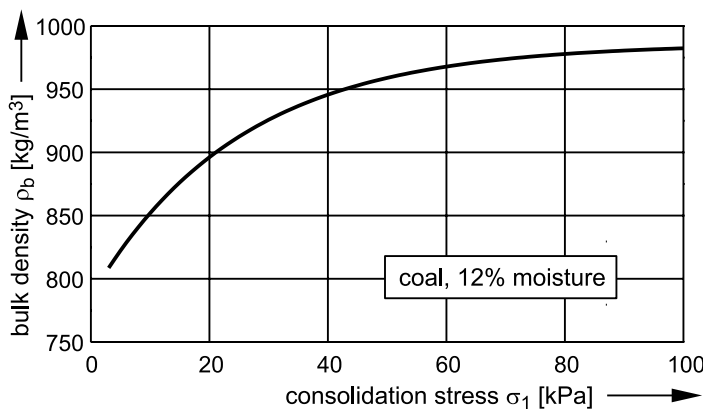


Fig. 4.18. Example: Bulk density, ρ_b , of coal with 12 % moisture as a function of the consolidation stress, σ_1 [4.38]

Compressibility can be easily measured with a setup as shown in Fig. 4.19. The bulk solid is filled loosely in a mould, scraped off flush with the top of the mould, and then subjected to a vertical force, F , through a platen of area A (Fig. 4.19). This causes a vertical stress in the bulk solid specimen which is equal to the major principal stress, σ_1 , in the axis of the specimen. From the height, h , and the mass of the specimen the bulk density is calculated. A source of error is the friction at the side walls of the mould. This friction reduces the normal stress from top to bottom (see Sect. 9.2.2) so that the bulk solid specimen is consolidated less towards the bottom of the mould. Thus for a simple test as shown in Fig. 4.19 a cylindrical mould with smooth walls and small height/diameter ratio (e.g., < 0.3) should be used. To reduce the wall friction, the walls of the mould can be lubricated (walls coated with a thin layer of lubricant, and the lubricant covered with a thin foil).

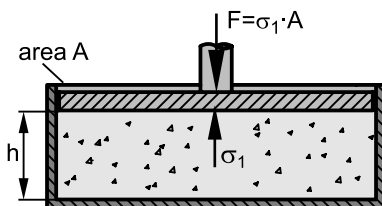


Fig. 4.19. Simple setup for a compressibility test

If a yield locus is measured, one obtains one value of bulk density, ρ_b , for one particular consolidation stress, σ_1 . Thus, the dependence of bulk density on consolidation stress can be obtained by measuring several yield loci at different consolidation stresses. The bulk density resulting from a yield locus test is typically somewhat larger than that from a compressibility test where the specimen is not sheared, but uniaxially consolidated (see Sect. 5.1.2).

For some applications it is of interest to know a characteristic value for the degree of compressibility. Compressibility can be an important parameter also for comparative tests. A single value describing compressibility can be obtained by measuring bulk density, ρ_b , at two different stress levels A and B. The consolidation stresses at these stress levels are called $\sigma_{I,A}$ and $\sigma_{I,B}$, respectively, where $\sigma_{I,A}$ is the smaller of the two consolidation stresses, $\sigma_{I,A}$ and $\sigma_{I,B}$. At both consolidation stresses the bulk density is measured, e.g., in a setup as shown in Fig. 4.19, or by measuring a yield locus at each of the two consolidation stresses.

With the bulk densities of the yield loci, ρ_A and ρ_B , the ratio ρ_B/ρ_A is determined as a characteristic value of compressibility. The larger the ratio, the larger is the increase in bulk density in the range of the consolidation stresses, $\sigma_{I,A}$ and $\sigma_{I,B}$. To ensure that the compressibility values of different bulk solid samples are comparable, it is important to use identical consolidation stresses, $\sigma_{I,A}$ and $\sigma_{I,B}$. The advantage of this procedure over the comparison of the bulk density of a loose specimen to its tap density is that here the bulk density is a result of a well-defined stress, whereby the loose density depends on how this loose state has been prepared (Sect. 6.3.7).

If the bulk density as a function of the consolidation stress is of interest, several pairs of values of bulk density and consolidation stress must be measured in the relevant stress range. The results should be indicated then in form of an equation adapted to the measuring points, which indicates bulk density as function of the consolidation stress. One finds an overview of meaningful equation types in [4.39]. A function, which can be adapted simply and usually describes bulk density in a limited stress range sufficiently well, is:

$$\rho_b = \rho_0 + a \cdot \ln\left(\frac{\sigma}{\text{Pa}}\right) \quad (4.1)$$

Here ρ_0 and a are parameters which have to be adapted. They both have the same units as the bulk density.

4.2 Selection of stresses

4.2.1 Yield locus (flowability)

4.2.1.1 Selection of stress level

Before beginning a test, the stress level, i.e., the appropriate consolidation stress, must be chosen. It is recommended that stresses similar to the stresses acting on the bulk solid in the application under consideration be selected. This can be the maximum stress in a silo, the stress in the hopper of a silo (especially for silo design for flow), the stress associated with storage of the bulk solid in IBCs or on pallets, the stresses in small containers (e.g., barrel, pail), or the stresses associated with dosage of very small masses (e.g., tabletting machine).

If similar materials must be compared on the basis of the test results, the stress level usually has no influence on the qualitative ranking of a set of products in terms of their flowability. Thus in most cases it is sufficient to adjust to the order of magnitude of the stresses of the application, because often the exact stresses acting in an application cannot be calculated and must be roughly estimated.

The measure of the stress level is the consolidation stress (major principal stress), σ_I , which depends on the geometry of the system and the flow properties. Stresses acting in a specific system can be calculated, or at least assessed, based on appropriate theories (see Chap. 9). However, for comparative tests a rough estimation of the relevant consolidation stress is usually sufficient. Some support in the assessment of stresses is given by appropriate computer programs (e.g. [4.40]).

For a very simple assessment of consolidation stress, σ_I , Table 4.1 can be used. It shows values of consolidation stress characteristic for specific applications. Since stresses in a bulk solid usually result from forces due to gravity, bulk density, ρ_b , plays an important role: The greater the bulk density, the greater the stresses (consolidation stresses) acting in the bulk solid. Furthermore, consolidation stress increases with the mass of the bulk solid in a specific application: The stresses in small containers are usually less than those in large silos. When regarding silos and hoppers it has to be

considered that flow problems usually arise in the vicinity of the outlet opening, where (especially in the discharge state) stresses are small and independent of the silo filling height or silo capacity (see Sect. 9.1.2; assessment of stresses at the outlet: Sect. 9.2.4). Thus in most cases it is not practical to measure the flow properties at the maximum stress occurring in the vertical section of the silo.

Table 4.1. Consolidation stress, σ_l , as a function of application and bulk density, ρ_b (for rough assessment of consolidation stress).

Application	Bulk density ρ_b [kg/m ³] from ... to				
	0 ... 50	150 ... 300	300 ... 600	600 ... 1200	1200 ... 2500
Containers up to 20 liters, dosage equipment	400 Pa	800 Pa	1600 Pa	2500 Pa	4 kPa
Containers up to 100 liters	800 Pa	1500 Pa	2500 Pa	5 kPa	10 kPa
IBCs, sacks packed on pa- lets, transport containers	1500 Pa	2500 Pa	5 kPa	10 kPa	20 kPa
Vertical section of silos	Stress depends on silo dimensions; for assessment of stresses see equations in Sect. 9.2.1.				
Outlet openings of silos and hoppers	Stress depends on outlet dimensions; for assessment of stresses see equations in Sect. 9.2.4.				

When selecting consolidation stress one must consider that lower limit of adjustable normal stresses depends on the type of shear tester. A lower limit for a typical Jenike-type shear tester is a consolidation stress of about 3 kPa, whereby the ring shear tester (Fig. 4.9) allows testing at smaller stresses. Thus, the numbers given in Table 4.1 have to be adjusted to the capabilities of the particular shear tester.

There is, of course, almost no application which can be characterized completely by only one consolidation stress. The stresses in a silo depend on location (hopper, cylinder). Furthermore, the stresses in a container or silo are strongly dependent on shape (e.g., height-to-diameter ratio) and other parameters (e.g., wall roughness). This section provides the user with a guide for rough assessment of the appropriate stress level for the tests.

In practice it can happen that the flow properties of a bulk solid must be determined generally, i.e., without knowing the application. Furthermore, sometimes the stresses acting in an application are not known and cannot be assessed. In such cases it is recommended that a consolidation stress ranging from 4 kPa to 8 kPa, which is the stress range for many applications, be used.

After the consolidation stress, σ_l , has been selected, the normal stresses for preshear and shear to failure have to be determined.

4.2.1.2 Normal stress at preshear and shear to failure

The relevant consolidation stress, σ_I (= major principal stress at preshear), of a yield locus can be determined only after the yield locus has been constructed; i.e., **after** the test. In contrast to normal stress at preshear, σ_{pre} , consolidation stress, σ_I , cannot be determined exactly before the test (except for the cases that a preliminary test is run, or the normal stress can be adjusted during the test as described in Sect. 4.2.1.3).

The consolidation stresses of similar bulk solids that are presheared with identical normal stresses, σ_{pre} , usually do not differ much. In addition, slightly different consolidation stresses usually affect the flowability value only slightly. Therefore, it is generally sufficient, for comparative tests, to select the same normal stress at preshear, σ_{pre} , for each bulk solid sample, and thus to accept slightly different consolidation stresses, σ_I .

The exact relationship between σ_I and σ_{pre} depends on the bulk solid and the stress level. Thus there exists no generally accepted calculation procedure by which one could compute the necessary normal stress at preshear, σ_{pre} , for obtaining exactly a desired consolidation stress, σ_I , before the test. For a rough estimate, the following equation can be used:

$$\sigma_{pre} = k \cdot \sigma_I \quad (4.2)$$

with $k = 0.3 \dots 0.7$ (usually). A fairly realistic value for a rough assessment is $k = 0.5$.

After the normal stress at preshear, σ_{pre} , is chosen, the normal stresses at shear, $\sigma_{sh,i}$, are specified. The normal stress at shear, $\sigma_{sh,i}$, should not be greater than about 80% of the normal stress at preshear, σ_{pre} . The adjustable minimum normal stress is dependent on the shear tester, e.g., with the Jenike tester the minimum stress is given by the mass of the bulk solid above the shear plane and all other parts supported by the bulk solid specimen. However, if possible, the points of incipient flow should not be located to the left of point B where the yield locus touches the Mohr stress circle defining the unconfined yield strength, σ_c (Fig. 4.20). On the other hand, the point of incipient flow with the lowest normal stress, $\sigma_{sh,i}$, should not be located at much greater normal stresses than point B, because in this case the yield locus must be extrapolated too far in the direction of lower stresses to be able to construct the Mohr stress circle for σ_c . The latter leads to an increase in uncertainty when determining the unconfined yield strength, σ_c . The range of normal stress at shear, $\sigma_{sh,i}$, arising from these considerations is indicated in Fig. 4.20.

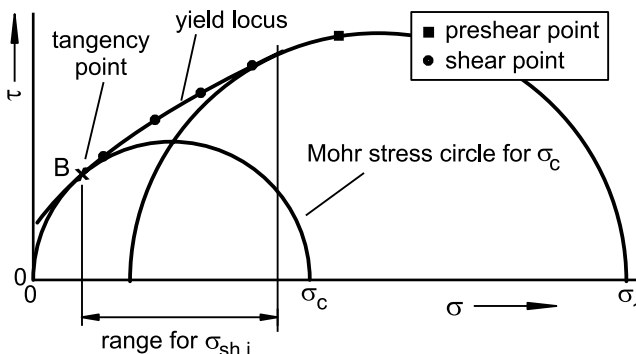


Fig. 4.20. Desired range of the normal stress for shear to failure, $\sigma_{sh,i}$

The rule that no measuring points to the left of the point where the yield locus touches the Mohr stress circle defining σ_c be used originates from the operation of the Jenike shear tester [4.8,4.13]. With the Jenike shear tester one observes a strong curvature of the yield locus towards lower shear stresses to the left of point B, i.e., at high ratios of shear stress to normal stress (Fig. 4.21). The curvature is increasingly pronounced with increasing distance from point B. One reason for this effect is that a part of all Mohr stress circles touching the yield locus to the left of point B is located to the left of the τ axis, i.e., at negative normal stresses. Thus tensile stresses are acting in the bulk solid, but bulk solids usually can transfer only small tensile stresses. Furthermore, to the left of point B the direction of the major principal stress at shear to failure is increasingly inclined to the direction of the principal stress at preshear. This is expected to lead to a further reduction of the shear stress at failure, because bulk solids show anisotropic behavior [4.26] (for more information about this see Sect. 5.3). Another reason for the curvature of the yield locus is probably the constructional conditions of the Jenike Shear Tester [4.15], where the shear lid can tilt at large ratios of shear stress to normal stress [4.15].

The exact values of the normal stresses at shear do affect the results, in particular the value of the unconfined yield strength, σ_c , somewhat [4.41]. The reason is that a yield locus is usually slightly curved [4.42,4.43], especially to the left of point B (see above). Thus by measuring only some individual points on the yield locus, which is commonly done for practical reasons, one obtains an approximation of the yield locus. If one of the shear points is located clearly left to point B and thus shifted towards the σ axis due to the curvature of the yield locus at small stresses (as depicted in Fig. 4.21), one would obtain an approximated yield locus with its left part shifted to lower shear stresses. This would lead to a smaller value of unconfined yield strength, σ_c . To avoid this, shear points to the left of point B

have to be omitted [4.13]. The better way would be to select appropriate normal stresses prior to the test.

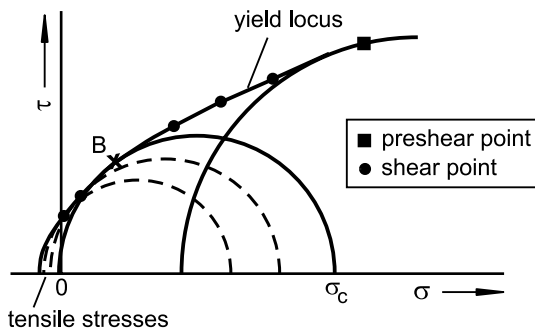


Fig. 4.21. Yield locus with shear points and corresponding Mohr stress circles to the left of point B, where the yield locus touches the Mohr stress circle defining the unconfined yield strength, σ_c .

The rules outlined above are especially important when the shear test results have to be applied quantitatively. Regarding silo design for flow according to Jenike's theory (Chap. 10), a too small value of unconfined yield strength would lead to an underestimation of the minimum outlet size to avoid flow obstructions. However, practical experience has shown that shear points to the left of the tangency point B can be tolerated as long as the curvature of the approximated yield locus is not increased significantly.

When comparative tests have to be run and it is important to identify even small differences in flow behavior, one should select **identical normal stresses at shear**, $\sigma_{sh,i}$, for all yield loci [4.44]. These stresses should cover the desired range of normal stresses at shear according to Fig. 4.20 in order to avoid extensive extrapolation of the yield locus to the left, which reduces the accuracy when determining the unconfined yield strength, σ_c . However, when running comparative tests with identical normal stress at preshear, points to the left of point B can be tolerated since they are not expected to have an influence on the ranking of the flowabilities of the tested samples.

The magnitude of the unconfined yield strength, σ_c , and the normal stress, σ , of the tangency point B, which both depend on the bulk solid's flow properties as shown in Fig. 4.22, are not known prior to a shear test. Therefore one must guess the lower limit for normal stress at shear, σ_{sh} , before beginning the test. Table 4.2 provides a guideline for choosing the lower limit.

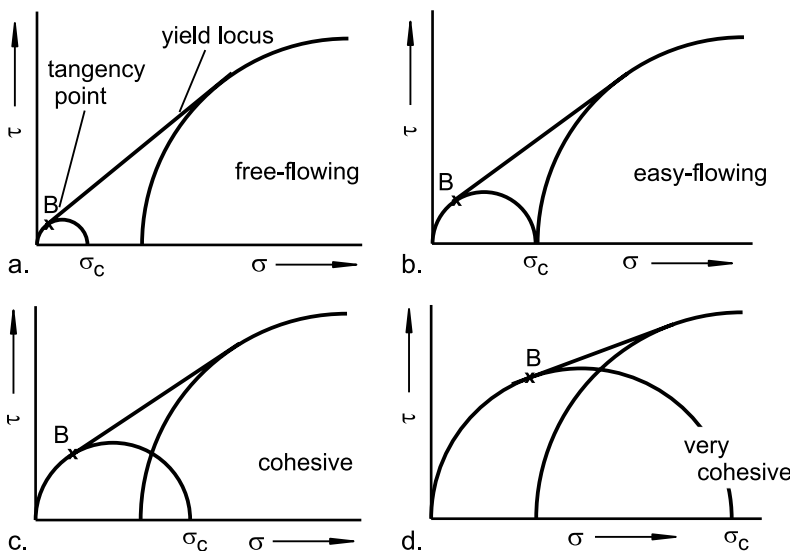


Fig. 4.22. Position of tangency point B for different values of the flowability. Point B is the point where the Mohr stress circle defining the unconfined yield strength, σ_c , touches the yield locus, for different flow behavior.

Table 4.2. Values for the assessment of the lower limit of normal stress at shear to failure. The examples are valid for a range of normal stresses at preshear from approx. 2 to 10 kPa.

Expected flow behavior	Lower limit of σ_{sh}	Examples
Free-flowing	(< 0.10) σ_{pre}	Dry sand, refined sugar, plastic pellets, salt
Easy-flowing to slightly cohesive	($0.10 \dots 0.25$) σ_{pre}	Pulverized brown coal, detergent powder
Cohesive	($0.25 \dots 0.4$) σ_{pre}	Moist coal 0 – 5 mm, flour, icing sugar
Very cohesive	(> 0.4) σ_{pre}	Moist flue gas desulfurization gypsum, zinc oxide, sewage sludge, moist clay, TiO_2

Table 4.2 shows that with free-flowing products, where the Mohr stress circle defining the unconfined yield strength is very small, the lowest normal stress at shear, σ_{sh} , can be 10% of the normal load at preshear, σ_{pre} . With more poorly flowing products a lower limit of 40% and more can be appropriate. For the case where an assessment of flow behavior is not possible, it is recommended to start with the assumption of a slightly cohesive

material and choose a minimum normal stress at shear, $\sigma_{sh,j}$, of about 20% of the normal stress at preshear, σ_{pre} .

The normal stresses for shear to failure, $\sigma_{sh,i}$, should be distributed equidistantly between the chosen minimum normal stress and around 80% of the preshear normal stress. To limit the time for testing on the one hand, and to obtain a yield locus with sufficient accuracy on the other hand, it is usually sufficient to select three different normal stresses, $\sigma_{sh,i}$, for shear to failure. This means that the lowest normal stress, $\sigma_{sh,1}$, is equal to the lower limit of the normal stresses at shear. The greatest normal stress at shear, $\sigma_{sh,3}$, is equal to the maximum value, which is 0.8 σ_{pre} . Then $\sigma_{sh,2}$ is equal to the mean value of $\sigma_{sh,1}$ and $\sigma_{sh,3}$. If more than three different normal stresses have to be used, the stresses have to be determined accordingly. In any case it makes sense to distribute the stresses equidistantly.

4.2.1.3 Automatic selection of stresses at preshear and shear

The preceding section explained the selection of normal stresses. Especially important is the selection of the normal stresses at shear to failure, which should be within the range defined in Fig. 4.20. In the present section a procedure for the ring shear tester presented in Sect. 4.1.2 is described which allows automatic determination of normal stresses at preshear and at shear to failure during a test [4.45, 4.46]. The procedure consists of two parts:

- automatic selection of normal stress at preshear based on the consolidation stress,
- automatic selection of normal stresses at shear to failure.

With automatic selection of normal stress at preshear, during the preshear process the computer program controlling the ring shear tester [4.45] assumes the probable size and position of the Mohr stress circle representing steady-state flow. Furthermore, the program assumes the position of the preshear point (i.e., the pair of values of normal stress and shear stress at steady-state flow) on this Mohr stress circle, which usually is somewhat to the left of the circle's zenith.

Fig. 4.23 shows the procedure: At the beginning of preshear, the normal stress, σ_{start} , is selected. σ_{start} is somewhat lower than the desired consolidation stress, σ_I . With increasing shear stress, the assumed Mohr stress circle increases, and so does its major principal stress, σ_I . If shear stress, τ , increases to the extent that the major principal stress might become greater than the desired consolidation stress, normal stress is reduced. The stress path (Fig. 4.23, dashed) demonstrates how shear stress and normal stress might develop during preshear. After steady-state flow is attained, the con-

trol program has adjusted the preshear normal stress, σ_{pre} , which would lead to the desired consolidation stress, σ_1 , if the assumptions regarding the position of the Mohr stress circle and the position of the preshear point are correct.

In Fig. 4.23 several Mohr stress circles which would result in steady-state flow if steady-state flow were to occur at lower shear stresses (for bulk solids with less internal friction than the bulk solid regarded here) are plotted (dotted). One can see that the higher the shear stress at preshear, the lower is the normal stress adjusted.

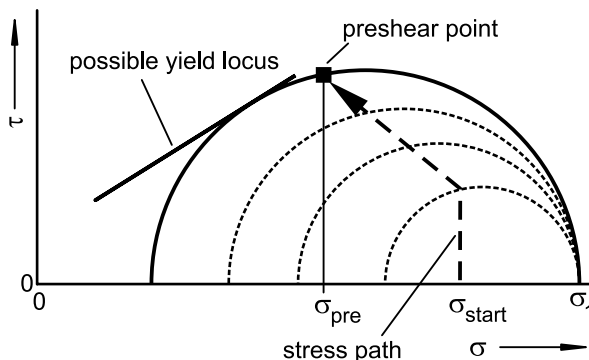


Fig. 4.23. Determination of the normal stress at preshear, σ_{pre} , during preshear

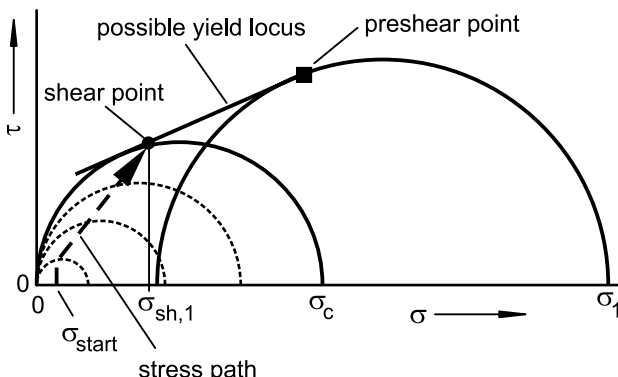


Fig. 4.24. Determination of the smallest normal stress at shear to failure, $\sigma_{sh,1}$, during shear to failure

With normal stresses at shear (incipient flow) automatically selected, the bulk solid specimen is first presheared. For measurement of the first point of incipient flow, normal stress, σ_{start} , is adjusted (Fig. 4.24) to a very low value amounting to a few percentage points of normal stress at preshear,

σ_{pre} , taking into account the minimum adjustable normal stress. During shear, the possible position of the point of incipient flow (i.e., the pair of values of shear stress and normal stress at incipient flow) relative to the Mohr stress circle defining the unconfined yield strength, σ_c , is assessed. The point of incipient flow should not be to the left of the tangency point B of the yield locus with this Mohr stress circle (see Fig. 4.20 and remarks in the preceding section). Thus, the point of incipient flow should be located on the right side of the point of tangency, but not too distant from this point in order to avoid having to extrapolate the yield locus toward much lower stresses. The latter would reduce the accuracy of the unconfined yield strength determined. To match a point fulfilling these conditions, the normal stress at shear is increased with increasing shear stress until incipient flow prevails. The stress path in Fig. 4.24 (dashed) shows how normal and shear stress develop during the test.

The normal stress at the moment of incipient flow is taken as the minimum normal stress at shear, $\sigma_{sh,I}$, of the yield locus. The other normal stresses at shear, $\sigma_{sh,i}$, are then distributed equidistantly between minimum normal stress and maximum normal stress at shear, which is set to 80% of normal stress at preshear (see preceding section).

With the procedure outlined above the yield locus can be measured alone after the desired consolidation stress (major principal stress) has been fixed. Thus the operator does not need to worry about normal stresses at preshear and shear to failure.

4.2.2 Time yield locus (flowability after time consolidation)

4.2.2.1 Selection of stress level

The choice of stress level follows the same procedure as for a yield locus test (see Sect. 4.2.1.1).

4.2.2.2 Normal stresses at preshear and shear to failure

Since a yield locus must be measured prior to the time consolidation test, the same normal stress as at preshear, σ_{pre} , is applied for the time consolidation test. After the consolidation time t , the specimen must be sheared to failure. It is recommended that a normal stress equal to one of the normal stresses, σ_{sh} , used for the measurement of the corresponding yield locus be selected for shear. For measuring the point of incipient flow the same applies as for measurement of a yield locus: The measured point of incipient flow should not be located to the left of the point where the time yield locus touches the Mohr stress circle defining the unconfined yield strength,

σ_c , but not too far removed from this point in order to avoid having to extrapolate the yield locus toward much lower stresses. Well selected shear points are shown in Fig. 4.13.

If three points of incipient flow (three different normal stresses at shear, $\sigma_{sh,1} < \sigma_{sh,2} < \sigma_{sh,3}$, see Sect. 4.2.1.2) have been determined for the yield locus, and the amount of time consolidation cannot be assessed prior to the time consolidation test, it is recommended to choose the mean normal stress at shear, $\sigma_{sh,2}$, for the time yield locus test. On the basis of the results of this preliminary time consolidation test the optimal normal stress for shear can be determined. If only a very small time consolidation effect is expected, the lowest normal stress, $\sigma_{sh,1}$, can be applied for shear. If much consolidation over time is expected, it is recommended that the highest normal stress for shear, $\sigma_{sh,3}$, or an even higher normal stress be applied. In any case several bulk solid specimens should be set up for each particular consolidation time in order to have the opportunity to vary the normal stress at shear to failure.

4.2.2.3 Automatic selection of the normal stress at shear to failure

The optimal normal stress at shear for a time consolidation test can be determined during shear in the same way as described for the yield locus test (see Sect. 4.2.1.3). The goal of the procedure is to adjust a normal stress, σ_{sh} , which is somewhat greater than the normal stress at the tangency point B, where the Mohr stress circle defining the unconfined yield strength, σ_c , touches the yield locus. At shear to failure, first a low normal stress, σ_{start} , is selected (Fig. 4.25).

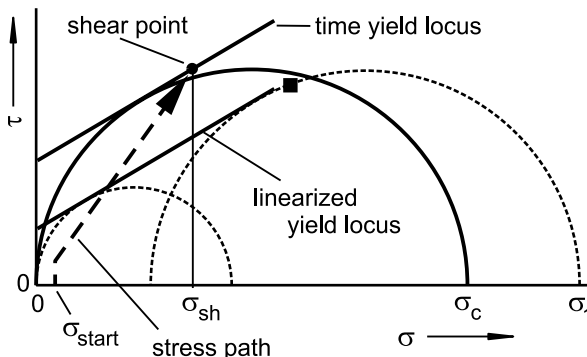


Fig. 4.25. Determination of the normal stress at shear to failure, σ_{sh} , during the measurement of a point of a time yield locus

During the shear process, the normal stress is increased as shear stress increases, until finally failure is attained. For assessment of the position of the shear point relative to the Mohr stress circle defining the unconfined yield strength, σ_c , it is assumed that the time yield locus is parallel to the linearized (instantaneous) yield locus.

4.2.3 Wall yield locus (wall friction)

4.2.3.1 Selection of wall normal stresses

Wall friction should be measured at normal stresses similar to the normal stresses acting between wall surface and bulk solid in the application under consideration. If wall friction is measured within a comparative test series where one yield locus is measured for each sample, the highest wall normal stress of the wall yield locus ($\sigma_{w,I}$ in Fig. 4.15) should be chosen equal to the consolidation stress, σ_I , of the yield locus.

Only when no yield loci, but only wall yield loci, are measured, the relevant stress level must be assessed; i.e., the maximum wall normal stress, $\sigma_{w,I}$, must be chosen. This can be done in the same way as determining the relevant consolidation stress, σ_I : First the consolidation stress, σ_I , relevant to the application under consideration is determined with the help of the tables in Sect. 4.2.1.1. Then the maximum wall normal stress, $\sigma_{w,I}$, is set equal to the consolidation stress, σ_I .

If the wall friction of a bulk solid must be determined “generally”, i.e., without knowing the application, or if the stresses acting in an application are not known and cannot be assessed, it is recommended that a maximum wall normal stress in the range from 4 kPa to 8 kPa be selected. This is the stress range pertinent to many applications.

Since wall friction angles are often dependent on wall normal stress, the wall friction angle should be measured at different wall normal stresses. It is common to measure at six wall normal stresses. After selection of the maximum wall normal stress, $\sigma_{w,I}$, as outlined above, the minimum stress, $\sigma_{w,6}$, is set to about 5% to 10 % of the maximum wall normal stress, $\sigma_{w,I}$, whereby the range of adjustable stresses of the shear testers has to be taken into account. In [4.13] it is recommended to ignore the result of the first test point measured at the maximum wall normal stress, $\sigma_{w,I}$.

4.3 Application-related measurement of flow properties

4.3.1 Comparative tests

With comparative tests, the quality of a product, for example, can be checked regularly, or products can be optimized in terms of their flowability. Depending on the application, different types of measurement can be useful:

- Flowability, ff_c , resulting from a yield locus test quantifies instantaneous flow behavior, i.e., the behavior of a bulk solid that has not been stored at rest for a longer time.
- Flowability, ff_c , resulting from a time consolidation test (caking test) quantifies flow behavior of a bulk solid after long-term storage at rest. With such a test the influence of conditions during storage (air humidity, temperature) also can be studied, if the bulk solid specimen is placed in a time consolidation bench and stored under defined ambient conditions (e.g., in a climate chamber).
- The wall friction angle, φ_x , quantifies the effort required to move a bulk solid across the surface of a specific wall material. Wall friction is not often measured for comparative studies, but a wall friction test can provide important answers, for example, whether or not a bulk solid will flow across the wall of a hopper or a chute.

When selecting the normal stresses the guidelines given in Sect. 4.2 should be considered.

4.3.2 Silo design for flow

In addition to determining flowability as part of comparative tests, surely silo design for flow pursuant to Jenike's theory [4.8] (see Chap. 10) is the most frequent application of shear testers. For this the flow properties of the bulk solid based on consolidation stress, σ_l , must be known. These data are determined by measuring several yield loci in the relevant stress range.

It is usual to measure three or four yield loci at different consolidation stresses for silo design for flow [4.8,4.13]. Consolidation stresses must be chosen so that stresses acting in the lower part of a hopper are covered. These stresses are proportional to bulk density, ρ_b . In Table 4.3 suitable values of consolidation stress σ_l of the yield locus with the lowest consolidation stress are presented. The consolidation stress of this yield locus is known as $\sigma_{l,min}$. The values in Table 4.3 correspond to recommendations for the Jenike shear tester [4.13].

Table 4.3. Consolidation stress, $\sigma_{I,min}$, of the yield locus with the smallest consolidation stress [4.13]

Bulk density ρ_b [kg/m ³] from... to	< 300	300 ... 800	800 ... 1600	1600 ... 2400	> 2400
Smallest consolidation stress $\sigma_{I,min}$ [kPa] (approximately)	1.5	2.0	2.5	3.0	4.0

The consolidation stresses, σ_I , of the other two or three yield loci should be two, four, or eight times as high as the minimum consolidation stress, $\sigma_{I,min}$, listed in Table 4.3. If a bulk solid flows relatively easily, measurement of the fourth yield locus is usually not necessary. For poorly flowing bulk solids the first yield locus is often not required. This follows from the procedure for silo design for flow according to Jenike [4.8] (Chap. 10).

If measurement of time consolidation is also necessary, time yield loci corresponding to individual yield loci must be determined. Consolidation times must be chosen based on the problem under consideration.

Wall friction, which is very important for silo design, is measured according to Sect. 4.1.4. The highest wall normal stress should be approximately equal to the consolidation stress of the yield locus with the second lowest consolidation stress [4.13].

5 A more detailed look at properties of bulk solids

Some derivations and statements in the preceding sections are based on assumptions and simplifications on the bulk solids properties. This is usually not a disadvantage regarding the practical determination of flow properties with shear testers, but sometimes for the description of the behavior of a bulk solid in a specific apparatus or testing device a deeper insight into the processes within the bulk solid is desired. Unfortunately, for this general theories are still not available. Therefore in the following the behavior of bulk solids is discussed on the basis of experimental findings from research in bulk solids technology and simplified models.

5.1 Anisotropy and influence of deformation on stresses

The properties of a bulk solid in a specific situation are strongly dependent on the preceding deformation (e.g. uniaxial compression or steady-state flow) and the corresponding stresses. Even the deformation velocity, i.e., strain rate, plays a role [5.1], but this can often be neglected with regard to the small velocities usually occurring during bulk solids flow.

The influence of deformation can only be studied with a test apparatus allowing controlled deformation of a bulk solid specimen, e.g. a biaxial tester. In the biaxial tester shown in Fig. 5.1 [5.2,5.3] a rectangular bulk solid specimen is confined by rigid walls in all three dimensions. The walls in x and y directions can be moved forward and backward independent of each other. Thus the specimen can be deformed in x and y directions, while the distance between the confining walls in z direction is constant. The surfaces of the confining walls are lubricated and then covered with a thin rubber membrane. Thus the shear stresses acting on the confining walls can be neglected, and the normal stresses can be regarded as principal stresses. For the measurement of stresses in x , y and z directions the walls are provided with stress measuring cells (not drawn in Fig. 5.1). In another type of biaxial tester (flexible wall biaxial tester [5.4–5.6]) the bulk solid specimen is confined by rubber membranes instead of rigid walls. Here the

stress on the bulk solid is adjusted through a gas pressure acting on the rear side of the membranes. In order to keep the membranes plane, the deformation of the membranes is detected with contacts. If a deformation is detected, the gas pressure at the rear side of the membrane is regulated appropriately. An overview on different devices is given in [5.7].

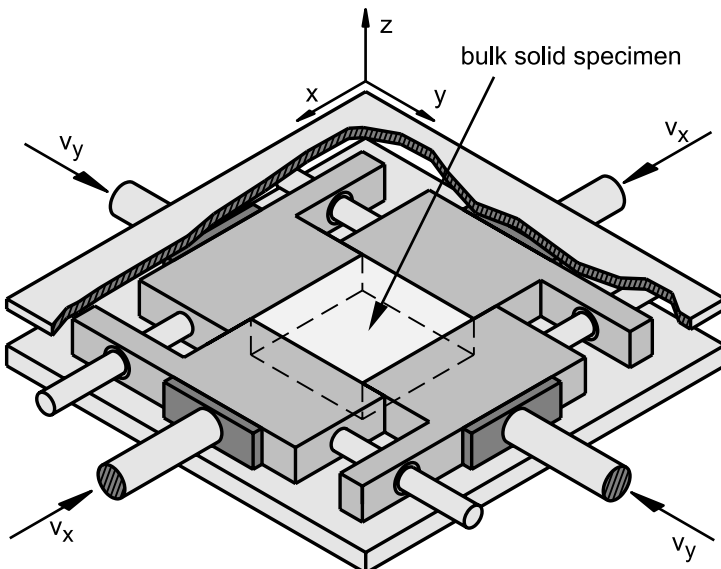


Fig. 5.1. Biaxial tester [5.3]

Some basic methods to deform a bulk solid specimen in a biaxial tester are depicted in Fig. 5.2. All start with a specimen having the same dimensions in x and y direction after filling. Uniaxial compression in x direction (procedure I) or in y direction (procedure III) can be studied. Procedure II represents identical compression in x and y directions. Procedure IV is characterized by isochoric deformation (constant volume) of the specimen, which is realized by forward movement of the walls in x direction and retraction of the walls in y direction. When flowing at constant volume, in the ideal case constant stresses are developing. This is called steady-state flow.

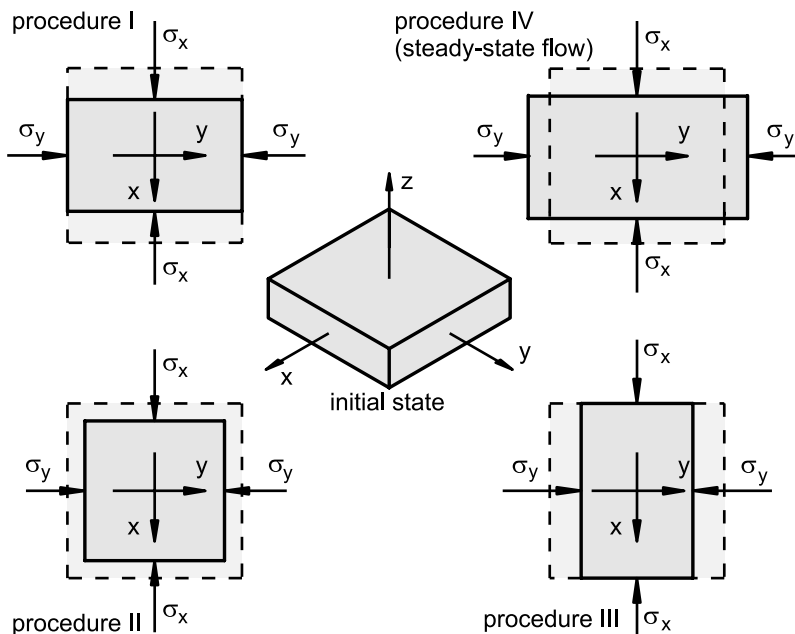


Fig. 5.2. Examples of deformation procedures of a biaxial tester [5.2,5.3]; the dashed lines show the shape of the bulk solid specimen before deformation.

5.1.1 Stresses

The influence of deformation on stresses will be outlined by regarding two examples of tests conducted with a biaxial tester [5.8]. Only the stresses in x and y directions (σ_x and σ_y), which are principal stresses in the biaxial tester, will be considered. The stress acting in z direction (σ_z) is also a principal stress, but it will not be taken into account here since it lies in most cases between the principal stresses acting in x and y directions and thus only plays a minor role (a survey on the principal stress in z direction at different types of deformation can be found in [5.5]). Thus, depending on the stress path, either σ_x or σ_y is identical to the major principal stress.

In the quadruple diagram in Fig. 5.3 stresses and strains measured during deformation of a bulk solid specimen are plotted. The four differently named axes of the quadruple diagram, which in fact consists of four diagrams, represent strain, ϵ , and normal stress, σ , in both x and y directions. The course of the strains in quadrant III is called the strain path, the course of the stresses in quadrant I is called the stress path .

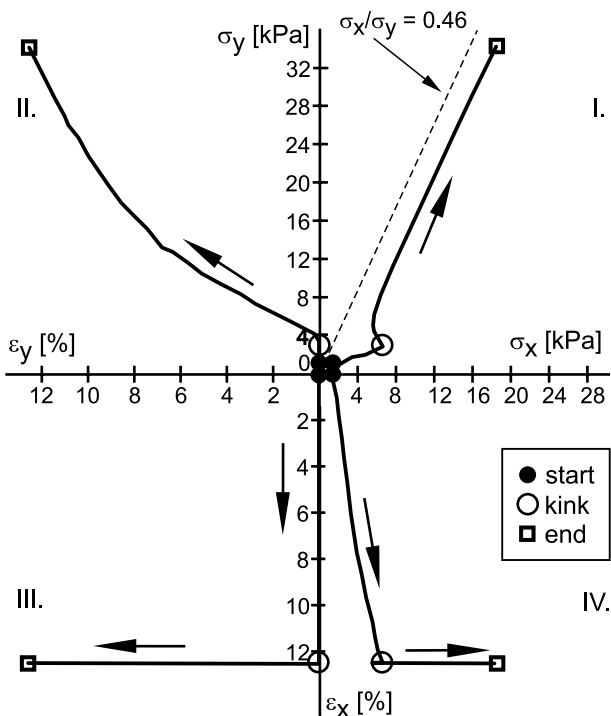


Fig. 5.3. Strains and stresses in a bulk solid specimen (limestone powder) during deformation in x and y directions plotted in a quadruple diagram. Applied strain path: First, uniaxial compression in x direction according to procedure I in Fig. 5.2, then uniaxial compression in y direction according to procedure III (compressive stresses and compressive strains are positive; arrows indicate direction of the stress path; constant strain rate 0.1 %/min; Roman numerals are used for numbering the quadrants) [5.8].

According to the stress path in Fig. 5.3, the bulk solid specimen (limestone powder) was deformed in two steps starting from its initial state (small stresses, $\sigma_x = \sigma_y = \text{approx. } 1.3 \text{ kPa}$): First the specimen was compressed in x direction, then in y direction. The applied strains, ε_x and ε_y , are plotted in quadrant III. The deformation can be characterized as uniaxial compression in x direction according to procedure I in Fig. 5.2 followed by uniaxial compression in y direction according to procedure III.

During compression in x direction the stresses σ_x and σ_y are proportional with σ_x being the major principal stress, σ_1 . The ratio σ_y/σ_x corresponds to the stress ratio, K , which prevails during uniaxial compression of a loose, uncompacted bulk solid and is a material parameter (see Sect. 2.3). The ratio σ_y/σ_x amounts to about 0.44 (value taken from data in [5.8]) shortly before the deformation direction is changed, i.e. close to the kink in the

stress path. After the kink the specimen is compressed in y direction only. This leads, after a short transition phase, to σ_y being the major principal stress, σ_I . Furthermore, again a nearly linear relationship between stresses σ_y and σ_x prevails, but no proportionality. The ratio of the minor to the major principal stress, σ_x/σ_y , decreases and amounts to about 0.54 at the end of the test. In other tests not reported here, where the same bulk solid was compressed uniaxially without changing the strain direction, at the same stress level a ratio of the minor to the major principal stress of about 0.46 was attained. One can see that in the test shown in Fig. 5.3 the stress path is parallel to the line $\sigma_x/\sigma_y = 0.46$ (broken line in Fig. 5.3), i.e., with increasing stresses the stress ratio asymptotically approaches this value [5.8–5.11].

Based on the test discussed above some qualitative statements regarding the behavior of bulk solids can be derived:

- Uniaxial consolidation of an initially loose and uncompacted bulk solid leads to a nearly constant ratio of the minor to the major principal stress. This is the known stress ratio, K , as described in Sect. 2.3.
- The ratio of the principal stresses is dependent on the previous deformation (the deformation history), i.e., the bulk solid is provided with a kind of memory. If a bulk solid specimen is compressed uniaxially, after having been compressed previously in a different direction, one will observe an initially strong, then smoother change of the ratio of the minor to the major principal stress (see Fig. 5.3, stress path after the kink in quadrant I). Thus a certain amount of deformation is required to change the stress ratio completely.

A second test is shown in Fig. 5.4. As in the first test the bulk solid specimen is first compressed uniaxially in x direction (according to procedure I in Fig. 5.2). After the kink in the deformation path the specimen is compressed in y direction, but simultaneously dilated in the x direction to the same extent (ε_x decreases, ε_y increases). Thus the specimen is subjected to isochoric deformation (deformation with constant volume as in steady-state flow) corresponding to procedure IV in Fig. 5.2. In quadrant IV of the quadruple diagram in Fig. 5.4 one can recognize that immediately after the kink the stress in x direction decreases sharply with decreasing strain, ε_x , and finally attains a constant value. The ratio of the minor to the major principal stress, σ_x/σ_y , amounts to about 0.09 at the end of the test. Similar values of the stress ratio have been found in other tests, where different strain histories were followed by isochoric deformation [5.8]. From this it can be concluded that the stresses prevailing at isochoric deformation (like steady-state flow) are less dependent on a bulk solid's history than stresses prevailing during uniaxial compression.

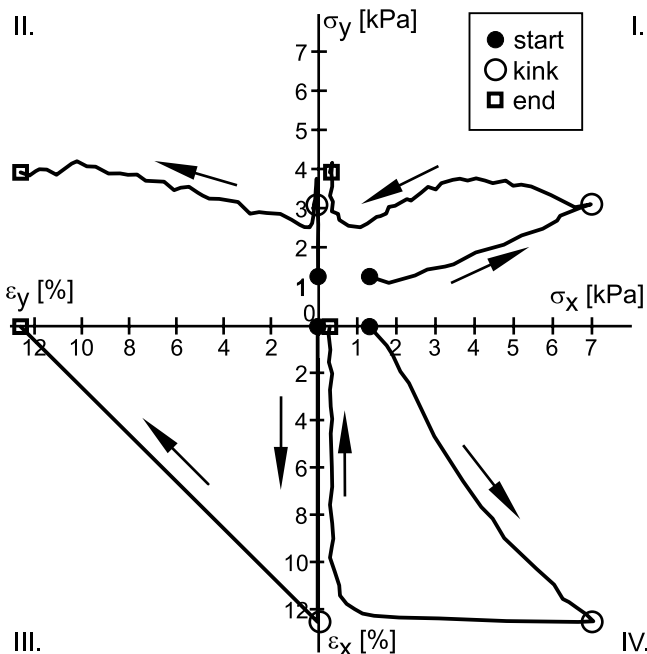


Fig. 5.4. Strains and stresses in a bulk solid specimen (limestone powder) during deformation in x and y directions plotted in a quadruple diagram. Applied strain path: First uniaxial compression in x direction, then isochoric deformation by compression in y direction and simultaneous dilation in x direction (compressive stresses and compressive strains are positive; arrows indicate direction of the stress path; constant strain rate 0.1 %/min) [5.8].

Different ratios of the minor to the major principal stress at different deformations are found more or less pronounced for every bulk solid. It is important in many applications, e.g. calculation of stresses acting in a hopper and the vertical section of a silo, to distinguish between the procedures “uniaxial compression” (corresponding to the stress state in the vertical section of a silo, see Chap. 9) and “steady-state flow” (nearly fulfilled when bulk solid flows in a mass flow hopper). The difference between the stress ratios of these procedures is demonstrated qualitatively in Fig. 5.5 by the corresponding Mohr stress circles. If in both procedures the major principal stresses, σ_1 , are the same (as in Fig. 5.5), the Mohr stress circle representing uniaxial compression is always located within the Mohr stress circle being touched by the effective yield locus and representing isochoric deformation or steady-state flow, respectively (see Sect. 3.2.3.3). The ratio of the minor to the major principal stress, σ_2/σ_1 , at uniaxial compression

(σ_{2B}/σ_1 in Fig. 5.5), i.e. the stress ratio K_0 , is therefore always greater than the ratio σ_2/σ_1 at steady-state flow (σ_{2A}/σ_1 in Fig. 5.5).

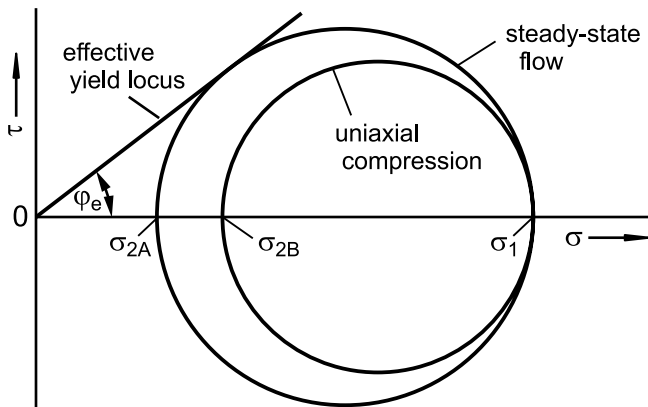


Fig. 5.5. Mohr stress circles representing uniaxial compression and steady-state flow in the x,y plane (qualitatively)

The common assumption that the powder is a continuum makes understanding of the reasons for the behavior discussed above more difficult. However, if the interactions of individual particles are considered, at least a simple qualitative model can be derived which helps one to understand a bulk solid's behavior when being deformed. The forces acting between individual particles of a bulk solid have been investigated experimentally (elasto-optic measurement of stresses [5.12,5.13]) as well as theoretically. The most common method for theoretical considerations is the discrete element method (DEM, e.g. [5.14–5.17]). With these means one can “look” into the bulk solid and investigate magnitude and direction of inter-particle forces. In the following a simplified interpretation of the bulk solid behavior shown in Figs. 5.3 and 5.4 will be presented based on particle interactions (Fig. 5.6).

If a bulk solid is subjected to a stress and/or deformed, the load acting on the bulk solid is transferred through individual particle contacts by normal and shear forces. If the bulk solid is considered as a continuum, it is assumed that the number of contacts in a volume element is large so the processes at individual contacts do not play a role. This leads to the assumption of a stress being homogeneously distributed across the area over which it is acting. But in reality particles in a bulk solid are distributed randomly, so in the direction of the applied stress some particles are close to each other, and others are more distant from each other. A possible initial situation of a loose bulk solid composed of spherical particles is shown

in Fig. 5.6.a. In reality the particles are distributed three-dimensionally, but for reasons of simplification this is reduced to a two-dimensional cutting plane as shown in Fig. 5.6. The distances between particles result from the actions of (not shown) particles behind and in front of the drawn cutting area. Especially with very fine-grained and/or moist bulk solids, where adhesive forces play an important role, stable structures with much larger voids than in Fig. 5.6 can exist.

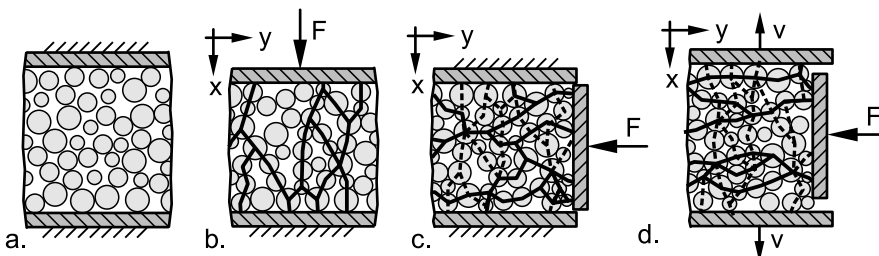


Fig. 5.6. Transmission of stresses in a bulk solid at different steps of deformation (simplified model); bold lines represent possible force chains; dashed lines represent force chains which were created by previous deformation. F : force in direction of compression; v : velocity of the side walls when retracted; a. loose bulk solid (initial state); b. uniaxial compression in x direction; c. uniaxial compression in y direction after previous compression in x direction; d. isochoric deformation with compression in y direction and dilation in x direction (after previous compression in x direction).

In Fig. 5.6.b the bulk solid specimen is uniaxially compressed in the x direction. This corresponds to the first deformation step in Fig. 5.3 (before the kink). Due to compression the particles approach each other, and this effect is more pronounced in the x direction (direction of deformation) than in the y direction. The force, F , or stress, σ_x , respectively, required to deform the bulk solid, can only be transferred from particle to particle through particle contacts. Lines connecting these contacts are called force chains or stress chains. Due to deformation in x direction, the force chains in Fig. 5.6.b are mainly oriented in the x direction, but have also components in y direction, which are responsible for the stress σ_y acting perpendicular to the direction of compression (see stress σ_x and smaller stress σ_y in Fig. 5.3, before the kink). The distribution of normal vectors at all particle contacts shows the highest values in directions around the direction of the major principal stress [5.12] so that the particles orient like columns [5.18]. In addition, if the bulk solid contains non-spherical particles (e.g. flat particles), it is to be expected that these particles will exhibit a preferred orientation after compression.

During the second step of deformation in Fig. 5.3 (uniaxial compression in y direction after previous compression in x direction) a ratio of the minor to the major principal stress develops which is different from that obtained in the first deformation step (first step: uniaxial compression of the loose, uncompacted bulk solid specimen in x direction). The second deformation step is represented in Fig. 5.6.c. Since the bulk solid is compressed in the y direction, new force chains are formed primarily in the y direction. Since the particle pattern is influenced by the previous compression in x direction (see dashed lines connecting particles along former force chains, Fig. 5.6.c), the number of particle contacts perpendicular to the direction of compression is greater than in Fig. 5.6.b where an initially loose bulk solid specimen is compressed. Thus in Fig. 5.6.c there are more stress chains with components perpendicular to the compression direction than in Fig. 5.6.b. With additional second deformation step the particles are increasingly displaced. Thus the influence of the first deformation step decreases, and the ratio of the minor to the major principal stress approaches the value which was also attained when compressing an initially loose bulk solid specimen (i.e., the first deformation step). Exactly this can be observed in Fig. 5.3.

A different result is obtained if the bulk solid specimen is in the first step compressed uniaxially in x direction, but in the second step subjected to isochoric deformation, i.e. compression in y direction and dilation in x direction, according to Fig. 5.4. Because of the dilation perpendicular to the compression direction, in the second step stress chains in x direction (resulting from the first deformation step) are cut due to particle distances increasing in x direction (Fig. 5.6.d), but at the same time the creation of new particle contacts in compression direction (y direction) is supported. Therefore the structure resulting from the first deformation step diminishes quicker than during the second step of the test of Fig. 5.3, i.e., the specimen “forgets” its history more quickly. This is demonstrated in Fig. 5.4 by the quick change of stresses after the kink where isochoric flow begins. Furthermore, after sufficient deformation isochoric flow leads to a more pronounced concentration of the force chains in deformation direction which goes along with a ratio of the minor to the major principal stress (here: σ_x/σ_y) being much smaller than the principal stress ratio attained after uniaxial compression.

Flow at constant volume and constant stresses as attained at the end of the test shown in Fig. 5.4 is called steady-state flow. When measuring a yield locus, the bulk solid specimen is consolidated in a defined way by shearing until steady-state flow is attained (preshear, see Chap. 3). The considerations in the previous paragraph show that this makes sense: During shear until steady-state flow (isochoric deformation) structures result-

ing from previous deformations (the history, e.g. the filling process at the preparation of a shear test) diminish or at least become less influential. Furthermore stress chains oriented in the major principal stress direction develop in the bulk solid.

Since deformation results in the formation of stress chains, a bulk solid gains anisotropic properties through anisotropic deformation (deformation varies with direction, e.g. uniaxial compression). After uniaxial compression, stiffness and compressive strength of a bulk solid specimen are greater in compression direction than perpendicular to this direction, because it has been subjected to a higher normal stress (namely the major principal stress) in direction of compression. The more different the strain and stress, respectively, in different directions, the more pronounced is the anisotropy after deformation. Thus steady-state flow (isochoric deformation) leads to a more anisotropic specimen than uniaxial compression [5.5]. If the bulk solid is composed of non-spherical particles it is likely that during the deformation the particles orientate primarily in a specific direction. This effect increases the anisotropic properties further [5.18]. Anisotropy resulting from deformation is called induced anisotropy [5.13,5.19].

Isotropic deformation can be realized by uniform compression of a bulk solid specimen in all directions, i.e., in x , y , and z directions. This would not be possible with the biaxial tester shown in Fig. 5.1, since it does not allow deformation in the z direction. For isotropic deformation a triaxial tester with cubical specimen [5.20,5.21] or cylindrical specimen [5.22–5.24] is required. Assuming that a bulk solid specimen is isotropic prior to deformation (i.e., no primary orientation of stress chains or particles), during isotropic deformation the same normal stress is acting in all directions and, thus, the three Mohr stress circles representing stresses in the three planes perpendicular to the x , y , and z directions (see Fig. 2.5) would be points (radius = 0). An orientation of the stress chains would not be expected.

It has to be mentioned that it is impossible to prepare an isotropic bulk solid specimen, because just by filling of a container or a test apparatus the particles are arranged in a specific way due to the force of gravity and geometrical conditions; non-spherical particles may have a specific orientation after filling [5.18,5.19]. This effect is demonstrated by tests on a device called a “Lambdameter” (Fig. 5.7) [5.25,5.26]. The Lambdameter allows one to determine the stress ratio, K , used for the representation of the ratio of horizontal stress to vertical stress in the vertical section of a silo (see Sects. 2.3 and 9.1.1; in some countries instead of K the Greek letter λ is used as the symbol for the stress ratio). In the Lambdameter the cylindrical bulk solid specimen is covered with a lid and loaded vertically by a vertical force, F . This results in the vertical stress, σ_v , acting in the

bulk solid specimen. The horizontal stress, σ_h , is measured by means of strain gauges fixed to the side walls of the measuring ring (for more details refer to [5.25,5.26]).

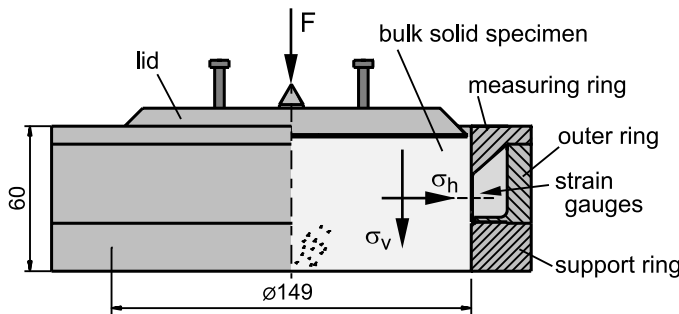


Fig. 5.7. Setup of the Lambdameter [5.25,5.26] (dimensions in mm)

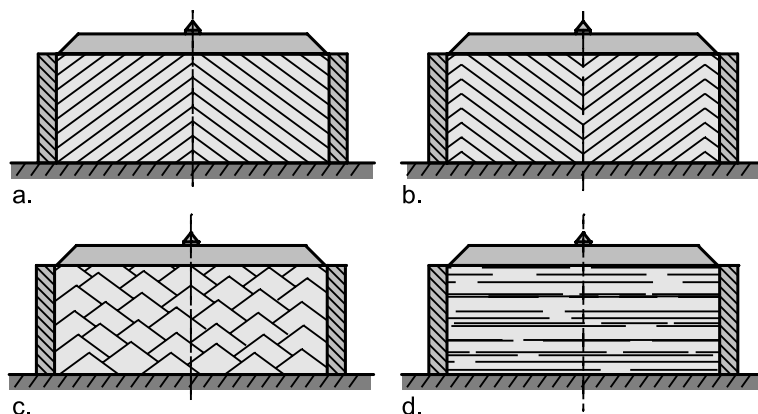


Fig. 5.8. Lambdameter after filling following different filling procedures: The lines in the bulk solid represent the shape of the bulk solid surface during filling [5.26]. a. centered filling; b. peripheral filling; c. filling in small portions; d. uniform filling with a sieve (horizontal surface)

For the tests the Lambdameter was filled with a bulk solid following different procedures:

- Centered filling through a funnel led to a growing conical pile with the bulk solid sliding downwards on the surface of the pile (Fig. 5.8.a).
- Peripheral filling created an annular pile (Fig. 5.8.b).
- Filling in small portions led to several small conical piles (Fig. 5.8.c).
- Filling through a sieve resulted in an always horizontal surface (Fig. 5.8.d).

Depending on the filling procedure the shape of the bulk solid surface during filling was different as indicated by the lines within the bulk solid specimen in Fig. 5.8. After filling excess material was scraped off flush with the top of the measuring ring, the lid placed on the bulk solid specimen and loaded with the vertical force, F . The ratios of horizontal to vertical stress measured for different bulk solids depend on the filling procedure (Table 5.1). With the coarse products (glass spheres, granular limestone) the smallest stress ratios, K , were obtained by filling through a sieve, and peripheral filling led to the largest values. Clearly the filling procedure influences the structure of the bulk solid and, thus, the primary orientation of the stress chains. An important parameter is the shape of the bulk solid's surface (Fig. 5.8) on which particles slide downwards during filling. This creates a certain structure in the bulk solid which results in different horizontal stresses being measured. This effect can be found even with the glass spheres where a specific orientation of individual particles can be excluded (e.g. orientation of the longitudinal particle axes parallel to the surface of the bulk solid filling). It is worth mentioning that with the cohesive limestone powder only a weak dependence of stress ratio on filling procedure was found. The probable reason for this is that after filling the cohesive limestone powder contains relatively large voids (high porosity) due to the influence of the interparticle forces. Thus, when the vertical stress is increased, the bulk density changes rapidly, especially compared to the two other products, and the particles have the ability to rearrange and to form new stress chains. Therefore the history "filling" has less influence.

Table 5.1. Ratios of horizontal to vertical stress at uniaxial compression measured with the Lambdameter (Fig. 5.7) for different filling procedures (Fig. 5.8); applied vertical stress $\sigma_v = 35$ kPa [5.26]

Filling procedure	Measured ratio σ_h/σ_v		
	Glass beads (1 mm)	Granular limestone (0.1 mm to 0.5 mm)	Limestone powder ($x_{50} = 4.7 \mu\text{m}$)
Centered (Fig. 5.8.a)	0.555	0.379	0.457
Peripheral (Fig. 5.8.b)	0.590	0.407	0.486
Portions (Fig. 5.8.c)	0.573	0.345	0.477
Uniform (Fig. 5.8.d)	0.460	0.301	0.470

From the dependence of the stress ratio on the filling procedure (Table 5.1) it can be concluded that a loose uncompacted bulk solid specimen can exhibit anisotropic behavior induced by the filling process. This anisotropy has an influence on the stresses at subsequent deformation (e.g. compres-

sion). The anisotropy, which is already existent before the specimen is deformed, is called inherent anisotropy [5.13,5.19].

5.1.2 Bulk density

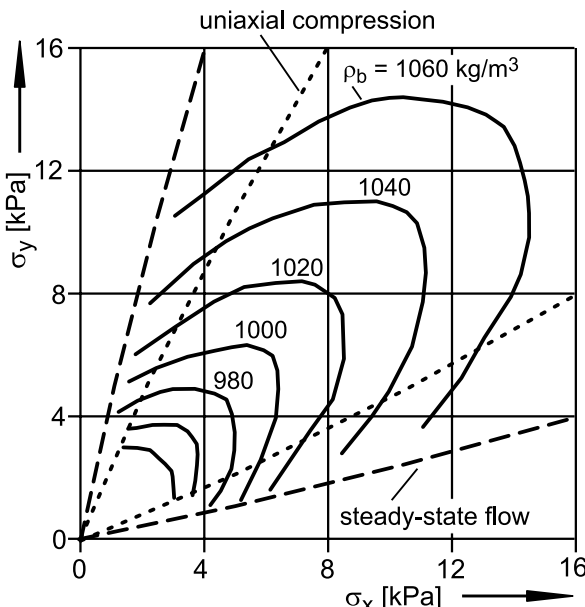


Fig. 5.9. Bulk density, ρ_b , as a function of the maximum principal stresses applied in x and y directions during compaction [5.5,5.6]. The dotted curves representing uniaxial compression have been added by the author (according to results of uniaxial compression tests in [5.5]).

The bulk density obtained after compression of a bulk solid specimen depends not only on the major principal stress, σ_I , but also on the compression procedure (e.g. uniaxial, isotropic) and the other principal stresses. Figure 5.9 shows results obtained with a flexible wall biaxial tester (see Sect. 5.1) where a rectangular bulk solid specimen can be deformed in x and y directions as with the biaxial tester in Fig. 5.1, but in contrast to Fig. 5.1, the walls of the flexible wall biaxial tester are formed from rubber membranes [5.5,5.6]. The axes of the diagram (Fig. 5.9) represent the stresses, σ_x and σ_y , acting in x and y directions. σ_x and σ_y are principal stresses. The stress in z direction is not considered here. The ratios of the principal stresses (σ_x/σ_y) obtained at steady-state flow (isochoric deformation) are plotted as dashed curves. These curves are limiting the range of

possible principal stress ratios at the end of compaction. Within this range curves for constant bulk density, ρ_b , are plotted.

It is obvious that uniform compression in x and y directions ($\sigma_x = \sigma_y$) requires clearly larger stresses to obtain a certain bulk density than uniaxial compression (dotted curves) or even compression with subsequent steady-state flow (dashed curves). Based on the simple particle model described in the previous section, the result can be interpreted as follows: The larger the difference between the principal stresses in x and y directions (and between the corresponding strains, respectively), the better the particles can move and thus rearrange to a denser packing, especially when the specimen can dilate in one direction such as at isochoric deformation. The latter has been demonstrated by the development of stress chains (Fig. 5.6). Thus it is to be expected that the higher the difference of stresses (and strains) in x and y directions (i.e. the higher the degree of anisotropy at compaction), the higher the resulting bulk density.

5.1.3 Unconfined yield strength (compressive strength)

Since particle arrangement depends on the deformation procedure during compaction (see previous section), it is to be expected that also the strength, which is based on the adhesive forces acting between particles, depends on the deformation procedure and, thus, may be anisotropic as a result of anisotropic deformation. This has been investigated experimentally by several authors [5.2,5.3,5.5,5.6,5.22,5.27–5.30]. Here results of Saraber et al. [5.30] and Harder [5.2,5.3] will be presented.

Saraber et al. [5.30] investigated the dependence of unconfined yield strength on the direction of stress application with a Jenike shear tester similar to earlier investigations of Molerus [5.27]. This was accomplished by rotating the direction of shear relative to the direction of preshear by an angle α . In Fig. 5.10 this is demonstrated for the angle $\alpha = 180^\circ$. In the diagram in Fig. 5.11 the values of unconfined yield strength, σ_c , resulting from yield loci measured for different angles α are plotted. Above angles α of about 30° the unconfined yield strength decreases strongly due to the reduction of the maximum shear stresses at shear to failure. With the simplified assumption that the major principal stress at preshear as well as at shear to failure is inclined by about 45° to vertical (this assumption is explained in Sects. 5.2.1 and 5.3.1), the angle β between the directions of the major principal stress at preshear and shear to failure can be assessed roughly as a function of α [5.31]. The plot of unconfined yield strength as a function of angle β (Fig. 5.11) shows that, up to an angle β of about 25° , no significant decrease of shear stresses at failure (τ_{sh}) and thus unconfined

yield strength is to be expected. If β exceeds 25° , unconfined yield strength decreases strongly until about $\beta = 60^\circ$. For angles β greater than about 60° no further reduction of unconfined yield strength can be observed.

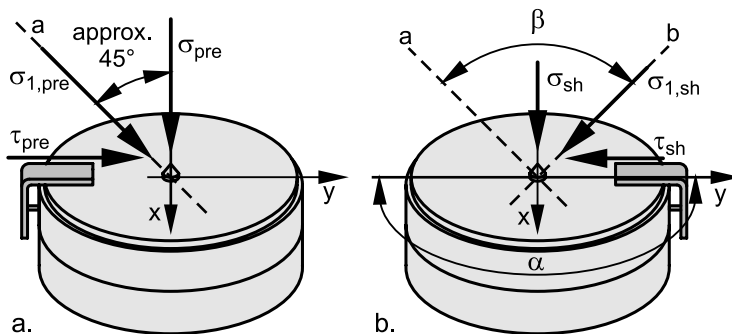


Fig. 5.10. Preshear (a) and shear to failure (b) with a Jenike shear cell. For shear to failure the lid of the shear cell and thus the shear direction was rotated by the angle α relative to the shear direction at preshear (Fig. b: $\alpha = 180^\circ$). β is the assumed angle between the directions of the major principal stresses, $\sigma_{1,pre}$ und $\sigma_{1,sh}$, at preshear and shear to failure. The shear stresses, τ_{pre} and τ_{sh} , indicate the direction of shear at preshear and shear to failure.

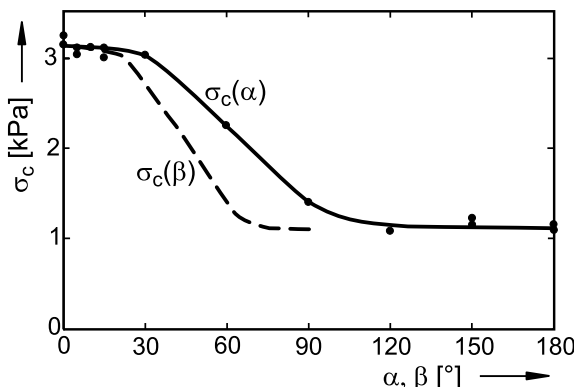


Fig. 5.11. Unconfined yield strength, σ_c , as a function of angles α (angle between the directions of shear) [5.30] and β (assumed angle between the major principal stresses at preshear and shear to failure) [5.31] (bulk solid: limestone powder).

Harder [5.3] investigated the influence of consolidation procedure on unconfined yield strength with the biaxial tester shown in Fig. 5.1. Starting from bulk solid specimens of both identical dimensions and identical bulk density (Fig. 5.2, initial state), the specimen was compacted (consolidated) following four different procedures in order to obtain the same final vol-

ume and same final bulk density, respectively. Procedure I represents uniaxial compression in x direction, procedure II uniform compression in x and y directions, and procedure III uniaxial compression in y direction. With procedure IV steady-state flow is attained at the end of consolidation when the specimen is compressed in x direction and simultaneously allowed to dilate in y direction. The major principal stress, σ_1 , acting at the end of the consolidation process is equal to σ_x for procedures I and IV, σ_x and σ_y for procedure II, and σ_y for procedure III.

After consolidation the specimen is unloaded. To measure a Mohr stress circle representing incipient flow (failure), the stress in y direction is adjusted to the desired value of the minor principal stress and kept constant. Then the confining walls in x direction are driven forward until the stress in x direction, σ_x , passes a maximum. The maximum stress, σ_x , and the stress in y direction, σ_y , measured at the same time are the minor (σ_y) and major principal stress (σ_x) of a Mohr stress circle representing incipient flow. Repeating the test several times with identical consolidation procedure, but different minor principal stress (σ_y) at incipient flow, one obtains a couple of Mohr stress circles for incipient flow. The common tangent to these circles is the yield locus. Knowing the yield locus, the unconfined yield strength, σ_c , is determined.

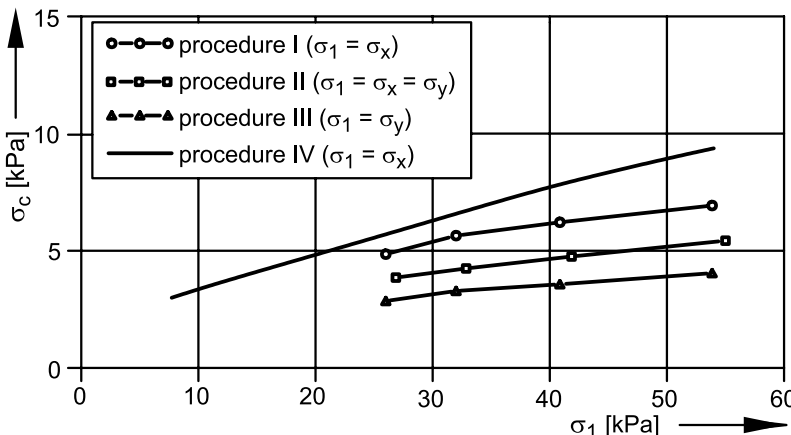


Fig. 5.12. Unconfined yield strength, σ_c , vs. major principal stress, σ_1 , of limestone powder measured after different consolidation procedures (see Fig 5.2) [5.2,5.3]

The unconfined yield strength, σ_c , determined with the discussed consolidation procedures is plotted in Fig. 5.12 versus the major principal stress at consolidation, σ_1 . The main results regarding the influence of the consolidation procedure are:

- In case of identical directions of the major principal stress at consolidation and at measurement of strength (failure) (procedures I, II and IV), the procedure where steady-state flow is attained (procedure IV) leads to the largest value of unconfined yield strength at all consolidation stresses, σ_I . The unconfined yield strength after uniaxial compression (procedure I) is smaller, and even smaller strength is obtained after uniform compression in x and y directions (procedure II, i.e. isotropic compression in the x,y plane). This result is in accordance with the findings for bulk density (Fig. 5.9) and the simplified particle model in Fig. 5.6: The more the principal stresses and the corresponding strains, respectively, are different from each other, the denser the particles are packed (higher bulk density) and the more pronounced the orientation of the stress chains in the direction of the major principal stress. A higher bulk density means that the particles are closer to each other. This increases the adhesive forces acting between particles (see Sect. 2.6) and thus the strength of the bulk solid.
- The comparison of procedures I and III, which differ from each other only in the direction of compression (i.e., the direction of the major principal stress), shows that the strength of a consolidated bulk solid specimen can be anisotropic. The greater value of unconfined yield strength is measured in the direction of the major principal stress at consolidation. Following the simplified particle model (Fig. 5.6.b), the reason for this can be seen in the stress chains which are primarily oriented parallel to the major principal stress at compression. As outlined above, the particles have more contacts in direction of the stress chains than in the perpendicular direction. This result corresponds to the findings of Saraber et al. [5.30] and Molerus [5.27].

5.2 Shear deformation, shear zones, localization

5.2.1 Idealization: simple shear and pure shear

Steady-state flow as explained in Sect. 5.1 by considering the biaxial tester is defined as isochoric flow under constant stresses. This type of flow (Fig. 5.13.a), which is achieved in the biaxial tester by compression in x direction and simultaneous dilation in y direction, is called pure shear. Here the strain rate, $\dot{\varepsilon}$, represents the momentary deformation per time unit.

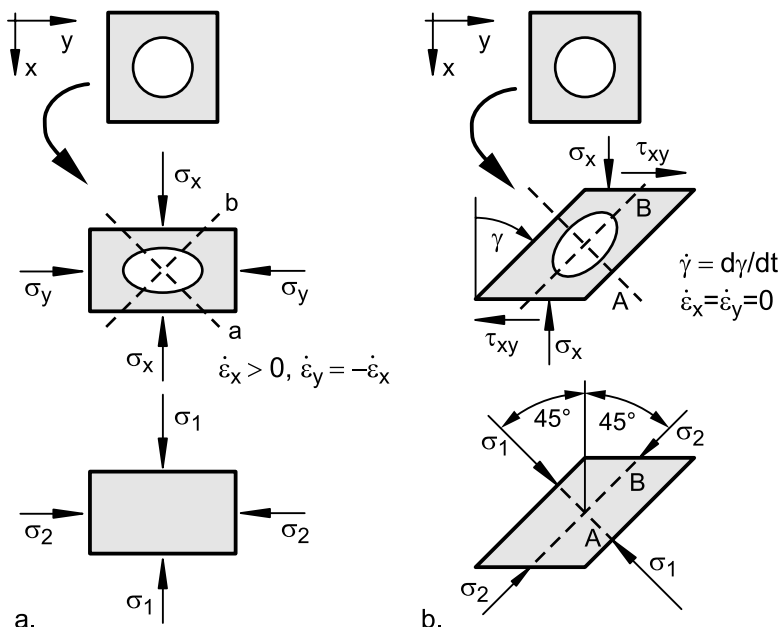


Fig. 5.13. Isochoric shear deformation (view on a cutting plane parallel to the x,y plane); a, b, A, and B characterize planes in the bulk solid specimen; in the bottom part of the figure the directions of the principal stresses are drawn under the assumption of isotropic material behavior; a: pure shear; b: simple shear

For the practical determination of flow properties, shear testers are used (see Chaps. 3 and 4). To obtain a consolidated bulk solid specimen in the shear cell, the material is subjected to shear deformation (preshear) until steady-state flow prevails. Shear deformation is achieved by moving the top and bottom of the shear cell, and thus the top and bottom of the bulk solid specimen, parallel to each other in opposite directions. In the ideal case shear deformation at steady-state flow can be characterized as simple shear, where no strain takes place in the x and y directions (Fig. 5.13.b). The momentary shear deformation at simple shear is represented by the shear rate, $\dot{\gamma}/2$.

Assuming isotropic material behavior (which is an idealization as outlined in the previous sections), the principal strain directions coincide with the principal stress directions. A principal strain direction is the normal direction of a plane on which the shear rate is zero (i.e. the plane does not rotate during deformation), in analogy to a principal stress plane where the shear stress is zero. Since in pure shear (Fig. 5.13.a) the volume is constant, the strains in x and y directions must have the same amount, but opposite direction. This results in a Mohr strain circle with its center at the

origin (Fig. 5.14.a) [5.32]. The intersections with the $\dot{\epsilon}$ axis represent strain rates in x and y directions. (Please note: The relations presented in Chap. 2 between directions in the Mohr stress circle and in the bulk solid specimen are also valid for the Mohr strain circle).

Since pure shear is regarded here as the same process as steady-state flow, the Mohr stress circle representing pure shear touches the effective yield locus. Assuming isotropic behavior, the major principal stress, σ_1 , has the same orientation as the strain in x direction. The planes of maximum shear stress τ_a and τ_b , which are also planes of maximum shear rate $(\dot{\gamma}/2)_a$ and $(\dot{\gamma}/2)_b$, are found in the Mohr stress circle rotated by 90° to the principal stress planes, thus in the bulk solid the planes of maximum shear stress (planes a and b in Fig. 5.13.a) are inclined by 45° to the x direction.

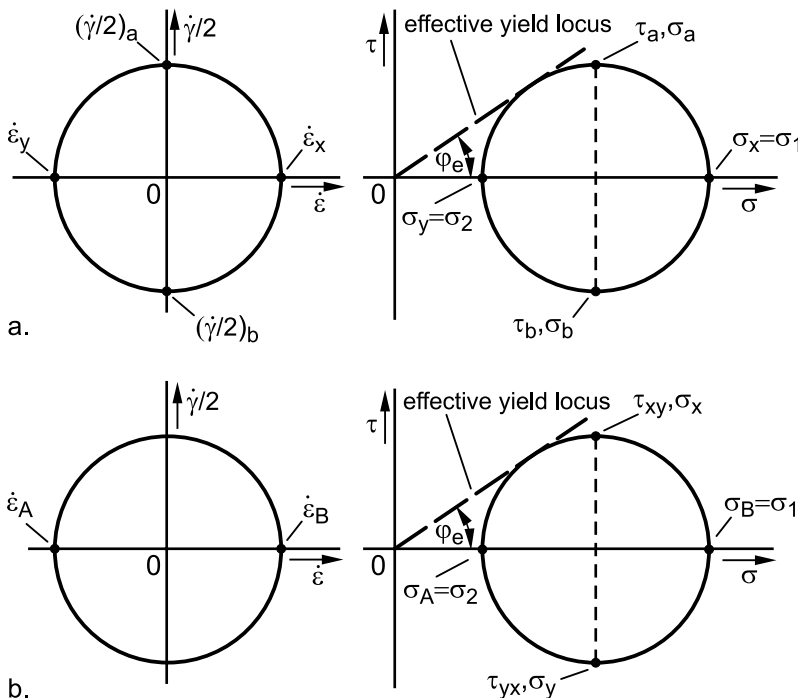


Fig. 5.14. Mohr strain circles (here the momentary strain per time unit is plotted) and Mohr stress circles for pure shear (a) and simple shear (b) according to Fig. 5.13

With simple shear (Fig. 5.13.b) the same Mohr strain circle is attained as in pure shear, but at simple shear the strain rates in x and y directions are zero (Fig. 5.14.b). Thus the intersections of the Mohr strain circle with the $\dot{\gamma}/2$ axis represent the conditions in x and y directions. Therefore the

greatest shear deformation or strain rate, respectively, is found in planes being perpendicular to the x and y axes (these are the horizontal and vertical planes in Fig. 5.13.b). The Mohr stress circle, which is drawn under the assumption of isotropic behavior, shows that in these planes the largest shear stresses are acting. Furthermore, the normal stresses in x and y directions are equal. The principal strain planes and principal stress planes A and B are inclined by 45° (in the Mohr circles by 90°) to the x and y axes, whereby the positive principal strain, $\dot{\varepsilon}_B$, and the major principal stress, $\sigma_I = \sigma_B$, are normal to plane B (see Fig. 5.13.b, bottom) [5.33,5.34].

Both pure shear (biaxial tester) and simple shear (shear tester) represent steady-state flow as defined in bulk solids technology. In both cases the bulk solid is compressed in one direction, and it dilates in the perpendicular direction (see deformation of the circle on the bulk solid element in Fig. 5.13). A difference between the shear processes is the rotation of material axes. During pure shear the orientation of material axes parallel to the principal strain directions remains constant whereby all other material axes are rotated. Thus the bulk solid rotates with respect to the plane of greatest shear deformation or greatest shear stress, respectively. During simple shear only the orientation of the material axes parallel to the applied shear deformation (y direction in Fig. 5.13.b) remains constant. Thus, in this case the bulk solid does not rotate with respect to the plane of greatest shear deformation or greatest shear stress.

It has to be added that the shear deformation of real bulk solids in real situations (shear tester, biaxial tester) can be different from the ideal cases “pure shear” and “simple shear” (e.g. [5.13,5.33,5.35,5.36]). One reason for this is the (local) concentration of the shear deformation in so-called shear bands. This effect is discussed in the following section.

5.2.2 Shear zones and shear bands

In recent years shear deformation in shear testers has been examined using DEM simulations (discrete element method) (e.g.[5.15,5.16, 5.37]), and there also has been some experimental work performed. In [5.32] the shear zones (i.e. zones where the shear deformation takes place) prevailing in the Jenike shear tester have been investigated using x-ray technique (Fig. 5.15). When an underconsolidated bulk solid specimen is presheared, a lens-shaped shear zone of nearly the same height as the shear cell prevails. The shape results from the fact that from geometrical considerations the bulk solid at the edges of the shear cell is not sheared. The large height of the shear zone results from the increasing consolidation of the initially underconsolidated specimen which goes along with an increase of the

shear stress, τ , until steady-state flow is attained (Fig. 5.15.a). If the height of the shear zone were smaller, only the bulk solid in the shear zone would become consolidated, but not the bulk solid above and below the shear zone. However the still unconsolidated bulk solid would not be strong enough to bear the increasing load caused by the increasing shear stress. Thus, the unconsolidated material flows (shear deformation), and the height of the shear zone increases. Therefore it can be stated that the height of a shear zone generally increases if the shear stress increases with increasing shear deformation [5.38].

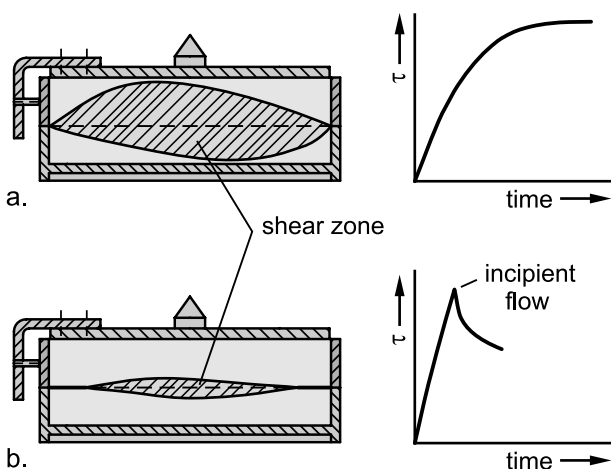


Fig. 5.15. Regions of shear deformation (shear zones) in the shear cell of the Jenike shear tester after shearing of an underconsolidated specimen (a) and an overconsolidated specimen (b) [5.32]. The shear zones were caused by the total shear deformation from the beginning to the end of a deformation. Thus the shear zones are not momentary, but integral shear zones.

When shearing an overconsolidated specimen (like shear to failure in a yield locus test, Sect. 3.2.1), the bulk solid starts for flow only after the applied shear stress is sufficiently large (Fig. 5.15.b). Incipient flow of an overconsolidated specimen is followed by decreasing shear stress and dilation of the bulk solid. The shear deformation is concentrated in a narrow shear zone. The reason for this is that as soon as the yield limit is attained in a region, however thin it is, the shear stress decreases and thus is not large enough to initiate flow also in the rest of the specimen where the bulk solid is still consolidated. In analogy to the “weakest link of a chain” the shear zone prevails where the yield limit is attained first with respect to the local strength of the bulk solid specimen and the stress distribution. The generalization of this result leads to the statement that decrease of

shear stress with increasing deformation leads to a concentration of the shear zone [5.38].

The shear deformation achievable with the Jenike shear cell is limited since the maximum horizontal displacement of the shear ring is twice its wall thickness. The region of shear deformation at preshear usually develops in the same manner as shown in Fig. 5.15.a. But if a bulk solid specimen is subjected to a larger shear deformation, which can be realized, for example, with a rotational shear tester, one observes that with increasing shear deformation the height of the shear zones decreases, i.e., the shear zone localizes. Figure 5.16 shows the development of the shear zone by deformation of a colored vertical particle layer. The local deformation, which was initially distributed uniformly across the height of the bulk solid specimen, concentrates increasingly until finally a very narrow so-called shear band is formed beneath the rough lid. One reason for the position of the shear band close to the lid is the increase of normal stress towards the bottom of the shear cell due to the force of gravity. The latter results in slightly smaller shear stresses required to deform the bulk solid close to the lid than in regions located further down.

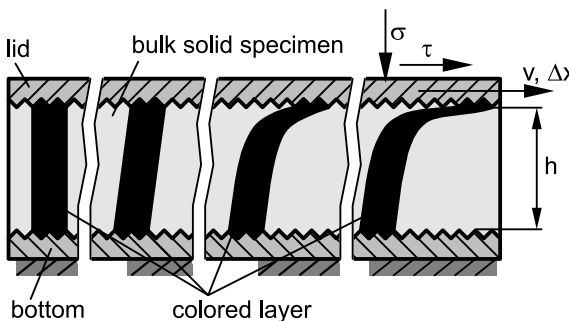


Fig. 5.16. Initially underconsolidated specimen in the shear cell of a ring shear tester after shear [5.39,5.40]. The shear deformation increases from the left (no shear displacement) to the right. v is the velocity of the lid relative to the bottom, Δx is the relative horizontal displacement, and h the momentary height of the bulk solid specimen. The specimen is subjected to a constant vertical stress, σ , during the test. The shear stress prevailing during shear is τ .

Formation of the shear band during preshear is neither a device-specific process nor limited to shear deformations similar to simple shear (Fig. 5.13.b). Shear bands can be found in many situations, e.g. in bulk solids flowing in the hopper of a silo, where the deformation is concentrated in shear zones between regions which are momentarily not deformed and flow downwards as almost rigid blocks (see Sect. 14.4). Even in a testing

device similar to the biaxial tester shown in Fig. 5.1 shear bands have been observed at a deformation according to procedure IV (Fig. 5.2) or pure shear, respectively [5.13,5.18]. The same has been found in a triaxial tester for similar deformation processes (e.g. [5.35]). The thickness of shear bands or shear zones, respectively, is according to the literature between five and twenty times the mean particle size (e.g. [5.13,5.18,5.36,5.41–5.43]) for bulk solids with a particle size of some 100 µm or more. With a cohesive limestone powder (mass median $x_{50} = 3 \mu\text{m}$) shear zones with a thickness of 200 times the mass median have been observed [5.39].

Considering the formation of shear zones and shear bands discussed above, it is unlikely that during shear deformation under constant stress (e.g. constant normal stress at preshear) steady-state flow prevails whereby the shear zone permanently comprises the whole specimen. Rather, with increasing shear deformation the shear zone is concentrated in a region of decreasing thickness (localization). Usually the localization goes along with the decrease of stresses.

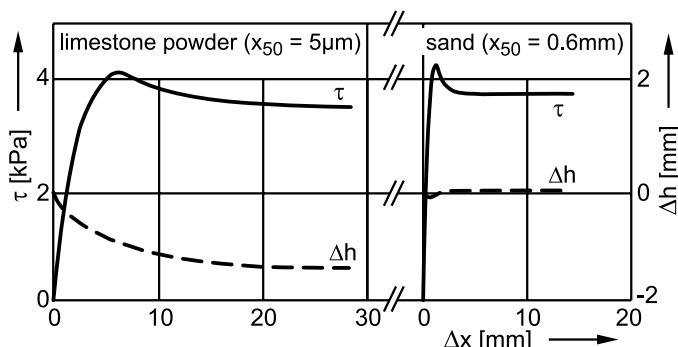


Fig. 5.17. Shear stress, τ , and variation of the specimen height, Δh , during large displacements, Δx , of the lid relative to the bottom of the shear cell of a ring shear tester. In both cases the initially loose (underconsolidated) specimen is sheared according to Fig. 5.16 under the normal stress $\sigma = 5000 \text{ Pa}$ (initial specimen height: $h_S = 12 \text{ mm}$).

In Fig. 5.17 typical courses of the shear stress during a shear deformation in accordance with Fig. 5.16 are plotted both for a fine-grained, cohesive bulk solid (limestone powder) and a free-flowing, nearly uncompressible one (sand). In both cases the shear stress at first increases, then passes a more or less pronounced maximum and decreases. Finally, after a certain displacement Δx of the top relative to the bottom, a constant shear stress prevails. Although the shear stress obviously does not become constant when the maximum shear stress is attained, but decreases, in the present

book the term “steady-state flow” is further used to characterize the flow of an initially underconsolidated specimen after the shear stress maximum has been attained (according to the common nomenclature in shear testing [5.55]). A further discussion of the term “steady-state flow” follows in Sect. 5.2.4.

The decrease of the shear stress and the localization depend on each other. For a shear deformation similar to Fig. 5.16 Beeler [5.38] formulated an equation describing the influence of the height of the shear zone, h_S , on the shear stress, τ :

$$d\tau = -\frac{1}{h_S^2} \left(v \frac{\partial \tau}{\partial \dot{\gamma}} + \Delta x \frac{\partial \tau}{\partial \gamma} \right) dh_S \quad (5.1)$$

The term $\partial \tau / \partial \dot{\gamma}$ gives the dependence of shear stress on shear rate (see Fig. 5.13.b), and the term $\partial \tau / \partial \gamma$ describes the dependence of shear stress on shear deformation. h_S is the thickness (height) of the shear zone, v the relative velocity, and Δx the relative displacement between top and bottom of the bulk solid specimen (Fig. 5.16). Following the principle of minimum energy (simplified: “The energy of a system approaches a minimum value at equilibrium”), the shear zone will prevail in a way that the shear stress becomes as small as possible, so the differential of the shear stress, $d\tau$, becomes negative. If the terms $\partial \tau / \partial \dot{\gamma}$ and $\partial \tau / \partial \gamma$ are negative, the shear stress decreases with decreasing height of the shear zone, h_S . This happens when an overconsolidated specimen is sheared (e.g. at shear to failure when measuring a point on a yield locus): Since the bulk solid specimen dilates at incipient flow, it holds that $\partial \tau / \partial \gamma < 0$. Neglecting the influence of shear rate, the shear stress can be minimized only if $dh_S < 0$, i.e., the height of the shear zone decreases. This corresponds to the narrow shear zone in Fig. 5.15.b.

The localization observed at steady-state flow (Fig. 5.16) can also be interpreted on the basis of Eq.(5.1): At small shear rates many bulk solids show negative ratios $\partial \tau / \partial \dot{\gamma}$, and these ratios are small compared to those of Newtonian liquids [5.1,5.44] (see Sect. 7.1.1). If such a bulk solid is sheared at constant relative velocity, v , applied to the bulk solid specimen from the outside, and the height of the shear zone decreases during shear, the shear rate in the shear zone increases and, thus, the shear stress decreases according to $\partial \tau / \partial \dot{\gamma} < 0$. Even the term $\partial \tau / \partial \gamma$ can be negative, e.g. due to a specific orientation of the particles forming “smoother” or “weaker” shear planes, on which the shear resistance is smaller compared to cutting planes with other orientations [5.33]. This effect has been demonstrated with tests on sand, where a primary orientation of the particles in the shear zone was found [5.13,5.18,5.45]. Therefore it can be concluded

that at steady-state flow the terms in the bracket in Eq.(5.1) can become negative, so that the shear stress is minimized by a decrease of the height of the shear zone ($dh_S < 0$).

During shear of an underconsolidated specimen (e.g. at preshear before steady-state flow prevails) a large shear zone develops (Fig. 5.15.a). Here the shear resistance increases with shear deformation, thus $\delta\tau/\delta\gamma > 0$. Neglecting the influence of the shear rate, the shear stress or the increase of the shear stress, respectively, can be minimized only when $dh_S > 0$, i.e., the height (thickness) of the shear zone increases.

Processes at large shear deformation have been investigated in geology (e.g. [5.38,5.46,5.47]). In Fig. 5.18 it is shown how shear stresses and shear zones develop in particle layers (results taken from laboratory tests where flow processes in simulated geological fault zones have been examined) [5.46]. When the particle layer is subjected to simple shear, one obtains a course of the shear stress versus displacement similar to Fig. 5.17. Based on the similarity of the shear stress curves it is assumed that the mechanisms during shear deformation are the same for the bulk solid and the particles in the simulated fault zone [5.47].

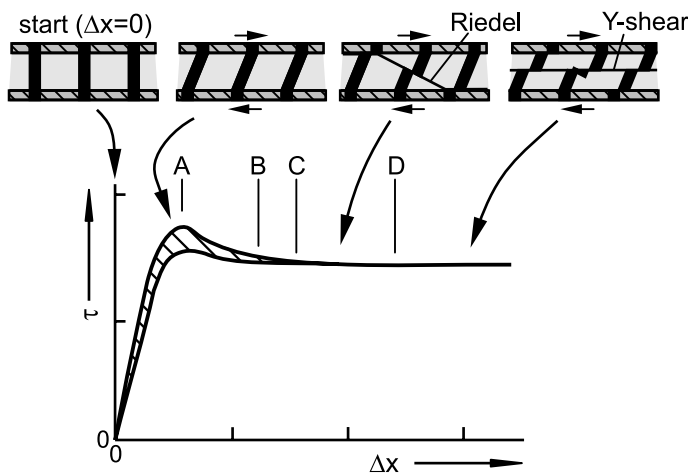


Fig. 5.18. Shear stress, τ , acting in a cohesionless particle layer (simulated geological fault zone) vs. horizontal displacement, Δx , of the top relative to the bottom (in principle) [5.46]. The hatched area represents the range of shear stresses measured with different bulk solids and different preconsolidation procedures (a loose particle packing obtained by careful filling results in less pronounced shear stress maxima). The shear deformation is indicated by the deformation of the black layers, which have been initially vertical (above the diagram).

Before the shear stress maximum (point A in Fig. 5.18) is attained, the shear deformation is distributed in the whole particle layer. This corresponds to Eq.(5.1): To the left of point A the shear stress increases, and thus the shear zone grows in order to reduce the increase of the shear stress ($d\tau_{xy} > 0$). After the shear stress maximum has been attained (A) the localization of the shear zone begins. According to Eq.(5.1) the shear stress is minimized by the concentration of the shear deformation to a smaller region ($d\tau_{xy} < 0$). Thus some inclined shear bands are formed (Riedel shears [5.48]), which are distributed in the whole particle layer after point B. After point C shear bands close to the confining walls of the particle layer can be observed (boundary shears), and beyond point D a final state with horizontal shear bands (Y shears) is attained. In this region two almost rigid blocks of bulk solid are moving across each other. The shear deformation is then concentrated in a horizontal shear band between the rigid blocks.

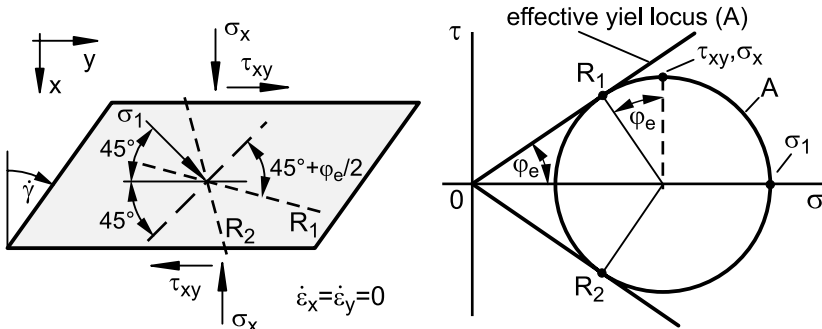


Fig. 5.19. Deformation of a bulk solid element by simple shear (the figure shows a cutting plane parallel to the x,y plane) and corresponding Mohr stress circle (stresses at point A in Fig. 5.18); R₁ and R₂ are “Riedel shears” [5.33,5.48,5.49]

The development of “Riedel shears” after point A (Fig. 5.18) is explained in Fig. 5.19. Assuming that at point A steady-state flow according to the effective yield locus plotted in Fig. 5.19 is attained (in analogy to Fig. 5.13.b and 5.14.b), the bulk solid can flow in those planes, where the pair of values of shear stress and normal stress is a point on the effective yield locus. This is the case for the planes marked as R₁ and R₂. These planes are inclined by $\pm(45^\circ + \phi_e/2)$ to the major principal stress plane, i.e., the plane where the major principal stress is acting. During further shear deformation, after point D in Fig. 5.18 horizontal shear bands are formed (Y shears). Figure 5.20 shows a possible Mohr stress circle (D) which results in a smaller shear stress $\tau_D < \tau_A$ although the vertical stress, σ_x , is still constant. Following Mandl’s [5.33] assumption that horizontal shear

planes are weaker than other planes (“horizontal plane of weakness”), the Mohr stress circle characterizing the stresses to the left of point D can be located partly above the yield limit for the horizontal shear plane. Thus the bulk solid has become anisotropic through the large shear displacement and formation of shear bands.

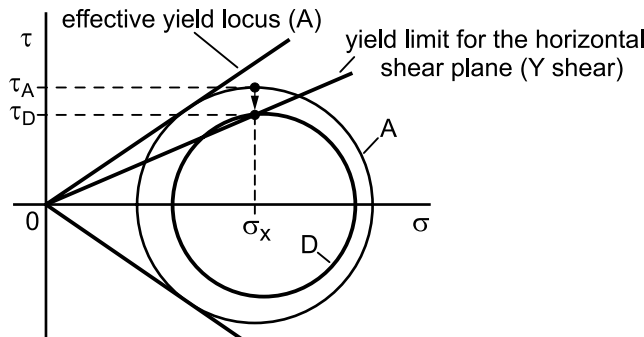


Fig. 5.20. Mohr stress circle (D) possibly attained after large shear deformation (after point D in Fig. 5.18). It is assumed that the bulk solid behaves anisotropically due to the existence of a weak horizontal shear plane (after Mandl [5.33]). For comparison, Mohr stress circle A taken from Fig. 5.19 and the corresponding effective yield locus are plotted.

The question remains whether the results obtained in geotechnical research (Figs. 5.18 to 5.20) can be applied to bulk solids technology. Reasons for this are, beside the similarity of the processes, the similar courses of the shear stress developing during shear (Fig. 5.17) as well as the formation of shear zones (Fig. 5.16), at least considering the uniform shear deformation at the beginning (Fig. 5.18, left of point A) and the narrow shear zone attained finally (Fig. 5.18, to the right of point D).

5.2.3 Dilatancy

The shear stress maximum, which can often be observed when cohesionless bulk solids are presheared (preshear for consolidation of a specimen in a yield locus test, Sect. 3.2.1), is to a major extent a result of the dilation during shear, which is clearly visible for the sand in Fig. 5.17 ($\Delta h > 0$). In contrast to cohesive, compressible powders, where the height of an initially loose specimen decreases during preshear (see limestone powder in Fig. 5.17), a cohesionless material like dry sand forms a relatively dense structure upon filling. The latter is possible because for non-cohesive bulk solids the interparticle adhesive forces are small compared to the particle

weights thus giving the particles high mobility. When such a dense structure is sheared according to Figs. 5.13.b and 5.16, respectively, the material dilates (principle of dilatancy). Only when an initially very loose packing of bulk material is sheared, it exhibits prior to the dilation a slight compaction due to the increasing load caused by the increasing shear stress (see initially negative Δh for the sand in Fig. 5.17).

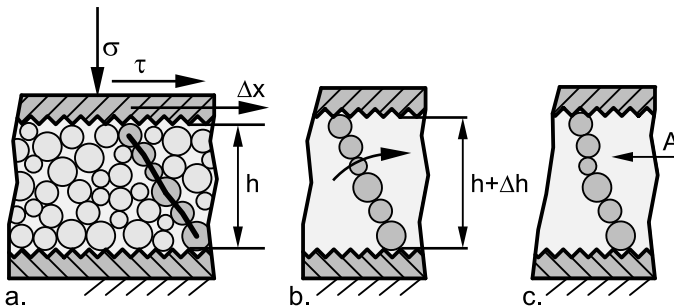


Fig. 5.21. Simple model of a shear zone demonstrating particle movement during shear deformation of a coarse bulk solid: Due to the shear deformation resulting from the horizontal displacement, Δx , of the top relative to the bottom of the bulk solid specimen (a), particle columns (bridges) forming the stress chains are rotated (b) thus increasing the height of the specimen, h . If the shear deformation proceeds, individual particles slide across each other (see position A in Fig. 5.21.c) [5.45,5.50].

The reason for the dilation is that during shear, particles have to move across other particles, i.e. they must be moved slightly upwards from their initial position in the dense packing (Fig. 5.21.a). In shear the applied load is carried by a network of stress chains that span the particle layer and are primarily oriented in the direction of the major principal stress. Considering the inclined stress chain marked in Fig. 5.21.a, the column of particles forming the stress chain becomes steeper with increasing shear deformation (see rotation indicated in Fig. 5.21.b). Thus the height, h , of the bulk solid specimen increases. As the particle column becomes steeper, at a certain position of the column the particles may slide across each other (A in Fig. 5.21.c) [5.45,5.50]. Thus the stress chain becomes ineffective. Shear deformation of a bulk solid is accommodated by a process in which individual stress chains continuously fail and new ones form and take their place [5.22,5.50]. The larger the particles, the greater is the expected vertical dilation, since the particles have to be lifted more to be able to flow across other particles, and the thickness of a shear zone is a multiple of the particle size, thus Δh is larger from geometrical reasons (Fig. 5.21.b).

After the initial dilation described above, the height of the bulk solid specimen remains constant upon further shear (see Fig. 5.17: sand). If shear is stopped and the specimen is unloaded from shear stress, the specimen deforms somewhat opposite to the former shear direction, which is partly caused by elastic recovery, and the specimen height decreases. The deformation at unloading can be interpreted considering the particle model shown in Fig. 5.21: Particle columns, which have become steeper during shear, rotate against the direction of the arrow in Fig. 5.21.b during unloading. Thus the specimen height is reduced.

Figure 5.22 shows results of a test performed by Mandl et al. [5.33], where the specimen (sand) was compacted prior to shear and, thus, shows a clearly visible dilation. Beside the measured values of shear stress, τ , and change of specimen height, Δh , the shear stress τ_d , required for the vertical dilation is plotted. This shear stress is a part of the overall shear stress, τ . It is assessed on the basis of an energy balance using the angle of dilatancy [5.33,5.51].

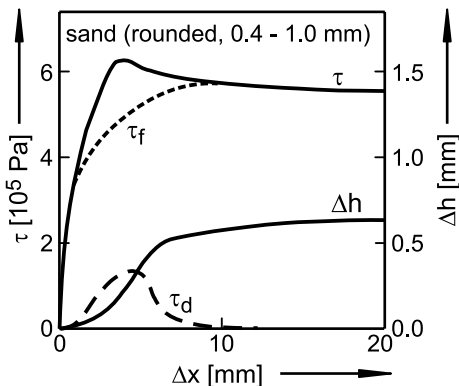


Fig. 5.22. Shear stress, τ , and variation of the specimen height, Δh , vs. horizontal displacement, Δx , of the top relative to the bottom of a ring shear cell after Mandl et al. [5.33]. τ_d is the shear stress portion resulting from the dilation of the specimen (calculated from a balance of energy). τ_f is the difference ($\tau - \tau_d$). (vertical normal stress applied during shear: $\sigma = 9.2 \cdot 10^5$ Pa; initial specimen height: $h = 12$ mm; sample was preconsolidated before shear by applying a vertical normal stress $\sigma = 1 \cdot 10^6$ Pa).

The angle of dilatancy, v , is a measure of the change of volumetric strain with respect to the change in shear strain. It can be derived by considering the deformation of a bulk solid element (Fig. 5.23) [5.13,5.39,5.52]. Δy is the displacement of the top of the initially rectangular bulk solid element relative to the stationary bottom during the time span Δt . Within this time span the height of the element increases by Δh (measured in the vertical

direction). According to the definition reported above, the angle of dilatancy, v , describes the momentary dilation related to the shear deformation by defining the direction of movement of the top of the bulk solid element relative to horizontal (y axis):

$$\begin{aligned}\tan v &= \lim_{\Delta y \rightarrow 0} \frac{\Delta h}{\Delta y} = \lim_{\Delta \gamma \rightarrow 0} \frac{\Delta h}{\Delta \gamma_{xy} \cdot h} \\ &= \lim_{\Delta \gamma \rightarrow 0} \frac{\Delta h / h}{\Delta \gamma_{xy}} = \frac{dh / h}{d\gamma_{xy}} \\ &= -\frac{d\varepsilon_x}{d\gamma_{xy}} = -\frac{\dot{\varepsilon}_x}{\dot{\gamma}_{xy}}\end{aligned}\quad (5.2)$$

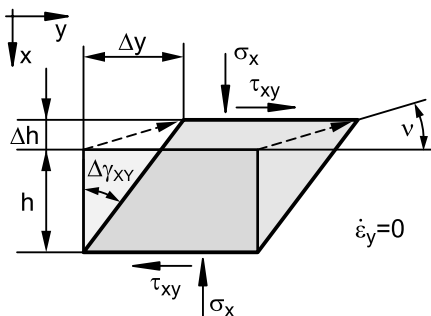


Fig. 5.23. Definition of the angle of dilatancy, v ; the figure shows a vertical cut through an initially rectangular bulk solid element before and after deformation [5.39, 5.52]

The minus sign in front of the strain $d\varepsilon_x$ results from the definition that compressive strain, ε , is positive (in analogy to compressive stress). Thus dilation of the bulk solid results in positive values of dh and positive angles v , but a negative strain $d\varepsilon_x$.

If during shear the bulk solid specimen dilates in the vertical direction, work is required to raise the top of the specimen by Δh against the vertical force, which is here equal to $\sigma_x \cdot A$. (A : area on which σ_x is acting). This work corresponds to the volumetric strain energy known from thermodynamics. If the force is constant, the work can be derived from the product of force and displacement in the direction of the force:

$$\Delta W_{Vd} = A \cdot \sigma_x \cdot \Delta h \quad (5.3)$$

The only way this work can be supplied to the bulk solid is the shear process, i.e., shear deformation and shear stress, respectively, applied from outside (e.g. by the drive moving the top of the specimen relative to the

bottom). Thus, at constant shear rate, dilation leads to an increase of shear stress. With additional shear stress resulting from the dilation, τ_d , the following additional work is provided within the time span Δt :

$$\Delta W_{Vs} = A \cdot \tau_d \cdot \Delta y . \quad (5.4)$$

Equating ΔW_{Vd} with ΔW_{Vs} , one obtains the momentary acting additional shear stress, τ_d , for the limit as Δy approaches zero ($\Delta y \rightarrow 0$):

$$\tau_d = \lim_{\Delta y \rightarrow 0} \sigma_x \frac{\Delta h}{\Delta y} = \sigma_x \tan v = -\sigma_x \frac{\dot{\varepsilon}_x}{\dot{\gamma}_{xy}} \quad (5.5)$$

Thus the overall shear stress, τ , applied to the bulk solid specimen can be divided into the portion related to dilation, τ_d , and a portion associated with friction on the shear plane, τ_f [5.33,5.51,5.53]:

$$\tau = \tau_f + \tau_d \quad (5.6)$$

With this simplified energy balance we neglect (as in [5.33]) energy that may be dissipated during dilation due to additional friction (e.g. by rearrangement of particles) [5.13,5.51].

In Fig. 5.22 the shear stress portions discussed above, namely τ_d and τ_f , are plotted as dashed curves. One can recognize that the maximum in the course of the overall shear stress, τ , results to a major extent from dilation of the specimen during shear. After the end of the dilation process the shear stress decreases further, which gives rise to the assumption that further mechanisms (e.g. the localization of the shear zone) are responsible for the shear stress decrease. Also the shear stress maximum observed with fine-grained, cohesive limestone powder (Fig. 5.17) is unlikely to result from dilation (the specimen height decreases with proceeding compaction), but follows from the effects related to localization of the shear zone (Sect. 5.2.2).

Dilation occurs also when a consolidated bulk solid specimen is sheared, e.g. at shear to failure in a yield locus test. Typical courses of shear stress, τ , and specimen height, h , during preshear and shear to failure of a cohesive bulk solid are plotted in Fig. 5.24. At the end of preshear the specimen is relieved from the shear stress which results in a slight reduction of specimen height as discussed above. During shear to failure, i.e., shear of an overconsolidated bulk solid specimen, the specimen dilates and thus its height increases (Fig. 5.24). Dilation of the specimen goes along with the decrease of bulk density within the shear zone and, thus, with weakening of the specimen resulting in decreasing shear stress. However, a portion of the observed dilation results from the fact that during shear to

failure additional space is required to allow particles to move across each other (as shown in Fig. 5.21 for preshear). This portion is assumed to be on the order of magnitude of the height decrease at the end of preshear when the specimen is relieved from the shear stress (Fig. 5.24).

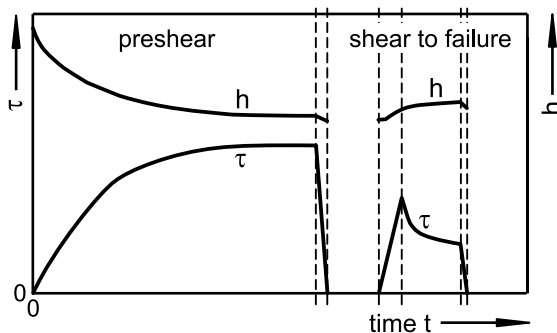


Fig. 5.24. Shear stress, τ , and specimen height, h , vs. time, t , during preshear and subsequent shear to failure of a cohesive bulk solid

If free-flowing bulk solids, which are nearly incompressible and thus their bulk density is nearly independent of the normal stress (e.g. glass beads), are sheared to failure, the observed dilation is primarily a result of the space required for shear deformation according to Fig. 5.21.

The present section can be summarized as follows: Because of the dilation occurring at shear to failure, the shear stress includes a portion according of Eq.(5.5). This is true for both free-flowing and cohesive bulk solids. Thus, generally it can be stated that at the beginning of a flow process, which does not result in an increase of the bulk density, dilation can be observed (see particle model in Fig. 5.21). On the contrary the transition from flow to a state of rest leads to a volume reduction [5.39].

5.2.4 Steady-state flow and dilation during flow property testing

In bulk solids technology the standard test method for determination of flow properties is the shear test (Sect. 3.2). To obtain a bulk solid specimen with defined conditions before measuring the strength, an underconsolidated specimen is sheared until steady-state flow prevails (preshear) [5.54,5.55]. Also the flow process in the hopper of a silo is approximated as steady-state flow [5.54,5.56].

In the previous sections it has been outlined that steady-state flow is an idealized flow process which in reality cannot proceed indefinitely. During

simple shear of a cohesive bulk solid (e.g. limestone powder, Fig. 5.17) one will find a point after which the shear stress decreases or at least does not increase further, i.e., the specimen is not consolidated further. At this moment the shear zone comprises a large part of the bulk solid specimen. Immediately after the shear stress maximum has been attained, localization of the shear zone begins, which leads more or less quickly to a more or less strong decrease of the shear stress. Thus the shear process is not a steady-state flow process with respect to constant stresses. However, the shear stress (especially when shearing fine-grained, cohesive powders) can remain for a certain period of time at the level of the maximum shear stress thus exhibiting a kind of shear stress plateau before the shear stress decreases (Fig. 5.25). Therefore the plateau corresponds to the concept of steady-state flow.

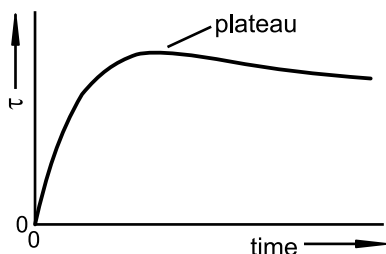


Fig. 5.25. Shear stress plateau (example) during preshear of a cohesive bulk solid

When measuring a yield locus, preshear is stopped as soon as the plateau described above is attained and the shear stress does not increase further [5.54,5.55]. When a Jenike shear tester is used, it is often not possible to observe the course of the shear stress during large shear deformation, because the shear displacement is limited. Thus the operator of a Jenike tester is usually satisfied when steady-state flow prevails within the available shear displacement. Preshear is stopped then and shear to failure is conducted (Sect. 4.1.1). Thus it becomes clear that in connection with the Jenike shear tester the term "steady-state flow" means the flow process in the vicinity of the shear stress plateau. This flow process is a good approximation to the ideal flow process "steady state flow" because the shear zone is still relatively large (Fig. 5.15.a) and localization just starts.

A major advantage of the preshear procedure, where the specimen is sheared until steady-state flow is attained, is that the shear stress plateau is reached only after the whole bulk solid specimen is sufficiently consolidated. Thus it is possible to monitor the state of consolidation by observing the shear stress.

The results and interpretations in the present and previous sections should not be understood as criticism of the common consolidation procedure applied with shear testers, namely the preshear procedure where a specimen is sheared until steady-state flow prevails. Discussion of the processes within the powder rather should help one to understand what happens in a bulk solid during shear, especially at large shear displacements, so that a user is provided with more background knowledge regarding performance and interpretation of shear tests.

An important result of the considerations above is that preshear should be stopped after the constant shear stress is attained and before the shear stress eventually starts to decrease (or at least before it decreases too much). In this state the localization effect is still limited. As outlined earlier in the present section, this is the common procedure with the Jenike shear tester where the shear deformation is limited and thus preshear is terminated as soon as the shear stress is constant.

The same procedure should be applied to rotational shear testers with unlimited shear displacement (ring shear tester, torsional shear tester) if steady-state flow is to be obtained under similar conditions as with the Jenike tester, and if the test results shall be comparable to those obtained with the Jenike tester. Sometimes it can be observed that the unlimited shear displacement encourages users to proceed with preshear until the region of Y shears (right of point D in Fig. 5.18) is attained, where the shear stress is constant at a lower level compared to the shear stress maximum. The reason given for this procedure [5.54,5.55] is that at the end of preshear steady-state flow and thus a constant shear stress has to be attained. The maximum in the course of the shear stress (the plateau in Fig. 5.25) is then interpreted according to [5.54,5.55] as an indication of an initially overconsolidated bulk solid specimen. Since the rules regarding constant shear stress and overconsolidation originate from the procedure for the Jenike shear tester, where the shear deformation is limited and the specimen is manually preconsolidated (twisting) prior to preshear, they should not be applied to another type of tester without appropriate adjustment. Since a rotational shear tester does not require a manual preconsolidation, the bulk solid is filled loosely into the shear cell so the stresses in the bulk solid are usually far below the stress applied at preshear. Thus there is no reason for overconsolidation. The maximum in the course of the shear stress (the plateau in Fig. 5.25) results rather from the localization discussed in Sect. 5.2.2 which commonly is not attained with the Jenike shear tester due to the limited shear deformation. The localization leads to a local weakening of the bulk solid specimen (decreasing shear resistance, “horizontal plane of weakness”, see Sect. 5.2.2). Thus with an excessively large shear deformation at preshear one obtains a smaller shear stress at

“steady-state flow” compared to the Jenike shear tester, so the shear stress maximum at shear to failure is also reduced. The latter has been investigated experimentally with a ring shear tester and a torsional shear tester [5.57,5.58].

As outlined in the previous paragraph, preshear should be stopped when constant shear stress is attained (i.e., on the shear stress plateau, Fig. 5.25, before the shear stress eventually decreases). This way the idealized flow process “steady-state flow” is very closely attained at the end of preshear. Only when free-flowing bulk solids with coarse particles are presheared, the possible influence of dilation has to be taken into consideration (Sect. 5.2.3). The dilation at the begin of shear results in a shear stress maximum which is passed within a shorter time than the shear stress plateau observed with more cohesive products. Nevertheless the specimen should be presheared until the shear stress does not increase further, which is the common procedure for the Jenike shear tester [5.54,5.55]. Since in this case the measured shear stress is equal (or close) to the maximum shear stress, it contains a portion τ_d which is the result of the dilation (see Fig. 5.22). Thus the shear stress at steady-state flow is overestimated somewhat. The shear stress maximum due to dilation can be reduced by careful filling without any compaction (no vertical stress, no vibration, no shocks) thus obtaining a very loose specimen. If one would measure the vertical strain in the bulk solid specimen during preshear, the shear stress portion τ_d could be assessed and subtracted from the measured overall shear stress [5.51]. The result would be the shear stress τ_f according to Fig. 5.22. Preshear had to be terminated then on the plateau in the course of τ_f .

Since dilation also emerges at shear to failure, a portion of the maximum shear stress measured at incipient flow is a result of the dilation (τ_d , see Sect. 5.2.3). Thus the yield locus contains the influence of the dilation. The latter seems to be reasonable, because whenever a bulk solid starts to flow the material in the shear zone must dilate against the normal stress acting in the direction of the dilation.

5.3 Yield locus

Construction of a yield locus according to Jenike (Chap. 3), which is widely applied, is based on assumptions and thus should be regarded as an approximation. This is not a disadvantage because the method has proven itself, e.g. by the fact that the flow properties obtained this way have been applied successfully for the design of thousands of silos. Nevertheless, some of the assumptions are discussed in the following in order to provide

more information on the interpretation of test results. More considerations on the interpretation of shear test results can be found in publications of Jenike [5.54,5.59], Schwedes [5.32,5.60], and Molerus [5.27].

5.3.1 Preshear point, shear points and Mohr stress circles

Following Jenike's evaluation method, the shear points (maximum shear stress at shear to failure) are located on the yield locus [5.54,5.55], and the Mohr stress circle representing steady-state flow is tangent to the yield locus (see Fig. 3.16). The position of the shear points is based on the assumption that the failure planes, i.e. the planes where incipient flow takes place, are oriented horizontally and, thus, are parallel to the direction of the applied shear stress. Only in this way can the applied normal stress and the measured shear stress at shear to failure form a point on the yield locus. Since a direct shear tester like the Jenike shear tester or a ring shear tester does not provide information about the stresses acting in other directions than the horizontal plane, the Mohr stress circle representing the stresses at incipient flow cannot be determined without assumptions, i.e., the stress circle is not defined unambiguously [5.27,5.32,5.56].

One way to get more information for the evaluation is the inclusion of the deformation of the bulk solid specimen. The orientation of the failure plane where incipient flow takes place is determined under the assumption of coincidence of the principal strain axes with the principal stress axes [5.32,5.39,5.52]. This is accomplished by measuring the change of specimen height, Δh (dilation), and relative displacement, Δy (Fig. 5.23), vs. time during shear to failure (note: the dilation in y direction is zero). The angle of dilatancy, ν , is then calculated with Eq.(5.2). Knowing ν , the Mohr strain circle, or, more exactly, the strain rate circle (circle of momentary strain rates), can be drawn (Fig. 5.26). Point $(\dot{\epsilon}_x, \dot{\gamma}_{xy}/2)$ of the circle represents the conditions in horizontal planes of the bulk solid specimen. In the Mohr strain circle the angle between this point and the axis of major principal strain, $\dot{\epsilon}_1$, is $(90^\circ + \nu)$. If coincidence of principal stress and principal strain axes is assumed, the same angle can be found in the Mohr stress circle between the axes of major principal stress and normal stress (σ_x) acting in the horizontal plane. With this additional information the Mohr stress circle representing incipient flow and running through the measured shear point (σ_x, τ_{xy}) can be drawn (Fig. 5.26).

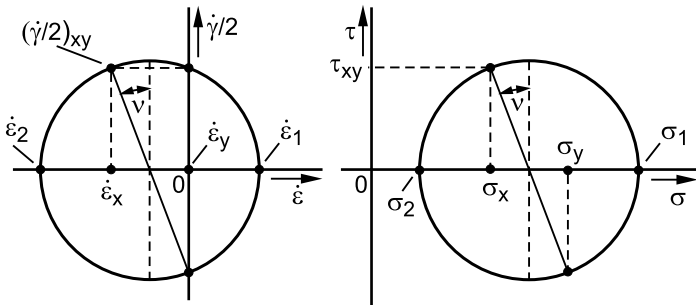


Fig. 5.26. Determination of the measured shear point (incipient flow) on the Mohr stress circle under assumption of coincidence of principal stress and principal strain axes [5.32,5.39,5.52]

When measuring points on a yield locus at different normal stresses σ_{sh} , the angle of dilatancy, v , becomes larger with decreasing ratio σ_{sh}/σ_{pre} , i.e., the ratio of the normal stress at shear to failure to the normal stress at preshear [5.31,5.39]. Knowing the angle of dilatancy, one obtains a Mohr stress circle for every shear point. An example is shown in Fig. 5.27.

The Mohr stress circle representing steady-state flow is drawn according to Fig. 5.14.b where the preshear point forms the zenith of the stress circle. This construction corresponds to Fig. 5.26 for $v = 0$ (steady-state flow = flow at constant volume). The yield locus is then drawn as a curve being the common tangent of the Mohr stress circles for incipient flow. An example is shown in Fig. 5.27 [5.39]. It is obvious that the yield locus is located above the shear points.

If a yield locus test is evaluated as outlined above (Fig. 5.27), one obtains similar or greater values of the effective angle of internal friction, φ_e , and larger values for the unconfined yield strength, σ_c [5.32,5.39,5.52]. However, this evaluation procedure is not commonly used. On the one hand, it is too difficult and expensive to determine the angle of dilatancy sufficiently accurate, e.g. because the deformation in a shear tester is not sufficiently homogeneous [5.32,5.52], and some types of shear testers like the Jenike shear tester are not provided with a means to measure the dilation. On the other hand it cannot be excluded that with this evaluation procedure the unconfined yield strength is overestimated [5.32,5.39], especially regarding silo design where sufficiently safe results are obtained with the Jenike shear tester and the common evaluation procedure (e.g. sufficiently large outlet dimensions to avoid arching). For other applications of shear test results, e.g. comparative tests, the common evaluation procedure leads to applicable results, so the additional effort for the determination of the angle of dilatancy does not seem to be necessary.

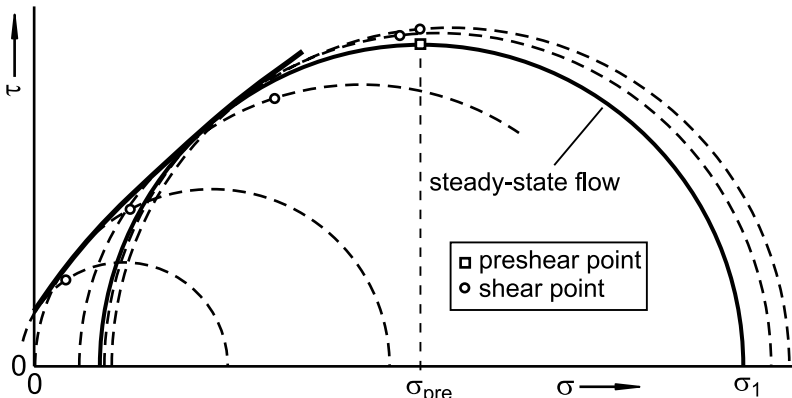


Fig. 5.27. Example of a yield locus constructed under the assumption of coincidence of principal stress and principal strain axes [5.39]. The dashed circles are stress circles representing the stresses at incipient flow, the solid circle is the Mohr stress circle for steady-state flow. Here for shear to failure different normal stresses up to the normal stress at preshear, σ_{pre} , have been applied.

When a yield locus is constructed according to Jenike's assumptions, the Mohr stress circle representing steady-state flow runs through the preshear point and touches the yield locus to the left of the preshear point (Fig. 3.16) [5.54,5.55]. The point of tangency is by definition the end point e of the yield locus.

The condition that the Mohr stress circle for steady-state flow touch the yield locus, is an approximation which is required so as to have sufficient information to construct this circle. Actually it is to be expected that the Mohr stress circle for steady-state flow, which represents stresses in the flowing bulk solid, is located somewhat below the corresponding yield locus, which is valid for incipient flow. Since the bulk density in the shear zone of a flowing bulk solid is smaller than the bulk density in a bulk solid at rest (at the same normal stress), dilation takes place due to the initiation of flow. The effect of dilation increases the shear stress (see remarks on the effect of dilation on shear stress in Sect. 5.2.3 and 5.2.4). Furthermore in a bulk solid at rest the particles are closer to each other and thus the adhesive forces are larger than in the shear zone of a flowing bulk solid. Accordingly one finds shear stress maxima when a bulk solid specimen, previously presheared under the normal stress σ_{pre} , is sheared to failure at a normal stress σ_{sh} to the right of the end point e (end point e see Fig. 3.16). Even at shear to failure under the normal stress $\sigma_{sh} = \sigma_{pre}$ the maximum shear stress is usually larger than the shear stress at steady-state flow [5.39,5.61]. Shear points to the right of the end point are included in Fig. 5.28 (and previously shown in Fig. 5.27).

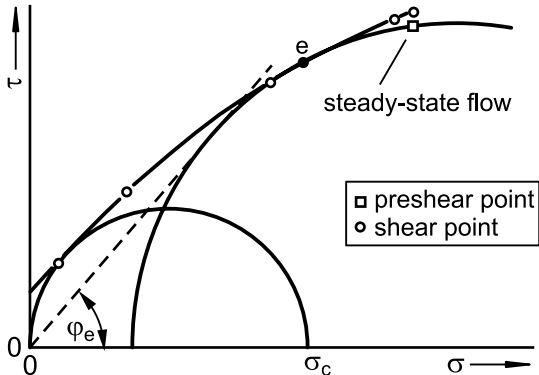


Fig. 5.28. Yield locus constructed from the measured points of Fig. 5.27 following Jenike's evaluation procedure [5.39].

If the test points of Fig. 5.27 are evaluated according to Jenike [5.54,5.55], the yield locus shown in Fig. 5.28 is obtained. In this case the point e is defined as the end point of the yield locus, but as outlined in the previous paragraph shear stress maxima at shear to failure (i.e., points of incipient flow) can be measured also to the right of the end point e [5.39,5.61]. Thus the yield locus extends beyond point e, i.e., it is unlikely that point e is the real end point of the yield locus.

Although the assumption of the yield locus being tangent to the Mohr stress circle for steady-state flow is an approximation, this does not seem to be necessarily a point of criticism, because the evaluation procedure due to Jenike has been proven over the years to be sufficiently accurate. The latter has been demonstrated by the successful application of the results, e.g. for the design of silos.

5.3.2 Tensile strength and cohesion

The tensile strength, σ_t , of a bulk solid is defined by the end point of the yield locus at negative stresses. The shear stress at the intersection of the yield locus with the shear stress axis is called cohesion, τ_c (see Sect. 3.2.3.3). With most shear testers it is not possible to measure points of the yield locus at very small or negative stresses because such stresses cannot be applied, e.g. in the Jenike shear cell the lower limit of normal stresses amounts to some 100 Pa, dependent on the bulk density and design of the shear cell [5.62]. In this case the cohesion can be determined only by extrapolating the yield locus towards small normal stresses. Since a yield locus is increasingly curved towards small stresses, the value of the cohesion cannot be determined very exactly this way and is usually less accurate.

rate than the unconfined yield strength, σ_c . Thus the unconfined yield strength should be preferred over the cohesion if different bulk solids have to be compared regarding their flow behavior.

A ring shear tester, where the shear zone is just below the annular lid, offers the possibility to install a device which exerts an upward directed force to the lid (see force F_A in Fig. 4.9). This force counteracts the weight of all parts resting on the bulk solid specimen. Thus very small normal stresses can be applied so that shear points can be measured at normal stresses of some 10 Pa or less (depending on the tester design and the bulk density) [5.31,5.62]. Therewith the cohesion can be determined without much extrapolation as shown in Fig. 5.29. It has to be mentioned that the Mohr stress circles measured at small normal stresses are crossing the region of tensile stresses (Fig. 5.29). Since the tensile strength of bulk solid is much smaller than its compressive strength (unconfined yield strength), the yield locus must be increasingly curved downwards with decreasing normal stresses.

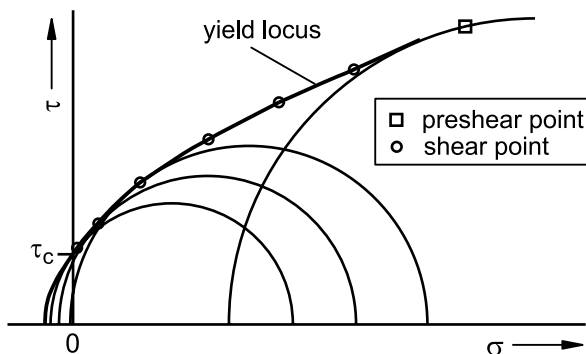


Fig. 5.29. Yield locus with shear points and preshear point; the shear points at small normal stresses are accompanied by the corresponding Mohr stress circles which are partially located in the negative stress region (evaluation according to Jenike like in Fig. 5.28 [5.54,5.55]).

It was shown in [5.31,5.63,5.64] that even shear points at negative normal stresses (tensile stresses) can be measured if the lid of the shear cell is appropriately formed and/or covered with an appropriate adhesive. A yield locus with shear points at negative normal stresses is shown in Fig. 5.30. The tensile strength, σ_t , was measured by first preshearing the bulk solid specimen and then pulling the lid upwards without applying a shear deformation. Therefore the same consolidation procedure was applied prior to measurement of tensile strength as prior to measurement of a point on the yield locus. Thus it is possible to combine the measured tensile

strength with the yield locus. If the specimen had been consolidated in a different way for the tensile strength test, e.g. by uniaxial compression, as in Fig. 2.19 (Sect. 2.7), the combination with the yield locus would be meaningless because of the different consolidation procedures (see Sect. 5.1.3 where the influence of the consolidation procedure is discussed).

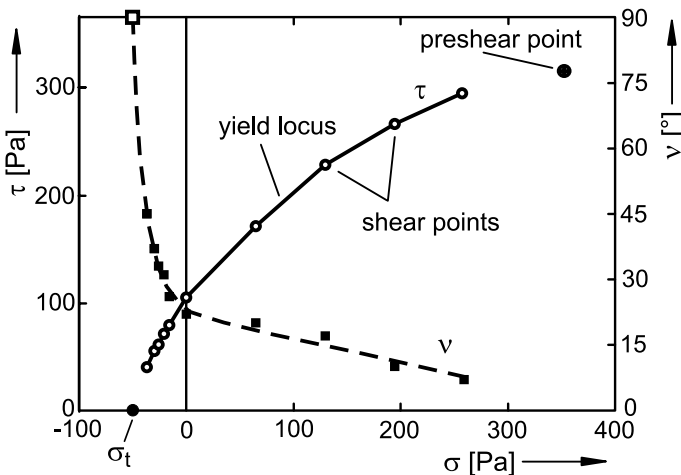


Fig. 5.30. Points on a yield locus of limestone powder and corresponding angles of dilatancy, v , at positive and negative normal stresses (i.e., at compressive and tensile stresses); the point representing the tensile strength, σ_t , was measured by lifting the lid of the shear cell [5.31].

When a consolidated specimen is subjected to a negative normal stress (smaller in absolute value than the tensile strength) and subsequently sheared to failure, the shear stress passes a maximum similar to shear to failure at positive normal stresses (Fig. 5.31). After the maximum the shear stress does not stop decreasing, and the bulk solid in the shear zone dilates increasingly. Finally the strength of the dilated bulk solid becomes too small to withstand the applied tensile stress so the shear cell lid with some bulk solid adhering to it (i.e., the bulk solid located above the shear zone) separates from the rest of the bulk solid specimen. The latter is indicated in Fig. 5.31 by the sudden increase of the measured value of specimen height, h [5.31].

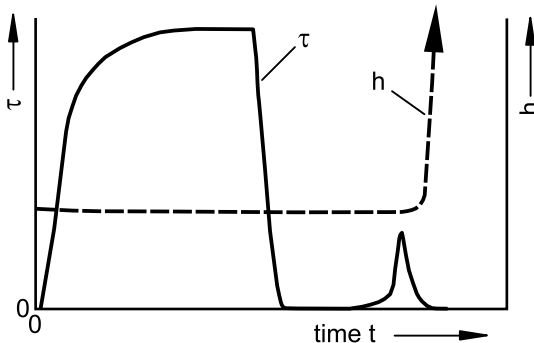


Fig. 5.31. Shear stress, τ , and specimen height, h , at preshear and shear to failure vs. time, t . For shear to failure a negative normal stress (tensile stress) of 20 Pa was applied. After incipient flow and the corresponding shear stress maximum, respectively, was attained, the bulk solid started to dilate until the lid of the shear cell lifted (the upward movement of the lid was indicated by the rapid increase of the measured specimen height, h) [5.31].

In Fig. 5.30 the angle of dilatancy, v , measured for the individual shear points and calculated according to Eq.(5.2), is plotted. The angle of dilatancy of the tensile strength measurement is 90° , because $\Delta h > 0$ and $\Delta y = 0$ (Fig. 5.23, Eq.(5.2)). As already mentioned (Sect. 5.3.1), the angle of dilatancy increases with decreasing ratio of normal stress at preshear to normal stress at shear to failure. This effect is especially pronounced in the range of negative normal stresses.

Assuming isotropic behavior with coincidence of principal stress and principal strain axes (Sect. 5.3.1, Fig. 5.26), the direction of major principal stress can be assessed as a function of the angle of dilatancy (see Fig. 5.32). At steady-state flow, where $v = 0^\circ$, the pair of values of normal stress at preshear and shear stress form the zenith of the Mohr stress circle (like at simple shear, Fig. 5.14.b). In the stress circle the angle between the major principal stress and the zenith is 90° , thus the principal stress plane is inclined by $90^\circ/2 = 45^\circ$ to horizontal. At shear to failure the angle between the major principal stress and the shear point is $(90^\circ + v)$ in the Mohr stress circle, and $(45^\circ + v/2)$ in the bulk solid. Thus the angle between the major principal stresses at preshear ($\sigma_{I,pre}$) and shear to failure ($\sigma_{I,sh}$) is $v/2$ (Fig. 5.32.b).

It was demonstrated in Sect. 5.1.3 that one obtains a smaller unconfined yield strength if the difference between the directions of the major principal stresses at preshear and shear to failure is large (e.g. $> 25^\circ$ for limestone powder, see Fig. 5.11). Thus it has to be expected that the points on the yield locus (shear points) measured at negative normal stresses are influenced by this effect, especially the value of tensile strength, where the

major principal stresses at preshear and at the measurement of strength are inclined by 45° to each other. Therefore the measurement of points on a yield locus at negative normal stresses does not seem to be useful, particularly since tensile stresses are difficult to apply with a shear tester, and only small tensile stresses can be realized [5.31].

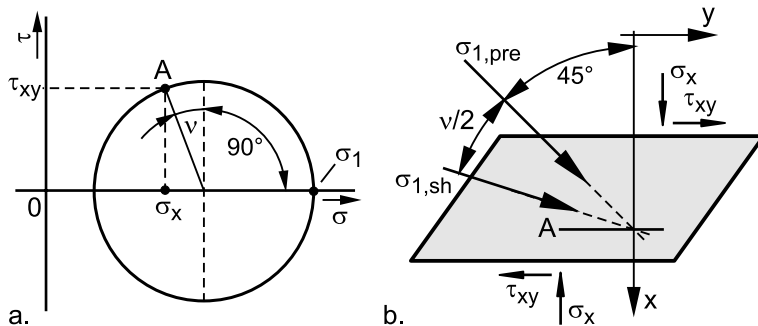


Fig. 5.32. a. Mohr stress circle with shear point (incipient flow) drawn under the assumption of coincidence of principal stress and principal strain axes (see Fig. 5.26); b. bulk solid element (vertical cutting plane) with directions of the major principal stresses at preshear ($\sigma_{1,pre}$) and shear to failure ($\sigma_{1,sh}$). Plane A represents the horizontal plane where the measured shear stress, τ_{xy} , is acting.

At shear to failure at positive normal stresses the angles of dilatancy are small so the principal strain axes at preshear and shear to failure are not inclined to each other by more than $v/2 = (10^\circ \dots 20^\circ)$. For the limestone powder (Fig. 5.11) it was found that the influence on the test results is small if $v/2$ is less than 20° [5.28,5.30]. Unfortunately more detailed investigations on this topic are not available. So it can be concluded that for a usual yield locus test, where cohesion is not of interest, shear points at very small normal stresses should be avoided. Information on the selection of normal stresses is given in Sect. 4.2.1.

In the literature methods for the direct measurement of cohesion or tensile strength in specially suited test devices are proposed (see Sect. 6.3.8, 6.3.12 and 6.3.13). In most of these devices the bulk solid is consolidated by uniaxial compression, which is likely to lead to smaller strength and greater scatter of the results than a consolidation procedure where steady-state flow is attained. More details about these test methods are given in the sections mentioned above.

It can be concluded from the considerations in the present section that tests at very small or negative normal stresses are more difficult and require more effort than at the stresses commonly applied in shear testers,

and such tests can be performed only with a small number of testers, which have to be specially designed or modified for these tests.

However, since the quantities cohesion and tensile strength do not play an important role when bulk solids are handled (in particular, tensile stresses seldom occur in bulk solids flow) and are not required, for example, for the design of bins and silos, there is usually no need to measure them.

5.3.3 Flow properties at very small stresses

In some situations a bulk solid must flow under stresses clearly smaller than 100 Pa, e.g. when very small containers (a few cm³) or dies of tabletting machines are filled. Thus it would be interesting to know the flow properties in this stress range. However, the design of most testers does not allow measurements in this stress range, for example, just by filling powder layers of a few millimeters height, stresses greater than 100 Pa (depending on the bulk density) are possible. Additional stresses may arise due to the weight of parts carried by the bulk solid specimen (e.g. a lid placed on top of the specimen as with the Jenike shear cell). Thus the lower limit of adjustable normal stresses depends on the tester. For the Jenike shear tester it amounts to several 100 Pa, i.e., the smallest consolidation stress, σ_l , of a yield locus is some 1000 Pa [5.62].

Because of the difficulty to measure flow properties at very small stresses, flow properties are usually measured at higher stresses and then extrapolated towards small stresses. Linearity is usually assumed for yield loci, flow functions and steady-state yield loci. The assumption of linearity can be justified by particle interactions [5.65,5.66], and seems to be reasonable in the range of sufficiently high stresses. However at very small stresses the assumption of linearity can be incorrect. The latter has been demonstrated by measurements at very small stresses using a specially designed ring shear tester [5.31,5.63,5.64]. Some results, namely the flow function and the steady-state yield locus, are discussed in the following.

The flow function represents the unconfined yield strength, σ_c , as a function of consolidation stress, σ_l . As an example in Fig. 5.33 the flow function of a cohesive limestone powder at small consolidation stresses is shown. Although the slope of the flow function is small at higher consolidation stresses, the unconfined yield strength decreases clearly with decreasing consolidation at small stresses (say below 500 Pa) where the flow function is close to the line $ff_c = \sigma_c/\sigma_l = 1$. If one were to measure points of the flow function only at stresses higher than, for example, 1000 Pa, extrapolation of the flow function to the left would result in an overestimation of the unconfined yield strength at small consolidation stresses.

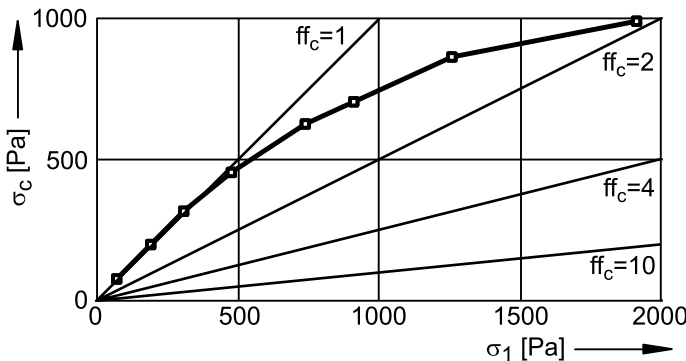


Fig. 5.33. Flow function of limestone powder ($x_{50} = 4.7 \mu\text{m}$) at small consolidation stresses [5.31,5.63,5.64]; lines of constant flowability, ff_c

The yield locus corresponding to the lowest point of the flow function in Fig. 5.33 is shown in Fig. 5.34. Evaluation of the yield locus according to Jenike (shear points are points on the yield locus) results in an unconfined yield strength which is slightly higher than the consolidation stress, and a Mohr stress circle representing steady-state flow which is partially located in the range of negative normal stresses (i.e., $\sigma_2 < 0$). Similar conditions have been found for all yield loci measured with limestone powder at consolidation stresses smaller than 500 Pa. Obviously the unconfined yield strength determined from the instantaneous yield locus can be slightly larger but not much larger than the consolidation stress. Thus at small stresses the flow function is close to the line $ff_c = 1$.

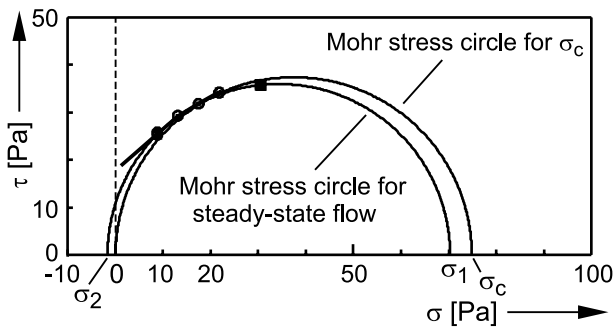


Fig. 5.34. Yield locus of limestone powder ($x_{50} = 4.7 \mu\text{m}$) at a very small consolidation stress (about 70 Pa) [5.31,5.63,5.64]

It has to be mentioned that the yield locus presented in Fig. 5.34 is not exactly covered by Jenike's definitions. According to Jenike, the end point of the yield locus is the point where the yield locus touches the Mohr stress

circle representing steady-state flow (point e in Fig. 3.16). The Mohr stress circle defining σ_c in Fig. 5.34 touches the yield locus to the right of point e, i.e., where it is not defined. Furthermore, it is not possible to draw the effective yield locus (line through the origin and tangent to the Mohr stress circle for steady-state flow) and to determine the effective angle of internal friction, φ_e , because σ_2 is negative for steady-state flow conditions (Fig. 5.34). However, yield loci like that in Fig. 5.34 are sometimes obtained from shear tests (even at higher consolidation stresses than in Fig. 5.34). Considering that with shear testers points of incipient flow (characterized by failure and decrease in bulk density) can be measured even to the right of point e (e.g., Fig. 5.28), and that the determination of a yield locus is based on assumptions (Sect. 5.3.1), it may be reasonable to evaluate yield loci even if this results in $\sigma_2 < 0$ and $\sigma_1 < \sigma_c$, respectively.

The steady-state yield locus is the common tangent of all Mohr stress circles for steady-state flow. In [5.27,5.65,5.66] it is assumed (based on particle interactions) that the steady-state yield locus is a straight line which can be extrapolated to small and negative normal stresses. The assumption of a straight steady-state yield locus can be verified in the range of consolidation stresses typically applied in shear tests (= stress range where tests can be performed with common shear testers, i.e. stresses higher than a few 1000 Pa). In Fig. 5.35.a a steady-state yield locus and Mohr stress circles for steady-state flow are shown for the limestone powder considered in Figs. 5.33 and 5.34. In fact the straight-lined steady-state yield locus is tangent to the Mohr stress circles measured at higher stresses (even to those measured at higher stresses than those drawn in Fig. 5.35.a). But below a consolidation stress (major principal stress) of about 0.5 kPa the Mohr stress circles are clearly below the straight-lined steady-state yield locus. Thus it is likely that the steady-state yield locus is curved in the low stress region.

Although the test results do not support the assumption of a straight-lined steady-state yield locus [5.27,5.65,5.66] in the full range of stresses, the observed behavior seems to be plausible. If the straight-lined steady-state yield locus would be valid even for negative normal stresses, Mohr stress circles would exist which were located (partially or totally) within the range of negative normal stresses (tensile stresses, $\sigma < 0$). Thus it would be possible to obtain steady-state flow when shearing a bulk solid specimen under a negative normal stress. This is contradicted by Fig. 5.35 where the minor principal stresses of the measured Mohr stress circles for steady-state flow remain close to $\sigma = 0$ (Fig. 5.35.b) and do not move farther in negative σ -direction with decreasing major principal stress, σ_1 , as one would expect from a linear steady-state yield locus. Another contradiction is the result of Fig. 5.31 where during shear to failure the bulk solid

specimen dilated until the lid of the shear cell with the bulk solid above the shear zone was lifted by the applied tensile stress so that steady-state flow could not be attained. Considering these observations, the deviation from the straight-lined steady-state yield locus is obviously a result of the inability of bulk solids to withstand considerable tensile stresses (this argument is similar to that regarding the curved shape of a yield locus at small stresses, see Sect. 5.3.2).

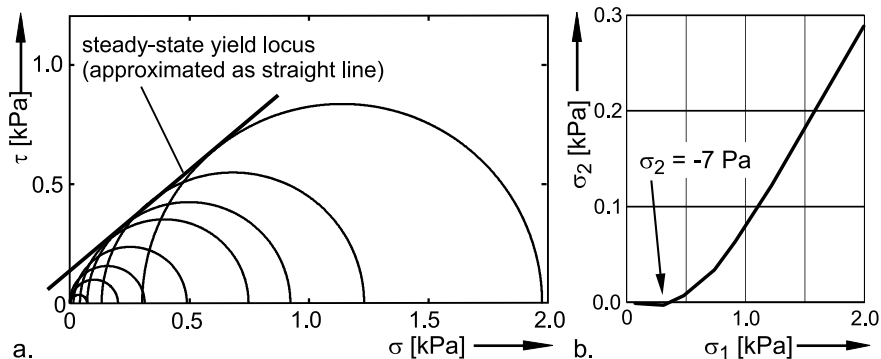


Fig. 5.35. a. Mohr stress circles for steady-state flow at different consolidation stresses; steady-state yield locus approximated by a straight line (limestone powder, $x_{50} = 4.7 \mu\text{m}$); b. minor principal stress vs. major principal stress at steady-state flow [5.31,5.63,5.64]

The sensitivity to tensile stresses at steady-state flow is demonstrated by the following simplified consideration: If a bulk solid specimen is subjected to a tensile stress and sheared (Fig. 5.36.a), the major principal stress, σ_1 , is negative and inclined to the vertical. In Fig. 5.36.b two particle layers within the shear zone are considered. Since a bulk solid has certain elasticity, the interactions with the particles above and below the two layers in Fig. 5.36.b are substituted by tension springs simulating the negative major principal stress.

When the powder is sheared, the particles are moved relative to each other. Thus, particle contacts are replaced by others. Due to the tensile stresses considered here, the total number of contacts decreases. The latter is a result of the elastic tension, here simulated by the tension springs: As soon as two adjacent particles loose contact, the adhesive force (e.g. van-der-Waals force) between these particles decreases sharply, and the particles are pulled away from each other by the force of the springs (i.e., the powder under tension). The increased distance between the particles leads to (1) the number of contacts decreasing with time, and (2) new contacts with smaller adhesive forces. Hence, the tensile stress transferable by the

powder decreases with increasing shear deformation. Finally the powder specimen fails because it cannot withstand the applied tensile stress (an example of this is shown in Fig. 5.31 where the lid of the shear cell with some adhering powder layers is lifted during shear to failure).

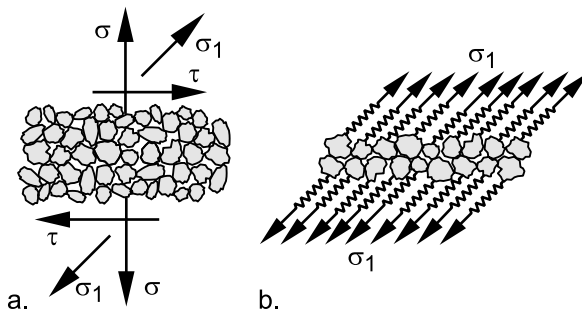


Fig. 5.36. a. Stresses during shear of a bulk solid specimen subjected to a tensile stress ($\sigma < 0$); b. simple particle model with tension springs

The particle model demonstrates that shear deformation under considerable tensile stresses leads to increasing dilation of the specimen. Thus steady-state flow is not possible. Therefore Mohr stress circles which are located in total (or at least to a major part) in the tensile stress region ($\sigma < 0$) do not exist. This is clearly demonstrated by the Mohr stress circles (left part of Fig. 5.35.a) and the minor principal stresses (Fig. 5.35.b) at small major principal stresses: When the major principal stress decreases, the minor principal stress remains in the vicinity of zero. Thus the steady-state yield locus is not linear, but curved downwards in the range of small stresses.

From the considerations in the present section it can be concluded that extrapolation of flow properties toward very small stresses can be difficult. On the other hand, measurements at very small stresses, especially if accurate results are desired, are time-consuming and difficult [5.31] so that at present routine tests at very small stresses do not seem to be practical.

5.4 Influence of velocity

For the measurement of flow properties with shear testers, usually shear velocities (relative velocity between top and bottom of the bulk solid specimen; specimen height is typically on the order of a few centimeters) of about 1 mm/s to 2 mm/s are applied. Since the yield limit (yield locus) is measured, the transition from a state of rest to a state of flow (incipient

flow) is of interest. This transition can be easily determined at small velocities because there is sufficient time to observe the measured shear stress and inertia forces can be neglected. Also in most practical situations (bins, hoppers, silos) a bulk solid flows with relatively small velocities below 1 m/s.

Compared to liquids, shear stresses in bulk solids are much less sensitive to shear velocity. For small flow velocities (say < 1 m/s) this influence is usually neglected. On the other hand, the stress level (liquids: pressure level) does not have much influence on the shear stresses in a liquid, but is the dominant quantity regarding shear stresses developing in bulk solids. Since in a flowing bulk solid particles (= solid bodies) move relative to each other, parallels to solid friction can be found, where, for example, microscopic deformations at contact points play an important role. Depending on the material behavior, shear stress can increase or decrease. Measurements have shown that shear stress can change on the order of several percent per decade increase in shear velocity. More pronounced effects on shear stress are observed during sudden changes of shear velocity, which therefore have to be avoided when measuring flow properties of bulk solids. The velocity influence is discussed further in Sect. 7.1.1.

For rapid flow of bulk solids, i.e. flow at velocities of several m/s, other mechanisms have to be taken into account, which are not discussed here. At these velocities collisions between particles play an increasing role, and shear stress usually increases with velocity [5.43].

6 Discussion of testers and test procedures

Shear testers are the standard testers in bulk solids technology. Although the results are based on assumptions and approximations, e.g., assumptions for evaluation of a yield locus (Sect. 5.3), relatively much is known about conditions in the bulk solid specimen from hundreds of publications on the results of research projects carried out in many countries. In addition, decisions on the design of hoppers and silos, and, thus, on large investments, are based on the results obtained with shear testers.

If test results are needed for comparison of bulk solids rather than for equipment design, often simple test methods (“simple testers”) are sought. In addition, sometimes shear testers are regarded with a certain amount of reserve since at first sight the presentation of test results with yield loci and Mohr stress circles is complicated. Thus, for the assessment of flowability sometimes other test devices than shear testers are used. Some of these simple test devices are based on other test methods and measure other physical quantities. Because it is often claimed that flow properties, or at least the flowability of powders and bulk solids, can be measured with such simple testers, one must assess their quality by applying the same criteria as for shear testers. The latter is done in the present chapter.

6.1 Influences on test results

6.1.1 Procedure and principal stresses

Since test results depend on a number of influencing variables and conditions, test methods with clearly defined conditions should be preferred. Based on the properties of bulk solids discussed in Chap. 5, one can derive basic rules for the measurement of flow properties, e.g., unconfined yield strength, σ_c , which is especially important for silo design for flow as well as for the determination of flowability:

- The consolidation procedure should end with steady-state flow since this eliminates the influence of deformation history (filling, preceding deformation), and one obtains the greatest strength at a given consolidation pressure.

tion stress (greater than after uniaxial or biaxial consolidation, see Fig. 5.12). Furthermore, steady-state flow prevails only after the whole bulk solid specimen is sufficiently consolidated, so the state of consolidation can be checked by observing the stresses during consolidation.

- Here the term “steady-state flow” means that the stresses (if a shear tester is used: shear stress) do not increase further during consolidation (preshear). If this is observed, the consolidation process has to be stopped. The specimen should not be deformed further to the point that the stresses decrease, e.g., due to localization (Sect. 5.2), and become constant at a lower level of stress. The latter would lead to too small stresses at failure (shear tester: too small shear stress at incipient flow) and, thus, to too small values of unconfined yield strength, σ_c .
- The major principal stresses should have the same orientation at consolidation (preshear) and at measurement of strength (shear to failure).
- During a test the deformation rate (e.g., shear velocity of a shear tester) must not change suddenly.

These conditions are largely fulfilled with shear testers. The principal stresses at preshear and shear to failure have similar orientations if the normal stress at shear to failure is sufficiently high (see Sect. 5.3.2). For instance, in the shear cell of the Jenike shear tester (Fig. 6.1) the major principal stress is inclined to vertical by about 45° at preshear ($\sigma_{I,pre}$), and by slightly larger angles at shear to failure ($\sigma_{I,sh}$). For such small differences the influence of the principal stress orientation is small and, thus, can be neglected (Sects. 5.1.3 and 5.3.2). The condition “consolidation until steady-state flow is attained” is also fulfilled with a shear tester if the test is run correctly.

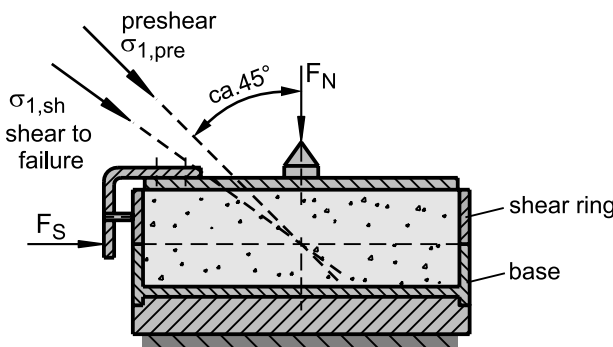


Fig. 6.1. Directions of the major principal stresses at preshear ($\sigma_{I,pre}$) and shear to failure ($\sigma_{I,sh}$) in the shear cell of a Jenike shear tester (qualitatively)

In contrast to a shear tester, the uniaxial compression test (Sect. 3.1, Fig. 3.1) does not fulfill all conditions listed above. The principal stresses at consolidation as well as at strength measurement are oriented vertically, but the consolidation procedure is uniaxial compression. This corresponds to procedure I in Sect. 5.1 (Fig. 5.2) which is likely to lead to a too small value of unconfined yield strength, σ_c , compared to a procedure where steady-state flow is attained at the end of consolidation.

Another advantage of the procedure “consolidation until steady-state flow is attained” compared to uniaxial compression is that less scatter of test results can be expected: Since preshear is only terminated when shear stress does not increase further, the actual state of consolidation can be observed. As long as no insufficiently consolidated regions exist in the bulk solid specimen, the shear stress will increase further. Inhomogeneities (e.g., voids or regions of low density), which can form when the specimen is filled into the test container, are removed to a certain extent by the shear deformation at preshear.

A condition of great importance is the defined state of consolidation prior to measurement of strength. Thus, if the strength of a consolidated specimen has been measured once, the specimen must be consolidated again before its strength can be measured a second time. Therefore, when measuring a yield locus with a shear tester, the specimen must be pre-sheared prior to shear to failure (see procedure described in Fig. 3.14).

Sometimes procedures are published which do not follow this principle. Enstad et al. [6.1] described a procedure where a specimen is presheared with a Jenike shear tester only once. Subsequently it is sheared to failure several times at different normal stresses without being presheared in between (Fig. 6.2.a). Since shear to failure goes along with dilation of the bulk solid specimen, the specimen is less consolidated after shear to failure than before. Thus, the shear stresses at incipient flow of the second and all following shear points are too small, i.e., several points of the yield locus are shifted towards lower shear stresses.

A similar effect takes place with the procedure described in [6.2,6.3], where the bulk solid specimen is first presheared with a translational shear tester (equipped with a shear cell similar to the Jenike shear cell). After steady-state flow is attained, the normal stress is continuously reduced (Fig. 6.2.b). With decreasing normal stress, the measured shear stress also decreases. The idea behind this procedure is that the stress path in the σ,τ diagram is identical to the yield locus. However, a yield locus represents failure conditions, and, as outlined in the paragraphs above, failure changes the density and, thus, the state of consolidation of the bulk solid specimen. If the stress path in Fig. 6.2.b would be a yield locus, the state of failure without any change of density and strength had to be preserved dur-

ing a certain time period. This is unlikely to occur because the bulk solid specimen dilates when being sheared under normal stresses smaller than the normal stress at preshear, σ_{pre} , so the state of consolidation deviates increasingly from its initial state obtained with preshear. Therefore, it is to be expected that the yield locus is shifted towards smaller stresses [6.4–6.7].

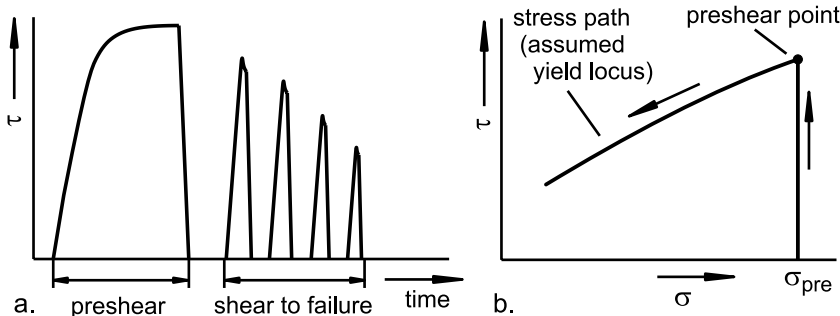


Fig. 6.2. a. Shear stress vs. time when the specimen is presheared once and subsequently several points of incipient flow are measured [6.1]; b. stress path in a σ,τ diagram when measuring a yield locus following the procedure described in [6.2,6.3] (direction given by arrows). After steady-state flow is attained (preshear point), the normal stress is continuously reduced which leads to dilation and decrease of shear stress (see stress path).

Considering the problems of the procedure in Fig. 6.2.b, Haaker et al. [6.6, 6.7] modified a shear cell (similar to a Jenike shear cell) to keep the specimen volume constant during shear to failure. Thus the dilation at shear to failure could be avoided, i.e., the properties of the specimen remained nearly constant. With this cell it was possible to measure a complete yield locus in one test with a procedure similar to that in Fig. 6.2.b. The test results agreed well with yield loci measured in the usual way (preshear and shear to failure, Fig. 3.14). However, this procedure is not commonly applied because it requires a more complicated tester compared to standard shear testers (Jenike tester, ring shear tester). Thus, shear testers are usually operated following the procedure proposed by Jenike, where a specimen is presheared prior to shear to failure.

6.1.2 Stresses in the measuring plane

Stresses in the measuring plane, e.g., the failure plane within the bulk solid specimen, must be known in order to obtain a quantitative result. For instance, in the shear cell of a Jenike shear tester (Fig. 6.1) the measuring

plane is located at the separation between the shear ring and the base. With a slight rise of the shear ring prior to the shear test, any contact between these rings is avoided. Therefore, any measured shear force is not affected by possible friction forces between the rings. This also applies to the normal force [6.8]. With this procedure, the **average** normal stress and **average** shear stress in the measuring plane are clearly known.

Further, the stresses anywhere in the measuring plane should be equal (homogeneous stress distribution). If this was not the case, the bulk solid at the consolidation stage (preshear) would be consolidated differently at various locations and one would measure subsequently (at shear to failure) the average strength of the variable range of consolidation within the bulk solids sample.

Inhomogeneities of stresses can be found, for example, in the Jenike shear cell close to the walls of shear ring and base, especially, as viewed in shear direction, in the front and rear parts of the specimen [6.9]. Since the inhomogeneities are limited to small regions, one obtains sufficiently reliable results. The latter has been demonstrated by comparative tests with more sophisticated testers [6.6, 6.10–6.15].

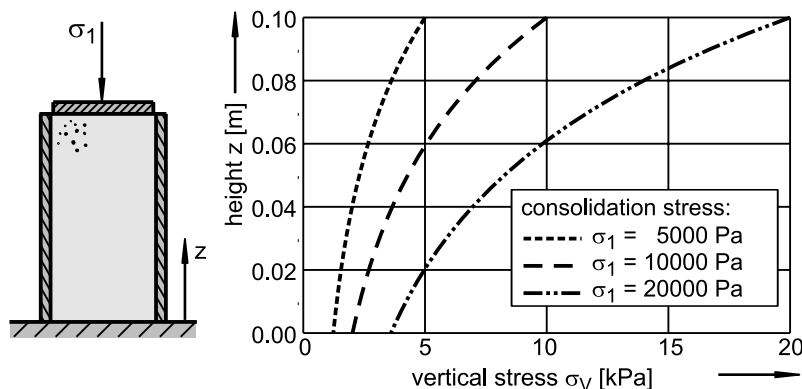


Fig. 6.3. Vertical stress at uniaxial compression in a hollow cylinder (specimen diameter 5 cm, specimen height 10 cm, wall friction angle $\varphi_x = 30^\circ$, stress ratio $K = 0.4$, bulk density $\rho_b = 1000 \text{ kg/m}^3$)

The problem of testers in which the stresses acting in the specimen are not known exactly is demonstrated by the uniaxial compression test (see Sect. 3.1, Fig. 3.1). The vertical stress in the specimen, σ_v (= consolidation stress, σ_1), decreases downwards due to friction at the cylinder wall (Fig. 6.3). The stress decrease depends on the bulk solid properties (stress ratio, wall friction angle), i.e., neither the course nor the mean value of the vertical stress is known. The calculated stresses in Fig. 6.3 (for the calculation

of stresses refer to Sect. 9.2) demonstrate that the relative decrease of vertical stress, σ_V , towards the bottom of the cylinder is larger, the greater the consolidation stress. Furthermore, the decrease of vertical stress is especially pronounced in the top part of the specimen. Thus, the applied vertical stress is acting only close to the top platen. If subsequently the compressive strength is measured, failure will occur more likely in the less consolidated bottom part of the specimen. This leads to underestimation of the bulk solid's strength.

6.2 Requirements for testers to measure flow properties

To obtain a quantitative statement regarding the flowability of a bulk solid, as described in Sect. 3.1.4, a defined measurement of strength is required following the above mentioned defined consolidation of the test specimen. Only in this way can test results be applied quantitatively (e.g., for silo design for flow), and a comparison of the flow properties of bulk solids is possible independent of the test apparatus.

If one does not need a quantitative statement, then all tests are in principle possible where a test specimen is somehow consolidated and its strength subsequently somehow determined. As indicated in the previous sections, the effects of wall friction, anisotropy, etc., may reduce the accuracy and, thus, the applicability of the results.

Further useful features of a test apparatus are:

- Variation of consolidation stress: This allows adjustment of consolidation stress to the situation where a bulk solid is stored or handled. Thus the test results are more representative of the actual problem which is especially important if the test results have to be applied quantitatively.
- Measurement of time consolidation: Often problems occur in situations where the bulk solid has been stored at rest for a long time period in a silo, an IBC, or even in a small container. Possible problems due to time consolidation are the formation of lumps, or the formation of flow obstructions such as stable arches. Time consolidation can be quantified only by time consolidation tests. It cannot be determined from the instantaneous properties.

Based on these features as well as on the requirements outlined in Sect. 6.1, a list of criteria can be developed for a test apparatus which provides quantitative results of flowability and other flow properties as defined in Chap. 3. The last two criteria (6 and 7) should be regarded as desirable capabilities which are not necessary if only flowability has to be determined.

1. Consolidation procedure with subsequent measurement of strength.
2. Consolidation of the bulk solid test specimen until steady state flow has been reached (preshear).
3. Not too much difference in directions of load application, i.e., similar orientations of the major principal stresses during consolidation and measurement of strength
4. Reproducible load application of the bulk solid specimen for consolidation (4a) and for measuring strength (4b).
5. Known average stresses in the measuring plane with possibly the most uniform stress distribution for consolidation (5a) and for measuring strength (5b).
6. Possibility for varying consolidation stresses (adjustment to application of test results).
7. Possibility for measuring increase of strength with time (time consolidation; if required for the application).

6.3 Measuring techniques and equipment (overview)

In the following, some measuring techniques and equipment for the evaluation of the flowability of bulk solids are explained based on earlier publications of the author [6.16,6.17]. The test methods have been selected with the intention to demonstrate the variety of physical principles applied. Some of the techniques are applied in practice, others have been proposed in publications. Apparatus that will only be used in the framework of research (e.g. [6.6, 6.11–6.13,6.15,6.18]) are not included (overview: see [6.10,6.19,6.20]). The inclusion of a particular tester in the following survey does not mean that this tester makes sense from the point of view of bulk solids mechanics. On the other hand, there may exist useful testers which are not listed here.

The measuring techniques are going to be discussed with respect to their application for the determination of flowability, ff_c , as defined in Sect. 3.1.4, whereby the criteria listed in Sect. 6.2 are applied. In order to be complete, techniques will also be included which do not cover a measurement of flowability according Sect. 3.1.4, but assist in evaluation of the flow properties established by other means. Such techniques may be useful, for example, if a specific application is simulated by the measuring technique but the technique does not fulfill the criteria defined in Sect. 6.2.

It must be accepted that any schematic listing of the many measurement techniques will not be precise in all aspects. An apparently poor evaluation does not necessarily exclude application of the equipment for special pur-

poses. Thus, nobody shall be prevented from purchasing or using any of the techniques discussed here. When in doubt, before the procurement of any new equipment one must review what must be measured and whether that piece of equipment can produce the required information, such as stress levels, condition of the bulk solids, storage time, etc. It is recommended to experiment with different types of equipment.

The explanation of the measuring technique is presented in a simplified schematic form for the most important measurement value. Subscript "V" indicates a consolidation of the bulk solid specimen for the measurement, subscript "M" indicates the measured value (such as m for mass, F for force, M for moment, p for pressure, α for angle, d for diameter, t for time and ρ_b for bulk density). " F_N " indicates a normal force which is applied to the bulk solid specimen during the test. After a short description of the measuring principles and some general comments, a table follows with a listing describing the compliance with criteria 1 to 7 from Sect. 6.2. If any criterion is not applicable, a “–” sign is noted in the column.

Evaluation of the correctness of a measuring technique (“general comments” in Sects. 6.3.1 to 6.3.20) establishes, in comparison with the Jenike shear tester, that the criteria of a measurement technique mentioned in Sect. 6.2 are (nearly) completely fulfilled. The use of the term “quantitative statement” means that these measurements have similar values for strength as obtained from the Jenike shear tester. “Limited quantitative statement” means that the measured values differ somewhat from those obtained with the Jenike shear tester, while one of the criteria 1 to 7 from Sect. 6.2 is not or not completely met. “Qualitative statement” means that at least two of the criteria are not met, so that the results deviate more from the truth (e.g. due to unknown stresses, or the influence of other parameters such as permeability).

Assessment of the measuring techniques focuses on the test principle and the physical processes in the bulk solid specimen. Other criteria, e.g., user-friendliness, quality of the apparatus, appropriate design, are not taken into account. These points have to be considered on each type of tester. Even shear testers can lead to incorrect results, such as by inappropriate design (e.g., if test results are influenced by friction in the shear cell or in bearings, or if normal stresses cannot be adjusted accurately), inappropriate test procedure (e.g., incomplete preshear, or too large shear deformation, see Sect. 5.2), or inappropriate operation (e.g., by ignoring the prescribed test procedure) [6.21,6.22].

6.3.1 Funnel

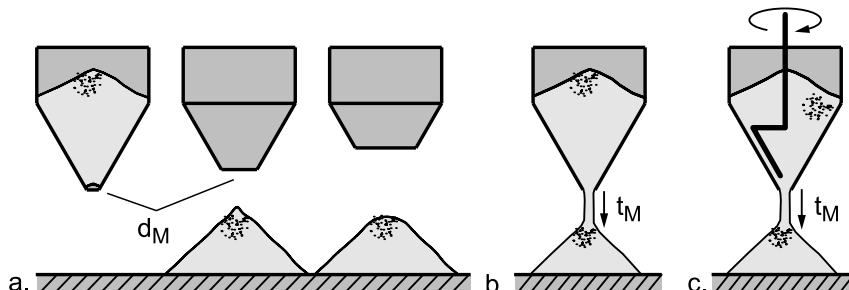


Fig. 6.4. a. Funnels with varying outlet diameters, b. funnel for measuring time of discharge; c. like b., additionally equipped with a stirrer acting as discharge aid

Description:

Bulk solids are fed through a funnel with varying outlet diameters (Fig. 6.4.a). Measurement of flowability is the minimum size of the outlet, d_M , at which flow occurs [6.23].

Alternative: measurement of the time, t_M , required to discharge the solids through a given outlet size (Fig. 6.4.b). Sometimes discharge aids (e.g., stirrer in Fig. 6.4.c) are installed to avoid flow obstructions with cohesive bulk solids. The shorter the time, the better the rating of flowability [6.24, 6.25].

General comments:

This is a simple comparison test without a quantitative statement concerning flowability and time consolidation. The filling method (influence of the operator) as well as the flow regime (mass flow or funnel flow, see Sect. 10.1) may affect the measurement. Furthermore, the mass flow rate is influenced by the permeability of the bulk solid, since a slight vacuum prevails in the bulk solid flowing downwards the hopper. Due to the vacuum, air flows from the outlet upwards into the bulk solid (countercurrent air flow) [6.26] (see Sect. 12.1). For the same reason the actual filling height plays a role: At small filling levels air can flow from the top into the bulk solid in the hopper thus reducing the air flow from the outlet. If discharge aids are used, the result (t_M) is affected by its design and operation (e.g., stirrer speed).

Table 6.1. Evaluation (funnel)

Criterion	1	2	3	4a/4b	5a/5b	6	7
Fulfillment	no	–	–	–	–	–	no

6.3.2 Angle of repose

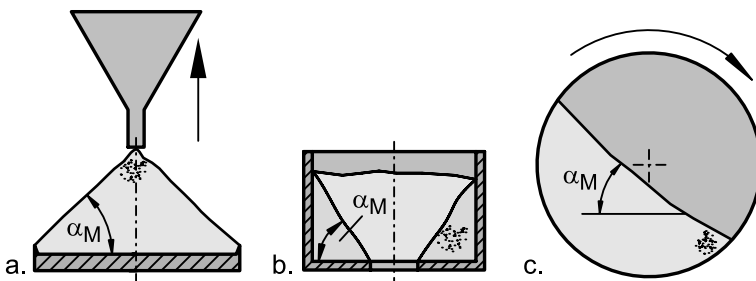


Fig. 6.5. Measurement of angle of repose; a. poured angle of repose (conical pile); b. drained angle of repose; c. dynamic angle of repose

Description:

Angle of repose, α_M , is the slope of a more or less conical pile of loose, uncompacted bulk solid [6.27,6.28] (Fig. 6.5.a). The pile is usually formed by pouring the bulk solid through a funnel which is located above a bottom plate. The funnel can be either fixed or moved upwards while the pile is formed in order to keep the distance between the tip of the pile and the funnel constant. To avoid the influence of the surface of the bottom plate, it is provided with a protruding outer edge to retain a layer of bulk solid [6.24].

A different approach is the measurement of drained angle of repose [6.26,6.29,6.30], which is the slope angle, α_M , of the material remaining in a container with flat bottom and central outlet after discharge (Fig. 6.5.b). Other test set-ups allow measurement of the drained angle of repose on plane or convex surfaces, whereby different surface shapes result in different angles [6.30].

Dynamic angle of repose (Fig. 6.5.c) is measured in a slowly rotating cylinder with horizontal axis [6.24,6.30]. Depending on the revolving speed and the bulk solid properties one obtains a more or less varying surface slope [6.30]. Especially with cohesive materials it can be observed that the bulk solid does not flow downwards continuously, but in avalanches, i.e., the bulk solid does not slide continuously across the surface (see Sect. 6.3.3). The latter makes the determination of angle of repose more difficult.

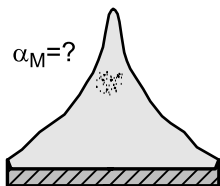


Fig. 6.6. Conical pile with varying angle of repose often observed with cohesive bulk solids [6.30]

General comments:

This is a simple comparison test without a quantitative statement concerning flowability and time consolidation. The slope angle in Fig. 6.5.a results from material properties at very low compaction, which occurs at the surface of the pile. Furthermore, since the bulk solid is falling from above and then sliding downwards on the surface, dynamic effects may play a role. No statement is possible about the behavior of the material under greater stresses (as in a bin, silo, or container) or about time consolidation. With cohesive powders heaps with a peaked tip often can be observed (Fig. 6.6).

When measuring drained angle of repose (Fig. 6.5.b), the bulk solid is somewhat consolidated by the stresses acting in the test mold after filling. The larger the stresses (e.g., due to a high bulk density or a large filling height), the steeper the slope angle of the remaining material.

In general, angle of repose is dependent on the test procedure (e.g., the way the heap is formed) and, thus, it is not an intrinsic property of the bulk solid [6.24,6.30]. This is also true for the dynamic angle of repose, which depends on the revolving speed, [6.30], the degree of air entrainment due to the constant movement of the material, which can lead to a state of fluidization, and the ratio of particle size to cylinder diameter [6.31]. Even segregation and agglomeration can occur in the revolving cylinder thus influencing the result.

Table 6.2. Evaluation (angle of repose)

Criterion	1	2	3	4a/4b	5a/5b	6	7
Fulfillment	no	-	-	-	-	-	no

6.3.3 Avalanching

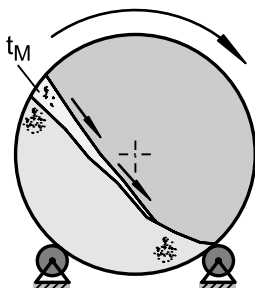


Fig. 6.7. Avalanching in a revolving cylinder

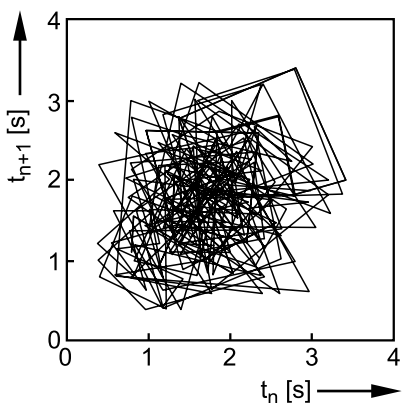


Fig. 6.8. Result of an avalanching test (strange attractor) ([6.32,6.33])

Description:

The set-up of the avalanching test is similar to the measurement of dynamic angle of repose. The bulk solid in the revolving cylinder forms an inclined surface on which material flows downwards (Fig. 6.7). Avalanches can be observed especially with cohesive bulk solids. Since avalanching is a chaotic process, it is not possible to predict the magnitude of the avalanches. As common in chaos research, a “strange attractor” is plotted for representation of the results (Fig. 6.8) [6.34]. During an avalanche test, the time, t , between two successive avalanches is measured. This time is a measure of the size (mass) of the avalanche. To obtain the strange attractor, time t_{n+1} is plotted vs. time t_n with n being the number of the avalanche. The larger the scatter of times, t_n , the larger the area where points (t_n, t_{n+1}) are found. The size of this area and the position of its center are considered as a measure for flowability.

General comments:

Here the same comments as given for the dynamic angle of repose (Sect. 6.3.2) are valid. Depending on the bulk solid, the constant movement of the material may lead to segregation, agglomeration, or air entrainment resulting in fluidization. In [6.35] it is reported that the avalanching test did not show differences between cohesive powder samples of different flowability according to another measuring technique.

Table 6.3. Evaluation (avalanching)

Criterion	1	2	3	4a/4b	5a/5b	6	7
Fulfillment	no	–	–	–	–	–	no

6.3.4 Imse test

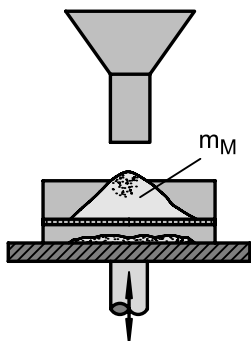


Fig. 6.9. Principle of the Imse test

Description:

Bulk solid is put into a funnel located on top of a sieve: the funnel is then slowly raised (Fig. 6.9). Subsequently the sieve is vibrated with the aid of a vibrating table. A measure of flowability is the mass m_M which is left on the sieve (smaller mass = better flowability) [6.36].

General comments:

This is a simple comparison test (initially for cement) without a quantitative statement concerning flowability and time consolidation. Similar to the funnel test (Sect. 6.3.1), the results are dependent on the experimenter (process of filling) and on the degree of aeration. No statement is possible for the material under greater stresses as they occur, for example, in a silo.

Table 6.4. Evaluation (Imse test)

Criterion	1	2	3	4a/4b	5a/5b	6	7
Fulfillment	no	–	–	–	–	–	no

6.3.5 Carr flowability index

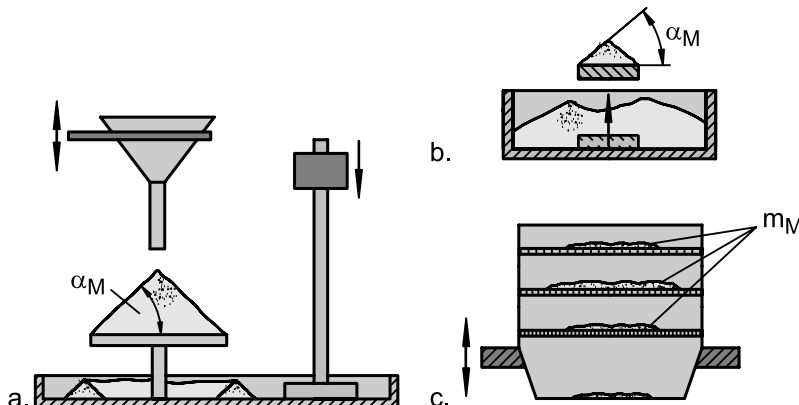


Fig. 6.10. Tests for determination of the Carr index [6.37–6.41]; a. angle of repose (with angle of fall); b. angle of spatula; c. sieving

Description:

This is a combination of different tests; in order to determine flow behavior the following measurements are made [6.37–6.41]:

- Figure 6.10.a: The angle of repose, α_M , of the material is measured after it has been poured from a vibrating funnel onto a round platen (see Sect. 6.3.2). For determination of a floodability index, the so-called angle of fall is measured, which is the slope angle, α_M , after the platen has been shocked five times by a falling weight.
- Angle of spatula (Fig. 6.10.b): The slope angle, α_M , of the material on a spatula is measured, after the spatula has been lifted up with material outside the container (similar to the determination of drained angle of repose, Sect. 6.3.2).
- Screening of bulk solids with a defined oscillation over a predetermined time span on three sieves with different openings (Fig. 6.10.c), and then determining the mass m_M of bulk solid left on each screen.
- Determination of loose (specimen filled loosely into the test container) and tapped bulk density; alternative (for larger solids): computation of a characteristic value describing the width of the particle size distribution.

Each one of the above tests (excluding the angle of fall) provides a number between 0 and 25. The sum of the four tests becomes the flowability index. Further tests (e.g., determination of the fall angle) allow determination of the floodability index indicating the tendency of the bulk solid to flood due to interstitial gas overpressure.

General comments:

This is a qualitative comparison test for fine-grained bulk solids without a quantitative statement concerning flowability and time consolidation as defined in Sect. 3.1.

Table 6.5. Evaluation (Carr flowability index)

Criterion	1	2	3	4a/4b	5a/5b	6	7
Fulfillment	no	-	-	-	-	-	no

6.3.6 Stirrer

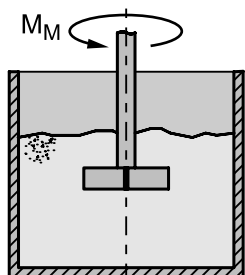


Fig. 6.11. Stirrer

Description:

The bulk solid is filled in a container equipped with a stirrer (Fig. 6.11) which can have vertical or inclined stirrer blades of various shapes. Flowability is assessed by the torque, M_M , measured as a function of time or rotational speed, or by the energy transferred to the bulk solid [6.42]. Sometimes the vertical force on the stirrer is measured.

General comments:

The material is tested in a moving and aerated mode. The stresses acting in the shear zone of complicated geometry are not known. Therefore, a quantitative statement cannot be made concerning flowability and time consolidation as defined in Sect. 3.1. Due to the action of the stirrer, fluidization or agglomeration may arise thus influencing the test result.

Table 6.6. Evaluation (stirrer)

Criterion	1	2	3	4a/4b	5a/5b	6	7
Fulfillment	no	-	-	-	-	-	no

6.3.7 Compressibility test

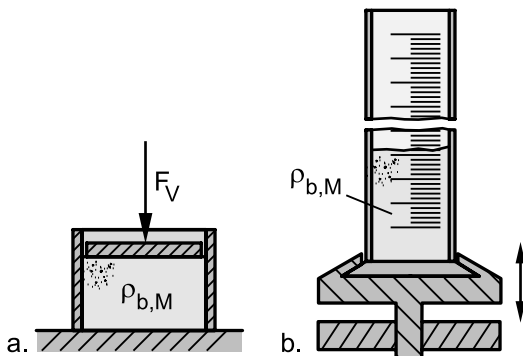


Fig. 6.12. a. Principle of a compressibility test; b. determination of tapped density in a tap vial

Description:

A bulk solid sample is compacted under increasing vertical stress or vertical force, F_V , respectively (Fig. 6.12.a). From the increase in bulk density, ρ_b , as a function of the vertical stress the flow behavior is evaluated (poorer flow behavior with increasing compressibility) [6.43]. An often used method is the determination of compressibility from only two quantities: the bulk density of the specimen poured loosely into the test container (aerated or loose bulk density, ρ_{b0}) and tapped density, ρ_t . The tapped density is determined with a tap vial (Fig. 6.12.b) [6.44–6.46]. Here the specimen is poured into a test cylinder which is then tapped against a hard surface a specified number of times. The tapped density, ρ_t , is determined from the mass and final volume of the specimen.

From the aerated and tapped densities different parameters can be derived, e.g., compressibility index, K_I (also known as Carr compressibility index), and Hausner ratio, H [6.24,6.30,6.47]:

$$K_I = \frac{\rho_t - \rho_{b0}}{\rho_t} \cdot 100\% \quad (6.1)$$

$$H = \frac{\rho_t}{\rho_{b0}} \quad (6.2)$$

A compressibility index $K_I = 0$ or a Hausner ratio $H = 1$, respectively, indicate an incompressible bulk solid ($\rho_t = \rho_{b0}$). This is interpreted as the best possible flowability. The larger the values of K_I or H , the poorer the flowability.

General comments:

This test is based on the influence of interparticle adhesive forces on bulk density: in loose bulk solids of poor flowability relatively large voids (high porosity) are formed due to the action of adhesive forces. This is not the case with free-flowing bulk solids. Thus it is to be expected that poorly flowing bulk solids are more compressible.

The test results are device-dependent [6.24,6.46], e.g., the diameter of the test cylinder and the magnitude of the taps play a role. Inertia forces acting on the bulk solid due to the taps depend on the stiffness of both the apparatus and the bulk solid. Thus, the compressibility test is a qualitative comparison test for fine-grained bulk solids without a quantitative statement concerning flowability and time consolidation as defined in Sect. 3.1.

Table 6.7. Evaluation (compressibility test)

Criterion	1	2	3	4a/4b	5a/5b	6	7
Fulfillment	no	–	–	–	–	–	no

6.3.8 Cohesion tester, flowability test

Description:

The “Warren Spring Bradford cohesion tester” [6.48,6.49] consists of a cylindrical test mold containing the bulk solid specimen (Fig. 6.13.a). First the specimen is vertically compacted (force F_V). After removal of the vertical load, a vaned paddle is lowered into the bulk solid (arrow v) until the top edge of the vanes is level with the surface of the bulk solid, and then rotated. From the maximum torque (M_M) measured at failure a shear stress is calculated and interpreted as cohesion (see Sect. 3.2.3.3).

A similar test is the “Flowability Test” (Fig. 6.13.b) [6.50]: The bulk solid specimen is first consolidated by applying a vertical force (F_V) on the top platen, while a stirrer is already within the bulk solid specimen. The plate is subsequently raised and the stirrer is slowly turned. The torque, M_M , is measured over the turning angle. Flowability is assessed based on the measured torque, e.g., the maximum torque at failure [6.50].

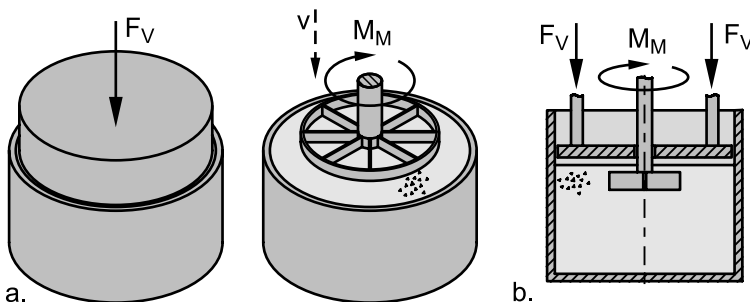


Fig. 6.13. a. Warren Spring Bradford cohesion tester [6.48,6.49]; b. flowability test [6.50]

General comments:

The bulk solid is consolidated uniaxially (no steady-state flow). The direction of the major principal stress at failure is inclined to the major principal stress at consolidation (vertical) by at least 45° . When turning the vaned paddle or stirrer, respectively, a force is applied by the vanes or stirrer blades only locally, so the deformation depends on radius. The stresses in the complex shear plane (plane of failure) are not known. Thus the test can be regarded as a qualitative comparison test concerning cohesion.

Table 6.8. Evaluation (cohesion tester, flowability test)

Criterion	1	2	3	4a/4b	5a/5b	6	7
Fulfillment	yes	no	no	yes/yes	yes/no	yes	yes

6.3.9 Penetration test

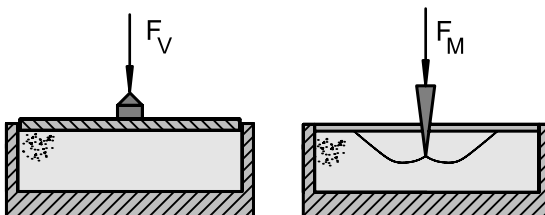


Fig. 6.14. Penetration test

Description:

The bulk solid test specimen is compacted vertically (force F_V , Fig. 6.14). Subsequently, a pointed probe is pushed from the top into the material, and the penetration force, F_M , is measured. With sufficient force fail-

ure occurs along curved slip lines. The bulk solid strength is determined from the force measured at the moment of failure [6.51].

General comments:

This is a qualitative comparison test concerning flowability. Measurement of time consolidation (qualitative) is possible. However, there is no quantitative statement concerning flowability and time consolidation. The stresses in the shear plane (curved slip lines) are not known.

Table 6.9. Evaluation (penetration test)

Criterion	1	2	3	4a/4b	5a/5b	6	7
Fulfillment	yes	no	no	yes/yes	yes/no	yes	yes

6.3.10 Uniaxial compression test

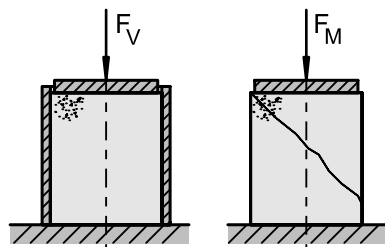


Fig. 6.15. Uniaxial compression test

Description:

See the description of the uniaxial compression test in Sect. 3.1; for applications refer to [6.12, 6.52–6.55]. In order to minimize the effect of friction between the solids and the cylinder wall (see Fig. 6.3), the wall must be “friction-free”. This may be nearly achieved if the wall is covered with a layer of rubber or plastic and a lubricant is placed between the wall and the layer [6.52].

General comments:

If the walls are friction-free (lubricated), this test results in a limited quantitative statement concerning flowability and time consolidation for cohesive bulk solids with a tendency for smaller strength values because of the consolidation procedure “uniaxial compaction” (see Sect. 6.1). If the walls are not friction-free, the consolidation stress may strongly decrease downwards (see Fig. 6.3) thus leading to a severe underestimation of the strength (tests results reported in [6.56] show that in this case the measured strength can be 50% or less compared to the results of a shear tester), so

that the measured strength additionally depends on the wall friction angle. Further, even with lubricated walls, there is a danger of non-homogeneity (no homogenizing effect of steady-state flow, see Sect. 6.1.1). A useful application of the uniaxial compression test is the measurement of time consolidation of coarse solids (with lubricated walls, see description).

Table 6.10. Evaluation (uniaxial compression test)

Criterion	1	2	3	4a/4b	5a/5b	6	7
Fulfillment	yes	no	yes	yes/yes	yes*/yes	yes	yes

* if wall friction is eliminated by lubrication

6.3.11 Monoaxial shear test

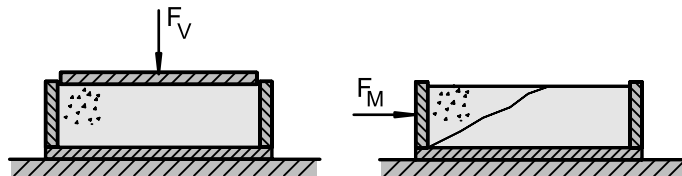


Fig. 6.16. Principle of the monoaxial shear test

Description:

This test is similar to the uniaxial compression test: The bulk solid specimen is compressed in the vertical direction (force F_V), and then, after removal of the vertical load, stressed in the horizontal direction by pushing a side wall into the material (Fig. 6.16). From the force F_M measured at the moment of failure the unconfined yield strength is calculated [6.10,6.57].

General comments:

Compared to the uniaxial compression test, the measured strength is additionally decreased through the anisotropic effects caused by the difference in direction of 90° between consolidation and strength measurement (see procedure III in Fig. 5.12, Sect. 5.1.3). Thus, it is not possible to establish a quantitative statement concerning flowability and time consolidation.

Table 6.11. Evaluation (Monoaxial Shear Test)

Criterion	1	2	3	4a/4b	5a/5b	6	7
Fulfillment	yes	no	no	yes/yes	yes*/yes*	yes	yes

* if wall friction is eliminated by lubrication

6.3.12 Powder bed tester with tensile strength test

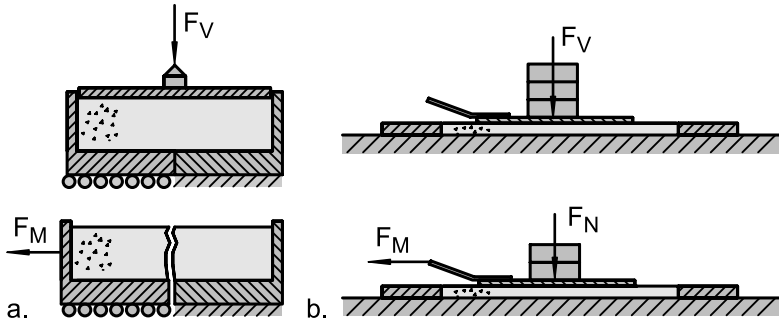


Fig. 6.17. Principle of the powder bed tester [6.58]; a. tensile strength test; b. shear test

Description:

This is a combination of two measurement techniques [6.58,6.59]:

- Determination of tensile strength (Fig. 6.17.a): The bulk solid specimen is placed in a vertically split cell and compacted in the vertical direction (force F_V). Subsequently, after removal of load the test specimen is pulled horizontally, and the pull force at failure, F_M , is measured. From F_M the tensile strength is calculated. This measuring technique is in accordance with a test principle proposed earlier by Ashton et al. [6.60,6.61]
- Figure 6.17.b: A sliding skid (i.e., a rectangular platen with a rough underside) is placed on top of a 3 mm layer of bulk solid. This layer is then consolidated by vertical force, F_V , by placing weights on the skid. Subsequently, the skid is pulled horizontally over the test specimen at a lower vertical stress (normal force $F_N < F_V$), and the pull force at failure, F_M , is measured

From the results of both measurements (sometimes several measurements are necessary) a yield locus is determined. The curved shape of the yield locus is approximated by the Warren Spring equation [6.60]:

$$\left(\frac{\tau}{\tau_c} \right)^n = \frac{\sigma}{\sigma_t} + 1 \quad (6.3)$$

The Warren Spring equation contains three parameters, i.e., tensile strength, σ_t , cohesion, τ_c , and an exponent, n , having values between 1 and 2. In [6.60] it is stated that n characterizes the flowability.

General comments:

This results in a qualitative statement regarding flowability. The sample is consolidated uniaxially as with the uniaxial compression test (no steady-state flow), resulting in a lower measured strength. This effect is increased further through anisotropic effects due to the different directions of consolidation and measurement of strength (90° inclination between the orientations of major principal stresses in the tensile strength test; 45° in the shear test with the skid) [6.10,6.20,6.62,6.63]. The value of tensile strength depends on the height of the bulk solid specimen [6.64].

Table 6.12. Evaluation (powder bed tester, tensile strength test)

Criterion	1	2	3	4a/4b	5a/5b	6	7
Fulfillment	yes	no	no	yes/yes	yes*/yes	yes	yes

* if wall friction at consolidation prior to the tensile strength test can be neglected

6.3.13 Uniaxial tensile strength test

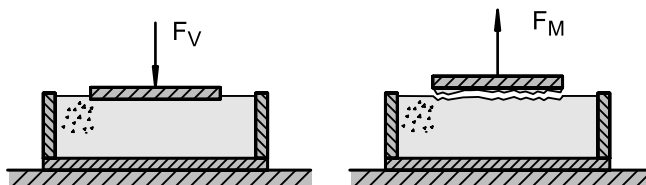


Fig. 6.18. Principle of uniaxial tensile strength test [6.65–6.67]

Description:

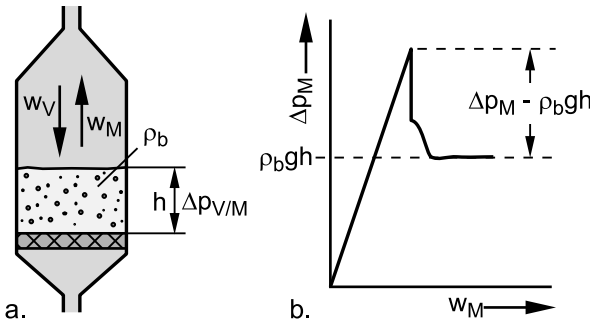
The bulk solid test specimen is compacted by a plate in the vertical direction (Fig. 6.18, force F_V). Subsequently the plate is raised. Since its underside is coated with an adhesive, a layer of particles adheres to the plate, i.e., failure takes place within the bulk solid. From the difference of the maximum force measured at failure, F_M , and the weight of the plate with the adhering bulk solid, tensile strength is calculated.

General comments:

This results in a qualitative statement regarding flowability. The sample is consolidated uniaxially as with the uniaxial compression test (no steady-state flow). In contrast to the tensile strength test discussed in Sect. 6.3.12 (Fig. 6.17.a), the orientations of the major principal stresses at consolidation and measurement are identical. Therefore larger values of tensile strength are to be expected [6.65]. However, the measuring technique only works if the tensile strength between the adhesive and the bulk solid is larger than the tensile strength of the bulk solid.

Table 6.13. Evaluation (uniaxial tensile strength test)

Criterion	1	2	3	4a/4b	5a/5b	6	7
Fulfillment	yes	no	yes	yes/yes	yes/yes	yes	yes

6.3.14 Tensile strength test with gas flow**Fig. 6.19.** a. Principle of the tensile strength test with gas flow; b. gas pressure vs. time during measurement of tensile strength [6.68–6.70]

Description:

A cylindrical container with porous bottom (Fig. 6.19.a) is filled with the bulk solid specimen which must be fine-grained and fluidizable. First the specimen is fluidized by an upward gas flow. Afterwards the direction of gas flow is reversed (gas velocity w_V). The specimen is then consolidated due to the resulting pressure drop, Δp_V , and its weight, so it is assumed that the consolidation stress at the bottom is $(\Delta p_V + \rho_b gh)$. For measurement of strength, the specimen is subjected again to an upward directed gas flow which is slowly increased (gas velocity w_M) until the pressure drop, Δp_M , passes a maximum (Fig. 6.19.b) similar to the maximum pressure drop at the onset of fluidization known from fluidized bed technology (see Sect. 7.2.4). The maximum goes along with fracture starting at the bottom of the specimen. Subsequently the pressure drop decreases to $\rho_b gh$. The maximum difference ($\Delta p_M - \rho_b gh$) is interpreted as the tensile strength of the bulk solid specimen [6.68–6.70].

General comments:

This provides a qualitative statement regarding flowability. The sample is consolidated uniaxially as with the uniaxial tensile strength test (Sect. 6.3.13, no steady-state flow). The consolidation stress increases from top to bottom, so the effect of friction along the cylinder walls must be taken into account, i.e., the consolidation stress is unlikely to be equal to $(\Delta p_V + \rho_b gh)$. The latter can be demonstrated by including the pressure drop into

the Janssen equation (see Sect. 9.2.2). During measurement of tensile strength, the vertical tensile stress increases from top to bottom (Fig. 9.12). Only if any wall friction effects can be neglected in the presence of vertical tensile stresses (i.e., no adhesion to the wall; no residual wall normal stresses resulting from the consolidation process) is the tensile strength at the bottom equal to $(\Delta p_M - \rho_b g h)$.

Table 6.14. Evaluation (tensile strength test with gas flow)

Criterion	1	2	3	4a/4b	5a/5b	6	7
Fulfillment	yes	no	yes	yes/yes	no/yes*	yes	no

* if wall friction effects during strength measurement can be neglected

6.3.15 Johanson Hang-up Indicizer™, similar techniques

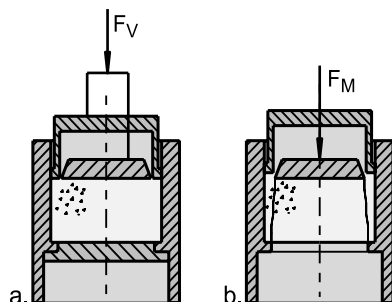


Fig. 6.20. Principle of Johanson Hang-up Indicizer™ [6.71–6.73]

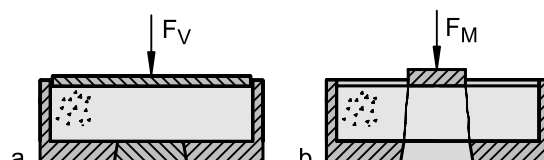


Fig. 6.21. Principle of Compact Strength Tester [6.74,6.75]

Description:

In the automatic Johanson Hang-up Indicizer™ (Fig. 6.20) a cylindrical bulk solid specimen is compressed in axial direction (force F_V) via an upper piston consisting of two concentric areas. Subsequently, after removal of the load, the piston at the bottom of the specimen is removed and the inner part of the upper piston pushes on the test specimen until failure occurs. From failure force, F_M , the unconfined yield strength, σ_c , or an index describing the bulk solid's ability to form stable arches or ratholes in silos,

is calculated [6.71–6.73]. The assumptions for calculation of stresses and unconfined yield strength have not been published by Johanson. Van der Kraan [6.75] presented a reconstruction of Johanson's assumptions.

A similar measuring principle is realized with the manually-operated Compact Strength Tester (Fig. 6.21) [6.74,6.75]. The ratio of specimen diameter to height is greater than for the Indicizer, so the vertical stress at consolidation is more uniform over the specimen height. Another tester following the same principle is the Bates/Ajax Uniaxial Direct Shear Tester [6.74,6.75].

General comments:

This results in a qualitative statement regarding flowability and time consolidation. The stresses at consolidation and during strength measurement are not fully known and are not homogeneous. The consolidation stress decreases downwards due to wall friction (see Fig. 6.3) depending on the bulk solid properties (ratio of horizontal to vertical stress, wall friction angle) and the specimen's geometry (height-to-diameter ratio). The effect is small with very small height-to-diameter ratios as in Fig. 6.21, but increases with larger ratios, whereby a reduction to about 60% of the stress applied on the top is possible [6.76]. Thus, neither the stress distribution nor the average stress values in the specimen is specifically known. During measurement of the bulk solid's strength, the vertical stress decreases downwards towards zero (free surface), and, thus, the specimen is subjected along its height to a variable stress. Consequently, the bulk solid's strength, as measured with the devices under consideration, is an “average value”, which results from various consolidation and stress levels that are not clearly defined.

Further, there are influences of anisotropy (different directions of principal stresses during consolidation and strength measurement) and of the consolidation procedure “uniaxial compression”, see Sect. 6.1. In [6.75] the dependence of test results on geometry (e.g., diameters of bottom opening and piston, specimen height) has been demonstrated. According to comparative measurements [6.56,6.73,6.77], the values of a bulk solid's strength are likely to be lower in comparison to a shear tester (Jenike shear tester, Schulze ring shear tester).

Table 6.15. Evaluation (Johanson Hang-up Indicizer™, similar measuring techniques)

Criterion	1	2	3	4a/4b	5a/5b	6	7
Fulfillment	yes	no	no	yes/yes	no/no	yes	yes*

* long-term storage under consolidation stress

6.3.16 Quality control tester

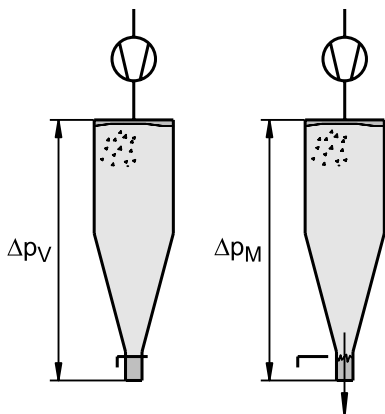


Fig. 6.22. Principle of the quality control tester [6.78]

Description:

A model silo (Fig. 6.22) is filled with bulk solid. The outlet opening is closed off with a porous slide gate. The solids are compacted by an air stream flowing from top to bottom. The pressure differential across the bulk solid column, Δp_V , is measured and considered as consolidation pressure. In order to measure the strength of the bulk solids, the silo is again subjected to an air pressure after the slide gate is opened. The air pressure is gradually increased until flow (of the bulk solid) is established. The maximum pressure differential, Δp_M , becomes a measure of strength [6.78].

General comments:

This provides a qualitative statement regarding flowability. There are possible influences from the flowing air, such as transport of fine particles and change in moisture content. Stresses in the failure plane (near the outlet) are not known.

Table 6.16. Evaluation (quality control tester)

Criterion	1	2	3	4a/4b	5a/5b	6	7
Fulfillment	yes	no	yes	yes/yes	no/no	yes	no

6.3.17 Biaxial compression test

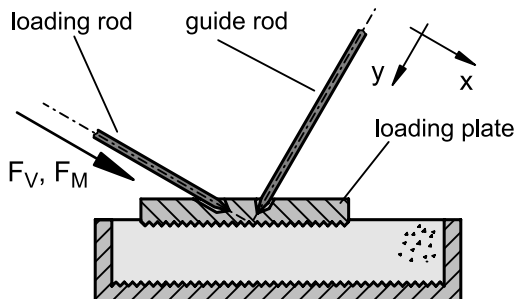


Fig. 6.23. Principle of the biaxial compression test [6.79,6.80]

Description:

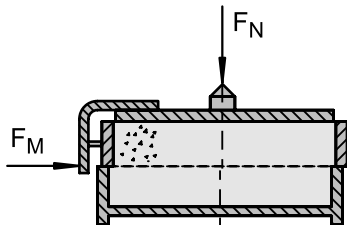
The bulk solid in the flat test mold is consolidated by moving a loading plate with rough underside linearly in x direction (Fig. 6.23) until the desired consolidation stress is acting in the x direction (force F_V in the loading rod). Afterwards the loading plate is further pushed in x direction, but simultaneously the guide rod is driven backwards (i.e., in negative y direction) to such an extent that the desired consolidation stress in x direction and the force F_V , respectively, remain constant. Thus steady-state flow (i.e., flow at constant stresses) prevails. Subsequently the bulk solid is unloaded from the stresses in x and y directions. For measurement of unconfined yield strength, after removal of the guide rod the loading plate is again driven in x direction until failure takes place. From the maximum force in the loading rod, F_M , measured at failure, the unconfined yield strength is calculated [6.79,6.80]. For a time consolidation test, the specimen is first consolidated as outlined above. Subsequently, the guiding rod is fixed and the specimen is subjected to a static consolidation stress during the desired consolidation period. Finally the strength is measured as described above.

General comments:

This provides a quantitative statement regarding flowability (steady-state flow is attained at the consolidation procedure). If isotropic behavior (coincidence of major principal strains and stresses) is assumed, the major principal stresses at consolidation and at strength measurement have the same orientation. Similar to the uniaxial compression test, here the consolidation stress and unconfined yield strength are directly applied or measured, respectively.

Table 6.17. Evaluation (biaxial compression test)

Criterion	1	2	3	4a/4b	5a/5b	6	7
Fulfillment	yes	yes	yes	yes/yes	yes/yes	yes	yes

6.3.18 Jenike shear tester**Fig. 6.24.** Shear cell of the Jenike shear tester

Description:

see Sect. 4.1.1 and [6.8,6.26,6.81,6.82].

General comments:

This results in a quantitative statement regarding flowability and time consolidation. The operation of Jenike shear tester requires training, which means that the results are operator sensitive. Since the Jenike tester is manually operated and for each test point a new sample has to be prepared (see Sect. 4.1.1), the time required for measurement of a complete yield locus is about one to two hours.

Some proposals exist to reduce the time for testing (see Sect. 6.1.1), but are likely to decrease accuracy. Another possibility with reduced accuracy is measurement of only one point on the yield locus (one point test [6.84]). However, since preparation of a test specimen requires relatively much time, these methods do not save much time compared to a complete yield locus test performed in an automatic rotational shear tester (e.g. [6.4]).

Table 6.18. Evaluation (Jenike shear tester)

Criterion	1	2	3	4a/4b	5a/5b	6	7
Fulfillment	yes	yes	yes	yes/yes	yes/yes	yes	yes

6.3.19 Torsional shear tester

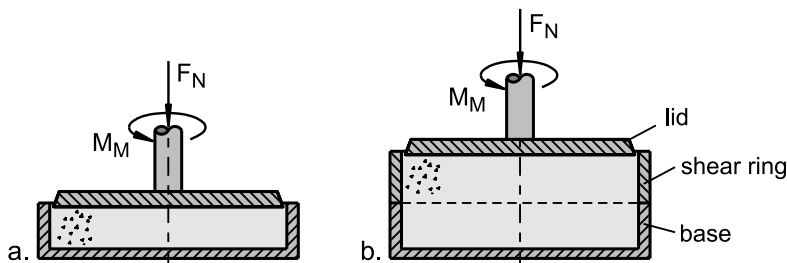


Fig. 6.25. a. Shear cell of a torsional shear tester [6.85]; b. torsional shear tester with split level shear cell [6.57,6.86,6.87]

Description:

The test sample is contained in a cylindrical shear cell (Fig. 6.25.a). Through a round, roughened lid on top of the sample a normal force, F_N , is applied. By rotation of the lid relative to the shear cell, a shear deformation is developed and torque, M_M , is measured. The shear stress acting in the sample is calculated from the measured torque. The design of Fig. 6.25.b consists of a shear ring and a base (similar to the Jenike shear cell), which enables rotation of lid and shear ring relative to the base. As with the Jenike Tester, the test sample is being presheared and sheared to failure, so a yield locus can be developed.

General comments:

This provides a quantitative statement regarding flowability and time consolidation, whereby the deformation varies with radius in the cell; at the perimeter it is maximum, in the center it is zero, i.e. no shear deformation in the rotational axis [6.19,6.85]. From comparative measurements it is known that the results of a torsional shear tester can differ from those of the Jenike tester [6.73, 6.85], so the test procedure often applied with torsional shear testers [6.86] is likely to play an important role [6.22] (the test procedure begins with a relatively large shear deformation which can result in lower shear stresses, see Sect. 5.2.4).

Table 6.19. Evaluation (torsional shear tester)

Criterion	1	2	3	4a/4b	5a/5b	6	7
Fulfillment	yes	yes	yes	yes/yes	yes/yes*	yes	yes

* with limitations due to the variation of deformation with radius [6.19] and the recommended test procedure [6.22].

6.3.20 Ring shear tester

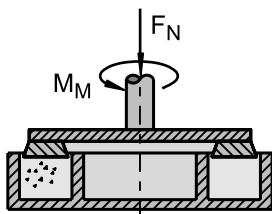


Fig. 6.26. Shear cell of a ring shear tester (e.g. [6.83–6.85])

Description:

This is similar to the torsional tester, but here the sample is contained in an annular trough. The normal force, F_N , is applied through a roughened annular lid. To shear the bulk solid sample, the trough rotates relative to the lid. The torque, M_M , necessary for shearing is measured. As with the Jenike tester, the test sample is being presheared and sheared to failure, so a yield locus can be developed.

For more details refer to Sect. 4.1.2 and [6.83–6.85].

General comments:

This results in a quantitative statement regarding flowability and time consolidation. Compared to the torsional tester, inhomogeneity of the deformation, which results from the dependence of shear stress on radius, is less strong and can be neglected if the ratio of the inner to the outer shear cell diameters is sufficiently large [6.19,6.85]. With proper test procedure and correct design of the ring shear tester, test results close to those achieved with the Jenike shear tester can be obtained [6.21,6.84,6.85], but the reproducibility is clearly better [6.48].

Table 6.20. Evaluation (ring shear tester)

Criterion	1	2	3	4a/4b	5a/5b	6	7
Fulfillment	yes	yes	yes	yes/yes	yes/yes*	yes	yes

*with sufficiently large ratio of inner to outer shear cell diameter and appropriate test procedure test results similar to those of the Jenike shear tester are obtained [6.84].

6.4 Remarks on reliability and accuracy

The various types of shear testers raise the question of whether the same results are obtained with different testers. Usually the Jenike shear tester is regarded as the standard due to its historical position. However, with respect to its difficult operation, one must ask how much longer this tester can be considered as the only standard. On the other hand, much research work on the Jenike tester has been carried out, including comparative tests with more sophisticated testers, and this work has shown that the Jenike tester leads to sufficiently accurate and applicable results if it is operated in the correct way. This is confirmed by the successful application of the Jenike tester for silo design for more than four decades.

An international collaborative project of the European Federation of Chemical Engineers carried out comparative tests over several years focused on operation of the Jenike shear tester. The test procedures were discussed and improved again and again until finally a generally agreed procedure, the “Standard Shear Testing Technique...” [6.8], was published. A defined limestone powder (CRM-116, $x_{50} = 4.1 \mu\text{m}$) was used for the shear tests. Samples of this powder and results from five of the laboratories involved in the study [6.88] are available from the European „Institute for Reference Materials and Measurements” [6.89]. These “certified” results are commonly regarded as “correct”, so that everyone has the possibility of comparing their own test results with certified values. The results are presented as normal and shear stresses for preshear and shear to failure, and shear stresses are given as mean values with their 95% confidence intervals, which are on the order of $\pm 7\%$ to $\pm 12\%$ of the corresponding mean. The intervals may appear large at the first sight, but it has to be remembered that they are mostly a result of differences between the laboratories. Multiple tests of individual laboratories showed smaller confidence intervals [6.48,6.88].

Generally, comparative tests of different testers should always be considered with care. For instance, such tests are useful only if the selected bulk solids are appropriate for the testers involved in the study (e.g., the particles must not be too large for any tester). If yield loci are measured, identical sets of normal stresses for preshear and shear to failure should be selected for all testers (see Sect. 4.3.1).

Several papers have been published on comparative tests where different testers and test procedures have been investigated (e.g., [6.21,6.22, 6.48,6.56,6.73–6.75,6.85,6.90]). The problem with this type of tests is that their results cannot necessarily be understood as generally valid. For instance, one can find papers where results of the Jenike shear tester are

compared to those of ring shear testers (e.g., Schulze ring shear tester [6.84]). Several tests have shown similar results for both testers [6.21,6.48,6.84,6.91,6.92], but if inappropriate test procedures have been applied, or the testers have not been designed carefully, differences (typically: smaller shear stresses and, thus, smaller values of unconfined yield strength) have been found [6.22,6.93]. Regarding the torsional shear tester (design according to Peschl [6.86]) results have been published where, compared to the Jenike shear tester, smaller values of unconfined yield strength have been measured [6.22,6.73,6.74], but in other studies the differences are small [6.48]. Another example is the Johanson Hang-up Indicizer™: According to [6.56,6.73,6.77], it gives smaller values of unconfined yield strength than the Jenike shear tester or the Scnulze ring shear tester.

Even a ranking of different bulk solids regarding flowability can be dependent on the tester. Markefka et al. [6.90] tested samples of lactose powders with gradually varied fines content using different measuring techniques (ring shear tester, avalanching, stirrer, and compressibility). Only the shear tester showed a steady decrease of flowability with increasing fines content. In tests conducted by Margreiter [6.94], the results of a shear tester and a stirrer partly showed the opposite trend regarding flowability of the tested samples. Also investigations of Bell et al. [6.74] demonstrate that with so-called simple testers the ranking of different bulk solid samples regarding flowability can depend on the measuring technique.

Even with biaxial testers (see Sect. 5.1), which are sophisticated testers intended to induce defined stresses and deformations, different flow functions have been measured. A flow function (i.e., unconfined yield strength as a function of consolidation stress) of limestone powder CRM-116 measured by Maltby [6.95] lies within the range of the certified results of the Jenike shear tester [6.48], but van der Kraan [6.75] found clearly higher values of unconfined yield strength. With another type of biaxial tester (Fig. 5.1) and a different limestone powder, Harder [6.11] found good agreement with results from a Jenike shear tester and a ring shear tester.

To give an idea of the situation, in Fig. 6.27 the unconfined yield strength, σ_c , measured with the above-mentioned limestone powder CRM-116 is plotted versus consolidation stress, σ_l . Data points for the Jenike shear tester have been determined from mean values given in the certified results. The other results are taken from different publications (see legend of Fig. 6.27), which have been mentioned above. The diagram clearly demonstrates that it is quite possible that different testers and test procedures, respectively, can lead to different results. Possible sources of differences are discussed in the sections where the testers are described.

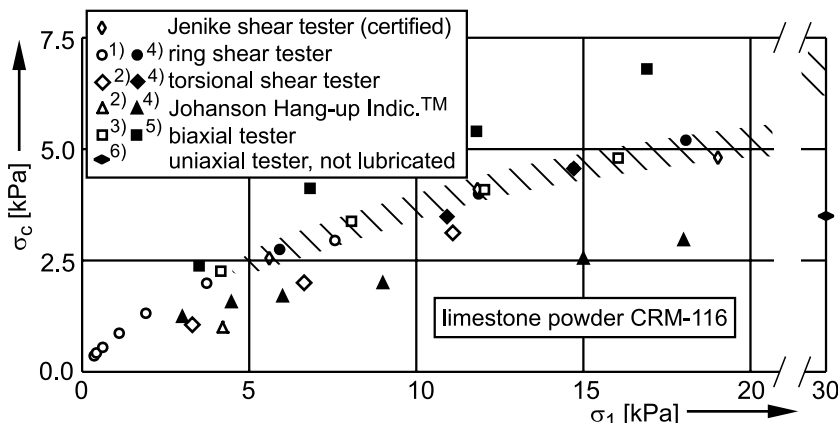


Fig. 6.27. Points of the flow function of limestone powder CRM-116, measured in different labs with different testers. Data sources: 1: [6.84,6.91]; 2: [6.73,6.74]; 3: [6.95]; 4: [6.48]; 5: [6.75]; 6: [6.56]; the hatched area indicates the range around the certified results obtained with a Jenike shear tester. It is the author's intention that the hatched area represents the flow properties of CRM-116 and should be matched with other shear testers. For consolidation stresses smaller than 5 kPa no certified results are available since the range of stresses realizable with the Jenike tester has a lower limit of several kPa. The test results of the ring shear tester (1) indicate the course of the flow function in the low stress region.

The examples discussed above demonstrate that measurement of flow properties is not trivial. As outlined in Chap. 5, several conditions can influence the test results. Therefore, not only for quantitative application, e.g., silo design, but also for quality control, product design etc. appropriate testers should be selected which allow well-defined test conditions. Thus the criteria listed in Sect. 6.2 are generally useful for the selection of appropriate test equipment.

So-called simple tests (e.g., angle of repose, funnel) do not fulfill these criteria. As a rule, these testers usually **are** not simple regarding what happens within the bulk solid specimen (what can be simple, for example, in a chaotic process?), but just **seem** to be simple at first sight, because there is no theory available describing what happens within the specimen, and, thus, the user is not in a situation to be confronted with theories.

Accuracy and reproducibility of flow property testers cannot be quantified without considering the bulk solid. Fine powders usually result in smooth curves, e.g., when being sheared with a shear tester. Other bulk materials lead to fluctuating signals up to slip-stick oscillations, which makes it difficult to find unique test results, i.e., accuracy and reproducibility are reduced. If the measuring technique is sensitive to the operator, this too may decrease accuracy and reproducibility.

6.5 Measurement of adhesive forces

Since the flow properties of a bulk solid are strongly dependent on inter-particle adhesive forces, it is of interest to measure adhesive forces directly. In earlier investigations centrifuges were used for this (Fig. 6.28). A certain amount of particles is first pressed with a defined force (i.e., the centrifugal force) against a rigid wall. Subsequently, after the wall has been reversed, the centrifugal force acts in a direction to pull the particles from the wall.

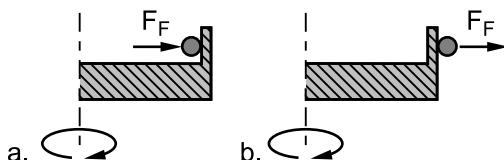


Fig. 6.28. Measurement of adhesive forces in a centrifuge (in principle); a. a particle is pressed against a rigid wall due to the centrifugal force, F_F ; b. after the rigid wall is reversed, the centrifugal force, F_F , acts in a direction to separate the particle from wall [6.96]

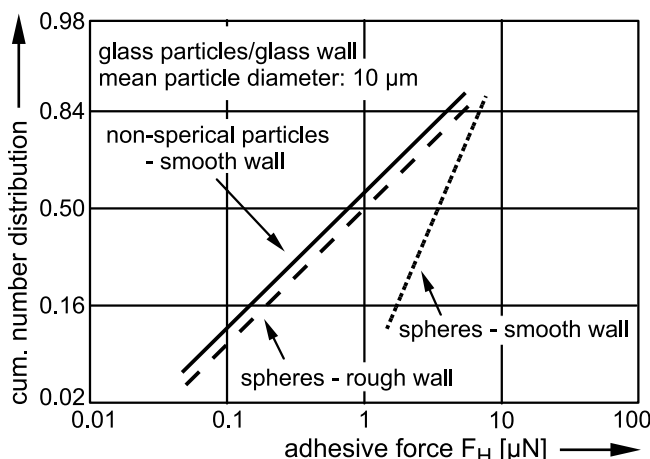


Fig. 6.29. Adhesive forces, measured with a centrifuge (taken from [6.96])

Because each particle has a different shape and surface topography, different adhesive forces are measured even for particles of identical size. Thus, a distribution of adhesive forces is obtained for each particle size (Fig. 6.29) so a sufficient number of tests must be performed to obtain a representative statement. Therefore it is often easier to measure flowability of a

bulk solid sample than to measure adhesive forces. This is especially the case if specific conditions, e.g., temperature or moisture, must be met.

The results in Fig. 6.29 demonstrate the influence of surface roughness (see Sect. 2.6): The greatest adhesive forces, F_H , have been found for glass spheres and a smooth wall. The smooth surfaces make possible small distances between particle and wall, and, thus, large van der Waals forces. If the surface roughness of either the wall (diagram: rough wall) or the particles (diagram: non-spherical particles) is increased, the adhesive forces, F_H , become smaller due to the increased distance.

For a couple of years now adhesive forces have been measured with atomic force microscopes (AFM). The heart of the AFM is a microscale elastic cantilever with a sharp tip (Fig. 6.30.a). When the tip is brought into proximity to a sample surface, forces (van der Waals forces, electrostatic forces, etc.) between the tip and the sample lead to deflection of the cantilever. Typically, the deflection is measured using a laser spot reflected from the top of the cantilever into an array of photodiodes. The forces acting on the tip are dependent on its distance to the surface. Thus, the topography of a sample can be determined by moving the tip across the surface and measuring the distance-dependent force through the deflection of the cantilever.

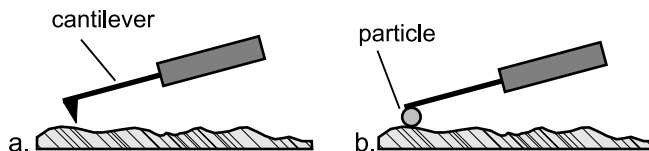


Fig. 6.30. Principle of measurement with an atomic force microscope; a. surface topography; b. adhesive force

The sensitive force measuring system of the AFM can be applied to determine adhesive forces of particles. For this measurement a particle is fixed on the cantilever (Fig. 6.30.b) [6.97] and pressed against a solid surface or another particle with the positioning system of the AFM. Subsequently, the particle is pulled away from the contact and the required force – the adhesive force – is measured. As with the centrifuge, multiple measurements with an AFM result in a distribution of adhesive forces, so a correlation to strength parameters exists (e.g., the tensile strength of a powder [6.70]). However, the application of adhesive force measurements on determination of flowability of bulk solids seems to be too expensive and time-consuming for practical applications.

6.6 Summary

The flowability of bulk solids can be characterized by the relationship between defined quantities “unconfined yield strength” and “consolidation stress”. For these measurements reliable testers are available, especially shear testers, which can be regarded as the standard testers in bulk solids technology. These testers yield useful and quantitatively applicable results, which is demonstrated by the fact that thousands of properly working silos and other bulk handling equipment have been designed based on shear test results.

If accurate physical quantities are not required, e.g., for comparative tests, measuring techniques can be applied which only give a qualitative statement, but are easier to operate. When selecting such a device, one should favor testers where the results are not affected by other conditions and quantities, e.g., filling procedure, wall friction angle, fluidization of the specimen, tester dimensions in relation to particle size. Furthermore, the measuring technique should cover the boundary conditions of the application (e.g., stress level in a container where the bulk solid is to be stored).

The criteria listed in Sect. 6.2 are fulfilled best by shear testers. Since measurement with a Jenike shear tester requires much skill and time, nowadays automated shear testers are preferred. Automated testers (usually rotational shear testers) reduce the influence of the operator and, thus, increase reproducibility.

Even for qualitative applications, e.g., comparative tests, shear testers should be preferred, because the purpose of such tests is usually not to distinguish between easy-flowing and cohesive bulk solids, but to identify even small differences in flow behavior, e.g., if small amounts of flow agents are added to a powder. For this application high reproducibility is required, which can only be obtained with defined conditions.

7 Properties exhibited by some bulk solids

In the present chapter effects are described which sometimes occur in flowing bulk solids. Furthermore, means and conditions are described that have an influence on the flow of bulk solids. Since most effects are related to specific materials, one cannot draw general conclusions from them, but the knowledge of such effects helps to assess the flow behavior of bulk solids.

7.1 Effects in flowing bulk solids

7.1.1 Slip-stick behavior

Slip-stick friction (also known as stick-slip friction) is a phenomenon occurring in many physical systems where surfaces are sliding against each other. Slip-stick leads to spontaneous, jerking movements or self-excited oscillations with constant or varying frequency, e.g., when playing a violin, rubbing a wet finger on the rim of a glass, squealing brakes or tires, and grinding of teeth. Even earthquakes, where tectonic plates are suddenly displaced relative to each other, result from slip-stick friction.

7.1.1.1 Conditions for slip-stick oscillations

Slip-stick friction can occur between surfaces of rigid bodies, within a bulk solid (internal friction), and between a bulk solid and the surface of a rigid body (wall friction). In Fig. 7.1.a to c a simplified model is shown for each case where a body (mass m in Fig. 7.1.a, the upper part of the bulk solid in Fig. 7.1.b, or the entire bulk solid layer in Fig. 7.1.c) is moved to the right, i.e., in x direction. The body is coupled by an elastic spring to a driving system moving at constant velocity, v . The spring constant, c , represents the stiffness of the system. The normal stress, σ , acting on the contact planes results from the weight of mass m (Fig. 7.1.a) or the vertical stress exerted on the bulk solid through a top plate, respectively (Figs. 7.1.b and c). To move solid bodies or particles (which are also solid bodies) across

each other or across a plane solid surface, the friction between them has to be overcome and, thus, a sufficient shear stress, τ , must be applied.

Slip-stick oscillations are caused, as the term slip-stick says, by an alternating slipping and sticking of surfaces being in contact and moved parallel across each other, e.g., as in Fig. 7.1.a. During a stick period, the shear stress, τ , increases until the static friction is overcome (Fig. 7.1.d). Thus, the mass suddenly starts to move. This is accompanied by a sudden decrease of shear stress, τ , due to the change from static friction to usually smaller kinematic friction. As shown in Fig. 7.1.d, the sudden decrease of shear stress is associated with an abrupt displacement in x direction (see coordinate x vs. time) and a peak in the velocity, dx/dt , of mass m . The reason for the sudden acceleration is that immediately at the onset of motion only a portion of the force, F , which at this moment is still transferred by the spring, is needed to overcome the reduced friction, so the excess force accelerates the mass. Thus, the system releases energy (previously stored as elastic energy in the spring and other elastic components) to accelerate the mass.

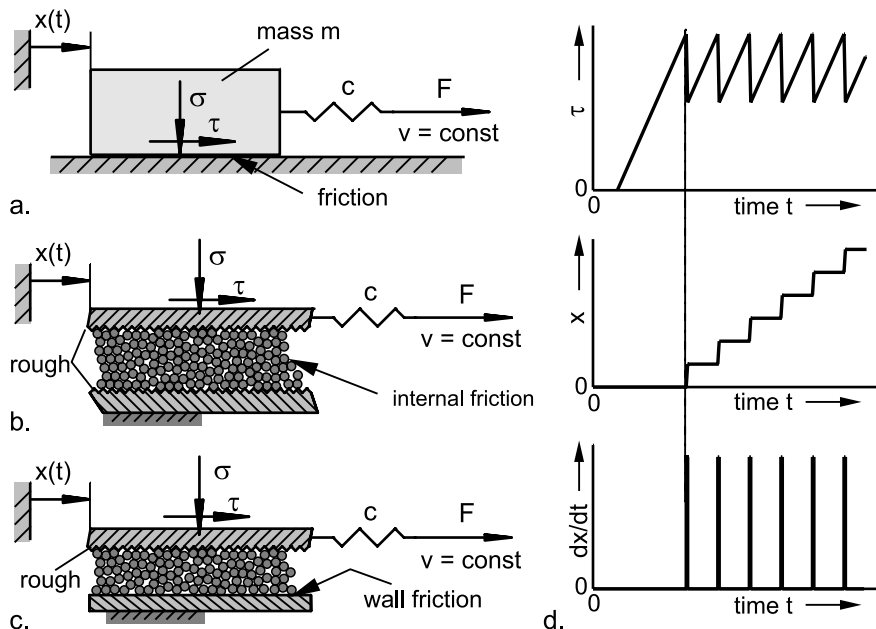


Fig. 7.1. a. Friction between solid bodies; b. internal friction in a bulk solid; c. friction between a bulk solid and a solid surface; d. shear stress, τ , displacement, x , and velocity, dx/dt , of the moving body in the presence of slip-stick friction

Depending on the properties of the system (damping, elasticity, masses, and, in case of a system according to Figs. 7.1.b or c, properties of the bulk solid) the effect described above can happen periodically thus resulting in oscillations. If the relative motion stops after a certain period of movement, the surfaces stick to each other again. Then the cycle starts again, i.e., the shear stress increases again until static friction is overcome and so on. The result is a “saw tooth” type shear stress pattern (Fig. 7.1.d) due to alternating slip and stick periods.

A simple mechanical system, which has been investigated experimentally, is the friction-excited oscillator (Fig. 7.2.a) [7.1]. A mass, m , rests (sticks) on a moving belt and is coupled to its surroundings by a spring and a damper. If the belt moves with constant velocity, u , the mass moves with the same velocity in x direction. After a certain time the spring is stressed so much that the spring force is equal to the maximum static frictional force between mass and belt. Thus, the mass starts to move (slip) relative to the belt with the relative velocity, v_r . If the coefficient of kinematic friction is smaller than the coefficient of static friction, μ_0 (idealized friction behavior as shown in Fig. 7.2.b), at this moment the spring force is greater than the frictional force (kinematic friction). The difference between spring force and frictional force accelerates the mass in negative x direction, so the spring releases elastic energy and the spring force decreases.

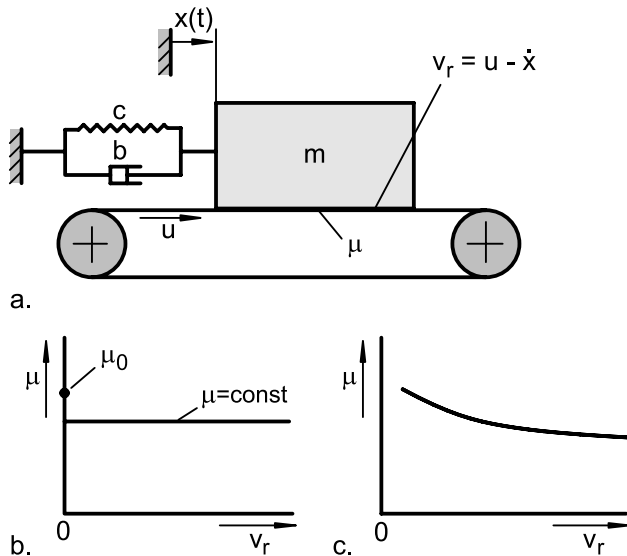


Fig. 7.2. a. Friction-excited oscillator with damper and spring; b. coefficient of friction vs. relative velocity, v_r ; simplified behavior: $\mu = \text{const.}$ for $v_r > 0$; c. real behavior: $\mu \neq \text{const.}$ for $v_r > 0$

While the mass is slipping relative to the belt, the friction on the belt decelerates the mass and subsequently accelerates it in x direction until the relative velocity, v_r , is zero and, thus, stick is attained again. This slip-stick mechanism can only occur if the friction force is reduced after the onset of relative motion. This means for the idealized friction behavior according to Fig. 7.2.b, that the coefficient of kinematic friction is smaller than the coefficient of static friction, μ_0 . Additionally, the system must have the ability to oscillate (e.g., damping must be sufficiently small) [7.1–7.3]. Thus, generally slip-stick behavior is a result of both **material properties** and **system properties**. Therefore, if slip-stick oscillations emerge in a specific situation (e.g., during shear in a particular shear tester), there is no reason that that slip-stick will necessarily occur in a different situation (e.g., with another type of shear tester, or in a silo). If, on the other hand, in a specific situation no slip-stick oscillations can be observed, this is no reason to exclude them from other situations.

Friction between rigid bodies is characterized by the coefficient of friction, μ . For the idealized frictional behavior according to Fig. 7.2.b as assumed above for the friction-excited oscillator, the coefficient of friction can be described as a very simple function of the relative velocity, v_r , between mass and belt. However, in reality bodies already start to move very slowly against each other due to creeping at the contacts when subjected to a force parallel to the frictional plane (even if the force is smaller than the maximum friction force). Thus, when the coefficient of static friction is measured and an increasing force is applied, a very small relative velocity, v_r , is present [7.4]. Furthermore, the coefficient of static friction depends on the time of (stationary) contact [7.5]. Thus the coefficient of static friction, μ_0 , is not a fixed value [7.6].

Steady-state kinematic friction is a process where materials are moved across each other with constant relative velocity. Here often a decrease of the coefficient of kinematic friction, μ , with increasing relative velocity, v_r , can be observed in a certain range of relative velocities (see Fig. 7.2.c) (e.g., [7.7]). Alone this effect, without the presence of a large coefficient of static friction, can cause slip-stick, because, for example, in a system as shown in Fig. 7.2 the increasing relative velocity yields a decrease of the coefficient of kinematic friction. Therefore, the material-specific condition for the occurrence of slip-stick must exceed the simple condition “static friction > kinematic friction”. Here the condition “decrease of the coefficient of friction with increasing relative velocity” is required.

Slip-stick behavior emerging while shearing a bulk solid with a shear tester leads to more or less regular shear stress oscillations (Fig. 7.3), whereby mostly the “saw tooth” pattern described above prevails. This is characterized by a relatively slow increase of shear stress followed by a sudden

drop. The frequency depends on several parameters; one of them is the shear velocity. Within the common range of shear velocities of about 1 to 2 mm/s often frequencies in the range of 1 to 10 Hz are observed. Slip-stick is more often observed during wall friction tests, where a bulk solid specimen is moved across the surface of a rigid body, than during yield locus tests, where the bulk solid is deformed internally (examples of bulk solids where slip-stick oscillation have been observed: cement, wheat flour, starch, milk powder, rice). Also when flowing in a silo or when being compressed (e.g., tabletting) slip-stick can result in jerking motion, thumps, or even in audible oscillations called “silo noise” (Chap. 14).

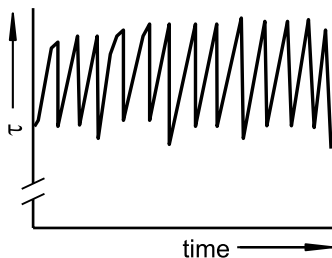


Fig. 7.3. “Saw tooth“ type pattern of shear stress, τ , vs. time which is typical for slip-stick friction

The frictional behavior of bulk solids is to some extent similar to that of solid bodies as discussed in Fig. 7.2. The influence of shear velocity, v_s , i.e., the velocity of the upper part of a shear cell relative to the lower part, is demonstrated in the following by the results of a study carried out with a ring shear tester (Sect. 4.1.2, Fig. 4.9) [7.3]. Subjected to a constant normal stress $\sigma = 5000$ Pa, a specimen was first sheared until constant shear stress was attained. Then the shear velocity, v_s , was varied in steps in the range from 0.05 mm/min to 30 mm/min. In Fig. 7.4 shear stress, τ , and specimen height, h , obtained with PE powder and limestone powder, are plotted versus time, t .

The PE powder dilates (h increases) if the shear velocity increases, and compacts if the shear velocity decreases. With the limestone powder this effect could not be measured with a displacement transducer having a resolution of 1.5 μm . In Fig. 7.5 the steady-state shear stress, τ_{ss} , of both powders is plotted versus the shear velocity, v_s . Limestone powder shows a decrease of shear stress with increasing shear velocity (approx. 1.5% per decade). In contrast to this, PE powder shows an increase of shear stress of approx. 4% per decade in the range of velocities investigated here.

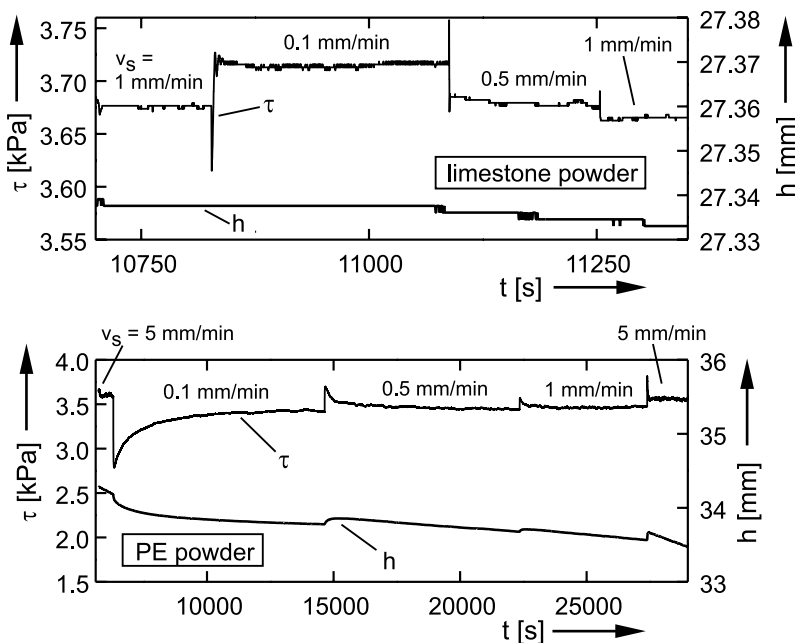


Fig. 7.4. Shear stress, τ , and specimen height, h , as a function of time, t , at step-wise varied shear velocity, v_s (normal stress $\sigma = 5000$ Pa) [7.3]

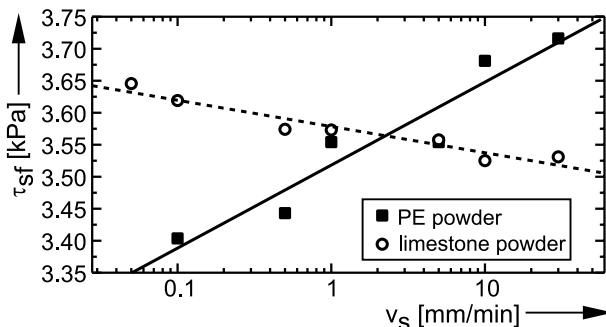


Fig. 7.5. Steady-state shear stress, τ_{sf} , vs. shear velocity, v_s (individual measurements and regression lines; normal stress $\sigma = 5000$ Pa) [7.3]

If a system exhibits slip-stick oscillations, a shear stress $\tau > 0$ acts during the stick period, but beside creeping no relative motion occurs. In order to investigate the influence of the duration of the stick period on the static friction which has to be overcome subsequently, so-called "slide-hold-slide tests" (SHS tests) were conducted. At first the powder specimen is sheared until steady-state flow (shear stress τ_{sf}) is attained. Then the motor is stopped and restarted after a defined period, the holding time, Δt [7.8,7.9].

The measured shear stress, τ , and the specimen height, h , are plotted versus time, t , in Fig. 7.6.

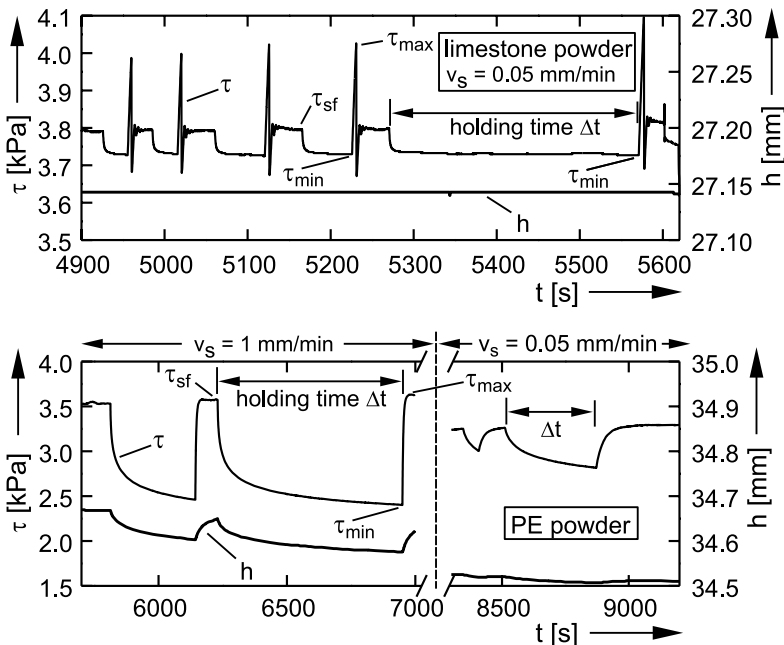


Fig. 7.6. Shear stress, τ , and specimen height, h , vs. time, t , during a slide-hold-slide test; normal stress 5000 Pa, shear velocity at sliding 0.05 mm/min (limestone powder, PE powder) and 1 mm/min (PE powder) [7.3]

During the holding time, Δt , the shear stress decreases to the value $\tau_{min}(\Delta t)$ due to relaxation resulting from viscoplastic deformation of the particle contacts, and the rate of decrease becomes slower and slower with time (see curves $(\tau_{min}-\tau_{sf})/\tau_{sf}$ plotted in Fig. 7.7; the shear stress decreases during the holding time nearly linearly with the logarithm of the holding time). Simultaneously the height of the powder specimen, h , decreases (clearly visible for PE powder). After the holding time, when the specimen is sheared again the shear stress exhibits a maximum, τ_{max} , which is higher than the shear stress, τ_{sf} , observed at steady-state flow prior to the holding time. During further shear, finally steady-state flow as observed prior to the holding time is attained. The longer the holding time, the larger the maximum shear stress, τ_{max} (see curves of $(\tau_{max}-\tau_{sf})/\tau_{sf}$ in Fig. 7.7). While with limestone powder and wheat flour a pronounced shear stress maximum could be observed, PE powder exhibited only a weak shear stress maximum. The maximum shear stress increases nearly linearly with the

logarithm of the holding time (as, for example, in [7.8,7.9]). Since the maximum shear stress takes place at the onset of shear, it corresponds to the static friction discussed above. The results in Fig. 7.7 clearly show the dependence of the maximum shear stress on the duration of the contact. Thus, it is demonstrated that the coefficient of static friction is not a fixed value for a specific material or material combination.

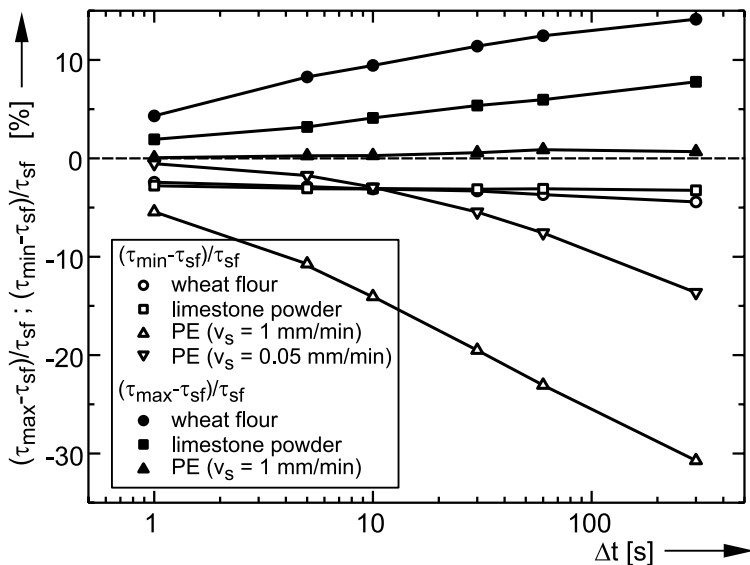


Fig. 7.7. Relative shear stress differences, $(\tau_{max} - \tau_{sf})/\tau_{sf}$ and $(\tau_{min} - \tau_{sf})/\tau_{sf}$, vs. holding time, Δt

As an example of slip-stick oscillations shear test results of wheat flour are plotted in Fig. 7.8 [7.3]. The slip-stick oscillations are characterized by a “saw tooth” pattern as discussed above, i.e., a nearly linear increase of shear stress, τ , followed by a sudden drop during the slip period. The slope of the increasing shear stress is a function of the stiffness of the system (bulk solid specimen, shear tester). Thus smaller shear velocities, v_s , yield larger amplitudes and shear stress maxima, respectively. One reason for this is the increase of the stick periods with decreasing shear velocity. The stick periods act similar to holding times (see Fig. 7.7) thus resulting in an increase of static friction. The higher the static friction, the more elastic energy is stored in the system and can be released at the start of slip thus resulting in a larger acceleration and a stronger decrease of the shear stress during slip (smaller values of shear stress minima). While the shear stress maxima represent static friction, the shear stress minima are not only dependent on the powders properties, but also on the dynamic behavior of the

system. Thus, the minima can be smaller or greater than the shear stress described by kinematic friction, i.e. the steady-state shear stress when no slip-stick oscillations take place.

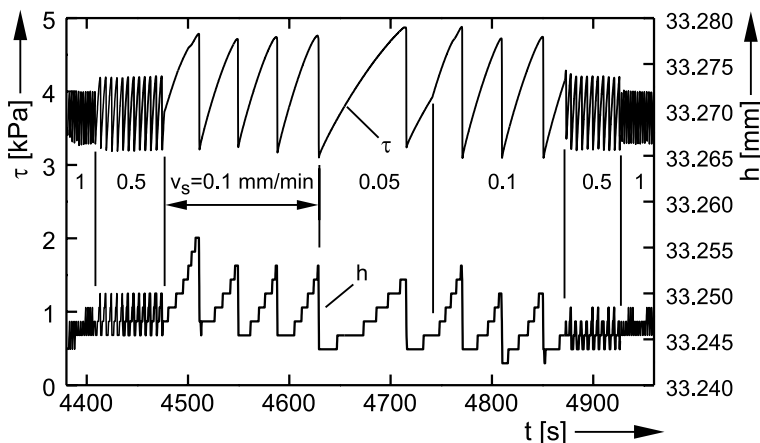


Fig. 7.8. Shear stress, τ , and specimen height, h , vs. time, t , during slip-stick friction (wheat flour); the shear velocity, v_s , was varied stepwise; the small steps in the h curve are artifacts due to the resolution.

During the test shown in Fig. 7.8 the specimen height, h , decreases sharply at every slip, and increases nearly linearly during the increase of the shear stress (stick period). The decrease of the specimen height, h , during a slip is similar to the decrease during the holding time of the SHS tests (Fig. 7.6, PE powder). At both processes the decrease of the shear stress goes along with a compaction. At the increase of shear stress, which starts at slip-stick directly after the slip and at SHS tests after the restart of the motor drive (i.e. directly after the holding time), the powder dilates. This behavior corresponds to the effect of dilatancy described in Sect. 5.2.3 which results in an increase of the specimen height at beginning shear deformation, and a decrease if the specimen is relieved of shear stress. Since during the increase of height additional energy has to be supplied to the specimen (Sect. 5.2.3), at least a part of the shear stress increase during the stick period (Fig. 7.8) is assumed to result from this effect.

With respect to the bulk solid properties, only the maximum values of shear stress have a physical meaning. They characterize static friction and, thus, the onset of plastic flow. The minimum values of shear stress are not meaningful. They do **not** characterize kinematic friction. Thus these values should not be used for any other application.

7.1.1.2 Shear testing of materials exhibiting slip-stick friction

If slip-stick friction emerges when measuring a yield locus with a shear tester (Fig. 7.9), the shear stress oscillations result in a certain reduction of accuracy and reproducibility. The following measures are recommended in order to obtain meaningful test results:

- The shear velocity should be reduced so that the measuring system of the shear tester is able to properly resolve the oscillations. However, a reduction of shear velocity leads to higher amplitudes (see Fig. 7.8).
- Preshear should be stopped after the shear stress oscillations show constant maximum values. This is regarded as semi-steady-state flow (see Fig. 7.9). The level of the maximum shear stress is then taken as the shear stress at preshear for evaluation of the yield locus.
- If at shear to failure slip-stick oscillations emerge as shown in Fig. 7.9, the largest local maximum shear force is used for calculation of a point on the yield locus.

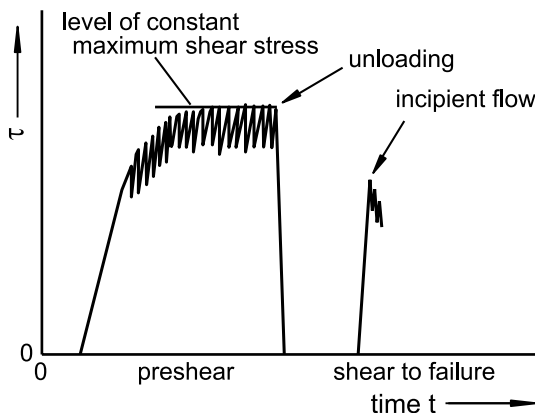


Fig. 7.9. Slip-stick friction during preshear and shear (yield locus test)

Since the amplitude of slip-stick oscillations decreases with increasing shear velocity (Fig. 7.8), it is sometimes possible to reduce the oscillations by a moderate increase of shear velocity to such an extent that a shear test can be performed in the usual way.

If slip-stick friction takes place during a wall friction test, the common test procedure (see Sect. 4.1.4) results in the shear stress pattern shown in Fig. 7.10. The stepwise decrease of shear stress, τ_w , results from the stepwise decrease of normal stress, σ_w . The frequency and amplitude of slip-stick oscillations depend on normal stress and shear velocity.

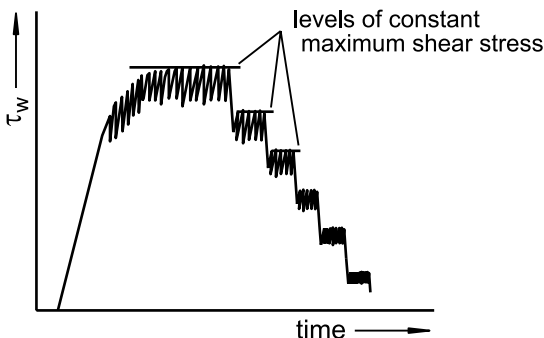


Fig. 7.10. Shear stress in a wall friction test where slip-stick friction occurs

If slip-stick friction occurs during a wall friction test, similar measures are recommended as for a yield locus (see above). At each level of normal stress semi-steady-state flow will prevail, where the shear stress oscillations show constant maximum values (Fig. 7.10). For applications where the maximum wall friction angle is of importance (e.g. mass flow design, Sect. 10.1) the wall yield locus should be constructed with these maximum values. The minimum values of the shear stress oscillations are not meaningful (see Sect. 7.1.1.1.).

7.1.2 Variation of wall friction with displacement

Some combinations of bulk solid and wall material exhibit a change of wall friction angle with shear displacement, i.e., with increasing relative displacement between bulk solid and wall. In Fig. 7.11 are shown results of wall friction tests for especially large relative displacements, Δx [7.10]. The coefficient of wall friction of millet against perspex decreases with increasing shear displacement. Cleaning of the plate resulted in the (higher) wall friction angle observed initially. This indicates that a greasy layer may have formed on the wall surface.

The formation of thin layers adhering to a wall surface can be observed also with certain types of corn and plastic pellets. It can result in a reduction of wall friction angle as in Fig. 7.11 (millet), which is likely to happen especially with initially rough surfaces (e.g., concrete). Also several crystalline products (such as sugar or sodium) tend to form a thin, hardly visible layer on the wall surface. The layer consists of very fine particles which originate, for example, from attrition of the particles, and can lead to a drastic increase of wall friction angle. For example, with the combination of sugar with smooth wall materials (e.g., plastic coating, cold-rolled stainless steel) the author has observed an increase of wall friction angle

from initially about 15° to 20° (clean wall surface) to more than 30° (nearly invisible layer of sugar on the wall surface).

Wall friction angle can change with increasing displacement also due to wear of the wall surface. The wall friction coefficient measured with sand on a stainless-steel surface (Fig. 7.11) increased from about 0.17 to 0.58 and remained at this level even after the wall surface had been cleaned which is an indication of the change of the wall surface.

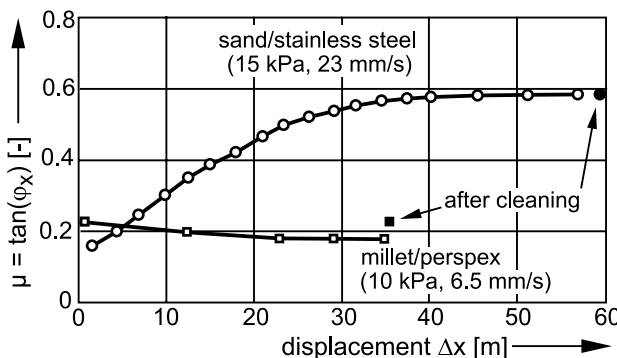


Fig. 7.11. Variation of coefficient of wall friction with displacement, Δx (results taken from [7.10])

If the wall friction angle measured in a test apparatus changes with displacement, the same is to be expected in an equivalent application, e.g., on a hopper wall or on a chute. Thus, when measuring wall friction, attention has to be paid to possible changes of wall friction angle, i.e., the wall friction test must be conducted (or repeated without cleaning the wall material sample between repetitions) until the shear stress does not change further. When applying the measured wall friction angles, e.g., for mass flow design or structural silo design, the total range of measured wall friction angles has to be considered in order to obtain sufficient function and stability for the new equipment in the initial condition as well as after a longer operating time.

7.2 Parameters and conditions influencing flow behavior

7.2.1 Particle size distribution

Adhesive forces acting between individual particles have considerable influence on the flow behavior of bulk solids. Most important for the flow behavior of bulk solids are the forces due to liquid bridges (if sufficient

moisture is present) and van der Waals forces (dominant force in dry, fine-grained bulk solids). Both forces are proportional to particle diameter (see Fig. 2.14, Sect. 2.6). Similar dependencies as in Fig. 2.14 can be found also for adhesive forces between individual particles.

Since in a particle bed the number of contacts per unit area is inversely proportional to the square of the particle diameter, the strength of a bulk solid increases with decreasing particle size, and, thus, flowability decreases (see Sect. 2.7). Examples of the influence of particle size are presented in Sect. 8.5.

Since nearly all bulk solids are composed of particles of different size, fineness cannot be defined exactly by only one parameter, e.g., the median (x_{50}) of the particle size distribution. Therefore, flow properties also do not correlate with only one particular parameter of the particle size distribution so other parameters such as the width of the particle size distribution have to be considered. Unfortunately, the prediction of, for example, flowability on the basis of a particle size distribution is difficult and can sometimes be misleading. Thus, an accurate measurement of bulk solid properties is essential. Nevertheless, the following qualitative rules often apply:

- Flowability of bulk solids having a particle size distribution of similar shape increases with increasing median, x_{50}
- Flowability of bulk solids having the same median, x_{50} , increases with decreasing width of the particle size distribution.

Further measurements and consideration on the influence of the particle size on the flow properties can be found, e.g., in [7.11].

7.2.2 Flow agents

Flow agents are used to improve the flow behavior of bulk solids. This is achieved by a reduction of interparticle adhesive forces.

Coarse, dry products with particles larger than about 100 µm often exhibit good flow behavior because adhesive forces are insignificant compared to gravity forces. For such products flow agents are applied mainly to reduce the tendency to form stable lumps (caking, time consolidation). Flow agents used here are often so-called release agents which prevent the particle surfaces from direct contact, e.g. beeswax as release agent for gummi bears, or talcum powder for animal feed pellets containing molasses.

With very fine-grained, dry bulk solids (“powders”) poor flow behavior is often observed which results from interparticle van der Waals forces. Here highly-dispersed powders like Aerosil® (highly-dispersed silicon di-

oxide), as well as products such as magnesium carbonate, magnesium stearate or lactose are added to reduce adhesive forces. Usually only a small percentage of flow agent is added (typically up to 1 % by weight). The flow agent particles should then adhere to the particles of the bulk solid as shown in Fig. 7.12.b.

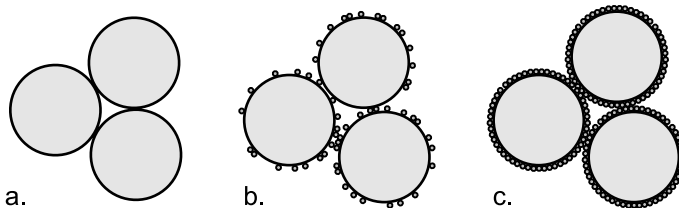


Fig. 7.12: Particle arrangements (sectional view) with and without flow agent (highly-dispersed powder); a. particles without flow agent; b./c. with flow agent; in Fig. c the surface is covered completely.

The effect of flow agent particles is similar to that of an increased surface roughness: The adhesive forces are reduced due to the increased distance between particles. Thus, the term „roller bearing effect“, which is sometimes used for explanation, does not describe correctly what happens. The effect of distance, e.g. due to surface roughness, is outlined in Sect. 2.6 (see Fig. 2.15). Results of an assessment of adhesive forces when a flow agent particle is considered are shown in Fig. 7.13. Adhesive force, F_H , has been calculated for the ideal case that a flow agent particle (radius r) is located between a smooth spherical particle (radius R) and a smooth wall [7.12]. If the distance between wall and flow agent particle is kept constant, the distance between the wall and the spherical particle (radius R) increases with increasing radius, r , of the flow agent particle. Compared to the curves in Fig. 2.15, which were calculated based on the same parameters for a hemispherical roughness, the adhesive forces in Fig. 7.13 are slightly smaller because the distance between the wall and the spherical particle is greater for the same value of r (distance $r + a_0$ in Fig. 2.15 and $2r + a_0$ in Fig. 7.13).

A calculation based on the adhesive forces between two particles with a flow agent particle in between [7.13] is a somewhat more realistic approach than the above calculation of forces between a particle and a wall. However, this calculation leads to slightly smaller adhesive forces, but shows the same general tendencies (Fig. 7.14).

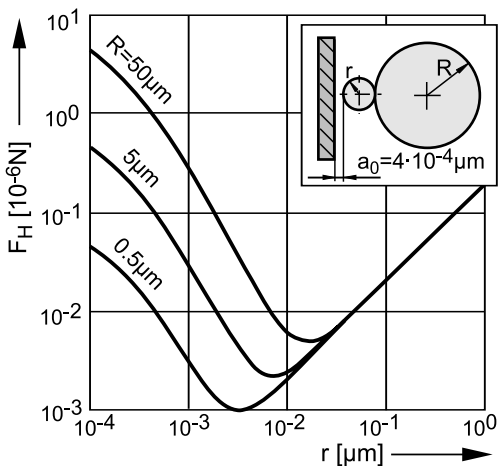


Fig. 7.13. Influence of radius, r , of a spherical flow agent particle on the adhesive force, F_H , between a spherical particle (radius $R = 0.5 \mu\text{m}$, $5 \mu\text{m}$, and $50 \mu\text{m}$) and a smooth wall at constant contact distance, $a_0 = 4 \cdot 10^{-4} \mu\text{m}$ (after [7.12]; calculated newly with parameters of Fig. 2.15)

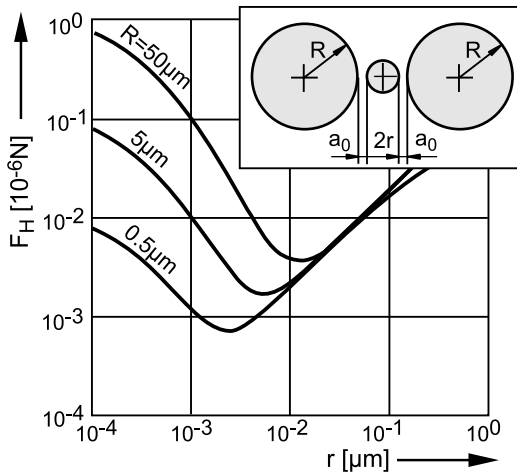


Fig. 7.14. Influence of radius, r , of a spherical flow agent particle on the adhesive force, F_H , between two spherical particles of equal radius, R ($R = 0.5 \mu\text{m}$, $5 \mu\text{m}$, and $50 \mu\text{m}$) at constant contact distance, $a_0 = 4 \cdot 10^{-4} \mu\text{m}$ (calculated after [7.13] with parameters of Fig. 2.15)

In the right part of the diagrams in Figs. 7.13 and 7.14, i.e., for greater values of the particle radius, r , of the flow agent, the adhesive force is increasing with r . Here the adhesive force of the flow agent particle itself is significant (see Fig. 2.14: the adhesive force increases with increasing particle

diameter). This demonstrates that flow agent particles must be sufficiently small in order to limit the adhesive forces of the flow agent particles themselves. According to Figs. 7.13 and 7.14, powders applied as flow agents should have particle diameters in the range of about 5 nm up to some 100 nm (depending on the particle size of the bulk solid to which the flow agent is added). However, general statements are difficult to make.

If a flow agent is added to a cohesive powder, one can expect an initially increasing improvement of flow behavior with increasing concentration of the flow agent, because the flow agent covers an increasing percentage of the particle surfaces. Thus, the probability of two adjacent particles of the cohesive powder being separated by one or more flow agent particles is increasing [7.12–7.15] (see Fig. 7.12.b). If the surface coverage is increased further until the flow agent influences all particle contacts, the best possible flowability is attained. A further increase of the flow agent percentage until the particle surfaces are totally covered (Fig. 7.12.c) does not improve flowability further, but can result in less favorable flow properties. One possible reason for the latter is the formation of larger contact areas between the particles being totally covered with flow agent particles [7.15].

Since flow agents are often based on nanosized particles, it has to be considered that these particles form stable aggregates, which adhere to each other thus forming less stable agglomerates with porous and branched structures (Fig. 7.15.a) [7.12].

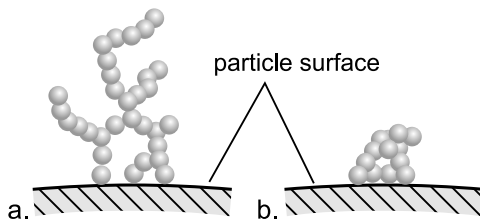


Fig. 7.15. Agglomerates of nanosized flow agent particles adhering at a particle surface during mixing [7.12]; a. at the beginning of the mixing process individual agglomerates, often exhibiting a branched structure, adhere to the particle surface; b. during further mixing the agglomerates break and smaller fragments adhere to the surface.

Insight into the complex behavior of nanosized flow agents is provided by the results of investigations on the action of different flow agents [7.12–7.15]: If a flow agent is mixed with a cohesive bulk solid, at first agglomerates of flow agent particles adhere to the particles (Fig. 7.15.a). Since the agglomerates have a relatively loose structure, they are neither very stable

nor adhere very firmly to the particle surface. Thus, during further mixing agglomerates either break thus forming smaller fragments (aggregates or smaller agglomerates) or separate from the particle surface. The fragments adhere more firmly to the particle surface than the initial agglomerates (Fig. 7.15.b) and, thus, cover the particle surface increasingly with increasing mixing time.

During the mixing process the flowability of the cohesive bulk solid is improved until a certain surface coverage is attained, i.e., a certain percentage of the particle surfaces is covered with the flow agent fragments. During further mixing the flowability does not increase although the surface coverage is increased further (the same effect has been observed for an increasing flow agent percentage, see above). Finally, after long mixing times, the flow agent can form a dense, smooth layer thus reducing the roughness of the particle surfaces [7.15]. This allows for smaller particle/particle distances and, therewith, a decrease of flowability.

The effect of a flow agent as discussed above is likely to be more pronounced if it is added to a bulk solid having smooth particles. If the particle surfaces are rough, the flow agent particles will preferentially collect within the valleys so the effect on interparticle distance is smaller.

Also liquids are used as flow agents, e.g., for cement grinding so-called “grinding aids” (e.g., triethanolamine, propylene glycol) are utilized, which reduce interparticle adhesive forces, for example, by forming adsorption layers with smaller Lifschitz-van der Waals constants, and thus reduce the tendency for agglomeration. Therefore these liquids act as flow agents.

The effect of flow agents cannot be predicted exactly. Thus, it is recommended to determine the optimal conditions by measuring flow properties (e.g., with a shear tester) of samples with different percentages of different flow agents. Furthermore, mixing time and process can play a role and, thus, should be considered.

7.2.3 Liquids, moisture

If a small amount of low viscosity liquid is added to a dry bulk solid which is wettable by the liquid, the liquid accumulates in narrow gaps between particles and forms liquid bridges (Fig. 7.16.a). The liquid bridges increase interparticle adhesive forces due to their surface tension and a possible negative capillary pressure (see Sect. 2.6). This results in an increase of the material’s strength and a pronounced decrease of flowability (Fig. 7.17). If further liquid is added, the liquid bridges grow and the first saturated regions appear (Fig. 7.16.b) so flowability decreases further but usually less

strong (Fig. 7.17). Finally the bulk solid is saturated with liquid (Fig. 7.16.c), i.e., the voids within the bulk solid are totally filled with liquid so that liquid surfaces and their surface tension disappear. As soon as saturation is attained, flowability increases sharply, and the moist bulk solid is transformed into a suspension. The moisture content at saturation is not one fixed value, but lies within a range as indicated in Fig. 7.17. The reason for this is explained in the following.

Saturation means that the degree of saturation, S , according to Eq.(2.25) is equal to 1:

$$S = \frac{V_{Liquid}}{V_{Voids}} = \frac{V_{Liquid}}{\varepsilon \cdot V} = 1 \quad (7.1)$$

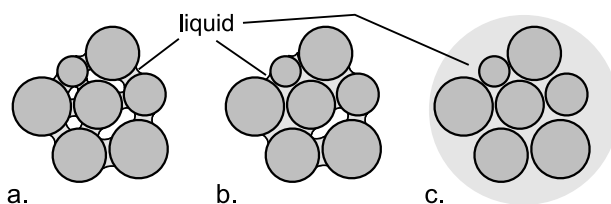


Fig. 7.16. Particles with different amounts of liquid; a. liquid bridges; b. liquid bridges and saturated regions; c. saturated bulk solid

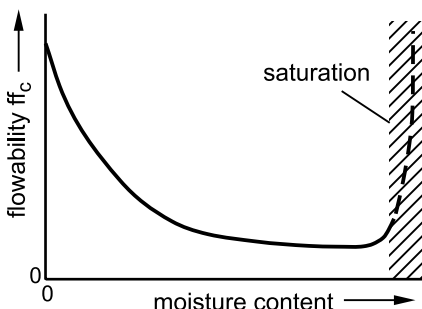


Fig. 7.17. Flowability as a function of moisture content (in principle)

The bulk density, and thus the porosity, ε , of a bulk solid can change. A very moist but not yet saturated bulk solid can be transformed into a saturated state alone by compaction, i.e., without further addition of liquid. This effect can be demonstrated, for example, on a beach during falling tide: when one starts to tap his foot on a section of moist sand, the initially stable sand below the foot begins to compact (ε decreases) and becomes a suspension (saturation). Thus it becomes clear that saturation can be at-

tained at different values of moisture content, dependent on the actual bulk density. This is indicated in Fig. 7.17 by the hatched area.

If a saturated bulk solid is dewatered, e.g., by gravity, the capillary pressure in the remaining liquid is greater than that in a liquid which has been added to an initially dry bulk solid (same moisture content in both cases). Due to the larger capillary pressure, the flow properties of the dewatered bulk solid are less favorable (e.g., tensile strength is larger) [7.11,7.16]. Handling of saturated bulk solid might cause unexpected problems because it initially appears to be good flowing (slurry), but soon after a small amount of liquid has drained off, a state just below saturation is attained where flowability is especially poor (Fig. 7.17).

Regarding the influence of moisture on the flow properties of bulk solids one has to distinguish between inherent moisture including pore fluid, i.e., moisture which is bound within the particles, and surface moisture, which forms liquid bridges and, thus, has a strong effect on flow properties. Especially when the flow properties of a bulk solid should be tested for a specific moisture content, but the bulk solid has lost moisture prior to the test (e.g., due to contact with the atmosphere) it has to be checked critically whether the addition of moisture can lead to the same conditions as prior to drying. Products like, for example, lignite contain relatively high inherent moisture. If after drying the same amount of moisture is added which previously had been removed by drying, the particles cannot take up their initial amount of inherent liquid. This results in excess surface moisture (sometimes saturation is attained) and flow properties which are different from the flow properties in the initial state.

Not only strength of a bulk solid is influenced by moisture, but also friction between a bulk solid and a rigid wall surface (wall friction). If a moist bulk solid is in contact with a surface (Fig. 7.18.a), liquid bridges are formed between particles and wall surface (Fig. 7.18.b), which result in adhesive force, F_H (Fig. 7.18.c). Thus, the contact force, F_K , between a particle and wall is not only caused by the normal force, F_N , resulting from the vertical stress, σ , applied to the bulk solid, but also by the adhesive force, F_H . Thus, as indicated in Fig. 7.18.c, $F_K = F_N + F_H$.

If the bulk solid is moved across the wall (velocity v , Fig. 7.18.a), those particles that are in contact with the wall surface have to move relative to the surface. Thus a sufficiently large tangential force, F_T , must act on each of these particles in order to overcome the friction force, F_R , between particle and wall surface. The friction force is equal to the contact force, F_K , multiplied by the wall friction coefficient, μ . Thus, without any external normal stress, σ , a force $F_T > 0$ is required to move the particle along the surface. The (mean) shear stress between the bulk solid and the wall, τ , which results from the tangential force, F_T , is plotted in Fig. 7.18.d versus

the externally applied normal stress, σ . With the assumption of a constant coefficient of friction, μ , the function $\tau(\sigma)$ is a straight line intersecting with the shear stress axis at a value $\tau > 0$. This line is a wall yield locus (Sect. 3.3.2), which does not run through the origin due to the adhesive forces caused by the liquid bridges. The shear stress at the point of intersection is known as adhesion, τ_{ad} (see Sect. 3.3.2, Fig. 3.29).

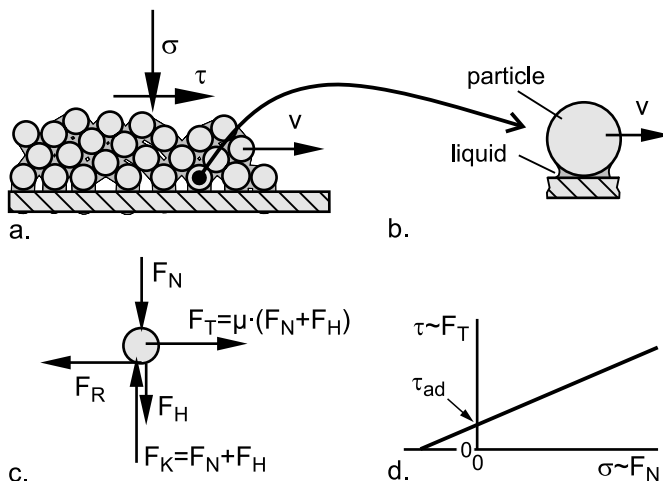


Fig. 7.18. Influence of moisture on wall friction; a. bulk solid is moved across a wall surface; b. liquid bridge between particle and wall surface (wetting liquid); c. forces acting on a particle being moved across the wall surface; d. shear stress, τ , required to move the bulk solid across the wall surface as a function of external normal stress, σ .

The influence of moisture content on wall friction angle of wettable wall materials is often similar to its influence on the bulk solid's strength or flowability, respectively (Fig. 7.17). Starting from dry product, wall friction angle increases at first steeply with increasing moisture content, then attains a plateau, and finally decreases if the moisture content approaches saturation.

On wall materials which are not or just poorly wettable (e.g., water in combination with PTFE or UHMW-PE) no adhesion enhancing liquid bridges can be formed. Here sometimes a decrease of wall friction angle with increasing moisture content can be observed. Some examples of the influence of the moisture content are given in Sect. 8.2.

7.2.4 Gas flow

If gas (e.g., air) flows through a layer of bulk solid, the behavior of the particle bed depends on the gas velocity. One has to distinguish between three regimes, namely the stationary particle bed, the fluidized bed, and pneumatic conveying. The transition between these regimes is shown in Fig. 7.19, where the pressure drop is plotted versus superficial gas velocity (i.e., the volume per unit time of gas divided by the cross-sectional area).

If a stationary particle bed is subjected to an upward directed gas flow with increasing velocity, the particle bed remains undisturbed (fixed bed) as long as the gas velocity is not too large. The pressure drop, Δp , across the bed increases with increasing gas velocity and acts against the gravity force, i.e., the flowing gas supports an increasing portion of the weight of the particle bed. When the gas velocity is sufficiently high and approaches the minimum fluidization velocity, w_L , the particle bed starts to expand slightly and becomes fluidized. At this stage the pressure drop is large enough to carry the weight of the particle bed. At the onset of fluidization a local maximum in the plot of the pressure drop may appear (see Fig. 7.19) which depends on the bulk solid and its degree of consolidation. The maximum results from expansion of the initially fixed particle bed, where adhesive forces must be overcome. When decreasing the gas velocity from the fluidized state no maximum can be observed since the bulk solid settles slowly and no adhesive forces have to be overcome. Furthermore, the pressure drop may be smaller when decreasing the gas velocity from a fluidized state because of the looser packing (see Fig. 7.19, increase and decrease of gas velocity is indicated by the arrows in the fixed bed region).

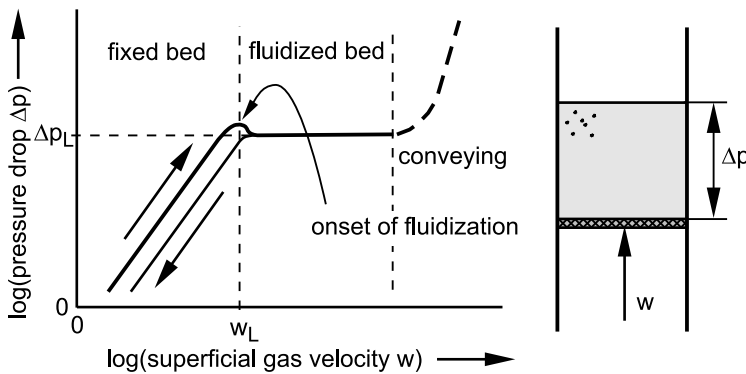


Fig. 7.19. Pressure drop, Δp , across a particle bed vs. superficial gas velocity, w (note logarithmic scaling). Δp_L is the pressure drop in the fluidized state (homogeneous fluidization). [7.17,7.18]

Further increase of superficial gas velocity ($w > w_L$) causes the particle bed to expand further, whereby the pressure drop, $\Delta p = \Delta p_L$, remains almost constant. In this regime the effect of gas velocity on pressure drop is compensated by the increasing permeability due to increasing voids (expansion). Only at much larger gas velocities individual particles are carried upwards which is equivalent to the onset of pneumatic conveying. From this point the pressure drop increases further with increasing gas velocity.

As long as the particles remain stationary (fixed bed), the gas flow does not change the flow properties. Only after the onset of fluidization the flow behavior changes dramatically since the aerated bulk solid behaves like a fluid, e.g., by forming a horizontal surface. Naturally, in this state the bulk solid flows better than in the non-fluidized state, which can be positive with respect to the initiation of flow (e.g., pneumatic discharge aids, see Sect. 12.2.1), but can also result in unwanted effects, e.g. uncontrollable outflow (flooding) resulting in dosage problems or dangerous situations. Based on such observations sometimes people characterize the flow behavior with terms like “flows like water”. However, it must be considered that this does not characterize the flowability, ff_c , of the bulk solid in an aerated state, but in a state of fluidization. A previously fluidized material can even exhibit poor flowability after settling and deaeration. With a shear tester the properties of a bulk solid are measured in a deaerated state.

If the superficial gas velocity is smaller than the minimum fluidization velocity (fixed bed, $w < w_L$), the pressure drop due to the gas flow counteracts the force of gravity and, thus, reduces the stresses acting in the particle bed, but not the flow properties of the bulk solid [7.19]. This effect can support the flow of a bulk solid in some situations, so that on first sight it might appear as if the gas flow would improve the flow properties. This, however, is usually not the case. This is illustrated by two examples in the following.

Example 1: Layer of bulk solid on an inclined porous surface (Fig. 7.20):

The pressure drop, Δp , across the layer of bulk solid (fixed bed, not fluidized) which is subjected to an upward gas flow from the porous bottom causes a force, F_p , which acts against that component of the gravity force, F_G , which is oriented perpendicular to the porous surface. Since this reduces the normal force, F_N , acting between the bulk solid layer and the porous surface, the maximum friction force, F_R , between the bulk solid and the surface is also reduced. The wall friction angle, φ_x , remains unchanged (if it is independent of the normal stress):

$$F_R = F_N \cdot \tan(\varphi_x) \quad (7.2)$$

Since here the gas flow reduces the friction force, F_R , the layer of bulk solid can slide downwards on the surface at smaller inclination angles than without gas flow. Thus, the injected gas supports the flow of the bulk solid without changing its flow properties (here: wall friction).

If one would increase the gas velocity to such an extent that the bulk solid becomes fluidized, it would flow like a liquid across the porous surface. In this case the flow properties had been changed by the gas flow.

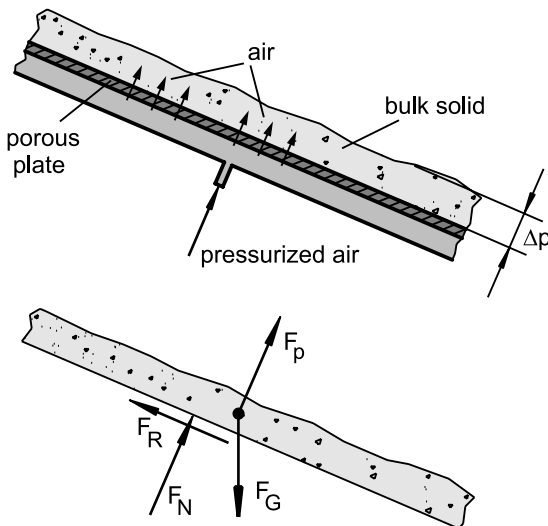


Fig. 7.20. Layer of bulk solid on an inclined porous surface; forces acting on the layer

Example 2: Bulk solid arch in a hopper (Fig. 7.21):

If air is injected into the hopper of a silo as shown in Fig. 7.21, most air flows towards the outlet opening if the filling level and, thus, the flow resistance, of the material in the silo shaft is sufficiently high. Fluidization of the bulk solid in the sense of a fluidized bed is usually neither intended nor attained (even if sometimes the word “fluidization” is used to describe the effect of air injection devices, e.g., pneumatic discharge aids). The effect of downward air flow on a stable arch in a hopper is illustrated in Fig. 7.21. The pressure drop, Δp , across the arch and the resulting force, F_p , act in the same direction as the gravity force of the arch. Therefore, the gas flow increases the arch supporting force, F_A , at the hopper wall. If the pressure drop across the arch is sufficiently large, the major stress in the arch overcomes the strength of the bulk solid (unconfined yield strength, σ_c) and the arch fails.

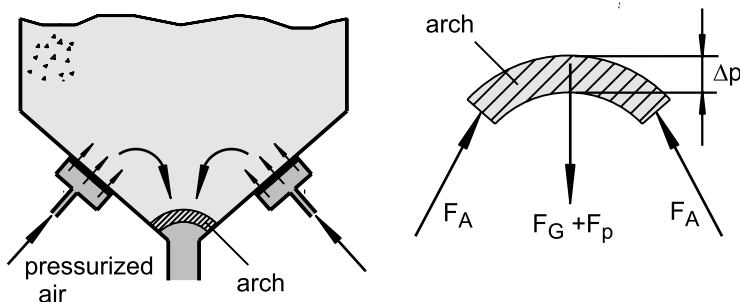


Fig. 7.21. Flow promotion by injection of air

A further example where flow properties are not changed by gas flow is the effect of the gas pressure gradient in a hopper on the discharge rate. This is discussed in Sect. 12.1.

A classification of dry bulk solids regarding their fluidization behavior has been published by Geldart [7.20]. It is shown in Fig. 7.22 with boundaries according to Molerus' calculations [7.17,7.18].

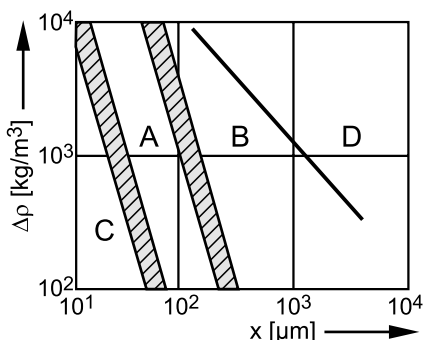


Fig. 7.22. Geldart's classification of fluidization behavior with boundaries according to Molerus [7.17,7.18]

Geldart identified four regions (A to D) in which the fluidization characteristics can be distinctly defined based on particle size, x , and the difference, $\Delta\rho$, between solid density and fluid density (note that the boundaries are not sharply defined):

- Easy to fluidize, sometimes simply by shaking or stirring; considerable expansion of the fluidized bed; slow settling of the bed when the gas flow is stopped. Strong tendency for flooding.
- Not as easy to fluidize as group A, small expansion of the bed at fluidization, deaerates and settles quicker than A, therefore there is only a low flooding tendency.

- C. Small particles, cohesive behavior due to the dominance of interparticle adhesive forces. Fluidization cannot be attained without further assistance, e.g., by stirring. Air flow results in formation of stable channels, while material between the channels remains stationary (similar to a fixed bed). Low tendency to flooding.
- D. Coarse particles, very large gas velocities required for fluidization. Due to their very low gas flow resistance, these products settle and deaerate very quickly. Thus, flooding is unlikely to occur.

The above consideration shows that air injection influences the behavior of group A products the most. Such products are fine-grained, but not too fine bulk solid, e.g., with particle diameters from about $20\text{ }\mu\text{m}$ to $100\text{ }\mu\text{m}$ and solid densities in the range from about 2000 kg/m^3 to 3000 kg/m^3 . For group B products air injection can also be applied, but this is often not economical because of the larger required air flow rates. The same is even more true for group D. If, however, the particles are too small (group C), channels are formed by the air which inhibit a homogenous permeation of the particle bed. Thus, the mechanisms shown in Figs. 7.20 and 7.21 are unlikely to work well with group C products.

7.2.5 Particle shape

Although particle shape affects flow properties, general statements about this effect cannot be made. When considering coarse particles (say larger than 0.5 mm), one often finds that smooth, spherical particles flow better than rough, sharp-edged, non-spherical particles. For cohesive bulk solids a statement is not that easy since the interparticle adhesive forces play the major role. A pronounced roughness can hinder the ability of particles to approach each other as smooth particles can, so the rough particles may exhibit a more favorable flow behavior (see Sect. 2.6 and effect of flow agents in Sect. 7.2.2).

Whereas it is possible to characterize all kinds of typical bulk solids with the usual test procedures (e.g., shear testers), the same is much more difficult for not too fine-grained (estimate: particles larger/longer than roughly 1 to 2 mm) fibrous and flaky particles of small thickness. These products can result in severe handling problems. Typical examples taken from recycling processes are shredded tires (high portion of fibers and steel wires) and shredded foil (plate-like particles of small thickness). Fibrous and flaky materials have to be handled in many other industries, e.g., when producing fiber-reinforced plastics, brake pads or chipboards. Since theoretical approaches to describe the behavior of these materials are not

known, their behavior is discussed in the following based on observed phenomena and a simple model.

Flow problems with fibrous and plate-like particles often appear when the material is subjected to high stresses. A practical example is shown in Fig. 7.23, where discharge by an elongated feeder (chain feeder) results in severe compaction of the bulk solid near the outlet at the front wall and, thus, excessive driving forces, F_h . In this region the longitudinal axes of the particles are preferentially oriented perpendicular to the assumed direction of major principal stress. The flow properties of such products cannot be measured with shear testers because they exhibit reasonable flow behavior in the loose state, but become less favorable with increasing load (as demonstrated in Fig. 7.23). This behavior is discussed in the following by measurements with a test mould shown in Fig. 7.24 [7.21].

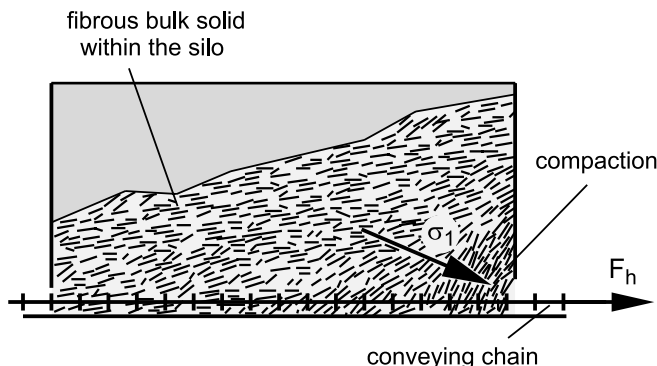


Fig. 7.23. Discharge of a bulk solid composed of thin, flexible flakes with a chain feeder, compaction at the front wall; possible direction of the major principal stress, σ_I , in the region of compacted material

With the test set-up the compressibility and elasticity of the bulk solid are measured by loading and unloading the bulk solid specimen through the vertically movable lid (Fig. 7.24.a). From the applied vertical force and the displacement of the lid, the vertical stress, σ_v , and strain, ε_v , are calculated. Since during compaction elastic deformation is superimposed by plastic deformation, the elasticity is measured while unloading the lid, i.e. during elastic recovery.

A second application of the test mould follows the principle shown in Fig. 7.24.b. The bulk solid specimen is at first subjected to a vertical stress, σ_I . Subsequently the lid is fixed in position, the closing plate at the bottom of the test mould is removed, and the center part of the lid, the circular loading plate, is moved downwards (force F_D) until the material fails (flows). The force required to initiate flow, the failure force, $F_{D,max}$, is re-

garded as a measure of the strength or the flow resistance, respectively, of the bulk solid. The test simulates conditions similar to those at the outlet of the silo shown in Fig. 7.23. However, as outlined in Sect. 6.3.15, where a similar procedure is used for the measurement of flowability, this test can only give qualitative results.

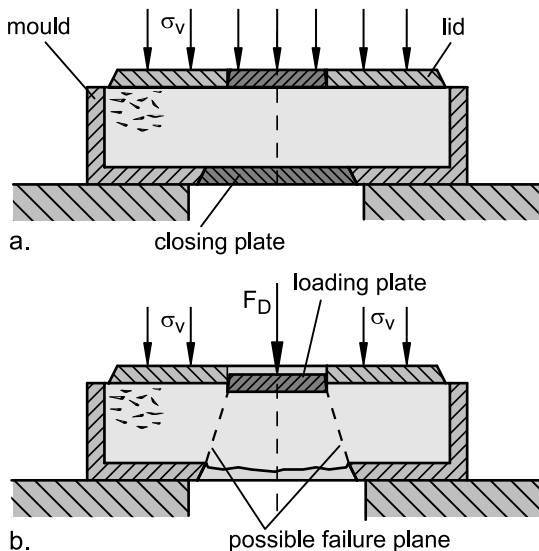


Fig. 7.24. Test mould: a. compaction; b. measurement of failure force, F_D (in principle)

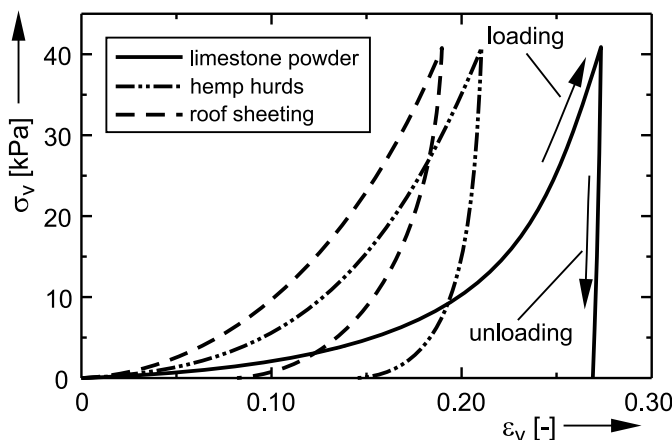
In a test series different products composed of fibers and flakes have been investigated. For comparison, a typical cohesive bulk solid, namely limestone powder, was also tested. Table 7.1 shows the characteristics of the individual bulk solids.

For compressibility and elasticity measurements the bulk solid specimen is first consolidated by a vertical stress of about 40 kPa, and subsequently unloaded. Examples of the measured stress-strain relationships are shown in Fig. 7.25.

The relatively fine-grained, cohesive limestone powder exhibits pronounced compressibility which is indicated by the large strain, ε_v , at maximum stress. The typical progressive slope of the stress-strain curve results from increasing bulk density, which makes the bulk solid increasingly stiff and, thus, makes further compression increasingly difficult. While unloading the specimen from the vertical stress, elastic recovery takes place with a stress-strain curve being clearly steeper than during loading.

Table 7.1. Bulk solids

Bulk solid	Description	Particle size and shape
Limestone powder	Typical cohesive bulk solid	$x_{50} = 4.7 \mu\text{m}$, round/cubical
Pig hair	Native product	Short hairs, length 1 to 2 mm, diameter < 0.1 mm
Hemp hurds	Native product (core fiber from the woody stalk)	Slim, partly cylindrical particles with tapered ends, length ca. 10 – 30 mm, diameter ca. 2.5 mm
Decorative overlay for furniture (shred)	Recycled material (cutting mill)	Thin plates of irregular, polygonal shape, thickness ca. 0.2 – 0.5 mm, length and width up to ca. 8 mm (median ca. 3 mm)
Plastic coffee cups (shred)	Recycled material (cutting mill)	Thin plates of irregular, polygonal shape, thickness ca. 0.2 mm, length and width up to ca. 8 mm (median ca. 2.5 mm)
Roof sheeting (shred)	Recycled material (cutting mill)	Thin plates of irregular, polygonal shape, thickness ca. 1.5 mm, length and width up to ca. 8 mm (median ca. 2.9 mm)

**Fig. 7.25.** Vertical stress, σ_v , vs. vertical strain, ε_v , while loading and unloading a specimen within the test mould

The shredded products (roof sheeting and hemp hurds) exhibit a clearly larger recovery strain (up to 53% of the total strain) than limestone powder. The reason for this is their particle shape: Both products consist of relatively flexible, plate-like particles, which form a very dense packing under load, and the particles change their orientation and adjust their shape as they “snuggle up” to each other. While unloading the specimen, the slope of the stress-strain curve becomes flatter with decreasing stress, i.e.,

the specimen becomes less stiff (this effect can also be observed with the limestone powder, Fig. 7.25, but clearly less pronounced), and the particles return to their initial shape to a certain extent, i.e., the plastic deformation of the particles is limited. Thus, the plastic deformation of the total bulk solid specimen results primarily from an increase in bulk density and only to a smaller extent from the plastic deformation of the particles.

Failure force, $F_{D,max}$, is measured in a test mould as shown in Fig. 7.24.b (diameter 250 mm, height 128 mm; diameter of loading plate 80 mm, diameter of bottom opening 100 mm). The bulk solid specimen is subjected to a vertical stress of 40.7 kPa. Subsequently, after removal of the closing plate, the loading plate is moved downwards (force F_D). The force-displacement curves for this step are shown in Fig. 7.26.

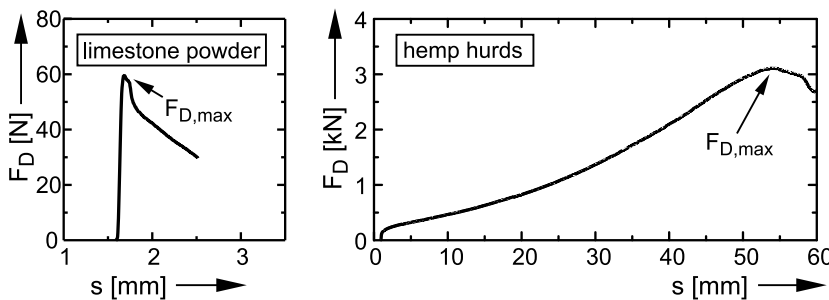


Fig. 7.26. Vertical force, F_D , vs. vertical displacement, s , of the loading plate, measured with limestone powder and hemp hurds; diameter of the loading plate 80 mm, diameter of the bottom opening 100 mm, bulk solid specimen consolidated with $\sigma_v = 40.7$ kPa [7.21].

The limestone powder shows a steep increase of the force, F_D . Failure of the specimen occurs at about $F_{D,max} = 60$ N (this force corresponds to a vertical stress beneath the loading plate of about 12 kPa). After failure the force decreases sharply (Fig. 7.26). The failure force, $F_{D,max}$, measured with hemp hurds is greater than 3000 N (corresponding to a vertical stress below the loading plate of about 600 kPa) and, thus, clearly larger than that measured with limestone powder. Furthermore, a significant vertical displacement of the loading plate is necessary until failure occurs. A completely different behavior is found for the roof sheeting particles, which exhibit a similar stress-strain relationship at compaction (Fig. 7.25): Immediately after the closing plate is removed, the roof sheeting particles flow through the bottom opening, i.e., $F_{D,max} = 0$.

The results reported above (and further measurements [7.21]) show that bulk solids composed of fibrous and plate-like particles with a sufficiently small ratio of thickness to length, and a length of at least several millime-

ters, require relatively large failure forces, $F_{D,max}$, which can amount to more than fifty times the force required for cohesive limestone powder. On the other hand, even these products show reasonable flow behavior in a loose, uncompacted condition. Obviously a mechanism is acting in these products which results, in contrast to typical bulk solids like limestone powder, in increasing strength while the material is increasingly stressed by the loading plate.

An explanation for this behavior can be given by a simple model: The load applied through the lid and the loading plate when compressing the material before the failure force is measured (Fig. 7.24.b) results in vertical stress acting in the bulk solid specimen. Thereby horizontally oriented particles tend to remain in their orientation, but particles having an inclined orientation are likely to approach a more horizontal orientation (Fig. 7.27). Flexible, thin particles may become bent in this situation, so only a part of such a particle adjusts to a more horizontal position (this effect is not depicted in Fig. 7.27). The result of the deformation is a more intensive overlap of the particles and, thus, an increase of the transferable friction force.

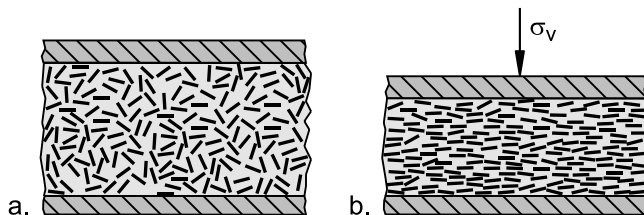


Fig. 7.27. Orientation of plate-like particles (schematically); a. before compaction; b. after compression in the vertical direction (vertical stress, σ_v)

When the loading plate is moved downwards to measure the failure force, $F_{D,max}$, a failure plane as indicated in Fig. 7.24.b develops. If it is assumed that after compaction the particles are primarily oriented horizontally (Fig. 7.28.a), the particles must adjust their orientation to the failure plane. This is demonstrated in Figs. 7.28.b and c where the possible formation of a shear zone is shown for two plates which are moved vertically against each other. Stiff particles must change their orientation according to Fig. 7.28.b to form a shear plane. If particles are sufficiently flexible, the particle shape can adjust to the direction of the shear plane (Fig. 7.28.c). In both cases individual particles have to be extracted from the bond of horizontally oriented particles left and right of the developing shear plane, i.e., friction acting on the particle surface has to be overcome.

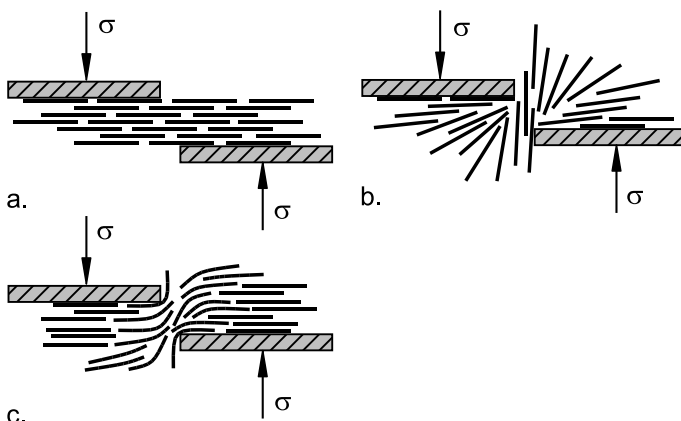


Fig. 7.28. Orientation of particles along the shear plane while measuring failure force according to Fig. 7.24.b; a. after compaction, i.e., before the loading plate is moved downwards; b. formation of a shear plane in case of stiff particles; c. formation of shear plane in case of flexible particles

Transferring the model of Fig. 7.28 to conditions in the test mould (Fig. 7.24.b) it becomes clear that formation of a failure plane is made difficult by the following mechanisms:

- The bulk solid cannot expand unhindered in the region where the failure plane forms to provide sufficient space for rearrangement of the particles (Figs. 7.28.b and c).
- The increasing vertical force, F_D , exerted through the loading plate increases the normal stress between the particles and, thus, an increasing shear stress is required to move the particle surfaces relative to each other. Therefore, formation of a failure plane becomes more difficult with increasing vertical force, F_D .

Due to these mechanisms the specimen gains in strength as a result of the increasing force, F_D , exerted through the loading plate: If F_D is increased, the friction forces between the particles increase which requires a higher force F_D to form the failure plane and so on. In other words: The force which should initiate failure increases the strength of the material further. This effect leads to the high values of $F_{D,max}$ as measured with some of the investigated materials (Table 7.1) in the test mould according to Fig. 7.24.b.

A typical bulk solid, here represented by limestone powder, does not exhibit this behavior since the particles neither arrange in a specific orientation nor overlap to a noteworthy extent. Thus, a typical bulk solid fails in a situation as in Fig. 7.24.b as soon as the strength of the material is over-

come. As outlined above, with fibrous and flaky particles (e.g., hemp hurds, shred coffee cups and shred overlay, see Table 7.1) the increasing force, F_D , increases the frictional forces between particles and, thus, increases the strength of the material. For this effect the ratio of particle thickness to length must be sufficiently small. This is obviously not the case for the shredded roof sheeting (Table 7.1). Also the pig hair (Table 7.1), a product consisting of thin, relatively short fibers, exhibited a behavior similar to the limestone powder despite its fibrous character. Here the rearrangement of particles for the formation of the failure plane is facilitated by the small particle dimensions.

Based on test results and further theoretical considerations not discussed here [7.21], it can be concluded that with fibrous and flaky particles more problems and differences from the behavior of typical bulk solids have to be expected,

- the larger the ratio of particle length to thickness;
- the larger the friction coefficient between the particle surfaces,
- and the smaller the porosity, ε .

Furthermore, observations from practical handling situations (e.g., Fig. 7.23) and the tests described above (Fig. 7.24) show that high stresses and local stress concentrations should be avoided when storing, discharging or conveying fibrous or flaky particles.

Shear testers and other test devices (e.g., uniaxial compression test), where a specimen is first consolidated and then relieved from the consolidation stress before strength is measured, should not be used for those bulk solids whose behavior is dominated by fibrous and flaky particles such as hemp hurds. If these test principles are applied, the bulk solid specimen will show a pronounced expansion due to elastic recovery (as can be seen in Fig. 7.25 for the hemp hurds) when being unloaded after the consolidation step (unloading means reduction of the normal stress for shear to failure in a shear test, Fig. 3.12, or relief from the consolidation stress and removal of the hollow cylinder in case of a uniaxial compression test, Fig. 3.1). Thus, the properties of the specimen change during unloading, and strength is measured on a specimen of higher porosity which is likely to be less consolidated than at the end of the consolidation process. However, wall friction tests, where a bulk solid specimen is moved across the surface of a wall material sample (Fig. 3.27), can be conducted with these materials.

8 Examples of measured flow properties

The flow properties of powders and bulk solids depend on several parameters, e.g., particle size distribution, moisture, temperature. Often flow properties vary with stress level. Flow agents, added to a bulk solid, can improve flow behavior. Besides flow properties, in specific situations other effects may be of interest, e.g., attrition of particles when flowing in a silo. In the present chapter such effects are demonstrated on the basis of measured flow properties.

Although the examples presented in the following cannot be applied directly on other bulk solids, they should point out which effects can be expected and how these effects can be quantified with appropriate testing equipment.

8.1 Flow agent

Flow agents are applied to improve the flow behavior of bulk solids (see Sect. 7.2.2). An example is shown in Fig. 8.1, where the flowability, ff_c , of a crystalline bulk solid is plotted versus flow agent concentration. The product had to be improved by the addition of a flow agent because it exhibited a strong time consolidation effect. To find the optimal concentration, samples with different percentages of flow agent were prepared. With each sample a yield locus (instantaneous properties) as well as a time yield locus for a storage time of 22 hours ($t = 22$ h) has been measured with a shear tester. As can be seen from Fig. 8.1, the sample with the concentration 0.55 % resulted in the largest flowability both for instantaneous conditions and after time consolidation. An increase of flow agent concentration beyond 0.55 % led to a reduction of flowability.

This example illustrates how one can quantitatively predict the effect of a flow agent on flowability. Another example is shown in Fig. 8.2, where a mixture of pepper extract (liquid) and salt was tested both with and without a flow agent ($MgCO_3$). The product without flow agent looked less dry and showed a strong tendency to form agglomerates, which is a typical indication of a less favorable flow behavior. This is in accordance with the

test results obtained at a relatively small consolidation stress (approx. 1000 Pa, Fig. 8.2), where the material with flow agent showed a smaller unconfined yield strength, σ_c , and thus a higher flowability, ff_c , than the product without flow agent.

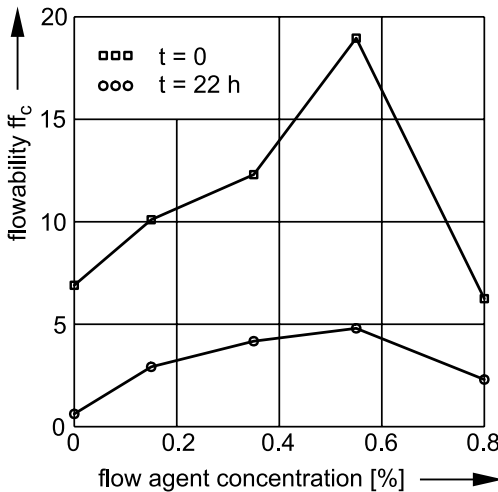


Fig. 8.1. Flowability, ff_c , of a crystalline product as a function of flow agent concentration (instantaneous behavior, $t = 0$, and behavior after 22 hours storage under consolidation stress) [8.1]

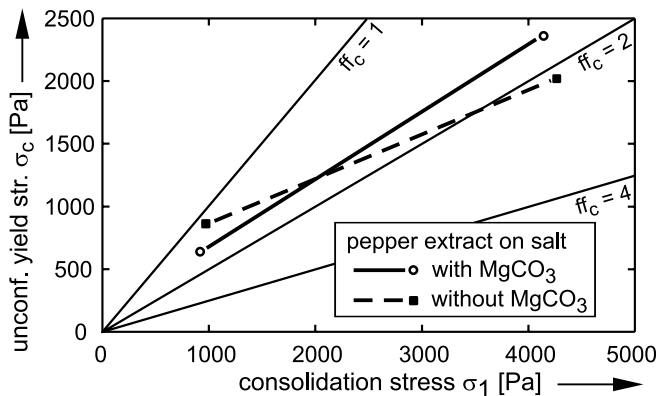


Fig. 8.2. Unconfined yield strength, σ_c , of pepper extract on salt, with and without flow agent ($MgCO_3$); lines of constant flowability, ff_c

However, shear tests on the same samples at a higher consolidation stress of about 4000 Pa (Fig. 8.2) showed slightly higher flowability of the product without flow agent compared to the product with flow agent. Thus, the

flow agent improves flowability only at small stresses. If the material has to be handled or stored at higher stresses (e.g., in a large container or silo) the flow agent (and flow agent concentration) according to the test results in Fig. 8.2 does not help. Thus, the flow agent should be left off, or it should be checked based on shear tests if a different flow agent concentration could improve flowability at higher stresses. However, if the product is handled at small stresses (e.g. in a small dosage system), the flow agent will improve the flow behavior.

8.2 Moisture content

If moisture is added to a bulk solid, it forms liquid bridges between particles and, thus, increases interparticle adhesive forces (Sect. 7.2.3). Additionally moisture can result in specific mechanisms depending on the bulk solid, e.g., chemical reactions or forming a solution on the particle surface with subsequent crystallization, which can result in severe time consolidation.

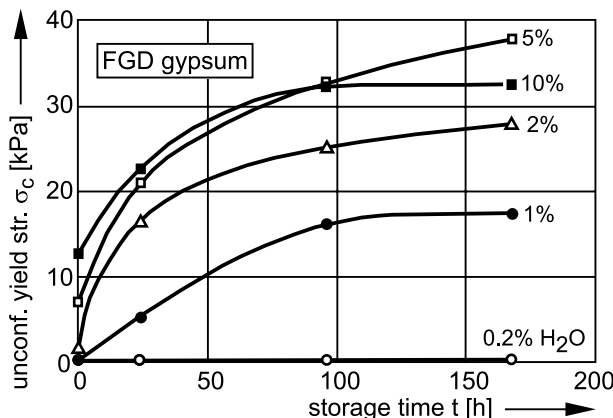


Fig. 8.3. Unconfined yield strength, σ_c , of FGD gypsum (flue gas desulfurization gypsum) of varied moisture content as a function of storage time at rest, t ; consolidation stress $\sigma_l = 26$ kPa [8.2]

An example of a moist bulk solid is gypsum from flue gas desulfurization plants (FGD gypsum). In Fig. 8.3 the unconfined yield strength, σ_c , of samples with different moisture content is plotted versus storage time at rest. Each measurement point in the diagram is the result of either a yield locus (storage time $t = 0$, i.e., instantaneous behavior) or a time yield locus ($t > 0$). The results obtained for $t = 0$ demonstrate the increase of uncon-

fined yield strength with moisture content which is a result of liquid bridges. While the unconfined yield strength of the almost dry sample (moisture content 0.2%) does not increase with storage time, a strong increase is found for higher values of moisture content. Only for the highest moisture content investigated (10%) the unconfined yield strength after longer storage time was below that obtained for 5% moisture which indicates that the time consolidation effect might decrease with a further increase of moisture content.

An example of the influence of moisture on wall friction angle is given in Fig. 8.4, where the wall friction angle of FGD gypsum is shown for two wall materials versus moisture content. The wall friction angle measured against mild steel (with mill scale) first increases with increasing moisture content and remains constant from 5 % to 10 % moisture. The reason for the increase of wall friction with moisture content is the increasing influence of adhesive forces due to liquid bridges between particles and wall surface (see Sect. 7.2.3). The other wall material, a plastic lining (UHMW-PE: ultra-high molecular weight polyethylene), is poorly wettable by water. Here no liquid bridges which increase the adhesive forces can form, but the liquid instead reduces the wall friction, possibly by forming a liquid film on the particle surfaces. The meaning of these results regarding silo design is that with mild steel no mass flow hopper of acceptable steepness can be realized, whereas an appropriate lining (here: UHMW-PE) could solve the problem.

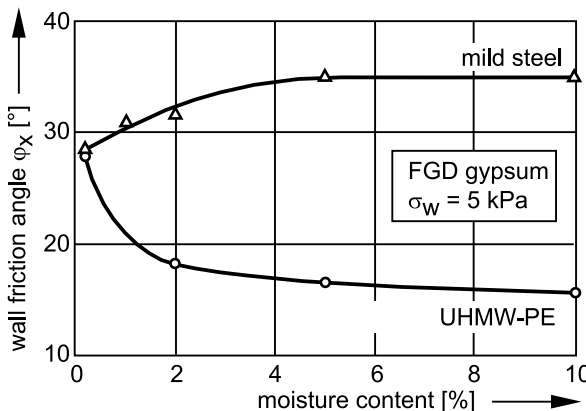


Fig. 8.4. Wall friction angle, φ_x , of FGD gypsum as a function of moisture content [8.2]

8.3 Temperature

A material exhibiting time- and temperature-dependent flow behavior is sulfur. In Fig. 8.5 is shown an open stock-pile, where sulfur granules (lens-shaped particles) are stored directly after being formed from molten sulfur [8.3]. The instantaneous behavior of the sulfur granules can be characterized as free-flowing, but due to the high temperature of the freshly produced pellets a strong time consolidation can be observed, which is demonstrated in Fig. 8.5 by vertical walls of up to 14 m height.

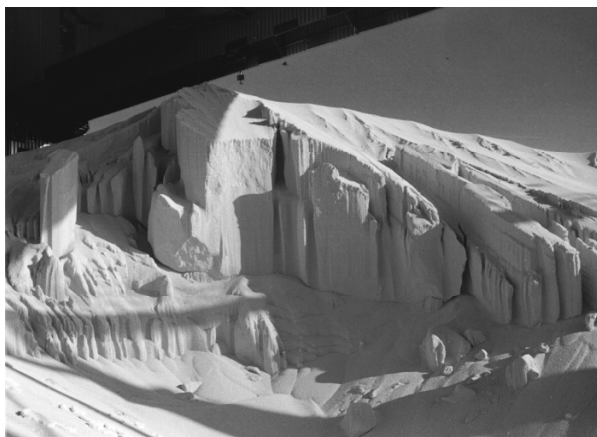


Fig. 8.5. Sulfur granules in an open stock-pile; height of the pile about 14 m [8.3]

Spherical sulfur granules, produced in a different process and having a diameter of several millimeters, had to be stored in a large silo (10 000 tons). For the silo design the flow properties had been measured [8.3]. Especially important was the measurement of consolidation with time, since the material had to be stored in the silo for long periods. As an example, in Fig. 8.6 the unconfined yield strength, σ_c , and flowability, ff_c , are plotted versus temperature. The individual specimens were stored in an oven for 14 days subjected to a consolidation stress of $\sigma_l = 117$ kPa. The large consolidation stress had been chosen to simulate storage conditions in the large silo.

For storage temperatures up to 40°C no time consolidation effect could be measured, i.e., the sulfur remained free-flowing even after storage under load over a period of 14 days (unconfined yield strength $\sigma_c = 0$; flowability $ff_c \gg 10$). At 50°C a slight time consolidation effect was measured, but the flowability was still reasonable ($ff_c = 7$). For temperatures above 60°C unfavorable small flowabilities close to 1 were obtained. Based on these results it was decided to cool the sulfur down to at least 50°C to

55°C before charging it into the silo. Flow problems due to time consolidation have not been observed in the new silo [8.3].

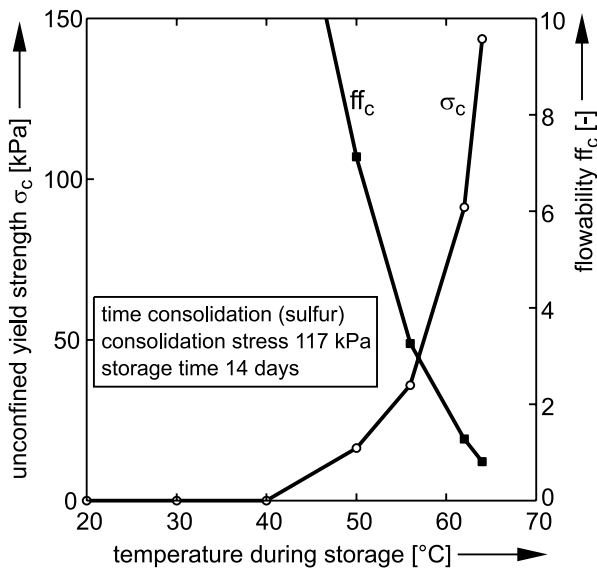


Fig. 8.6. Time consolidation of sulfur granules [8.3]

8.4 Time consolidation

Time consolidation is exhibited by a wide range of products and is, dependent on the application, an important quantity. Especially for silo design the time consolidation should be known, because only then are statements on the formation of arches after long periods of storage at rest possible. Also the usually unwanted formation of lumps (caking), e.g., in packages or IBCs, is a result of time consolidation.

Time consolidation is the increase of unconfined yield strength, σ_c , with storage time at rest, t . An example of this is shown in Fig. 8.3 (Sect. 8.2) where unconfined yield strength is plotted versus time for samples of FGD gypsum with different moisture content. The results for 0.2 % moisture demonstrate that bulk solids exist which do not exhibit any time consolidation effect. The curves measured for the other values of moisture content (Fig. 8.3) represent the typical pattern which can be observed with most bulk solids exhibiting time consolidation: The initially steep slope of the

curves becomes increasingly smaller with time, and often a constant strength is attained after a certain storage time.

In Fig. 8.7 the instantaneous flow functions and time flow functions of two samples of FGD gypsum (different from the FGD gypsum in Fig. 8.3) are plotted. Flow functions represent the dependence of unconfined yield strength, σ_c , on consolidation stress, σ_1 . The time flow functions have been determined for a storage time of 5 days. They are clearly steeper than the (instantaneous) flow functions. This can also be observed with several other bulk solids, especially in case of a very distinctive time consolidation effect. Thus, a time flow function should not be assumed as being parallel to the flow function.

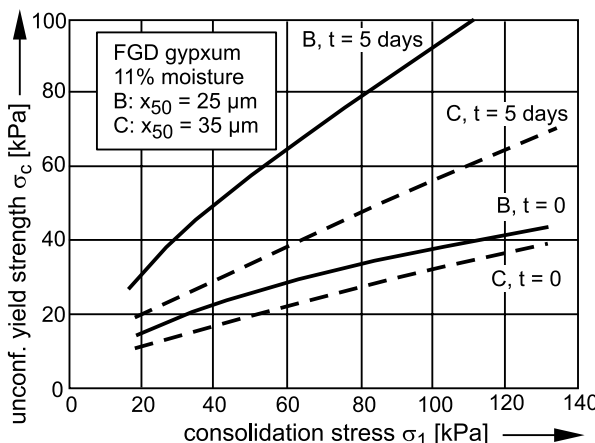


Fig. 8.7. Instantaneous flow functions and time flow functions of two different samples of FGD gypsum [8.2]

Examples of time consolidation can also found in Figs. 8.1 and 8.6. In Fig. 8.1 the possible effect of a flow agent on time consolidation can be seen. In Fig. 8.6 the unconfined yield strength and flowability of sulfur granules are plotted as a function of temperature for a storage time of 14 days.

8.5 Particle size

In most cases the flow properties of bulk solids become more unfavorable (e.g., smaller flowability) with increasing fines content. A general statement is not possible, especially if the fineness is characterized by only one particular parameter of the particle size distribution (e.g. mass median, x_{50}), since also shape and width of the particle size distribution play a role.

However, for similar products with a particle size distribution of similar shape a correlation of a fineness parameter with flowability is often found.

Due to segregation effects (see Chap. 13), fineness can vary even if the same product is always charged into a bin. If, for example, coarser particles are located primarily in the vicinity of the bin wall, whereas an increased amount of fine particles is found at the center, properties such as flowability or wall friction angle of the material may vary across the cross-section of the bin. Obviously it is important to use the correct properties – which requires the correct particle size distribution – depending on how the results are to be used.

An example on the influence of fineness is shown in Fig. 8.7, where the flow functions and time flow functions of two types of FGD gypsum of different particle size distribution (B: $x_{50} = 25 \mu\text{m}$; C: $x_{50} = 35 \mu\text{m}$) are plotted. Not only is the flow function of the finer material located at higher values of unconfined yield strength, σ_c , than that of the coarser product, but also the time flow function, where the effect is even stronger compared to the flow function. Thus, in this example the smaller particle size leads to higher strength and a stronger time consolidation effect.

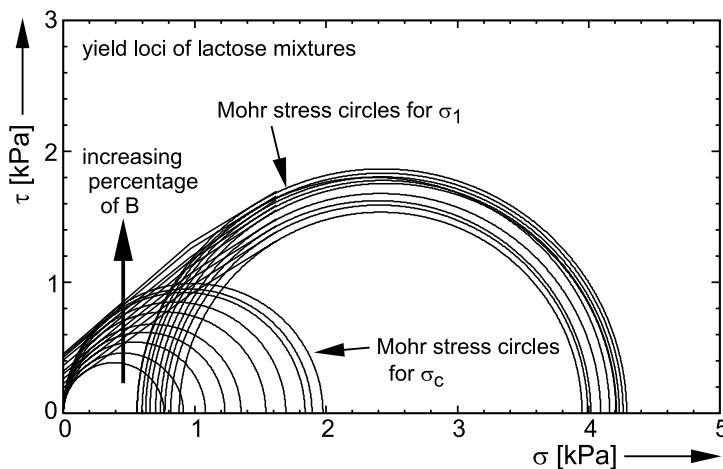


Fig. 8.8. Yield loci of mixtures from two types (A and B) of lactose (type B is finer than A)

Another example of the influence of particle size is shown in Fig. 8.8. Mixtures from two types of lactose (A and B) with different percentages of finer component B have been prepared. With each mixture a yield locus has been measured with a ring shear tester. The larger the percentage of the finer component B, the more the yield locus is shifted towards higher shear stresses and, thus, the larger the unconfined yield strength, σ_c , and

the smaller the flowability, ff_c (see Table 8.1 and Mohr stress circles for σ_c in Fig. 8.8). The results show a continuous decrease of flowability with increasing fines content. Additionally, it is obvious that the flowability does not decrease much further if the percentage of component B is greater than 40 %. The reason for this is that the finer component dominates flow behavior from a certain concentration, so a further increase of its percentage does not change the flow behavior significantly.

Table 8.1. Flow properties of mixtures from two types (A and B) of lactose; (type B is finer than type A)

Percentage of B	σ_1 [Pa]	σ_c [Pa]	ff_c [-]
50 %	4288	1976	2.17
45 %	4158	1893	2.20
40%	4261	1840	2.32
35 %	4232	1693	2.50
30 %	4210	1541	2.73
25 %	4208	1352	3.1
20 %	4090	1229	3.3
15 %	4015	1082	3.7
10 %	3991	914	4.4
5 %	3948	767	5.1

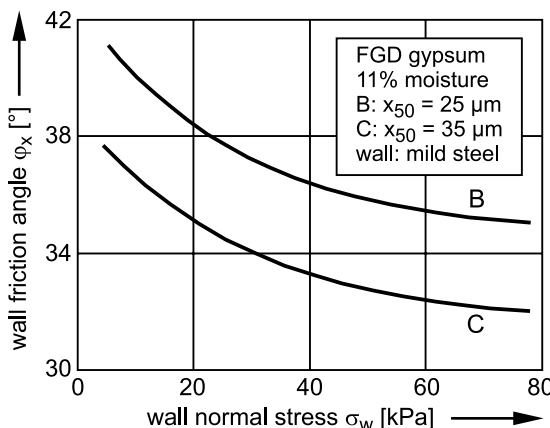


Fig. 8.9. Wall friction angle, φ_x , of moist FGD gypsum of different particle size measured against mild steel [8.2]

Also the wall friction angle can depend on the particle size distribution. In Fig. 8.9 wall friction angles, φ_x , are plotted which have been measured with the FGD gypsum samples from Fig. 8.7 against mild steel. In the entire range of investigated wall normal stresses, σ_w , the wall friction angle of

the finer FGD gypsum sample B is about 3° larger than that of sample C. The reason for this is the increasing influence of adhesive forces between particles and wall surface with decreasing particle size (see Sect. 7.2.3). The decrease of wall friction angle with increasing wall normal stress is discussed in Sect. 8.8.

8.6 Attrition

Some bulk solids are sensitive to attrition, i.e., the generation of fines due to particle breakage or abrasion. To avoid or at least reduce attrition, the bulk solid must be handled gently. When the material is discharged from a bin or a silo, the stresses in the flowing material must be kept sufficiently small. The upper limit of acceptable stresses can be found by attrition tests with a shear tester according to Sect. 4.1.6.

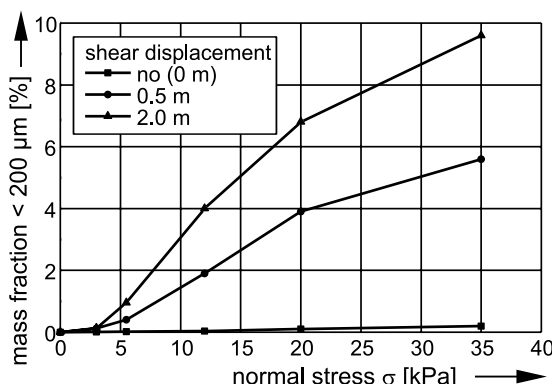


Fig. 8.10. Attrition of granulated sugar [8.4]

Results of attrition tests on granulated sugar performed with a ring shear tester are shown in Fig. 8.10. The fraction of fines smaller than $200 \mu\text{m}$ is taken as a measure of the fines generated during shear deformation. In the diagram the fines fraction is plotted versus normal stress, σ , for different values of shear displacement (i.e., the relative circumferential displacement between top and bottom of the ring shear cell). A static load without shear deformation generates only a negligible amount of fines (see Fig. 8.10: no shear displacement). Only if the material is subjected to shear deformation, larger amounts of fines are generated for normal stresses, σ , larger than 3 kPa . Following these results, a silo for the storage of granulated sugar was designed so that the flowing bulk solid was not subjected to stresses greater than 3 kPa [8.4].

Another example of the design of a silo based on attrition tests is reported in [8.3] (sulfur granules). A sample problem on this topic is given in Chap. 15 (sample problems 2 and 3).

Attrition tests can be utilized not only for silo design, but also for comparative tests. A possible application is the optimization of a product regarding its resistance to attrition. The advantage of the test procedure outlined above is that the bulk solid specimen is subjected to a defined and reproducible load.

8.7 Bulk density

The bulk density, ρ_b , of fine-grained or cohesive bulk solids is strongly dependent on consolidation stress, σ_1 , whereas free-flowing, coarse materials are usually almost incompressible. In cohesive products the adhesive forces are large compared to the gravity force, so a loose packing with large stable voids (high porosity) can be formed when such a material is poured loosely into a container. Only when the material is subjected to larger stresses, the porosity can be reduced and, thus, the bulk density can be increased. As an example, in Fig. 8.11 the bulk density, ρ_b , of a cohesive limestone powder is plotted versus consolidation stress, σ_1 . The data points are the results of yield locus tests performed with two ring shear testers.

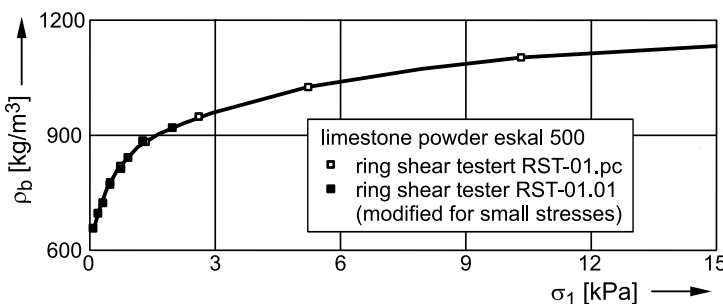


Fig. 8.11. Bulk density, ρ_b , of limestone powder eskal 500 ($x_{50} = 5 \mu\text{m}$) vs. consolidation stress, σ_1 [8.5]

In the stress range from about 60 Pa to 15 kPa the bulk density increases from about 650 kg/m^3 to 1100 kg/m^3 . Due to the decreasing slope of the curve more than 50% of the density change takes place below 1500 Pa. With increasing bulk density the material becomes increasingly stiff. If one would increase the stress range of Fig. 8.11 towards very large stresses,

one would attain the range of tabletting and briquetting where the curve would become almost horizontal.

In Fig. 8.12 the bulk density, ρ_b , of moist coal as used, for example, for combustion in power plants is plotted versus consolidation stress, σ_1 . The shape of the curve is in principle the same as found for limestone powder (Fig. 8.11), but here a broader stress range is considered.

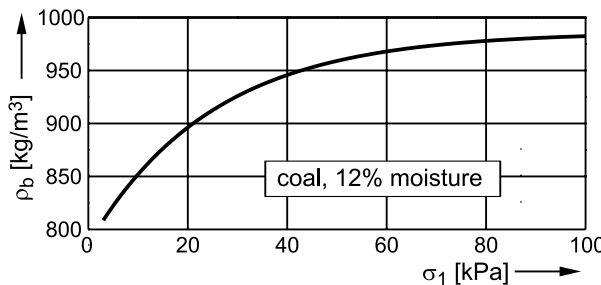


Fig. 8.12. Bulk density, ρ_b , of moist coal vs. consolidation stress, σ_1 [8.6]

Knowledge of bulk density, ρ_b , as a function of consolidation stress, σ_1 , is useful, for example, to assess the mass contents of a bin. As an example, in the following a silo for limestone powder is considered (different from the product in Fig. 8.11). For reasons of simplification, the silo is assumed to consist only of a cylindrical shaft of 4 m diameter and 20 m filling height [8.6]. Knowing the flow properties and wall friction angle, stresses in the silo can be assessed with Janssen's approach (see Sect. 9.2.1), and by taking into account the dependence of bulk density on stress. This way the bulk density is determined for any position in the silo, so that a more realistic assessment of the mass of the silo contents is possible. In Fig. 8.13 the assessed contents (mass) is plotted versus filling level. For reasons of comparison, the results of calculations based on constant bulk density are added. For this both the bulk density from DIN 1055-6 (1987) [8.7], and the bulk density in a loose, uncompacted state (aerated density) have been used. As one would expect, with the aerated density the mass of the silo contents is clearly underestimated, namely by 30%. The value taken from DIN 1055-6 (1987) results in an underestimation of only about 10%. However, the bulk density of bulk solids depends on their particle size distribution (beside other parameters): If the limestone powder is finer, the bulk density is likely to be smaller. Thus it is recommended to measure the bulk density for each particular case in order to obtain more realistic results (as shown in Fig. 8.13).

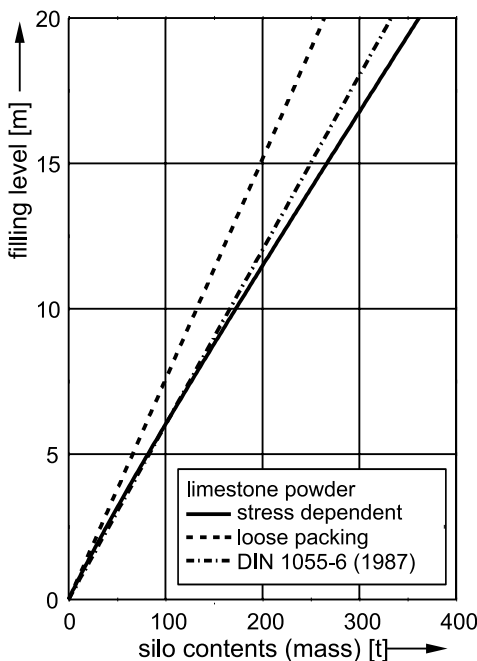


Fig. 8.13. Influence of assumed or measured bulk density, ρ_b , on calculated silo contents (limestone powder) [8.6]

8.8 Stress dependency of wall friction

If the wall friction angle is stress-dependent, usually a decrease of wall friction angle with increasing wall normal stress is observed, e.g., when measuring a wall yield locus. This effect typically takes place if the adhesive forces between wall surface and particles are large. The adhesive forces superimpose the applied normal stress and, thus, increase the shear stress significantly (see Sect. 7.2.3). In this case the wall yield locus does not run through the origin, but intersects with the shear stress axis at positive shear stress (Fig. 8.14).

With increasing wall normal stress the ratio of adhesive forces to wall normal stress becomes smaller, because the adhesive forces do not increase proportionally to the applied normal stress. Thus, the influence of adhesive forces on shear stress decreases, and the wall friction angle, φ_s , which is determined for each point on the wall yield locus from the ratio of shear stress to normal stress, decreases with increasing wall normal stress, σ_w (see Sect. 3.3.2). An example of this effect is shown in Fig. 8.14, where

both the wall yield locus and the wall friction angle are plotted for moist coal against mild steel. In the stress range of Fig. 8.14 the wall friction angle decreases from about 34° for $\sigma_w = 1 \text{ kPa}$ to 24° for $\sigma_w = 100 \text{ kPa}$. Under no circumstances should this difference be neglected when applying the wall friction angle, even if at first sight the shape of the wall yield locus does not give an indication of strong stress dependence. For instance, mass flow design requires the wall friction angle measured at relatively small wall normal stresses (usually $< 10 \text{ kPa}$) occurring in the lower part of the hopper, whereas for structural design the wall friction angles at relatively high stresses in the vertical section have to be applied.

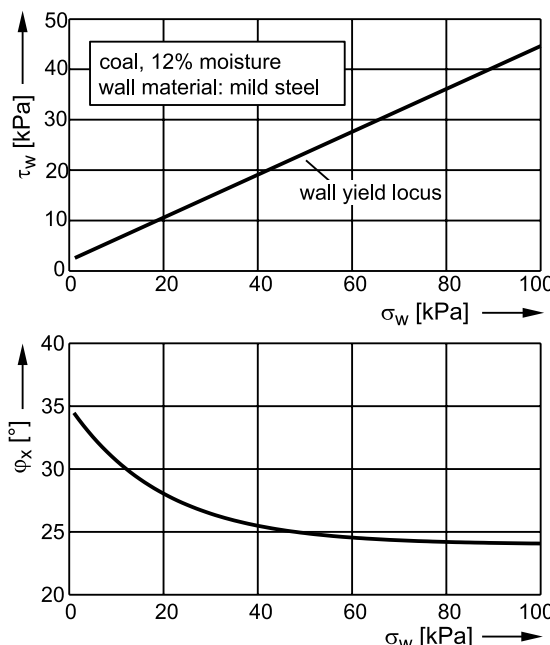


Fig. 8.14: Wall yield locus of moist coal; wall friction angle, φ_x , vs. wall normal stress, σ_w [8.6]

The FGD gypsum in Fig. 8.9 and many other moist bulk solids exhibit a similar behavior as moist coal. On the contrary, significant stress dependence is rarely seen with dry, not too fine-grained bulk solids in combination with hard wall materials (steel, aluminum, concrete). Here the influence of adhesive forces is small and, thus, affects the wall friction angle only slightly. However, even with dry bulk solids a stress dependent wall friction can occur if either the bulk solid or the wall is soft and plastically deformable. This is the case, for example, for hard, brittle particles and a

wall material made from plastic (or a wall with a relatively soft coating), where at high wall normal stresses the edges of the particles can penetrate into the wall resulting in an increased wall friction angle.

8.9 Influence of wall material on wall friction angle

Wall friction depends on the properties of both the bulk solid and the wall material. Important parameters of the wall material are its surface structure (e.g., roughness and microstructure), hardness and chemical composition (influence on wettability). Forming (e.g., when a conical hopper is formed from a metal sheet) can change the surface structure causing the wall friction angle to increase. Important parameters of the bulk solid are its particle size distribution, surface structure of the particles, particle hardness, moisture, and chemical composition.

Investigations of several combinations of bulk solids and wall materials have shown that one can recognize tendencies regarding the influence of the parameters mentioned above, but general statements cannot be made [8.8–8.11]. To illustrate this, in Fig. 8.15 the wall friction angle, φ_x , of salt is shown as a function of roughness, R_a , of the wall material [8.12, 8.13]. Furthermore, the maximum slope, Θ_c , of a conical hopper to achieve mass flow (see Chap. 10) is plotted. The wall materials are steel sheets of different roughness depending on the surface treatment (hot- and cold-rolled sheets from mild steel and stainless steel, surface treatment e.g. by grinding, polishing, sand-blasting). It is clearly evident that the wall friction angle in principle increases with increasing roughness, R_a , but for the same roughness one can find different wall friction angles. Thus other parameters are likely to play a role.

The variation of hopper slope angles for mass flow, Θ_c , is even larger than that of the wall friction angles, φ_x (Fig. 8.15). Thus, the selection of a wall material based alone on one roughness parameter (e.g., R_a) appears to be risky (e.g., for $R_a = 3 \mu\text{m}$ hopper slope angles, Θ_c , from 6° to 16° can be found, see Fig. 8.15).

An example of the influence of chemical composition of the wall material is shown in Fig. 8.4. The wall friction angle of moist FGD gypsum against the poorly wettable wall material UHMW-PE is clearly smaller compared to the easily wettable mild steel.

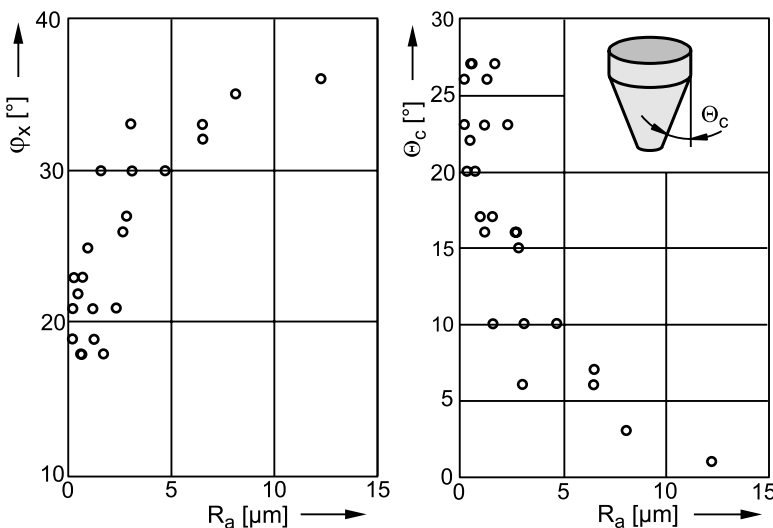


Fig. 8.15. Wall friction angle, ϕ_x , and hopper slope angle for mass flow, Θ_c , of salt for wall materials of different roughness parameter, R_a (stainless steel and mild steel, different surface treatments) [8.12,8.13]

Wall friction angle is of essential importance not only regarding the flow of a bulk solid (e.g., mass flow), but also regarding structural silo design. It is recommended to measure the wall friction angle for each particular case since many different parameters play a role. Although there is a lot of experience with many combinations of bulk solids and wall materials, only tendencies regarding the influence of individual parameters (roughness, moisture, ...) can be given in the following, whereby for almost all statements one can find a particular example to prove the opposite:

- Wall friction angle often decreases with decreasing wall surface roughness [8.9].
- Polishing of (already relatively smooth) wall surfaces is not always useful, because despite the reduction of surface roughness the wall friction angle can increase [8.10,8.11].
- Grinding of a wall surface usually leaves grooves, which can result in a significant increase of wall friction angle. This effect is especially important for wall materials which are relatively smooth prior to grinding (e.g., cold-rolled stainless steel).
- In case of parallel grinding grooves, one can often find a dependence of wall friction angle on the direction of flow. Flow parallel to grooves usually results in the lowest, and flow perpendicular to the grooves in the highest, wall friction angles.

- The influence of surface roughness is less pronounced with very fine-grained, cohesive bulk solids (e.g., $x < 50 \mu\text{m}$) than with coarse bulk solids.
- The finer the bulk solid, the larger the wall friction angle (usually).
- Smooth wall materials are less appropriate for hard, sharp-edged particles, because their edges can penetrate into the wall material and thus increase wall friction. The same is true for soft coatings and liners.
- For moist, adhesive bulk solids wall materials of low wettability are advantageous.
- Several crystalline products (e.g. sugar) tend to form a thin, almost invisible layer on the wall surface, which can lead to an increase of wall friction angle. The effect is especially strong with smooth wall materials.

9 Stresses

The knowledge of the stresses prevailing in bulk solids, especially when being stored in bins and silos, is extremely important when considering the following topics:

- Silo design for flow (e.g., design procedure according to Jenike)
- Load assumptions for structural silo design (e.g., [9.1–9.3])
- Loads on feeders and inserts
- Limitation of stresses acting in a bulk solid (e.g., to avoid particle damage)
- Adjustment of the stress level of shear tests (or other flow property tests) to the situation in the application under consideration.

Furthermore, the possibility exists to calculate stresses for other applications, for example, consolidation of powders in dies, or movement of bulk solids plugs in tubes. Following some basic considerations of stress states in bulk solids, methods for assessment of stresses in silos and factors influencing the stresses are explained in the present chapter.

9.1 Stress states in silos

9.1.1 Ratio of horizontal to vertical stress

Previously in Sect. 2.3 it was explained that within a bulk solid different stresses can act in different directions, and in Sect. 5.1 the influence of deformation on stresses was discussed. One specific case of deformation, namely uniaxial compression, which represents, for example, deformation in the vertical section of a silo, is presented in an idealized manner in Fig. 9.1.a where an element of bulk solid is confined in a cylinder with frictionless, perfectly rigid walls. In the vertical direction the stress $\sigma_z = \sigma_v$ is applied to the bulk solid causing the horizontal stress, $\sigma_x = \sigma_h$. The ratio of horizontal to vertical stress, σ_h/σ_v , is called the lateral (or horizontal) stress ratio, K , being first introduced in soil mechanics and as well being used in the new European silo code [9.2,9.3] where it is called “lateral pressure ra-

tio" (in the former version of DIN 1055 part 6 [9.1] the lateral pressure ratio was designated as λ). The special case of a frictionless wall (as shown in Fig. 9.1) is indicated by index "0":

$$K_0 = \lambda_0 = \frac{\sigma_h}{\sigma_v} \quad (9.1)$$

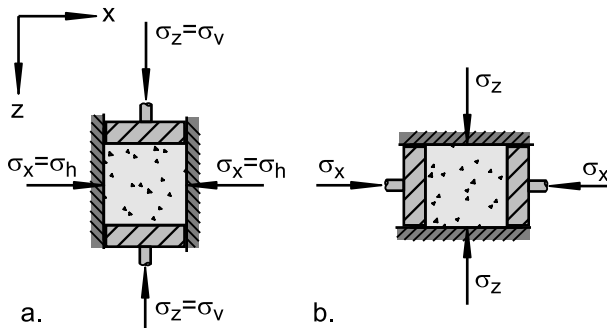


Fig. 9.1. Bulk solid element confined by parallel, frictionless walls; a. vertical compression; b. horizontal compression

Generally the lateral stress ratio, K , prevails whenever a bulk solid is consolidated uniaxially, i.e., when the bulk solid is compressed in one direction while no deformation occurs in the perpendicular direction. The stress perpendicular to the direction of consolidation can be assessed by multiplying the consolidation stress by the stress ratio, K . The latter is independent of the direction of consolidation although the term "horizontal stress ratio" seems to contradict this. Thus, it follows for the horizontal consolidation shown in Fig. 9.1.b (frictionless walls; stresses σ_x and σ_z are principal stresses; gravity force neglected):

$$K_0 = \lambda_0 = \frac{\sigma_z}{\sigma_x} \quad (9.2)$$

As already explained in Chap. 2, in bulk solids technology the bulk solid is mostly regarded as being a continuum. If differently inclined cutting planes within the bulk solid element are considered, one can show that different shear and normal stresses act on those planes. An indication of this fact is figure 9.1 showing that stresses are not the same in all directions. As outlined in Sect. 2.3.1, stresses acting in different cutting planes are represented by the Mohr stress circle (Fig. 9.2). For every Mohr stress circle with a radius greater than zero one can find a maximum normal stress. This stress is called the major principal stress, σ_1 . The smallest normal stress, called the minor principal stress, σ_2 , is acting perpendicular to σ_1 .

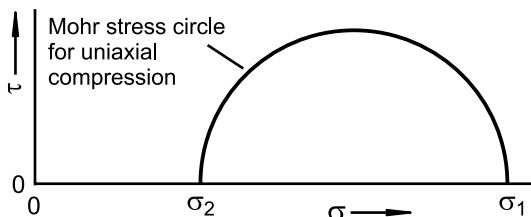


Fig. 9.2. Mohr stress circle (upper half) for uniaxial consolidation

The principal stresses act on the principal stress planes. The shear stresses on these planes are zero (intersections of the Mohr stress circle with the σ -coordinate, Fig. 9.2). Also the stresses presented in Fig. 9.1 are principal stresses, for example, in Fig. 9.1.a the consolidation stress, σ_v , is identical to σ_1 , and σ_h acting in the perpendicular direction is identical to σ_2 . Thus, the stress ratio, K_0 , in Eq. 9.1 is the ratio of the minor to the major principal stress.

The lateral stress ratio is used in silo technology to describe the ratio of the wall normal stress to the mean vertical stress in the silo's vertical section. The bulk solid is compressed vertically by gravity, but strain in the horizontal direction is prevented. Thus, the deformation in the vertical section is comparable to that in Fig. 9.1.a. Since the silo walls are not frictionless as the walls in Fig. 9.1.a, the vertical and horizontal stresses are principal stresses only along the silo axis, but not at the silo walls. Therefore, the lateral stress ratio, K , in a silo's vertical section is dependent on the wall friction angle and, thus, somewhat different from K_0 [9.4].

The value of the lateral stress ratio differs with the bulk solid. While the stress ratio of a perfectly rigid, inelastic solid body would be equal to zero, and that of a Newtonian fluid equal to one, the values for bulk solids at rest (e.g., in a silo's vertical section) are usually between 0.3 and 0.6 [9.4], very rarely beyond these limits.

It has to be mentioned that the above statement is valid for bulk solids which had been compressed in only one direction starting from a very loose state of packing. If a bulk solid is, for example, compressed in two steps, first in z -direction and second in x -direction, a ratio σ_z/σ_x will be achieved after the second step which is not identical to the ratio that would have been achieved without the first compression step. The reason for this is the fact that any deformation causes a specific particle arrangement. Depending on the following deformation this arrangement is more or less preserved and has an influence on the stress relations (see Sect. 5.1.1). Measurements of the deformation behavior and approaches to describe it can be found in [9.5,9.6].

9.1.2 Stresses in silos

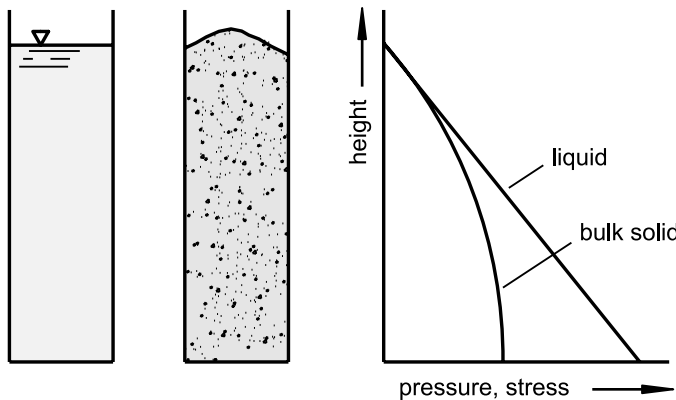


Fig. 9.3. Pressure and stress, respectively, in liquids and bulk solids

As it is known from the friction between solid bodies, bulk solids at rest can also transmit shear stresses (contrary to Newtonian fluids). While pressure increases linearly with depth in a liquid container (Fig. 9.3), the shear stress exerted from the bulk solid onto the container wall – i.e. the friction at the container wall – carries part of the bulk solids weight. As a consequence the stress in a container filled with a bulk solid is increasing less and less in downwards direction.

A typical silo consists of a vertical section (vertical section, cylinder section) and a hopper. The stress conditions in the hopper are more complex than in the vertical section. If a previously empty silo is filled with a bulk solid, a stress distribution results as shown in Fig. 9.4.a [9.7]. In the vertical section both the wall normal stress, σ_w , and the mean vertical stress, σ_v , are increasing in the downward direction and tend to approach an asymptotic value. The ratio of the wall normal stress to mean vertical stress is given by the lateral stress ratio, K (Sect. 9.1). The major principal stress, σ_I , is oriented vertically along the silo axis and deviates more and more from vertical towards the silo walls. This state of stress is called “active state of stress” or “active stress field”. The direction of the major principal stress is represented in Fig. 9.4 by major principal stress lines.

At the transition to the hopper the wall normal stress has a discontinuity caused by the sudden change of wall inclination. Further downwards in the hopper both the vertical stress and the wall normal stress are decreasing and approach zero at the hopper apex (the outlet is assumed as infinitely small), but depending on the vertical stress at the transition, the silo shape, and the bulk solid’s properties the stresses in the hopper either increase in the first instance and then decrease, or decrease continuously from the

transition to the apex as in Fig. 9.4.a (the stress distributions plotted in Fig. 9.4 shall be regarded as qualitative examples). In general the stresses in vertical direction are larger than those in horizontal direction. Along the hopper axis the major principal stress is oriented vertically, i.e., an active state of stress (active stress field) prevails as in the vertical section. The stress field in the hopper prevailing after filling is also referred to as “filling state of stress” or just “filling conditions”.

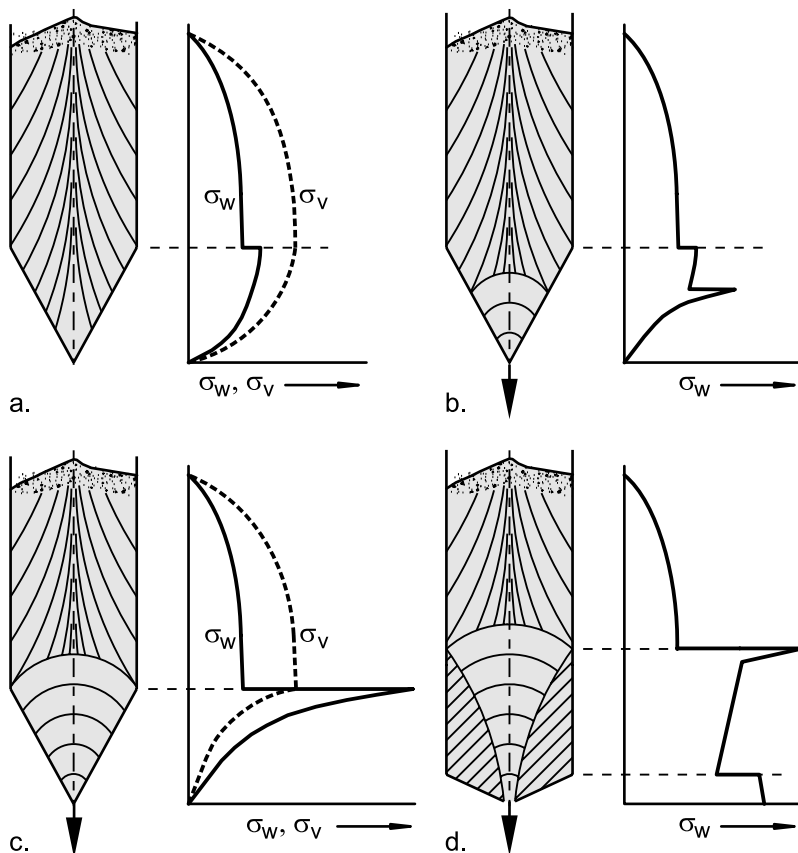


Fig. 9.4. Qualitative distributions of wall normal stress, σ_w , and mean vertical stress, σ_v (dashed, only in Figs. a and c), vs. the vertical coordinate (within the silos lines of major principal stress, σ_I , are plotted; stagnant zones are hatched [9.7,9.8]; the hopper outlet in Figs. 9.4.a to c is assumed to be infinitely small). a. Filling conditions prevailing during initial filling of an empty silo; b. emptying conditions in the lower part of the hopper; c. emptying conditions in the entire hopper; d. emptying conditions in a funnel flow silo (mixed flow according to [9.3]).

When material is discharged from a mass flow silo the first time after it has been filled, after a short transition period the entire contents of the silo moves downward. Due to the convergent flow zone in the hopper the bulk solid is compressed horizontally, while it dilates in the vertical direction due to the downwards flow. As a result the larger stresses act in the horizontal direction, and the major principal stress along the hopper axis is oriented horizontally. This stress field is called “arched” (according to the shape of the lines of major principal stress in the hopper, which are increasingly inclined towards the wall; see Fig. 9.4.c) or “passive” stress field. Other designations are “passive state of stress”, “emptying state of stress” or just “emptying conditions”. Figure 9.4.b shows the situation a very short time after the onset of discharge, where the passive stress field has developed only in the lower part of the hopper. A bit later compared to the situation in Fig 9.4.b, the passive stress field is fully developed (Fig. 9.4.c). Here the stresses in the hopper decrease remarkably towards the apex. In the lower part of the hopper the so-called “radial stress field” develops where the local stress is nearly proportional to the distance from the hopper apex. In the emptying state the stresses close to the outlet are independent of the stresses in the upper part of the hopper and, therefore, also independent of the silo’s dimensions or level of filling.

The deformation of the bulk solid while flowing in the hopper approximately corresponds to steady-state flow (flow at constant stresses and constant bulk density, i.e., compression in one direction and dilation in the perpendicular direction). The ratio of the minor and major principal stresses at steady-state flow cannot be described with the lateral stress ratio, K , which is valid only for uniaxial compression. Figure 9.5 shows an example of a stress circle for steady-state flow and a stress circle for uniaxial consolidation as discussed above. It can be clearly seen that for identical major principal stresses, σ_1 , a smaller minor principal stress, σ_2 , results for steady-state flow compared to uniaxial consolidation (for further explanations regarding the influence of deformation on stresses refer to Sect. 5.1). Thus, the ratio of the minor to the major principal stress in the hopper axis is similar to that of steady-state flow.

$$\frac{\sigma_2}{\sigma_1} = \frac{1 - \sin \varphi_e}{1 + \sin \varphi_e} \quad (9.3)$$

In the silo’s vertical section the active state of stress remains during emptying, as long as no local convergences exist (reduction of the cross-section due to inserts, dents, etc.). The transition from the active to the passive state of stress is called “switch”. Considering the arched principal stress lines in the hopper, the switch takes place in an arched region origi-

nating from the cylinder/hopper transition (see Fig. 9.4.c). The switch is accompanied by a local peak of the wall normal stress. Since the passive stress field and the stress peak are not a result of dynamic forces, they are preserved even when discharge is stopped.

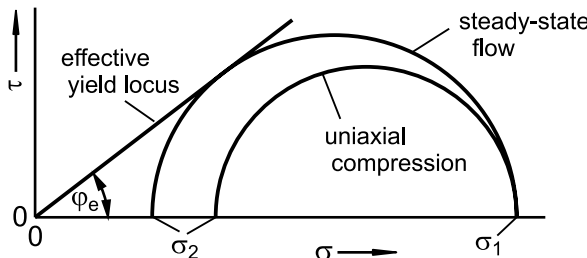


Fig. 9.5. Mohr stress circles representing steady-state flow and uniaxial consolidation

The switch stress peak develops while starting discharge from a silo which has been freshly filled from completely empty (Fig. 9.4.a). From the beginning of discharge the passive stress field develops in the hopper starting at the outlet and, thus, the switch region and the stress peak travel up (Fig. 9.4.b) until they become caught at the cylinder/hopper transition (Fig. 9.4.c). The passive stress field does not establish in the entire hopper immediately after the start of discharge, but only after a certain amount of bulk solid has been discharged (depending, for example, on the bulk solid's properties and hopper dimensions). One reason for this is that a bulk solid dilates somewhat at the onset of flow.

In funnel flow stagnant zones are formed which remain at rest while the material in the flow zone is flowing downwards (Fig. 9.4.d). If the boundary between a stagnant zone and the flow zone meets the silo wall within the vertical section, a stress peak occurs due to the "switch" from active to passive stress field caused by the convergent flow zone beneath the top of the stagnant zone. For the sake of completeness it has to be mentioned that the large wall normal stress along the hopper walls of the funnel flow silo in Fig. 9.4.d results from the shallow slope of the hopper walls.

The stress peak has to be considered when designing a silo for strength [9.1]. Compared to mass flow, this is more difficult in funnel flow, because the stress peak acts in the sensitive vertical section where its position cannot be accurately predicted [9.9]. In addition, the stress peak can be asymmetric with respect to the perimeter, and it can change its position with time. Thus, the complete vertical section has to be designed accordingly [9.1]. Silo damages resulting from unexpected stress peaks are reported in [9.10]. Some bulk solids (e.g., crystalline sugar) have the ten-

dency to form very steep flow zones in funnel flow silos (Fig. 9.6.a). The boundary between stagnant and flow zones does not meet the silo wall, or it meets the silo wall only near to the surface where the stresses are small. Thus, no (or no significant) stress peak develops at the silo wall.

Figure 9.6.b shows a funnel flow silo with eccentric outlet causing an eccentric flow zone (eccentric flow, Sect. 9.4.2). Although a stagnant zone is formed only on the left side, the principal stresses change their direction over the total width of the silo due to the transition from active to passive stress field (switch). Thus, a stress peak is to be expected also at the right side [9.10]. The same would happen if the silo in Fig. 9.6.b were a mass flow silo with a steep hopper wall, i.e., an inclined wall instead of the stagnant zone. Thus it becomes clear that a switch, i.e., the transition from an active to a passive state of stress, results in a pronounced local increase of wall normal stress where the transition zone meets the silo wall. Therefore, a stress peak can occur at the upper edge of a hopper (Fig. 9.4.c), and also along vertical walls without any stagnant zones located directly at these walls (Fig. 9.6.b).

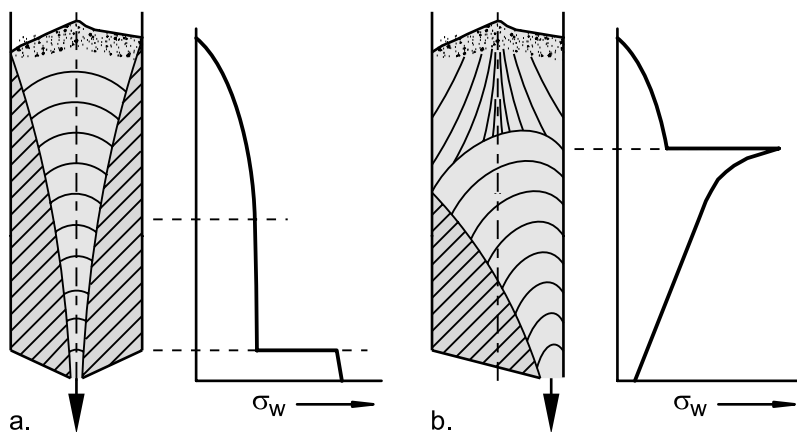


Fig. 9.6. Wall normal stresses σ_w (at the right silo wall) during discharge; lines of major principal stress in the flowing bulk solid; stagnant zones are hatched; a. funnel flow with steep flow zone (pipe flow according to [9.3]), b. funnel flow with eccentric flow zone (eccentric pipe flow according to [9.3]).

The stress peak can be explained by the orientations of the principal stresses (Fig. 9.7): In the vertical section the major principal stress, σ_1 , is oriented more or less vertically (see lines of principal stress in Fig. 9.4.c). Thus the vertical stress is greater than the horizontal stress. The principal stresses, σ_1 and σ_2 , acting along the silo axis are plotted in Fig. 9.7 as arrows (see bulk solid elements right to the silo), with the length of an arrow

being a qualitative measure of the magnitude. When flowing in the hopper the bulk solid is compressed in the horizontal direction, but it can dilate vertically. Thus, the horizontal stress is larger than the vertical stress in the hopper, and along the hopper axis the minor principal stress, σ_2 , acts vertically and the major principal stress, σ_1 , horizontally. Since at the transition from active to passive stress field the vertical stresses from above have to be in equilibrium with the vertical stresses from below, a significant increase of the horizontal stress occurs as can be seen from the peak in the wall normal stress (e.g., Fig. 9.4.c). Even though the principal stresses are increasingly inclined to the vertical and the horizontal, respectively, with increasing distance from the axis, this does not change anything in the principal validity of this consideration.

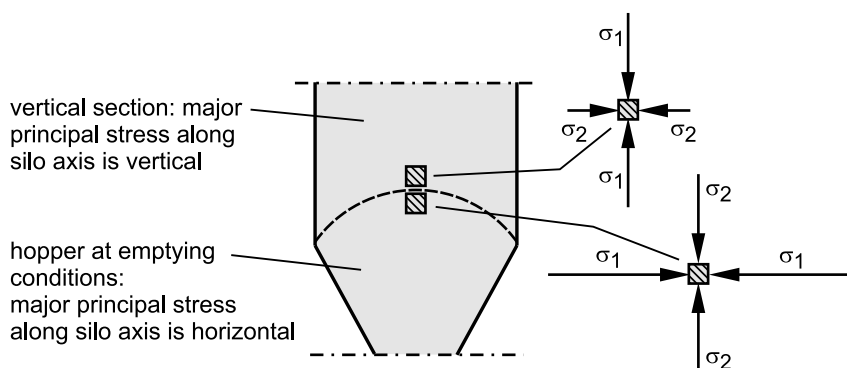


Fig. 9.7. Principal stresses at the transition from the vertical section to the hopper of a mass flow silo (major principal stresses acting along the silo axis above and below the transition from active to passive stress field are plotted as arrows with the length of an arrow being a qualitative measure of the magnitude).

An estimation of the magnitude of the stress peak is in principle possible, for example, with the approaches derived by Enstad [9.11], Walters [9.12,9.13], and Jenike [9.14]. Silo codes such as the German code DIN 1005 part 6 or the present Eurocode [9.1–9.3] contain equations for calculation of the stress peak; however, it is reasonable to assume that the stress-strain behavior of the bulk solid has an influence on the stress peak. A stiff, incompressible bulk solid will lead to a more pronounced local peak stress than a fine-grained, compressible material. The latter needs more deformation for reorientation of the major principal stresses (active → passive) and, thus, must flow further downwards in the hopper until the passive state of stress is fully attained. Therefore it is to be expected that the stress peak is less sharp and has a smaller maximum, but will act over a larger area.

9.2 Assessment of stresses

Following the considerations in the previous section, it becomes clear that for the assessment of stresses acting in silos three conditions have to be considered:

- Stresses in the vertical section
- Stresses in the hopper (active state of stress, filling conditions)
- Stresses in the hopper (passive state of stress, emptying conditions)

Stresses in silos have been investigated starting more than one hundred years ago, experimentally and theoretically. At first stresses in vertical channels were considered (Roberts [9.15,9.16], Janssen [9.17], Koenen [9.18]). Later stresses acting in hoppers were also considered. Well-known approaches are those of Jenike [9.19,9.20], Walker [9.21,9.22], and Walters [9.12,9.13]. The first theoretical approaches were based on slice element methods which considered the force equilibrium on a slice element of infinitesimal thickness in the vertical section [9.12,9.17] and the hopper, respectively [9.13,9.21,9.22].

The procedure for calculation of stresses in a hopper during emptying conditions (passive state of stress) derived by Jenike [9.19,9.20] is based on differential equations being solved with the method of characteristics. In addition, this approach allows designing silos for the hopper inclination for mass flow to occur and the minimum outlet dimensions to prevent arching and ratholing (see Chap. 10). Jenike presented the results of his calculations in the form of diagrams.

From more recent investigations those of Enstad [9.11] and Benink [9.23] should be mentioned, who calculated emptying stresses in the hopper with slice element methods. Important for the calculation of the stresses in the filling state is the work of Motzkus [9.24,9.25]), who recognized the assumptions of Walker and Walters as being unrealistic and introduced new and improved assumptions.

Also the method of finite elements (FEM) is used for calculation of stresses (e.g., [9.6,9.26,9.27]), whereby the bulk solid properties are given by constitutive models (sometimes also called constitutive laws). These constitutive models describe the stress-strain behavior of bulk solids. The necessary parameters have to be obtained by relatively extensive measurements. Thus, at present FEM seems to be too expensive for application to practical problems related to bulk solids.

A recent approach is the discrete element method (DEM, e.g., [9.28, 9.29,9.30]). In DEM the bulk solid is not considered as being a continuum but the interactions between individual particles are simulated. This re-

quires a high demand for processing power. Also the complex shapes of particles cannot be closely approximated. Thus, at present DEM is primarily suited to simulate situations in which the interactions of individual particles that are well defined regarding size and shape are important, and where the number of particles is limited (e.g., in a tumbling mill). With the increasing capacity of computers more applications can be expected in the future.

For practical applications slice element methods are still mainly used due to their relatively easy handling. Several codes [9.1–9.3,9.31,9.32] for the design of silos for strength are based on the equation of Janssen, which can be adapted to the situation in the silo by an equivalent selection of suitable parameters. For calculation of stresses in a hopper in the filling state (active state of stress) the slice element method of Motzkus [9.24,9.25,9.33] yields useful results, and for the emptying state (passive state of stress) the equations derived by Enstad [9.11] can be used (especially in the form presented by Arnold and McLean [9.34]).

The determination of stresses in a vertical section according to the method of Janssen [9.17] will be described in detail in the following section. Additionally the application of this method for other tasks (e.g., uniaxial consolidation of bulk solids) will be explained. Regarding the calculation of stresses in a hopper one is referred to the literature mentioned above (further surveys see [9.10,9.24,9.33]). For an estimation of stresses acting close to the outlet simple equations will be given. An estimation of stresses is also possible with the freeware program “Silo Stress Tool” of the author [9.35].

9.2.1 Stresses in vertical channels (Janssen's approach)

The classical method to calculate stresses in a silo's vertical section (active state of stress) was derived by Janssen [9.17]. He considered a slice element, i.e., an elemental section of the vertical section, of infinitesimal height, dz (Fig. 9.8). With the assumptions of constant vertical stress, σ_v , acting across the cross-section, and constant bulk density, ρ_b , equilibrium of forces in z -direction gives:

$$A\sigma_v + g \rho_b A dz = A(\sigma_v + d\sigma_v) + \tau_w U dz \quad (9.4)$$

Introducing the wall friction angle (assumed to be fully mobilized),

$$\tan \varphi_x = \tau_w / \sigma_h, \quad (9.5)$$

and the lateral stress ratio,

$$K = \sigma_h / \sigma_v, \quad (9.6)$$

one obtains a differential equation for the vertical stress, σ_v :

$$\frac{d\sigma_v}{dz} + \sigma_v K \frac{U}{A} \tan \varphi_x = g \rho_b \quad (9.7)$$

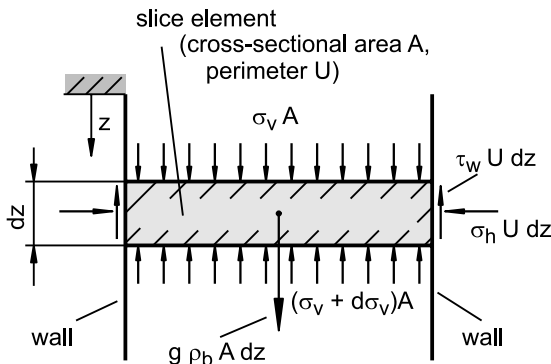


Fig. 9.8. Slice element (bulk solid) in the vertical section

Assuming constant values of parameters ρ_b , φ_x , and K , this is a first order differential equation which can be solved analytically. With the condition that a vertical surcharge stress, σ_{v0} , is acting on the top surface ($z = 0$), integration of the differential equation yields:

$$\sigma_v = \frac{g \rho_b A}{K \tan \varphi_x U} + \left[\sigma_{v0} - \frac{g \rho_b A}{K \tan \varphi_x U} \right] \cdot e^{\frac{-K \tan \varphi_x U z}{A}} \quad (9.8)$$

For the case that the stress on the top surface is zero ($\sigma_{v0} = 0$ at $z = 0$), Eq.(9.8) yields the well-known “Janssen equation”:

$$\sigma_v = \frac{g \rho_b A}{K \tan \varphi_x U} \cdot \left[1 - e^{\frac{-K \tan \varphi_x U z}{A}} \right] \quad (9.9)$$

σ_h and τ_w follow from Eq.(9.8) by substituting K and $\tan \varphi_x$, respectively, using Eqs.(9.5) and (9.6):

$$\sigma_h = \frac{g \rho_b A}{\tan \varphi_x U} + \left[K \cdot \sigma_{v0} - \frac{g \rho_b A}{\tan \varphi_x U} \right] \cdot e^{\frac{-K \tan \varphi_x U z}{A}} \quad (9.10)$$

$$\tau_w = \frac{g \rho_b A}{U} + \left[K \tan \varphi_x \cdot \sigma_{v0} - \frac{g \rho_b A}{U} \right] \cdot e^{\frac{-K \tan \varphi_x U z}{A}} \quad (9.11)$$

For large values of z the exponential functions in Eqs.(9.8) to (9.11) approach zero. Thus, the expression in front of the brackets is the final (asymptotic) stress, which is attained for $z \rightarrow \infty$. The final value of the vertical stress is:

$$\sigma_{v\infty} = \sigma_v(z \rightarrow \infty) = \frac{g \rho_b A}{K \tan \varphi_x U} \quad (9.12)$$

$\sigma_{v\infty}$ is independent of silo height and surcharge stress, σ_{v0} . It depends on the bulk solid's properties and the ratio A/U , which is $A/U = D/4$ in a cylinder of diameter D . Thus, according to Eqs.(9.9) to (9.11) the maximum possible stress in a cylindrical section, where usually no significant surcharge load is applied, is proportional to the silo diameter. Therefore slim silos can be high without getting too large stresses in the silo, whereas tanks for storing liquids (e.g., oil tanks) are preferably built with small heights and large diameters because of hydrostatic pressure.

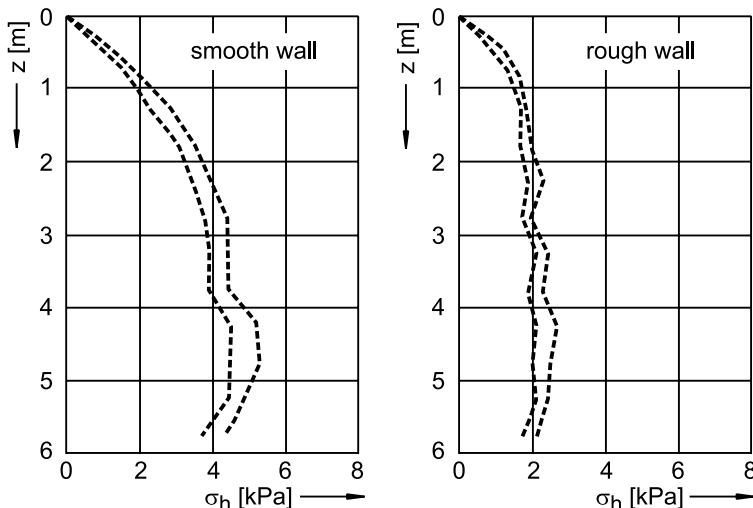


Fig. 9.9. Horizontal stress measured in the vertical section of a model silo (filling state) vs. coordinate z ; wall roughness was varied ($z = 0$ at the surface; lines represent the 95% confidence interval; bulk solid: semolina) [9.37]

The validity of Janssen's equation (9.9) has been proven in many experimental investigations, for example [9.7,9.10,9.36–9.38]. It is the basis of

most codes for the design of silos for strength (e.g., [9.1,9.2,9.31,9.32]). As an example, in Fig. 9.9 measured horizontal stresses, σ_h , are plotted [9.37]. One can recognize the typical distribution of horizontal stress with respect to height as predicted by Eq.(9.10). Furthermore, the influence of the angle of wall friction, φ_x , is demonstrated: The rough wall (larger angle of wall friction, φ_x) results in smaller horizontal stresses because it carries a larger part of the bulk solids weight than the smooth wall.

9.2.2 Further application of Janssen's equation

Janssen's equation can be applied not only to silos, but also to other situations where a bulk solid being confined in a rigid parallel channel is stressed in axial direction. An example of this is the uniaxial compression of a bulk solid specimen (Fig. 9.10). The stress being exerted by the punch at the top of the specimen is the surcharge stress denoted as σ_{v0} in Eq.(9.8). To generalize the representation, the vertical stresses, σ_v and σ_{v0} , are related to the final vertical stress, $\sigma_{v\infty}$, which would be attained at infinite depth, and the vertical coordinate, z , is related to the diameter, D , of the specimen. Applying this to Eq.(9.8) yields:

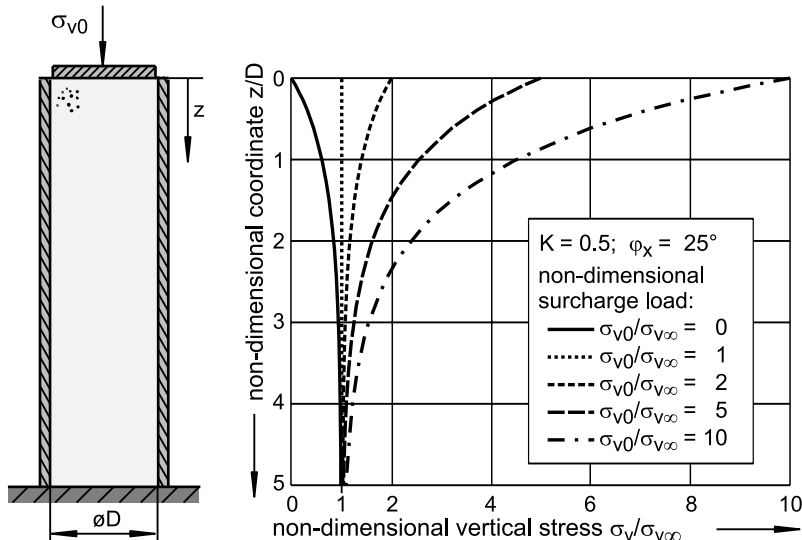


Fig. 9.10. Uniaxial compression of a bulk solid specimen; diagram shows the non-dimensional vertical stress vs. the non-dimensional vertical coordinate for different surcharge stresses, σ_{v0} .

$$\frac{\sigma_v}{\sigma_{v\infty}} = 1 + \left[\frac{\sigma_{v0}}{\sigma_{v\infty}} - 1 \right] \cdot e^{-4K \tan \varphi_x \frac{z}{D}} \quad (9.13)$$

The non-dimensional stress, $\sigma_v/\sigma_{v\infty}$, depends only on the surcharge load, $\sigma_{v0}/\sigma_{v\infty}$, and parameters K and φ_x . Thus, for geometrically similar containers and identical parameters ($\sigma_{v0}/\sigma_{v\infty}$, K , φ_x) identical non-dimensional stress distributions are obtained.

The non-dimensional stress according to Eq.(9.13) is plotted in Fig. 9.10 versus the vertical coordinate for different surcharge loads and typical values of K and φ_x ($K = 0.5$ and $\varphi_x = 25^\circ$). Since the exponential function rapidly gets small at large values of z/D , values of $\sigma_v/\sigma_{v\infty}$ close to 1 are attained at about $z/D = 3$ almost independent of the surcharge load. This demonstrates, for example, that it is not practical to choose too large ratios of height-to-diameter when consolidating bulk solids according to Fig. 9.10.

If a plug of bulk solid should be pushed upwards in a vertical channel (Fig. 9.11.a), the wall shear stress acts on the plug in the opposite direction, i.e., downwards. A derivation based on Fig. 9.8 (but with the shear stress acting downwards) yields a differential equation similar to Eq.(9.7), but with a negative sign before the term with the angle of wall friction. The solution of the modified differential equation is:

$$\sigma_v = -\frac{g \rho_b A}{K \tan \varphi_x U} + \left[\sigma_{v0} + \frac{g \rho_b A}{K \tan \varphi_x U} \right] \cdot e^{\frac{K \tan \varphi_x U z}{A}} \quad (9.14)$$

Without surcharge stress ($\sigma_{v0} = 0$) it follows:

$$\sigma_v = \frac{g \rho_b A}{K \tan \varphi_x U} \left[e^{\frac{K \tan \varphi_x U z}{A}} - 1 \right] \quad (9.15)$$

For the cylindrical plug in Fig. 9.11.a Eq.(9.15) can be transformed into a non-dimensional form by introducing $\sigma_{v\infty}$ according to Eq.(9.12):

$$\frac{\sigma_v}{\sigma_{v\infty}} = \left[e^{4K \tan \varphi_x \frac{z}{D}} - 1 \right] \quad (9.16)$$

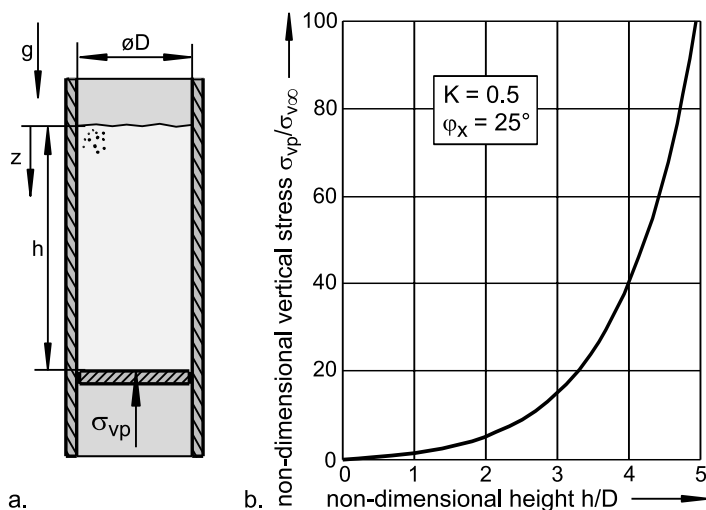


Fig. 9.11. a. Cylindrical plug (height h) pushed upwards with a piston; b. required vertical stress, σ_{vp} , at the bottom of the plug as a function of height, h (non-dimensional representation)

With Eq.(9.16) the vertical stress, σ_{vp} , at the bottom of the plug (i.e., at $z = h$, Fig. 9.11.a) can be calculated. This is the vertical stress which must be transferred through the piston to push the plug upwards. In Fig. 9.11.b the dimensionless vertical stress, $\sigma_{vp}/\sigma_{v\infty}$, is plotted versus the non-dimensional height of the plug, h/D . For $h/D = 5$ more than 100 times the vertical stress, $\sigma_{v\infty}$, according to Eq.(9.12) would be necessary. $\sigma_{v\infty}$ is the maximum vertical stress below a stationary column of bulk solid only subjected to the force of gravity (as in Fig. 9.10.a). Thus it becomes clear that it is not practical to push a plug of bulk solid with a large height-to-diameter ratio upward through parallel channels such as tubes.

If a gas flows through a stationary packing of bulk solid, the stresses in the bulk solid are influenced by the pressure gradient. This effect can be taken into account for a setup as shown in Fig. 9.12 by adding the pressure gradient, dp/dz , due to a vertical gas flow to the equilibrium of forces according to Eq.(9.4).

$$A\sigma_v + g \rho_b A dz - \left(\frac{dp}{dz}\right) A dz = A(\sigma_v + d\sigma_v) + \tau_w U dz \quad (9.17)$$

When the gas is flowing downwards, the gas pressure, p , decreases in z -direction, i.e. the pressure gradient is $dp/dz < 0$ (Fig. 9.12.a). When the gas is flowing upwards, p increases in z -direction ($dp/dz > 0$, Fig. 9.12.b). In the latter case the pressure gradient counteracts the gravity force. As long as the resultant of gravity force and pressure gradient acts downwards, the

shear stress acts upwards as in Fig. 9.8. If constant pressure gradients and constant bulk solids properties are assumed for the entire particle bed, in analogy to Eq.(9.9) the solution of the differential equation without surcharge load is:

$$\sigma_v = \frac{\left(g\rho_b - \frac{dp}{dz}\right)A}{K \tan \varphi_x U} \cdot \left[1 - e^{-\frac{-K \tan \varphi_x U z}{A}} \right] \quad \text{for } \left(g \rho_b - \frac{dp}{dz}\right) \geq 0 \quad (9.18)$$

The vertical stress according to Eq.(9.18) is plotted in Fig. 9.12.a versus the vertical coordinate. The shape of the curve is similar to that of the curve for $\sigma_{v0}/\sigma_{v\infty} = 0$ in Fig. 9.10. The final value of the vertical stress, $\sigma_{v\infty}$, which is the maximum vertical stress attained below a bulk solid column of infinite height, follows from Eq.(9.18) for $z \rightarrow \infty$:

$$\sigma_{v\infty} = \sigma_v(z \rightarrow \infty) = \frac{\left(g \rho_b - \frac{dp}{dz}\right)A}{K \tan \varphi_x U} \quad \text{for } \left(g \rho_b - \frac{dp}{dz}\right) \geq 0 \quad (9.19)$$

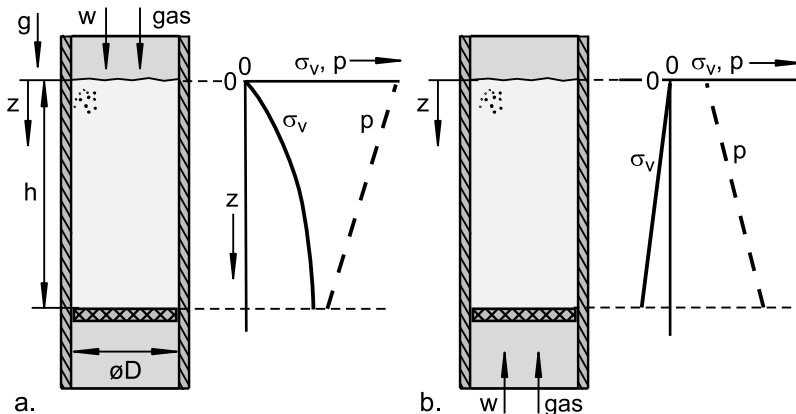


Fig. 9.12. Distributions of vertical stress and (absolute) gas pressure in a stationary particle bed (fixed bed) subjected to vertical gas flow (gas velocity: w). a. downward gas flow; b. upward gas flow where $g\rho_b < dp/dz$ (before the onset of fluidization)

At $g\rho_b = dp/dz$ the vertical stress is zero throughout the complete plug, because the gravity force equals the force resulting from the pressure gradient of the upward gas flow. If the pressure gradient exceeds the gravity force only slightly, the resultant force on the bulk solid acts upwards. Thus, a negative vertical stress (tensile stress) is acting within the material. In this situation a loosely packed, cohesionless bulk solid starts to dilate,

transforms into a fluidized bed, and due to the increased porosity the pressure drop decreases so that again $g\rho_b = dp/dz$ is fulfilled (onset of fluidization, see Sect. 7.2.4). A cohesive bulk solid can still be in the state of a fixed bed at considerable pressure gradients $dp/dz > g\rho_b$ even before the onset of fluidization. The reason for this is the ability of a cohesive bulk solid to transfer tensile stresses due to its tensile strength, which is dependent on the actual state of consolidation. For the calculation of vertical stress it is assumed that in the presence of vertical tensile stresses the (horizontal) wall normal stress and, thus, the shear stress transferred between the bulk solid and the confining walls, is zero, i.e., adhesion according to Fig. 3.29.b and possible residual stresses in the horizontal direction which can result from a preceding consolidation and remain even after the material is relieved from the consolidation stress (e.g., [9.4]) are excluded. Considering this condition ($\tau_w = 0$) and introducing the pressure gradient in the equilibrium of forces on a slice element according to Fig. 9.8, one obtains:

$$A\sigma_v + g\rho_b A dz - \frac{dp}{dz} A dz = A(\sigma_v + d\sigma_v) \quad (9.20)$$

Integrating this equation and solving for the vertical stress gives:

$$\sigma_v = \left(g\rho_b - \frac{dp}{dz} \right) \cdot z \quad \text{for } \left(g\rho_b - \frac{dp}{dz} \right) < 0 \quad (9.21)$$

According to Eq.(9.21) the vertical stress is zero at the upper surface and decreases linearly downwards, i.e., a tensile stress acts in the bulk solid which is maximum at the bottom (Fig. 9.12.b). If the tensile stress is sufficient to overcome the bulk solid's tensile strength, the onset of fluidization (see Sect. 7.2.4) will be reached and the fixed particle bed is transformed into a fluidized bed. The pressure difference being necessary for the onset of fluidization therefore depends on the actual yield limit and, thus, on the state of consolidation of the bulk solid. For the sake of completeness it has to be mentioned that with sufficiently cohesive bulk solids in an arrangement according to Fig. 9.12.b the complete bulk solid mass can also rise in form of a plug.

9.2.3 Bulk solid properties for calculation of stresses

To apply Janssen's equation the values of bulk density, ρ_b , angle of wall friction, φ_s , and lateral stress ratio, K , are needed. While both the bulk density and the angle of wall friction can easily be measured with shear testers, determination of lateral stress ratio is more difficult.

Janssen determined the lateral stress ratio by fitting Eq.(9.9) to the stresses measured in a model silo. This possibility is normally not available when calculating silo stresses. Thus, alternative methods are used.

Koenen [9.18] proposed to calculate the lateral stress ratio according to Rankine's coefficient of active earth pressure, K_0 , which is the ratio of the minor to the major principal stress (therefore index "0") in the active plastic state of stress. This is equivalent to the steady-state flow concept used in bulk solids technology (see Fig. 9.5, stress circle for steady-state flow):

$$K_0 = \frac{\sigma_2}{\sigma_1} = \frac{1 - \sin \varphi_e}{1 + \sin \varphi_e} \quad (9.22)$$

The application of Eq.(9.22) in combination with Janssen's equation implies firstly that the vertical and the horizontal stresses in the vertical section are principal stresses (which due the presence of wall friction is only possible along the axis of the vertical section), and secondly that the bulk solid is in an active plastic state of stress which is equivalent to steady-state flow. To eliminate the first incorrect assumption, equations for the calculation of the lateral stress ratio have been derived which consider friction at the wall (e.g., Walters [9.12]). The assumption of steady-state flow also cannot be correct, because steady-state flow could only be achieved if the bulk solid in the vertical section had the possibility to sufficiently dilate in the horizontal direction. This is normally not possible due to the stiffness of the silo walls [9.10,9.24,9.25,9.36].

As stated above, the bulk solid in the vertical section is compressed only in the vertical direction as a result of the gravity force, whereby almost no deformation takes place in the horizontal direction. Thus, the material is subjected to uniaxial compression. For certain major principal stresses, σ_1 , a larger minor principal stress, σ_2 , develops at uniaxial compression compared to steady state flow (e.g., [9.4,9.39]). Thus, the Mohr stress circle for uniaxial compression (active elastic state of stress) plotted in Fig. 9.5 lies below the Mohr stress circle representing steady-state flow (active plastic state of stress) and, thus, below the effective yield locus. Therefore, Eq.(9.22) predicts a too small lateral stress ratio for the vertical section.

Several publications exist in which other relations for the lateral stress ratio, K , have been derived. Surveys can be found in [9.5,9.24,9.36,9.40]. Often the coefficient of earth pressure at rest, K_0 , calculated according to an equation proposed by Kézdi [9.41], is used to describe the ratio, K , of horizontal to vertical stresses in the vertical section:

$$K = K_0 = 1 - \sin \varphi \quad (9.23)$$

φ is the angle of internal friction, which is often approximated by the effective angle of internal friction, φ_e , since this angle can be determined with shear tests. The advantage of Eq.(9.23) compared to Eq.(9.22) is the better agreement between calculated and measured values of lateral stress ratio [9.39]. But, strictly speaking, Eq.(9.23) is only valid for a particle bed having infinite dimensions in the horizontal direction, i.e., the influence of the wall is neglected as in Eq.(9.22). Also silo codes such as DIN 1055 part 6 (version from 1987) [9.1] are based on a slightly modified form of Eq.(9.23):

$$K = 1.2 \cdot (1 - \sin \varphi) \quad (9.24)$$

Eq.(9.24) leads to larger wall normal stresses and shear stresses in the upper silo part which leads to safer load assumptions compared to Eq.(9.23). For applications where the vertical stress is of importance (e.g., to determine the load on a feeder) it is recommended to use the smaller value of K resulting from Eq.(9.23), since it yields larger vertical stresses compared to the predictions of Eq.(9.24).

For rough estimates of the stresses in the vertical section a value of

$$K = 0.4 \quad (9.25)$$

is often recommended [9.42,9.43].

The values of the lateral stress ratio calculated according to Eq.(9.24) should be regarded as estimates. They cannot be correct in any case, since the lateral stress ratio in a real silo is dependent on other parameters (e.g., the angle of wall friction). A step forward to get more reliability is the recommendation in the new European silo code (DIN 1005-6:2005-03 [9.2], Eurocode [9.3]) to determine the lateral stress ratio from a uniaxial compression test in a modified oedometer (Fig. 9.13). In this test, in a similar form realized, for example, by Lohnes [9.44] and recommended by Nielssen and Kolymbas [9.45], a bulk solid specimen within a cylindrical mould is compressed vertically while measuring the resulting horizontal stress. With this test certainly not all parameters of influence are taken into account, but at least those parameters are considered which are based on the bulk solids properties. Measurements in a special tester designed by the author and called “Lambdameter” (see Sect. 5.1.1, Fig. 5.7) [9.4] demonstrate its applicability for the determination of the lateral stress ratio.

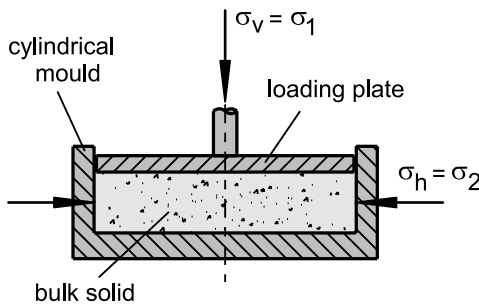


Fig. 9.13. Direct measurement of the lateral stress ratio (in principle)

In Fig. 9.14 lateral stress ratios, K , measured with the Lambdameter are plotted versus the effective angle of internal friction, φ_e . Additionally results calculated according to Eqs.(9.23) and (9.24) are drawn as dashed curves. Some measured values show a significant deviation from the predicted values. Generally the measured values of K are within a smaller range than the results obtained with the equations. The average value of the measurements is about $K = 0.5$. Note that bulk solids with a large effective angle of internal friction, φ_e , exhibit large deviations from the calculated values. Thus, the recommendation in [9.2,9.3] to measure the lateral stress ratio directly seems to be a significant improvement.

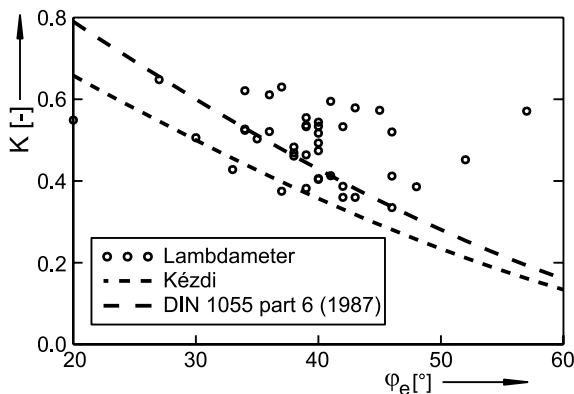


Fig. 9.14. Lateral stress ratio, K , measured with the Lambdameter and calculated from Eqs.(9.23) and (9.24) where the effective angle of internal friction, φ_e , is substituted for the angle of internal friction, φ [9.4]

9.2.4 Estimation of stresses at an outlet opening

The calculation of stresses in a hopper is too complex to be described here in detail. Moreover some numerical solutions are necessary. In Sect. 9.2 one is referred to appropriate literature and to a computer program provided by the author. To determine vertical stresses and wall normal stresses at an outlet opening, diagrams published by Jenike [9.19] or equivalent equations [9.8,9.34] can be found. A very rough estimate being at least valid for an idea of the order of magnitude of the vertical stress, σ_{va} , at the outlet of a mass flow hopper is possible with the following equations:

Conical hopper:

$$\sigma_{va} = 0.2 \cdot g \rho_b d \quad (9.26a)$$

Wedge-shaped hopper:

$$\sigma_{va} = 0.4 \cdot g \rho_b b \quad (9.26b)$$

d is the outlet diameter of a conical hopper, b the outlet width of a wedge-shaped hopper (see Sect. 10.3, Fig. 10.4).

The major principal stress at the outlet opening can be roughly estimated for emptying conditions with Eq.(9.3) in combination with the equations listed above by setting the vertical stress equal to the minor principal stress:

$$\sigma_I = \frac{1 + \sin \varphi_e}{1 - \sin \varphi_e} \cdot 0.2 \cdot g \rho_b d \quad (9.27a)$$

and

$$\sigma_I = \frac{1 + \sin \varphi_e}{1 - \sin \varphi_e} \cdot 0.4 \cdot g \rho_b b \quad (9.27b)$$

At filling conditions (i.e., after a silo has been freshly filled from completely empty) the stresses at the outlet opening depend on several conditions and cannot be calculated precisely. It is known from stress measurements (e.g., [9.25,9.33]) that the vertical stress at the outlet can be up to five to ten times larger compared to emptying conditions. Since at filling conditions the major principal stress in the hopper is oriented more or less vertically (see Fig. 9.4.a), the major principal stress does not differ much from the vertical stress.

9.2.5 Assessment of the stress distribution in a silo

To calculate stresses in a silo as shown by example in Fig. 9.15, the individual sections (vertical section, hopper, etc.) are considered one after the other, with the calculation starting at the upper surface and continuing downwards. Thus, at first the stresses in the vertical section are calculated with Janssen's equation. The vertical stress at the lower edge of the vertical section gets the designation σ_{v1} . Afterwards the stresses in the hopper for both filling and emptying conditions are calculated under consideration of the surcharge stress, σ_{v1} , resulting from the material in the vertical section. Suitable are, for example, the mentioned methods of Motzkus [9.24,9.25] and Enstad and Arnold/McLean, respectively [9.34]. The vertical stress at the lower edge of the hopper (designation σ_{v2} , Fig. 9.15) is then used as the surcharge stress for the calculation of the stresses in the lower vertical section (Janssen's equation with surcharge). The vertical stress at the outlet opening is σ_{v3} .

The procedure just mentioned for the calculation of stresses is used in the "Silo Stress Tool" software (freeware) [9.35]. The program enables estimation of stresses acting in simple silo forms as shown in Fig. 9.15 (circular/rectangular vertical sections, conical/wedge-shaped hoppers). However, the program is not suitable for the design of silos for strength since for this other calculation methods and safety factors as provided in related codes [9.1-9.3,9.31] have to be used.

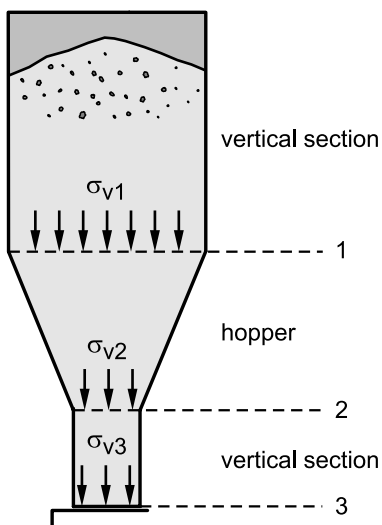


Fig. 9.15. Silo subdivided in sections for calculation of stresses

9.3 Loads on feeders

Most silos are provided with a feeder. The feeder must withstand the load resulting from the bulk solid in the silo, and it must be able to move the bulk solid beneath the outlet opening. Following a fundamental consideration of stresses at a silo's outlet opening, the principal procedure for estimating driving forces of feeders is explained by simple examples.

9.3.1 Vertical stress at an outlet opening

As outlined in Sect. 9.1.2, after a silo has been freshly filled from completely empty (filling conditions, active state of stress), the vertical stress at the outlet opening is larger than at emptying conditions [9.19,9.33,9.34, 9.42,9.46] (in experiments up to ten times larger stresses were measured for the filling state compared to the emptying state [9.19,9.33]). In Fig. 9.16.a the filling level, h_f , of a silo is plotted for filling and subsequent discharge. While filling the silo, the vertical stress acting on the feeder (Fig. 9.16.b) is increasing, but the increase per unit time becomes smaller due to the effect of the hopper and silo walls increasing with filling height. To discharge bulk solid, the feeder must be able to move the material which is subjected to the high vertical stress attained at the end of the filling process. Thus, high friction forces have to be overcome which results in a high driving force, F_h (Fig. 9.16.c). As soon as discharge has started, the passive stress field (emptying conditions) develops in the hopper which results in a sudden drop of the vertical stress, σ_v , at the outlet opening (Fig. 9.16.b) with the consequence of a lower driving force, F_h (Fig. 9.16.c).

The large driving force occurring at discharge following filling conditions can be avoided only by means of reduction of vertical stress:

- Continuous discharge during filling (especially while the hopper is filled) reduces the vertical stress in the hopper by transforming the active to a passive stress field; the discharge rate can be very small to limit the amount of discharged material, alternatively material can be discharged intermittently [9.46].
- If complete emptying of the silo is avoided, a material cushion remains in the silo so the passive stress field is preserved. During subsequent filling the stresses in the cushion may increase to a certain extent (dependent on the amount of material; it is advantageous to keep the entire hopper filled), but the stress at the outlet is considerably smaller compared to a silo being filled from completely empty. Further advantages of this method are the reduction of wear by avoiding material falling di-

rectly on the feeder during filling (important for coarse, hard materials). Fine-grained materials, which may be in a fluidized state just after being filled into a silo, are hindered from flooding through the silo outlet [9.46].

- The vertical stress at a silo outlet can be reduced with appropriate inserts (Sect. 9.4.1.2) [9.47] which have to be designed so that they do not cause flow problems such as stagnant zones or stable arches.
- A slide gate (or similar device) installed above the feeder should be closed during filling. If it is then opened just before the feeder is started, the bulk solid in the silo flows a bit downwards which leads to a reduction of the vertical stress due to the beginning transition from the active to the passive stress field as shown in Fig. 9.4.b.

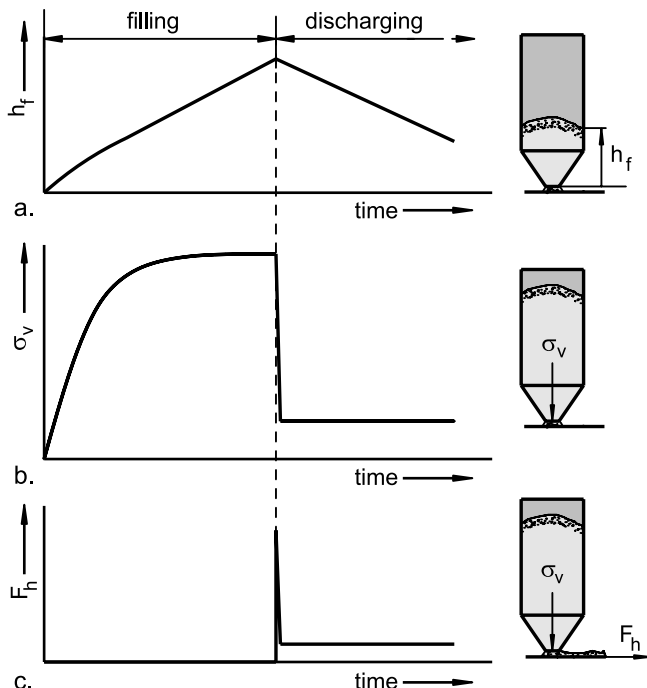


Fig. 9.16. Filling level, h_f , vertical stress at the outlet, σ_v , and driving force, F_h , during filling and subsequent emptying of a silo

If no means are taken to reduce the vertical stress, one must ensure that the vertical displacement of the silo during filling is not larger than the displacement of the feeder. This can happen, for example, when the silo is suspended in a steel frame, and the feeder (e.g., an en-masse feeder) is placed on a concrete foundation: The increase of the silo weight might lead

to a significant downward displacement of the silo, but there is only a small vertical displacement of the feeder due to its rigid foundation. Even when the displacement of the silo relative to the feeder is small ($< 1 \text{ mm}$), the vertical stress exerted by the bulk solid in the silo onto the feeder can reach a multiple of the vertical stress which normally prevails in the filling state [9.33]. Figure 9.17 shows qualitatively the vertical stress, σ_{vg} , acting on a feeder (filling conditions) as a function of the difference $\Delta z = z_a - z_s$ of the displacements of feeder (z_a) and silo (z_s): Positive values of Δz mean that the feeder is displaced downwards relative to the hopper as happens if the feeder is suspended flexibly (also feeders suspended from a hopper are likely to displace downwards relative to the hopper). In this case the vertical stress is slightly reduced (Fig. 9.17). On the other hand, an extreme increase of the vertical stress follows for negative values of Δz (decreasing distance between silo and feeder during filling) which, thus, have to be avoided.

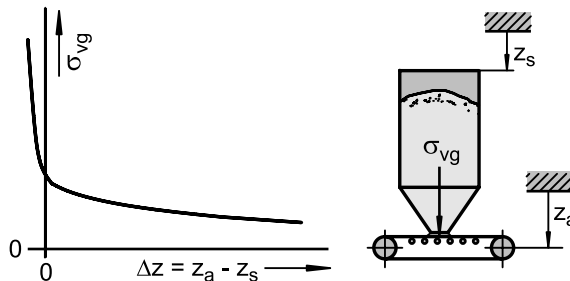


Fig. 9.17. Vertical stress, σ_{vg} , acting on a feeder, as a function of the vertical displacement, Δz , of the feeder relative to the silo during filling [9.33]

9.3.2 Estimation of driving forces

The driving power required by a feeder is the result of several conditions and processes, for example, friction within the feeder system (pulleys, chains, bearings, etc.), inertia forces, and others. In the following only the force required to move the material below the outlet opening of a bin is considered. Inertia forces can usually be neglected due to the small transport velocities typically occurring at discharge; internal friction forces of the feeder depend on the type of the feeder and can be estimated with help of characteristic values used in conveyor technology [9.48]. The driving force is then calculated as the sum of all friction forces which have to be overcome at discharge. For this the motion of the material beneath the outlet has to be considered.

For three types of feeders the calculation of the driving force is demonstrated in the following, i.e., belt feeder (Fig. 9.18), apron feeder (Fig. 9.19), and en-masse feeder (Fig. 9.20). Descriptions of the feeders are given in Sect. 12.3.2. All three feeders are positioned beneath the outlet slot of a wedge-shaped hopper. It is assumed that the hopper/feeder interface is designed to provide withdrawal over the entire outlet area (for details refer to Sect. 12.3.2). The vertical stress at the outlet opening, σ_{va} , can be estimated with the equations described in Sect. 9.2. The stress acting on the feeder is larger than σ_{va} due to the weight of the particle layer beneath the outlet opening. For the layer normally a linear (hydrostatic) increase of stress can be assumed, because wall friction does not need to be considered due to the height of the layer being small compared to its horizontal dimensions.

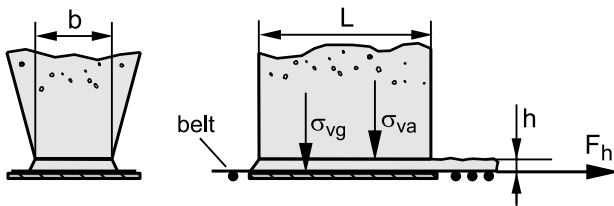


Fig. 9.18. Discharge with a belt feeder from a wedge-shaped hopper

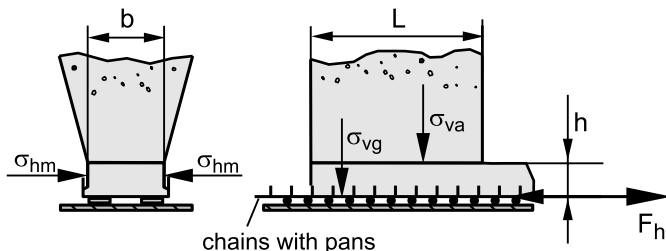


Fig. 9.19. Discharge with an apron feeder from a wedge-shaped hopper

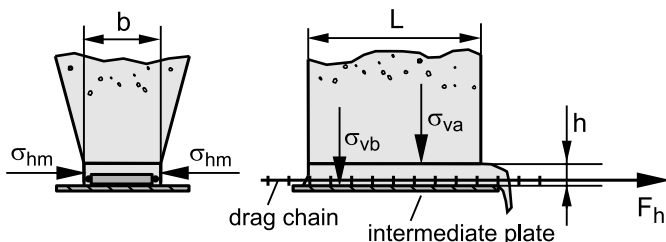


Fig. 9.20. Discharge with an en-masse feeder from a wedge-shaped hopper

First the belt feeder (Fig. 9.18) is considered. The maximum force which can be transmitted from the belt to the bulk solid is determined by the maximum friction force between belt and bulk solid [9.33]. The vertical stress, σ_{vg} , acting on the belt is given by

$$\sigma_{vg} = \sigma_{va} + \rho_b gh. \quad (9.28)$$

The vertical stress, σ_{va} , at the outlet opening can be assessed according to Sects. 9.2.4 and 9.2.5. The maximum possible driving force, F_h , of the belt feeder equals the friction force being transmitted by the belt:

$$F_h = \sigma_{vg} L b \tan(\varphi_{x,sg}) \quad (9.29)$$

$\varphi_{x,sg}$ is the angle of friction between bulk solid and belt.

Measurements on a model silo equipped with a belt feeder have shown that Eq.(9.29) really leads to an upper limit of the driving force, i.e., usually the driving force is smaller than the calculated value [9.33,9.49]. Figure 9.21 shows the measured maximum driving force of a belt feeder when discharging from a hopper at filling conditions. The data points correspond to the maximum in the course of the driving force, F_h , in Fig. 9.16.c. The slope of the hopper wall, Θ , and the shape of the transition from the hopper to the feeder had been varied in the experiments. The straight line in Fig. 9.21 corresponds to Eq.(9.29). Also in the literature, somewhat pure empirical equations for calculation of the driving force of belt feeders can be found, mostly resulting in smaller values of driving force ([9.42,9.46,9.50, 9.51], surveys in [9.33,9.49]).

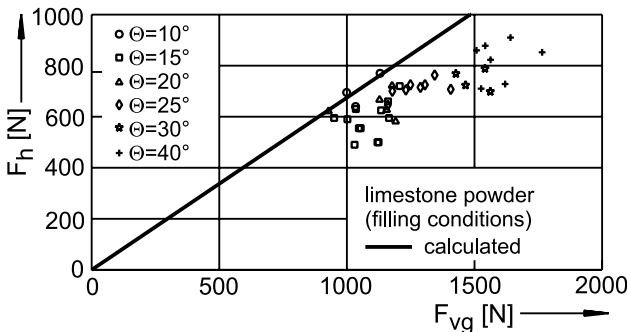


Fig. 9.21. Maximum driving force, F_h , as a function of the vertical force on the belt feeder, $F_{vg} = \sigma_{vg} \cdot L \cdot b$ (filling conditions in the hopper; different values F_{vg} result from different hopper wall slopes, Θ). The line represents the feeder force calculated with Eq.(9.29) based on the measured vertical stress [9.33].

The apron feeder shown in Fig. 9.19 is equipped with pans provided with flanges projecting upwards. Thus, the bulk solid cannot slip across the surface of the pans. For calculation of the driving force it is assumed that the pans transport a particle layer of height h horizontally. Thus, friction forces have to be overcome at the upper side of the layer (internal friction, i.e., friction within the bulk solid) and along the stationary vertical side walls (wall friction).

The vertical stress acting on top of the transported layer, σ_{va} , can be estimated with the equations described in Sect. 9.2. The stress, σ_{vg} , acting on the pans can be approximated with Eq.(9.28) thereby assuming hydrostatic increase of the vertical stress (i.e., no influence of wall friction on vertical stress). The stress acting on the side walls is, roughly equal to the mean vertical stress in the transported layer multiplied by the lateral stress ratio, K :

$$\sigma_{hm} = K \cdot \frac{\sigma_{va} + \sigma_{vg}}{2} \quad (9.30)$$

For the driving force it follows:

$$F_h = \sigma_{va} L b \tan(\varphi_{sf}) + 2\sigma_{hm} L h \tan(\varphi_{x,sw}) \quad (9.31)$$

The internal friction of the bulk solid at the upper side of the moved layer is assessed based on the angle of internal friction at steady-state flow, φ_{sf} . It takes into consideration that the bulk solids layers are sliding against each other as they do in a shear test during steady-state flow. It also would be possible to take the effective angle of internal friction, φ_e , instead of φ_{sf} , but φ_e can become rather large (e.g., $\varphi_e > 70^\circ$) for poorly flowing bulk solids (e.g., moist clay) leading to unrealistic high values of the calculated driving force. On the contrary, for easy flowing bulk solids the difference between the angles φ_e and φ_{sf} is quite small. Thus, both angles can be used. $\varphi_{x,sw}$ is the angle of wall friction for the bulk solid and the material of the side walls.

The driving force of the en-masse feeder (Fig. 9.20) is calculated similarly to that of the apron feeder. Here the bulk solid is shifted across the stationary intermediate plate, which results in additional friction to be overcome. The vertical stress acting on the intermediate plate, σ_{vb} , is calculated like the stress on the belt feeder according to Eq.(9.28). Then the driving force of the en-masse feeder is given by:

$$F_h = \sigma_{va} L b \tan(\varphi_{sf}) + 2\sigma_{hm} L h \tan(\varphi_{x,sw}) + \sigma_{vb} L b \tan(\varphi_{x,sb}) \quad (9.32)$$

Here $\varphi_{x,sb}$ is the angle of wall friction between the bulk solid and the bottom plate. The other parameters are the same as in Eq.(9.31).

When applying the equations derived above, it has to be considered that they are based on ideal assumptions. According to geometrical conditions larger driving forces can arise, for example, if the height of the transported layer is extremely small compared to its length, or if the layer must converge in conveying direction. The equations can be modified with respect to other feeders. To do so the situation in the hopper/feeder interface must be examined carefully and described with appropriate mathematical terms. However, if the conveying process is too complex it is not possible to derive reliable equations. For several types of feeders, which cannot be considered as shown above, equations for calculating driving forces exist, for example, for screw feeders [9.52–9.54] and vibratory feeders [9.55].

9.4 Disturbances to the stress distribution

The stresses acting on silo walls have to be known for the design of silos for strength. These are on the one hand the stress distributions following, for example, from Janssen's equation (Sect. 9.2.1) [9.17]. On the other hand, according to the flow pattern in a silo (e.g., the shape of stagnant zones, if any), deviations (e.g., asymmetric stress distributions) are possible from the stresses which are calculated on the basis of idealized considerations. If such effects are not taken into account for the design of a silo, they can have dramatic consequences on the stability of a silo. Some important reasons for non-uniform stress distributions are considered in the following

9.4.1 Local variations of the cross-section

9.4.1.1 Imperfections

A silo's vertical section with perfectly vertical walls results in a smooth stress distribution as predicted by Janssen's equation. This is not the case for a real vertical section which has more or less pronounced imperfections resulting in local convergences and divergences. When a bulk solid in the vertical section passes a local convergence when flowing downward, it is compressed horizontally. As a result, the horizontal stress increases locally [9.9,9.14,9.56]. This effect is taken into account in several silo codes by multiplying the horizontal stress determined for filling conditions with a factor larger than one [9.1-9.3].

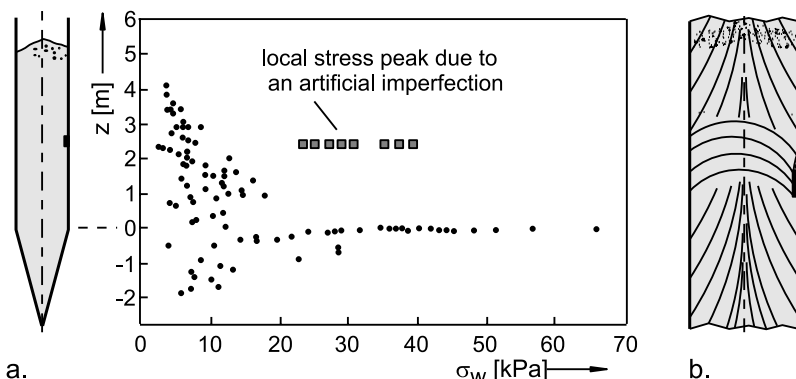


Fig. 9.22. Consequences of a local convergence on the wall normal stress; a. silo with artificial local imperfection and measured data of the wall normal stress, σ_w , (due to [9.57]); b. assumed lines of major principal stress in the region of the artificial imperfection

An example demonstrating the effect of a local convergence is shown in Fig. 9.22 [9.57]. The diagram (Fig. 9.22.a) shows measurements of wall normal stress, σ_w , in a silo which can be provided with an artificial imperfection. Without imperfection, the wall normal stress behaves as predicted by the theory: it increases from the top of the silo according to Janssen's equation, shows a pronounced stress peak at the transition, and decreases in the hopper. If the artificial imperfection is installed, the wall normal stress exhibits a strong local increase by a factor of up to about four (see squares in the diagram). The reason for this is the deformation of the bulk solid: To flow around the artificial imperfection, the bulk solid is compressed in the horizontal direction. This is roughly equivalent to the situation at the transition from a vertical section to a hopper in a mass flow silo (see Sect. 9.1.2, Fig. 9.4.c). The more the cross-section is reduced by the imperfection, and the less compressible a bulk solid, the more probable that a passive stress field develops across the complete width of the vertical section. For this case Fig. 9.22.b shows possible lines of major principal stress which are oriented predominantly horizontally in the region of the local convergence.

If the local reduction of the cross-section is small compared to the entire cross-section of the vertical section, and if the bulk solid is sufficiently compressible, it is to be expected that a passive stress field develops only close to the local imperfection, because in this case the deformation of the bulk solid can be compensated by a local increase of the bulk density. Thus, small local convergences following from irregularities of the silo wall will lead to lower local stress increases than larger construction parts

as in Fig. 9.22. Such parts which project into the silo (e.g., level probes, temperature sensors, nozzles, ladders, horizontal weld beads,...) are subjected to large loads resulting from the local change of the state of stress. The loads on those parts cannot be determined based on stresses following from Janssen's equation, because this equation does not consider local stress increases. Unfortunately, general procedures for the assessment of loads on such parts are not available.

9.4.1.2 Inserts

Inserts can be installed in a silo's vertical section (or other vertical channels), where they cause local convergences as discussed in the previous sections, or in a hopper. To date no generally valid equations exist for calculation of loads on inserts, and in several silo codes (e.g., DIN 1005 part 6 [9.1,9.2], Eurocode [9.3]) loads on inserts are not included. The reason for this situation is given by the complex relationship between the flow pattern and the resulting stress distribution, which had already been subject of many investigations (e.g., [9.47,9.58,9.59]). To describe some basic effects of inserts, results obtained by Strusch [9.47] are described in the following. Strusch measured insert loads and stresses in a model silo with wedge-shaped hopper, rectangular vertical section and wedge inserts of different dimensions and positions (Fig. 9.23).

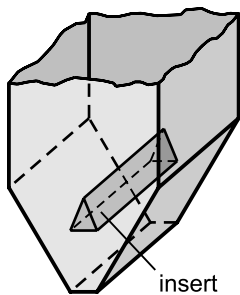


Fig. 9.23. Wedge insert

A sufficiently large insert installed in a vertical section causes convergent flow and, thus, leads to similar conditions as in hoppers. On the other hand, very small inserts cause only small convergences and, thus have only a local effect as already discussed in the previous section (imperfections). In the following only large inserts are regarded. In addition, mass flow will be assumed because only in mass flow is the flow zone precisely defined.

Strusch [9.47] found particularly large insert loads and wall stresses when the insert was installed in the vertical section and the silo was emp-

tied. For filling conditions and for inserts installed in the hopper section, lower loads and stresses were observed in most cases. The reason for the large loads in the vertical section at emptying conditions is the transition from active to passive stress field due to the transition to convergent flow (similar to the mass flow hopper in Fig. 9.4.c, and the imperfection in Fig. 9.22.b). In Fig. 9.24.a the lines of major principal stress are depicted for the case that a wedge insert is installed along the axis of a vertical section and material is discharged (emptying conditions). Between insert and silo wall the cross-section converges downwards. Thus, a passive state of stress develops as in a mass flow hopper. This goes along with the transition from active to passive stress field (the switch) causing a peak of the wall normal stress, σ_w , at the transition from a vertical section to a mass flow hopper (see diagram in Fig. 9.24.a showing the distribution of wall normal stress and vertical stress). In the region of the insert the wall normal stress and the vertical stress decrease downwards. The stresses acting on the side walls of the insert will develop similar to the stresses on the opposite silo wall, i.e., they are largest at the tip of the insert and decrease downwards [9.47]. Beneath the insert the state of stress turns again into an active state of stress.

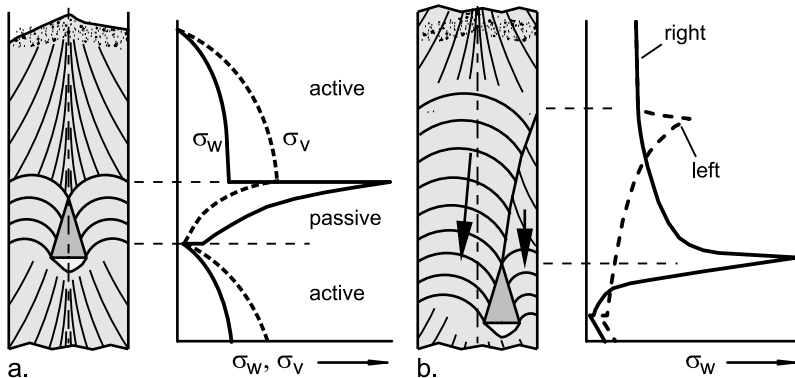


Fig. 9.24. Wedge insert in a vertical section of rectangular cross-section; distribution of the wall normal stresses, σ_w , and the mean vertical stresses, σ_v (dashed; only in Fig. a) versus silo height; the lines of major principal stress, σ_I , are plotted as assumed by the author (stresses qualitatively according to [9.47]); a. insert along the silo's axis of symmetry, b. insert laterally displaced, flow velocity is indicated by the length of the arrows.

If the insert is laterally displaced from the axis of symmetry, both the insert loads and the silo wall stresses become asymmetric. Furthermore, the insert shown in Fig. 9.24.b leads to an asymmetric velocity profile. At the level of the lower edge of the insert, the vertical stress in the area to the left

of the insert is greater than that on the right due to the larger width of the flow channel (in a converging channel the radial stress field develops where the stress is proportional to the local width). The larger vertical stress on the left side of the insert causes the material below to flow faster than that on the right side and, thus, finally results in a higher flow velocity of the material on the left side of the insert compared to the right side. The asymmetric velocity distribution still exists above the insert and is more and more equalized in the upward direction. Strusch [9.47] identified a boundary layer between the zone with the lower velocity on the right side and the zone with the higher velocity on the left side (see Fig. 9.24.b, where the boundary layer is indicated by a line starting from the tip of the insert).

For the zone of higher velocity (left) the zone with the lower velocity acts similar to a stagnant zone. Thus, convergent flow emerges in the faster flowing zone, which goes along with the development of a passive state of stress (see lines of major principal stress in this area, Fig. 9.24.b). At the top level of the converging flow zone a switch region develops indicated by a peak wall normal stress on the left silo wall. In the slower flowing zone (right side) no convergent flow takes place so the active state of stress is likely to be preserved. The stress in the slower zone increases in the downward direction due to the normal and shear stresses transferred through the boundary layer (especially important are the nearly vertically acting shear stresses due to the relative velocity of the zones). Since a converging channel is formed by the insert and the silo wall, the stress state in the slower flowing zone switches from active to passive at the level of the upper edge of the insert. The switch region goes along with a significant stress peak at the right silo wall. The stresses then rapidly decrease between insert and silo wall in the downward direction. Due to the smaller width between insert and silo wall the wall normal stresses are reduced to smaller values in comparison to the situation on the left side (radial stress field: stresses are proportional to local hopper width). Similar is the development of the vertical stress. The asymmetric vertical stresses have been mentioned already before as being the reason for the asymmetric flow profile.

The stress distributions caused by the insert (Fig. 9.24) demonstrate that in the area of the insert significantly larger stresses prevail than in a vertical section without insert, where the maximum vertical stress is given by $\sigma_{v\infty}$ according to Janssen's equation (Eq.(9.12), Sect. 9.2.1).

A quantity for the representation of the vertical load on inserts is the so-called specific insert load, $\sigma_{vE,spec}$, which is equal to the vertical load, F_V , acting on the insert (Fig. 9.25) divided by the base area of the insert [9.47]:

$$\sigma_{vE,spec} = \frac{F_V}{b_E \cdot L} \quad (9.33)$$

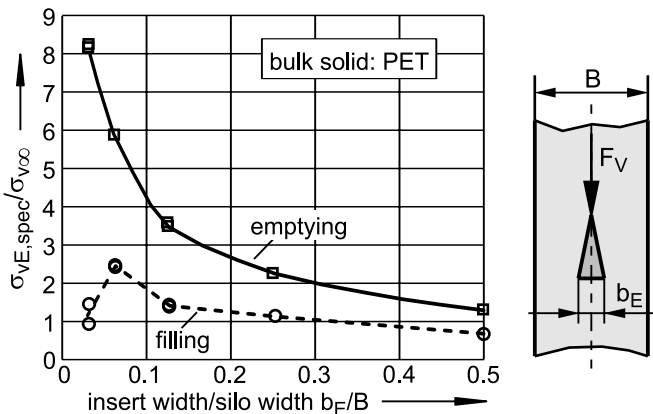


Fig. 9.25. Ratio $\sigma_{vE,spec}/\sigma_{v\infty}$ as a function of the ratio of insert width, b_E , to silo width, B , according to test results of Strusch [9.47] (insert in the vertical section)

b_E is the width of the insert, L the length of insert and silo (Fig. 9.25). The specific insert load has the unit of stress (force per area). In the diagram of Fig. 9.25 the ratio of the specific insert load, $\sigma_{vE,spec}$, to the maximum vertical stress in the vertical section, $\sigma_{v\infty}$, according to Eq.(9.12) is plotted versus the ratio of insert width, b_E , to silo width, B , for both filling and emptying conditions as measured by Strusch in a specific test arrangement [9.47]. It can be clearly seen that in the emptying state the specific insert load increases disproportionately with decreasing insert width. Furthermore, the specific insert load is larger in the emptying state than in the filling state for the range of parameters investigated (filling conditions will not be further discussed here, for further information refer to [9.47]). According to Fig. 9.25, in the emptying state the specific insert load is up to eight times $\sigma_{v\infty}$. Thus, a calculation of vertical insert loads based on the vertical stress according to Janssen's equation ($\sigma_{v\infty}$) multiplied by the base area of the insert would underestimate the real loads.

Especially small inserts (small ratio b_E/B in Fig. 9.25) exhibit large specific insert loads. This can be explained by the fact that the stresses acting on the insert are largest at the top edge of the insert and decrease downwards (Fig. 9.24.a). If a small insert is regarded as being the tip of a large insert, it will become clear that the average of the stresses acting on an insert becomes larger with decreasing insert width.

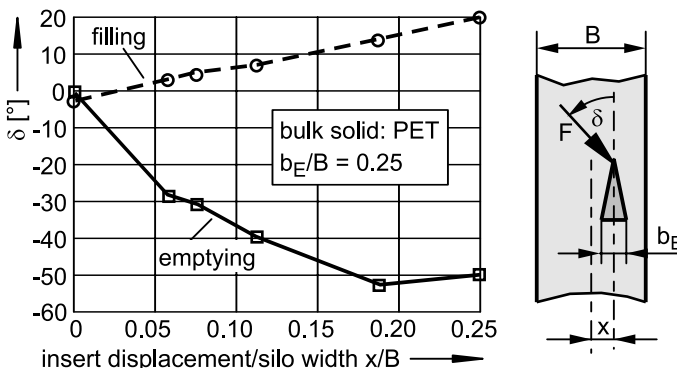


Fig. 9.26. Inclination to the vertical, δ , of the total force, F , acting on the insert as a function of the ratio of insert eccentricity, x , to silo width, B , according to measurements of Strusch [9.47] (insert within the vertical section)

The orientation of the force, F , acting on the insert is almost vertical at symmetrical conditions (Fig. 9.25). Small deviations can be caused, for example, by eccentric filling of the silo [9.47]. If the insert is displaced from the axis of symmetry, the insert load also becomes asymmetric. The direction of the total force, F , acting on the insert is plotted in Fig. 9.26 versus the ratio of insert eccentricity, x , to silo width, B . The inclination, δ , of the force to the vertical is increasing with increasing insert eccentricity, x . For emptying conditions δ is smaller than 0° , i.e., the force has a horizontal component acting from right to left. The reason for this is the stress peak developing on the right side of the insert (see Fig. 9.24.b). Values of δ smaller than -45° indicate that the horizontal component of force F is larger than the vertical component. Thus, horizontal loads on inserts can be larger than vertical loads [9.47].

In the filling state the angle, δ , is slightly increasing with increasing insert eccentricity, x . The reason for this is that on the left side larger stresses develop due to the larger distance between insert and wall compared to the situation on the right side.

If an insert is located in the hopper of a silo, in most cases the insert load is smaller compared to that on the same insert located in the vertical section. This is true especially for emptying conditions in a mass flow silo where the passive stress field prevails in the entire hopper. Thus, no switch stress develops at the upper edge of the insert (Fig. 9.27.b). The stresses between insert and hopper wall decrease stronger in the downward direction compared to the hopper without an insert, because the width of the flow channels left and right to the insert is smaller than the width of the hopper (compare distributions of wall normal stress with and without insert, Fig. 9.27.b). Beneath the insert the stresses converge towards the

stresses which would be acting there without the presence of an insert, i.e., radial stress field prevails, where the stresses are proportional to the local width of the hopper.

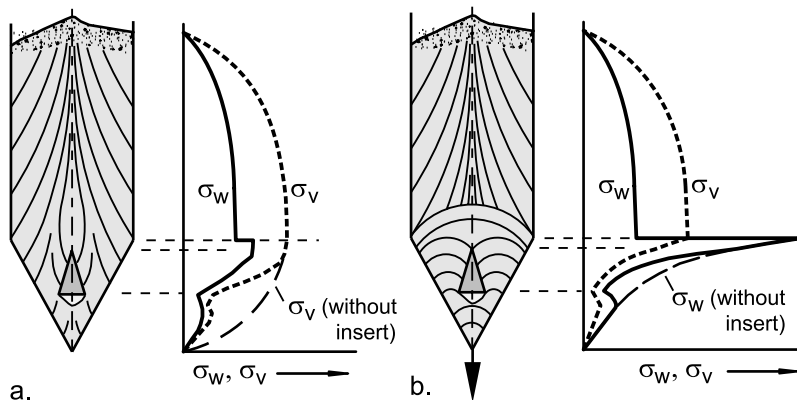


Fig. 9.27. Wedge insert in a wedge-shaped mass flow hopper; qualitative distributions of the wall normal stress, σ_w , and the mean vertical stress, σ_v , vs. silo height; the lines of major principal stress, σ_I , are plotted as assumed by the author; a. filling conditions, b. emptying conditions.

Also for filling conditions (Fig. 9.27.a) a reduction of the stresses in the region of the insert can be observed, whereby the active state of stress is preserved. Only the orientation of the principal stresses is slightly changed due to the presence of the insert. In contrast to emptying conditions, where the stress in the lower part of the hopper is proportional to the local width and does not depend on the conditions further up in the silo, at filling conditions the stresses in the hopper depend on the surcharge load caused by the material in the vertical section. Thus, the stresses beneath the insert are significantly reduced compared to the situation without insert (Fig. 9.27.a). This is above all important when the vertical stresses at the outlet should be reduced by the insert, for example, to decrease the load on a feeder.

9.4.2 Eccentric flow

The situation of an asymmetric flow zone, i.e., the bulk solid flows predominantly on one side of the silo, is called eccentric flow. The problems of eccentric flow are – besides the disadvantages of funnel flow – that within the silo a stress distribution develops that is asymmetric with respect to the perimeter. This has to be considered for structural design of a silo [9.9].

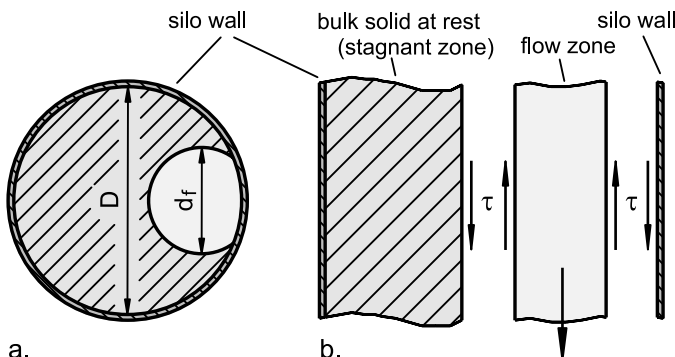


Fig. 9.28. Eccentric flow in a silo's vertical section (schematically); a. axial section; b. vertical section through the silo axis

Fig. 9.28 schematically shows a cylindrical section (diameter D) with an assumed flow zone (diameter d_f). The bulk solid flowing downwards exerts shear stresses not only on the silo wall, but also on the bulk solid that is at rest (stagnant zone), i.e. the flow zone transmits part of its weight to the silo wall and to the bulk solid in the stagnant zone. The shear stresses are depicted in Fig. 9.28.b showing their directions on the sectional planes. Thus, the flow zone can be regarded as being a “silo in a silo” with the diameter d_f . From Janssen’s equation (see Sect. 9.1.2) it is known that the maximum vertical and horizontal stresses being achieved in a cylinder are proportional to its diameter. Thus, in the flow zone of diameter d_f smaller stresses prevail than in the stagnant zone.

The distribution of wall normal stress, σ_w , developing during eccentric flow is schematically depicted in Fig. 9.29 (equivalent measurements see, e.g., [9.60, 9.61]). In the region of the flow zone significantly smaller wall normal stresses prevail than in the remaining part, but on either side of the flow zone slightly larger stresses occur [9.27, 9.62–9.64]. Due to this non-uniform load, the silo wall becomes flattened in the region of the flow zone (larger radius of curvature) and nearby slightly more bended (smaller radius of curvature). This behavior is most obvious if the silo is fabricated from metal. Thus, the silo wall is subjected to bending moments in different directions.

In reality the situation is more complex than shown in Figs. 9.28 and 9.29: The stresses in the flow zone and in the stagnant zones influence each other, the diameter of the flow zone can change with height (normally the diameter is increasing with height), and dependent on the shape of the flow zone it can happen that further up in the silo the stresses in the flow zone are the larger ones [9.60]. Furthermore, the flow zone can change its shape and position with time. Surveys of experimental and theoretical in-

vestigations about eccentric emptying are given by Hampe [9.10] and Rombach [9.27]. Calculation procedures can be found, for example, in [9.65–9.67]. Some silo codes contain procedures for the consideration of loads due to eccentric flow (e.g., [9.1–9.3]).

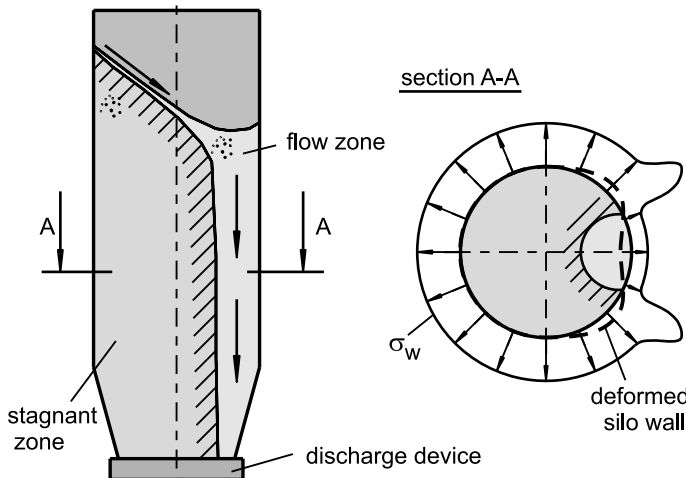


Fig. 9.29. Schematic distribution of the wall normal stresses σ_w and deformation of the silo wall at eccentric emptying

Reasons for eccentric flow can be:

- Funnel flow silo with asymmetric flow zone, for example, due to an eccentric outlet opening or an asymmetric hopper (Fig. 9.30.a). Note that even in a symmetrical funnel flow silo asymmetric flow zones may prevail, for example, due to segregation during filling.
- Multiple outlet openings, from which discharge does not occur simultaneously (Fig. 9.30.b./c.)
- Not fully opened gate (Fig. 9.30.d)
- Feeder withdrawing the material only from a part of the outlet opening (Fig. 9.30.e)

Also in a mass flow silo asymmetric stresses can occur around the perimeter when the bulk solid is not flowing uniformly over the cross-section. In this case the faster flowing bulk solid is supported by the slower flowing bulk solid as if it were a stagnant zone. An example is shown in Fig. 9.24.b, where the different flow velocities are caused by an insert. Also a feeder withdrawing asymmetrically can lead to different flow velocities within the bulk solid: The belt feeder in Fig. 9.31 withdraws material preferentially from the rear part of the outlet slot. This causes significantly dif-

ferent wall normal stresses, σ_w , at the front and rear walls of the silo, whereby in the lower part of the hopper the stresses are smaller where the downward velocities are larger.

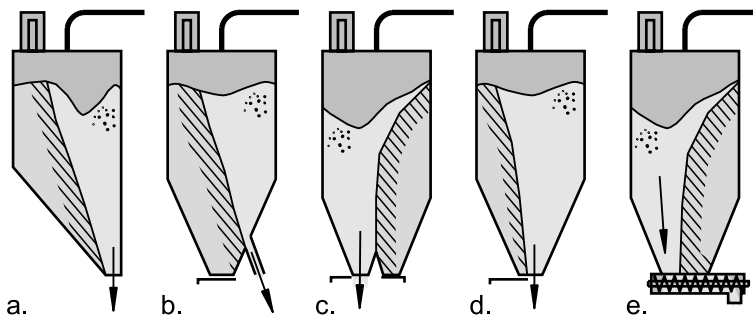


Fig. 9.30. Reasons for eccentric flow; a. asymmetric hopper; b./c. multiple outlet openings; d. not fully opened gate; e. feeder withdrawing the material only from a part of the outlet opening

The distributions of stresses caused by eccentric emptying are most important for the structural design of a silo. Due to the asymmetric load bending moments and stresses are created which do not occur under symmetrical load [9.9]. For instance, if thin-walled cylindrical metal silos are deformed by eccentric loads as outlined above (Fig. 9.29), the radius of curvature of the cylindrical wall is increased in the area of the flow zone, so the vertical buckling strength is reduced.

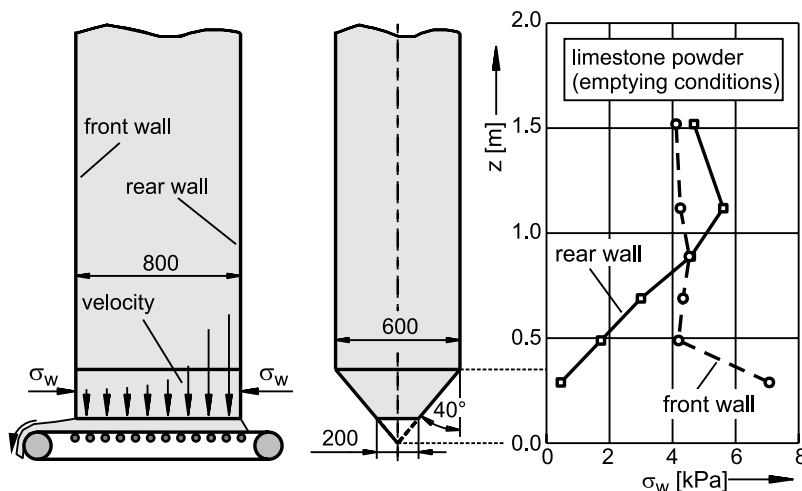


Fig. 9.31. Stresses while discharging with a belt feeder [9.33]

If the position of the flow zone changes with time the stress distribution also changes. As an example, in Fig. 9.32 a cylindrical silo provided with an orbiting screw feeder is shown. The screw rotates with respect to the silo axis while discharging (see Sect. 12.3.2.10). The bulk solid flows from above into the screw and, thus, forms an eccentric flow zone, the extension and shape of which depends on the geometry of the screw and on bulk solids properties. Due to the eccentric flow zone the silo walls will be stressed and deformed similar to the situation in Fig. 9.29, but since the screw is rotating with respect to the silo axis, the flow zones and the local stresses and deformations are traveling around the silo axis [9.68]. Thus, any point of the silo wall is subjected to alternate bending moments. This also takes place with other discharge techniques where the position of withdrawal is moving, for example, with inverted cone silos used for the homogenization of raw mix or cement (Sect. 12.3.2.8) [9.64,9.69].

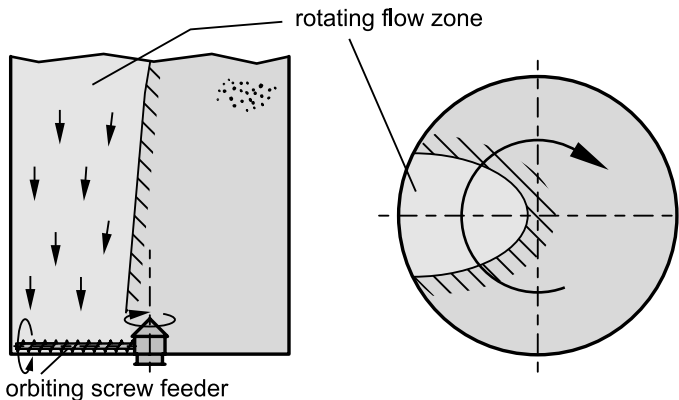


Fig. 9.32. Flow zone rotating around the vertical silo axis while discharging with an orbiting screw [9.68]

10 Silo design for flow

Since poorly designed silos can lead to shut-down periods in production plants as well as to product degradation due, for example, to segregation or too long residence times, silos should be designed by considering the bulk solid properties. As with other components in the design of process plants, reliable design criteria for silos are available. In the present chapter the well known design procedure due to Jenike [10.1,10.2] is described, which is based on the bulk solid's properties. The expense to measure bulk solid properties that are necessary for silo design for flow is normally small compared to the costs which arise due to quality problems, production stoppages, building adjustments or complete reconstructions if such properties are ignored.

10.1 Flow profiles: mass flow and funnel flow

When a bulk solid discharges under gravity from a silo, one must distinguish between mass flow and funnel flow (also known as core flow or plug flow), see Fig. 10.1. In a mass flow silo every particle of the bulk solid in the silo is moving whenever the outlet is opened provided that arching does not occur. Mass flow is only possible if the hopper walls are steep and/or low enough in friction. If the hopper wall is too flat or too frictional, funnel flow will occur. In a funnel flow silo (Fig. 10.1.b/c) at first only the bulk solid in a channel above the opening flows downwards – if anything discharges. The bulk solid located in the stagnant zones (also designated as dead zones), which develop at the silo periphery starting at the hopper walls directly above the opening, can be discharged only if the silo is emptied completely. The stagnant zones can reach the top level of the filling with the result that a flow funnel is formed at the surface (this type of funnel flow is called pipe flow in [10.3]). Thus, in this case funnel flow can easily be detected. It is also possible that the stagnant zones exist only in the lower part of the silo, because the boundary between the flowing bulk solid (flow channel) and the stagnant zones intersects the silo wall beneath the top level of the filling (this type of funnel flow is called mixed

flow in [10.3]). In this case a clear recognition of the flow profile is not possible by only looking from above on the filling (Fig 10.1.c). Additionally the stagnant zones can be asymmetrical (even if the silo is symmetric with a centric outlet) thus causing disadvantageous loads on the silo walls (Sect. 9.4.2). Even more asymmetric flow may prevail in a silo with an eccentric flow zone (eccentric pipe flow according to [10.3], Fig. 10.1.d) caused, for example, by an eccentric outlet opening in combination with too shallow hopper walls (more reasons for eccentric flow are shown in Fig. 9.30).

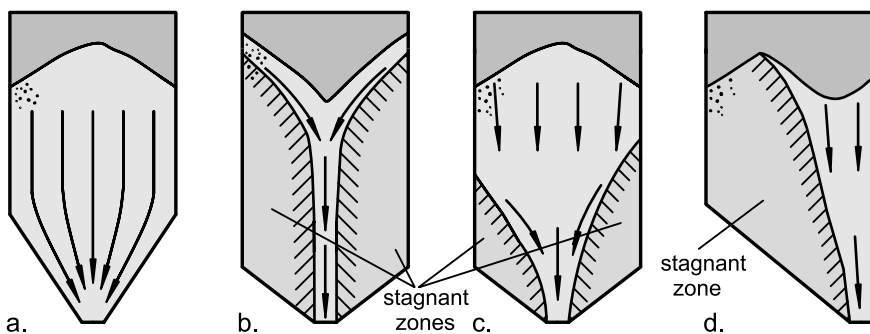


Fig. 10.1. Flow profiles: a. mass flow; b. funnel flow with stagnant zones up to the level of filling (pipe flow [10.3]); c. funnel flow with stagnant zones in the lower silo part (mixed flow [10.3]); here the stagnant zones are asymmetric; d. funnel flow with eccentric flow zone (eccentric pipe flow [10.3])

In a mass flow silo the complete mass of filling is in motion whenever bulk solid is discharged. However the velocity can be – and almost always is – different across the cross-section of the silo. If a uniform velocity distribution is assumed at the opening, a velocity distribution develops in the hopper with the highest values at the hopper axis and the lowest at the walls. Figure 10.2 depicts the vertical velocity components in a mass flow silo. The velocity at the wall is smaller the more frictional and flatter the hopper wall is. If the hopper wall is too frictional or too flat, no movement at the wall is possible, and, thus, a stagnant zone develops (funnel flow).

The velocity distribution in the hopper still exists in the lower part of the vertical section, but with increasing distance from the upper corner of the hopper it turns into plug flow. The height of this transition zone is typically about 0.7 to 1.0 times the diameter of the vertical section, D .

In funnel flow silos, where stagnant zones exist only in the lower part of the silo (Fig. 10.1.c), the velocity distributions above the stagnant zones are similar to those found in mass flow silos above the hopper. Therefore,

observation of the level of filling does not always give the correct indication of the flow profile.

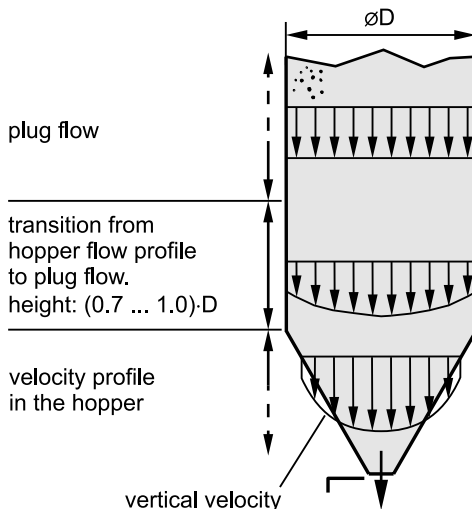


Fig. 10.2. Distribution of vertical components of velocities in a mass flow silo

10.2 Flow problems in silos

Problems often occurring during the storage of bulk solids in silos were described briefly in Sect. 1.1 (Fig. 1.2). Most of the mentioned problems are connected with funnel flow (Fig. 10.1). Therefore, many of the problems shown in Fig. 1.2 can be avoided if the silo is designed for mass flow:

- Ratholes (also called pipes) are formed from consolidated stagnant zones. Therefore, they are only possible in funnel flow (Fig. 1.2.c).
- The residence time distribution in a mass flow silo is narrow (“first in – first out”). Thus, the unfavorable long and unknown residence times occurring in a funnel flow silo (Fig. 1.2.b) can be avoided.
- Flooding often is the result of an insufficient deaeration of the bulk solid, and, therefore, it occurs when the residence time is too short. Especially in a funnel flow silo the residence time can be very short when the bulk solid is discharged during filling. As a result of the stagnant zone, the bulk solid just fed in appears after a very short time at the silo outlet (Fig. 1.2.d). Compared to a funnel flow silo, at identical mass of

filling and identical discharge rates the residence time in a mass flow silo is much longer (additional remarks regarding flooding: Sect. 12.1)

- Segregation during filling, where different fractions separate across the surface of the silo filling, has a strong influence on the transient composition of the bulk solid discharged from funnel flow silos (Fig. 1.2.e). In contrast to this, in a mass flow silo the bulk solid is often sufficiently remixed in the hopper section (for means to reduce segregation refer to Chap. 13).

Thus, in mass flow silos only the potential problem of arching remains where a stable arch forms above the silo outlet so that discharge is stopped. Coarse grained bulk solids can build up arches due to interlocking and wedging of particles (Fig. 10.3.a). This kind of arching can be avoided if the diameter of the circular outlet of a conical hopper is at least 6 to 10 times the maximum particle size, x_{max} . The width of the rectangular outlet of a wedge-shaped hopper should be at least 3 to 7 times x_{max} (the outlet dimension depends on particle size distribution and particle shape [10.4]; a narrow particle size distribution and sharp-edged particles will tendentially increase the probability of arch formation due to interlocking and wedging. Even if the outlet is large enough to avoid the formation of a stable arch, it may result in pulsating flow. With the maximum values given above satisfactory flow may be obtained with a wide range of different materials). With fine-grained and cohesive bulk solids the reason for arching is the cohesive strength (compressive strength, unconfined yield strength) of the bulk solid due to adhesive forces between individual particles. Even in this case arching can be avoided by a sufficiently large outlet opening. The calculation procedure will be explained in this section.

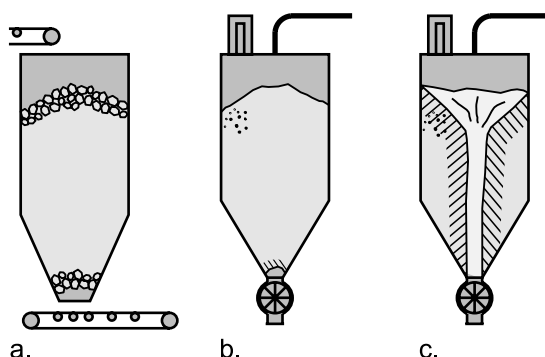


Fig. 10.3. a. Arching due to interlocking and wedging of coarse-grained bulk solids; b. arching due to the cohesive strength of a bulk solid; c. ratholing (piping)

In case of a funnel flow silo, all problems mentioned above, which are characteristic of funnel flow, can occur (e.g., segregation or a wide residence time distribution). To ensure at least unobstructed flow, arching as well as ratholing (piping) (Fig. 10.3.c) must be avoided. A stable rathole develops in a funnel flow silo if only the bulk solid vertically above the outlet discharges, whereby the rest of the bulk solid – the material in the stagnant zones – remains stationary in the silo due to its cohesive strength, thus building the walls of a stable rathole. If the bulk solid tends to time consolidation, the strength of the stationary material in the stagnant zones increases with time, and as a result, the tendency for ratholing is also increased. In the extreme case the bulk solid can be discharged only with major effort (e.g., manually loosened and discharged from the silo top with truck mounted vacuum equipment). Like arching, ratholing can be avoided with a sufficiently large outlet opening. The calculation procedure will also be explained in this section.

10.3 Jenike's procedure for silo design

The design procedure developed by Jenike [10.1] has been applied with great success for more than 40 years. It allows determination of the hopper slope required for mass flow and outlet dimensions for unobstructed gravity flow, i.e., no arching in mass flow silos and neither arching nor ratholing in funnel flow silos.

After Jenike's fundamental approach had been published, further procedures regarding silo design were presented by other researchers, for example, those of Enstad [10.5] and Molerus [10.6]. Nevertheless, Jenike's design procedure is still the most applied one and, thus, is explained in the following in a simplified form.

For the design procedure the quantities characterizing the flow properties of the bulk solid have to be known (Chap. 3). Essentially, these are the bulk density, ρ_b , the effective angle of internal friction, φ_e , characterizing the internal friction of the bulk solid, the unconfined yield strength, σ_c , and the angle of wall friction, φ_x . The angle of wall friction is the major property for mass flow hopper slope design, whereas the unconfined yield strength is the decisive property considering arching. It has to be mentioned that all flow properties mentioned above depend on the stress level being represented by the major consolidation stress, σ_I (see Fig. 3.22). They can be measured with shear testers (Chap. 4).

10.3.1 Design of mass flow silos

The basic geometrical shapes investigated by Jenike are the conical hopper and the wedge-shaped hopper (Fig. 10.4). Also asymmetric wedge-shaped hoppers are treated and instructions are given for asymmetric conical hoppers. However both shapes have no advantages – and several significant disadvantages (see Sect. 11.2.1) – considering discharge behavior or best use of space compared to the equivalent symmetric hoppers. To neglect the influence of the front walls, it is supposed for the wedge-shaped hopper that the length, L , of the rectangular outlet is at least three times its width, b ($L > 3b$). The goal of the design process is the determination of the hopper slope necessary for mass flow and the minimum outlet size to prevent flow problems due to arching or ratholing.

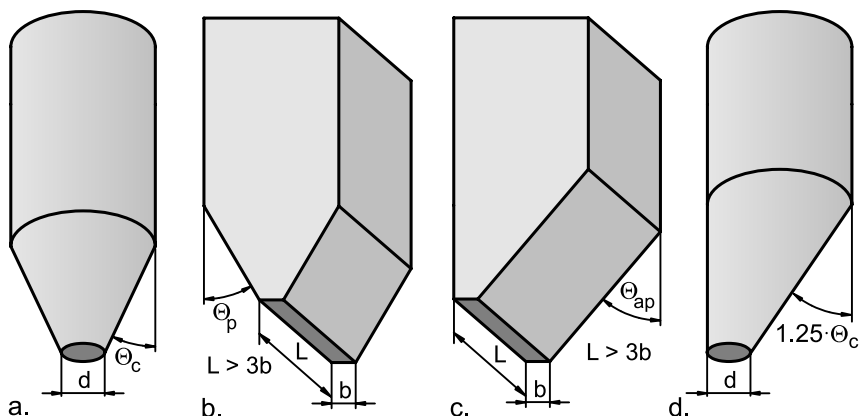


Fig. 10.4. Basic silo shapes: a. conical; b. wedge-shaped; c. asymmetric wedge-shaped; d. asymmetric conical

Jenike's approach is based on the calculation of stresses in hoppers. With the conditions of equilibrium applied to an infinitesimal volume element of bulk solid in the hopper, he derived two partial differential equations. The properties of the bulk solid are taken into account by parameters obtained from yield loci. For the flowing bulk solid steady-state flow conditions are assumed where the ratio of major to minor principal stress is defined by the effective angle of internal friction, φ_e , or the effective yield locus, respectively. Incipient flow (being important for arching and ratholing not to occur) is characterized by an equation for the linearized yield locus. With further simplifying assumptions Jenike postulated that the major principal stress σ_I in the lower hopper part is proportional to the distance, r , from the virtual hopper apex ("radial stress field") [10.1]:

$$\sigma_I = r \cdot g \cdot \rho_b \cdot s(\Theta', \Theta, \varphi_x, \varphi_e) \cdot (1 + \sin \varphi_e) \quad (10.1)$$

As an approximation the bulk density, ρ_b , is assumed to be constant. Angle Θ' and radius r determine the position of the bulk solid element in the hopper (polar coordinates; see Fig. 10.5), whereas Θ is the inclination of the hopper wall to vertical. Thus, function s depends on the bulk solid's properties, φ_e and φ_x , the hopper slope, Θ , and coordinate, Θ' .

A solution of the system of differential equations exists only for specific combinations of parameters, Θ , φ_e , and φ_x . Thus, only for these conditions mass flow will occur. If the hopper wall is not steep enough, no solution exists fulfilling the condition of bulk solid moving along the hopper wall (mobilization of wall friction), and, thus, a stagnant zone will form (funnel flow). With the solution of the system of differential equations function s in Eq.(10.1) is also known. Thus, besides others, the major principal stress in the hopper can be calculated.

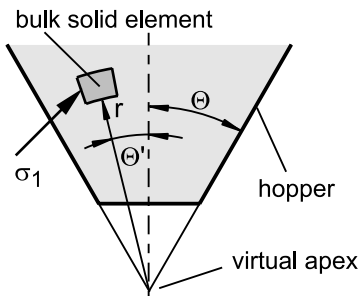


Fig. 10.5. Polar coordinates in a hopper

In Fig. 10.6 the combinations of parameters which lead to solutions of the system of differential equations, and, thus, to mass flow for conical hoppers, are indicated as “mass flow” region. The mass flow region is separated from the funnel flow region (where no solutions of the differential equations are found) by the mass flow boundaries, which depend somewhat on the effective angle of internal friction, φ_e , characterizing the internal friction at steady-state flow. In Fig. 10.7 the boundaries for wedge-shaped hoppers are shown which are not theoretically determined boundaries, but modified based on Jenike's practical experience (the theoretically obtained boundaries are located more to the right, but are not sufficient to obtain mass flow at all conditions). In both figures the angle of wall friction, φ_x , is plotted versus the slope of the hopper wall, Θ , from vertical (Θ_c for conical hoppers, Θ_p for wedge-shaped hoppers).

Conditions within the mass flow boundaries (Figs. 10.6 and 10.7) lead to mass flow whereas conditions outside represent funnel flow. Knowing the angle of wall friction, φ_x , and the effective angle of internal friction, φ_e , the maximum inclination, Θ , of the hopper wall for mass flow to occur can be determined from the mass flow boundaries. For the case of a conical hopper, a safety margin of 3° to 5° [10.1] should be subtracted from the maximum inclination because the mass flow boundaries have been calculated for ideal conditions (a safety margin of 2° to 3° may be sufficient if the properties of the bulk solid and the wall surface are well-defined and do not change with time, and the maximum wall friction angles have been determined accurately). All boundary lines have a similar shape indicating that the maximum hopper slope for mass flow is steeper (Θ smaller) the larger the angle of wall friction, φ_x .

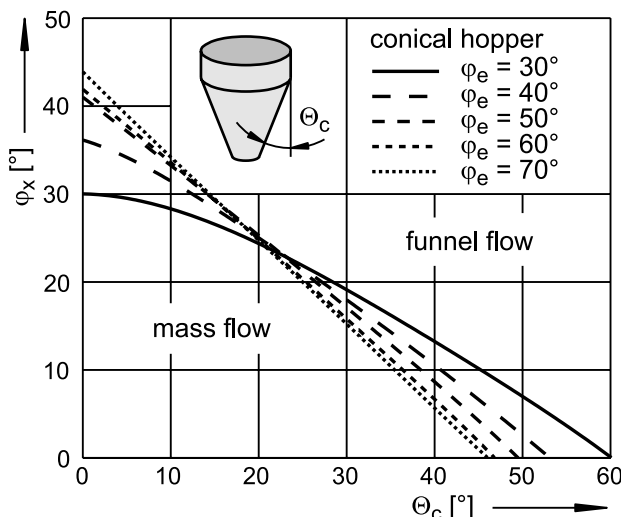


Fig. 10.6. Mass flow diagram (conical hopper)

For identical material properties (φ_x , φ_e), the wedge-shaped mass flow hopper can be flatter (larger angle Θ) than a conical mass flow hopper; the difference is normally in the range of 8° to 12° . This can be explained by the fact that at identical hopper inclination the cross-section of a conical hopper is reduced more in the direction of flow than that of a wedge-shaped hopper. The inclined wall of an asymmetric wedge-shaped hopper can even be flatter (Fig. 10.4.c; diagram with mass flow boundary: see Sect. 10.5). The maximum wall inclination of an asymmetric conical hopper (Fig. 10.4.d) follows from a multiplication of the maximum angle of inclination of a symmetric conical hopper, Θ_c , by 1.25 [10.1].

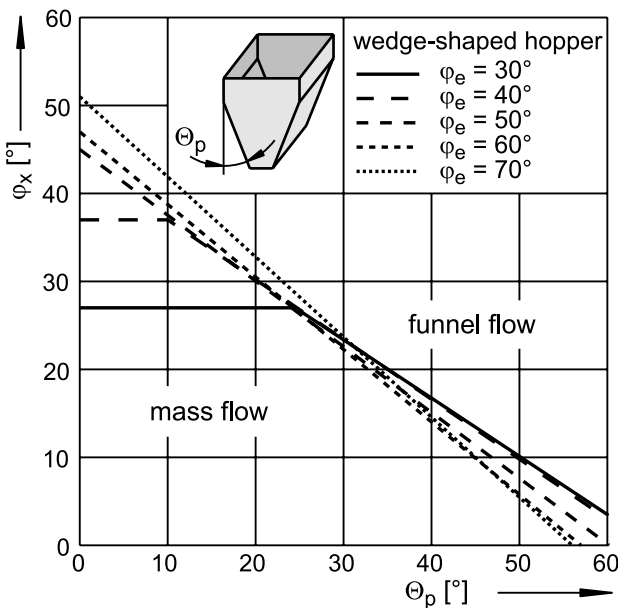


Fig. 10.7. Mass flow diagram (wedge-shaped hopper, $L > 3b$)

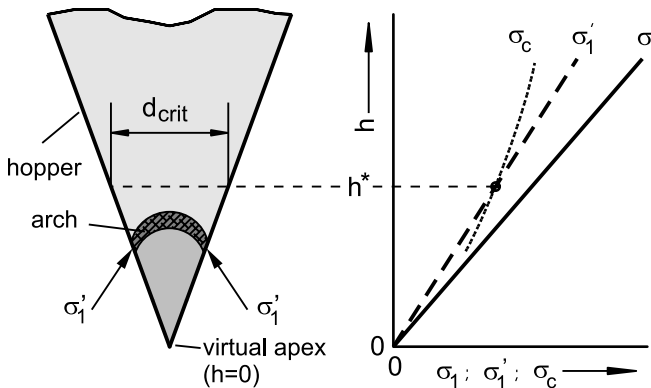


Fig. 10.8. Model for determination of minimum outlet size, d_{crit} , to avoid arching

For the next step, i.e., determination of the minimum size of the outlet opening to avoid arching, the stresses in the hopper are considered. When bulk solid is discharged from a mass flow silo, the radial stress field develops in the hopper (Sect. 9.1.2). The major principal stress, σ_1 , of the radial stress field is (at least at a sufficient distance from the silo's vertical section) proportional to the local hopper diameter which in turn is proportional to the distance, r , to the virtual hopper apex. Thus, σ_1 tends towards zero at the hopper apex (Fig. 10.8). The major principal stress, σ_1 , is acting

as the consolidation stress which determines the local properties of the bulk solid.

For each major principal stress (= consolidation stress), σ_1 , the unconfined yield strength, σ_c , can be measured (Chap. 3). The relation $\sigma_c(\sigma_1)$ is called the (instantaneous) flow function (Fig. 10.9). The flow function should not be mixed up with the yield locus: Each yield locus provides one pair of unconfined yield strength, σ_c , and consolidation stress, σ_1 , values, i.e., one point on the flow function. According to the flow function (Fig. 10.9), in Fig. 10.8 for every consolidation stress, σ_1 , the corresponding value of unconfined yield strength, σ_c , is plotted.

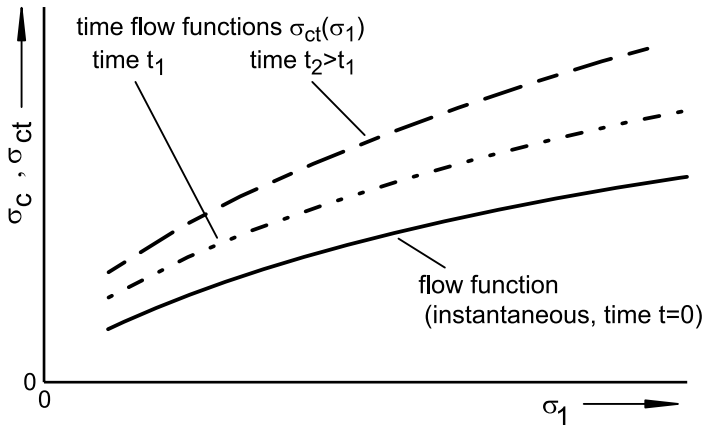


Fig. 10.9. Flow function and time flow functions

If a cohesive arch has formed in a hopper (Fig. 10.8), a force resulting from the weight of the bulk solid is transferred to the hopper walls. This effect is represented by the major stress required to support a stable bulk solid arch, σ'_1 , which is comparable to the bearing stress of a road bridge. Jenike calculated σ'_1 by assuming that the bulk solid arch has a smooth shape with a constant thickness in vertical direction, and that the arch must carry only its own weight, i.e., any load from the material above the arch is neglected. With further assumptions it follows for the major stress in a stable arch [10.4]:

$$\sigma'_1 = \frac{2r \cdot \sin \Theta \cdot g \cdot \rho_b}{1 + m} \quad (10.2)$$

m is a parameter describing the hopper shape: $m = 0$ for wedge-shaped hoppers and $m = 1$ for conical hoppers. The term $(2r \cdot \sin \Theta)$ represents the local hopper diameter, d , for the conical hopper and the local width, b , for the wedge-shaped hopper (silo shapes: see Fig 10.4). Coordinate r meas-

ures the distance from the hopper apex to the support of the arch (similar to Fig. 10.5, but along the hopper wall, i.e., $\Theta' = \Theta$).

A stable arch is only possible in that part of the hopper where the unconfined yield strength is greater than the stress that would exist in a stable arch ($\sigma_c > \sigma_l'$), i.e., beneath the point of intersection of the σ_c curve with the σ_l' line (Fig. 10.8). Above the point of intersection the unconfined yield strength is smaller than the major stress in the arch, i.e., the material will flow. The intersection point defines that position in the hopper (height h^* , Fig. 10.8) where the hopper diameter is equal to the so-called critical outlet diameter, d_{crit} , which must be exceeded if arching is to be avoided. If the outlet opening is smaller than d_{crit} (i.e., lower in the hopper), flow promoting devices have to be installed between the actual outlet opening and the critical diameter, d_{crit} (height h^*). The equivalent procedure for a wedge-shaped hopper with a rectangular outlet leads to a critical outlet width, b_{crit} . Since here the influence of the front walls (friction!) is neglected, the length, L , of the outlet must be at least three times its width, b .

Some bulk solids have the tendency to consolidate with time when stored at rest, for example, in a silo (time consolidation, Sect. 3.1.2). In analogy to the (instantaneous) flow function which characterizes the instantaneous behavior (unconfined yield strength directly after consolidation, i.e., after the storage period $t = 0$), time flow functions $\sigma_{ct} = \sigma_c(\sigma_l, t)$ exist which represent the unconfined yield strength after certain consolidation periods. Two time flow functions are plotted in Fig 10.9 being valid for two storage periods at rest, t_1 and $t_2 > t_1$. If the time flow function line would be transferred into Fig. 10.8, a point of intersection of σ_l' and σ_{ct} would result located further upwards, i.e., at $h > h^*$. Thus, a larger critical diameter, d_{crit} , would result. This leads to the well known effect that with increasing time of storage at rest larger outlet diameters are necessary to avoid arching.

For the practical determination of critical outlet dimensions Jenike proposed a procedure outlined in the following. It is based on the fact that both stresses σ_l' and σ_l are proportional to the local hopper diameter which in turn is a function of the distance, r , to the hopper apex (see also Eqs.(10.1) and (10.2)). Thus, at the hopper wall ($\Theta' = \Theta$) the ratio σ_l/σ_l' , called the flow factor, ff , is constant.

$$ff = \frac{\sigma_l}{\sigma_l'} = const = (1 + m) \cdot s(\Theta, \varphi_x, \varphi_e) \cdot \frac{1 + \sin \varphi_e}{2 \sin \Theta} \quad (10.3)$$

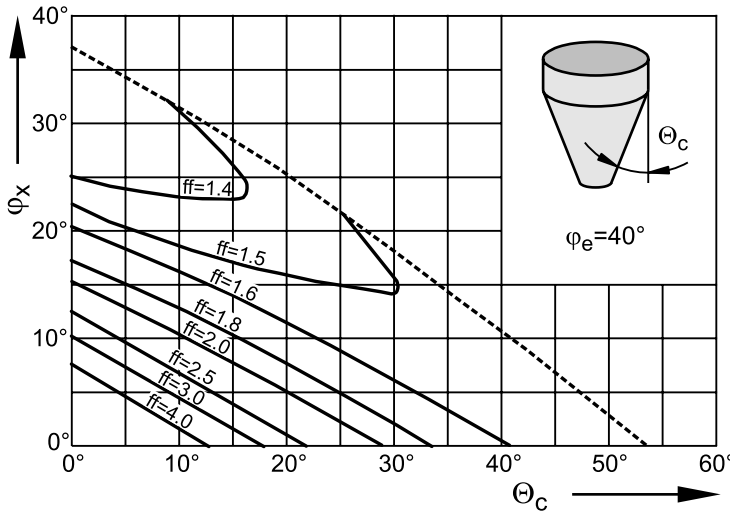


Fig. 10.10. Flow factor, ff , for conical hoppers and $\varphi_e = 40^\circ$ [10.1]

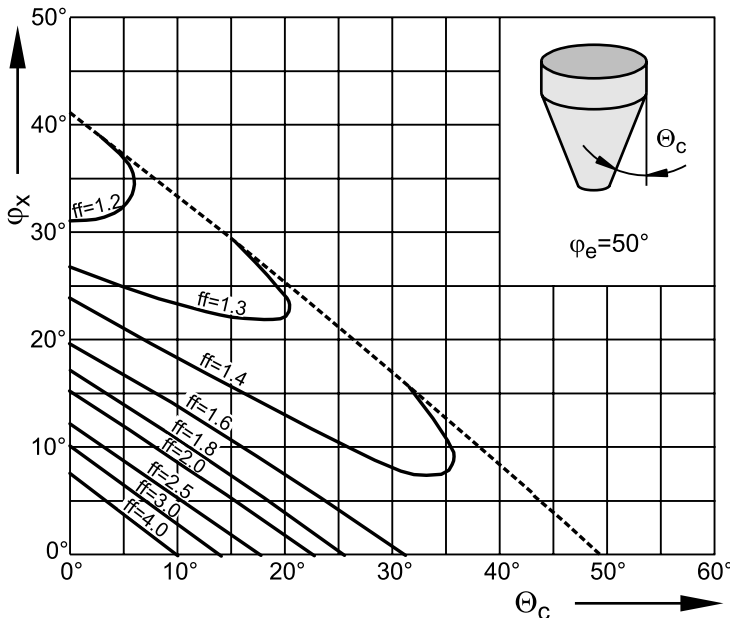


Fig. 10.11. Flow factor, ff , for conical hoppers and $\varphi_e = 50^\circ$ [10.1]

The flow factor ff is dependent on the flow properties (φ_x , φ_e) and the hopper shape (m , Θ). Knowing function s (Eq.(10.1)), the flow factor can be calculated. Jenike provided diagrams for an easy determination of the flow factor. Each of the diagrams is valid for a specific hopper geometry (e.g.,

conical) and a fixed value of the effective angle of internal friction, φ_e , being varied from diagram to diagram in steps of 10° . Two of these diagrams (valid for conical hoppers) are shown in Figs. 10.10 and 10.11. The solid curves represent constant values of ff , as given by the labels. For values in between and φ_e values which are not multiples of 10° , the flow factor values must be obtained by interpolation. The mass flow boundary is also plotted in each diagram (dashed curve). Further diagrams are presented in Sect. 10.5. The complete set of diagrams is given in Jenike's Bulletin 123 [10.1]. Equations approximating ff and the maximum hopper wall angles for mass flow are published in [10.7].

For determination of critical outlet dimension to avoid arching a σ_c, σ_I diagram as shown in Fig. 10.12 is used. Additionally, the major stress in the arch, σ'_I , is plotted in this diagram, which, according to Eq.(10.3), is directly proportional to σ_I .

$$\sigma'_I = \frac{\sigma_I}{ff} \quad (10.4)$$

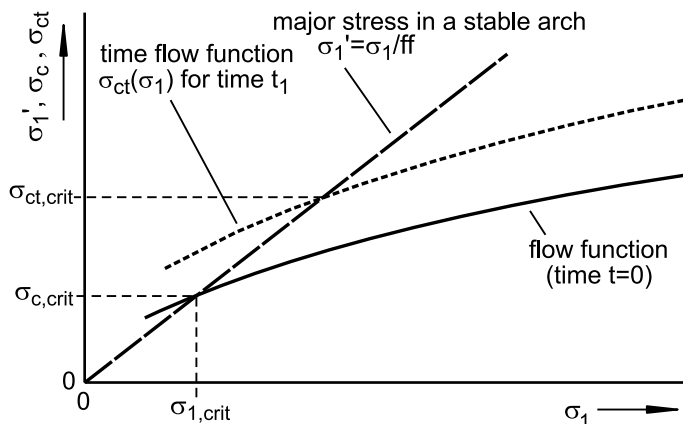


Fig. 10.12. Flow function and time flow functions; major stress in a stable arch, σ'_I

With the measured flow properties, the hopper inclination, Θ , determined at the mass flow design, and Jenike's diagrams [10.1] (e.g. Fig 10.10), the flow factor, ff , can easily be determined.

The point of intersection of the major stress in the arch, σ'_I , and the flow function in the σ_c, σ_I diagram (Fig. 10.12) is equivalent to the point of intersection in Fig. 10.8. The coordinates of the intersection point are provided with the index "crit" (unconfined yield strength, $\sigma_{c,crit}$, and consolidation stress, $\sigma_{I,crit}$). Finally the equivalent local hopper diameter, the critical diameter, d_{crit} , has to be calculated. To do so Eq.(10.2) is rearranged, and the

major stress in the arch, σ_l' , is replaced by the unconfined yield strength, $\sigma_{c,crit}$, (at the point of intersection is $\sigma_l' = \sigma_{c,crit}$). With

$$d = 2r \cdot \sin\Theta \quad (10.5a)$$

and

$$b = 2r \cdot \sin\Theta \quad (10.5b)$$

it follows for the critical outlet width, b_{crit} , of a wedge-shaped hopper:

$$b_{crit} = \frac{\sigma_{c,crit}}{g \cdot \rho_b} \quad (10.6a)$$

The critical outlet diameter, d_{crit} , of a conical hopper is:

$$d_{crit} = 2 \frac{\sigma_{c,crit}}{g \cdot \rho_b}. \quad (10.6b)$$

A more precise calculation yields the following equations:

$$b_{crit} = H(\Theta_p) \frac{\sigma_{c,crit}}{g \rho_{b,crit}} \quad (10.7a)$$

and

$$d_{crit} = H(\Theta_c) \frac{\sigma_{c,crit}}{g \rho_{b,crit}}. \quad (10.7b)$$

For bulk density, ρ_b , the value $\rho_{b,crit}$ corresponding to $\sigma_{l,crit}$ is used. The function $H(\Theta)$ takes into account the hopper geometry (conical or wedge-shaped; wall inclination Θ_c and Θ_p , respectively). $H(\Theta)$ is plotted in Fig. 10.13 (for approximate equations for $H(\Theta)$ refer to [10.7]).

In a similar way the outlet dimensions can be determined which are required to avoid arching after longer periods of storage at rest (= no bulk solid is discharged). For this case the point of intersection of the major stress in the arch and the time flow function for the storage time in question, $\sigma_{ct} = \sigma_c(\sigma_l, t)$, has to be determined (Fig. 10.12).

If a silo has been designed for a specific storage time at rest, some bulk solid must be discharged after this time to avoid arching. During discharge, the particles in a mass flow hopper are moved relative to each other so existing particle contacts are replaced by new ones. Thus, any time consolidation that prevailed during the storage at rest diminishes, i.e., the bulk solid behaves again as prior to the storage period. To obtain this effect, only a portion of the silo contents has to be discharged, because in a mass

flow silo the whole contents are in motion during discharge (this is discussed further in Sect. 10.4).

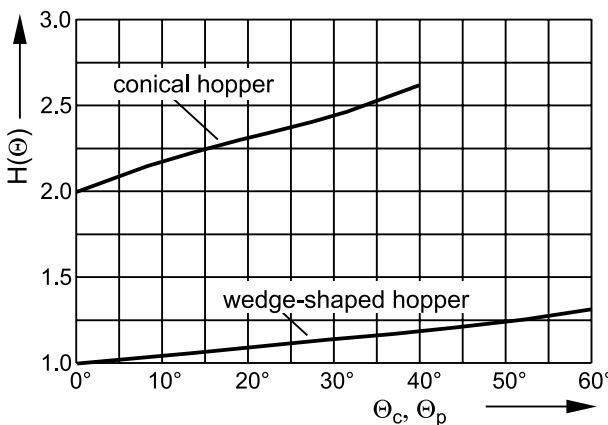


Fig. 10.13. Function $H(\Theta)$ [10.1]

Since the design procedure outlined above is based on the radial stress field, i.e., stresses prevailing in the hopper after the bulk solid has moved downwards (emptying state, Fig. 9.4.c), the calculations are not valid for the filling state which develops when bulk solid is fed into an empty silo without any discharge. In the filling state the stresses in the hopper can be larger than in the emptying state (see Fig. 9.4) thus leading to a stronger consolidation of the bulk solid.

In practice often an iterative procedure is necessary for silo design. Both the hopper angle for mass flow and the flow factor, ff , depend on the effective angle of internal friction, φ_e , and the angle of wall friction, φ_x , which often are stress-dependent (see Figs. 3.22 and 3.29). At the start of the design process the outlet dimensions and, thus, the major principal stress at the outlet, are not yet known. Therefore, values for φ_e and φ_x have to be estimated. After the critical outlet dimension has been determined and the major principal stress at the outlet is known, φ_e and φ_x can be determined for the conditions at the outlet. If these values are not equal to the estimated values, the design process has to be repeated with the new values, and so on until finally the estimated values are equal to the calculated values. The same procedure must be followed if a critical outlet dimension is determined with a time flow function.

If the angle of wall friction is stress-dependent, one must find the wall friction angle for a given value of the major principal stress, $\sigma_{I,crit}$. This is accomplished by considering the situation at the hopper wall close to the outlet. The major principal stress, σ_I , is inclined by the angle α to the wall

normal stress, σ_w (Fig. 10.14.a). The major principal stress for the critical outlet diameter is $\sigma_I = \sigma_{I,crit}$ (see above). The effective angle of internal friction corresponding to this major principal stress, i.e., $\varphi_{e,crit} = \varphi_e(\sigma_{I,crit})$, follows from the measured yield loci. Since steady-state flow is assumed in the hopper, a stress circle with the major principal stress $\sigma_I = \sigma_{I,crit}$ being tangent to the effective yield locus for $\varphi_e = \varphi_{e,crit}$ represents the stresses at the outlet (Fig. 10.14.b).

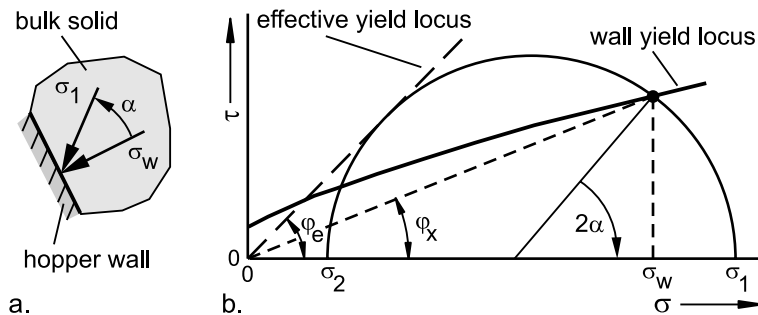


Fig. 10.14. Determination of the wall normal stress in a mass flow hopper; a. wall normal stress, σ_w , and major principal stress, σ_I , at hopper wall; b. Mohr stress circle representing the stresses at the wall

Additionally, the wall yield locus is plotted in the σ, τ diagram. Its right point of intersection with the Mohr stress circle characterizes the normal and shear stresses at the hopper wall (Fig. 10.14.b). Thus, the angle of wall friction, φ_x , for the stress conditions at the outlet can be easily determined from the slope of a straight line running through the origin and the right point of intersection. The right intersection point must be used here because in the emptying state the major principal stress is horizontal at the axis of symmetry and slightly inclined downwards at the wall. Thus the angle between the major principal stress and the wall normal stress is small. On the other hand, the angle between the minor principal stress and the wall normal stress is larger as can easily be seen on the stress circle in Fig. 10.14.b. The angle between the directions of the major principal stress, σ_I , and the wall normal stress, σ_w , can also be obtained from the stress circle where it appears as 2α (drawn in the opposite direction of rotation than in the bulk solid, see Fig. 10.14; for more details refer to Sect. 2.3.1).

Alternatively to the σ, τ diagram shown in Fig. 10.14.b, the wall normal stress at the outlet can also be determined with diagrams provided by Jenike [10.1].

10.3.2 Design of funnel flow silos

To avoid the problems typically occurring in funnel flow silos (e.g., segregation, degradation, ratholing; see Sects. 1.1 and 10.2), mass flow should be used. Funnel flow may only be acceptable if “friendly” bulk solids are stored which do not exhibit such problems. In the following it will be shown how funnel flow silos have to be designed for trouble-free operation.

The walls of a funnel flow silo are flatter than those of a mass flow silo, but should be steep enough to ensure that the silo can be cleared completely alone by gravity. For cohesive bulk solids, the maximum inclination of the hopper walls to vertical, θ_{cd} , can be assessed according to Jenike [10.1] as a function of the angle of wall friction, φ_x :

$$\theta_{cd} = 65^\circ - \varphi_x \quad (10.8)$$

This value is only a rough estimate for poorly flowing bulk solids. Having easy-flowing bulk solids (i.e. granules), even flatter hoppers can be sufficient (e.g., with an inclination from horizontal of about $\varphi_x + 10^\circ$). Pre-requisite for complete clearance by gravity is that the strength of the bulk solid is too small to support a stable rathole.

For the design of funnel flow silos to avoid ratholing two procedures are outlined in the following. The approach according to Jenike's first edition of Bulletin 123 (1964 edition [10.2]) assumes that the stresses at the wall of a stable rathole are independent of the filling level. This procedure is referred to as giving a lower bound of the maximum diameter of a stable rathole which may only be approached when the bulk solid is withdrawn during filling [10.14]. If the latter is not the case, the procedure may significantly underestimate the maximum rathole diameter. Thus, Jenike presented another approach in the 1980 edition of Bulletin 123 [10.1]. This approach leads to an upper bound of the rathole dimension. It is based on the assumption that the bulk solid is consolidated by filling stresses which depend on the filling height.

The “lower bound” approach of Jenike from 1964 [10.2] is based on the following considerations: If a stable rathole of diameter D is formed within the bulk solid above the outlet (Fig. 10.15), a circumferential compressive stress, σ_l' , is acting close to the surface of the rathole wall. The reason for this stress is that the bulk solid tends to flow into the interior of the rathole. If the unconfined yield strength, σ_c , of the bulk solid exceeds the circumferential stress, σ_l' , the bulk solid cannot start flowing, and, thus, the rathole remains stable.

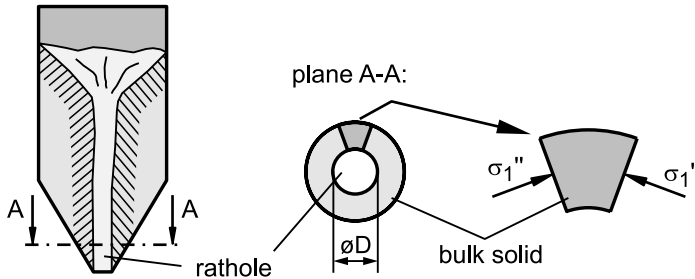


Fig. 10.15. Stable rathole and circumferential stress. σ_I''

The circumferential stress, σ_I'' , depends on the rathole diameter, D , and can be calculated as follows [10.1,10.4]:

$$\sigma_I'' = \frac{D \cdot g \cdot \rho_b}{f(\varphi_i)} \quad (10.9)$$

The function $f(\varphi_i)$ is depicted in Fig. 10.16. The angle φ_i is the local slope of the yield locus, which is approximated by the slope of the linearized yield locus, φ_{lin} . As can be seen in Eq.(10.9), the circumferential stress, σ_I'' , is proportional to the rathole diameter, D .

To be able to compare the circumferential stress to the unconfined yield strength, σ_c , the consolidation stress σ_I (major principal stress) acting at the surface of the rathole has to be known. Then with the flow function the corresponding unconfined yield strength can be determined. For this procedure the lower part of the rathole, i.e., the part directly above the outlet opening, is considered. If the rathole is not stable in this region, the bulk solid will also flow in the upper silo parts. The consolidation stress above the outlet has been derived [10.4] to be:

$$\sigma_I = \frac{1 + \sin \varphi_e}{4 \cdot \sin \varphi_e} \cdot D \cdot g \cdot \rho_b \quad (10.10)$$

The major principal stress, σ_I , and the circumferential stress, σ_I'' , near the surface of a rathole are proportional to the rathole diameter, D . The ratio of σ_I to σ_I'' is called the “flow factor for ratholing”, ff_p :

$$ff_p = \frac{\sigma_I}{\sigma_I''} = \frac{1 + \sin \varphi_e}{4 \cdot \sin \varphi_e} \cdot f(\varphi_i) \quad (10.11)$$

If the calculation leads to a value of $ff_p < 1.7$, a fixed value of $ff_p = 1.7$ has to be used.

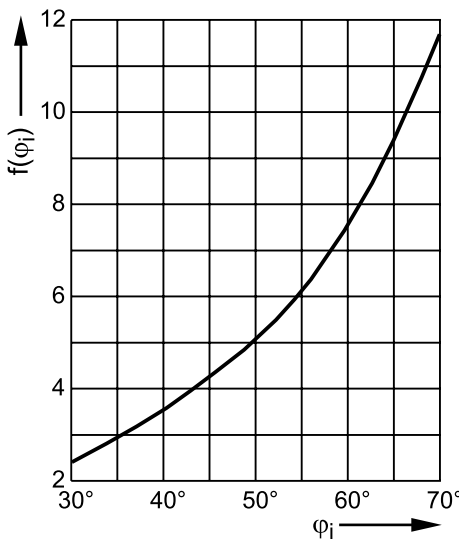


Fig. 10.16. Function $f(\phi_i)$ [10.2]

For the design of a funnel flow silo to avoid ratholing the circumferential stress, σ_1'' , has to be drawn in a σ_c, σ_1 diagram (Fig. 10.17). The flow factor, ff_p , needed for this is calculated with Eq.(10.11).

$$\sigma_1'' = \frac{\sigma_1}{ff_p} \quad (10.12)$$

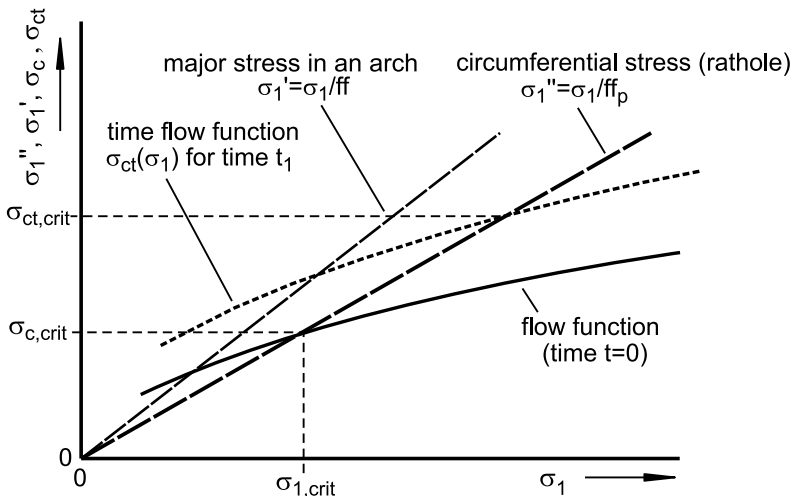


Fig. 10.17. Flow function and time flow functions; circumferential stress, σ_1''

The coordinates of the point of intersection of the circumferential stress with the unconfined yield strength are designated by the index “crit” (unconfined yield strength, $\sigma_{c,crit}$, and consolidation stress, $\sigma_{l,crit}$). Finally the appropriate outlet diameter, D_{crit} , is calculated. In doing so the circumferential stress, σ_l , in Eq. (10.9) is replaced by the unconfined yield strength, $\sigma_{c,crit}$, at the point of intersection. Considering the bulk density, ρ_b , the “critical” value corresponding to $\sigma_{l,crit}$ is used:

$$D_{crit} = f(\varphi_i) \frac{\sigma_{c,crit}}{g \cdot \rho_b \cdot \sigma_{l,crit}} \quad (10.13)$$

The points of intersection of the circumferential stress with time flow functions lead to critical outlet dimensions required to avoid ratholing after the equivalent storage times at rest.

Since the design procedure outlined above is based on stresses prevailing in the emptying state, i.e. after some bulk solid has been discharged, the calculations are not valid for the filling state. The filling state develops when bulk solid is fed into an empty silo while no material is discharged from the silo. In this case larger stresses prevail close to the outlet leading to a higher degree of consolidation. As outlined above, a second design procedure [10.1] allows for estimation of the maximum rathole diameter under consideration of the stresses prevailing in the filling condition (upper bound of rathole diameter) [10.14]. This procedure is described in the following.

First the maximum consolidation stress (major principal stress) for filling conditions is estimated with Janssen’s equation [10.8]. Although this equation is valid for vertical sections only, it is also applied here for reasons of simplification to estimate stresses in the hopper. This results in a distribution of vertical stress as depicted in principle in Fig. 10.18. Since for filling conditions the major principal stress, σ_l , is oriented more or less vertically in the entire silo (see Sect. 9.1.2), it is approximately equal to the mean vertical stress, σ_v . Thus, the maximum consolidation stress at the bottom of the silo, which is the critical stress, $\sigma_{l,crit}$, is obtained with Janssen’s equation (see Eq. (9.9)) for $z = h_f$ (h_f : height of filling, see Fig. 10.18):

$$\sigma_{l,crit} = \sigma_v = \frac{\rho_b g A}{K \tan \varphi_x U} \cdot \left[1 - e^{-\frac{K \tan \varphi_x U h_f}{A}} \right] \quad (10.14)$$

Parameters A , U , K , φ_x , and ρ_b represent conditions within the vertical section. If the lateral stress ratio is not known it may be estimated according to Sect. 9.2.3 with $K = 0.4$ or $K = 0.5$.

For the major consolidation stress, $\sigma_{I,crit}$, according to Eq. (10.14), the corresponding values of the unconfined yield strength, $\sigma_{c,crit}$, may be determined from the measured instantaneous flow function or time flow function (Fig. 10.17). Also the values of ρ_b and φ_{lin} corresponding to $\sigma_{c,crit}$ have to be determined. Then the upper bound value of the critical outlet diameter, D_{crit} , to avoid ratholing can be calculated with Eq.(10.13).

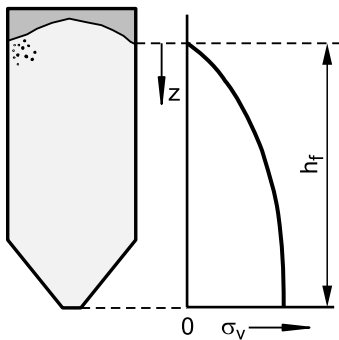


Fig. 10.18. Distribution of vertical stress, σ_v , in a funnel flow silo for filling conditions (stresses in the hopper approximated with Janssen's equation, see Sect. 9.2.1)

Since for a conical funnel flow hopper the critical outlet diameter to avoid ratholing is always larger than the one to avoid arching ($D_{crit} > d_{crit}$), only a design to avoid ratholing is necessary. For a wedge-shaped funnel flow hopper the calculated critical value D_{crit} has to be applied on the diagonal of the rectangular outlet. Therefore, the width, b , of the outlet is not necessarily large enough to avoid arching. Thus, the critical width, b_{crit} , of the rectangular outlet must be determined with the design procedure to prevent arching (see Sect. 10.3.1), whereby the values $ff = 1.7$ and $H(\Theta) = 1.15$ have to be used [10.1].

The description of the determination of critical outlet dimensions for ratholing not to occur might lead to the impression that a funnel flow silo can be operated without any problems as a mass flow silo. This, however, is not the case because of the potential problems related to funnel flow (see Sects. 1.1 and 10.2; e.g. segregation). Additionally, the time consolidation in a funnel flow silo cannot be limited by discharge of a part of the silo contents in regular time intervals, because in contrast to a mass flow silo the particles in the stagnant zones are not moved during discharge. Thus, time consolidation is not reduced. Therefore it can be stated: If a bulk solid that is affected by time consolidation is stored in a funnel flow silo (which generally should be avoided), the silo has to be cleared completely after the storage period for which the outlet opening has been designed.

10.4 Application of results

The essential results of silo design for flow are the inclinations of the hopper walls for mass flow to occur, and the outlet dimensions for avoiding arching and ratholing. In Fig. 10.19.a possible critical outlet dimensions are plotted versus storage time at rest, t , for a bulk solid showing time consolidation. Typically the values of d_{crit} (outlet diameter of a conical hopper) are about twice as large as the values of b_{crit} (outlet width of a wedge-shaped hopper). The critical rathole diameter, D_{crit} , is often clearly larger than d_{crit} , especially if the upper bound values are considered. With many bulk solids exhibiting time consolidation the increase of critical outlet dimensions with time becomes smaller with increasing storage time (as shown in Fig. 10.19.a).

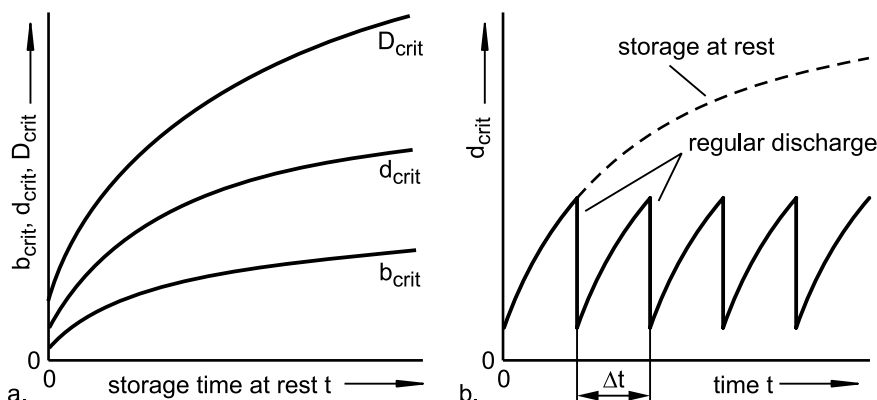


Fig. 10.19. a. Possible critical outlet dimensions versus storage time at rest, t ; b. critical outlet diameter, d_{crit} , vs. time when bulk solid is discharged in regular time intervals, Δt ; each discharge cycle reduces the strength of the bulk solid to its instantaneous value, and, thus, the critical diameter to $d_{crit}(t = 0)$. For comparison the critical diameter for storage at rest, i.e. without intermediate discharge, is plotted (dashed curve).

If the critical outlet dimensions as shown in Fig. 10.19.a are known, it is possible to quantitatively predict the necessary outlet size as a function of storage time at rest. It is also possible to determine the maximum storage time at rest for given outlet dimensions so that arching and ratholing do not occur. After this maximum storage time the material has to be set in motion, for example, in the case of a mass flow silo, by discharge of a portion of the silo filling, which can be fed again into the silo. Thereby the effect of the time consolidation is completely reduced, and, thus, the behavior of the bulk solid is characterized by its instantaneous flow properties (i.e., the

flow properties according to the storage time at rest $t = 0$) so that the critical dimensions for $t = 0$ are valid again (Fig. 10.19.b). It should be noted that this procedure does not work with funnel flow silos, because the material in the stagnant zones remains stationary during discharge of only a portion of the silo filling. Thus, time consolidation in the stagnant zones continues and the critical rathole diameter, D_{crit} , increases further. Therefore a funnel flow silo must be completely discharged in order to limit the effect of time consolidation and, thus, the critical rathole diameter, D_{crit} .

Besides the determination of hopper inclination and outlet dimension, further statements are possible when the bulk solid's properties are known. Two examples are described in the following (for further examples refer to [10.9,10.10]):

- One can determine hopper slope angles and outlet dimensions for different hopper shapes and different wall materials. Thus a comparison of capital costs is possible considering different shapes and materials [10.9,10.11]. For example, it can be stated whether lining of the hopper walls (e.g., with cold-rolled stainless steel) is advantageous considering costs in a specific application.
- If the flow properties fluctuate (e.g., due to variable moisture contents [10.12,10.13]), the most unfavorable situation can be predicted. If the silo is designed for this situation, trouble-free operation considering all possible flow properties is to be expected.

10.5 Design diagrams

Jenike published diagrams required for silo design in Bulletin 123 "Storage and Flow of Solids" [10.1]. It is strongly recommended to use this Bulletin if silos have to be designed.

Supplementary to Sect. 10.3.1, in the present section some often used diagrams are presented to give an overview of the influence of bulk properties and silo shape on the flow factor and the hopper slope for mass flow.

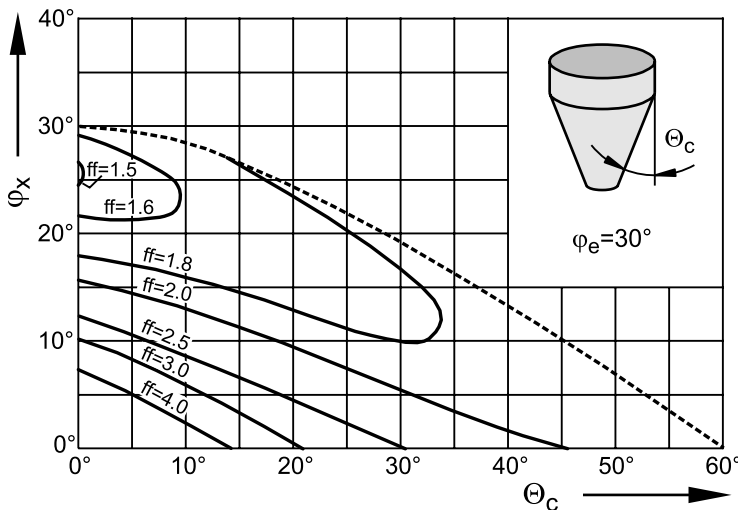


Fig. 10.20. Flow factor, ff , for conical hoppers and $\varphi_e = 30^\circ$ [10.1]

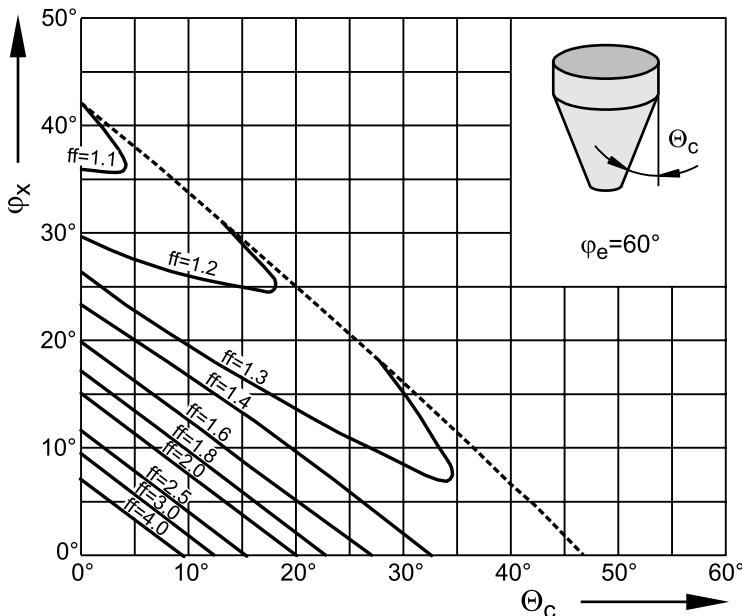


Fig. 10.21. Flow factor, ff , for conical hoppers and $\varphi_e = 60^\circ$ [10.1]

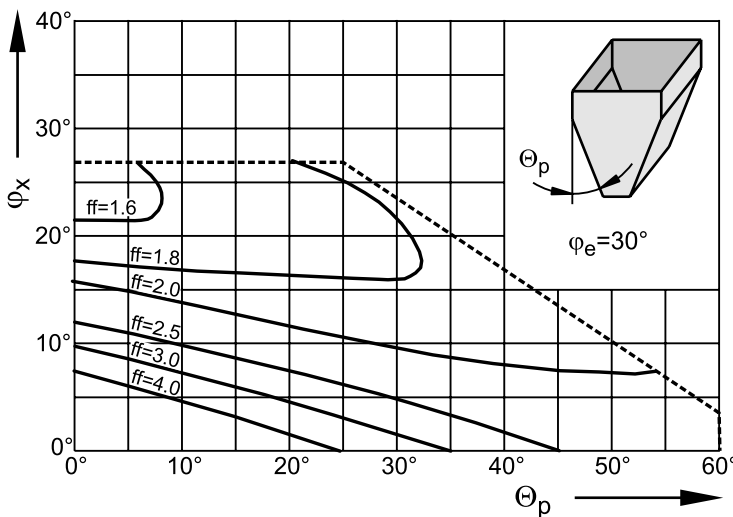


Fig. 10.22. Flow factor, ff , for wedge-shaped hoppers and $\varphi_e = 30^\circ$ ($L > 3 b$) [10.1]. In this and the next diagrams the curves for constant flow factors are plotted only for the mass flow range according to the mass flow boundaries proposed by Jenike (dashed lines).

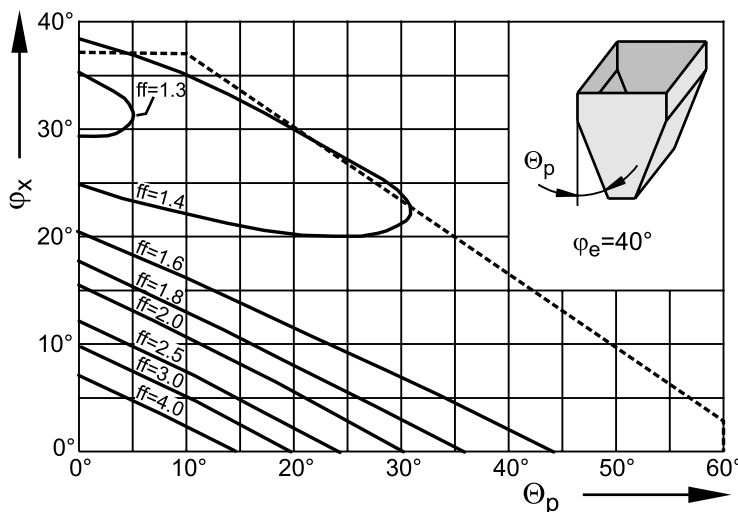


Fig. 10.23. Flow factor, ff , for wedge-shaped hoppers and $\varphi_e = 40^\circ$ ($L > 3 b$) [10.1]

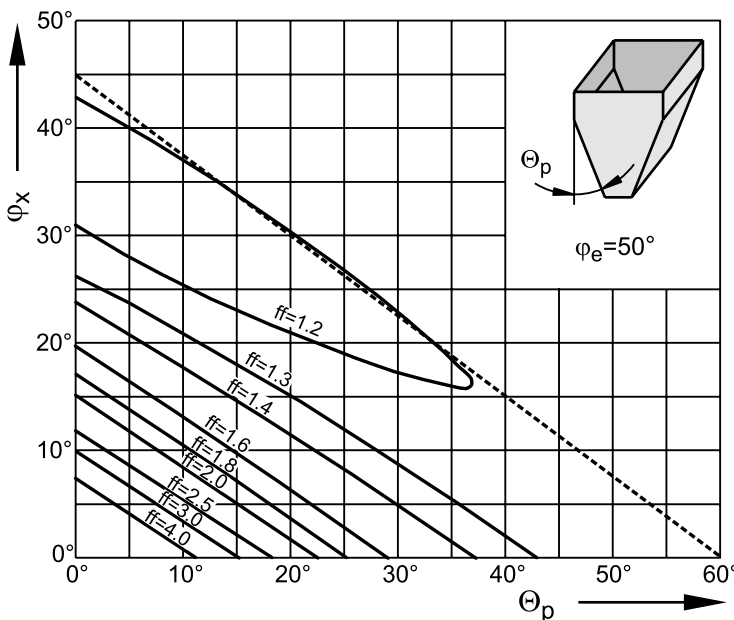


Fig. 10.24. Flow factor, ff , for wedge-shaped hoppers and $\varphi_e = 50^\circ$ ($L > 3 b$) [10.1]

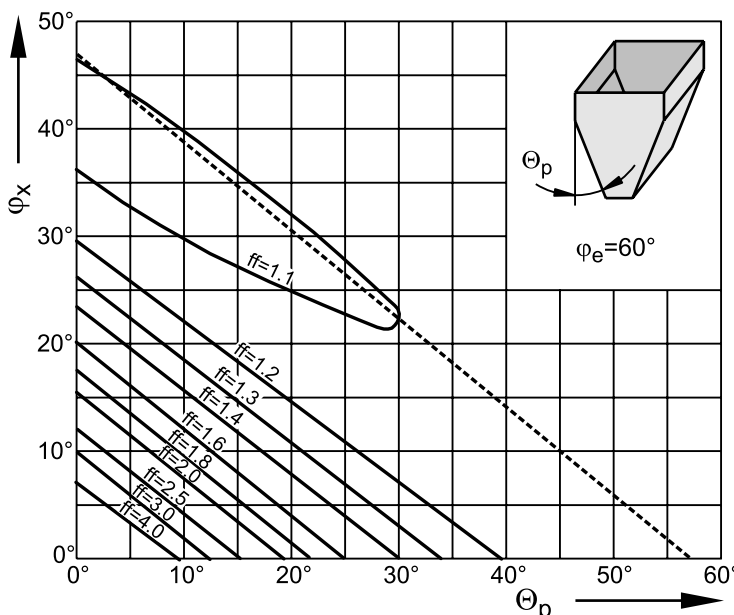


Fig. 10.25. Flow factor, ff , for wedge-shaped hoppers and $\varphi_e = 60^\circ$ ($L > 3 b$) [10.1]

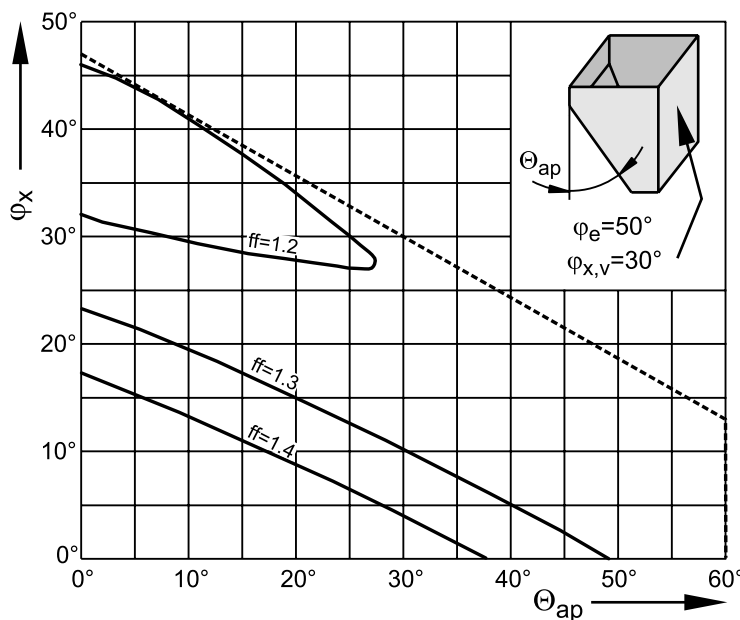


Fig. 10.26. Flow factor, ff , for asymmetric wedge-shaped hoppers; the angle of wall friction at the vertical wall is $\varphi_{x,v} = 30^\circ$; $\varphi_e = 50^\circ$ ($L > 3 b$) [10.1]

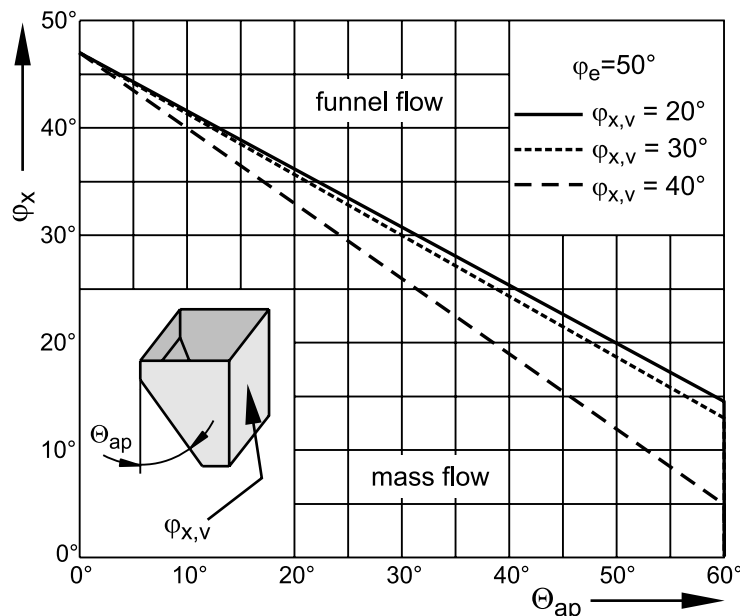


Fig. 10.27. Mass flow boundaries for asymmetric wedge-shaped hoppers; $\varphi_{x,v}$ is the angle of wall friction at the vertical wall; $\varphi_e = 50^\circ$ ($L > 3 b$) [10.1]

11 Silo configurations

The silo design procedure outlined in the previous chapter predicts the slope of hopper walls for mass flow to occur and the minimum outlet dimensions to avoid arching and ratholing for the basic silo shapes. These values can also be applied to various other hopper shapes and inserts, and they influence the complete concept of a silo including the selection of feeders and flow promoting devices. For specific tasks many different peculiar shapes exist which are distinguished by special inserts, typical operation procedures, etc. With the aid of selected examples it will be demonstrated some of the possibilities for silo design which exist when the specific bulk solid properties are known.

11.1 Influence of flow properties on silo configuration

Figure 11.1 shows a diagram with different combinations of the quantities determined with the silo design procedure due to Jenike [11.1], i.e., the maximum hopper wall slope for mass flow, Θ_c , and the minimum outlet diameter, d_{crit} , for arching not to occur in a conical hopper. According to the values of Θ_c and d_{crit} , different silo configurations are appropriate.

The easy-flowing bulk solid A (e.g., plastic granules) having a small angle of wall friction needs only a relatively shallow hopper (large value of Θ_c) for mass flow, and a small outlet opening to avoid arching. Here for feeding and dosing a rotary valve feeder may be useful. Bulk solid B requires a larger effort: For mass flow the hopper has to be steeper, and a larger outlet diameter (2000 mm) is necessary to avoid arching. With respect to the large outlet diameter, a bin activator might be an appropriate discharger. Bulk solid C is characterized by an extremely large angle of wall friction with the result that even in the steepest hopper mass flow cannot be achieved. Thus, a silo without hopper is required ($\Theta_c = 0^\circ$), and the feeder must be directly attached to the cylindrical section. The feeder must be able to discharge bulk solid from the entire cross-section of the silo which can be accomplished, for example, with a properly designed large multiple screw feeder.

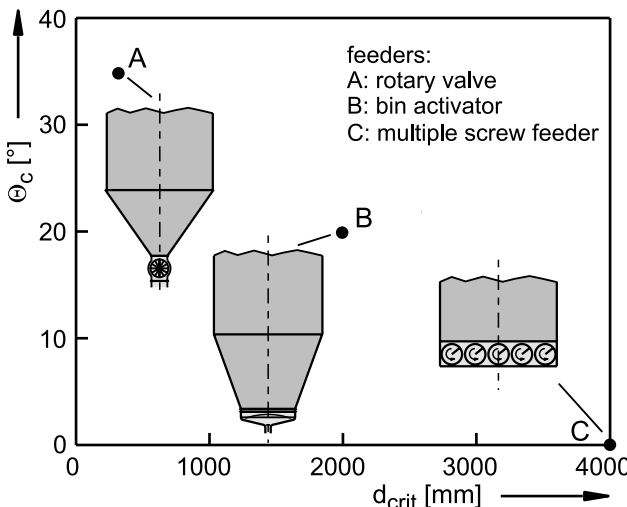


Fig. 11.1. Silo configurations as a function of the results of silo design for flow

11.2 Hopper configurations

11.2.1 Hopper shape

The design procedure due to Jenike [11.1] yields the basic geometrical data for conical and wedge-shaped hoppers (Fig. 11.2.a/b), i.e., the wall slope, Θ_c , and the outlet diameter, d , of a conical mass flow hopper, and the wall slope, Θ_p , and outlet width, b , of a wedge-shaped hopper. In addition, guidelines for the design of asymmetric wedge-shaped hoppers are given for a reduced parameter set (Fig. 11.2.c: slope Θ_{ap} , outlet width b). Considering the wedge-shaped hopper it is assumed that the length, L , of the rectangular outlet is at least three times its width, b . Only then can the influence of the end walls close to the outlet be neglected.

The maximum wall slope of an asymmetric conical hopper (Fig. 11.2.d) should not exceed $1.25 \cdot \Theta_c$ (Sect. 10.3.1) [11.1]. The relatively steep inclination is necessary since this hopper shape tends to funnel flow with a flow zone along the steeper side of the hopper.

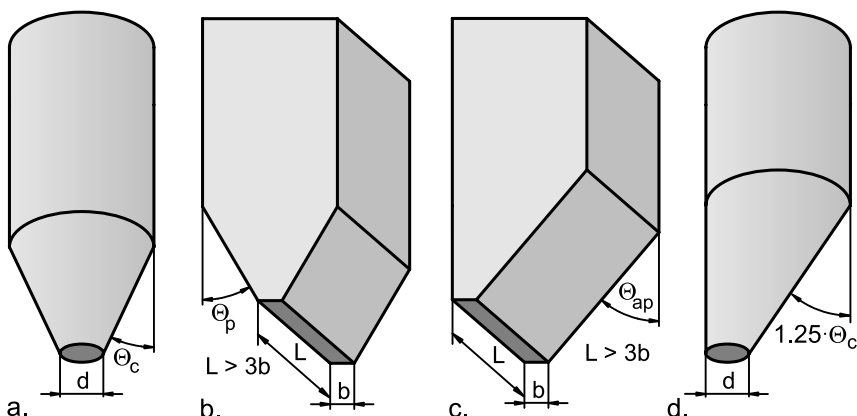


Fig. 11.2. Hopper shapes (basic shapes); a. conical; b. wedge-shaped; c. asymmetric wedge-shaped; d. asymmetric conical

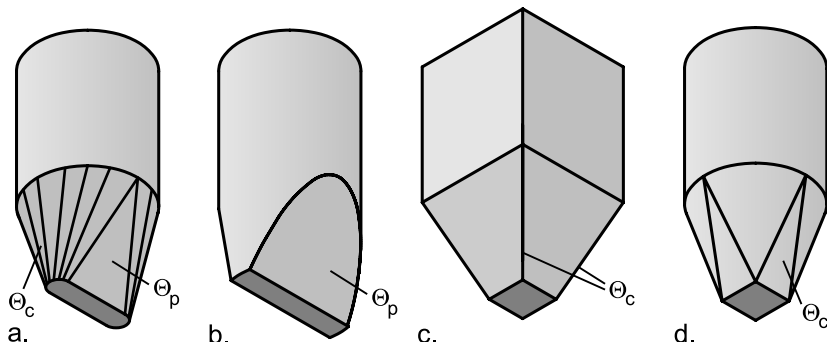


Fig. 11.3. Modified hopper shapes [11.2]; angles (Θ) indicate the maximum slope to the vertical for mass flow.

The design quantities for the basic hopper shapes as shown in Fig. 11.2 can also be applied to other hopper shapes. In Fig. 11.3 further possibilities are shown [11.1,11.2]. If a cylindrical vertical section is combined with a wedge-shaped hopper, designs according to Fig. 11.3.a and b are possible. Also in these applications the length, L , of the rectangular outlet has to be at least three times its width, b . If the end walls are inclined as in Fig. 11.3.a, their slope must not exceed Θ_c , i.e., the maximum wall slope of a conical hopper.

The pyramidal hopper (Fig. 11.3.c) is disadvantageous if mass flow is to be obtained, because the bulk solid has to flow downwards in the valley formed by pairs of adjacent hopper walls, where friction has to be overcome on two sides. To get mass flow in a pyramidal hopper, the valleys should be rounded, and the inclination of the valleys to the vertical (i.e.,

the valley angle, Θ_v) must conform to the maximum wall slope of a conical mass flow hopper, Θ_c . Since the walls of a pyramidal hopper are steeper than the valleys, a pyramidal hopper designed for mass flow is always steeper and, thus, higher than an equivalent conical hopper. The valley angle, Θ_v , can be calculated from the angles of inclination of the adjacent walls, Θ_1 and Θ_2 (all measured to the vertical):

$$(\tan \Theta_v)^2 = (\tan \Theta_1)^2 + (\tan \Theta_2)^2 \quad (11.1)$$

A mass flow hopper according to Fig. 11.3.d also has to be steeper than a conical mass flow hopper. This hopper realizes the transition from a cylindrical section to a square outlet. The slope of the plane hopper walls to the vertical should not be larger than Θ_c .

Comparing the hoppers shown in Figs. 11.2 and 11.3 considering their wall steepness required to achieve mass flow, variants c and d in Fig. 11.3 have to be steepest. The conical hopper (Fig. 11.2.a) can be somewhat flatter. The lowest steepness is possible for a symmetric wedge-shaped hopper (Fig. 11.2.b) and its modifications (Fig. 11.3.a/b).

In some industries still today asymmetric hoppers are favored (e.g., pyramidal hopper with four differently inclined walls). Following the principles of bulk solid mechanics, no argument can be found for those geometries. Asymmetric hoppers should only be used if due to space requirements no alternative exists.

If mass flow has to be achieved in an asymmetric hopper, the height of this hopper is always larger than the height of an equivalent symmetric hopper [11.3]. Clearly the comparison of the variants in Fig. 11.2.a and d demonstrates this conclusion. Also with respect to arching asymmetric mass flow hoppers do not provide advantages. As in equivalent symmetric hoppers, the bulk solid flows in a convergent manner towards the outlet. Thus, the principal stress lines (i.e., lines indicating the orientation of the principal stresses) and possible arches exhibit asymmetric shapes (compare Fig. 11.4.a/b).

Also in the case of funnel flow, asymmetry is of no help when ratholing has to be avoided (Fig. 11.4.c/d.). Only with a not too poorly flowing bulk solid might it be possible that flow obstructions occur somewhat less often in asymmetric funnel flow silos compared to symmetric ones, because less friction has to be overcome at the silo wall (Fig. 11.4.d) compared to the friction within the bulk solid (Fig. 11.4.c). Furthermore, if a stable rathole forms as in Figs. 11.4.c and d, a flow promoting device (e.g., a hammer) applied from the outside of the silo will have a stronger effect on the rathole wall in the asymmetric silo than in the symmetric silo, where the distance from the silo wall to the rathole is greater. However, in general the

same problems will occur in asymmetric and symmetric funnel flow silos (e.g., segregation, wide residence time distribution, ratholing). Thus, a mass flow silo is the better alternative. Furthermore, asymmetric hoppers can lead to an unfavorable asymmetric load distribution in the silo shell which has to be considered for silo design for strength (see Sect. 9.4.2).

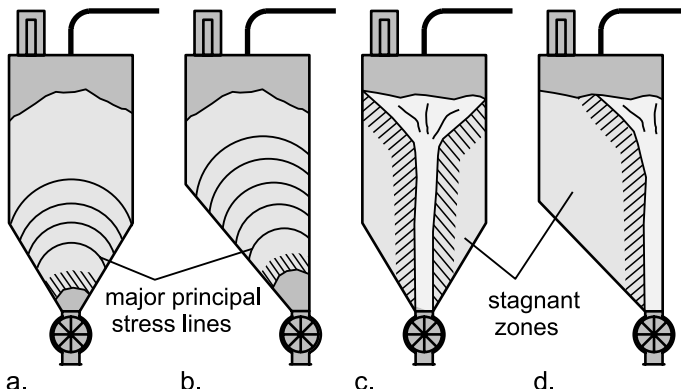


Fig. 11.4. Symmetric and asymmetric hoppers; a./b. arching; c./d. ratholing

11.2.2 Transitions and inclined walls

Even if the hopper walls are steep enough for mass flow, stagnant zones may build up due to poorly designed transitions to downstream equipment, inappropriate wall surfaces, or eccentric discharge by feeders (regarding feeder design refer to Sect. 12.3.1).

In Fig. 11.5 two transitions from a hopper to a feeder (or any other downstream equipment) are shown. In case of Fig. 11.5.a the cross-section is reduced abruptly thus forming a horizontal edge on which stagnant zones can form – even if the hopper slope fulfills the requirement for mass flow. Also less obvious stepwise reductions of the cross-section must be avoided, because a protrusion with a width of only a few particle diameters is sufficient for the formation of a stagnant zone. Therefore, possible reasons for stagnant zones can be gaskets or welds protruding inside, poorly fitted flanges, partially closed slide gate, etc. Figure 11.5.b illustrates a more expensive solution by using an intermediate transition hopper. The transition hopper is designed for mass flow. Thus, stagnant zones cannot form. At flange connections it is always advisable to make the inner diameter of the lower flange (e.g., the transition diameter of the downstream element) larger than the inner diameter of the upstream flange so that a

protrusion of the downstream flange can be excluded from consideration of possible manufacturing tolerances.

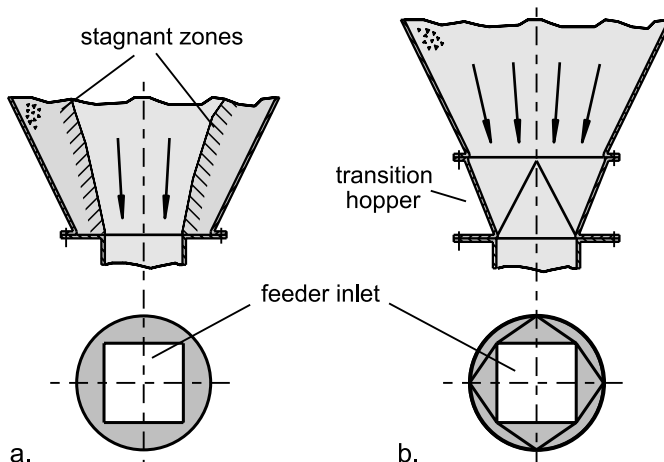


Fig. 11.5. Transition from hopper to feeder; a. abrupt reduction of cross-section leads to stagnant zones; b. transition hopper designed for mass flow

When a hopper is provided with a liner, care has to be taken that the liner does not cause stagnant zones due to protrusions. If (metal or plastic) sheets must overlap, they should be arranged as shingles (Fig. 11.6.b). Otherwise, the edges of the sheets will protrude into the bulk solid (Fig. 11.6.a) thus potentially leading to stagnant zones.

If metal sheets are butt welded, it is important that the welds, especially if they are not parallel to the flow direction, do not protrude into the bulk solid (Fig. 11.6.c), but are smooth and flush with the liner surface (Fig. 11.6.d). If necessary, the welds should be ground fine, but it is important that the liner's surface not become roughened due to the grinding action, because this might increase the angle of wall friction, and, thus, could be a reason for mass flow not to occur. For instance, the surface quality of stainless steel attained by cold-rolling is often advantageous considering wall friction, so this material is often used as a liner for hoppers. Grinding (even fine grinding) of these relatively smooth surfaces often leads to a significant increase of wall friction.

If the liner is fastened with screws protruding into the bulk solid, mass flow might be prevented (Fig. 11.6.e). Thus, it is preferable to use more appropriate fastening systems (e.g., countersunk screws, Fig. 11.6.f, or weld studs with special nuts and a cover made from the liner material, Fig. 11.6.g [11.4]).

Similar to protruding screws, devices for the measurement of temperature, humidity, pressure etc. can have a detrimental effect on flow if placed on sloping surfaces. Thus, such devices should, if possible, be placed on vertical surfaces.

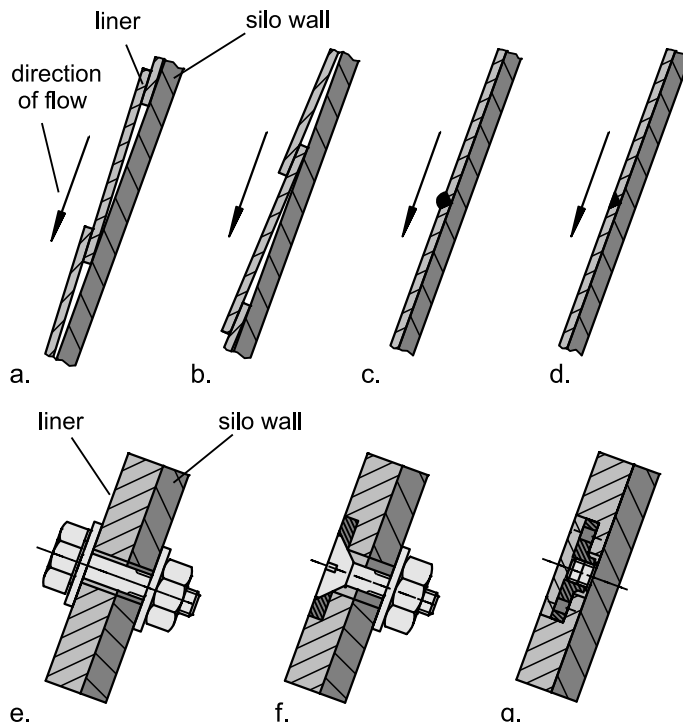


Fig. 11.6. Fastening and arrangement of liners [11.12]: a. unfavorable: overlap causing protrusions in flow direction; b. favorable: overlap like shingles; c. unfavorable: protruding welds oriented perpendicular to flow direction; d. better: flat, fine grinded welds; e. unfavorable: fasteners (here: screws) protruding inside; f. favorable: countersunk screw flush with liner [11.4]; g. favorable: weld stud with special nut, covered flush with the liner [11.4]

11.2.3 Multiple outlets

Occasionally multiple outlets are desired so as to allow discharge to several feeders or other downstream units separately from each other. To do so silos are equipped with multiple outlets (Fig. 11.7.a) or additional lateral outlets (Fig. 11.7.b). The disadvantage of these designs is that mass flow can only be achieved if bulk solid is discharged from all outlets at the

same time. If this is not the case, stagnant zones (funnel flow) can be created as shown by example in Fig. 11.7. It is absolutely advisable not to use multiple outlets if segregation has to be avoided (see Sect. 13.2.3), or if the bulk solid exhibits time consolidation and bulk solid is not discharged from all outlets. Even considering silo design for strength, the asymmetric flow profile is disadvantageous (see Sect. 9.4.2). In order to avoid the problems mentioned above, a mass flow silo should be provided with only one outlet. Further downstream the discharged material can be split with appropriate equipment into multiple streams without any negative impact on the flow profile in the silo.

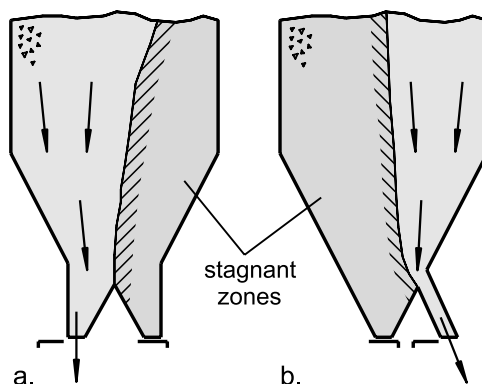


Fig. 11.7. a. Silo with multiple outlets; b. silo with additional lateral outlet

11.2.4 Special cases: hoppers with varying steepness

In certain conditions it is practicable to use a hopper in which the steepness is varied over its height. One possibility is the “expanded flow” hopper [11.1], being a combination of a mass flow and a funnel flow hopper (Fig. 11.8). The minimum diameter of the funnel flow hopper, which is located above the mass flow hopper, must be large enough for ratholing not to occur (minimum outlet diameter to avoid ratholing: D_{crit}). If the bulk solid exhibits time consolidation, D_{crit} must be calculated based on the maximum period of time between filling and **complete** discharge of the silo.

The mass flow hopper is designed for arching not to occur. For the calculation of the critical outlet diameter, d_{crit} , the time interval between two discharge sequences must be taken into account. Generally, one will obtain a value d_{crit} smaller than D_{crit} (see Sect. 10.4).

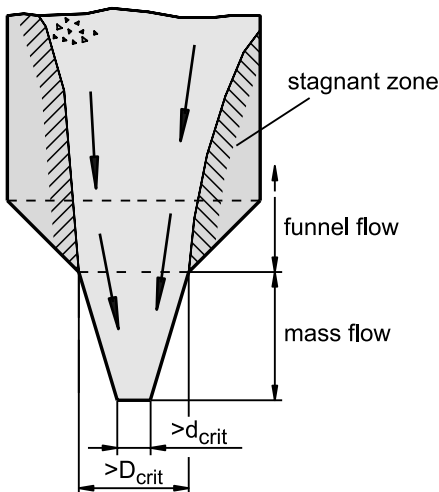


Fig. 11.8. Expanded flow: combination of a mass flow hopper and a funnel flow hopper [11.1]

Such a combination of mass flow and funnel flow makes sense only if the value of D_{crit} is distinctly smaller than the silo diameter, i.e., the time consolidation of the bulk solid in the stagnant zones during the maximum period of time between filling and complete discharge should not be excessive. If a silo is used continuously as a buffer which is never discharged completely, the expanded flow principle is only useful for bulk solids exhibiting little or no time consolidation effect.

Advantages of expanded flow are:

- reduced hopper height compared to a mass flow hopper,
- enlargement of the flow zone compared to a funnel flow silo having the same outlet dimensions,
- smaller outlet dimensions compared to a funnel flow silo designed to avoid ratholing ($d_{crit} < D_{crit}$).

If the wall friction angle is strongly dependent on the wall normal stress (i.e., the normal stress between bulk solid and wall), a hopper configuration according to Fig. 11.9 can be advantageous. In the emptying state of stress, the wall normal stress, σ_w , in a mass flow hopper decreases towards the hopper tip (see Sect. 9.1.2). The angle of wall friction of some bulk solids (e.g., moist coal) decreases with increasing wall normal stresses. Due to the downwards decreasing wall normal stress, the wall friction angle, φ_x , increases towards the hopper apex (diagram in Fig. 11.9). Increasing angles of wall friction require steeper hopper walls to obtain mass flow, i.e., the hopper slope to the vertical, Θ , becomes smaller towards the

outlet. If this effect is significant it is worthwhile to design the hopper with different slopes. The example hopper in Fig. 11.9 consists of three individual sections with slopes $\Theta_1 > \Theta_2 > \Theta_3$, which are calculated based on the wall normal stress acting at the lower end of each section. In contrast to the hopper in Fig. 11.9, a mass flow hopper with constant steepness and identical outlet dimensions had to be inclined by the angle Θ_3 with the consequence of a distinctly larger height.

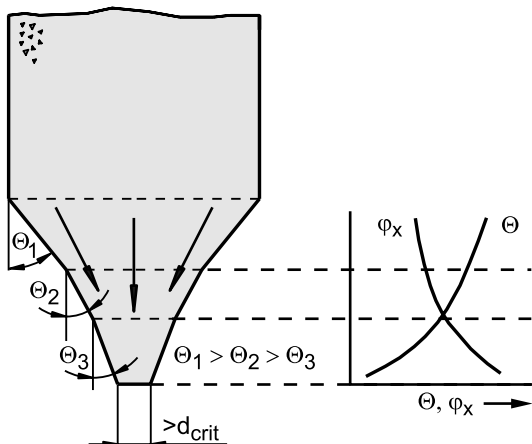


Fig. 11.9. Mass flow silo with varied hopper slope, Θ , due to a stress-dependent wall friction angle, φ_x

11.3 Inserts

Inserts (also called internals) are objects located inside a silo, for example, nozzles fixed at the silo wall, inverted cones, pipes, level sensors, or ladders. If inserts are required, it has to be considered that the loads on inserts and, thus, on their supports, can be extremely high (e.g. [11.5] and Sect. 9.4.1.2), and that the current existing theoretical knowledge is not yet sufficient for a safe design. Furthermore, the supports required to carry inserts can be detrimental to the flow pattern. Therefore the supports have to be designed carefully. For example, their surfaces must be sufficiently steep to avoid the formation of stagnant zones, and cross-sections must be large enough to avoid flow obstructions due to arching. Therefore inserts should only be used if their placement is absolutely necessary due to the given task, for example,

- measurement of temperature, humidity, etc.,
- change of the flow profile (e.g., transformation from funnel flow to mass flow; enlargement of the flow zone),
- reduction of segregation, abrasion, or vibrations,
- enlargement of the mass flow rate,
- addition of gases or liquids,
- influencing the stresses in the silo,
- mixing and homogenizing of bulk solids.

11.3.1 Inverted cones and wedges

Inserts like inverted cones or wedges locally reduce the cross-section of a silo (Fig. 11.10). The inclined walls of the insert act on the bulk solid similar to hopper walls. Thus, to avoid flow problems, inserts have to be designed for mass flow, and the minimum width between insert and silo wall must be large enough for arching not to occur. The following sections give an overview of typical applications of such inserts.

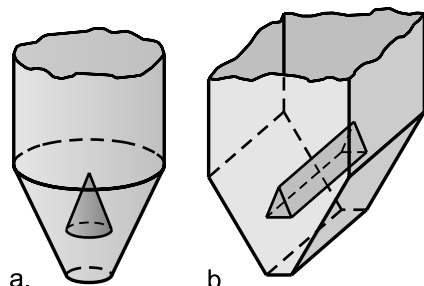


Fig. 11.10. Inserts: a. inverted cone; b. wedge

11.3.1.1 Gas injection

For the injection of gases into bulk solids the inserts shown in Fig. 11.10 can be used. The gas stream is introduced into the void within the insert (Fig. 11.11.a), from which it flows into the bulk solid distributed across the area covered by the insert thus keeping the local velocities small. Equivalent inserts are used, for example, for the cooling of bulk solids (e.g., plastic granules), or for flue-gas cleaning (e.g., in adsorbers filled with activated coke).

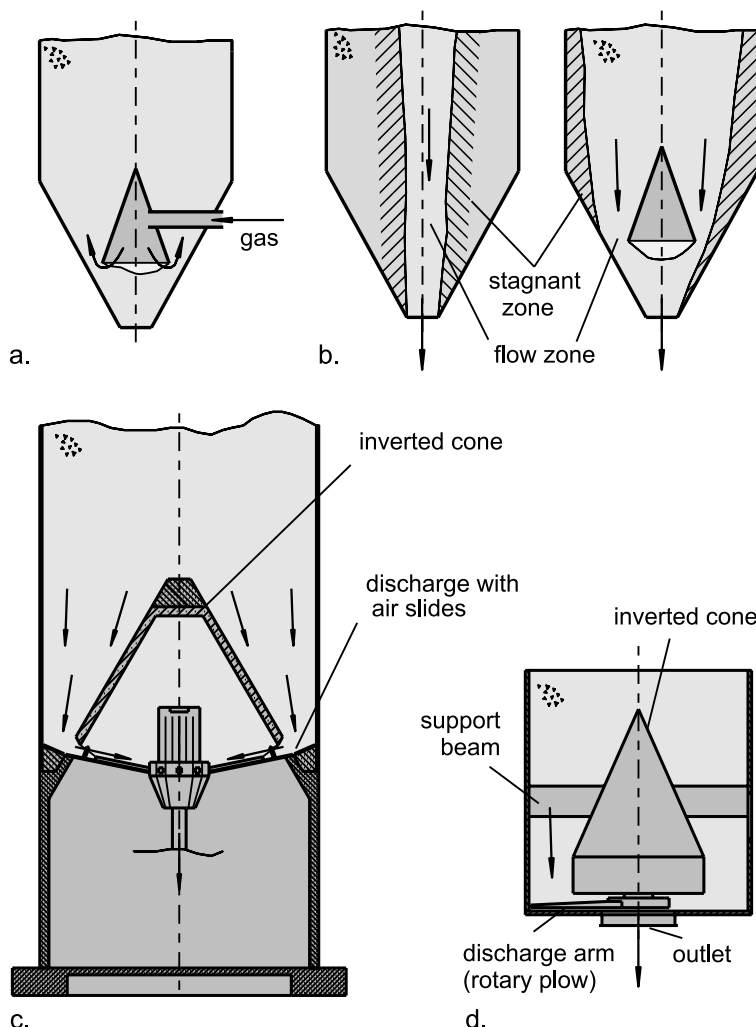


Fig. 11.11. Applications of inverted cone inserts: a. gas injection; b. enlargement of the flow zone; c. inverted cone silo; d. silo with rotary plow

11.3.1.2 Enlargement of the flow zone

An insert can be used to enlarge the flow zone in a funnel flow silo and, thus, to make stagnant zones smaller (Fig. 11.11.b) [11.6]. Since the bulk solid must flow around the insert, the size of the flow zone is necessarily increased. When the insert is correctly designed and placed, a distinct improvement of the silo usage compared to the silo without an insert can be

obtained. Under favorable conditions, which are not always met, segregation can be reduced (if the flow pattern approaches mass flow), and the probability of ratholing is reduced due to the increased cross-section of the flow zone. However, an insert can result in additional problems, for example arching between insert and silo wall, or asymmetric stresses (see Sect. 9.4.1.2). Thus, with respect to most reliable operation, a well-designed mass flow hopper (without insert) should be preferred. The insert can be regarded as a means of solving not too severe problems in not too large funnel flow silos.

For the storage of cement often large silos with a central inverted cone (inverted cone silo, Fig. 11.11.c) are used. Silo wall and insert form a hopper with annular cross-section. The bottom is provided with air slides which transport the bulk solid through multiple outlet openings located at the lower edge of the inverted cone (see Sect. 12.3.2.8).

Annular outlet slots being formed by a central inverted cone are also used in combination with different types of discharge devices, for example, rotary plow feeders [11.7] or traveling plow feeders (Sect. 12.3.2.9). A rotary plow feeder is depicted in Fig. 11.11.d (see also Fig. 12.25): The sickle-shaped discharge arm (Fig. 11.11.d) rotates close to the silo bottom around the central vertical axis and moves the bulk solid to the central discharge opening. To avoid stagnant zones, the slope of the inverted cone has to be sufficiently steep for mass flow to occur. Additional tasks of the inverted cone are (1) reduction of vertical stress at the silo bottom (see next section) to avoid too high driving torque of the discharge arm, and (2) prevention of unintended discharge of the bulk solid through the central outlet opening.

11.3.1.3 Reduction of stresses

The stresses in the lower part of a hopper are relatively large in the filling state of stress (i.e., after filling an empty silo), whereas in the emptying state of stress distinctly smaller stresses are found (see Sect. 9.1.2). The large filling stresses are disadvantageous for two reasons:

- Since the vertical stress acting on the feeder is very large in the filling state, the feeder has to be designed for an equivalent driving force. [11.7,11.8].
- The large filling stresses cause a much stronger consolidation of the bulk solid compared to the emptying stresses. Thus, the tendency for arching and ratholing is increasing if the bulk solid is subjected to filling stresses.

A possible means (besides others [11.7]) for stress reduction in the lower part of a hopper is placement of an insert above the outlet (e.g., as in Fig. 11.10). The insert reduces the load onto the bulk solid located beneath so that lower vertical stresses are obtained in the filling state. The influence of the insert on the stresses as well as the loads acting on such inserts is explained in more detail in Sect. 9.4.1.2.

11.3.2 Cone-in-cone insert

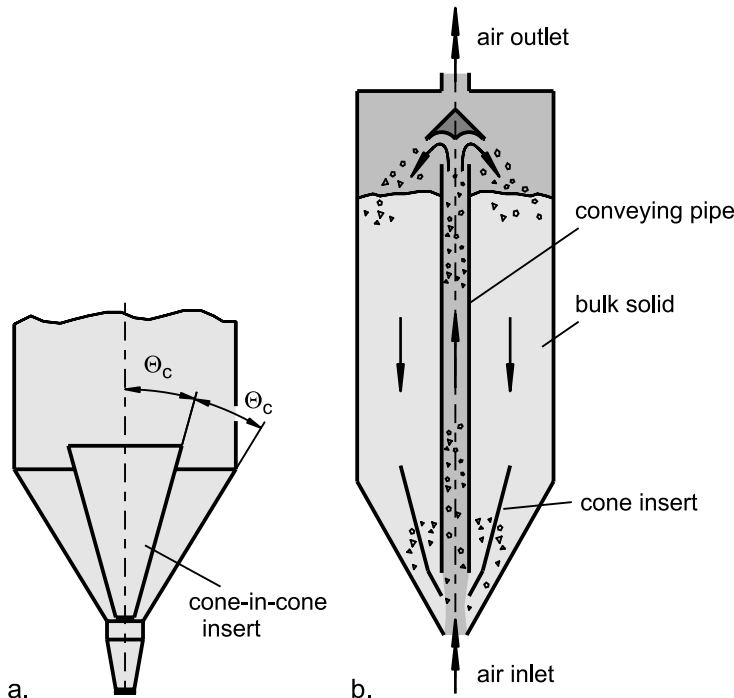


Fig. 11.12. a. Silo with cone-in-cone insert; b. pneumatic blending silo

With a cone-in-cone insert (Fig. 11.12.a), also known as "Binsert®" [11.9] and patented, it is possible to convert a funnel flow hopper into a mass flow hopper. The internal cone has to be designed in the same way as a normal hopper, i.e., its slope must not be larger than Θ_c to achieve mass flow. To obtain mass flow also in the annular space between the internal cone and the hopper, their walls should not be inclined to each other by more than Θ_c . Furthermore, it has to be ensured that arching cannot occur either within the cone insert or in the annulus. Therefore, it is not advisable

to use a cone-in-cone insert when bulk solids with poor flow properties and a considerable tendency to time consolidation have to be stored.

Normally the cone insert is designed in a way that within and outside the cone similar flow velocities prevail. It is also possible to adjust the ratios of the cross-sections at the upper and lower ends of the cone in such a way that different flow velocities, and, thus, different residence times prevail within and outside the cone. Thus, when the bulk solid is flowing in such a hopper, adjacent particles are separated from each other and subsequently combined with others. This is the principle of any mixing process. An application of this mixing technique is the pneumatic blending silo with cone insert shown in Fig. 11.12.b [11.10]. In the central pipe the bulk solid is conveyed pneumatically from the bottom to the top of the silo, so that the silo filling can be recirculated several times until the desired blend quality is attained.

11.3.3 Discharge tubes

Discharge tubes (Fig. 11.13) are vertical tubes placed above the outlet of a silo and typically provided with lateral openings. If the discharge rate is not too high (Fig. 11.13.a), the bulk solid in the discharge tube flows in a plug flow regime. The stresses acting on the material in the discharge tube can be calculated in analogy to a cylindrical section of a silo. Thus, the maximum possible vertical stress in the discharge tube is (see Sect. 9.2.1):

$$\sigma_{v\infty} = \frac{g \rho_b D_{tube}}{4 K \tan \varphi_x} \quad (11.2)$$

D_{tube} is the internal diameter of the discharge tube. $\sigma_{v\infty}$ is the stress acting at infinite depth, but is usually nearly attained at a depth being equivalent to about three times the tube diameter, D_{tube} .

In the plug flow regime no bulk solid flows through the lateral openings into the discharge tube, although the stresses in the silo (i.e., outside the discharge tube) are essentially larger than within the discharge tube. The explanation for this is given in Fig. 11.14, where a section of a discharge tube is shown. If bulk solid were to flow through the lateral opening, a converging flow zone would be created as bulk solid flows towards the lateral opening. This would result in a passive state of stress similar to the flow zone in a funnel flow hopper (Sect. 9.1.2, Fig. 9.4.d), where the major principal stress is oriented more or less perpendicular to the direction of flow.

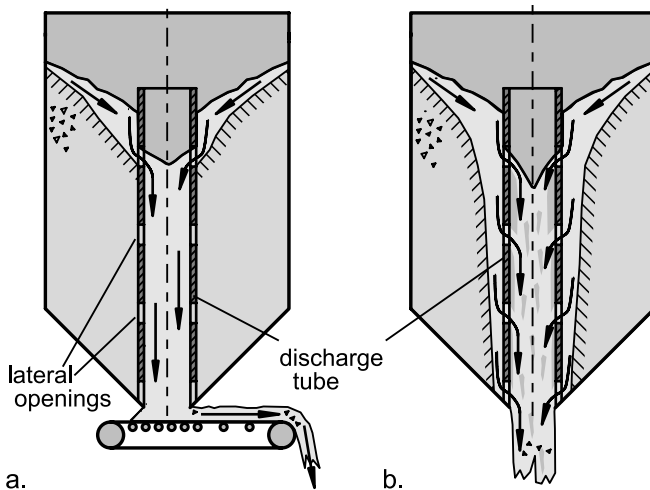


Fig. 11.13. Operating modes of discharge tubes; a. plug flow; b. accelerated flow [11.11]

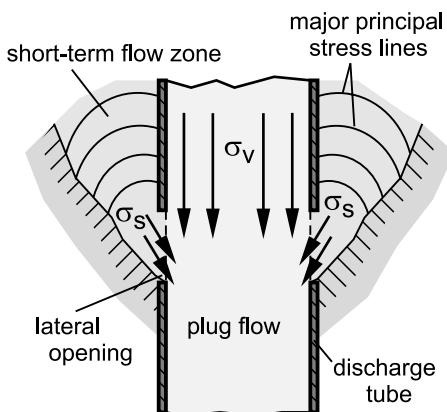


Fig. 11.14. Situation at lateral openings of a discharge tube during plug flow; flow zone and lines of major principal stress

The stress acting in the flow direction (σ_s in Fig. 11.14) would then be clearly smaller than the vertical stress, σ_v , in the discharge tube so the bulk solid cannot flow through the lateral opening and displace material in the plug flow zone. Thus, only at the initial discharge after having filled a previously empty silo an insignificant amount of bulk solid might flow through all lateral openings into the discharge tube until the conditions of Fig. 11.14 are met (therefore the flow zone is designated as “short term flow zone” in Fig. 11.14). Afterwards the bulk solid exclusively flows through the uppermost of the lateral openings which are located beneath

the silo's fill level. Therefore, when discharging a silo with a discharge tube, the bulk solid flows only in regions where the stresses are small, namely close to the top surface of the filling and within the discharge tube. In the same silo, but without a discharge tube, the bulk solid had to flow under considerably higher stresses. However, it has to be noted that the use of a discharge tube leads to funnel flow, whereby the flow zone is defined by the discharge tube. Considering the potential flow problems associated with funnel flow, it is not advisable to use discharge tubes for bulk solids exhibiting poor flow properties and/or time consolidation.

If the discharge rate is high, for example, if the bulk solid flows out unrestricted as in Fig. 11.13.b, the mass flow rate through the uppermost lateral opening below the silo's fill level is not sufficient to fill the discharge tube completely. As a result, bulk solid flows into the discharge tube also through lower lateral openings so that plug flow may develop only in the lower part of the discharge tube. In the extreme case of unrestricted discharge, the bulk solid falls downwards in the entire discharge tube and, thus, gets accelerated, which causes a significant increase of the porosity. Thus, plug flow is impossible, and the bulk solid flows into the discharge tube through many or all (depending on the geometrical conditions, for example, height and diameter of the discharge tube) of the lateral openings as depicted in Fig. 11.13.b. The discharge rate can be increased by a factor of more than two compared to a silo without a discharge tube [11.11].

If the discharge tube is used as shown in Fig. 11.13.a (plug flow), the following benefits can be realized:

- Reduction of attrition, which is especially important for sensitive bulk solids (see Chap. 15, sample problem 3).
- Vibrations (silo honking) occurring during discharge are often proportional to the mass of the flowing bulk solid. A carefully designed discharge tube leads to a reduction of vibrations [11.8,11.13–11.14] (see Chap. 14).
- If the silo is filled and later discharged via a discharge tube, segregation can be reduced [11.11] (see Chap. 13).
- Reduction of stresses acting on silo walls [11.15–11.17].

The last mentioned effect is explained in the following. In Fig. 11.15.a a flat-bottom silo is shown where the stagnant zone acts like a hopper. At the top level of the hopper a stress peak develops as is the case with the transition from a vertical section to a hopper (see Fig. 9.4.d). Since the shape of the stagnant zone is neither stationary nor predictable, the position of the stress peak in a funnel silo is unknown; this is contrary to a mass flow silo where it always coincides with the transition from the vertical section to

the hopper. If the wall of a funnel flow silo is damaged due to the local peak stress, one possibility of correcting this problem (in conjunction with repairing the damaged wall) is the placement of a discharge tube above the outlet, which due to this application is called “antidynamic tube” (the stress peak is sometimes called “dynamic peak” or “dynamic overpressure” because it exists only after discharge has started, see Sect. 9.1.2). If the bulk solid is discharged through the antidynamic tube (Fig. 11.15.b), the bulk solid at the cylinder wall is at rest over the entire height of the filling. Thus, no stress peak can develop.

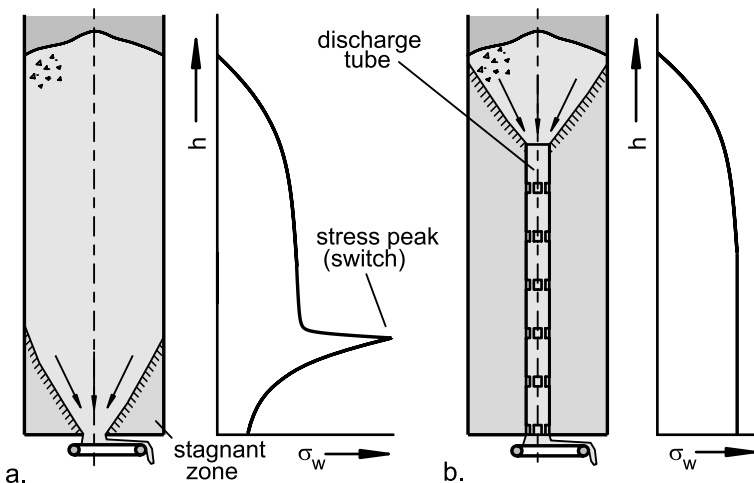


Fig. 11.15. a. “Dynamic” stress peak caused by a stagnant zone; b. discharge tube acting as “antidynamic tube” to avoid the stress peak

Various types of silos used for blending, mixing or homogenizing make use of modified discharge tubes. Since the bulk solid flows due to gravity, these silos are often called gravity blenders, whereas the tubes are called “blending pipes”. The blending process is realized by drawing off the bulk solid from different locations within the silo and combination of the individual streams. If required, blending efficiency can be improved by recirculation of the material. Figure 11.16.a depicts an example of a gravity blender with multiple blending pipes [11.18,11.19], which are provided with lateral openings at different positions. Other types of gravity blenders have a central blending pipe (Fig. 11.16.b), whereby the lateral openings are provided, for example, with baffles protruding into the tube. The baffles disturb plug flow and thus provide space for the material to enter the discharge tube through the lateral openings. Furthermore, the baffles reduce the vertical stresses above the lateral openings since they act as hop-

per walls. Thus, as in a hopper, a passive state of stress with small vertical stresses develops (see stresses in a mass flow hopper, Fig. 9.4.c). Therefore the mechanism shown in Fig. 11.14 is disturbed and bulk solid flows into the discharge tube through all lateral openings.

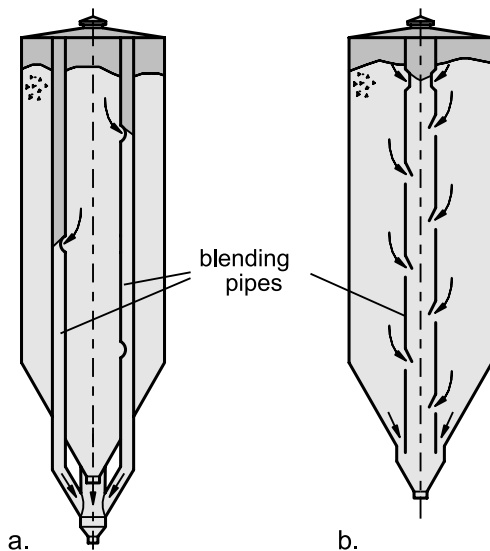


Fig. 11.16. Gravity blenders [11.18,11.19]; a. multiple blending pipes; b. central blending pipe

12 Discharge of bulk solids

For simple applications it can be sufficient that the bulk solid flows out freely from a hopper or a bin. Here, only the achievable maximum discharge rate is of interest. However, in most cases controlled discharge is desired so appropriate feeders are required. Most feeders are either conveyors being modified for the requirements of silo discharge, or special discharge devices.

Discharge aids, or flow promoting devices, are used to initiate flow (e.g., in the case of arching and/or ratholing), or to improve flow (e.g., to change the flow pattern from funnel flow to mass flow, or to increase the discharge rate). Some discharge devices or feeders also act as discharge aids by initiating flow within the silo. In the present chapter the distinction between discharge devices (including feeders) and discharge aids follows from their main function.

Furthermore, means such as the improvement of the flow properties of a bulk solid (e.g., addition of a flow agent, Sect. 7.2.2) or installation of inserts (e.g., inserts increasing the flow zone, Sect. 11.3) are often considered as discharge aids. However, in the present chapter only those discharge aids are discussed which are attached to the silo with the aim to initiate flow by supplying energy to the bulk solid.

12.1 Maximum discharge rate

The unrestricted rate of discharge of a bulk solid under gravity (i.e., when an outlet is opened) is dependent on several parameters, e.g., the bulk solid's properties, the size and shape of the outlet, the hopper inclination, and, in the case of funnel flow, the shape of the stagnant zones [12.1,12.2]. The conditions of unrestricted discharge can also be fulfilled in the presence of a feeder if the desired discharge rate exceeds the unrestricted discharge rate. Thus, if a feeder is installed, it should be ensured that the unrestricted discharge rate exceeds the range of adjustable feeding rates.

With fine-grained bulk solids the influence of air flow has to be considered [12.3–12.9]. In the vertical section of a silo the bulk solid stress is in-

creasing in the downward direction. Thus, if material is discharged and the filling level of the silo is kept constant, the bulk solid in the vertical section is compressed when flowing downwards. Thus, a gas overpressure, $p_e > 0$, develops (Fig. 12.1). Dependent on the boundary conditions (permeability of the bulk solid, discharge and filling rate, etc.) more or less gas will flow upwards through the bulk solid.

Since in the hopper the stresses decrease in the downward direction (see Fig. 12.1), the bulk solid dilates when flowing downwards, i.e., the bulk density, ρ_b , decreases and the porosity, ε , increases. Thus, the gas in the voids expands which results in the development of an underpressure ($p_e < 0$, Fig. 12.1). The underpressure causes gas to flow following the pressure gradient. At sufficiently large filling heights most of the gas will enter the hopper through the outlet opening since the flow resistance of the bulk solid above the hopper is definitely larger. The pressure gradient in the hopper acts opposite to the gravity force resulting in a decrease of the mass flow rate. Often a pulsating outflow can also be observed similar to liquid outflow from a bottle held with the opening downwards.

Just as unfavorable as an underpressure in the hopper is an overpressure below the outlet, which, for example, may develop when feeding a positive pressure pneumatic conveying line. Therefore, overpressure directly at the hopper outlet and countercurrent gas flow must be avoided or at least reduced, for example, by using double-flap gate valves or rotary valves (Sect. 12.3.2.7).

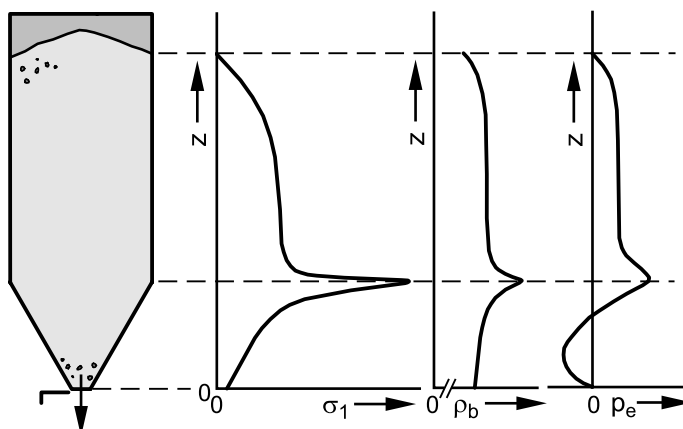


Fig. 12.1. Qualitative distributions of major principal stress, σ_1 , bulk density, ρ_b , and gas overpressure, p_e , vs. vertical coordinate, z , during discharge of a fine-grained bulk solid from a mass flow silo (assumption: before the discharge started, the gas pressure in the silo was equal to atmospheric pressure, i.e., $p_e = 0$)

To decide which bulk solids have to be regarded as fine-grained or coarse-grained with respect to their behavior during discharge, the well known Geldart diagram (see Sect. 7.2.4, Fig. 7.22) can be used as a guideline. Geldart classified dry bulk solids considering their gas permeability into four groups A to D. The behavior of group A materials is most influenced by gas flow. These bulk solids can easily be fluidized and are fine-grained, but not that fine-grained that adhesive forces play a dominant role.

12.1.1 Discharge rate of coarse-grained bulk solids

Due to the many influencing parameters it is impossible to exactly predict mass flow rates. Many equations can be found in the literature which have been developed empirically or with dimensional analysis [12.1,12.2, 12.10]. Many equations are based on an analogy to the outflow of liquids under gravity conditions. For a large tank that is open at the top and has a hole a distance h below the water surface the velocity, w , of the liquid flowing from the hole follows the well-known Torricelli equation (without friction):

$$w = \sqrt{2gh} \quad (12.1)$$

Having a bulk solid instead of a liquid the stress („pressure“) is not proportional to height, h , but to the diameter, d , of the outlet opening. Thus, the velocity, w , reads:

$$w \propto \sqrt{gd} \quad (12.2)$$

To obtain the mass flow rate the outflow velocity has to be multiplied by the cross section, A , of the flowing bulk solid, and the bulk density, ρ_b :

$$\dot{m} = A \cdot \rho_b \cdot w \propto A \cdot \rho_b \cdot \sqrt{gd} \propto \rho_b \cdot \sqrt{g} \cdot d^{2.5} \quad (12.3)$$

As early as 1852 Hagen [12.11] postulated that d in Eq.(12.3) has to be reduced because the cross section of the outflowing bulk solid is smaller than the cross section of the outlet opening. Therefore, a term kx being proportional to the particle diameter, x , is subtracted from d .

$$\dot{m} \propto \rho_b \cdot \sqrt{g} \cdot (d - kx)^{2.5} \quad (12.4)$$

This equation shows the basic structure of many equations for the estimation of the mass flow rate of coarse-grained, cohesionless bulk solids. Some of the established equations are mentioned in the following.

For circular outlet openings and coarse-grained bulk solids Beverloo [12.12] stated:

$$\dot{m} = C \rho_b \sqrt{g} (d - kx)^{2.5} \quad (12.5)$$

C and k are fitting parameters. With different bulk solids Beverloo found a range of about $C = (0.55 \dots 0.65)$ and $k = (1.5 \dots 3.0)$.

A similar estimate is given by the British Materials Handling Board [12.13,12.14] for coarse-grained (less than $3\% < 250 \mu\text{m}$), free flowing bulk solids. It is distinguished between circular and rectangular outlet openings:

Circular outlet openings (diameter d):

$$\dot{m} = 0.58 \rho_b \sqrt{g} (d - kx)^{2.5} k_\Theta \quad (12.6)$$

Rectangular outlet openings (width b , length $L > 3b$):

$$\dot{m} = 1.03 \rho_b \sqrt{g} (L - kx)(b - kx)^{1.5} k_\Theta \quad (12.7)$$

In Eq. (12.6) and in Eq. (12.7) k is dependent on the particle shape ($k = 1.6$ for spherical and $k = 2.5$ for non-spherical particles). The hopper inclination, Θ , is taken into account by the factor k_Θ :

$$k_\Theta = (\tan \Theta)^{-0.35} \text{ for hopper inclinations } \Theta < 45^\circ$$

$$k_\Theta = 1 \text{ for } \Theta \geq 45^\circ.$$

Compared to openings with horizontal orientation (such as a typical silo outlet opening, Fig. 12.1), smaller mass flow rates are attained with outlet openings in inclined or vertical walls. For instance, a circular opening in a thin vertical wall delivers only about one third of the mass flow rate following from Eq. (12.5). With increasing wall thickness the discharge rate is further reduced [12.15].

An equation for the estimation of mass flow rates of cohesive coarse-grained bulk solids by considering the flowability was published by Johansson [12.14,12.23].

12.1.2 Discharge rate of fine-grained bulk solids

As stated in Sect. 12.1, gas pressure in a hopper plays an important role when fine-grained bulk solids are discharged. Thus, Eq.(12.5) to Eq.(12.7) cannot be applied. The influence of the pressure and the resultant gas flow is highest close to the outlet where the maximum pressure gradient, dp/dz , prevails (see Fig. 12.1) [12.9,12.16]. For the case of underpressure in the

hopper, the pressure gradient acts opposite to the gravity force ($dp/dz < 0$) and thus reduces the discharge rate. The influence of the pressure gradient can be considered in Eq.(12.5) as follows:

$$\dot{m} = C \rho_b \sqrt{g + \frac{1}{\rho_b} \frac{dp}{dz}} \cdot (d - kx)^{2.5} \quad (12.8)$$

The pressure gradient at the outlet cannot be predicted accurately, since exact values regarding porosity and permeability would be necessary. Due to the inhomogeneity of the bulk solid those values are very difficult to measure. Nevertheless equations can be found in the literature being based on the compressibility and the permeability of bulk solids (e.g., [12.17–12.19]). However, the gas pressure distribution in the bulk solid can change with time (see further down in this section) which has an influence on the mass flow rate.

If fine-grained bulk solids flow out freely from a hopper, dynamic arches can be created dependent on the actual pressure conditions. At the beginning of discharge, a dynamic arch moves upwards in the hopper until it remains at a certain position (Fig. 12.2). Single particles rain from the underside of the arch and are replaced by the bulk solid in the hopper slowly moving downwards (Fig. 12.2) [12.20,12.21]. In this situation the actual mass flow rate is independent of the size of the outlet opening. Also dynamic arches were observed by the author which moved upwards in a hopper and then suddenly collapsed. As a result the empty space beneath the dynamic arch was quickly filled with bulk solid leading to a large excess gas pressure, intensive aeration of the bulk solid, and an excessive discharge rate due to flooding (fast, unhindered outflow of the aerated bulk solid).

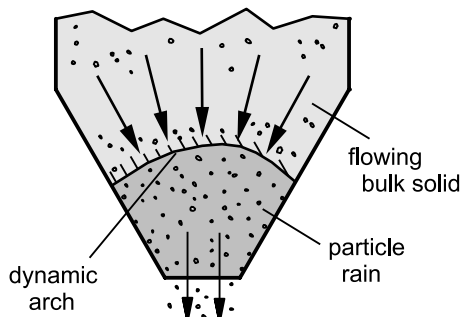


Fig. 12.2. Dynamic arch of a cohesive bulk solid at maximum mass flow rate (according to [12.20]; particles are shown magnified)

To increase the discharge rate of a fine-grained bulk solid, the pressure gradient at the outlet has to be reduced. This can be achieved by a sufficient increase of the outlet size (dimensions above the size of a dynamic arch) or by the injection of gas into the hopper [12.21,12.22]. When increasing the outlet size, the stresses and the bulk density decrease less towards the outlet opening (see diagrams in Fig. 12.1). Thus, dilation of the bulk solid and decrease of the gas pressure are less pronounced.

An example of the injection of gas is shown in Fig. 12.3 [12.21]. When discharging ground anthracite (a fine-grained bulk solid with 50% through 200 mesh) from a mass flow hopper, the discharge rate could not be increased above a certain limit. The bulk solid was raining from the underside of the filling onto the belt feeder leading to severe dust development (Fig. 12.3.a). The problem was solved with the help of a system for injection of air inside the hopper (Fig. 12.3.b). At bulk solid mass flow rates of up to 3.2 tons per hour an air volume flow rate of up to $3 \text{ dm}^3/\text{min}$ was added. This is equivalent to only 0.056 m^3 air per ton bulk solid and approximately equals the volume increase of the bulk solid during downward flow in the hopper.

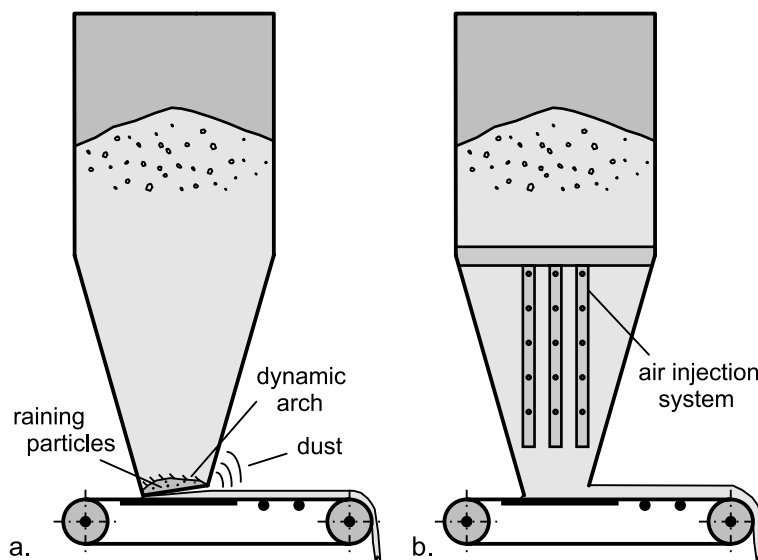


Fig. 12.3. Silo for ground anthracite; a. initial situation; b. after installation of an air injection system (according to [12.21]).

The addition of too much air in a situation as shown in Fig. 12.3 has to be strictly avoided, because that would lead to gas overpressure in the bulk solid. Then the gas gradient dp/dz in Eq. (12.8) would become larger than

zero and would enlarge the mass flow rate possibly leading to uncontrolled discharge of the aerated bulk solid (flooding).

If uncontrolled discharge can be avoided, for example, with a rotary valve connected to the outlet, or an extremely high discharge rate is demanded, the injection of large quantities of gas into the hopper with an accompanying gas overpressure in the bulk solid can be a suitable means for obtaining sufficiently large mass flow rates (e.g., in blow tanks of pneumatic conveying systems).

Gas overpressure can develop in a hopper also without air injection, for example, if the residence time of a fine-grained bulk solid in a silo is too short. Directly after being fed into the silo, the bulk solid located close to the top surface of the filling has small stresses. The stresses increase if further bulk solid is fed into the silo. Due to the increasing stress, the material is compressed so that gas overpressure prevails resulting in gas flowing from the bulk solid to the surrounding atmosphere (deaeration). The time required for deaeration, i.e., the reduction of the gas overpressure, depends on the permeability of the bulk solid, the filling rate, and the silo dimensions. If bulk solid is discharged before the gas overpressure has been reduced completely, it can happen that bulk solid with gas overpressure approaches the outlet opening. If the pressure gradient close to the outlet is sufficiently large, the gas flows towards the outlet with high velocities thus causing uncontrollable flooding from the outlet. Extremely unfavorable regarding deaeration are funnel flow silos, because in those silos the freshly filled bulk solid reaches the outlet much faster than in a mass flow silo of identical volume.

The process described above can be found with silos where large quantities of fine-grained bulk solids are continuously filled and discharged. The following example of a silo for the storage of ground ore demonstrates this effect. The dimensions of the silo are depicted in Fig. 12.4.a [12.3]. Beneath the rectangular outlet a feeder of appropriate dimensions is placed (feeder not shown in Fig. 12.4.a). In the diagram of Fig. 12.4.b the gas overpressure, p_e , is plotted versus the vertical coordinate, z , for different relative discharge rates, $\dot{m}_{rel} = \dot{m}/m_{tot}$. The relative discharge rates are equivalent to 100%, 300%, and 600% of the total mass, m_{tot} , in the silo discharged per hour. The upper filling level in the silo is kept constant by continuous feeding. At a relative discharge rate of 100% the gas overpressure, p_e , is increasing in the silo's vertical section with depth because the bulk solid is increasingly compressed. In the hopper the gas pressure is decreasing due to the dilation of the bulk solid, and reaches a small negative value (underpressure) in the lower part of the hopper. Thus, at the outlet a negative pressure gradient prevails, i.e., air flows countercurrent to the bulk solid into the hopper.

With the two larger relative discharge rates (300%, 600%) distinctly larger gas overpressures, p_e , develop, because the higher flow velocity results in a shorter residence time which does not allow sufficient deaeration. Furthermore, the bulk solid moves faster downwards than the air flows upwards relative to the bulk solid. Although the bulk solid dilates when flowing downwards in the hopper, a distinct gas overpressure remains leading to a large positive pressure gradient, dp/dz , close to the outlet and, thus, to larger gas velocities. If the relative gas velocity (relative to the bulk solid velocity) approximately reaches the velocity for minimum fluidization, flooding occurs.

A possible solution to solve the problem of excessive overpressures and flooding without reducing the discharge rate could be the installation of a system for the removal of air in the region of the highest gas overpressure, for example, with inserts like in Fig. 12.3.b.

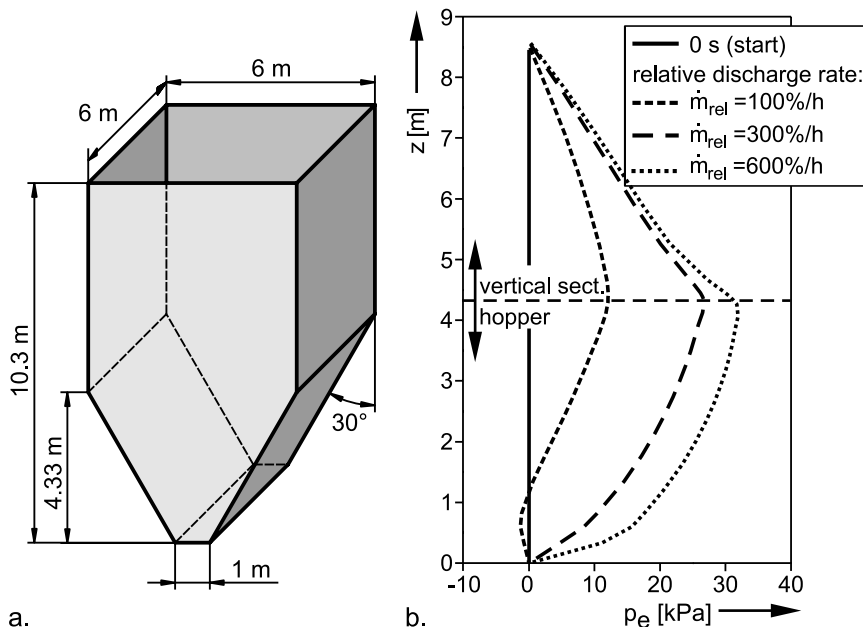


Fig. 12.4. a. Silo for ground ore; b. gas overpressure, p_e , for different relative discharge rates after having reached a steady state (constant filling level; results according to [12.3]).

The examples of gas pressures induced by flowing bulk solid show that when discharging fine-grained bulk solids problems can arise due to gas underpressure as well as due to gas overpressure. Furthermore, the stresses

and, thus, the gas pressures in a silo can change with time, for example, due to different filling levels and variable discharge and filling cycles.

Having very fine and cohesive bulk solids, i.e., group C materials according to Geldart's diagram (Sect. 7.2.4, Fig. 7.22), the occurrence of problems due to gas pressures becomes more unlikely with increasing distance from group A. The reason is the fact that those bulk solids tend to form channels during gas permeation (channelling). Due to the strong action of the adhesive forces relatively stable bulk solid regions are formed between which the gas can easily flow through void and fissures (channels). Additionally, the very cohesive group C materials require larger outlet openings for avoiding flow problems compared to group A materials. The larger outlet openings yield smaller flow velocities and higher stresses, i.e., the bulk solid dilates less in the lower hopper region.

12.2 Discharge aids

Discharge aids which initiate flow by transfer of energy can be roughly divided into the following two groups:

- Pneumatic discharge aids (e.g., air injection)
- Mechanical discharge aids (e.g., knockers, vibrators, agitators)

12.2.1 Pneumatic discharge aids

Pneumatic discharge aids (Fig. 12.5) initiate flow by the injection of air. In the systems according to Fig. 12.5.a to Fig. 12.5.e air is injected continuously at low flow velocities. This can be done as shown in Fig. 12.5.a through hopper walls made of porous material, but also through aeration elements placed at the hopper walls as in the Figs. 12.5.b to 12.5.e. Having a simple aeration box or aeration pads, the air enters the bulk solid through a porous material, for example, fabric weave or sintered material. Some types of aeration nozzles blow the air parallel to the wall into the bulk solid in order to activate a larger area of the silo wall. The vibrating aeration nozzle is provided with a flexible cap pressed against the silo wall. Air is flowing between wall and cap into the silo while the cap is excited to vibrate, i.e., the bulk solid is stimulated by vibration in addition to air flow.

Air injection causes local overpressures. Thus an air flow prevails in direction to lower pressures, for example, the ambient pressure at the outlet opening or at the surface of the filling, so the major portion of the air takes the path with the smallest air resistance. Thus, if the silo's filling level is

sufficiently high, and air is introduced into the lower part of the hopper (which is usually the case), the majority of the injected air flows towards the outlet opening. Thus, the air flow creates additional forces on the bulk solid in the direction to the outlet so that wall friction may be overcome, and arches and ratholes may be destroyed. Furthermore the air flow encourages bulk solids flow towards the outlet, being explained in Sect. 12.1.2 with the action of a gas overpressure in the hopper. This method of aeration is mostly advisable for group A materials according to Geldart's classification (Fig. 7.22). To get a similar effect with distinctly larger particles very high air velocities and thus uneconomically large air volume rates would be necessary [12.14]. Having very cohesive bulk solids (group C), the injection of air can also be problematic, since those bulk solids tend to channeling, i.e. voids and fissures are created in the bulk solid (e.g., close to the wall) through which the air escapes, while the rest of the bulk solid remains stationary.

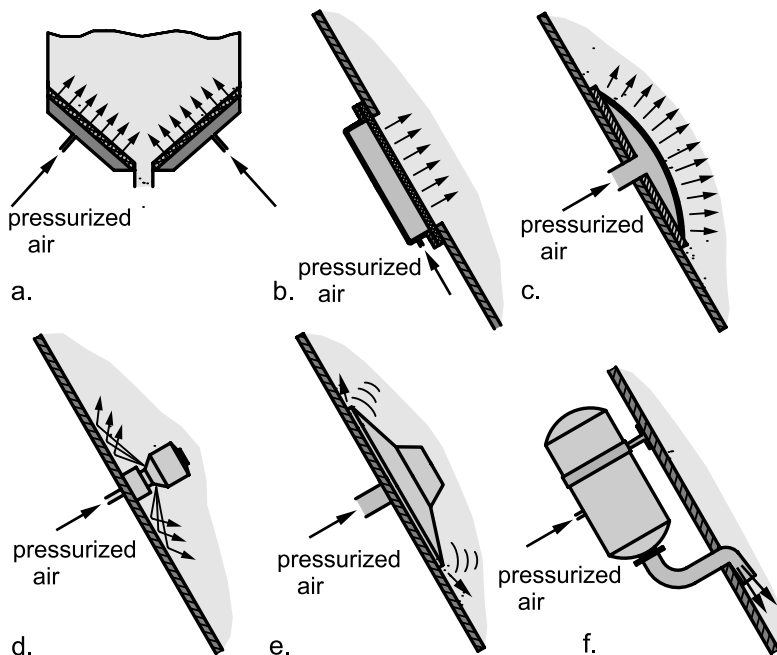


Fig. 12.5. Pneumatic discharge aids (examples); a. porous hopper; b. aeration box; c. aeration pad; d. aeration nozzle; e. vibrating aeration nozzle; f. air cannon

The action of air flow on a stable cohesive arch is explained in Sect. 7.2.4 (Fig. 7.21). The injected air is flowing downward towards the outlet thus exerting an additional force onto the arch which can be sufficient to col-

lapse the arch. The optimal position for air injection (e.g., for the devices according to Figs. 12.5.b to 12.5.e) is just above the possible arch. Thus the air flow resistance is limited which reduces the energy consumption [12.24].

There may also be an influence of air injection on the flow pattern. In a funnel flow silo into which air is injected far from the outlet (Fig. 12.6), the action of air close to the outlet (region A) may, for example, break an arch and initiate flow. However, the discharged bulk solid will be replaced primarily by the bulk solid flowing under the action of gravity from directly above the outlet (region B). Thus, the flow zone (region B) may be enlarged due to air flowing from the air injection device through the stagnant zones towards the flowing zone. However, experience shows that flow across the wall (approaching mass flow) is often achieved in a limited region only (see possible stagnant zone C, Fig. 12.6), especially if the wall steepness is far below that required for mass flow, and if the air flow rate is small. This also holds for porous hoppers having large diameters (Fig. 12.5.a): Even if air can flow through the entire hopper wall, the largest portion of air flows out in the vicinity of the outlet where the gas flow resistance towards the outlet is lowest. Following these considerations it is usually impossible to achieve flow across the entire hopper walls of a large funnel flow silo with the help of injected air. Furthermore, extremely high air flow rates would be necessary for this which might lead to uncontrollable flooding from the outlet, or even to fluidization of the bulk solid in the vertical section [12.24]. However, a quantitative statement is not possible. Flow across the wall initiated by air injection is more likely to occur in small hoppers and with high air flow rates.

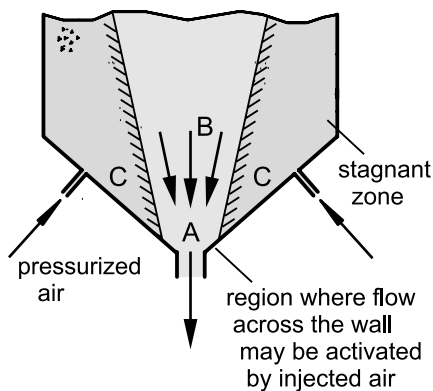


Fig. 12.6. On the influence of injected air on the flow profile

Besides continuous injection of air at small flow rates, the possibility exists to impulsively release compressed air stored in a pressure vessel (volumes of 2 to 500 liters, pressure up to 10 bars) through one or more nozzles into the silo. Equivalent discharge aids (Fig. 12.5.f) are known under different commercial names; often the term “air cannon” is used (survey and applications see [12.25]). The pressure impulse created by the air cannon generates a stress wave in the bulk solids structure propagating faster than the air pressure wave expanding in the pore structure of the bulk solid. Clearly a stress wave can be sufficient for the collapse of arches and ratholes [12.26–12.28].

Contrary to continuous air injection, air cannons can also be used for coarse-grained bulk solids (e.g., for flow problems resulting from time consolidation), since due to the impulsive injection of air a positive action can be achieved even if the air flow resistance of coarse-grained bulk solids is low. Also for the storage of poorly flowing bulk solids in large silos air cannons will be used since their range of action is large compared to the devices with a slow air injection (note that the required number and size of air cannons depends on bulk solid properties and silo dimensions).

When using air cannons it has to be kept in mind that problems can arise if the air cannons are not correctly applied and designed (dust generation due to too large air volumes; extremely high local stressing of the silo walls due to the pressure impulse [12.29], especially when the bulk solid fails to move; excessive loads on the hopper walls or the feeder due to large amounts of material suddenly collapsing). A typical application of air cannons is the retrofitting of silos which exhibit flow problems and where no other means are possible or practicable. For new silos air cannons are significant if bulk solids with a strong time consolidation effect have to be stored.

12.2.2 Mechanical discharge aids

The simplest mechanical discharge aids are rods and similar means inserted into a hopper through the outlet opening or poke holes to encourage the bulk material to flow, or a hammer used for beating the hopper wall. Further development of these archaic methods led to the application of knockers and agitators. As an example Fig. 12.7 shows an agitator above a vertical axis rotary valve. The agitator blades ensure that the flow zone is not limited to the region above the eccentric inlet of the rotary valve, but covers the entire cross-section of the hopper. Agitators with horizontal axis are also available and applied, for example, in combination with screw feeders in metering devices to ensure that cohesive bulk solids flow into

the commonly narrow feeding screw. Generally the application of agitators is limited to small diameters because the driving torque increases progressively with agitator diameter.

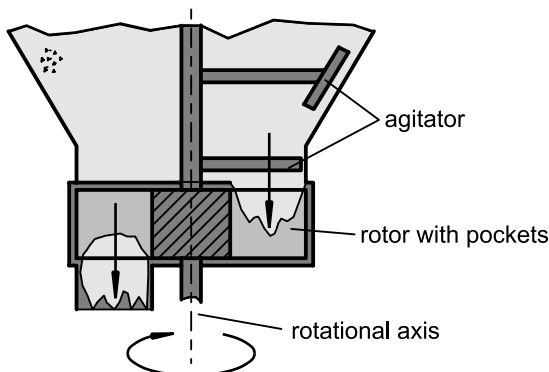


Fig. 12.7. Rotary valve with vertical axis and agitator [12.30]

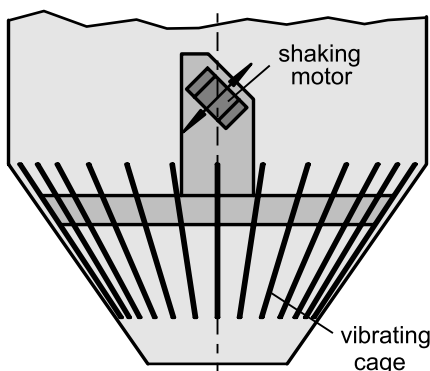


Fig. 12.8. Vibrating insert [12.14]

Vibrators are widely applied as mechanical discharge aids, and different forms of devices are available. Some of them transfer vibrations into the silo wall like knockers, but with higher frequencies. Others excite inserts located within the bulk solid, for example, a cage as shown in Fig. 12.8. Vibrations induced at the silo wall aid to overcome wall friction. Additionally, vibrations momentarily increase the stress in the bulk solid. If thereby the yield limit is attained, the vibration breaks stable arches or ratholes. However the design of vibrating devices mounted directly on a silo wall is difficult, because the properties of the silo structure have to be taken into account (e.g., wall thickness and stiffness), and a (conical) hopper is particular stiff close to its outlet (small radius of curvature) where stable

arches are formed predominantly. With vibrating inserts it has to be ensured that they do not act as a flow obstruction or as the basis for a stagnant zone, which is often the case at least when they are not active.

According to [12.31] the action of vibrations is best at frequencies above 100 Hz. It can be assumed that the effect of vibration decreases with increasing fineness and compressibility of the bulk solid, because the latter enhances absorption of the vibrations.

12.2.3 Application of discharge aids

All flow promoting devices should be used only during discharge. Vibration of a stagnant bulk solid as well as the action of agitators and knockers, or a continuous releasing of air cannons is likely to cause further consolidation and, thus, increasing flow problems.

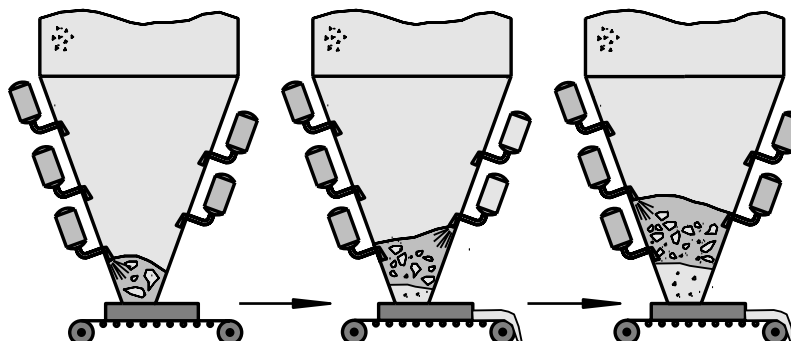


Fig. 12.9. Application of discharge aids; example: air cannon

Discharge aids have to be located so that they can act at the source of the flow problem, i.e., in the case of arching in the region where the arch is carried by the hopper wall, or if pneumatic discharge aids are used, somewhat above the arch. If severe problems are present, for example, due to a strong time consolidation effect leading to large stable arches or ratholes, discharge aids are needed in a larger part of the hopper (Fig. 12.9). Since air cannons have a larger range of action compared to other discharge aids, their use is specially favored for this application. It is best to use them one after the other starting at the lowest position. Thus, the consolidated material will be loosened in steps (Fig. 12.9). This is advantageous because the bulk solid falls down in portions and builds up a cushion of material above the outlet opening so the danger of damage to the feeder or hopper is reduced. Furthermore, the bulk solid portions activated by the discharge aid can easily fall into existing voids. If this is not possible the bulk solid

could fail to move which would result in excessive local stresses and additional consolidation.

Apart from air cannons, most discharge aids seem to be most suitable for the elimination of smaller flow problems in silos or hoppers that are not too large. The reasons for this are:

- Aeration elements (Fig. 12.5.b to e) have only a small range of action. Thus, many elements and a large amount of air would be necessary if larger problems exist (e.g., large arches). The dimensions of aerated hoppers (Fig. 12.5.a) are limited.
- The action of knockers and vibrators attached to a silo wall depends on the oscillatory behavior of both the silo structure (e.g., wall material, wall thickness) and the bulk solid. Therefore, this method is most applicable for smaller metal silos having thin walls.
- The size of agitator blades is limited due to the necessary driving torque increasing tremendously with diameter.

Although discharge aids can provide satisfactory solutions of problems, they can also create additional problems, e.g., irregular flow due to collapsing arches and ratholes, flooding of the bulk solid as a result of the injected air (pneumatic discharge aids), consolidation of the bulk solid due to inappropriate operation. Thus, when designing new facilities preference has to be given to adjust the silo to the measured flow properties in such a way that discharge aids are not necessary. However, if a bulk solid shows a strong time consolidation effect, the installation of discharge aids can be useful to reduce the size of the feeder (see Sect. 12.4).

12.3 Feeders and other discharge devices

Discharge devices are well known devices as, for example, belt feeders, apron feeders, en-masse feeders, vibratory feeders, rotary valves, and screw feeders being attached to the outlet of a silo. Shut-off devices (e.g., slide gates, clamshell gates) can also be regarded as discharge devices since they allow a certain (often poor and accompanied by problems, see Sect. 12.3.1.1) regulation of the discharge.

12.3.1 Rules for design regarding mass flow

Even in an appropriately designed mass flow hopper with sufficient steepness (Sect. 11.2), mass flow can be achieved only if the bulk material is

withdrawn from the entire outlet opening. Therefore, mainly two rules, which are described in the following sections, have to be followed when designing feeders:

1. Any planes which are not sufficiently steep to avoid the formation of stagnant zones have to be avoided.
2. The feeder must be able to discharge bulk solid from the entire outlet opening.

12.3.1.1 Rule 1

Feeders have to be designed so that all surfaces being in contact with the bulk solid are sufficiently steep to avoid the formation of stagnant zones. An example of this situation is the double gate shown in Fig. 12.10.a. If one of the butterfly valves is closed, a stagnant zone will form on the stationary saddle between the valves, and the plate of the closed valve. An alternative is the design according to Fig. 12.10.b where a single blade diverter is installed below a butterfly valve. All surfaces being in contact with the bulk solid are sufficiently steep to avoid stagnant zones.

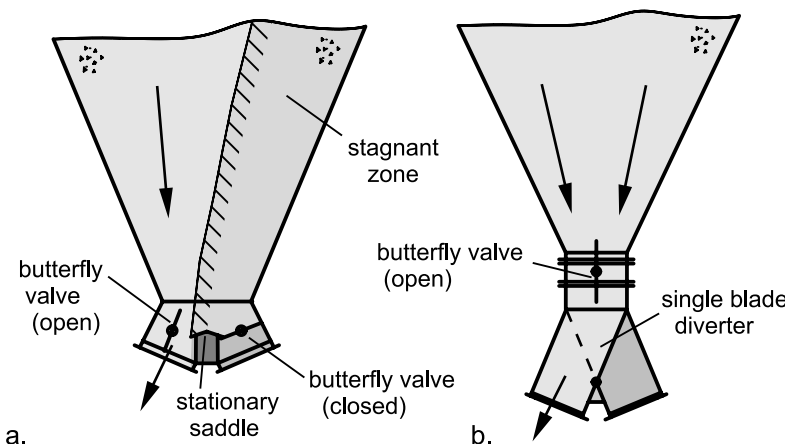


Fig. 12.10. a. Diverter with two butterfly valves; stagnant zone forms on the closed valve; b. butterfly valve with downstream single blade diverter

If converging sections are within a feeder as in the case of the rotary valve shown in Fig. 12.11, the minimum cross-section has to be sufficiently large to avoid arching. Furthermore, inclined walls within a feeder must be steep enough to avoid the formation of stagnant zones which can extend up into the hopper and the vertical section thus changing the flow pattern from mass flow to funnel flow.

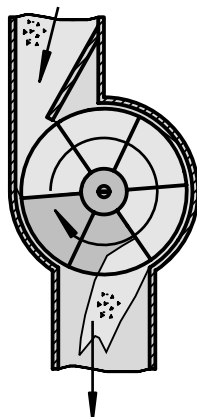


Fig. 12.11. Rotary valve with converging inlet section (as used, for example, for granules)

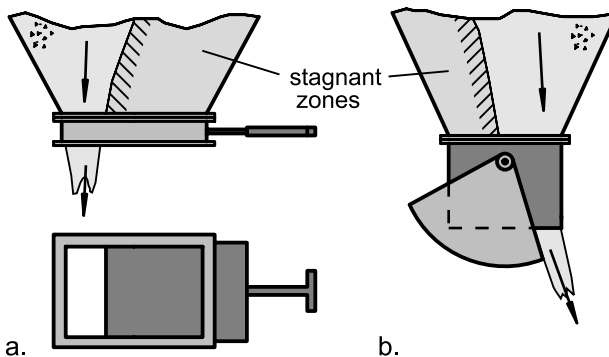


Fig. 12.12. Formation of stagnant zones due to partly opened gates: a. slide gate; b. clamshell gate

Another example of the formation of stagnant zones is the slide gate shown in Fig. 12.12.a being only partly opened. Originating from the slide plate a stagnant zone is formed leading to funnel flow with all known disadvantages (flow problems, segregation,...). The same problem will occur with any configuration of valves and gates (e.g., clamshell valve, Fig. 12.12.b), which are not opened completely during discharge. Therefore, if mass flow is desired, gates have to be opened completely for discharge, and it must be ensured that there are no protrusions into the flowing bulk solid.

12.3.1.2 Rule 2

Many types of feeders tend to discharge the bulk solid only from a portion of the outlet. An example is the screw feeder (Fig. 12.13). The major element of a screw feeder is the rotating screw, consisting of a central shaft to which a helical flight is fitted, conveying the bulk solid in a trough with circular or U-shaped cross section.

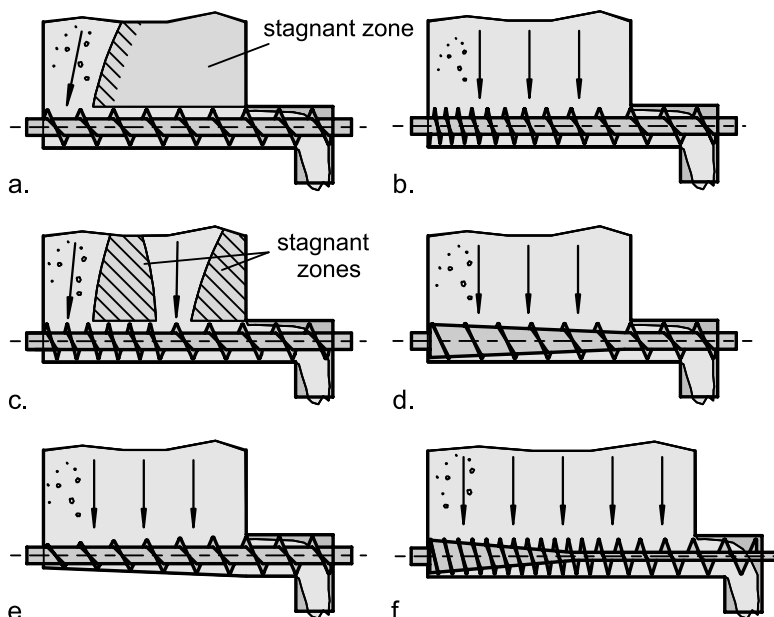


Fig. 12.13. Configurations of screw feeders [12.32–12.34,12.40]

The screw feeder shown in Fig. 12.13.a withdraws the bulk solid preferentially only from the rear end of the outlet slot so a stagnant zone is formed (funnel flow) even if the silo is designed as a mass flow silo. The reason for this behavior is the fact that the screw fills completely at the rear part of the outlet, and the screw conveys this bulk solid towards the exit beneath the bulk solid resting above the front part. This behavior can be avoided by designing the helical flights in such a way that the conveying capacity is increasing in the conveying direction, for example, by an increasing pitch of the screw helix as shown in Fig. 12.13.b (design guidelines in [12.35]). Using this method the screw can discharge bulk solid across the entire length of the outlet slot. The increase of the pitch of the screw should be continuous. If there are too long sections with constant capacities (Fig. 12.13.c), stagnant zones can be formed [12.32,12.34].

Other possibilities to realize increasing capacity are to decrease the shaft diameter in the conveying direction (Fig. 12.13.d), or increase the flight diameter (Fig. 12.13.e). The last option is less convenient because the width of the trough also has to be enlarged in the conveying direction which itself requires an equivalent fitting of the hopper geometry. For outlet slots with a large length-to-width ratio it is useful to start with a decreasing shaft diameter at constant pitch followed by an increasing pitch at constant shaft diameter (Fig. 12.13.f) [12.40].

12.3.2 Types of discharge devices (selection)

In the present section feeders and other discharge devices used for different purposes are described. Crucial points are less the technical details of the apparatuses than the influences of the discharge devices on flow of the bulk solid in the silo, especially with regard to the achievement of mass flow. As will be demonstrated, the above-described principle of increasing capacity to achieve withdrawal of the bulk solid from the entire outlet can be applied to several types of discharge devices.

12.3.2.1 Screw feeders

Screw feeders (Fig. 12.13) are often used for fine-grained and powdery bulk solids (e.g., sawdust, maize, cement, sand, coal dust). Since the bulk solid is subjected to shear deformation and internal friction within a screw feeder, they are less suitable for friable materials. The same holds for very abrasive bulk solids leading to wear of the feeder. Hot bulk solids (up to 800°C) can be conveyed by screw feeders provided with a hollow shaft that is cooled from the inside.

Sticky and adhering bulk solids tend to clog a screw and rotate with it as one mass without being conveyed. To avoid this situation the screw helix should be as smooth as possible (stainless steel, coatings, if possible with poor wettability), and the trough should be rough. For very adhesive bulk solids shaftless screws are used, or parallel screws which overlap and thus clean each other. A screw feeder can be manufactured dust-, gas-, and pressure-tight.

Normally screw feeders applied for silo discharge have a diameter of a few 100 mm; however, some can be found having outer diameters of more than 1000 mm. Typical speeds of rotation are 15 to 80 rpm in exceptional cases also up to 250 rpm. The speed of rotation should not be too high since then the bulk solid cannot flow easily into the screw due to high cen-

trifugal forces. The driving power of screw feeders is relatively high. Design data can be found, for example, in [12.32,12.35, 12.36].

The design of screw feeders for obtaining uniform withdrawal is explained in Sect. 12.3.1.

12.3.2.2 En-masse feeder

The conveying element of the en-masse feeder (Fig. 12.14.a) is a single- or double-strand drag chain arranged between two end sprockets located within a trough. Usually an intermediate plate is arranged beneath the upper strand in the region of the silo outlet opening. The bulk solid is discharged by the upper strand moving the material across the intermediate plate. Then the bulk solid falls onto the bottom of the trough where it is transported to the feeder's outlet by the lower strand.

The en-masse feeder is a very robust feeder. Normally the drag chains are forged and hardened, and the trough can be lined with wear resistant material. The en-masse conveyor is applicable for fine and coarse (up to particle sizes of 100 mm), abrasive, hot (up to 1000°C), sticky and adhesive bulk solids, but not for friable materials. The trough can be manufactured pressure shock resistant (up to 3.5 bars) and gas-tight. The width of the drag chains ranges from 100 mm to 1800 mm. Discharge should be regulated by variation of the chain speed.

An en-masse feeder has the tendency to discharge bulk solid from the rear part (with respect to the transport direction) of the silo outlet opening where the drag chain enters the outlet area and is immediately “filled” with bulk solid. Thus, in the rest of the outlet area no further bulk solid can be discharged by the already “filled” drag chain so a stagnant zone is formed (Fig. 12.14.a). A possibility to avoid the stagnant zone by discharging bulk solid from the entire outlet is the installation of guide plates directly above the drag chain (Fig. 12.14.b) [12.37]. These sloped plates form an outlet slot of increasing width in direction of conveying. This way the width of the layer of material transported by the drag chain is increasing in conveying direction, i.e., an increasing mass of bulk solid is transported (increasing capacity). When designing the guide plates it has to be ensured that the minimum width of the slot is sufficiently large to avoid arching, and that the inclination of the guide plates is sufficient for mass flow (Note that this method might not work well with fluidized bulk solids or those exhibiting a very low angle of repose. These materials may enter the space below the guiding plates.). Alternatively to guide plates, the inlet section of an en-masse feeder can be equipped with layer-height limiters which are described in the following section.

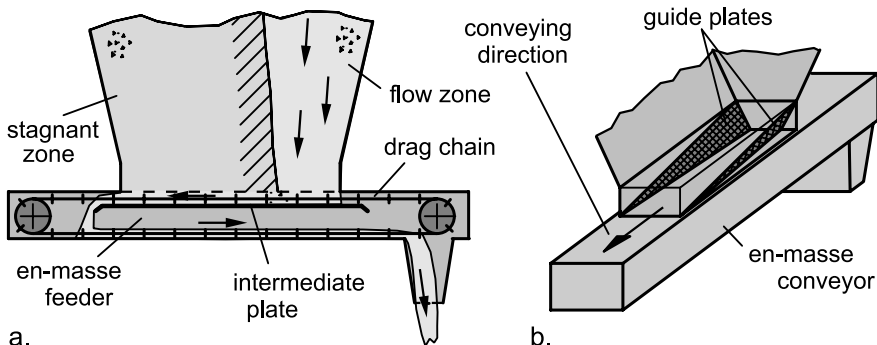


Fig. 12.14. a. Funnel flow caused by an en-masse feeder; b. en-masse feeder with guide plates (cross-hatched) [12.37]

12.3.2.3 Belt feeder

A belt feeder (Fig. 12.15.a and 12.3) consists of an endless strap of flexible material (usually woven fabric covered with rubber; occasionally belts made from other materials are found, for example, woven wire) which is stretched between the driving drum and the tension drum [12.14]. Between these drums the belt is supported by idlers; at smaller stresses the belt can also glide on a smooth metal plate (slider bed). Beneath the outlet opening of the silo the distance between the idlers is smaller to carry the additional vertical load due to the silo. Often belts used for discharge are flat, i.e., the belt surface forms a plane surface and does not form a trough as often seen with belt conveyors.

The driving power of belt feeders is small compared to other feeders [12.38,12.39]. The width of the belt can be up to 5 m for special applications; in most cases the width is smaller than 1 m. The belt velocity is on the order of 0.025 to 0.5 m/s which makes possible discharge rates of up to some 1000 tons per hour [12.41]. Belt feeders can be used for free-flowing, cohesive, fibrous and even friable materials (the latter in contrast to screw feeders or en-masse feeders), but it is not advisable to use standard belt feeders for sticky or hot ($>160^{\circ}\text{C}$) bulk solids. Furthermore, the sometimes not insignificant wear of the belt has to be considered.

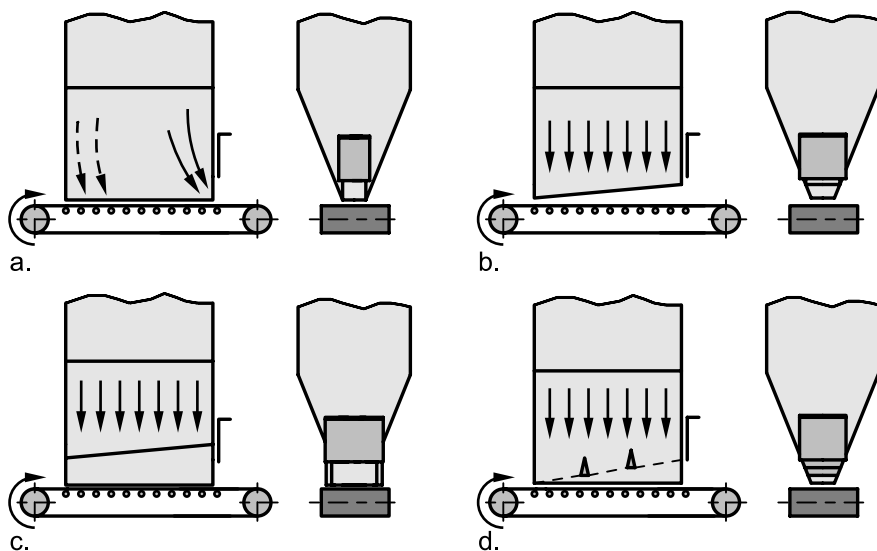


Fig. 12.15. Discharge with a belt feeder: a. non-uniform discharge; a smooth belt and a large layer height preferentially results in discharge from the front end; a rough belt leads to discharge from the rear end (dashed arrows); b. uniform discharge due to a tapered outlet; c. uniform discharge due to a hopper with tapered lower edge and vertical walls; d. uniform discharge due to layer-height limiters (rough belt)

Belt feeders have the tendency to withdraw bulk solid preferentially from one end of the outlet. A smooth belt and a tall gate opening at the front end result in preferential withdrawal from the front part of the outlet slot (Fig. 12.15.a, solid arrows). The bulk solid is more discharged from the rear part of the silo if the conveyor belt is rough and/or the gate is opened less (dashed arrows) [12.38,12.42,12.43]. Other parameters determining the flow pattern are the angle of internal friction (large internal friction promotes discharge of the bulk solid from the front part), and for the case that the outlet is provided with vertical side skirts, the wall friction angle of the side skirts (large friction angle at the side skirts promotes discharge of the bulk solid from the front part of the outlet slot). The large number of influencing parameters makes it impossible to predict exactly the flow pattern, which is, as stated above, usually non-uniform for a standard interface as shown in Fig. 12.15.a. Thus, to withdraw material from the entire outlet slot, it is essential to apply the principle of increasing capacity. This can be achieved by sloping the lower edge of the hopper thus realizing a taper in both plan and elevation, Fig. 12.15.b. As a result, an increasing amount of bulk solid can be transported by the belt feeder in direction of conveying (increasing capacity).

In the example of Fig. 12.15.c vertical walls (non-parallel side skirts) are attached to the hopper of Fig. 12.15.b restricting the taper in plan and resulting in uniform withdrawal if the gate is properly adjusted [12.43]. Since a misadjusted gate can result in non-uniform withdrawal even if the interface is properly designed as in Fig. 12.15.c, in general the discharge rate should be adjusted by belt speed rather than by the position of the gate. Attention has to be paid when discharging cohesive bulk solids since their flow pattern is very sensitive to gate adjustment, and often it takes a very long time until a steady flow pattern is attained [12.38,12.42].

Another possibility to get a more uniform withdrawal from a long outlet slot is the placement of inserts acting as layer-height limiters (Fig. 12.15.d). Due to the inserts the height of the horizontally transported layer increases in conveying direction thus providing the desired increasing capacity. This method can also be applied to apron feeders or en-masse conveyors [12.38,12.42]. The inserts have to be designed so that neither arches nor stagnant zones can be formed on them.

Prerequisite for success of the means shown in Fig. 12.15.b to d is that the angle of friction between the belt and the bulk solid is sufficiently large to withdraw material from the rear part of the outlet slot. If the friction is too small, the material will still be discharged preferentially from the front part (Fig. 15.12.a, solid arrows).

12.3.2.4 Apron feeder

Apron feeders discharge bulk solid similar to belt feeders, whereby the bulk solid is carried by a “steel belt” composed of overlapping steel pans being laterally connected with chains driven by sprockets. Depending on the design, chain and pans are carried by rollers attached to the pans or chain elements, or by rollers fixed at the feeder’s frame.

Depending on the application, pans of different type are used. They can be almost flat, but also arched or provided with flanges to obtain a “deep” pan [12.14]. An apron feeder is suited for extreme operation conditions, i.e. for coarse, very abrasive and sharp-edged bulk solids with particle sizes of up to 1000 mm and temperatures of up to 1100°C. Furthermore it can be used for poorly flowing, wet, fine grained bulk solids which require large outlet dimensions and have a large angle of internal friction (large driving force), for example, moist clay or filter cake.

Apron feeders are available in lengths from 2 m to 15 m and widths up to 4 m. The operating speed is usually on the order of 0.01 to 0.5 m/s [12.44,12.45]. The driving power is significantly larger compared to belt feeders.

To ensure withdrawal from the entire outlet opening, identical means have to be applied as described for the belt feeder and the en-masse feeder. The discharge rate should be adjusted by the chain speed, as is recommended for belt feeders (Sect. 12.3.2.3), and not by variation of the layer height.

12.3.2.5 Vibratory feeder

A vibratory feeder (Fig. 12.16) consists of an elastically supported trough located beneath the outlet of a silo. The trough is excited to oscillate by an appropriate drive, e.g. an eccentric-mass mechanical drive, an electromagnetic drive, or, applied less often, a positive mechanical drive with a crank. Vibratory frequencies range from 5 Hz to 100 Hz [12.14,12.46,12.47]. Discharge rate is dependent on the angle of slope of the trough (0° to -15° , measured from horizontal), the bulk solid properties, and the layer height [12.48]. By changing the amplitude (electromagnetic drives) or the frequency (all types of drives), the discharge rate can be regulated. Advantages of a vibratory feeder are its simple construction, low maintenance requirements, and low driving power.

Vibratory feeders tend to discharge the bulk solid preferentially from the front part of the outlet, which often causes stagnant zones if the material is discharged from elongated outlets (Fig. 12.16.a). Withdrawal from the entire outlet can be only achieved by decreasing the ratio of the outlet length to layer height to a value less than 1 (Fig. 12.16.b) [12.34,12.49]; with a ratio of about 0.5 a uniform withdrawal can be achieved [12.50]. Furthermore, the drive of the vibratory feeder has to be adjusted in amplitude and frequency in such a way that the bulk solid beneath the silo outlet is actually transported on the trough according to the principle of vibratory conveying. If the adjustment is insufficient, one can observe indeed that bulk solid is discharged, but this is based on the reduction of the angle of repose by the vibration, i.e., the bulk solid only moves on the surface of the trough filling, but not on the bottom of the trough (Fig. 12.16.c). Thus, similar to Fig. 12.16.a, discharge takes place only in the front part of the outlet. Therefore it is essential to consider the discharge behavior when adjusting the mass flow rate by variation of amplitude or frequency of vibrations.

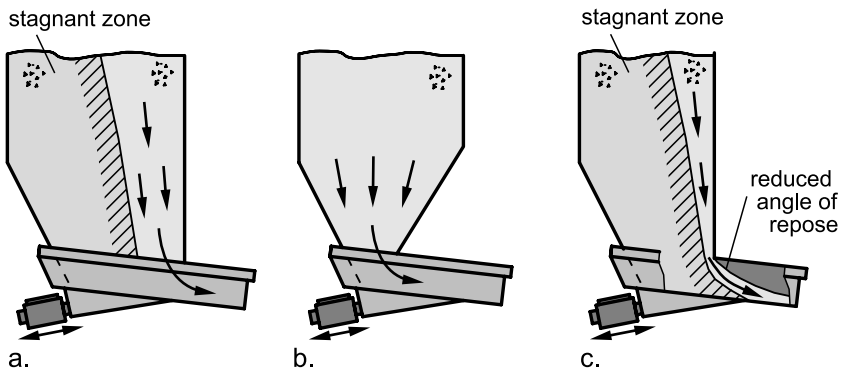


Fig. 12.16. Vibratory feeder; a. discharge only from the front part due to an inappropriate long outlet slot; b. uniform discharge due to a sufficiently small length of the outlet in conveying direction; c. misadjusted vibratory feeder resulting in funnel flow

12.3.2.6 Bin activator and similar principles

The principle of a bin activator is shown in Figure 12.17.a. It consists of a relatively shallow hopper flexibly suspended below the silo outlet. The hopper, which is provided with a convex baffle, is excited to horizontal vibrations by an externally mounted vibrator motor. Thereby the bulk solid flows through the annular gap between baffle and hopper, and further on the shallow hopper walls to the outlet. The shapes of hopper and baffle depend on the manufacturer; baffles in the form of an inverted cone or a pyramid are also available, and hoppers can be conical or dished, or a combination of both. Since a bin activator both initiates flow and discharges material, it can be considered both as discharge aid and discharge device.

Variations of the bin activator are shown in Figs. 12.17.b to d. The model in Fig. 12.17.b is provided with a longitudinal insert fixed to an axis-symmetric hopper. The inserts form parallel outlet slots through which material is withdrawn. Furthermore, this model is equipped with two frequency-regulated drives for better control of the discharge rate.

The version in Fig. 12.17.c is provided with a rectangular frame carrying adjustable blades vibrating with the (rectangular) hopper. Due to the adjustability of the blades the discharge rate can be influenced. In contrast to the bin activators considered so far, the hopper of the system shown in Fig. 12.17.d is fixed to the silo outlet, i.e., it is not flexibly supported, and, thus, a flexible seal is not required. This version has advantages when considering the danger of leakage and the effects of pressure shock. The in-

verted cone insert can be lifted and vibrated vertically with a vibratory drive. The material is then discharged through the annular gap between the inverted cone and the silo hopper. The discharge rate depends on the operational settings (amplitude and position of the cone).

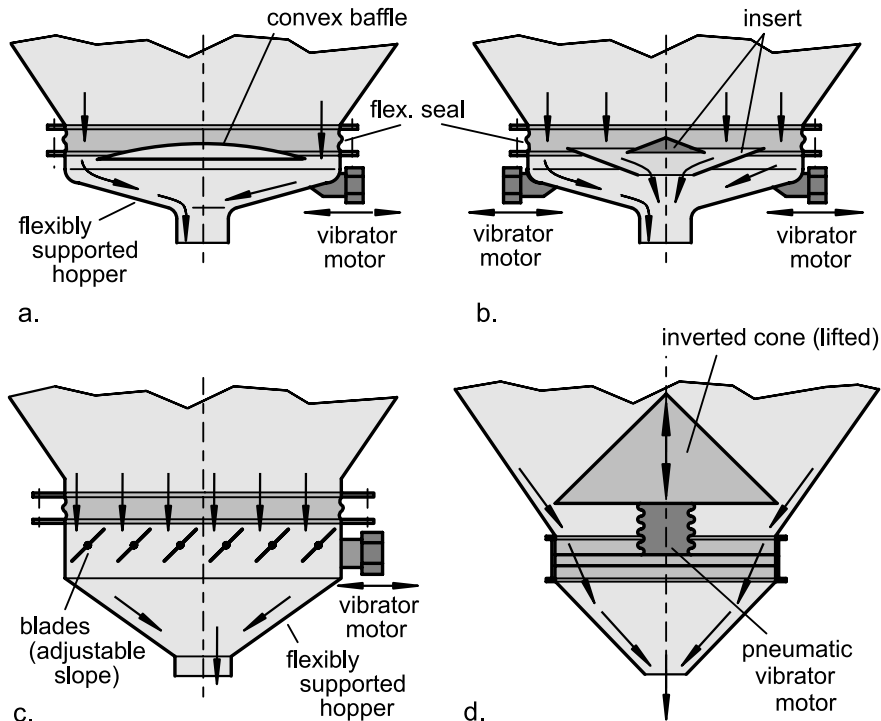


Fig. 12.17. Bin activator and similar principles (simplified presentation); a. bin activator with convex baffle (e.g., [12.77]); b. with insert and additional discharge at the center (type Silo-Tray [12.51]); c. with adjustable blades (type Hogan [12.52]); d. with agitated conical insert (type Matcon [12.53])

One can expect that the devices described above withdraw the material from the entire outlet of the silo if it is ensured that the flow rate is not restricted by downstream equipment. The latter can happen if, for example, a conveying or dosing device is installed downstream, which limits the mass flow rate to a value smaller than the mass flow rate that could be delivered by the bin activator at its present operational settings (such a combination is often used because the feeding accuracy of the devices discussed here is very limited). This situation is shown in Fig. 12.18 for a rotary valve attached to a bin activator. Due to the limitation of the discharge rate by the rotary valve, the bin activator may fill completely with the bulk solid, and

a possible result is the formation of an eccentric flow zone. The stagnant material in the hopper thus becomes increasingly consolidated due to the effect of the vibration. To avoid such situations, one has to take care that the entire amount of bulk solid entering the vibrating hopper from the top is discharged. If this cannot be realized, a buffer with level control has to be installed between the bin activator and the downstream equipment. Then the bin activator is activated only to fill the buffer.

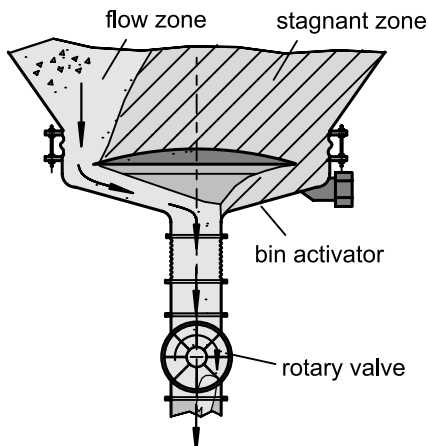


Fig. 12.18. Funnel flow inside a vibrating hopper due to a following conveying equipment (here: rotary valve)

12.3.2.7 Rotary valve

Two versions of rotary valves (rotary feeders) are shown in Figs. 12.7 (vertical driving shaft) and 12.11 (horizontal driving shaft). In the case of Fig. 12.11 the bulk solid flows by gravity from above into the pockets of the rotor and is then transferred by the motor-driven rotor to the outlet section.

The rotor of the rotary valve in Fig. 12.7 transfers the bulk solid horizontally from the eccentric inlet opening to the outlet which is displaced by 180° to the inlet [12.30]. To avoid stagnant zones in the hopper due to the eccentric feeder inlet, the driving shaft is elongated upwardly and provided with an agitator rotating directly above the rotary feeder. If necessary further agitators can be applied further up as discharge aids (see Sect. 12.2.2).

Rotary valves are used to feed bulk solids in systems with different gas pressure, for example, from atmospheric pressure into a pneumatic conveying line, or from pressurized systems (e.g., pneumatic sifters) to atmos-

pheric pressure. Thereby pressure differences of up to about 3.5 bars can be overcome without the presence of much air leakage [12.54].

Standard rotary valves are used for relative easy flowing, fine-grained bulk solids at temperatures of up to 600°C. The power required to drive rotary valves is low. At speeds of rotation of 5 rpm to 90 rpm and rotor diameters of more than 500 mm mass flow rates of up to 1000 m³/h can be achieved depending on the actual type of the rotary valve.

In rotary valves with a horizontal axis the mass flow rate at first increases nearly linearly with the speed of rotation [12.55]. At higher speeds of rotation the mass flow rate decreases because the centrifugal force acting against the gravity force increases and the time available for filling the pockets of the rotor becomes smaller. In rotary valves with a vertical shaft the centrifugal force has no negative influence on the mass flow rate because it does not counteract flow of the bulk solid into the pockets [12.57].

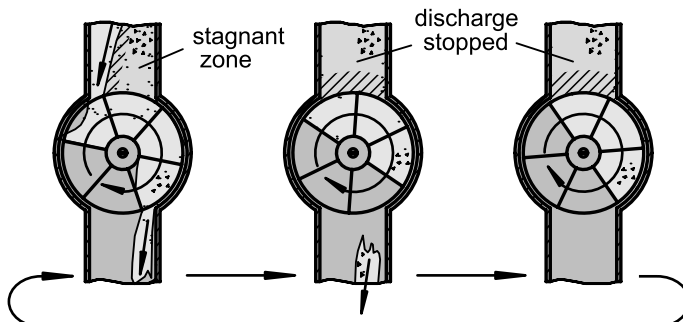


Fig. 12.19. Discharge of an easy flowing bulk solid with a rotary valve

Under specific conditions a rotary valve can result in eccentric or intermittent discharge from a hopper. A free-flowing bulk solid fills the pockets of the rotor as soon as they enter the inlet area of the rotary valve. The bulk solid is therefore primarily discharged from the left part of the silo outlet as shown in Fig. 12.19. The problem of eccentric discharge can be avoided by the addition of an inclined plate in the infeed section as in Fig. 12.11 (consider angle of inclination and smallest cross section, as discussed in Sect. 12.3.1.1), or by a sufficiently tall section of constant diameter (height should be 1 to 3 times the diameter, depending on the bulk solid) directly above the rotary valve so that the flow zone is likely to cover the entire cross-section at the top of this section.

With hard, brittle bulk solids, intermittent flow which might be caused by a rotary valve as depicted in Fig. 12.19 can lead to undesirable vibrations of the silo. In this case continuous discharge can be achieved by a ro-

tor with an increased number of (smaller) pockets, and by a higher rotational speed.

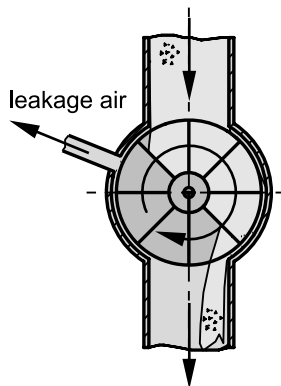


Fig. 12.20. Rotary valve with leakage air vent

When feeding a (fine-grained) bulk solid with a rotary valve into a system of higher gas pressure (e.g., a pneumatic conveying line), one must ensure that air leakage due to the pressure gradient is minimized. Otherwise the upwards flowing gas can reduce the discharge rate to an unacceptable extent [12.56] both by reducing the fill efficiency of the pockets, and by causing an upward gas flow within the hopper (countercurrent air flow, see Sect. 12.1.2). Air leakage results from air flowing through the rotor casing clearance and air transported in the empty pockets on the return side of the rotor. To minimize air leakage, the rotary valve must be kept in a sufficiently tight condition (maintenance!), and especially with fine powders a venting system is helpful. The venting system in Fig. 12.20 (body vent) is connected to an external vent line, which may be connected to a filter or to the top (roof) of the silo. Since the air flow in a vent line, which is essentially a pneumatic conveying system, is usually small, they tend to become blocked by dust. Thus, regular maintenance is important.

12.3.2.8 Air-assisted discharge

Fine-grained bulk solids (mainly group A materials according to Geldart's diagram, Fig. 7.22) can easily be loosened and transported by the continuous introduction of air (or any other gas). This effect is described in connection with pneumatic discharge aids, which are primarily used to initiate and support bulk solids gravity flow (Sect. 12.2.1), whereby the systems discussed in the present section are based on the idea of air-assisted (gravity) conveying on slightly inclined, nearly horizontal surfaces.

The principle of air-assisted gravity conveying on an air slide is depicted in Fig. 12.21. The air slide consists of a porous material (e.g., woven fabric, woven steel laminate, sintered material made from metal or plastics) supporting the bulk solid. Pressurized air is then supplied to the plenum chamber beneath the porous plate [12.14,12.58]. Thus the bulk solid is subjected to a continuous upward flow of gas. Depending on the air flow rate, this can lead to reduction of the normal stress (resulting in smaller frictional forces), loosening of the material, and even to fluidization, so that the bulk solid flows along the air slide being inclined of up to 15° to the horizontal.

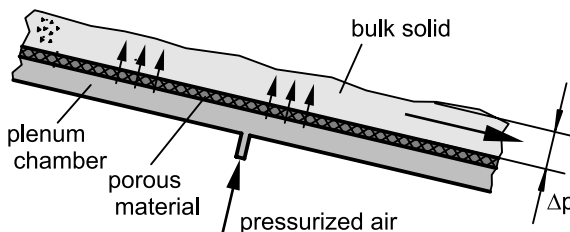


Fig. 12.21. Principle of air-assisted conveying on an air slide

The principle of the air slide is also used to discharge fine-grained bulk solids from silos. Figure 12.22 depicts the placement of air slides beneath a (relatively small) outlet opening of a silo. The aerated area is divided into two sections: section 1 beneath the silo outlet, section 2 next to section 1 in the transport section. The sections are supplied with pressurized air independent of each other. Fluidization in the original sense as being realized in the air slide of Fig. 12.21 is difficult to achieve in section 1 due to the column of bulk solid above it, but the air injected in section 1 flows towards the control gate and causes a force on the bulk solid in the same direction due to the air flow resistance. However, in section 2, i.e., between silo outlet and control gate, fluidization is possible due to the small layer height. The fluidized material flows towards the control gate, where the mass flow rate is adjusted by the control gate.

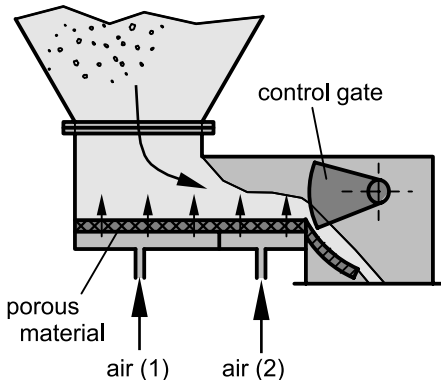


Fig. 12.22. Discharge with air slides

Air slides are also applied to discharge huge silos (diameter up to 25 m; height up to 50 m) used for the storage and homogenization of, for example, cement or raw mix. In earlier times, these silos were mostly built with a shallow bottom provided with one or more outlet openings. Around each outlet opening the bottom is sloped by 10° to 15° to horizontal and equipped with air slides which are intended to transport the material to the outlet opening. For the task of homogenization, for example, for the compensation of variations in the compositions of raw mix, the silo bottom is divided into segments which can be aerated separately. This allows discharging the bulk solid from different silo regions one after the other which results in the homogenizing effect.

Since about 1980 homogenizing silos are more and more built as inverted cone silos (Fig. 12.23) [12.59–12.61]. In the center of the silo a huge inverted cone made from concrete is placed forming an annular hopper with the outer wall of the silo. In the lower part of the cone wall four or more apertures are provided acting as outlet openings from which the bulk solid is discharged with air slides. Depending on the number of apertures, further air slides are spread over the bottom of the annular outlet slot. Their intention is to transport the bulk solid towards the outlet openings. For homogenization only the air slides in one or two particular sections (e.g., only the air slides being associated with one outlet opening) are activated simultaneously, and in regular time intervals other sections are activated following a specific pattern. Thus, flow zones form temporarily in which bulk solid from different layers having different compositions flows downward and, thus, is mixed [12.62]. The non-symmetrical flow zone and its regularly changing position have to be taken into account when designing the silo for strength [12.63,12.64].

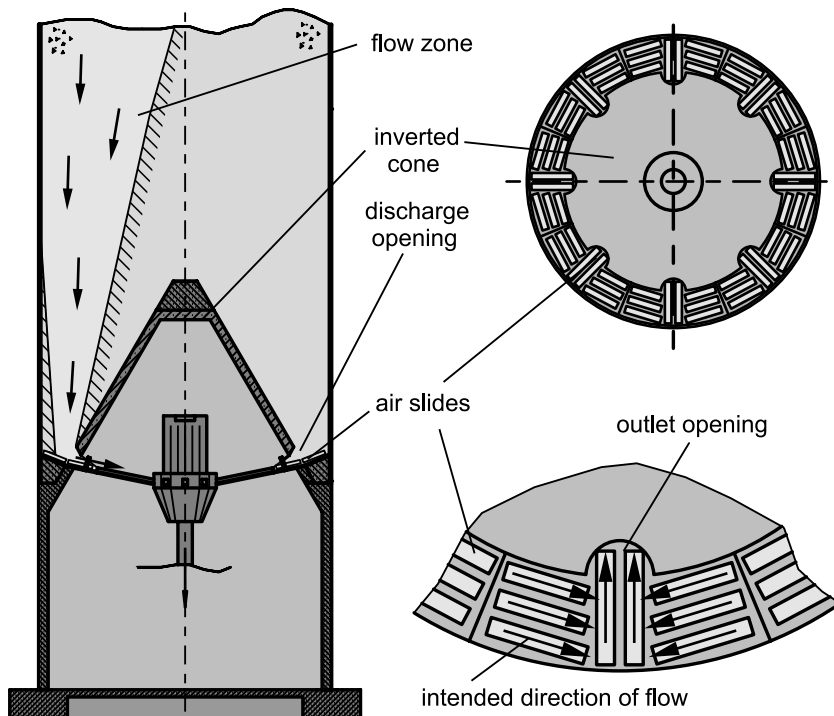


Fig. 12.23. Inverted cone silo [12.62]: vertical section (left) and top view (top right); magnified area around an outlet opening with the intended conveying direction of the air slides (bottom right). Shape of the flow zone assumed according to [12.63].

When using a silo to store a poorly flowing bulk material tending to time consolidation, it must be designed for mass flow to avoid flow problems. Considering a silo equipped with air slides, this can only be achieved when the material is withdrawn along the entire length of the air slides. Experience has shown that with long air slides material is not withdrawn uniformly with respect to the length of the air slide. Furthermore, in such a situation a stagnant zone is likely to be formed over the rear part of the air slide (i.e., the part being more distant from the silo outlet, see Fig. 12.24). The reason for this is the fact that for transport over the entire length of the air slide a layer of bulk solid of the same length as the air slide had to be moved on the air slide beneath the bulk solid resting above. The necessary forces are not attainable with significant air mass flow rates and realizable air pressures (silo walls are loaded by bulk solid stresses and gas pressure!). Additionally, the air will preferentially leave the plenum chamber of the air slide where the flow resistance towards the outlet opening is

smallest, i.e. in regions close to the outlet opening. Thus, in the region farthest from the outlet opening the minimum air flow rate is to be expected. A higher air flow rate in those areas can be achieved by subdivided air slides with separate air supply as shown in Fig. 12.24. Also steeper air slides are likely to increase the size of the flow zone.

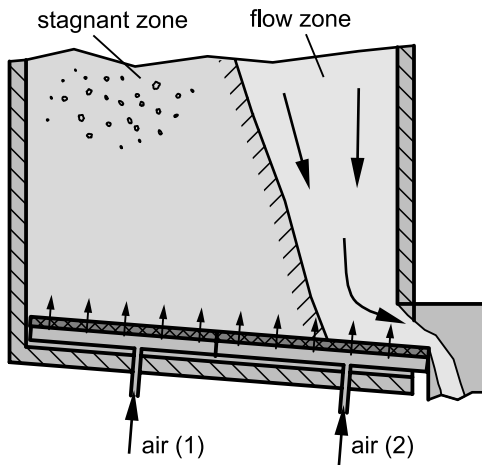


Fig. 12.24. Possible stagnant zones when a bulk solid is discharged with long air slides

12.3.2.9 Rotary plow feeder, rotary discharge machine

Rotary plow feeders with one plow as shown in Fig. 12.25 are mostly used for the discharge of poorly flowing bulk solids. A rotary plow feeder consists of an inverted cone insert (mostly stationary; sometimes rotating [12.65], usually accompanied by a cylindrical part at its lower end) above a central outlet opening, and a curved plow located directly above the silo bottom. The curved plow rotates around the central, vertical axis, and moves the bulk solid through the vertical clearance between insert and silo bottom into the discharge opening. The insert prevents uncontrollable discharge of the bulk solid through the central outlet opening. Additionally it reduces the load on the plow and, thus, the driving torque, since it forms a hopper of annular cross-section with the (vertical or inclined) outer wall, where the stress decreases in the downward direction as typical for hoppers (see Sect. 9.1.2)

Rotary plow feeders are available with diameters from 1 m to about 8.5 m. At low speeds of rotation of a few revolutions per minute volume flow rates from $0.5 \text{ m}^3/\text{h}$ to more than $6000 \text{ m}^3/\text{h}$ are achievable. Rotary

plow feeders are considered to be robust and suitable for abrasive and poor flowing bulk solids [12.65–12.67]. To prevent arching, the minimum width of the annular hopper has to be considered which is usually found at the lower edge of the insert. Depending on the manufacturer and the dimension of the rotary plow feeder, the minimum width of the hopper can amount up to 1.5 m.

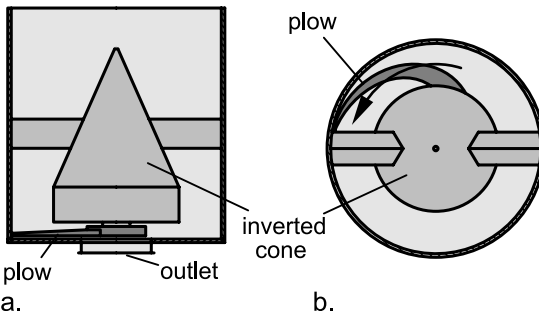


Fig. 12.25. Principle of a rotary plow feeder with one plow: a. vertical cut; b. top view

A rotary discharge machine, sometimes also called a rotary plow feeder, consists of discharge wheel carried by a wagon traveling on rails beneath a roof-shaped insert parallel to the outlet slot of the silo (Fig. 12.26). The discharge wheel moves the material through the vertical clearance between insert and silo bottom onto a belt conveyor located beneath. In addition to discharge machines reclaiming bulk solid from both sides as shown in Fig. 12.26, devices also exist which only reclaim from one side.

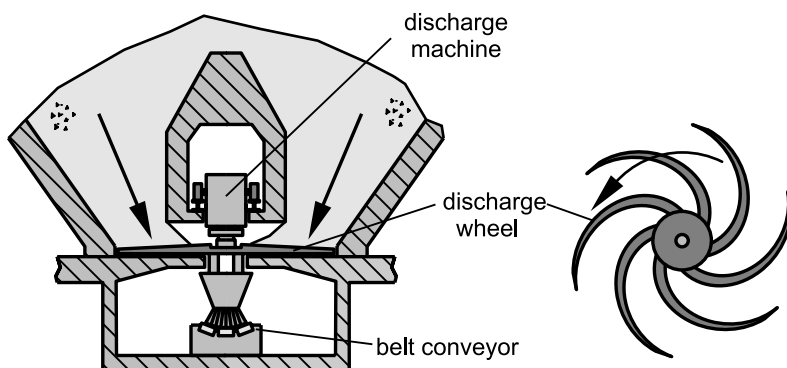


Fig. 12.26. Principle of a rotary discharge machine reclaiming from two sides (sectional plane perpendicular to the direction of travel), top view of the discharge wheel

Rotary discharge machines are used for large silos with lengths of the outlet slot of more than 20 m (e.g., coal silos of power stations), and also to reclaim bulk solid from large stockpiles. The discharge wheels can have diameters from 2 m to 5 m. Thus, mass flow rates of more than 3000 t/h are realizable [12.68]. Rotary discharge machines are considered as being extremely robust. Besides easy-flowing bulk solids also coarse (particle sizes up to several 100 mm), poorly flowing, and sticky bulk solids can be discharged.

Similar designs also exist for the discharge from huge circular silos with inverted cone insert (similar to the silo with the rotary plow, Fig. 12.25, but with larger diameter). Thereby the rotary discharge machine rotates beneath the inverted cone around the vertical axis of the silo. The discharge wheel reclaims the bulk solid from the annular slot between inverted cone and silo wall (similar to the rotary plow in Fig. 12.25), and feeds it onto a radially oriented belt conveyor rotating around the silo axis with the discharge machine [12.68,12.69].

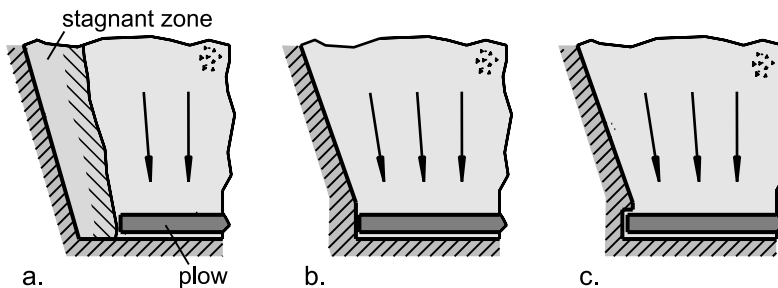


Fig. 12.27. Arrangement of hopper wall and plow (or discharge wheel)

Since rotary plows and discharge wheels cannot simultaneously withdraw bulk solid from the entire (annular or longitudinal) outlet slot, mass flow is achieved only in an integral view, i.e., after one revolution of the rotary plow in the case of Fig. 12.25, or after bulk solid has discharged from the entire length of the outlet slot in the case of a rotary discharge machine, respectively. Furthermore, for mass flow it has to be ensured that the bulk solid is discharged from the entire width of the outlet slot. If this is not the case as shown in Fig. 12.27.a, stagnant zones are formed close to the silo wall, which is especially a problem when storing poorly flowing bulk solids and those with a tendency for time consolidation. The reason for the stagnant zone in Fig. 12.27.a is that the distance between the tip of the plow and the hopper wall is too large. To avoid this, the clearance between plow and silo wall must be sufficiently small, and, if the rotary plow feeder is located beneath a hopper as in Fig. 12.27, a sufficiently high section

with vertical walls (Fig. 12.27.b) or an undercut (Fig. 12.27.c) should be added.

12.3.2.10 Feeders for large outlet openings

Very cohesive bulk solids can exhibit such poor flow behavior that outlet diameters of several meters are required. Sometimes even any hopper of reasonable dimensions would cause flow problems, so a silo without hopper is a possible option. Such silos are sometimes also built with the intention to save height. In these cases feeders are needed which have the ability to withdraw the bulk solid from a large cross-section. Some examples of those feeders are presented in the following.

A multiple screw feeder consists of parallel screws within a common housing. In Fig. 12.28 a multiple screw feeder for very large outlet dimensions is presented (up to 6 m side length). The discharge screws withdraw the material and transport it towards the central transverse outlet slot, below which a collecting screw is located. For this the discharge screws are provided with flights of different orientation left and right of the outlet slot in order to obtain opposite conveying directions. Increasing capacity is realized by decreasing the shaft diameter in the conveying direction (similar to the single screw feeders, Sect. 12.3.1.2). Above the outlet slot the cross-section of the screw is enlarged to cover the outlet slot. This prevents the collecting screw from being filled completely by too much material entering the screw from the region above the collecting screw.

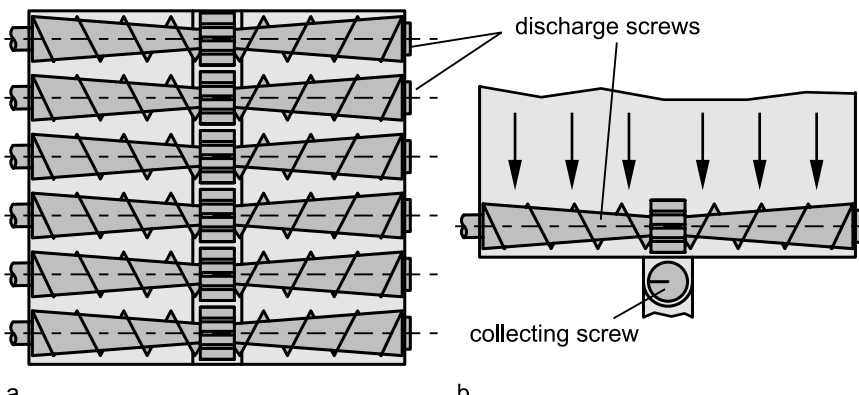


Fig. 12.28. Multiple screw feeder with collecting screw [12.70]; a. view from the top; b. vertical cut

Besides the standard version with screws placed beside each other as in Fig. 12.28, also interlocking screws (all of the same geometry) are applied

which minimize rotation of the bulk solid with the screw by “cleaning” each other and, thus, preventing the screw from becoming logged with sticky, adhering bulk solid. A bottom surface adjusted to the screws keeps residual amounts of bulk solid small when the silo is discharged completely. This is significant if the silo is used for different bulk solids.

Often multiple screw feeders of smaller dimensions than in Fig. 12.28 and rectangular cross-section are applied. Here the collecting screw or an outlet without further screw feeder is normally located at one end of the feeder. Multiple screw feeders are suitable for cohesive, poorly flowing bulk solids with not too large particles.

An alternative for the discharge of bulk solids from large cross-sections is the system with oscillating bars [12.71] (Fig. 12.29). It consists of parallel bars, which slowly oscillate (oscillating rotational motion) to promote flow. In the closed position, the bars act as a closed gate and prevent discharge (Fig. 12.29.a). The discharge rate can be adjusted by speed and opening angle of the bars. The discharged material falls into a collecting hopper (Fig. 12.29.b). The oscillating bar discharger can be used for the discharge of easy flowing bulk solids, for cohesive, adhering materials as well as for products like shredded foil. Devices with dimensions of 5 m by 6.5 m have been realized [12.71]. It is important for poorly flowing bulk solids that the collecting hopper beneath the oscillating bars is not filled to such an extent that flow problems (arching, ratholing) will arise there.

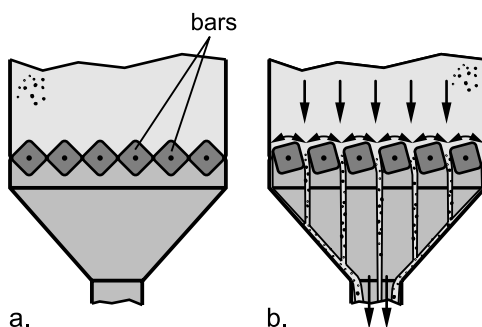


Fig. 12.29. Discharge system with oscillating bars; a. bars closed; b. discharge by oscillating rotation of the bars [12.71]

Besides the continuous activation of the entire outlet area (multiple screw feeder, oscillating bar discharger) discharge devices exist which momentarily withdraw bulk solid only from a part of the outlet area, but within a certain time period the entire outlet is activated (similar to the rotary plow feeder described in Sect. 12.3.2.9). The orbiting screw feeder (Fig. 12.30) represents this group of discharge devices. The orbiting screw rotates

around its axis to withdraw the bulk solid and transport it to the central outlet opening. Simultaneously, the screw rotates around the vertical silo axis. Thus, the screw is orbiting around the silo axis and discharges bulk solid from every region of the silo within a certain time period. The drives mostly are placed along the silo axis. Orbiting screw feeders are applicable to outlet diameters from 2 m to 20 m [12.72,12.73].

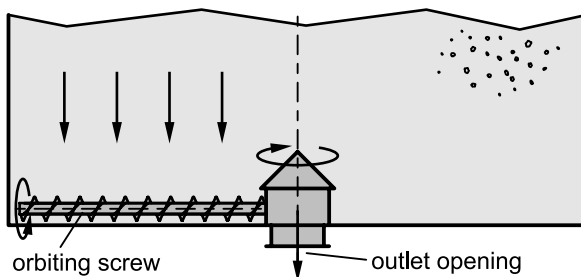


Fig. 12.30. Orbiting screw feeder [12.72]

The orbiting motion of the version shown in Fig. 12.30 is load dependent, because instead of adjusting its speed a constant torque is exerted on the screw in the desired direction. Therefore, the orbiting speed and, thus, the time for one revolution is dependent on operating conditions (e.g., vertical stresses, strength of the bulk solid). This way excessive forces and torques, respectively, are avoided, and the screw construction can be relatively light. Other versions of orbiting screws are driven with constant speed [12.34,12.74], which results in heavy structures, limits on the screw length, and high driving torques especially if the screw is driven from the silo center. The latter can be avoided by a drive which is rotating with the screw at the perimeter of the silo [12.74], but this leads to a very expensive construction of the silo wall which has to be undercut.

The usually conical covering of the drive and the outlet opening in the center of the silo in principle form a hopper with the silo wall already discussed with respect to inverted cone silos and rotary plows (Sects. 12.3.2.8 and 12.3.2.9). If the ratio of outlet diameter to cone diameter is small, this effect can be neglected, but at smaller ratios the possibility of arching has to be checked.

To withdraw material over the entire length of the screw, the capacity of an orbiting screw must increase in the conveying direction, for example, due to an increasing pitch [12.74,12.75] (Sect. 12.3.1.2). However, since a screw withdraws only from the region above it, an eccentric flow zone with varying location prevails (similar to the central cone silo, Sect. 12.3.2.8), which leads to a non-symmetric, fluctuating load on the silo

walls which has to be considered for silo design for strength [12.64,12.76] (see Sect. 9.4.2).

12.4 Feeder dimensions and placement of discharge aids

For reliable operation of a silo, the hopper steepness and outlet size have to be determined based on the flow properties of the bulk solid (see Chap. 10). Knowing these parameters, different concepts can be considered for the hopper shape and selection of feeders and, if required, discharge aids. Some design concepts are presented in the following by considering a conical mass flow hopper. For an example bulk solid, in the diagram in Fig. 12.31 the minimum outlet diameter, d_{crit} , required to prevent arching is plotted as a function of storage time at rest, t (i.e., the time between two consecutive discharge operations). Since the bulk solid shows a strong time consolidation effect (i.e., increase of unconfined yield strength with storage time at rest), the critical diameter, d_{crit} , increases strongly with time, t . The maximum storage time at rest expected for maintenance work or holidays is t_1 .

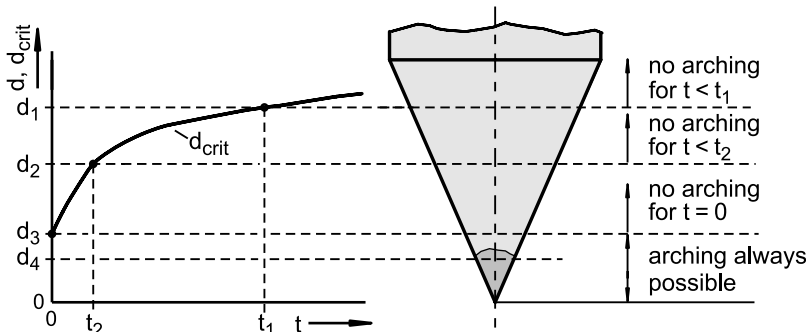


Fig. 12.31. Minimum outlet diameter, d_{crit} , vs. storage time at rest, t ; conical hopper and critical diameters for storage times $t = 0$, t_1 , and t_2

Concept 1: Outlet diameter, d_1 , according to the maximum storage time at rest, t_1 ; $d_1 = d_{crit}(t = t_1)$

In this case, the outlet diameter $d_1 = d(t = t_1)$ is large enough to prevent arching even after the expected maximum storage time at rest. In the example under consideration the maximum storage time is t_1 which requires the outlet diameter $d_{crit}(t_1) = d_1$ (Fig. 12.31). A hopper with this outlet diameter is shown in Fig. 12.32.a. A feeder of appropriate size (diameter d_1) has to be fitted to the outlet. The choice of the feeder type depends on the

outlet size, bulk solid (particle size, stickiness, flowability, moisture) and other requirements (e.g., accurate dosage, pressure shock resistance).

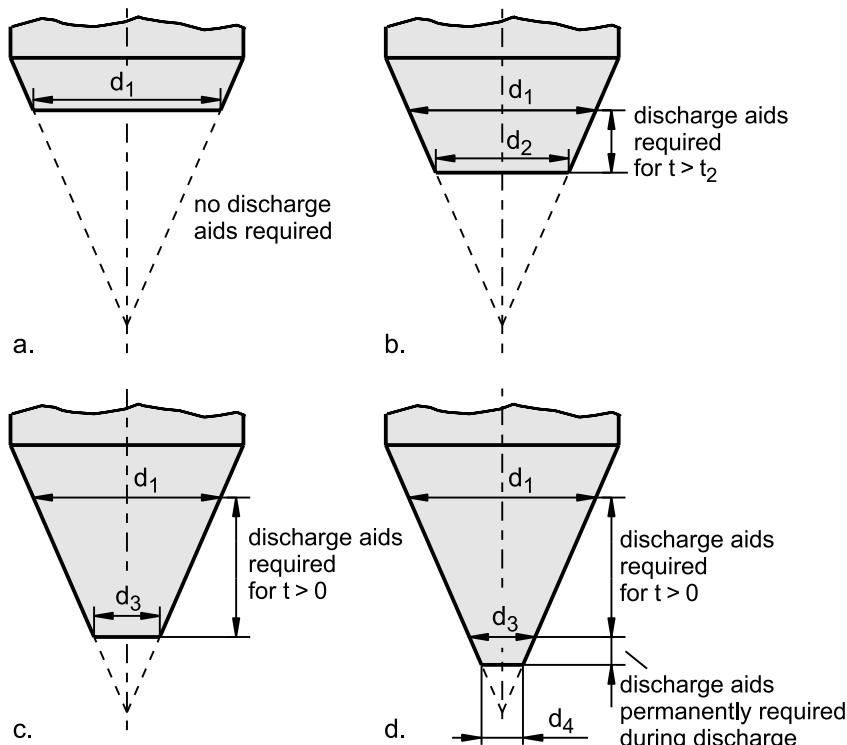


Fig. 12.32. Concepts for mass flow hoppers

Concept 2: Outlet diameter, d_2 , according to storage time $t_2 > 0$ and $t_2 < t_1$; $d_{crit}(t = 0) < d_2 < d_{crit}(t = t_1)$

If the outlet diameter d is chosen according to d_2 (Fig. 12.32.b), the outlet is large enough to prevent arching for storage times at rest up to t_2 (see Fig. 12.31). If the bulk solid is stored at rest over a longer period up to t_1 , stable arches can form. Hence, discharge aids are required in the region between the outlet and the diameter d_1 to initiate flow after storage time t_2 was exceeded ($t > t_2$; Fig. 12.32.b). Due to their large range of action air cannons would be a possible solution. Discharge aids are only required to initiate flow after storage times at rest greater than t_2 ; they are needed neither to initiate flow after shorter storage periods ($t < t_2$), nor to maintain flow because time consolidation is no longer a consideration after the material has been caused to flow.

The choice of the outlet diameter $d_3 = d_{crit}(t = 0)$ (Fig. 12.32.c) is the limiting case of concept 2. Here the discharge aids must always be used to initiate flow if the bulk solid has been stored at rest for a period $t > 0$. To maintain flow a further use of the discharge aids is not necessary.

Concept 3: Outlet diameter $d_4 < d_{crit}(t = 0)$

For an outlet diameter $d_4 < d_{crit}(t = 0)$ (see Figs. 12.31 and 12.32.d) arching is possible even without time consolidation. Therefore, discharge aids have to be used between the outlet and that position where the hopper diameter is equal to the minimum diameter, d_1 , to avoid arching after the maximum storage time at rest, t_1 . Discharge aids located below diameter $d_3 = d_{crit}(t = 0)$ have to be used continuously during discharge, while discharge aids above that diameter (as in concept 2) have to be used only to initiate flow after a storage time $0 < t < t_1$.

The three concepts described above are only valid for mass flow silos. In the case of mass flow only the problem of arching exists; ratholing is only possible in funnel flow silos. In a mass flow silo the whole contents of the silo are in motion during discharge. Thus, time consolidation is completely overcome. In a funnel flow silo stagnant zones are formed in which the bulk solid remains at rest even during discharge, and these stagnant zones are moved only when the silo is emptied completely. Thus, bulk solid can stay in the stagnant zones over very long times and, therefore, is consolidated increasingly so that it builds up stable ratholes. Furthermore, when comparing funnel flow silos and mass flow silos, the following has to be considered:

- The minimum outlet diameter to avoid ratholing usually is larger than the minimum outlet diameter to avoid arching [12.33] (see Sect. 10.3.2). Thus, a funnel flow silo must be provided with a larger outlet diameter, or discharge aids have to be placed in the hopper up to a larger height (= larger diameter).
- In mass flow silos the maximum storage time at rest equals the maximum time interval between two consecutive discharge sequences. On the contrary, in funnel flow silos the time interval between two complete emptying sequences has to be considered as the maximum storage time at rest, since bulk solid in stagnant zones is at rest nearly up to the end of the emptying process. Thus, much longer (often not predictable) storage times have to be considered when designing a funnel flow silo. This leads to larger outlet openings or to the necessity to apply discharge aids in a significantly larger area of the hopper compared to a mass flow silo.

Following these arguments, funnel flow silos should be chosen only if the bulk solid exhibits no or limited time consolidation, and when the further

disadvantages of funnel flow silos (segregation, wide residence time distribution, etc., see Sect. 10.2) can be accepted.

It is impossible to give a general assessment of the concepts for mass flow silos discussed above. Concept 1 is the simplest one considering performance and operation, because discharge aids are not necessary. As described in Sect. 12.2, discharge aids cannot be designed quantitatively, so their selection and sizing is mainly based on experience. Additionally the application of discharge aids can lead to disadvantages (e.g., irregular flow, flooding). Therefore, generally concept 1 should be considered first.

In the case of bulk solids exhibiting poor flow behavior and pronounced time consolidation effects, the minimum outlet diameter required to avoid arching even after a short storage time at rest (e.g., a few hours or days) may amount to several meters. If a feeder of appropriate dimensions is not available or seems to be too expensive, concept 2 might be a solution. Here both the outlet diameter and the feeder size are chosen large enough to avoid arching without time consolidation. Discharge aids ensure that flow is initiated after storage at rest. The possible disadvantages combined with the use of discharge aids (e.g., irregular flow) occur only after a long storage time at rest and, thus, might be acceptable depending on the application.

In the case of concept 3 (see Fig. 12.32.d) some discharge aids have to be used continuously during discharge. Continuously operating discharge aids (e.g., aerated hopper and other aeration devices, vibrator) are suitable for this application. Discharge aids operating in a discontinuous way (e.g., air cannons) might result in irregular flow. Therefore, concept 3 should be used only for those bulk solids which can be handled reliably by continuously operating discharge aids. Concept 3 should not be used for bulk solids with poor flowability, pronounced time consolidation effect, or a tendency for flooding.

13 Segregation

Powders and other bulk solids tend to segregate when the particles are different, for example, in size, shape, and/or density. Most segregating materials are free-flowing or slightly cohesive so that the particles can easily separate from each other. On the contrary, the behavior of poorly flowing bulk solids (materials containing fine particles or moisture) is dominated by interparticle adhesion forces, which reduce the mobility of individual particles and, thus, the tendency to segregate.

Usually one wishes to avoid, or at least reduce segregation, since many downstream processes require a product with constant composition, for example, if the bulk solid must be filled into packages for customers in small quantities of equal composition, or if in a process (e.g., grinding or combustion) steady-state conditions can be attained only with a feed of constant composition. Furthermore, segregation can result in inaccurate volumetric dosing due to a fluctuating bulk density.

13.1 Segregation mechanisms

The processes of segregation are complex and thus cannot be predicted quantitatively. Bulk solids segregate mostly due to differences in particle size, particle density, particle shape, and/or particle surface roughness. Nevertheless it is significant for the interpretation of segregation processes to know the principles of the segregation mechanisms. Some of the observed effects, which partly have been investigated scientifically, will be described in the following. It has to be mentioned that the nomenclature of the effects and their classification is described using various terms in the literature [13.1–13.8], and that often more than only one of the mentioned effects appear simultaneously.

13.1.1 Sifting and other segregation mechanisms on inclined surfaces

If particles slide downwards on the surface of a bulk solids heap or any other inclined surface of a particle bed, smaller particles have a higher probability to be caught by a sufficiently large cavity on the surface than larger particles. Thus, smaller particles remain in the cavities whereas the larger particles predominantly slide or roll down to the base of the heap (Fig. 13.1). The surface of the heap acts similar to a sieve through which the smaller particles fall [13.1,13.9–13.11]. Thus, this effect is called sifting.

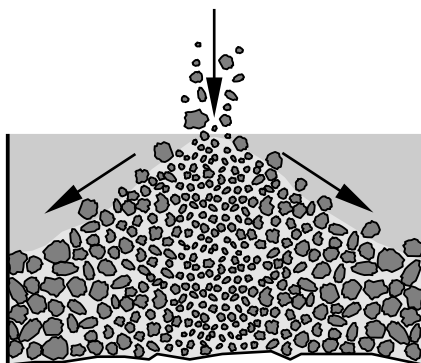


Fig. 13.1. Segregation by particle size on a heap surface due to the sifting effect (here: heap formed by central filling of a silo)

The sifting effect is the more pronounced the more the particles differ regarding their size. In the case of a small percentage of fine particles, these particles will collect close to the top of the heap. If the percentage of fine particles is significant, many of these fine particles will also reach the base of the heap. If the bulk solid contains only a small amount of relatively large particles, these particles are likely to collect at the base.

Besides the sifting effect other segregation effects take place on inclined particle bed surfaces. If some of the particles can form a larger angle of repose than other particles, the heap will be steeper in the upper part (Fig. 13.2). Particles with the larger angle of repose mainly rest in the upper, steeper part of the heap, while particles with the lower angle of repose will be found further downward [13.1]. The reasons for different angles of repose are manifold, for example:

- Sharp-edged particles form a steeper angle of repose than rounded particles (Fig. 13.2.a). Rounded particles that are large enough compared to

the other particles roll on the heap downwards. The larger the downwards rolling particles, the larger their kinetic energy, and, thus, the easier they can pass local surface irregularities and obstacles and finally reach the base of the heap [13.12].

- Fine bulk solids are poorly flowing due to the strong influence of adhesive forces. Therefore, they can form steeper heaps compared to coarse, better flowing bulk solids (Fig. 13.2.b).
- Fine, easy-to-fluidize bulk solids form flatter surfaces compared to coarse, slightly fluidizable bulk solids.

Also mass flow rate has an influence on segregation on inclined surfaces. The larger the mass flow rate, the larger the thickness of the particle layer sliding downwards on the inclined surface. Thus, fines have to move farther down before they can rest on the stationary heap surface. Therefore, more fines reach the base of the heap which results in a less pronounced segregation effect.

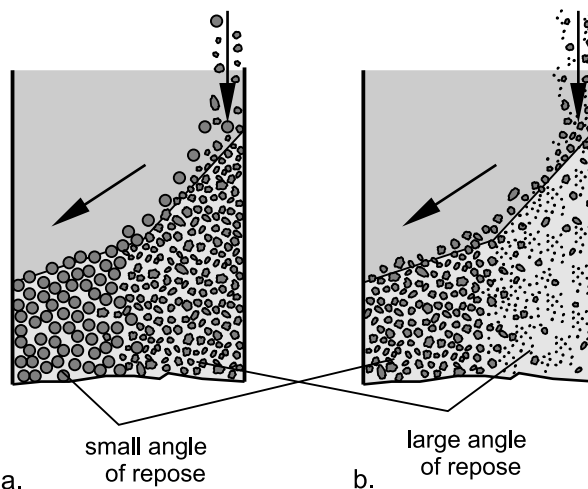


Fig. 13.2. Segregation due to different angles of repose resulting from particle shape (a) and fines content (b)

At low concentrations of coarse and heavy particles those particles sink in the bulk solids surface like meteorites (Fig. 13.3). They can form craters and will rest there causing those particles to be collected in the center of the heap. Depending on the material's properties (elasticity, damping) those particles can also jump back from the crater and will finally be found at the base of the heap [13.2,13.5].

In all instances where bulk solid is moving along repose slopes segregation has to be taken into account, for example, when filling bulk solid into a silo, a container or a package. Even in mixers with agitated containers (e.g., rotating drums) bulk solid is moving on inclined surfaces so that often an increased number of coarse particles is found at the base.

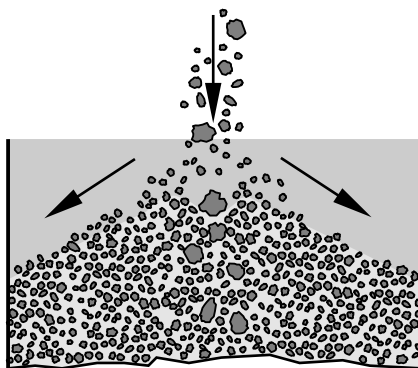


Fig. 13.3. Collection of coarse particles beneath the fill point due to the formation of a crater

13.1.2 Percolation in particle beds

If a particle bed is deformed, the particles move relative to each other. Thereby small cavities are formed between individual particles into which smaller particles can penetrate [13.1,13.13]. Since the gravity force is the dominant external force in most processes, the small particles migrate preferentially downwards within moving bulk solid layers. Also the sifting effect described in the previous section can be related to percolation. The particle movement necessary for percolation takes place in different situations, for example:

- If a container filled with a bulk solid is shaken or vibrated vertically, the particles move up and down. Small particles can enter momentarily formed gaps beneath larger particles. Thus, the large particles cannot return to their initial position. Therefore, coarse particles move upwards successively while fine particles collect at the base of the container (Fig. 13.4).
- If a pile is formed from a single point fill, avalanching might occur on the inclined surface. Thereby in the center of the heap stationary layers are formed, which become unstable with increasing thickness and thus

intermittently slide downwards like avalanches across the surface of the stationary particle bed (Fig. 13.5.a). Within the avalanche a velocity gradient and, thus, a shear deformation develop. As a result, the smaller particles migrate into the lower layers of the avalanche due to the percolation effect described above (Fig. 13.5.b). This way every avalanche forms an inclined layer of high fines concentration covered by a layer consisting primarily of coarser particles. In a vertical cut through a pile the structure of a “Christmas tree” can be recognized (Fig. 13.5.a). Since in addition to percolation with the avalanche segregation due to sifting also takes place (see previous section), more fines will be found close to the center of the pile than in the periphery.

- Segregation due to percolation can also occur within funnel flow silos, where the fine particles can percolate from the flow zone into stagnant zones (or into slower moving material) [13.2].

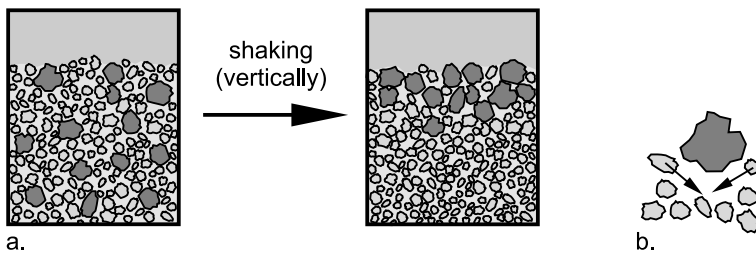


Fig. 13.4. a. Segregation due to percolation in containers shaken vertically; b. mechanism: fine particles enter gaps which form beneath coarse particles when these move upwards as a result of shaking. Thus, coarse particles are lifted successively.

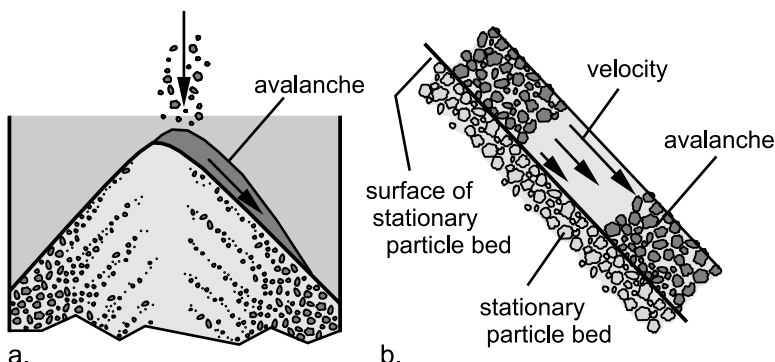


Fig. 13.5. Segregation on a pile due to percolation and sifting; a. formation of an avalanche; the bulk solid already filled in shows the structure of a “Christmas tree”; b. velocity gradient and percolation in the avalanche

The consequences of sifting and percolation are mostly determined by differences in the particle size. Particle shape is important for the segregation along heap surfaces, for example, round particles have the ability to roll. Even at particle size ratios of 1:1.3 segregation effects can be noticed [13.14]; with increasing width of the particle size distribution the segregation effect becomes stronger. In wet bulk solids and those with particle sizes below about 100 µm [13.14,13.15] the mobility of single particles is reduced due to adhesive forces thus leading to a reduced tendency for segregation. Precise statements regarding particle size are not possible, since particle size distribution and other parameters that influence flow properties are also of importance. Segregation due to percolation is distinctly noticeable when the percentage of fines is low.

13.1.3 Effect of air resistance

The velocity of a particle relative to a gas is definitely influenced by the air resistance of the particle. The ratio of air resistance to gravity force increases strongly with decreasing particle size. Thus, the steady-state settling velocity of particles in the gravity field decreases significantly with decreasing particle size (Table 13.1). This effect plays an important role even for particle sizes of 50 to 100 µm, but becomes significant at particle sizes below 10 µm. Thus, small particles suspended in a gas cannot move with noticeable velocities relative to the gas and can be easily carried away by a gas stream.

Table 13.1. Steady-state settling velocities of spherical particles under gravity in dry air at 20°C (solid density 2700 kg/m³)

Particle diameter d [µm]	Steady-state settling velocity w_g [mm/s]
1	0.082
10	8.2
25	51

If a stream of particles, for example, when filling a container, is initially directed horizontally (or in an inclined direction), different trajectories result as a function of particle size. Fine particles are more affected by air resistance than coarser particles and, therefore, fines do not travel as far as coarser particles. Also particle shape may influence air resistance. Thus, whenever a bulk solid moves with a horizontal velocity component

through a gas, segregation due to different trajectories is likely to happen. However, if the particles form a dense stream which drags gas with it, only the trajectories of particles at the edge of the stream are affected by their individual air resistance [13.2].

Figure 13.6.a shows a pile formed by discharge from an inclined chute. Due to the discussed effect of air resistance on trajectories, coarse particles will predominantly collect at the side far from the chute. Additional segregation occurs due to sifting as described in Sect. 13.1.1.

If a silo is filled from the side (Fig. 13.6.b), fines may be distributed asymmetrically in the entire silo due to the effect of different trajectories. If the coarse particles flow noticeably better than the fines, eccentric flow may take place during discharge with the effect that at the beginning of discharge primarily the coarse fraction is discharged [13.1,13.6].

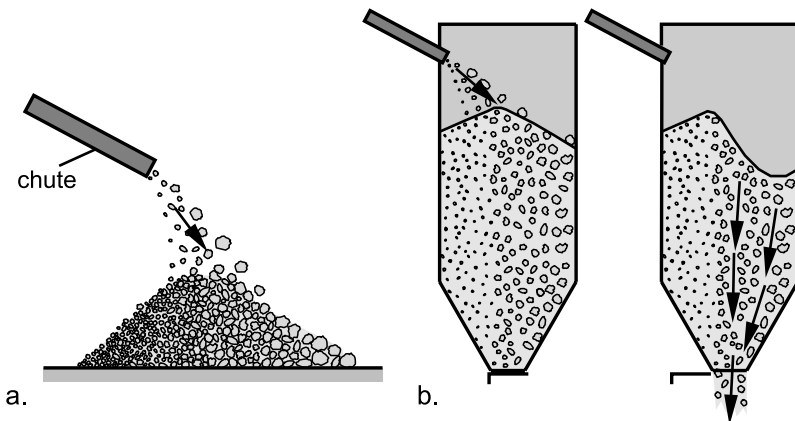


Fig. 13.6. Trajectory segregation; a. formation of a pile by discharge from a chute; b. silo filling and discharge; eccentric flow due to segregation

When material is transferred from a chute onto a belt conveyor having a different direction as in Fig. 13.7, the effect of particle size dependent trajectories leads to material on the belt being segregated over its cross-section. The segregation effect is further increased due to the situation on the chute where the fines collect close to the bottom of the chute due to percolation (Sect. 13.1.2). Since the particles close to the bottom move slower than the (coarse) particles further up, the trajectories of the fines are additionally shortened compared to those of the coarse particles [13.2,13.5].

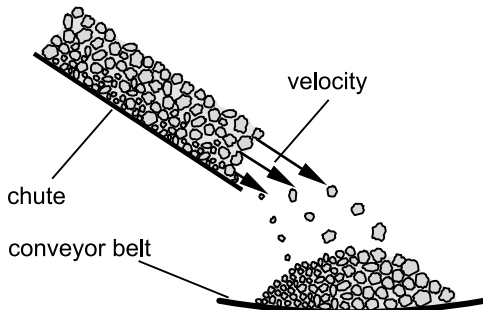


Fig. 13.7. Segregation on a belt charged from the side (conveying direction of the belt conveyor is perpendicular to the drawing plane)

The effect of particle size on settling velocity is also noticeable when charging a silo vertically from the top (Fig. 13.8). If, for example, a bulk solid is pneumatically conveyed into a bin, sufficiently coarse particles follow the gas stream down to the surface of the filling and remain there. On the contrary, fine particles (rough estimate: particles smaller than 50 ... 100 μm [13.2,13.10]) are entrained in the gas stream which is turned outward towards the walls as it approaches the surface of the material already in the bin, and finally directed upwards. Since the gas velocity is reduced towards the bin wall due to the increased cross-section of the gas stream, particles drop out and settle on the surface of the filling, so smaller particles settle more distant from the fill point. Thus, the finest particles will be deposited close to the bin wall. Sometimes it can be noticed that very fine particles adhere directly to the wall, form a particle layer, and finally fall down when the layer exceeds a specific thickness.

Even if a bulk solid is charged into a silo alone by gravity, i.e. without an air stream resulting from a pneumatic conveying system, the particle stream drags a stream of air with it. This air follows a similar path as in Fig. 13.8. This leads to the same segregation mechanism as discussed above, but the effect is less intense due to the smaller air velocity compared to charging from a pneumatic conveying system.

The distribution of fine and coarse particles over the cross-section depends on several parameters and cannot be predicted quantitatively. An important quantity is the height of the bin. If the bulk solid is blown into the silo tangentially, an increased amount of coarse particles will be deposited at the silo periphery (non-symmetrical with respect to the perimeter), whereas more fines will be found close to the silo axis. If the conveying air leaves the silo at the top through a filter vent which is periodically cleaned, an increased amount of fines will be found directly below the filter.

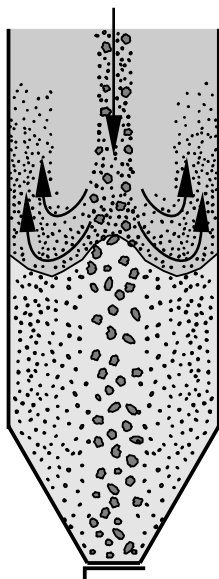


Fig. 13.8. Segregation as a result of fines being entrained in flowing air (upward air flow may result from pneumatic conveying or, in case of gravity filling, from air entrained in the particle stream)

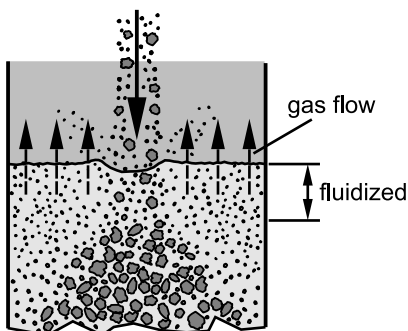


Fig. 13.9. Segregation due to a fluidized layer near the surface of the silo filling

If the bulk solid charged into a silo consists of a mixture of coarse and fine particles, and if the fines are easily fluidized, a layer of fines can remain at the surface of the silo filling (Fig. 13.9) [13.6,13.1]. This happens if the particle stream fed into the silo drags a significant stream of air with it. After the material stream has landed, the air escapes from the bulk solid. Additionally, the bulk solid already resting in the silo de-aerates due to the vertical stresses increasing with increasing filling height [13.16]. Both effects lead to an upwards flowing air stream which can be sufficient to keep

the upper layer of fines in a state of fluidization, whereby coarse particles sink downwards through the fluidized layer. Thus a higher percentage of fines accumulates near the surface. If the silo is charged periodically, several layers with fines may be generated. Contrary to all other segregation effects mentioned so far leading to segregation over the horizontal cross-section, here a vertical segregation takes place, which results in a fluctuating fines content of the discharged material.

13.2 Techniques to reduce segregation

The segregation mechanisms explained in Sect. 13.1 mostly take place when the bulk solid is moving, especially when filling, for example, a container or a bin. As an example, Fig. 13.10 shows a simple package filling process where a mixture is prepared and then filled into a transport container from which it is finally discharged in portions. The individual packages contain the predetermined composition only if the bulk solid discharged from the transport container exhibits a constant composition. However, transport containers are often provided with relatively shallow hoppers leading to funnel flow as the one in Fig. 13.10 where at first material from the center is discharged followed by material from stagnant zones at the periphery. Since most of the segregation effects discussed in Sect. 13.1 lead to transverse segregation over the cross section, the composition of the bulk solid discharged from the intermediate container varies with time.

To reduce segregation in bins, basically three strategies can be followed which will be discussed in the next sections:

- Modification of the bulk solid to reduce its tendency for segregation
- Optimization of the filling process
- Remmixing material that has been segregated during filling

If a mixture exhibits a strong tendency to segregate, an additional solution might be to produce a mixture of exactly the required mass only when it is needed. This means, for example, for the package filling process, that for each package an individual mixture has to be prepared. Since the introduction of such a procedure is a decision of process design, it will not be discussed any further.

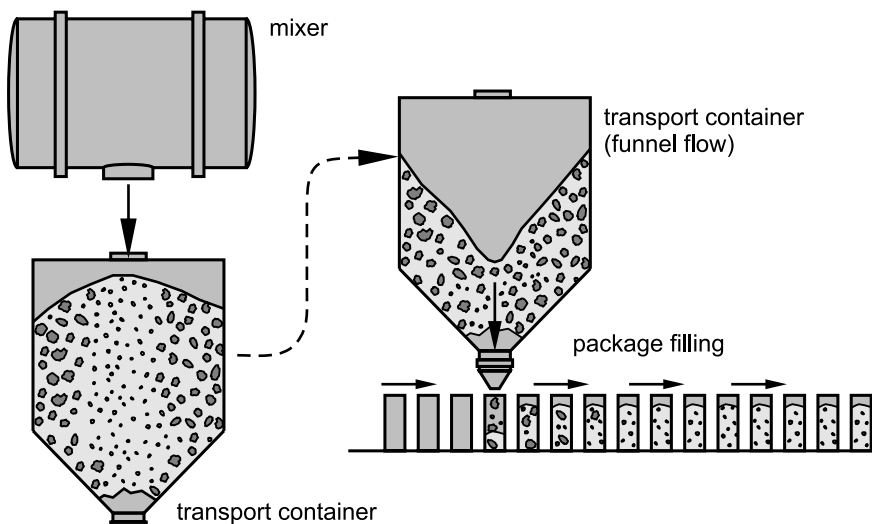


Fig. 13.10. Mixing and filling process

13.2.1 Modification of the bulk solid

It is often not possible to modify an already existent product, but during the development of new products the possibility of segregation problems should be considered and counteracted by appropriate measures. The following modifications reduce the tendency to segregation:

- Reduction of differences regarding particle size, particle shape, and particle density which are the main causes of segregation.
- Reduction of flowability by increasing interparticle adhesive forces: This reduces the mobility of the particles and thus the possibility for segregation. The adhesive forces can be enlarged by adding liquid (water, oil) or by reducing the particle sizes (having particles with sizes $< 50 \mu\text{m}$ the tendency for segregation due to sifting or percolation is remarkably reduced) [13.2,13.7]. However, these modifications are often not practical with respect to process conditions and desired properties of the end product, and may lead to flow problems due to reduced flowability.
- Compact binding of the components of the mixture, for example, due to coating of one component with another component.

13.2.2 Optimization of the filling process

To avoid segregation during charging a bin, the mechanisms described in Sect. 13.1 have to be avoided or at least reduced. Segregation due to sifting takes place when a bulk solid flows along an inclined surface of a particle bed. To avoid this, the formation of inclined surfaces such as repose slopes have to be avoided, i.e., a bin has to be charged uniformly over its entire cross-section. This can be realized with rotating chutes (Fig. 13.11.a) which are used, for example, to charge blast furnaces, where a homogeneous distribution of particles over the cross-section is essential for uniform gas flow in the particle bed. Due to the variable inclination of the rotating chute, the material can be charged to concentric rings of any diameter thus keeping the surface almost horizontal. However, this option is usually too expensive for most bins and silos. An alternative solution is a dispersion baffle (Fig. 13.11.b) which distributes the flow stream over a broader area of the bin's cross-section. For this method it is essential that the flow stream is directed vertically to the center of the baffle, and not segregated over its cross-section. Otherwise it cannot be ensured that the bulk solid is distributed in all directions both uniformly and with identical composition. If the material would be thrown on the dispersion baffle from a belt conveyor or an inclined chute as shown in Fig. 13.11.c, trajectory segregation (Sect. 13.1.3) would result above the baffle causing an inhomogeneous distribution of fines in the bin. To avoid this, the bulk solids stream could be both centered and mixed in a vertical mixing tube (similar to a static mixer) located above the dispersion baffle (Fig. 13.11.d).

When the bulk solid falls from the dispersion baffle as in Fig. 13.11.b, it can segregate in the radial direction due to different trajectories depending on particle size, shape, and density (Sect. 13.1.3) [13.1,13.2]. An additional cylindrical skirt can be used to constrain the dispersed material so that it falls downwards almost vertically (Fig. 13.11.e). Thus, trajectory segregation is widely reduced, but on the surface of the bin a ring-shaped pile is formed which is a possible source of segregation due to sifting on its repose slopes. Fines will then be found predominantly below the top edge of the annular pile, whereas coarse particles will concentrate along the vertical axis and the periphery of the bin.

Other ideas to avoid or reduce repose slopes during filling are, for example, multiple fill points through which the bin is charged simultaneously (Fig. 13.11.f), a horizontal perforated plate beneath the silo roof, which is charged from above and causes a particle rain distributed on the bin's cross-section, or traversing belt conveyors [13.1,13.2,13.17]. However, these methods can be quite expensive, and it cannot be guaranteed that the bulk solid is not segregated over the cross-section of the bin. This is espe-

cially true if a material stream, which is segregated over its cross-section, is dispersed (dispersion baffle, perforated plate) or split up (multiple fill points).

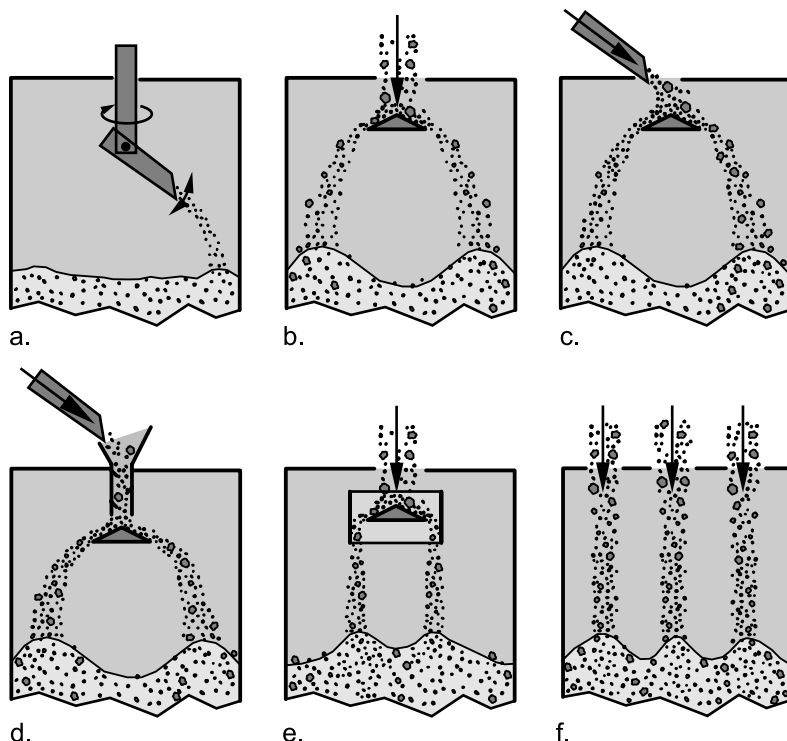


Fig. 13.11. Methods for distributed fill; a. rotating chute with variable inclination; b. dispersion baffle charged from above; c. unfavorable: dispersion baffle beneath an inclined chute; d. dispersion baffle with mixing tube beneath an inclined chute; e. dispersion baffle within a cylindrical skirt; f. multiple fill points

If a bulk solid containing particles smaller than 50 to 100 μm is subjected to a gas stream, segregation can occur due to the air resistance of the particles (see Sect. 13.1.3). To reduce this segregation, the gas velocity has to be decreased. When pneumatically conveying a material containing fine particles into a silo and going in at 90° either to the side wall or the top, segregation over the cross-section has to be expected (Figs. 13.12.a and 13.8). The situation may be somewhat better when introducing the material stream tangentially. A more significant improvement can be achieved by directing the conveying pipe upward against a deflector plate, placed in the center of the silo top, from where the material is distributed over the cross-section (Fig. 13.12.b) [13.2]. Of course, a more efficient reduction of the

gas velocity in the silo is achieved when using a mechanical conveyor instead of a pneumatic conveying system [13.18,13.19]. A similar effect can be obtained by separating particles from the air stream, for example, by a cyclone (Fig. 13.12.c), before the bulk solid is fed into the silo.

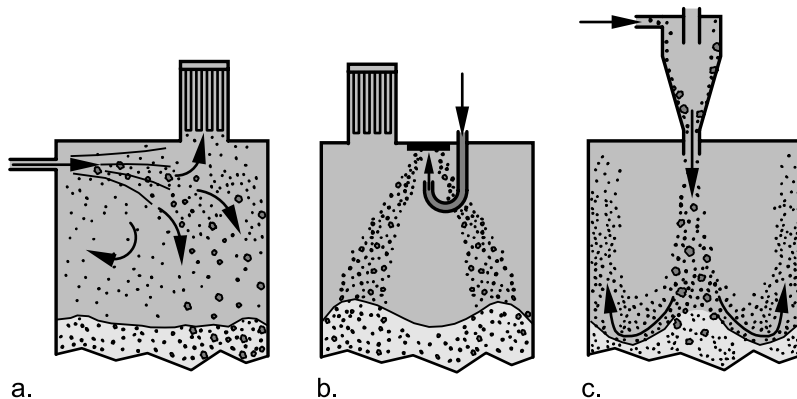


Fig. 13.12. Segregation due to the effect of air resistance when pneumatically conveying a bulk solid into a bin; a. bulk material going in at 90° to the silo wall thus segregating over the cross-section; b. reduction of segregation by directing the material stream upward to a deflector plate; c. reduction of segregation by separating particles from the air stream with a cyclone

Even if the particles are separated from the conveying air before being fed into a bin, segregation due to entrainment of particles in a gas stream can occur, but the effect is limited to smaller particles according to the dependence of the settling velocities on the particle size (see Table 13.1, Sect. 13.1.3). If the bulk solid falls, for example, from a cyclone (Fig. 13.12.c) vertically into a bin, air is dragged along with the bulk solid stream, so a gas stream is generated in the downward direction. The gas stream is rerouted on the surface of the particle bed and finally moves upward near the wall of the bin. As outlined in Sect. 13.1.3 (Fig. 13.8), the air stream causes segregation by transporting fine particles to the periphery. In this case a reduction of gas velocities within the bin can be achieved by dispersing the fill stream on a flat cone (Fig. 13.13.a). However, trajectory segregation may still occur since the particles are discharged from the cone in an inclined direction.

Another solution to reduce gas velocities is the installation of a helical slide (Fig. 13.13.b) [13.17,13.19] on which the bulk solid slides downwards relatively slowly. Thereby, less air is entrained in the material stream. Sometimes filling tubes (Fig. 13.13.c) are used to reduce segregation. A filling tube, which is provided with lateral openings similar to a

discharge tube (see Sect. 11.3.3), is charged from the top. The bulk solid then falls downwards and leaves the tube through those lateral openings which are just above the momentary filling level. This way the particle stream is diverted and decelerated. Thus, the particles in the bin may be less agitated so segregation effects based on this phenomenon are reduced. However, in [13.20] a situation is described where the installation of a discharge tube could not significantly reduce segregation (see Sect. 13.2.3).

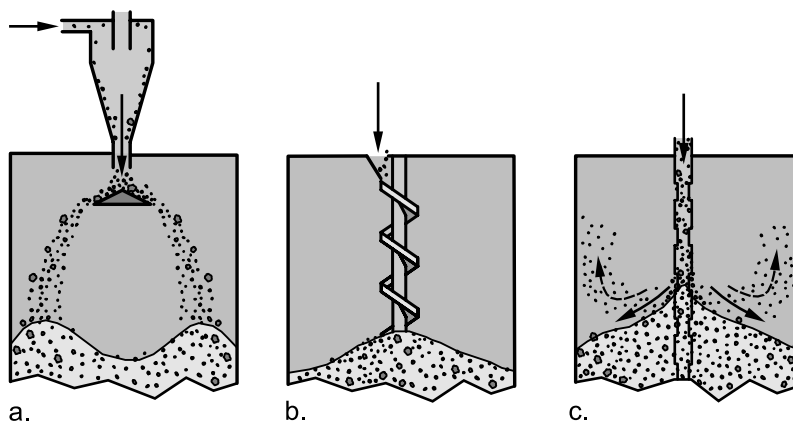


Fig. 13.13. Methods to reduce segregation resulting from the effect of air streams; a. separation of particles from the air stream with a cyclone, dispersion of the material stream on a flat cone; b. helical slide; c. filling tube

To avoid vertical segregation due to a fluidized surface layer (Sect. 13.1.3, Fig. 13.9), the bulk solid must be as deaerated as possible when charged to a bin. Thus, the bulk solid should be transferred by a helical slide (Fig. 13.13.b) rather than falling downwards. Direct feed from a pneumatic conveying line as in Fig. 13.12.a should be avoided. More favorable is a system separating the particles from the conveying air (e.g., Fig. 13.13.a), or the application of mechanical conveyors. According to [13.1], vertical segregation due to a fluidized surface layer can be reduced by accelerating the deaeration process, which decreases the height of the fluidized layer. Here a frame with vertically oriented rods is vibrated horizontally (Fig. 13.14). Thus close to the vibrating rods longitudinal voids are formed through which air can escape faster than through the particle bed.

The effectiveness of the methods to reduce segregation during filling cannot be predicted quantitatively. In each particular case one should check which of the possible means is applicable to attain the required product homogeneity which itself has to be defined for each application. However, experience suggests that apart from expensive solutions like, for

example, a rotating chute with adjustable inclination, it is often not possible to obtain the demanded product homogeneity by only applying the means discussed above. Thus, as a standard solution it has been established to accept segregation resulting from the filling process, and to remix the segregated components at the discharge process (see next section).

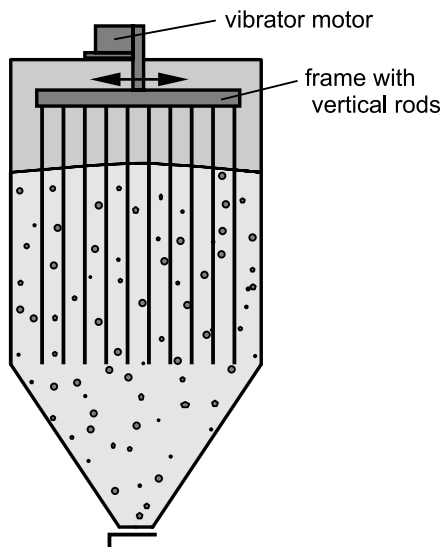


Fig. 13.14. Device for accelerated deaeration [13.1]

13.2.3 Remmixing

If materials have segregated while filling a bin, the bin has to be designed so that during discharge the segregated material is remixed. In case of segregation over the cross-section of a bin or a silo, this can be achieved with a mass flow pattern (Fig. 13.15.a) where material from the total cross-section moves towards the outlet thus being remixed. On the contrary, in case of a funnel flow pattern at first the material would be discharged which is within the flow zone developing above the outlet, whereas the material at the periphery (stagnant zones) is discharged later. Thus, funnel flow results in an unsteady, fluctuating product composition at the outlet.

In case of vertical segregation caused by a fluidized surface layer (see Fig. 13.9) a mass flow pattern does not reduce the segregation since it would lead to discharging sequential layers with fine or coarse particles.

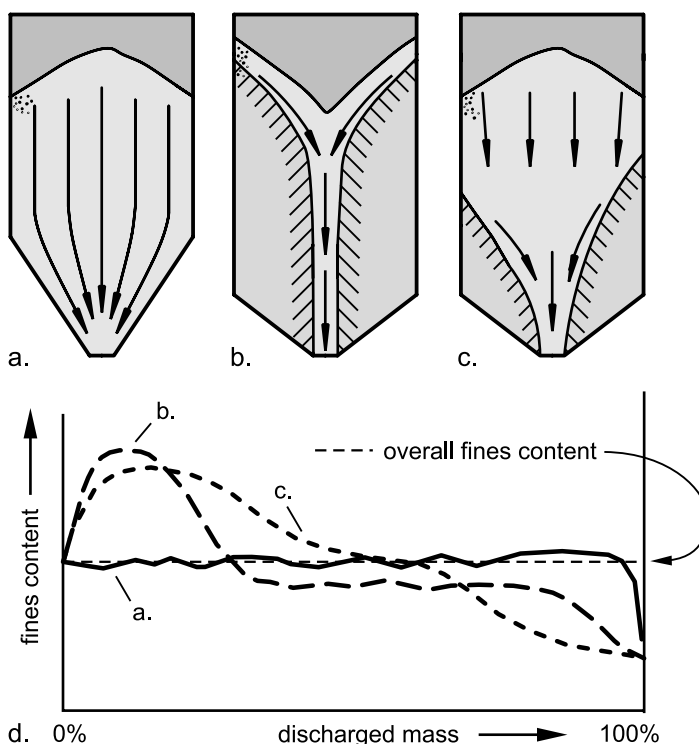


Fig. 13.15. a. mass flow; b./c. funnel flow with differently shaped stagnant zones; d. fines content vs. discharged mass during complete emptying (in principle)

The influence of the flow profile on the fines content of the discharged material is shown qualitatively in Fig. 13.15.d for the case of segregation over the cross-section of the silo (fines concentrated in the center). In the case of mass flow (Fig. 13.15.a) a relatively uniform composition of the discharged bulk solid can be expected due to remixing in the hopper. In funnel flow at first the bulk solid located close to the silo axis flows out, and the stagnant zones will be discharged later starting from the top. Depending on the shape of the stagnant zones, different behavior of the composition at the outlet can be observed (compare curves b and c in Fig. 13.15.d). For the case of a flow pattern according to Fig. 13.15.b with a narrow, steep flow zone, the stagnant zone is discharged layer by layer. Since the layers cover a large portion of the silo's cross-section, the mean fines content of each layer does not deviate very much from the overall fines content. Thus, to a certain extent remixing takes place while these layers are discharged (see long horizontal section of curve b in Fig. 13.15.d). Nevertheless, at the beginning of discharge (high fines concentration in the initial flow zone above the outlet) and towards the end (small fines concen-

tration in the region close to the hopper wall) larger deviations from the overall fines content have to be expected.

To attain mass flow, the hopper walls must be sufficiently steep and low in friction. The necessary hopper angle can be determined with Jenike's theory for silo design based on the flow properties of the bulk solid [13.21] (Chap. 10). Although mass flow is the preferable flow pattern to reduce segregation, it has to be considered that the velocity profile in the hopper as well as in the lower part of the silo's vertical section is less uniform than that in the upper part, where nearly plug flow prevails (see Sect. 10.1, Fig. 10.2), i.e. the material near the hopper walls moves slower than that in the axis. At the end of discharge, when the filling level approaches the upper edge of the hopper, the velocity profile becomes more pronounced. The reason for this is that at high filling levels the column of bulk solid in the vertical section forces the material in the hopper to flow more uniformly over the cross-section. Thus, if the silo is discharged completely, towards the end material in the center flows out faster than that near the walls, so that finally material is discharged that was initially located near the walls. For the case of the mass flow silo in Fig. 13.15.a, the latter results in a reduced percentage of fines at the end of discharge. Thus, even in a mass flow silo a certain degree of segregation can be observed, which however is small compared to a funnel flow silo. To reduce segregation resulting from the velocity profile in the hopper, the height of the vertical section should be large with respect to its diameter, i.e., a slim silo is more favorable than a squat one. Also, the silo should not be emptied completely any more often than necessary. The minimum fill level should be about 0.75 times the diameter of the cylindrical section above the top of the hopper [13.5].

The discharge device under the hopper must be designed to discharge the material uniformly across the outlet. Otherwise it may happen that at first material is withdrawn primarily from a region with, for example, an increased fines concentration due to the segregation during filling.

Moreover, a silo with only one outlet is preferable. In case of multiple outlets it is always doubtful if all outlets deliver the identical composition. This only can be achieved if the filling and the resulting segregation are absolutely symmetrical with regard to the outlet openings, and if the bulk solid is discharged from outlet openings both simultaneously and with the same discharge rate. From Fig. 13.16.a it becomes immediately clear that segregation from side to side due to unsymmetrical filling results in different compositions being discharged from both outlet openings even if the discharge rates are identical. On the other hand, if the silo is filled symmetrically but the outlets are discharged at different rates, material of different composition will appear at the outlets, because the flow velocities of the

bulk solid being different at the outlets are equalized further up in the silo. Thus, material from a larger part of the silo's cross-section flows towards the outlet discharged at a higher rate (Fig. 13.16.b).

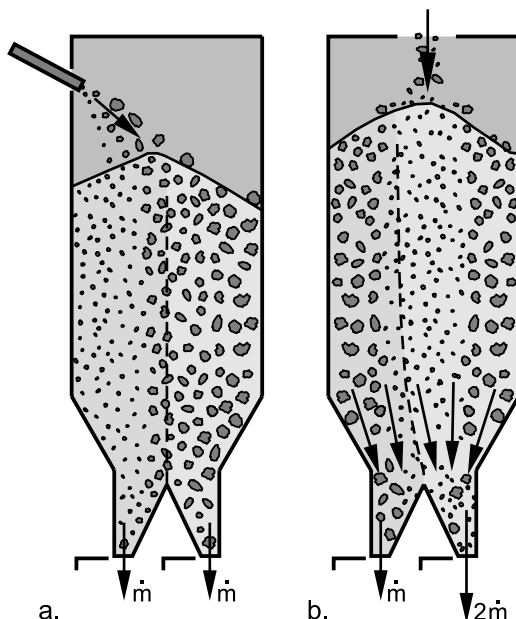


Fig. 13.16. Silo with two outlet openings; a. unsymmetrical filling, symmetrical discharge; b. symmetrical filling, unsymmetrical discharge

Mass flow can also be achieved with a cone-in-cone insert, the so-called Binsert® (Sect. 11.3.2, Fig. 11.12.a) [13.22,13.23]. For this application the hopper of the silo does not have to be as steep as in the case without the inner cone. Thus, the inner cone is also an appropriate means to turn funnel flow hoppers causing segregation problems into mass flow hoppers. Whether an existing hopper can be modified this way can be decided based on the flow properties of the bulk solid.

A mass flow pattern is the most reliable means to reduce segregation. Since mass flow can only be achieved in steep hoppers, due to reasons of economy and available space sometimes easier, less expensive solutions to influence the flow profile are sought.

A typical approach is place an inverted cone within the hopper (Sect. 11.3.1.2, Fig. 11.11.b). Such an insert enlarges the diameter of the flow zone of a funnel flow silo, but a mass flow pattern is usually not attained. The enlarged flow zone contains material from a larger portion of the cross-section, at first glance promising more favorable conditions for re-

mixing in the first sequence of the discharge process. But since stagnant zones are likely to exist in the silo, at the end of the discharge process material will appear at the outlet which was initially located near the silo walls and, thus, may have a composition much different than the overall composition of the silo contents. A general assessment of the efficiency of an inverted cone insert is not possible, since its effect depends not only on the formation of stagnant zones, but also on the distribution of the segregated components. An improvement is likely to be noticeable when stagnant zones almost disappear due to the insert (see measurements reported in [13.24]). If this cannot be ensured, the insert will likely have little effect on the reduction of segregation (see later in the present section) [13.20].

Discharge tubes (see Sect. 11.3.3) can also help to reduce segregation. A discharge tube is placed vertically above the outlet and provided with lateral openings (Fig. 13.17). While discharging the silo, material flows only near the surface of the silo filling and within the discharge tube. Thus, the discharge tube leads to funnel flow which is normally said to be unfavorable regarding segregation. But since the flow zone is defined by the discharge tube and, thus, small compared to the cross-section of the silo, the silo is discharged through the discharge tube in layers from top to bottom. Measurements on silos with discharge tube [13.24,13.25] have shown that deviations from the overall composition mostly occur at the beginning and end of discharge, when the silo is completely emptied. When the discharge process is started, the material initially located within the discharge tube and within a conical region above the discharge tube is discharged (regions A and B). Towards the end the material resting near the hopper walls is discharged (region D). If, for example, segregation with respect to particle size takes place and the silo is center filled, coarse particles rest predominantly near to the silo wall. Thus, compared to the overall composition, the concentration of fines is higher in regions A and B, and lower in region D. Since region C is discharged successively from top to bottom, coarse particles from the periphery and fine particles from near the discharge tube are remixed so that the composition of the discharged material does not deviate much from the overall composition. However, since the material moves over the inclined surface of the stationary material below while discharging region C, segregation due to sifting cannot be excluded.

If a discharge tube is used to reduce segregation, the ratio of silo height to silo diameter should be as large as possible, and the diameter of the discharge tube should be small compared to the silo diameter in order to keep regions A, B, and D small with respect to the silo volume.

Comparing the means to reduce segregation by remixing, it follows that the most satisfactory effect can be expected from a mass flow pattern. Inverted cone inserts and discharge tubes can reduce segregation, but often

not to the same extent and less predictable, and, if not properly designed, they might be ineffective [13.20,13.24].

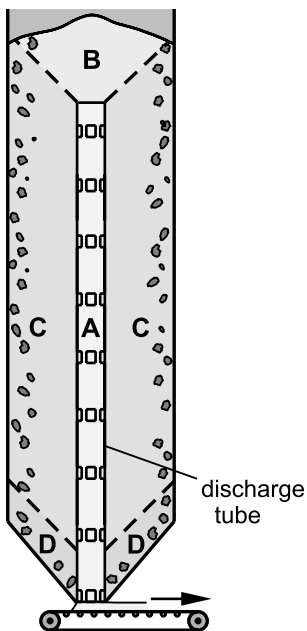


Fig. 13.17. Funnel flow silo with discharge tube; sequence of discharge: A, B, C, D [13.25]

A full-scale investigation of the segregation of plaster (fine-grained bulk solid, approx. 30 % $> 90 \mu\text{m}$) showed the effect of different means for the reduction of segregation [13.20]. Loading silos (diameter 3200 mm, height of vertical section 11700 mm) exhibiting a funnel flow pattern and leading to segregation had been modified in different ways. Figure 13.18.a shows the original shape of the silos. The variant in Fig. 13.18.b is provided with an enlarged outlet opening and a bin activator. The enlarged outlet opening increases the diameter of the flow zone, which is done in Fig. 13.18.c by an inverted cone insert. Another variant is equipped with a filling tube (Fig. 13.18.d; see also Fig. 13.13.c) and pneumatic discharge aids located at the hopper walls. Furthermore, a mass flow hopper was designed based on the flow properties of the plaster (Fig. 13.18.e). Since the hopper slope required for mass flow is rather steep, a discharger with a large diameter (bin activator) is used to limit the height of the hopper.

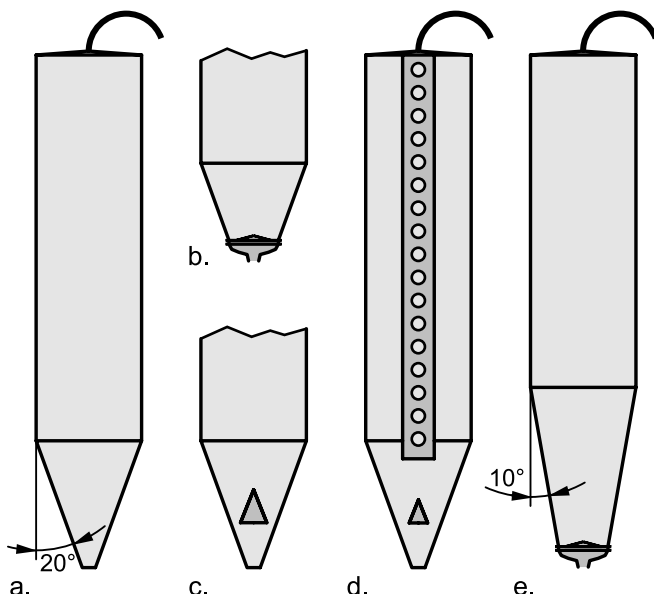


Fig. 13.18. Investigated variants of loading silos for the storage of plaster [13.20]; a. original funnel flow silo; b. funnel flow silo with bin activator; c. funnel flow silo with inverted cone insert; d. funnel flow silo with filling tube and pneumatic discharge aids (not shown); e. mass flow silo with steeper hopper

The original silo (Fig. 13.18.a) was charged from a pneumatic conveying line in two steps, first at an intermediate position in the cylindrical section, then from the top. As a result of the relatively small particle size, segregation was due to the entrainment of particles in air currents according to Fig. 13.8 leading to an increased amount of fines near the wall. In Figure 13.19 the sieve residue on 90 µm (i.e., the fraction of particles > 90 µm) is plotted versus the discharged mass. The original silo exhibits typical behavior of a funnel flow silo: At the beginning primarily material initially located near the silo axis (more coarse particles) is discharged, followed by that from near the silo wall (more fine particles). The peak in the plot at about 60 tons results from the change of the fill point from the intermediate position to the top.

The variants presented in Figs. 13.18.b to d did not lead to much improvement. Since funnel flow still prevailed, the material initially resting close to the wall was discharged latest. Also the filling tube could not avoid the problem of an increased concentration of fines at the silo wall. Only with the mass flow silo (Fig. 13.18.e) could a sufficiently constant composition of the discharged bulk solid finally be achieved. Towards the end of emptying an increase of the fines (decrease of residue on 90 µm)

can be detected probably being caused by the velocity profile in the hopper (as previously discussed in the present section) in combination with the increased fines concentration near the silo wall.

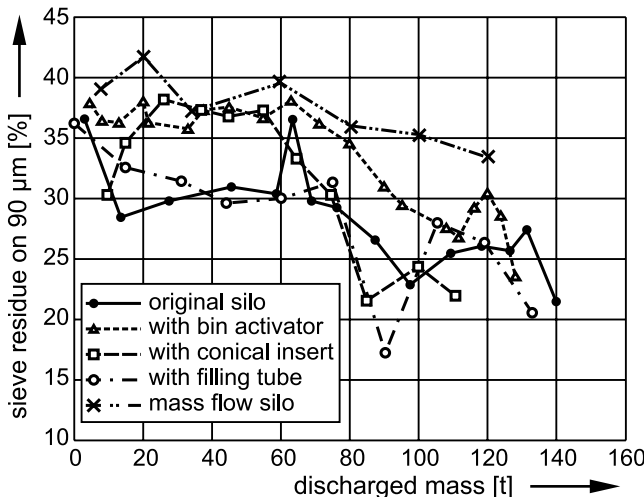


Fig. 13.19. Results of segregation tests on full-scale silos [13.20]: sieve residue on 90 μm vs. the discharged mass (complete emptying). Note: the mean value of the sieve residue on 90 μm of the total mass varied slightly from test to test

13.3 Sampling

When samples are taken to assess the composition of a bulk solid and to find evidence of segregation, the common guidelines for sampling have to be adhered to [13.26, 13.27]:

- The samples must be large enough to contain a sufficient number of particles of each component. Only then is a statistically reliable statement possible.
- If a sample is too large for analysis, it must be reduced into smaller representative samples but it is imperative that the sample used for analysis be representative of the initial sample. For an accurate reduction, devices like, for example, rotating sample dividers should be used. In no case should a reduced sample be taken for analysis from the initial sample at an arbitrary position, for example, from the top, because segregation is likely to occur also in the sample container.

- If a sample is taken from a bulk solids stream, possible segregation perpendicular to the flow direction has to be taken into account. This is demonstrated by Fig. 13.7: If a sample is taken from only a part of the bulk solids stream supplied from the chute, it contains either a too high or a too low percentage of fines due trajectory segregation. The situation at the discharge of the belt conveyor is even more complex, because the material on the belt is segregated from side to side and probably also top to bottom. Thus, a sample which is not taken from the entire cross-section of a bulk solids stream is worthless.
- If the concentration of a material stream is fluctuating, samples have to be taken in sufficiently short time intervals. Otherwise one cannot detect fluctuations of higher frequencies.

13.4 Final remarks

Whenever a bulk solid flows or is transported, handled or processed, segregation may occur. Particularly significant are the effects emerging while filling bins or containers.

In principle, the tendency of a bulk solid to segregate can be reduced by modifying the product, but this, however, is often limited or just impossible with respect to costs and the required product properties. The means to avoid segregation while filling a bin are restricted, unpredictable regarding their efficiency, and sometimes too expensive. Thus, as a standard solution, a bin should be designed so that the segregated components are remixed while discharging the bin. Therefore, in most cases a mass flow pattern is the optimal solution.

14 Silo quaking and silo honking

14.1 Phenomenon

The flow of bulk solids in silos can be accompanied by dynamic pulsations and self-excited vibrations [14.1]. The frequency of the pulsations can be larger than 1 Hz; sometimes vibrations in the audible range (> 20 Hz [14.2, 14.3]) occur where the amplitudes are low [14.4]. The latter is called silo noise, silo honking or silo music: The noise often appears intermittently with a sound similar to that of a truck horn. Distinct shocks appearing at irregular intervals of seconds to hours can also occur, which are called silo quaking or silo thumps. Depending on the properties of the ground supporting the silo, shocks can spread out far into the surroundings. Thus, silo quaking and silo honking can affect the environment (Fig. 14.1), are unpleasant for personnel nearby and can damage a silo structure.

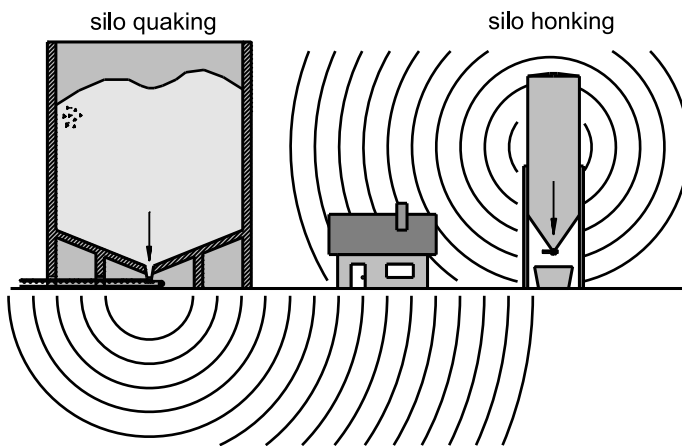


Fig. 14.1. Silo quaking and silo honking

As will be explained in the following the reason for silo quaking and silo honking is the sudden acceleration and subsequent deceleration of a suffi-

ciently large mass of bulk solid. For reasons of simplification all mentioned effects – including vibrations – will be summarized as shocks.

Probably many silos exhibit shocks of more or less intensity. Those phenomena are called silo quaking or silo honking only if they are so strong that people become aware of them. Not every bulk solid will excite severe shocks, which have been observed mostly with hard, brittle and coarse grained bulk solids (maize [14.5,14.7], corn [14.1,14.4,14.5,14.7, 14.8], cement clinker [14.5,14.6,14.9], coal [14.1,14.4,14.8,14.10–14.13], iron ore [14.4,14.14], rape seed [14.2], polymer-granules [14.15–14.18], sand [14.19,14.20], salt [14.8]), but also with some fine-grained materials (cement [14.18], fly-ash [14.21], starch [14.18]). Silo honking appears in combination with shocks and was found, for example, with polymer granules and starch [14.14–14.18].

Silo shocks may be due to many different mechanisms, most of which have been neither sufficiently investigated nor completely understood. Therefore, no standard solutions are available to avoid them. In the following sections known phenomena are described, explained and classified, whereby the slip-stick effect will be considered as being an important prerequisite for shocks. In some cases the latter may lead to interpretations being different from statements found in the literature.

14.2 Shocks as a result of sudden flow

Shocks are originated by bulk solids regions which suddenly start to flow (acceleration) and just as suddenly are stopped (deceleration). Those regions can be a relatively small part of the contents of squat silos (Fig. 14.2.a) or a large part of the contents of slender silos, where the bulk solid may flow across the entire cross-section of the vertical section (Fig. 14.2.b). The inertia force due to the deceleration of the bulk solid is mostly responsible for the effect of a shock on the silo structure or the surroundings, respectively. This force, which is acting mostly downwards, depends on the mass of the decelerated bulk solid and the strength of the deceleration mechanism. In general, the larger the filling mass and filling level, the larger masses are accelerated and decelerated, i.e. appearance and strength of silo shocks increases with silo dimensions and filling height, respectively (e.g., [14.1,14.4,14.6,14.14,14.22]). Strong shocks can occur especially in tall silos with a large ratio of height-to-diameter, because during acceleration the bulk solids column in the vertical section is moving downwards like a plug whereby only wall friction has to be overcome, i.e., no deformation takes place within the bulk solid. Thus, only a small part of

the available energy is dissipated in friction, and the strength of the shocks increases exponentially with filling height [14.8].

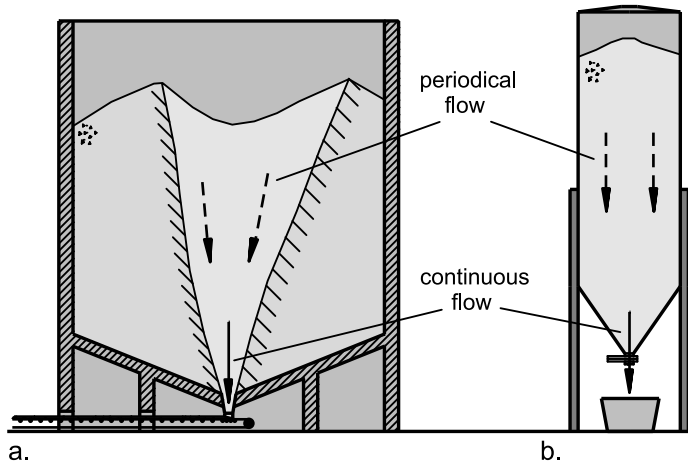


Fig. 14.2. Bulk solid regions suddenly moving downwards; a. squat silo with large cross-section; b. slender silo

In Fig. 14.3 the typical pattern of a silo's supporting force during a shock is plotted qualitatively. If a part of the silo filling suddenly starts to move downwards, it is subjected to inertia forces acting upwards thus reducing the silo's supporting force. At the subsequent impact on the (resting or slower flowing) bulk solid further down the moving material is suddenly decelerated leading to large inertia forces acting downwards. The result is a pronounced peak in the supporting force.

To put it simply, the strength of the deceleration mechanism depends on the stopping distance of the bulk solid. The stiffer the bulk solid (e.g., like the hard, brittle bulk solids mentioned in Sect. 14.1), the smaller the stopping distance and, thus, the larger the inertia forces acting downwards. With fine-grained, compressible bulk solids the deceleration is less strong and, as a consequence, the inertia forces are smaller. However, it must be considered that fine-grained bulk solids are increasingly compressed with increasing consolidation stress. Therefore, a fine-grained bulk solid becomes stiffer and less compressible when stored under higher stresses. Thus, such a bulk solid (e.g., cement) can exhibit shocks when stored in a huge silo where large stresses prevail, whereas the same bulk solid would flow without any shocks in a small silo.

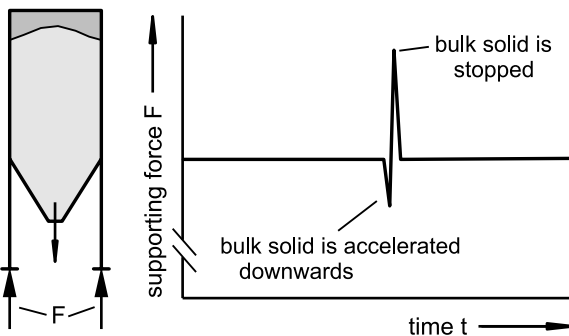


Fig. 14.3. Supporting force, F , vs. time during a shock (qualitatively)

Also the silo honking effect typically occurring in tall, slender metal silos (Fig. 14.2.b) originates from shocks within the bulk solid. Investigations on a silo filled with plastic pellets [14.16,14.23] have shown that the honking sound resulted from the vibration of the silo structure at its eigenfrequency of 292 Hz, excited by individual shocks over a period of a few seconds.

As simple as it is to identify irregular, intermittent flow as being the reason for silo quaking, it is difficult to find clear explanations why flow suddenly starts, or why pulsating flow occurs. Neglecting vibrations that are originated by a feeder at the outlet area of a silo (see Sect. 14.6.2), in principle it can be observed that material within a silo flows intermittently (e.g., upper part of the flow zone in Fig. 14.2.a; contents of the silo's vertical section in Fig. 14.2.b), whereas near the outlet continuous flow takes place. Intermittent flow can mean sudden flow periods with pauses in between (e.g., [14.6]), continuous pulsating flow (e.g., [14.24]) and, as a combination of both, pulsating flow only within certain intervals (e.g., [14.16,14.23]). In the following sections some explanations are presented that are based on the available literature and the author's experience (further surveys see [14.4,14.25,14.26]).

14.3 Sudden flow and pulsating flow caused by slip-stick friction

In the literature of the last few years the slip-stick effect is increasingly seen as the source of shocks in silos. If slip-stick takes place, the bulk solid flows in an intermittent, sometimes jerky, non-continuous manner due to the change between “stick” and “slip” periods. The slip-stick process is

explained in Sect. 7.1.1 where it is stated that two conditions have to be fulfilled for slip-stick to occur [14.27,14.28]:

1. Material behavior: The friction must decrease with increasing relative velocity (simplified: sliding friction must be smaller than static friction).
2. System behavior: The system must allow vibrations (e.g., sufficiently small damping, ability to store a sufficient amount of elastic energy).

When slip-stick friction has already been observed while measuring flow properties in a shear tester, it can be assumed that the bulk solid fulfills the first condition, and the system “bulk solid in the shear tester” fulfills the second condition. Whether shocks will occur with this bulk solid in a particular silo cannot be deduced from this because the second condition must also be fulfilled in the system “bulk solid in the silo”. When on the other hand no slip-stick friction is observed in a shear test, slip-stick in the silo cannot be excluded, because the system “bulk solid in the shear tester” may not allow vibrations (second condition not fulfilled), whereas the system “bulk solid in the silo” may allow vibrations.

In case of slip-stick friction (either within a bulk solid or between a bulk solid and an adjacent wall) stresses build up in the stick phase leading to a sudden accelerated movement after the static friction has been overcome (slip). Depending on the boundary conditions individual shocks as well as periodic shocks (vibrations) are possible. Different mechanisms where slip-stick plays a role are explained in the following sections.

14.4 Shear zones in silos

To understand the reasons for shocks in silos it is important to look closer at the flow mechanisms within a bulk solid. In a mass flow silo being discharged uniformly across the outlet the typical velocity profile shown in Fig. 14.4 develops. At a sufficient distance from the hopper almost plug flow prevails in the vertical section; however, close to the wall, depending on the wall roughness, a more or less pronounced shear zone may develop (e.g., [14.23]) where the velocity decreases somewhat towards the wall (not visible in Fig. 14.4).

In the mass flow hopper the vertical velocity (averaged over a long time period) is maximum in the center and minimum in the vicinity of the inclined hopper walls. The larger the friction at the hopper wall, and the closer the hopper inclination to the mass flow boundary, the more non-uniform the velocity profile. The velocity distribution in the hopper can

also be found in the lower part of the vertical section, where it is transferred into plug flow with increasing distance from the hopper. The height of this transition region is typically about 0.7 to 1.0 times the diameter of the vertical section, D .

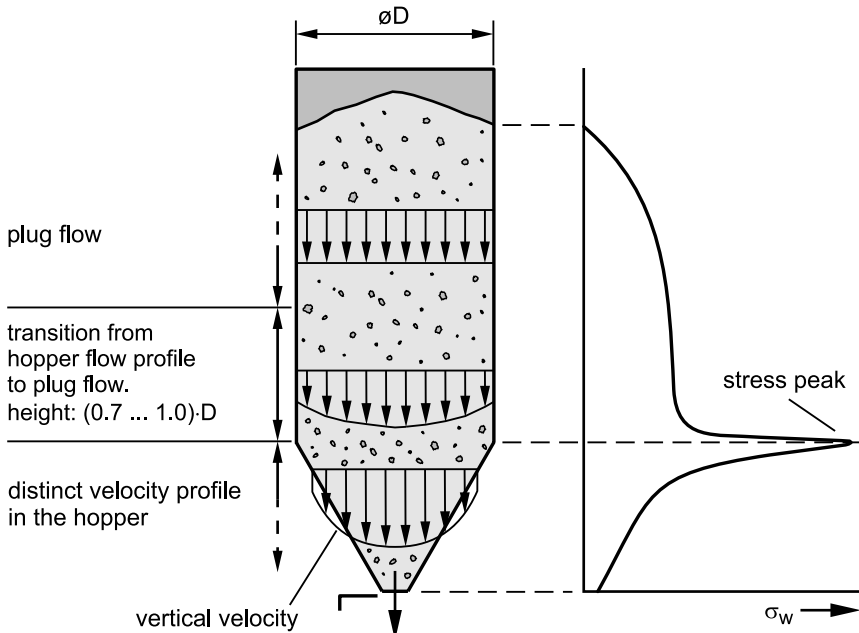


Fig. 14.4. Wall normal stress, σ_w , and distribution of vertical velocity (averaged over a longer period of time) in a mass flow silo (qualitatively)

In reality flow of a bulk solid in a hopper is more complex than it might appear from the averaged velocities in Fig. 14.4. Due to the converging cross-section of the hopper, shear deformations take place in the bulk solid when flowing downwards. Besides the hopper inclination, the wall friction angle also affects the shear deformation since a larger wall friction angle leads to larger differences of velocities and, thus, results in larger shear deformation.

If a bulk solid is subjected to a large shear deformation, the shear zone concentrates in limited regions (localization of the shear zone, e.g., [14.29], see Sect. 5.2). This also happens in the hopper of a silo. The effect was established by X-ray investigations where a hopper of a silo was radiographed while being discharged [14.30–14.32]. Shear zones could be identified which could be distinguished from the adjacent non-deformed zones by lower X-ray absorption due to their smaller bulk density (Fig.

14.5.a). The smaller bulk density in the shear zones results from dilation which is necessary for the particles to move across each other (Sect. 5.2.3).

The shear zones move downwards with the bulk solid, and the regions between the shear zones move as blocks parallel to the adjacent hopper wall. The momentary vectors of the velocities of the blocks between the shear zones are represented in Fig. 14.5.a by arrows (v). These vectors were estimated based on the movement of lead shot markers which had been positioned in the bulk solid prior to the test [14.30]. As qualitatively indicated in Fig. 14.5.a, the momentary velocity distribution is not symmetrical with respect to the hopper axis.

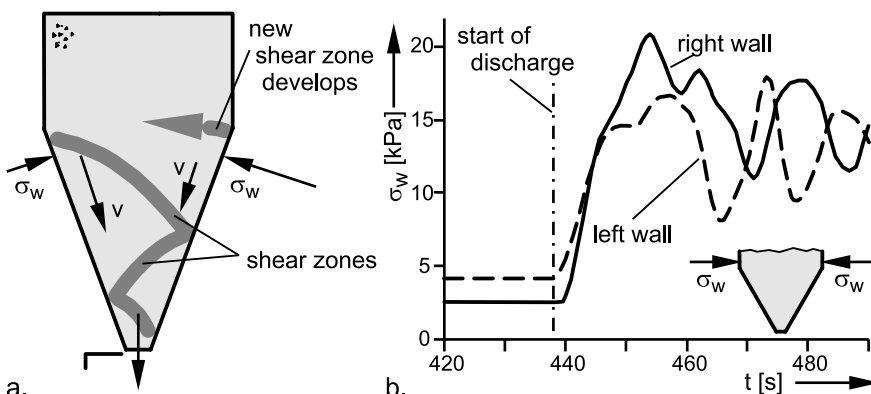


Fig. 14.5. Example of shear zones determined experimentally in a wedge-shaped mass flow hopper inclined at 20° from vertical (according to Fig. 5.b in [14.30]); a. momentary wall normal stress, σ_w , in the upper hopper area and velocities, v , depicted qualitatively (length of the arrows); b. measured wall normal stress, σ_w , at the lower edge of the vertical section as a function of time, t (similar silo shape as in Fig. 14.5.a; results according to Fig. 40 in [14.25]).

Shear zones can turn inactive on their way downwards, i.e., shear zones which have been formed at the transition from the vertical section to the hopper do not necessarily remain shear zones when approaching the outlet [14.32]. While material is discharged from the silo, again and again new bended shear zones are created at the transition from the vertical section to the hopper, expand towards the silo interior, and move downwards. Experiments on wedge-shaped hoppers have shown that there is a preference for the shear zones to be formed intermittently right and left, whereby their shape changes randomly [14.30]. The development of a new shear zone at the transition from the vertical section to the hopper goes along with a temporary increase of wall normal stress in this region (see arrows in Fig. 14.5.a which qualitatively represent the wall normal stress, σ_w) [14.25],

14.30]. In Fig. 14.5.b the wall normal stresses measured on another model silo with a wedge-shaped hopper are plotted versus time [14.25]. The stresses at the left and right walls of the vertical section a short distance above the transition show a fluctuating pattern with the maximum stress occurring intermittently on the left or the right side which indicates the formation of shear zones according to Fig. 14.5.a. The frequency of shear zone formation is proportional to the mass flow rate [14.25,14.33]. During further discharge the shear zone forming at the right side of the silo in Fig. 14.5.a will grow until being developed completely. Thereafter the next shear zone - this time starting on the left side – will be formed and the process outlined above will proceed in a mirror-image pattern.

Following the above arguments it can be stated that during discharge shear zones are formed intermittently which goes along with intermittent variations of local stresses and velocities. The pattern of shear zones can be more complex than depicted in Fig. 14.5.a (see [14.30–14.32]). In conical hoppers it has to be assumed that the shear zones are curved in all three dimensions.

In mass flow silos, shear zones develop not only within the bulk solid, but also between the bulk solid and the walls (of hopper and vertical section). Thus shear deformation of the bulk solid near the wall depends on wall friction. In case of a sufficiently small wall friction angle the bulk solid near the wall may move across the wall surface without being sheared internally. However, in the following all these situations are called shear zones at the wall. In Fig. 14.6.a the regions of possible shear zones in a mass flow silo are depicted according to the above considerations.

Regions of shear deformation in funnel flow silos are shown in Fig. 14.6.b. Shear zones within the bulk solid have to be expected in the converging part of the flow zone. Additionally, a shear zone develops between the stagnant zone and the flow zone. If the boundary between the stagnant zone and the flow zone meets the wall, and the filling level above the stagnant zone is sufficiently high, the material of the flow zone moves across the wall of the vertical section. Shear zones between bulk solid and silo wall prevail only in this region.

The fact that shear zones are formed is not sufficient for shocks to occur. But if at the same time the conditions for the appearance of slip-stick are fulfilled, shear deformation in the shear zones will not be smooth and regular, but jerky and accompanied by strong accelerations. If thereby large masses of bulk solid are moved, noticeable shocks are created.

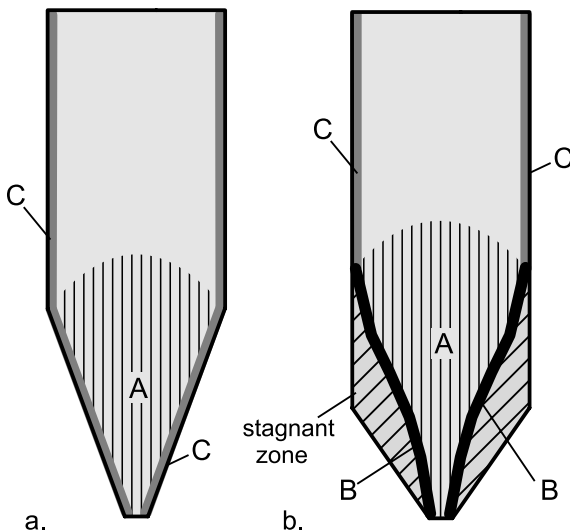


Fig. 14.6. Regions where shear zones can occur; a. mass flow silo; b. funnel flow silo (A: region of shear zones within the flowing bulk solid; B: shear zones at the boundary between stagnant zones and flow zones; C: shear zones at the wall; note that the hatch patterns do not represent the orientation of shear zones)

14.5 Silo shocks due to slip-stick friction

14.5.1 Shear zones in flowing bulk solid

Shocks and vibrations in mass flow silos, which are assumed to be caused by shear deformation within the bulk solid, are documented in several publications [14.1,14.4,14.12,14.13,14.22,14.25]. In mass flow silos the shear deformation takes place mostly in the hopper and in the lower part of the vertical section (Sect. 14.4).

If bulk solid is discharged from a mass flow hopper, shear zones develop within the hopper (shear zones A in Fig. 14.6.a). Having slip-stick friction, a relatively large stress must first build up along a shear zone before static friction is overcome and, thus, further (plastic) shear deformation can take place, i.e., the material in the shear zone can flow further. Since even at the occurrence of shocks the bulk solid is flowing continuously through the outlet opening, the following situation results [14.22, 14.25]: Below a certain region (e.g., region X in Fig. 14.7.a) the bulk solid flows, but above this region in the first instance the material remains stationary because in region X one or more shear zones exist, in which the

static friction has not yet been overcome. Thereby the stationary material will be supported less and less by the continuously flowing material below. Consequently the stresses in the flowing material decrease. The stationary bulk solid is supported increasingly by the silo walls (hopper and vertical section), thus leading to an increase of stresses in this region. Finally the stresses are sufficiently large to overcome static friction in the shear zones in region X. Thus, a sudden movement of the bulk solid above the considered region is initiated so that the bulk solid rapidly drops downwards and subsequently is just as suddenly decelerated by the material below (Fig. 14.7.b). The deceleration is then felt as a thump or a shock (see Sect. 14.2) and leads to compression of the bulk solid as well as to an increase of the stresses (even below region X). If then, due to the deceleration process, flow is stopped above a certain level (e.g., region X), the complete cycle will repeat.

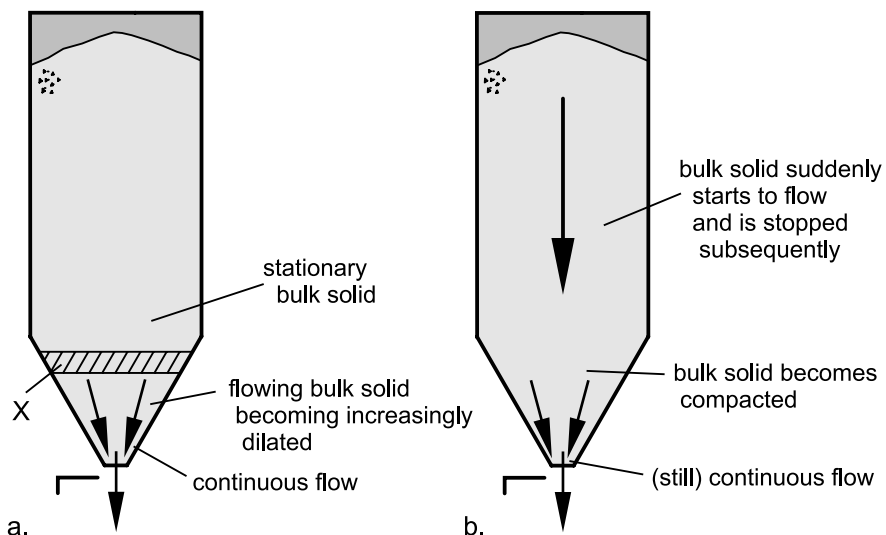


Fig. 14.7. Simplified model describing a shock cycle in a mass flow silo due to slip-stick friction within the bulk solid (region X); a. before a shock; b. during a shock

The further up in the hopper the region X where the shocks are initiated, the larger the shocks resulting from the described cycle. This statement is supported by the following reasons:

1. Stresses in the hopper increase upwards. At the transition from the vertical section to the hopper a stress peak also exists (Fig. 14.4). Thus, when static friction is overcome and the slip process starts,

more elastically stored energy can suddenly be released in the upper hopper region than in the lower hopper region to accelerate the bulk solid.

2. Bulk density increases in the hopper in the upward direction (as the stress). Thus, further up the bulk solid is stiffer. This results in a stronger deceleration and, thus, larger inertia forces.
3. Further up in the hopper the cross-sections are larger. Thus a larger mass of bulk solid is suddenly accelerated when static friction is overcome, and thereby the effect of the bulk solid above the shear zone is stronger.
4. A sudden acceleration of the bulk solid in the lower part of the hopper, which is less intense following the statements in the three paragraphs above, at first initiates flow in the hopper. When flowing in the hopper, the bulk solid is deformed horizontally due to the converging cross-section which results in the formation of the shear zones discussed in Sect. 14.4. Since the latter results in a certain damping effect and energy dissipation, it is likely that a sudden movement originated in the lower hopper region does not extend into the vertical section or initiates only a moderate movement of the material in the vertical section.
5. If a sudden movement of bulk solid in the lower hopper region is not sufficient to increase the stresses above this region to such an extent that static friction is also overcome there, the sudden movement cannot extend upwards. In this case the shock results from the deceleration of only a relatively small mass of bulk solid and, thus, is weak.
6. A sudden movement in a shear zone in the region of the transition from vertical section to hopper is particularly intense (see paragraphs 1 to 3) and leads directly to a sudden drop and a subsequent deceleration of the bulk solid in the vertical section which must overcome only the wall friction. Thus, in this case the most intense shocks of the silo have to be expected.

Measurements on a model silo [14.25] have confirmed that strong shocks occur especially when they are initiated in the region of the transition from the vertical section to the hopper, and when the filling level in the vertical section is large. For this case Fig. 14.8 qualitatively shows how the stresses change during a shock cycle. Directly after a shock the wall normal stresses in the hopper are relatively large. Then the stresses decrease with time starting from the bottom end of the hopper. The latter is demonstrated by the stress pattern measured between two shocks, where the stresses in the bottom part already have reached the values they had before the shock, while further up the stresses are still close to the values measured directly

after the shock. At the same time the wall normal stress measured at the lower edge of the vertical section has enlarged a bit. Thus the bulk solid will be supported less and less from below and has to be supported more and more by the walls of the vertical section. Finally the static friction in a shear zone in the region of the transition from the vertical section to the hopper is suddenly overcome. Thus, the bulk solid suddenly drops and is subsequently decelerated which causes a shock. Stresses in the hopper increase, whereas stresses on the wall of the vertical section decrease slightly.

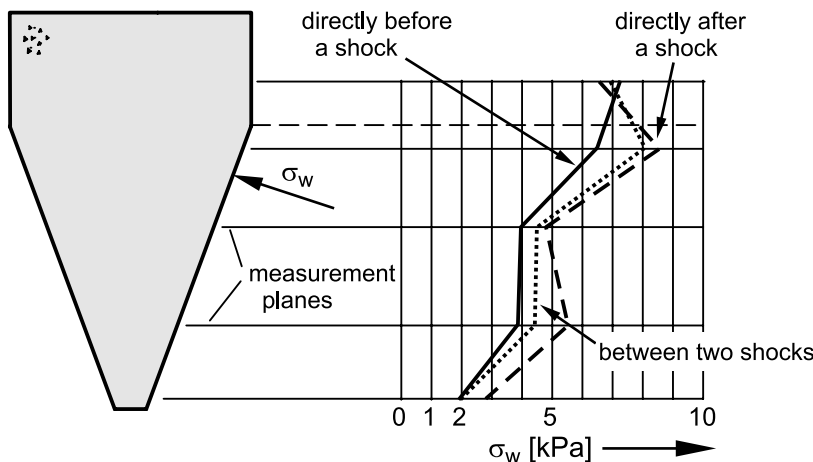


Fig. 14.8. Distribution of wall normal stress, σ_w , immediately before a shock, after a shock, and after half of the period between two shocks (taken from graphs in [14.25]); measured during discharge; vertical section was full.

In the literature similar models can be found where the region of the transition from vertical section to hopper is considered as being the reason for the shocks. In [14.4] the formation of rupture planes is claimed to be the reason for periodic stress variations. In [14.1,14.12] it is assumed that the bulk solid in the vertical section is less and less supported by the bulk solid in the hopper up to the point where it suddenly drops and, thus, initiates a shock. Also here it has to be expected that slip-stick is the precondition for the sudden acceleration of the bulk solid.

Test results [14.25] show that the intensity of shocks decreases with decreasing filling level. But even if the filling level falls into the hopper section, shocks (of low intensity) still occur. Thus it is demonstrated that in principle shocks can be initiated by shear zones located anywhere in the hopper; however, at low filling levels the shocks are weak and hardly noticeable in the surrounding. Another result of the tests in [14.25] is that the

conditions in the vertical section do not have a strong influence on the shocks: Neither increased wall friction nor inserts in the vertical section could reduce the shocks significantly or even avoid them. Thus it may be concluded that the shocks discussed in the present section result from the flow of the bulk solid in the hopper.

If sudden flow is initiated by the bulk material in the hopper as discussed above, the bulk solid in the vertical section follows whereby flow starts at the bottom of the vertical section and then propagates in the upwards direction, in that an acceleration wave [14.25] (unloading wave in [14.20]) travels up the material in the vertical section (Fig. 14.9). A deceleration wave follows [14.25] (compression wave in [14.20]) when the bulk solid is brought to a halt from the material below. The peak values of the deceleration wave are larger than those of the acceleration wave and increase in the vertical section from bottom to top [14.20]. The velocity of the waves is dependent, for example, on the stress, silo dimensions, wall friction, and the bulk solid itself. Measured wave propagation velocities range from 75 m/s [14.20] to 150 m/s [14.25]. It has to be mentioned that the statements in [14.20] and Fig. 14.9 apply for the case of shocks as a result of slip-stick friction at the wall of the vertical section (see Sect. 14.5.3.2), but the result is the same as discussed in the present section, namely the suddenly downwards moving bulk solid in the vertical section. Thus, similar situations can be expected here.

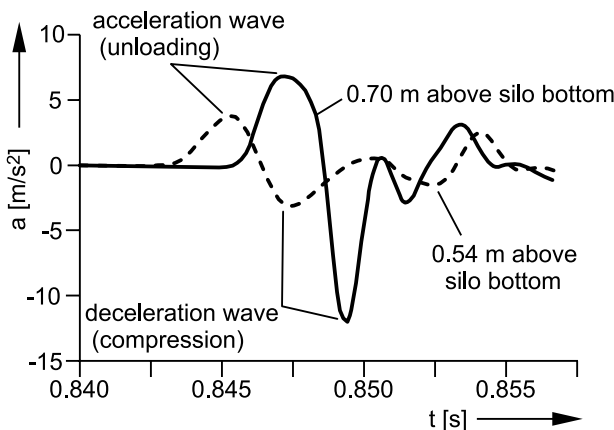


Fig. 14.9. Acceleration, a , of bulk solid during a shock; measured at two different levels, z , in the vertical section of a model silo according to Fig. 14.14.a [14.20]; positive accelerations act in direction of gravity.

The more intense the shear deformation of the bulk solid in the hopper, the more probable the occurrence of shocks based on shear zones within the

bulk solid. Model tests [14.4] have shown that a hopper that is in a borderline mass flow condition (i.e., the combination of hopper slope and wall friction angle is very close to the mass flow boundary; see Sect. 10.3.1) exhibited mass flow with a pronounced velocity profile and very small velocities at the wall. This situation led to regular shocks. With reduced wall friction the hopper exhibited a more uniform velocity profile being equivalent to a lower shear deformation in the bulk solid. No shocks were detected in this situation.

In [14.10] shocks in a silo storing coal which was discharged with an en-masse feeder are reported. Due to the design of the en-masse feeder the coal was mostly discharged from one end of the outlet slot (Fig. 14.10). Thus a non-uniform velocity profile was established in the silo. Due to the large differences in vertical velocity, v (see velocity distribution observed at section A), the bulk solid was subjected to large shear deformation. In a simplified view, at least one inclined zone of intense shear deformation was formed between the faster and slower flowing bulk solid. This inclined zone was considered as the origin of the shocks [14.10]. To reduce the shear deformation, the en-masse feeder was redesigned to achieve more uniform withdrawal. After the modification no shocks were observed. Obviously, the reason for the shocks was the large velocity gradient in the flowing bulk solid.

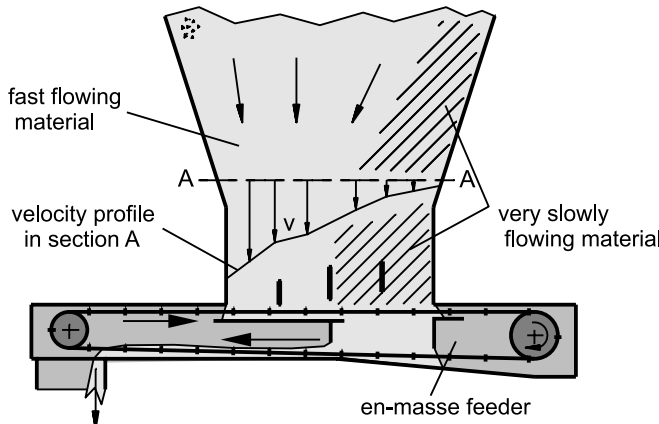


Fig. 14.10. Velocity profile (velocity v) due to non-uniform withdrawal by an en-masse feeder [14.10]

Silo quaking resulting from the effect described in the present section can also occur in funnel flow silos. When the boundary between the stagnant zone and the flow zone meets the silo wall in the lower part of the silo, as is shown in Fig. 14.6.b, a transition from a cylindrical flow zone to a con-

verging flow zone is formed. The situation at this transition is similar to that at the transition from the vertical section to the hopper of a mass flow silo. In the hopper shear zones are formed similar to the situation in a mass flow hopper (shear zones in region A, Fig. 14.6.b). Additionally, intense shear deformation takes place at the boundary between stagnant zone and flow zone (shear zones B, Fig. 14.6.b) being further possible sources for shocks.

For the shocks being described here and in the following subsections of Sect. 14.5 it holds that the time from incident to incident certainly can vary randomly, but the average time (with respect to many shocks) often is inversely proportional to the mass flow rate (e.g., [14.5,14.6,14.20,14.22, 14.25]). This relationship can be explained by the fact that the deformation of the bulk solid is proportional to the discharged mass. Thus, if a silo shock problem is investigated, it is more useful to know the mass discharged between two subsequent shocks than to know the time [14.25]. If the discharge rate is increased to very high values, the individual shocks can be transformed into a vibration of the system “silo with bulk solid” whereby the frequency is independent of the mass flow rate [14.24,14.25].

14.5.2 Unstable stagnant zones (funnel flow)

In a funnel flow silo only the bulk solid in the flow zone is moving, whereas the rest of the bulk solid remains stationary and forms stagnant zones. Typical reasons for funnel flow are too shallow or too rough hopper walls (Sect. 10.3.1), eccentric discharge due to inappropriate feeders or hopper/feeder interfaces (Sect. 12.3), or obstacles protruding into the silo (Sect. 11.2.2).

Stagnant zones can be unstable, i.e., it can happen that material from a stagnant zone suddenly starts flowing thus leading to a shock. This is equivalent to shear zones B (Fig. 14.6.b) occurring suddenly in the region of a stagnant zone. Even a sudden movement of the material across the hopper wall is possible. Different situations are described in the following subsections.

14.5.2.1 Hopper slope close to critical hopper slope for achieving mass flow

In Fig. 14.11 a funnel flow silo is shown where the hopper walls are slightly shallower than required for mass flow to occur. When, after filling, the bulk solid is initially discharged, at first a flow channel is formed where the material flows downwards. Depending on the flow properties of

the bulk solid, and also on the silo shape, filling method, momentary filling level, and other parameters, the shape of the flow zone will be more or less converging.

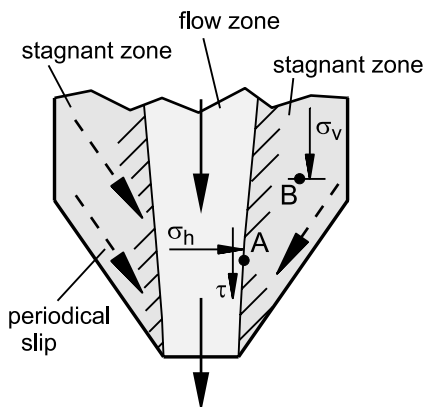


Fig. 14.11. Shocks due to sudden flow of stagnant zones across the hopper wall; at point A the flow zone exerts horizontal stress, σ_h , and shear stress, τ , onto the stagnant zone. At point B vertical stress, σ_v , is acting.

While discharging the silo, the bulk solid is moving downwards in the flow zone and is supported through normal and shear stresses (depending on the shape of the flow zone) by the stagnant zones (see point A in Fig. 14.11). Due to this support, the vertical stress, σ_v , in the stagnant zone is likely to increase (e.g., at point B in Fig. 14.11), whereas the stresses in the flow zone (e.g., the horizontal stress, σ_h) decrease. Thus, the bulk solid in the stagnant zone is subjected to an additional stress in the vertical direction, but less support in the horizontal direction. As a possible result of these modified stress conditions, the bulk solid in the stagnant zone will slip down the hopper wall. If additionally the static friction at the wall is significantly larger than the kinematic friction, the bulk solid in the stagnant zone will start to move suddenly due to the sudden release of stored energy (see explanations on sudden flow due to slip-stick friction, Sects. 14.3 and 7.1.1).

As a result of the sudden flow of the stagnant zone, the bulk solid in the flow zone is compressed and the bulk solid coming from the stagnant zone is decelerated more or less rapidly. Depending on the strength of the deceleration and the mass of the decelerated material, a more or less intense shock (thump) takes place as a result of inertia forces. At further discharge this cycle repeats: The compressed bulk solid in the flow channel supports the stagnant zones. With decreasing stresses and increasing dilation in the

flow zone the horizontal support decreases etc., and finally another shock will arise [14.1,14.4,14.11,14.13,14.14,14.34].

14.5.2.2 Unstable shape of stagnant zones

Shocks due to a sudden change of the flow profile can also arise in a funnel flow silo where slipping on the hopper wall is not possible, for example, in a silo with very shallow or rough hopper walls, or in a flat bottom silo. In a funnel flow silo, especially when storing free-flowing bulk solids, the stagnant zones are unstable. Due to the effects discussed in Sect. 14.5.2.1 (decreasing horizontal support of the stagnant zones), stagnant material may enter the flow channel more or less intermittently while the slip planes (shear zones) are within the bulk solid. Due to the acceleration and subsequent deceleration of the bulk solid shocks can be originated. In principle this effect is the same as that described in Sect. 14.5.2.1, but with the difference that here only a part of the stagnant bulk solid begins to move, and the material does not slip directly on the hopper wall.

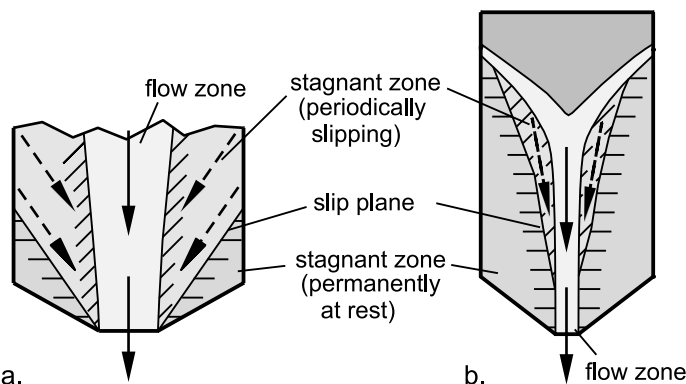


Fig. 14.12. Sudden flow of parts of stagnant zones; a. nearly the entire stagnant zone starts slipping; b. only a small part of the stagnant zone starts slipping

Two examples are shown in Fig. 14.12. In the case of Fig. 14.12.a at first only the bulk solid inside the flow zone moves downwards. Due to decreasing horizontal support and increasing vertical stress in the stagnant zones (Sect. 14.5.2.1), finally almost the entire contents of the silo begin to move by sliding down a slip plane (shear zone) within the bulk solid. This compacts the material in the flow zone, with the result that the moving material suddenly decelerates thus causing a severe shock.

In the case of Fig. 14.12.b only a small part of the stagnant zone is unstable. The resulting shocks will be stronger the greater the mass of bulk

solid that is accelerated and then decelerated intermittently. Therefore, for the case of Fig. 14.12.a more severe shocks are to be expected than for the case of Fig. 14.12.b

Stagnant zones can also be caused by protrusions into the flow channel, mismatched flanges, partially opened slide gates (Fig. 14.13), or feeders which do not discharge the bulk solid across the entire outlet opening (see Sect. 11.2.2 and 12.3.1). In some publications [14.4,14.14,14.34] it is argued that in the lower parts of the stagnant zones very large stresses (“excessive pressure concentration”) prevail being responsible for noticeable shocks. The large stresses in the stagnant zones are generated by the flowing bulk solid which exerts normal and shear stresses to the stagnant zones (see explanations in Sect. 14.5.2.1 regarding Fig. 14.11). Thereby the stresses in the flow zone decrease.

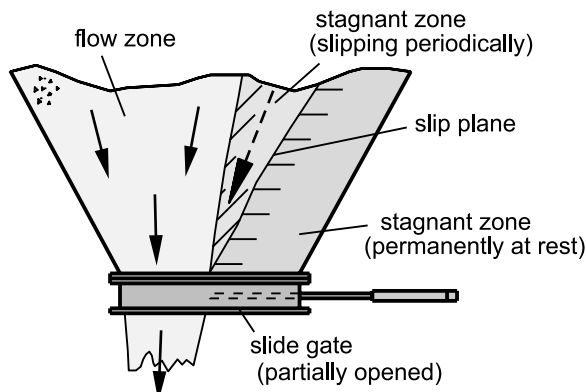


Fig. 14.13. Unstable stagnant zone above a slide gate that is only partially opened

Due to the high vertical stress in the stagnant zone – which is equivalent to high stored energy in this area – material from the stagnant zone can suddenly start to flow in the direction toward the adjacent flow zone (see Fig. 14.13). As described in Sect. 14.5.2.1, the flow zone will be compacted and the bulk solid which just had started to move is then stopped. This sequence can occur occasionally but also be repeated intermittently resulting in vibrations of the silo [14.4,14.14,14.34].

14.5.3 Flow at the silo wall

14.5.3.1 Hopper

In funnel flow the hopper walls are covered by stagnant zones. Thus, no flow takes place on the hopper walls as long as the filling level is suffi-

ciently high (only close to completely empty some material may slide across the walls). An exception to this is the effect described in Sect. 14.5.2.1.

The combination of bulk solid and wall material may lead to slip-stick friction in the vertical section as well as in the hopper. Since in several silos slip-stick in the vertical section has been found to be the reason for shocks [14.16,14.19,14.20, 14.23,14.24], it has to be assumed that in this case slip-stick friction simultaneously occurring in the hopper is less important. The reason for this is probably that, due to the complex flow situation in the hopper (Fig. 14.5), the effect is limited to individual blocks of bulk solid being separated by shear zones. In contrast to this, plug flow prevails in the vertical section so that a relatively large mass of bulk solid suddenly starts flowing at “slip” and is stopped subsequently thus leading to an equivalent large shock (see next section).

14.5.3.2 Vertical section

If the filling level in the vertical section above the hopper (and above the stagnant zones in funnel flow, respectively) is sufficiently high, nearly plug flow prevails during discharge (Fig. 14.4), i.e., the bulk solid in the vertical section moves downwards with an almost uniform velocity over the cross-section. Thus, the relative motion between the bulk solid and the wall (shear zone C in the vertical section, Fig. 14.6) plays an essential role regarding the occurrence of slip-stick.

If a silo is discharged, one expects that the material moves downwards in the hopper as well as in the vertical section. However, if slip-stick friction occurs at the walls of the vertical section, the bulk solid in the vertical section can move downwards only after the static friction at the wall is overcome, i.e., when the shear stress at the wall is sufficiently large. As long as this has not been achieved, the bulk solid in the vertical section is decreasingly supported from below since the bulk solid in the hopper is continuously flowing downwards. As a result the gravity force of the bulk solid in the vertical section is increasingly supported by friction at the vertical walls (shear stress). Thus, the shear stress at the vertical walls increases. After static friction has been overcome, the shear stress at the wall decreases according to the lower kinematic friction and, thus, only a part of the weight of the bulk solid in the vertical section can be supported by wall friction. The remaining part of the weight accelerates the bulk solid so that the bulk solid in the vertical section suddenly moves downwards and is subsequently stopped (decelerated) by the bulk solid below (the movement of the bulk solids in the vertical section is discussed in Sect. 14.5.1 and takes place here in a similar manner). The deceleration results in a se-

vere shock, due to which the bulk solid in the hopper is also compacted. Then it takes some time before the bulk solid in the hopper is dilated again (due to the continuing discharge), the support for the bulk solids column in the vertical section decreases again, and the next shock occurs. This mechanism is similar to the one discussed in Sect. 14.5.1 (Fig. 14.7), where slip-stick friction within the bulk solid is assumed as a source of shocks, whereas here slip-stick friction at the wall is considered.

The explanation in the previous paragraph is based on the idea that slip-stick friction at the wall of the vertical section leads to shocks without any influence of the flow process in the hopper. This idea is proven by measurements with the model silo shown in Fig. 14.14.a. The bulk solid (sand) within a hollow cylinder made from perspex is supported by a piston. While the piston is slowly moving downwards, severe shocks occur due to the jerky motion of the bulk solid [14.19,14.20]. The acceleration, a , measured in the bulk solid during deceleration increases exponentially with distance, z , from the piston (Fig. 14.14.b). The shock period, T , i.e., the time between two shocks, is inversely proportional to the velocity of the piston (Fig. 14.14.c). Similar results have been achieved with a larger model silo which was equipped with a hopper [14.20].

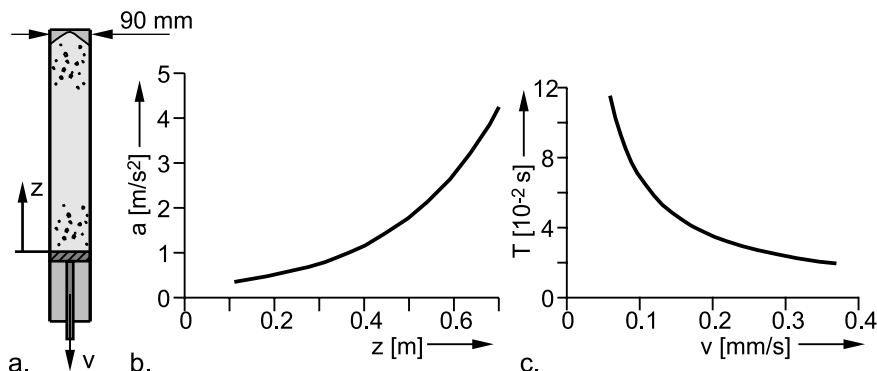


Fig. 14.14. a. Set-up for investigation of shocks induced in a cylindrical silo [14.19,14.20]; b. maximum acceleration, a , of the bulk solid during deceleration as a function of distance from piston, z (total height of the bulk solid column is about 0.8 m) [14.20]; c. shock period, T , as a function of piston velocity, v [14.20]

In another investigation [14.24] model silos with a cylindrical section (made from different wall materials), flat bottom and central outlet opening were used. The silos were resting on supporting springs so that the stiffness of the support and thus the eigenfrequency of the system “silo/bulk solid” could be varied. The investigations have shown that depending on the boundary conditions (eigenfrequency of the system, bulk

solid, wall material) the frequency of the shocks can be identical to the eigenfrequency of the filled silo (structural resonance); however, it can also be different from this value (in this case the silo follows the shocks induced by the bulk solid). Thus, the shocks and vibrations, respectively, are not only based on the structural resonance of the silo [14.24]. The shocks which resulted from slip-stick friction at the silo wall did not occur with all investigated combinations of bulk solid and wall material. Also Tejchman [14.16,14.23] observed shocks in a cylindrical model silo made from perspex. The shocks could be reduced to a large extent by increasing the roughness of the internal surface of the cylinder by lining it with sand paper or other materials with a rough surface structure. Even these results indicate that the reason for shocks is the slip-stick friction between bulk solid and wall.

In [14.16,14.23] Tejchman describes detailed investigations of silo shocks and silo honking occurring in aluminum silos storing polymer granulates (Fig. 14.15.a). During discharge at a rate of 12 t/h intense shocks were observed every 7 seconds. The shocks excited the silo structure to vibrate at its eigenfrequency of 292 Hz, whereby each shock resulted in a short, decaying honking sound. The filling level had no influence on this frequency, but honking only occurred at a sufficient filling level (in a similar silo the minimum filling level in the cylindrical section for honking to occur was about twice the cylinder diameter, but shocks could even be detected at smaller filling heights [14.18]). Measurements of the vertical strain, ε_v , of the cylinder wall (Fig. 14.15.b) show that vertical compression slowly increases before a shock and suddenly decreases to about 80 % of its maximum value during a shock. This result is in line with the mechanism explained at the beginning of this section. The shear stresses directed downwards on the silo wall increase up to the point where static friction is overcome. Due to increasing shear stresses the cylinder wall is increasingly stressed and, thus, increasingly compressed vertically. After static friction has been overcome, the lower kinematic friction immediately prevails. Just as suddenly both the vertical stress in the cylinder wall and the vertical compression are reduced. Acceleration measurements [14.16,14.23] showed extreme upward accelerations of the silo wall (above 500 g at level A; g = acceleration due to gravity; these accelerations decrease upwards), but the vertical displacement was only 0.02 mm to 0.04 mm [14.16] (Also if static friction is overcome only in a section of the cylinder wall, the wall may be accelerated upwards. As in a chain reaction this might lead to lower kinematic friction in other regions of the cylindrical section). Simultaneously with the upward acceleration the silo wall is also accelerated towards the interior (> 50 g at level A). Due to the acceleration the silo wall is caused to vibrate which in turn causes the honking

sound. The vibrations and the honking sound, respectively, decay within about 0.15 seconds.

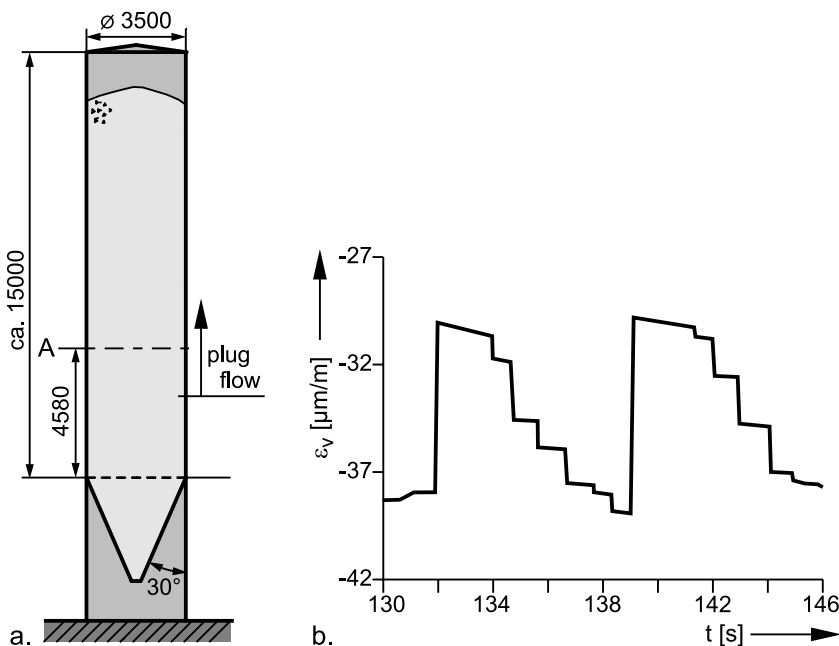


Fig. 14.15. a. Silo for storage of polymer granulates [14.16,14.23]; assumed plug flow region; b. vertical strain, ε_v , of the cylinder wall at level A vs. time measured before the silo was modified (data taken from [14.23] and smoothed by the author by omitting superimposed oscillations. Negative values of ε_v represent compression of silo wall; all dimensions in millimeters).

In the above mentioned investigations on a model silo [14.24] silo honking was also observed, which was found to be driven by the pulsating motion of the bulk solid and associated with resonance of the air column above the bulk solid bed. The frequency of the audible vibrations was in accordance with the resonance frequency of the air column above the particle bed and, therefore, was dependent on the filling level; however, the sound frequency was different from both the pulsation frequency of the bulk solid and the eigenfrequency of the silo. Whether silo honking, which is occurring in silos of industrial dimensions, results from the resonance of the air column above the bulk solid bed would be an interesting question for future research. However, even if silo honking due to the vibration of an air column was observed in [14.24], the author believes that the silo honking effect observed in practice can be explained plausibly by the mechanism described in Fig. 14.15.

Shocks (and associated honking) occurring at intervals of a few seconds have been observed in several aluminum silos storing polymer granulates (PET) [14.17, 14.18]. The silos were similar to that shown in Fig. 14.15. In one of the silos [14.17] the honking frequency was 330 Hz, and the vertical acceleration of the silo wall more than 400 g. The honking frequency was independent of filling level which is contrary to the assumption in [14.24] according to which the honking frequency should be dependent on the height of the air column above the bulk solids surface. Thus it is likely that the silo noise found in model tests [14.24] is caused by a different mechanism than silo honking found in real silos (e.g., [14.16, 14.17, 14.23]).

Based on the observation that shocks could be avoided by an increased roughness of the walls of the vertical section (see above), the silos shown in Fig. 14.15 have been modified [14.16, 14.23, 14.35]. The vertical section was provided with aluminum waffle sheets (roughness on the order of the particle size of the bulk solid) riveted to the interior surface, but it turned out that it was sufficient to line only the region marked in Fig. 14.16. In this region the most intense accelerations of the silo wall had been observed. With the modification the shocks were reduced and the associated silo honking was eliminated. Due to the large roughness at the silo wall a noticeable shear zone of a thickness of 0.15 m to 0.20 m was formed [14.16, 14.23].

If it is assumed that the shocks observed in the silo of Fig. 14.15 are caused by slip-stick friction at the cylinder wall similar to the other examples mentioned above [14.17, 14.19, 14.20, 14.24], increased roughness of the cylinder wall has the following effects:

- The region of the cylinder wall where slip-stick friction occurs is reduced.
- The region where plug flow has to be expected is reduced (Fig. 14.16). Since in the case of mass flow plug flow starts at some distance above the hopper (see Fig. 14.4), a plug of height about 10 m (Fig. 14.15.a) can be expected in the unmodified silo. After the modification the rough wall leads to a more pronounced velocity profile. Thus, plug flow may only be achieved at some distance above the waffle sheets, i.e., the plug is limited to the top part of the bulk solid in the vertical section and its height is only about 5 m (Fig. 14.16). In this region the normal and shear stresses are lower and the bulk solid is less compacted.
- If it is assumed that the shocks are caused in the plug flow region by slip-stick friction at the cylinder wall, the effect may be clearly reduced by decreasing the height of the plug flow region: The strength of the shocks becomes smaller because of, for example, the smaller accelerated mass, increased damping due to a reduced bulk density, reduced

stress level, and reduced absolute difference between the shear stresses of static and kinematic friction. The vertical force in the cylinder wall and, thus, the vertical compression of the cylinder wall exhibit only small changes after modification compared to the significant changes observed prior to modification (Fig. 14.15.b). Furthermore, at level A no significant vertical acceleration could be measured after the modification [14.16], i.e., in the lower part of the cylindrical section the wall was no longer excited to vibrate, and further up the excitation was considerably reduced. Near the silo no silo honking could be detected. However, measurements of sound pressure inside the silo (above the bulk solid) showed similar pressure maxima before and after the modification [14.16]. This leads to the conclusion that after the modification shocks still appeared in the upper part of the cylindrical section.

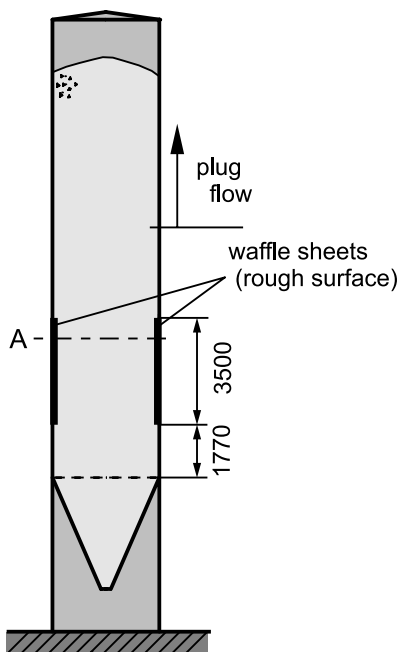


Fig. 14.16. Silo for storage of polymer granulates after modification [14.16, 14.23, 14.35]; assumed plug flow region (dimensions in millimeters)

It has to be noted that Tejchman [14.23] assumes, contrary to the explanations above, that shocks are not based on slip-stick friction but on stress fluctuations which are generated at the silo bottom and propagate upwards as stress waves. In the case of smooth walls the fluctuations are transmitted

to the silo wall whereas in the case of rough walls they are damped by the shear zone near the wall.

14.5.4 Combinations of different mechanisms

In the preceding sections each type of shear zone according to Fig. 14.6 is considered as being solely responsible for the occurrence of shocks. However, a combination of reasons is also possible. For example, in a mass flow silo slip-stick friction may take place within the bulk solid (hopper) as well as at the wall of the vertical section. In this combination a shock in the hopper could prompt static friction at the wall of the vertical section to be overcome, which could result in severe shocks possibly accompanied by silo honking. Unstable stagnant zones may also occur in combination with slip-stick friction at the wall of the vertical section. Likewise shocks in the flowing bulk solid combined with changeable stagnant zones and, should the occasion arise, also slip-stick friction at the wall of the vertical section could appear simultaneously.

14.6 Shocks and vibrations due to other reasons

14.6.1 Large discharge rate with respect to outlet size

Bulk solids can be discharged continuously from a silo (i.e., “steady state”) up to a specific mass flow rate. Larger mass flow rates initiate a pulsating discharge (Sect. 12.1), especially if the outlet dimensions are close to the critical dimensions to avoid arching [14.4]. The reason for the pulsating flow is the formation of arches, which only develop for a short time and collapse subsequently. The pulsations can be transmitted to the flowing bulk solid above, and hence to the silo structure. Since the pulsations may be damped with increasing distance from the outlet opening due to the deformation of the bulk solid in the hopper (energy dissipation), the resulting silo vibrations may be small if the outlet opening is small and, thus, the pulsating flow is originated only in a small region compared to the silo volume (similar to shocks being initiated in the lower hopper region due to slip-stick friction, see Sect. 14.5.1). However, in the case of a large outlet opening severe vibrations have been observed due to the described mechanism [14.4].

When fine-grained bulk solids are discharged from a silo, a gas under-pressure can arise in the hopper causing air to flow through the outlet opening into the bulk solid (see Sect. 12.1). If the desired discharge rate is

too high, the countercurrent air flow may lead to pulsating flow of the bulk solid (e.g., [14.36]). However, the strength of the vibrations resulting from pulsating flow is probably limited due to the damping of fine-grained bulk solids.

14.6.2 Cyclic excitation by a feeder

A feeder can initiate periodic changes of the flow velocity in a silo [14.4,14.37]. This can happen, for example, when a free-flowing bulk solid is discharged by a rotary valve (Sect. 12.3.2.7, Fig. 12.19). At small rotational speeds the pockets of the rotary valve are filled immediately when the pocket enters the region of the hopper outlet opening. Thus, the bulk solid is withdrawn intermittently from the hopper which can initiate vibrations, especially with brittle solids. However, those vibrations are likely to be relatively weak because the source of the periodic movement is in the lower hopper region.

In [14.4] vibrations in a silo for the storage of coal are described being initiated by a belt feeder. The belt was supported by idlers including the section below the discharge opening of the silo. Due to sag of the belt between the idlers, a cyclic motion was initiated when the material moved over the idlers which resulted in the vibration of the silo.

14.6.3 Collapsing arches and ratholes

If the outlet of a silo is too small, i.e., smaller than the critical arching or ratholing diameter, stable arches or ratholes can form. An arch or rathole may collapse through external excitation, for example, ambient vibrations, impact, or the action of flow promoting devices. The impact of the falling material causes a shock load on the silo structure. This case seems to be especially dangerous if the bulk solid from the lower part of the hopper has been discharged, for example, due to the action of flow promoting devices installed there, but a stable arch exists at some distance from the outlet opening (Fig. 14.17.a). Due to the large height of fall a particularly strong shock can be expected when the arch collapses.

Large regions of compacted bulk solid which have formed on one side of a silo (e.g., arising from non-symmetrical stagnant zones, Fig. 14.17.b), can suddenly collapse and start to flow initiated by, for example, vibrations or flow promoting devices. If subsequently flow is stopped by the silo walls, impact forces with a significant horizontal component can result. Such forces may be sufficient to cause the silo to fail.

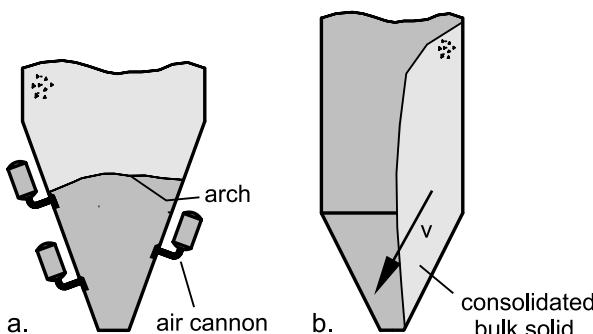


Fig. 14.17. a. Arch with a large distance to the outlet opening; material below has been discharged with the help of discharge aids (here: air cannons) located only in the lower part of the hopper; b. asymmetric region of compacted bulk solid; v is velocity of the material after initiation of flow.

14.7 Means for reducing silo quaking and silo honking

Standard solutions for the elimination of problems due to quaking or honking are not available because there are too many reasons for their occurrence. It is useful to learn as much as possible about the reasons for a particular problem before deciding on appropriate means. If distinct shocks occur, it is particularly helpful to measure the complete order of events simultaneously at different vertical positions in the silo (e.g., with accelerometers). If the measuring rate is sufficiently high, it can be detected where the process was initiated. The mechanisms described in the preceding sections show that the position of the greatest action (e.g., largest increase of stresses or strongest accelerations during the shock process) is not implicitly the position where a shock was initiated. Unfortunately a detailed investigation is often expensive or even not possible due to limited accessibility of the silo (need for scaffolding) and lack of time. If several of the possible reasons for shocks occur simultaneously, understanding and solution of the problem becomes even more difficult.

Several solutions for the elimination of silo quaking and honking have been reported elsewhere [14.1, 14.4, 14.6, 14.9–14.12, 14.14, 14.16, 14.23]. In the following these solutions are presented according to the source of the shocks or vibrations:

- A: Shear zones in the flowing bulk solid (Sect. 14.5.1)
- B: Unstable stagnant zones (Sect. 14.5.2)
- C: Flow at the silo wall (Sect. 14.5.3)
- D: Other reasons (Sect. 14.6)

Type D sources can be detected and eliminated relatively easily, e.g., by enlarging the outlet opening according to the required discharge rate (Sect. 14.6.1), by selecting or modifying a feeder with respect to more continuous withdrawal (Sect. 14.6.2), or by adjusting the silo or the operation of the silo, respectively, to the properties of the bulk solid (Sect. 14.6.3). The mechanisms described in Sect. 14.5 are more complex. Solutions are presented in the following sections.

14.7.1 Reduction of the accelerated mass

An effective solution for the elimination or reduction of shocks for the cases A, B, and C is the reduction of the mass which is accelerated and subsequently decelerated. This way not only inertia forces are reduced, but also stresses in the bulk solid which is a measure of the elastically stored energy (see Sects. 14.2 and 14.3).

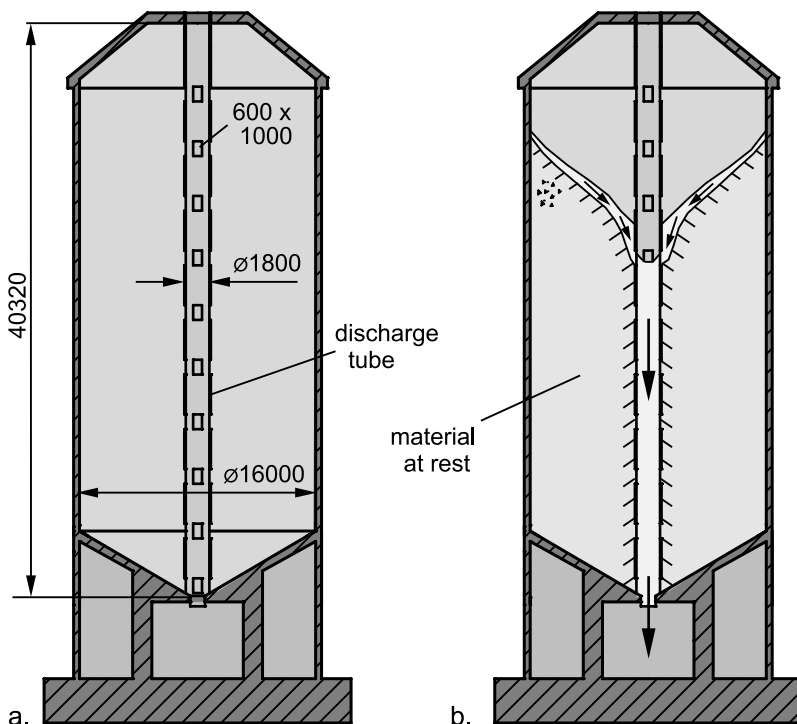


Fig. 14.18. Silo for storage of cement clinker equipped with a discharge tube; dimensions in millimeters [14.8,14.9]

The simplest method is the reduction of the filling height which, because it leads to a reduction of usable volume, is often not acceptable. Alternatively it is possible to reduce the mass of bulk solid that is in motion while discharging the silo. Here the principle of the discharge tube (see Sect. 11.3.3) can be applied for bulk solids with a sufficiently good flowability. The silo for the storage of cement clinker shown in Fig. 14.18.a was successfully retrofitted by this method [14.8,14.9]. Since the bulk solid enters the discharge tube only through the highest row of openings below the top surface of the silo contents, only the material within the discharge tube and near the top surface of the silo contents moves while discharging the silo (Fig. 14.18.b). Thus, a smaller mass of bulk solid is in motion during discharge compared to the situation in the silo prior to the installation of the discharge tube. Furthermore, the stresses within the moving bulk solid are considerably smaller. Alternatively to the situation in Fig. 14.18, discharge tubes can also be placed at silo walls, either inside or outside [14.3].

Another example of the reduction of the mass of flowing material is shown in Fig. 14.19 [14.1,14.8]. The silo storing 6000 t of coal exhibited severe shocks while being discharged simultaneously through all seven outlet openings that were evenly distributed over the cross-section. Since a mass flow hopper was placed above each outlet opening, the total silo contents came in motion when all openings were active. The shocks could be significantly reduced by only activating three outlet openings (in line through the silo axis) at the same time. Thereby a wedge-shaped flow zone was formed (Fig. 14.19.b).

Besides the reduction of the mass of the flow zone, the effect of this measure is probably also based on the following mechanisms:

- Above the hopper converging flow (Fig. 14.19.b) develops instead of plug flow. This increases the internal shear and, thus, energy dissipation in the material so that the acceleration and subsequent deceleration during a shock process are less severe.
- The stresses acting vertically on the (active) mass flow hoppers are significantly reduced due to the converging flow. Thus, the shear zones which develop in the top part of the hopper (according to region A in Fig. 14.6.a) are subjected to smaller stresses. Thus, if slip-stick friction in the shear zones in the hopper is the source of the shocks, less elastic energy is stored prior to a shock and released during a shock.

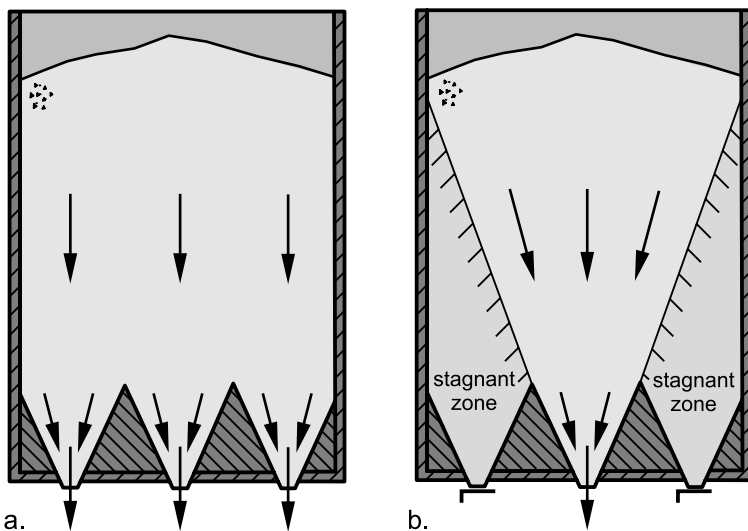


Fig. 14.19. Silo for storage of 6000 t coal [14.1,14.8] (vertical section through the silo axis); a. all (seven) outlet openings are active, plug flow in the vertical section; b. only three outlet openings in one line are active leading to funnel flow with a converging flow zone

14.7.2 Regular initiation of small shocks

In Fig. 14.20 one silo out of a battery of six used to store coal is shown. Severe shocks occurred with a period of two minutes when the filling level was above 50% [14.11,14.13,14.38]. Although the asymmetrical hoppers had relatively steep walls, mass flow was not achieved. Stagnant zones were caused by the shallower regions of the hopper, i.e., the less inclined parts of the walls as well as the valleys in the pyramidal hopper section being inclined by up to 28° to the vertical. However, due to the relatively steep walls the situation was close to the mass flow boundary (see Sect. 14.5.2.1).

Investigations of the shock process have shown that at first bulk solid in the upper hopper region was moving (region X, Fig. 14.20), and subsequently the material in the vertical section followed. Thus, possible reasons for the shocks were sudden flow of the bulk solid in the stagnant zones in region X (reason B, Sect. 14.5.2.1), or a sudden flow along shear zones in the flowing bulk solid in region X (reason A, Sect. 14.5.1). The shocks had been so strong that shocks in the other five silos were also ini-

tiated leading to a severe quaking of the complete building containing the silos.

To reduce the shocks four air cannons installed in the upper region of the hopper (region X) were activated in a period of one minute. Each time the air cannons induced a shock but it was less strong compared to the shocks occurring before, because due to the shorter time the stresses in the bulk solid could not increase that much (less elastically stored energy). This way it also could be avoided that one silo initiated shocks in the other silos. However, later the silos had been replaced by new silos [14.13].

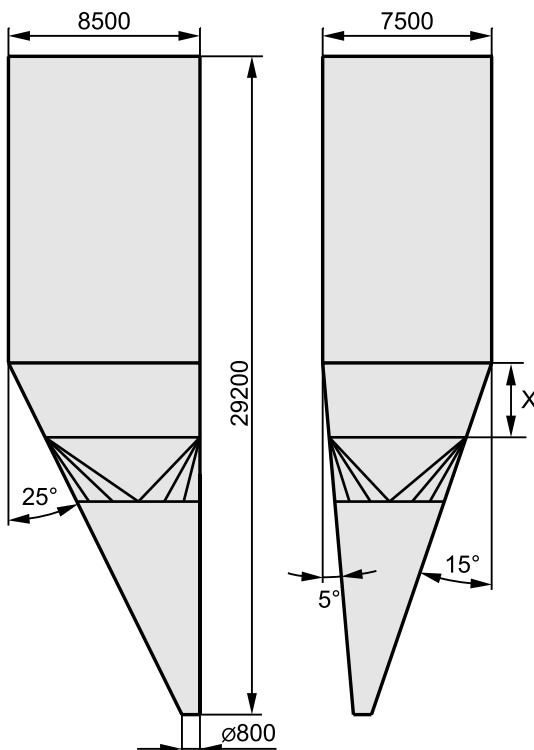


Fig. 14.20. Silo with asymmetric, partly pyramid-shaped hopper for storing coal (dimensions in millimeters) [14.11,14.38]

14.7.3 Increasing roughness of the vertical section

If shocks are caused by sudden flow of the bulk solid on the wall of the vertical section due to slip-stick (reason C, Sect. 14.5.3.2), a reduction of the shocks and, if the occasion arises, also an elimination of silo honking

can be achieved by increasing the roughness of the wall (see Fig. 14.16) [14.16, 14.23]. However, shocks due to shear zones in the hopper (reasons A and B) cannot be eliminated by an increased roughness of the wall [14.25]. Only a – presumably low – reduction of the effect seems to be possible since the rougher cylinder walls subject the bulk solid column to higher vertical shear stresses at the wall. Thus, it cannot be accelerated downwards as fast, so the vertical stress acting on the bulk solid in the hopper is lower.

14.7.4 Reduction of velocity gradients

If shocks are initiated by shear zones within the bulk solid (reason A), a reduction of the velocity gradients may eliminate the shocks. This is manifested by the example of the en-masse feeder shown in Fig. 14.10, where the shear deformation in the bulk solid was reduced by a modification of the feeder for more uniform withdrawal.

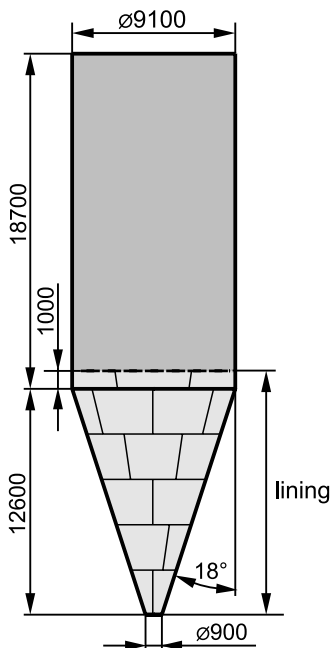


Fig. 14.21. Silo with a mass flow hopper for storage of coal (dimensions in millimeters) [14.13]

If in a mass flow hopper the combination of hopper inclination and wall friction is close to the mass flow boundary (i.e., close to funnel flow, see

Fig. 10.7), the velocity of the bulk solid at the wall is relatively small and, thus, the shear deformation is large. In this case smaller velocity gradients can be achieved by a reduction of the wall friction angle (e.g., with an appropriate lining or coating) which may be sufficient to eliminate shocks [14.4]. An example for this is given by mass flow silos for the storage of coal (Fig. 14.21) which were built to replace the funnel flow silos shown in Fig. 14.20. The hopper and the lower part of the vertical section were lined with cold-rolled stainless-steel sheets in order to obtain a small wall friction angle.

After these new silos came into operation, severe shocks occurred for many months [14.13]. Thereafter the shocks disappeared although obviously the same type of coal was stored and no changes were undertaken at the silo. From interviews of the staff it was found that initially the welds of the lining protruded into the hopper, but with time the coal smoothed the wall and, thus, the protruding welds. Therefore, the initial situation in the hopper might have been close to the mass flow boundary so that a large velocity gradient prevailed. Due to the increasing smoothness of the wall the distance to the mass flow boundary increased, the velocities became more uniform, and, thus, the shocks disappeared. This example clearly demonstrates how important it is to base mass flow design on wall friction tests on realistic wall material samples, and to pay attention to a sufficient standard of workmanship regarding the interior surface of the hopper.

14.7.5 Transforming funnel flow into mass flow

If in a funnel flow hopper the combination of hopper inclination and wall friction is close to the mass flow boundary and shocks occur due to intermittent flow of the stagnant zone (reason B, Sect. 14.5.2.1), mass flow can be achieved by reducing the wall friction with the result that also the shocks disappear [14.4]. Generally such borderline conditions, i.e., funnel flow hoppers with wall slopes close to the mass flow boundary, should be avoided.

15 Sample problems and solutions

15.1 General remarks

Most equations used in the present chapter are based on simplified assumptions. Thus, the presented results are not as accurate as they might seem with respect to the number of decimals. However, the results were not rounded so as to make the comparison with the reader's own calculations easier.

The bulk solid properties given in some sample problems may not be properties of real bulk solids, but are more favorable from didactic reasons. However, this should not reduce the benefit of the examples.

15.2 Sample problems

Sample problem 1: Stresses in the vertical section of a silo

Calculate the horizontal and vertical stresses acting in the vertical section of a silo (Fig. 15.1.a: rectangular cross-section of 3 m by 5 m, filling height 20 m) 5 m, 10 m, 15 m, and 20 m below the bulk solid surface, which is assumed to be horizontal and without surcharge load. Plot the stresses vs. coordinate z . What would be the magnitude of the vertical stress at infinite depth ($z \rightarrow \infty$)?

Given:

$$\rho_b = 1250 \text{ kg/m}^3, \varphi_x = 22^\circ, K = 0.5$$

Solution:

The stresses in the vertical section of a silo (parallel walls) can be calculated with the Janssen equation (Sect. 9.2.1, Eq.(9.9)):

$$\sigma_v = \frac{g \rho_b A}{K \tan \varphi_x U} \cdot \left[1 - e^{-\frac{-K \tan \varphi_x U z}{A}} \right] \quad (15.1)$$

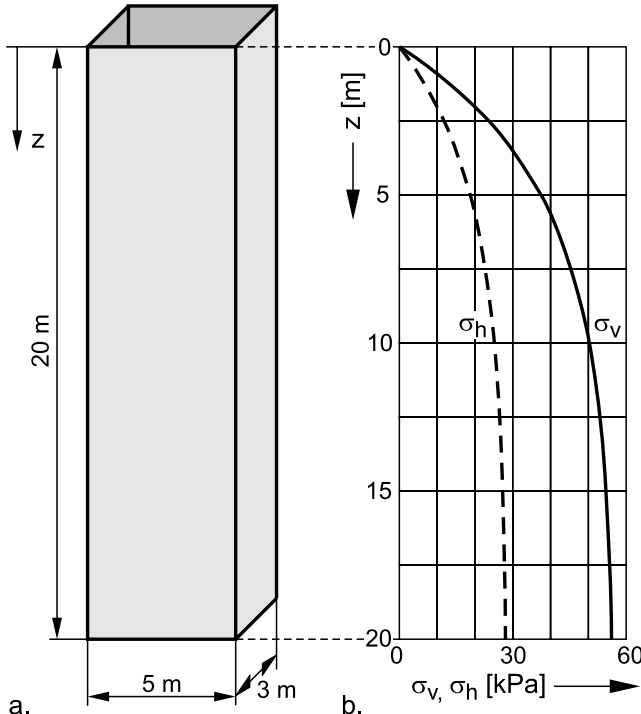


Fig. 15.1: a. Vertical section of a silo; b. stresses vs. vertical coordinate z

Beside the given bulk solid properties, the cross-sectional area $A = 15 \text{ m}^2$ and the circumference $U = 16 \text{ m}$ have to be entered. For the coordinate z , which is equal to zero at the top surface and increases downwards, the values 5 m, 10 m, 15 m, and 20 m have to be entered. For the calculation of the stress at infinite depth, i.e., $z \rightarrow \infty$, the exponential term becomes zero. Thus the vertical stress is equal to the term before the brackets in Eq.(15.1) (according to $\sigma_{v\infty}$ in Eq.(9.12)).

For the calculation of the horizontal stress, σ_h , the vertical stress is multiplied by the stress ratio, K (see Eq.(9.10)):

$$\sigma_h = K \cdot \sigma_v = \frac{g \rho_b A}{\tan \varphi_x U} \cdot \left[1 - e^{-\frac{-K \tan \varphi_x U z}{A}} \right] \quad (15.2)$$

The results are depicted in Table 15.1. In Fig. 15.1.b the stresses are plotted versus z . It can be clearly seen that already at a depth of 10 m about 90% of the stress acting at infinite depth ($z \rightarrow \infty$) is attained.

Table 15.1. Stresses in the vertical section

z [m]	σ_v [Pa]	σ_h [Pa]
0	0	0
5	37485	18743
10	50279	25140
15	54646	27323
20	56136	28068
$z \rightarrow \infty$	56908	28454

Sample problem 2: Maximum stress in a mass flow silo

In order to limit particle breakage and attrition, a particular product must not flow at stresses higher than 10 kPa. Since the product tends to segregate it is planned to store it in a mass flow silo.

Assess the maximum diameter, D , of the silo under consideration of the stress peak at the transition from the cylindrical section to the hopper.

Given:

$$\varphi_x = 30^\circ, \varphi_e = 42^\circ, \rho_b = 760 \text{ kg/m}^3, K = 0.4$$

Solution:

The maximum stress in the cylindrical section is the vertical stress, σ_v , for $z \rightarrow \infty$, following from Eq.(9.12):

$$\sigma_{v\infty} = \frac{g\rho_b D}{4K \tan \varphi_x} \quad (15.3)$$

At the transition to the hopper a stress peak develops (switch stress, see Sect. 9.1.2). Here the orientation of the principal stresses changes: The major principal stress along the axis of the cylindrical section is directed vertically, but it is oriented horizontally along the hopper axis. Assuming steady-state flow for the bulk solid in the hopper, according to Eq.(9.3) the ratio of vertical to horizontal stress at the hopper axis is:

$$\frac{\sigma_v}{\sigma_h} = \frac{\sigma_2}{\sigma_1} = \frac{1 - \sin \varphi_e}{1 + \sin \varphi_e} \quad (15.4)$$

Equating the vertical stress at the top of the hopper to the maximum vertical stress in the cylindrical part ($\sigma_{v\infty}$ according to Eq.(15.3)), the maximum

stress, namely the horizontal stress, $\sigma_{h,max}$, at the stress peak can be roughly assessed with Eq.(15.4):

$$\sigma_{h,max} = \sigma_{\infty} \cdot \frac{1 + \sin \varphi_e}{1 - \sin \varphi_e} \quad (15.5)$$

After substitution of Eq.(15.5) with Eq.(15.3), it follows for the silo diameter:

$$D = \frac{4K \tan \varphi_x}{g \rho_b} \cdot \frac{1 - \sin \varphi_e}{1 + \sin \varphi_e} \cdot \sigma_{h,max} \quad (15.6)$$

With the values given above the maximum silo diameter is calculated to be $D = 0.246$ m. Since the calculated diameter is very small, it is not practical to store the product in a mass flow silo. However, a funnel flow silo would also not be a reasonable solution, because similar stresses as in a mass flow silo, and even a stress peak, can occur (see Fig. 9.4). An alternative solution is considered in sample problem 3.

Sample problem 3: Discharge tube

The bulk solid of example problem 2 is to be stored in a silo provided with a discharge tube (Fig. 15.2) in order to limit particle attrition. The wall friction angle at the internal wall of the discharge tube is 25° . Find the maximum diameter, D_{tube} , of the discharge tube, and the maximum vertical distance, a , between the lateral openings.

Solution:

In a silo provided with a discharge tube according to Fig. 11.13.a (Sect. 11.3.3), the material flows only within the discharge tube and close to the top surface of the silo filling. Under the assumption that attrition is due to the major principal stress acting while in a flowing condition (see example in Sect. 8.6) which clearly will not occur outside of a discharge tube at the bottom of the silo, here the maximum stresses within the discharge tube and at the top surface have to be considered.

The maximum stress in a discharge tube is the vertical stress at infinite depth according to Eq.(11.2):

$$\sigma_{\infty} = \frac{g \rho_b D_{tube}}{4K \tan \varphi_x} \quad (15.7)$$

Thus the diameter is:

$$D_{tube} = \frac{4K \tan \varphi_x \cdot \sigma_{v\infty}}{g \rho_b} \quad (15.8)$$

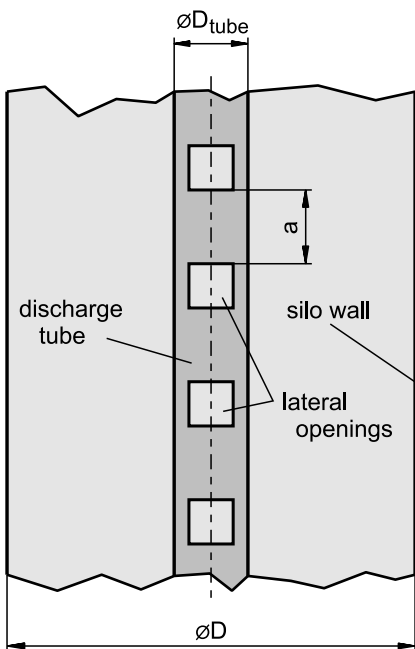


Fig. 15.2. Discharge tube in the vertical section of a silo

It follows $D_{tube} = 1.0$ m for the given bulk solid properties. Thus the diameter of a discharge tube must not be larger than one meter if the maximum stress of 10 kPa cannot be exceeded.

Before the bulk solid enters the discharge tube, it flows close to the top surface of the silo filling. The maximum depth, i.e. the maximum vertical distance to top surface, is defined by the vertical distance, a , between the lateral openings (Fig. 15.2). Flow at the maximum depth takes place when the filling level drops below the lower edge of a lateral opening and, thus, the next lower lateral opening becomes active. Since the vertical distance, a , is small with respect to the silo diameter, D , the vertical stress can be assessed without taking into account wall friction, i.e. the vertical stress is calculated similar to the hydrostatic increase of pressure in a liquid). The vertical stress is considered here because in a vertical section of a silo, the vertical stress is close to the major principal stress (Sect. 9.1.2). Thus, the vertical stress at a distance a below the top surface is approximately:

$$\sigma_v = g\rho_b a \quad (15.9)$$

After rearrangement of Eq.(15.9) it follows $a = 1.34$ m for the given bulk solid properties. Thus the maximum vertical distance between the lateral openings is fixed.

Sample problem 4: Driving force of a feeder

An en-masse feeder is mounted below the circular outlet opening of a silo with a conical hopper (Fig. 15.3). Assess the vertical stress acting on the en-masse feeder both in the filling state (after complete filling of the previously empty silo) and the discharge state. What is the driving force in both cases? The friction at the side walls of the feeder can be neglected.

Given:

$$\rho_b = 1400 \text{ kg/m}^3$$

$$\varphi_{sf} = 48^\circ$$

$$\varphi_{x,sb} = 30^\circ \text{ (friction bulk solid/bottom plate)}$$

$$d = 1 \text{ m} \text{ (outlet diameter of the conical hopper)}$$

$$a = 250 \text{ mm} \text{ (vertical distance between outlet opening and bottom plate)}$$

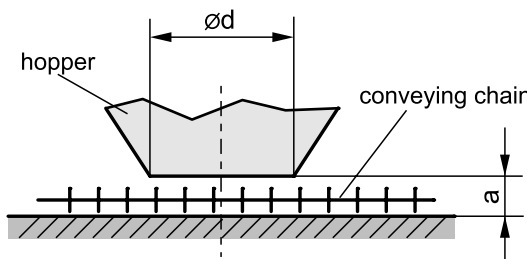


Fig. 15.3. Hopper outlet and en-masse feeder

Solution:

In Sect. 9.3 a simple method has been presented for assessment of the driving force of an en-masse feeder, i.e. the force necessary to move the chain below the outlet (Eq.(9.32)). Since en-masse feeders are mostly connected to rectangular outlet openings, Eq. (9.32) contains the dimensions of an outlet slot, namely length, L , and width, b . To adjust the equation to the present problem, the area of the outlet slot, $L \cdot b$, is replaced by the area of the circular outlet, $d^2 \cdot \pi / 4$. Furthermore, the friction at the side walls is neglected so that the second term in Eq.(9.32) can be omitted. Thus the driving force is:

$$F_h = \sigma_{va} \frac{\pi}{4} d^2 \tan(\varphi_{sf}) + \sigma_{vb} \frac{\pi}{4} d^2 \tan(\varphi_{x,sb}) \quad (15.10)$$

The vertical stress at the outlet opening can be roughly assessed for both the filling state and the discharge state with Eq.(9.26a) in Sect. 9.2.4:

$$\sigma_{va} = 0.2 \cdot g \rho_b d \quad (15.11)$$

With the given parameters it follows $\sigma_{va} = 2747$ Pa for the discharge state. The vertical stress in the filling state can be five to ten times the vertical stress in the discharge state (note that this is a rather crude approximation, see Sect. 9.2.4). Thus the vertical stress in the filling state can be up to $\sigma_{va} = 27470$ Pa.

Due to the weight of the bulk solid layer between outlet opening and bottom plate, the vertical stress acting on the bottom plate is greater than that at the outlet opening. Since the height/diameter ratio of the bulk solid layer is small, a hydrostatic increase of stress is assumed. The height of the bulk solid layer is equal to a (Fig. 15.3). Thus the vertical stress at the bottom plate is:

$$\sigma_{vb} = \sigma_{va} + g \rho_b a \quad (15.12)$$

If follows $\sigma_{vb} = 6180$ Pa for the discharge state and up to $\sigma_{vb} = 30900$ Pa for the filling state. After having determined all stresses in Eq.(15.10), the driving force, F_h , amounts to 5198 N for the discharge state and up to 37973 N for the initial discharge starting from the filling state.

Sample problem 5: Press

Cylindrical compacts (diameter $D = 8$ cm) have to be formed with a press (Fig. 15.4). Find the force F required to ensure that everywhere in the compact a vertical stress of at least 1.5 MPa is acting. This has to be calculated for compact heights, h , of 4 cm, 8 cm, 16 cm, 32 cm, and 64 cm (h : height after compaction). What can be concluded from the results with respect to the height of the compacts?

Given:

$$\rho_b = 600 \text{ kg/m}^3, \varphi_x = 23^\circ, K = 0.4$$

Solution:

The bulk solid in the press is compacted by the upper punch which exerts a vertical surcharge stress on the top surface of the bulk solid. Thus Eq.(9.8) has to be used for calculation of stresses:

$$\sigma_v = \frac{g \rho_b A}{K \tan \varphi_x U} + \left[\sigma_{v0} - \frac{g \rho_b A}{K \tan \varphi_x U} \right] \cdot e^{\frac{-K \tan \varphi_x U z}{A}} \quad (15.13)$$

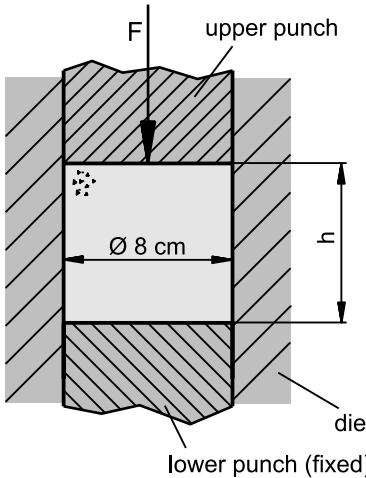


Fig. 15.4. Press with compact of height h

Since the vertical stress acting on the top of the compact is much higher than $\sigma_{v\infty}$ according to Eq.(9.12), the vertical stress will decrease from top to bottom. Thus the smallest vertical stress is acting at the bottom of the compact, i.e., at $z = h$ (z is the vertical coordinate increasing in the downward direction, see Fig. 9.8). For determination of the required surcharge stress, σ_{v0} , Eq.(15.13) is rearranged, whereby the ratio of cross-sectional area to circumference, A/U , is replaced by $D/4$:

$$\sigma_{v0} = \frac{g \rho_b A}{K \tan \varphi_x U} + \left(\sigma_v - \frac{g \rho_b A}{K \tan \varphi_x U} \right) \cdot e^{\frac{4K \tan \varphi_x h}{D}} \quad (15.14)$$

With the parameters given above and $\sigma_v = 1.5 \text{ MPa} = 1.5 \cdot 10^6 \text{ Pa}$ one obtains an equation for the surcharge stress, σ_{v0} , as a function of compact height, h :

$$\sigma_{v0} = 693 \text{ Pa} + \left(1.5 \cdot 10^6 \text{ Pa} - 693 \text{ Pa} \right) \cdot e^{8.49 \frac{h}{\text{m}}} \quad (15.15)$$

Force F , which has to be applied by the upper punch, is equal to the product of the cross-sectional area of the compact and the surcharge stress, σ_{v0} :

$$F = \sigma_{v0} \cdot \frac{\pi}{4} d^2 = 5.03 \cdot 10^{-3} \text{ m}^2 \cdot \sigma_{v0} \quad (15.16)$$

Note that “Pa” and “m” in the above equations are units. The results are shown in Table 15.2.

Table 15.2. Surcharge stress and vertical force for different compact heights, h

h [m]	σ_{v0} [kPa]	F [kN]
0.04	2106	10.6
0.08	2958	14.9
0.16	5833	29.3
0.32	22687	114.0
0.64	343300	1725.6

The conclusion from the results is that it is not possible to produce compacts with a large height/diameter ratio, because the required force increases exponentially with compact height (see Sect. 9.2.2).

Sample problem 6: Stresses in combined bins

Find the vertical and horizontal stresses acting at the top and bottom of the lower cylinder (Fig. 15.5.a) after filling, i.e., before discharge is started. Plot both the vertical and horizontal stress (σ_h and σ_v) versus height.

Given:

$$\rho_b = 850 \text{ kg/m}^3, \varphi_x = 25^\circ, K = 0.4$$

Solution:

The stresses in the upper cylinder are calculated like the vertical section of a silo (without surcharge load). The bulk solid in the lower cylinder is subjected to a surcharge load from material in the upper cylinder.

For the upper cylinder the Janssen equation without surcharge load according to Sect. 9.2.1, Eq.(9.9), is applied. Substituting the ratio of cross-sectional area to circumference, A/U , of the upper cylinder with $d_1/4$ gives:

$$\sigma_v = \frac{g \rho_b d_1}{4 K \tan \varphi_x} \cdot \left[1 - e^{-\frac{-4K \tan \varphi_x z_1}{d_1}} \right] \quad (15.17)$$

With the parameters given above one obtains the vertical stress at the bottom of the upper cylinder $\sigma_v(z_1 = h_1 = 4 \text{ m}) = 17.33 \text{ kPa}$. This stress is acting on the top level of the bulk solid in the lower cylinder as a surcharge

stress, σ_{v0} . The horizontal stress at the bottom of the upper cylinder results from multiplying the vertical stress with the stress ratio, K :

$$\sigma_h = K \cdot \sigma_v \quad (15.18)$$

With $K = 0.4$ Eq.(15.18) leads $\sigma_h(z_1 = h_1 = 4 \text{ m}) = 6.93 \text{ kPa}$.

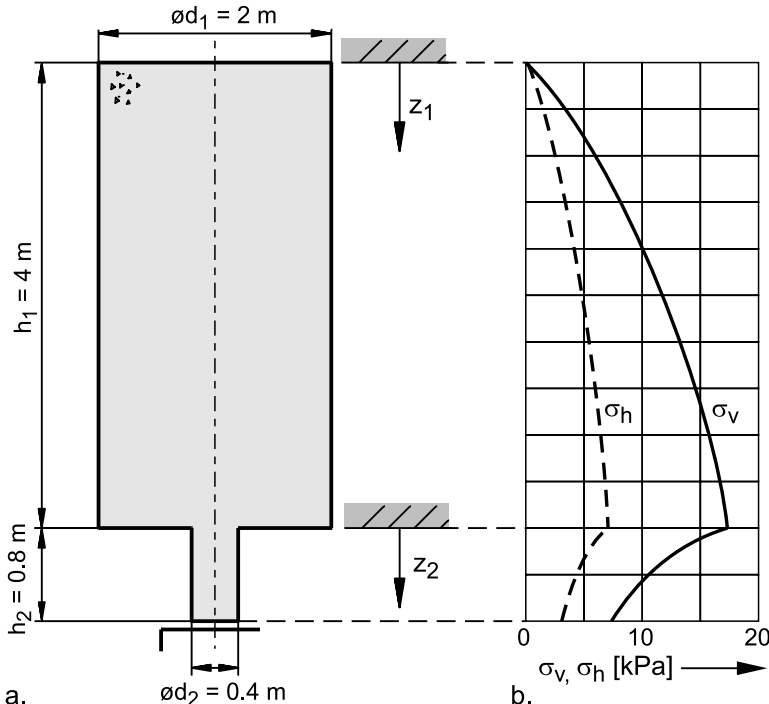


Fig. 15.5. a. Combination of two cylindrical bins; b. calculated vertical and horizontal stresses

The stresses in the lower cylinder are determined with the Janssen equation with surcharge load, Eq.(9.8). Substituting the ratio of cross-sectional area to circumference of the lower cylinder with $d_2/4$, Eq.(9.8) gives:

$$\sigma_v = \frac{g \rho_b d_2}{4 K \tan \phi_x} + \left[\sigma_{v0} - \frac{g \rho_b d_2}{4 K \tan \phi_x} \right] \cdot e^{\frac{-4 K \tan \phi_x z_2}{d_2}} \quad (15.19)$$

Note that Eq.(15.19) is valid only for the lower cylinder, and coordinate z_2 is zero at the top of the lower cylinder. With the surcharge stress $\sigma_{v0} = 17.33 \text{ kPa}$ and the other parameters given above one obtains the vertical stress at the bottom of the lower cylinder $\sigma_v(z_2 = h_2 = 0.8 \text{ m}) = 7.36 \text{ kPa}$.

The corresponding horizontal stress is $\sigma_h(z_2 = h_2 = 0.8 \text{ m}) = 2.94 \text{ kPa}$ according to Eq.(15.18).

Values of vertical and horizontal stresses in both cylinders can be calculated with Eqs.(15.17) to (15.19). The results are plotted in Fig. 15.5.b.

It has to be remarked that a compressible bulk solid is compressed even during filling due to increasing stresses. Compression of the bulk solid in the lower cylinder causes bulk solid located above the lower cylinder to flow downwards. Thus an arched stress field builds up in the flowing bulk solid similar to Fig. 9.4.d leading to a reduction of vertical stress at the transition to the lower cylinder.

Sample problem 7: Stresses in FIBCs and sacks on pallets

A bulk solid is stored in FIBCs (FIBC: flexible intermediate bulk container) or in sacks packed on pallets (Fig. 15.6) before being shipped to a customer. Since caking of the material during storage especially in the lower part of the FIBCs and in the sacks close to the pallet is observed, the problem is to be investigated. To do this, time consolidation tests have to be run where the storage conditions are simulated. What is the appropriate consolidation stress for the tests?

Given:

$$\rho_b = 980 \text{ kg/m}^3$$

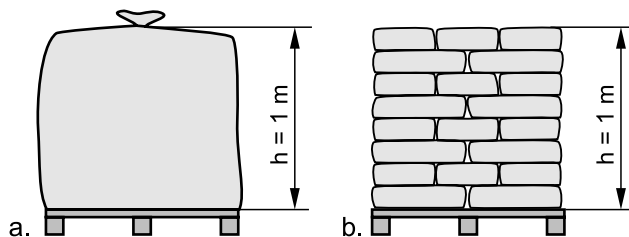


Fig. 15.6. a. FIBC (flexible intermediate bulk container); b. sacks on a pallet

Solution:

If a bulk solid is stored in a flexible container located on the ground, the flexible walls cannot support the bulk like stiff silo walls. Thus the vertical stress, which can be regarded approximately as the major principal stress, increases linearly with vertical coordinate z :

$$\sigma_v = g\rho_b z \quad (15.20)$$

Thus the maximum vertical stress is acting at the bottom of the FIBC. For a filling height $h = 1$ m Eq.(15.20) gives the vertical stress at the bottom $\sigma_v = 9.6$ kPa.

The same principle can be applied to the storage of sacks on pallets since the lowest layer of sacks supports all sacks located above. Thus the highest vertical stress is found in the lower part of a sack in the lowest layer. For a total height of 1 m (Fig. 15.6.b) one obtains the same maximum vertical stress as for the FIBC, i.e., $\sigma_v = 9.6$ kPa. To simulate these conditions in a time consolidation test, the consolidation stress should be about 9.6 kPa.

Sample problem 8: Discharge rate

A bulk solid is flowing through the outlet of a conical mass flow hopper. The outlet diameter is $d = 200$ mm, and the hopper slope is $\Theta_c = 20^\circ$ measured from vertical. Assess the maximum discharge rate (mass flow rate).

Given:

$\rho_b = 1450$ kg/m³, particle size: 5 mm (non spherical particles).

Solution:

The discharge rate from a circular outlet opening can be roughly assessed with Eq.(12.5):

$$\dot{m} = C \rho_b \sqrt{g} (d - kx)^{2.5} \quad (15.21)$$

With $C = 0.55$ and $k = 3$ and the parameters given above the mass flow rate is 36.8 kg/s and 132.4 t/h, respectively. Here the parameters C and k are chosen so that the result is conservative, i.e. the calculated discharge rate is at the lower boundary of Eq.(12.5).

A second method to assess the discharge rate from a mass flow hopper is provided by Eq.(12.6) where, in contrast to Eq.(12.5), the slope of the hopper wall is taken into account:

$$\dot{m} = 0.58 \rho_b \sqrt{g} (d - kx)^{2.5} k_\Theta \quad (15.22)$$

Parameter k is equal to 2.4 for non spherical particles. k_Θ depends on the hopper slope and is $k_\Theta = (\tan \Theta_c)^{-0.35} = (\tan 20^\circ)^{-0.35} = 1.424$.

Thus the discharge rate is 57.5 kg/s or 210 t/h, respectively. The difference from the results of Eq.(15.21) is mainly caused by consideration of hopper slope (factor k_Θ).

Sample problem 9: Selection of a wall material for mass flow

Segregation is observed in a funnel flow silo with conical hopper (hopper slope angle $\Theta_c = 20^\circ$). It has to be checked with laboratory tests if mass flow can be obtained with a coating (A or B) or a lining (cold-rolled stainless steel) of the hopper walls. The results of the wall friction tests are depicted in Table 15.3.

Table 15.3. Wall materials and wall friction angles, φ_x

Wall material	φ_x
Coating A	22°
Coating B	28°
Lining (stainless steel)	26°

Measurement of a yield locus in the relevant stress range gives the effective angle of internal friction $\varphi_e = 35^\circ$. Which of the tested wall materials is appropriate to enable mass flow with the present hopper slope? Find the maximum hopper wall slopes ensuring mass flow for the tested wall materials.

Solution:

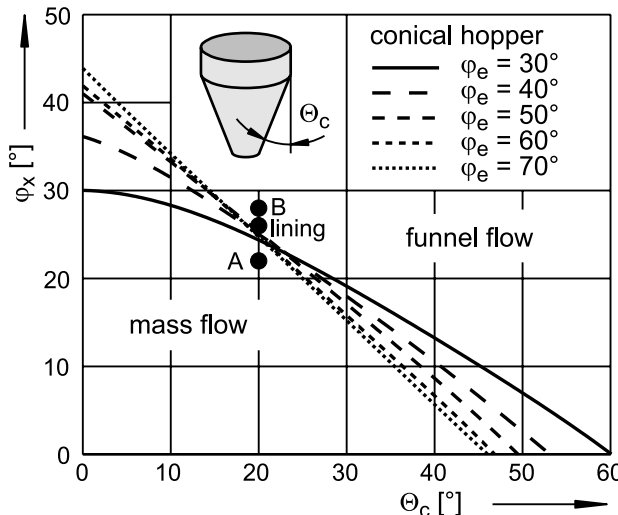
The pairs of values of the hopper slope, $\Theta_c = 20^\circ$, and the wall friction angles, φ_x , measured for the individual wall materials (Table 15.3) are plotted in the mass flow diagram for conical hoppers (Fig. 15.7). One can clearly see that mass flow will prevail only with coating A. The points representing coating B and the stainless steel lining are located in the funnel flow region.

The maximum hopper wall slope for mass flow can be determined with the mass flow diagram for conical hoppers (Fig. 15.7). Alternatively the flow factor diagrams can be used where the mass flow boundary is plotted in each diagram for one particular value of effective angle of internal friction, φ_e .

First the hopper slope angle, Θ_c , on the mass flow boundary is determined. The relevant boundary follows from the effective angle of internal friction, φ_e . In the case under consideration it has to be interpolated between the boundaries for $\varphi_e = 30^\circ$ and $\varphi_e = 40^\circ$. This yields the angles depicted in the second column of Table 15.4. Assuming that the properties of the bulk solid and the wall surface are well-defined and do not change with time (Sect. 10.3.1), the values have to be reduced by a safety margin of 2° to 3° . Thus the hopper slope angles should not be greater than the values given in the third column of Table 15.4.

Table 15.4. Wall materials and maximum hopper slope for mass flow

Wall material	Θ_c (boundary)	Θ_c (safety margin included)
Coating A	25°	22°
Coating B	13°	10°
Lining (stainless steel)	18°	15°

**Fig. 15.7.** Combinations of hopper wall slopes and wall materials (see black circles) in the mass flow diagram for conical hoppers.**Sample problem 10: Design of a mass flow silo**

The flow properties of a bulk solid have been determined with a shear tester in order to design a mass flow silo. As a result three yield loci and a wall yield locus have been measured. The wall friction angle, φ_x , is equal to 25° in the investigated stress range. The results of the yield locus tests are listed in Table 15.5.

Table 15.5. Flow properties

Yield locus no.	σ_l [Pa]	σ_c [Pa]	ρ_b [kg/m ³]	φ_e [°]	φ_{lin} [°]
1	4200	3100	880	50	26
2	8700	4350	935	50	36
3	14000	5760	965	50	39
4	27500	7050	980	50	40

Find the maximum hopper slope angles for conical and wedge-shaped hoppers. What are the minimum outlet dimensions to avoid arching?

Solution:

First the maximum hopper slope angles for mass flow have to be determined. Since the effective angle of internal friction, φ_e , is equal to 50° and thus constant in the investigated stress range, the flow factor diagram for $\varphi_e = 50^\circ$, which contains the mass flow boundary, can be used. Figure 15.8 shows the diagram for conical hoppers. For a wall friction angle $\varphi_x = 25^\circ$ one finds the value $\Theta_c = 20.5^\circ$ (point A) at the mass flow boundary. This value has to be reduced by a safety margin (assuming that the properties of the bulk solid and the wall surface are well-defined and do not change with time (Sect. 10.3.1), a safety margin of 2° to 3° may be sufficient). Thus a hopper slope angle $\Theta_c = 18^\circ$ is chosen (point B).

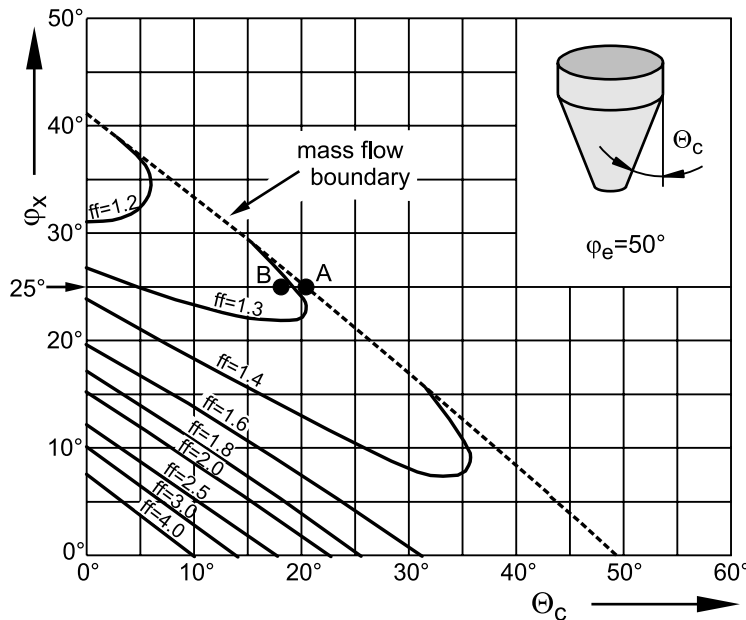


Fig. 15.8. Flow factor diagram for conical hoppers and $\varphi_e = 50^\circ$

The maximum hopper slope of a wedge-shaped hopper is determined in the same way using the flow factor diagram in Fig. 15.9. One finds a maximum hopper slope $\Theta_p = 26.5^\circ$ (see Fig. 15.9, point A). A safety margin need not be considered here because it is already contained in Jenike's mass flow boundaries for wedge-shaped hoppers (see Sect. 10.3.1).

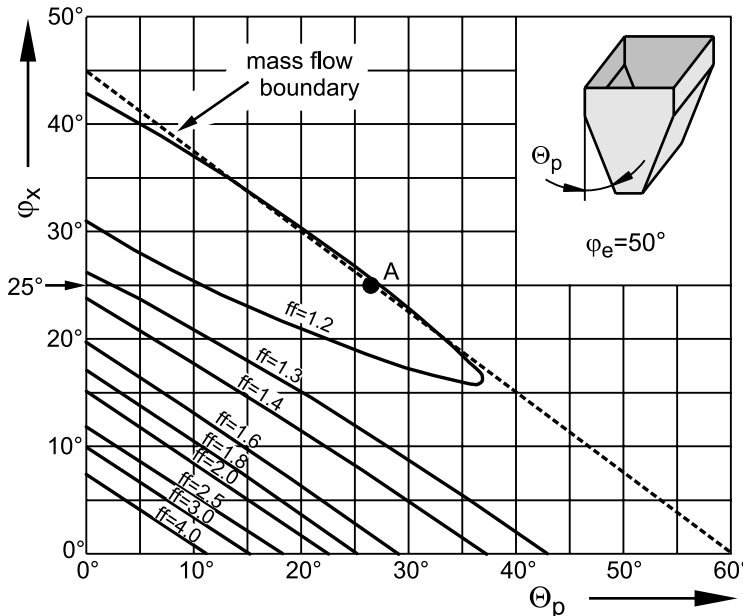


Fig. 15.9. Flow factor diagram for wedge-shaped hoppers and $\varphi_e = 50^\circ$

In the next step the minimum outlet dimensions to avoid arching are determined. Therefore the unconfined yield strength, σ_c , bulk density, ρ_b , and effective angle of internal friction, φ_e , are plotted against consolidation stress, σ_I (Fig. 15.10). It is recommended to draw the diagrams above each other with the same scale of the σ_I axis, and to use the same scale for σ_c and σ_I .

Then segments of straight lines or curves are plotted through the measured points. The points in Fig. 15.10 are connected by straight lines. Towards smaller and larger stresses the lines are extrapolated (broken lines), whereby the slope of the neighboring straight section is applied.

Next the bearing stress of a stable arch, σ_I' , must be plotted in the σ_c, σ_I diagram. The bearing stress is calculating with the equation (Sect. 10.3.1):

$$\sigma_I' = \frac{\sigma_I}{ff} \quad (15.23)$$

The flow factor, ff , has to be determined from the appropriate flow factor diagrams for both a conical and a wedge-shaped hopper. Thus for the points representing the wall friction angle and the chosen hopper slope angle (point B in Fig. 15.8, point A in Fig. 15.9) the flow factor, ff , is determined with the help of the curves for $ff = \text{constant}$ by interpolation or, which is easier to do, by setting ff equal to the next higher value of ff . The

latter provides some additional safety against arching and avoids a too small ff value caused by false interpolation.

Using the next higher value of ff , one obtains $ff = 1.3$ for the conical hopper (point B in Fig. 15.8) and $ff = 1.2$ for the wedge-shaped hopper (point A in Fig. 15.9). Thus the arch bearing stress can be plotted according to Eq.(15.23) as a straight line running through the origin for both hopper shapes (Fig. 15.10).

The bearing stress intersects with the part of the flow function extrapolated to the left. From the point of intersection one obtains the “critical” values of consolidation stress, $\sigma_{I,crit}$, and the corresponding values of unconfined yield strength, $\sigma_{c,crit}$, bulk density, $\rho_{b,crit}$, and effective angle of internal friction, $\varphi_{e,crit}$. For reasons of clarity the point of intersection and the determination of critical values is shown in Fig. 15.10 only for a wedge-shaped hopper, i.e. for $ff = 1.2$ (see squares in Fig. 15.10). The critical values, characterized with the index “crit”, represent the consolidation stress and flow properties at the outlet opening of minimum (critical) dimensions. Table 15.6 shows the critical values for both hopper shapes considered here.

Table 15.6. “Critical” parameters at the intersection of bearing stress and flow function (values taken from Fig. 15.10)

Hopper shape	$\sigma_{I,crit}$ [Pa]	$\sigma_{c,crit}$ [Pa]	$\rho_{b,crit}$ [kg/m ³]	$\varphi_{e,crit}$ [°]
Conical	3925	3025	877	50
Wedge-shaped	3500	2900	872	50

The minimum outlet dimensions to avoid arching are calculated from the critical values (Table 15.6) with Eqs.(10.7a/b):

$$d_{crit} = H(\Theta_c) \frac{\sigma_{c,crit}}{g\rho_{b,crit}} \quad (15.24)$$

$$b_{crit} = H(\Theta_p) \frac{\sigma_{c,crit}}{g\rho_{b,crit}} \quad (15.25)$$

Factor $H(\Theta)$ is taken from the diagram in Fig.10.13. The resulting minimum (critical) outlet dimensions are listed in Table 15.7.

Table 15.7. Function $H(\Theta)$ and minimum outlet dimensions

Hopper shape	$H(\Theta)$	$d_{crit}; b_{crit}$ [m]
Conical	2.30	0.81
Wedge-shaped	1.13	0.38

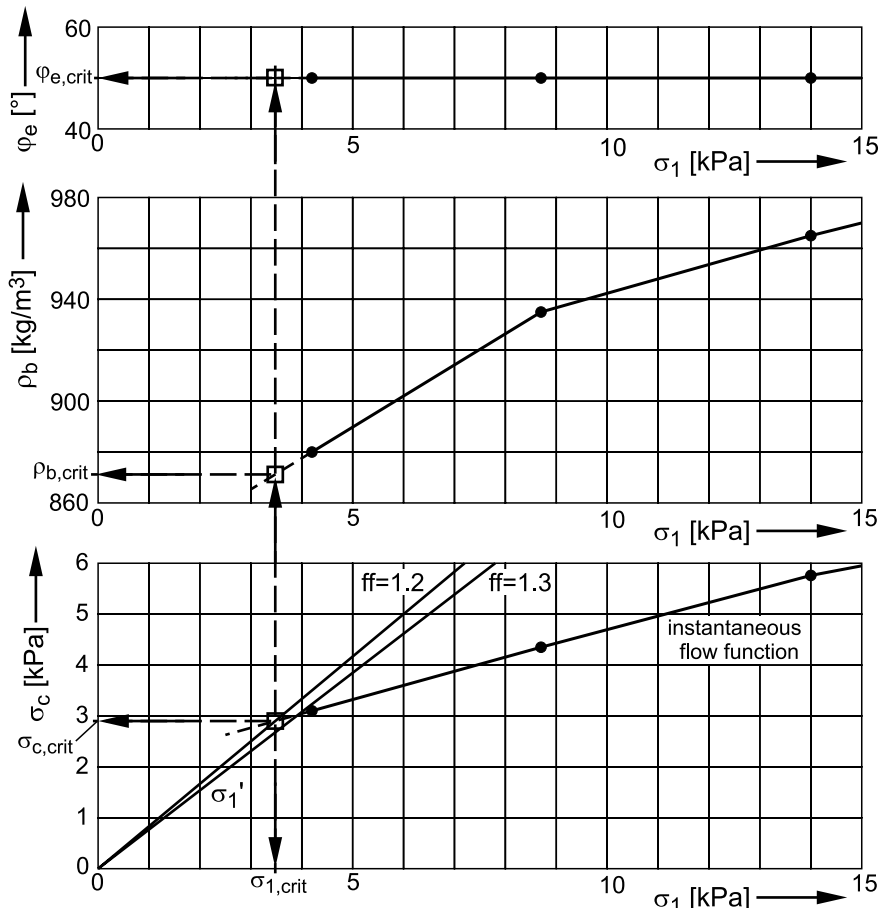


Fig. 15.10. Diagrams showing flow properties for the determination of minimum outlet dimensions to avoid arching (measured values are plotted as circles; squares represent critical values according to the point of intersection of the flow function with the major stress in a stable arch, σ_1')

Sample problem 11: Design of a funnel flow silo

A funnel flow silo with conical hopper has to be designed for the bulk solid of sample problem 10, whereby both the lower and upper bounds of the rathole diameter have to be determined. The bulk solid is assumed to exhibit no time consolidation. The diameter of the silo is $D = 3$ m, the maximum filling level for filling conditions, i.e., before material is discharged, is $h_f = 6$ m.

Solution:

The slope of the hopper walls must be sufficiently steep to ensure complete discharge by gravity. Thus Eq.(10.8) has to be applied:

$$\Theta_{cd} = 65^\circ - \varphi_x \quad (15.26)$$

With the wall friction angle $\varphi_x = 25^\circ$ it follows $\Theta_{cd} = 40^\circ$, i.e., the hopper walls have to be inclined by 40° from vertical to ensure complete emptying.

The minimum outlet dimension to avoid ratholing is calculated with both procedures outlined in Sect. 10.3.2, i.e., the lower bound value as well as the upper bound value of the rathole dimension is determined.

For the determination of the lower bound value the circumferential stress (major principal stress) in the rathole wall, σ_I'' , is plotted in the σ_c, σ_I diagram (Sect. 10.3.2):

$$\sigma_I'' = \frac{\sigma_I}{ff} \quad (15.27)$$

The flow factor for ratholing, ff_p , follows from:

$$ff_p = \frac{1 + \sin \varphi_e}{4 \cdot \sin \varphi_e} \cdot f(\varphi_i) \quad (15.28)$$

φ_i is approximated by the slope angle of the linearized yield locus, φ_{lin} . Following the table in sample problem 10, φ_{lin} is dependent on the consolidation stress. Since the critical consolidation stress, i.e. the consolidation stress corresponding to the minimum outlet dimensions, is not known prior to the design procedure, first φ_{lin} must be estimated. Assuming $\varphi_{lin} = 30^\circ$, one obtains $f(\varphi_i = \varphi_{lin} = 30^\circ) = 2.4$ from Fig. 10.16. Then Eq.(15.28) yields the flow factor $ff_p = 1.38$. Since ff_p should not be smaller than 1.7, it follows $ff_p = 1.7$. This allows one to plot the major stress in the rathole walls, σ_I'' , according to Eq.(15.27) in the σ_c, σ_I diagram (Fig. 15.11).

The intersection of the major stress in the rathole wall with the flow function yields a critical consolidation stress, $\sigma_{I,crit}$, and the corresponding critical values of unconfined yield strength, $\sigma_{c,crit}$, bulk density, $\rho_{b,crit}$, effective angle of internal friction, $\varphi_{e,crit}$ and the angle of the linearized yield locus, $\varphi_{lin,crit}$ (see squares in Fig. 15.11 and values in Table 15.8).

Table 15.8. “Critical” values at the intersection of the major stress in the rathole wall with the flow function

$\sigma_{I,crit}$ [Pa]	$\sigma_{c,crit}$ [Pa]	$\rho_{b,crit}$ [kg/m^3]	$\varphi_{e,crit}$ [°]	$\varphi_{lin,crit}$ [°]
6200	3650	910	50	30

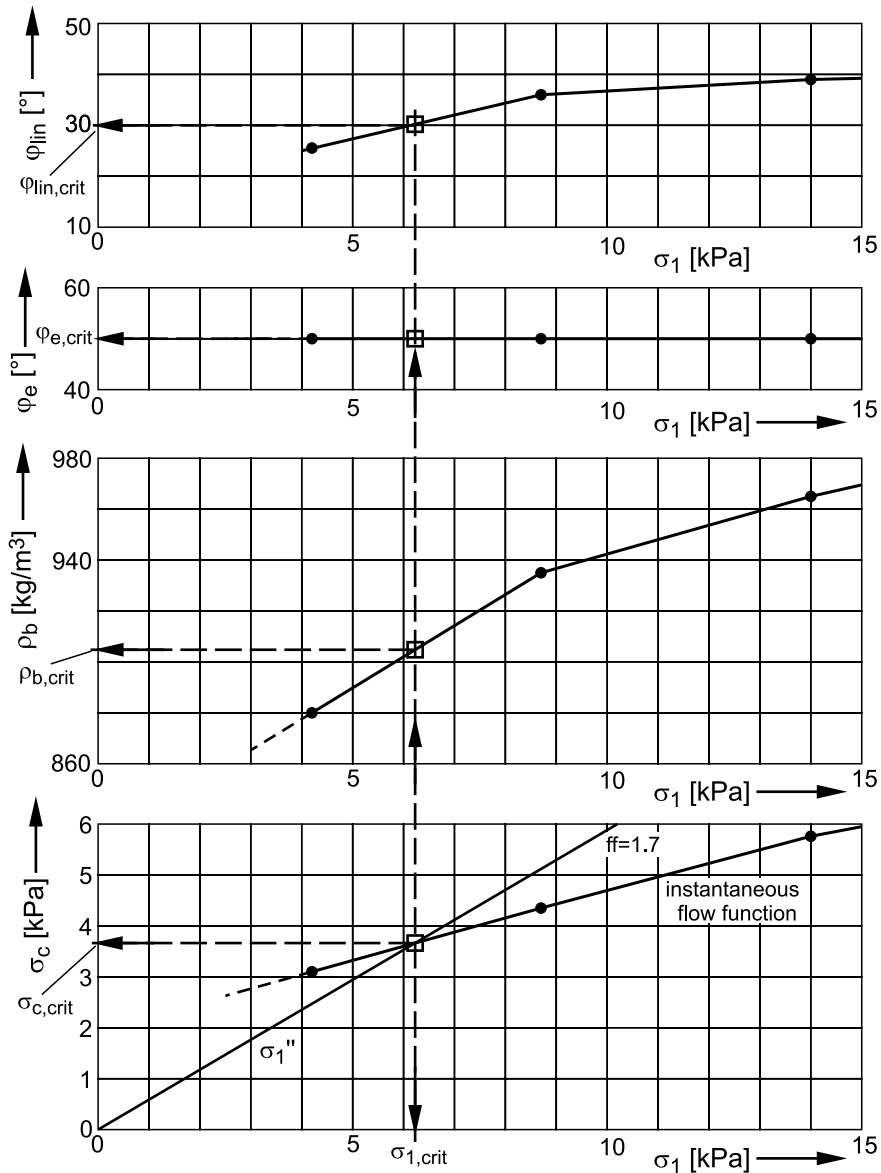


Fig. 15.11. Diagrams showing flow properties for the determination of the lower bound of the minimum outlet dimension to avoid ratholing (measured values are plotted as circles; squares represent critical values according to the point of intersection of the flow function with the major stress in the wall of a stable rathole, σ_1'')

The initially estimated value of φ_{lin} is equal to the finally determined value. If this were not the case, the design procedure would have to be repeated with the determined value $\varphi_{lin,crit}$ as the new estimated value. This has to be repeated until the estimated value is equal to the determined value of φ_{lin} (iteration).

The lower bound value of the minimum outlet dimension to avoid rat-holing is calculated from the critical values with Eq.(10.13):

$$D_{crit} = f(\varphi_i) \frac{\sigma_{c,crit}}{g \cdot \rho_{b,crit}} \quad (15.29)$$

With the critical values from Table 15.8 one obtains $D_{crit} = 0.98$ m. As expected, the critical outlet diameter to avoid ratholing (even the lower bound value) is larger than the outlet diameter d_{crit} required to avoid arching in a conical mass flow hopper (Table 15.7). However, it must be noted that the lower bound value of D_{crit} may be approached only if the silo is being discharged while being filled (see Sect. 10.3.2).

For determination of the upper bound value of the outlet dimension to avoid ratholing the filling stress at the bottom of the silo has to be estimated with Janssen's equation (see Sect. 10.3.2):

$$\sigma_{1,crit} = \sigma_v = \frac{\rho_b g A}{K \tan \varphi_x U} \cdot \left[1 - e^{-\frac{-K \tan \varphi_x U h_f}{A}} \right] \quad (15.30)$$

With maximum filling height, $h_f = 6$ m, ratio of cross-section to perimeter, $A/U = D/4 = 0.75$ m, wall friction angle, $\varphi_x = 25^\circ$, maximum bulk density in the investigated stress range, $\rho_b = 980$ kg/m³, and $K = 0.5$ (assumed; 0.4 or 0.5 are typical values of K , see Sect. 9.2.3) one obtains the critical consolidation stress $\sigma_{1,crit} = 26.14$ kPa. The maximum bulk density has been used because filling stresses are usually relatively high. Critical values of unconfined yield strength, $\sigma_{c,crit}$, bulk density, $\rho_{b,crit}$, and angle of the linearized yield locus, $\varphi_{lin,crit}$ (substitute for φ_i) corresponding to $\sigma_{1,crit}$ are then determined from the functions in Fig. 15.12 (see squares in the diagrams; values are listed in Table 15.9).

Table 15.9. “Critical” values for major stress at the bottom of the silo (filling conditions, filling height $h_f = 6$ m)

$\sigma_{1,crit}$ [Pa]	$\sigma_{c,crit}$ [Pa]	$\rho_{b,crit}$ [kg/m ³]	$\varphi_{lin,crit}$ [°]
26140	6900	979	40

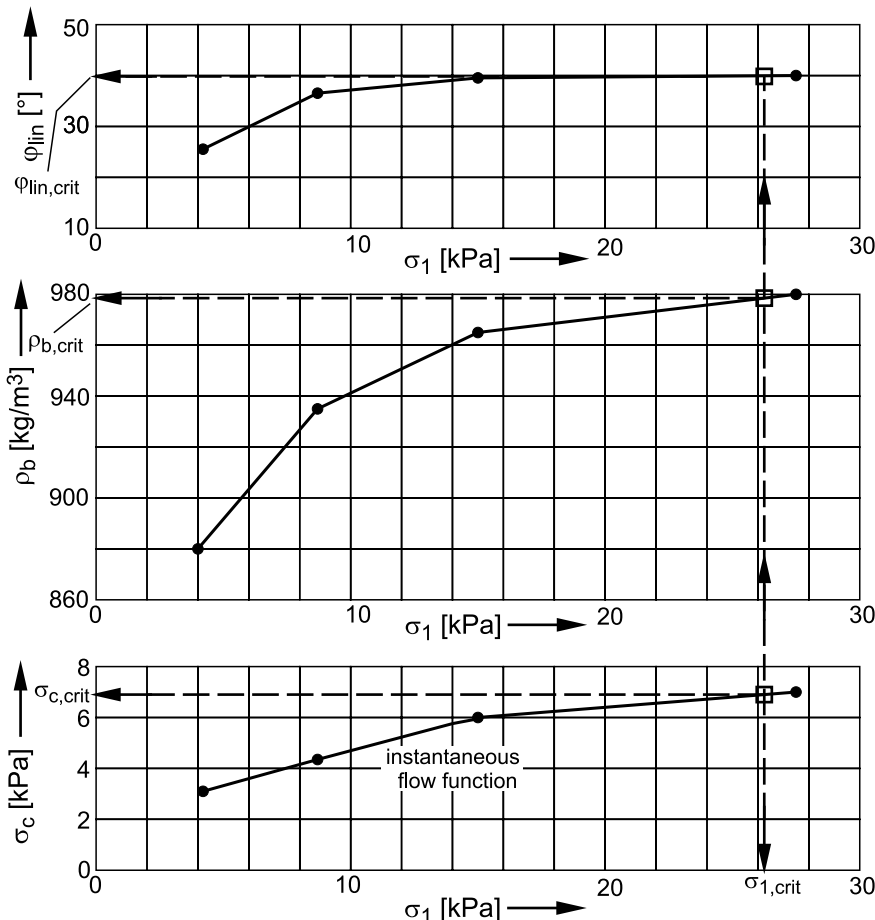


Fig. 15.12. Diagrams showing flow properties for determination of upper bound of minimum outlet dimension to avoid ratholing (measured values are plotted as circles; squares represent critical values according to the maximum consolidation stress for filling conditions)

The bulk density $\rho_b = 980$ kg/m³ used for estimation of major consolidation stress, $\sigma_{1,crit}$, is almost equal to the critical value in Table 15.9. Since bulk density increases from the top to the bottom of the silo filling according to the increase of consolidation stress (Fig. 10.18), the major consolidation stress at the bottom may be overestimated somewhat which provides some additional safety. If the bulk density used for the estimation of consolidation stress would have been smaller than the critical value, the calculation would have to be repeated with a higher bulk density.

The upper bound value of minimum outlet dimension to avoid ratholing is calculated from the critical values in Table 15.9 using Eq.(15.29). Thus the value of function $f(\varphi_i)$ has to be determined with Fig. 10.16: $f(\varphi_i = \varphi_{lin} = 40^\circ) = 3.6$. Finally one obtains the upper bound value $D_{crit} = 2.59$ m. This diameter is clearly larger than the lower bound value ($D_{crit} = 0.98$ m), which is a result of the higher consolidation stress in the state of filling (see Sect. 10.3.2).

Sample problem 12: Design of a silo under consideration of time consolidation

A mass flow silo with conical hopper has to be designed for the storage of a bulk solid tending to time consolidation. Arching has to be avoided even after three days storage at rest. The flow properties, which have been measured with a shear tester, are plotted in diagrams (Fig. 15.13). The wall yield locus (also shown in one of the diagrams in Fig. 15.13) does not run through the origin. Thus the wall friction angle, φ_x , is dependent on the wall normal stress.

Find the maximum hopper slope for mass flow and the minimum outlet opening to avoid arching for storage times up to three days.

Solution:

First the hopper slope for mass flow has to be determined. This is somewhat more difficult than in problem 10, because the wall friction angle, φ_x , as well as the effective angle of internal friction, φ_e , are dependent on the stress level. For mass flow design the flow properties (φ_x , φ_e) at the stresses acting close to the outlet opening have to be applied. Since the stress at the outlet opening is not known when starting the design procedure, the flow properties at the outlet have to be estimated.

In order to obtain a realistic estimation, the following procedure is recommended: The flow factor, ff , required to plot the ff line representing the major principal stress in the arch, is often on the order of 1.2 to 1.4. Thus one can plot a preliminary ff line, for example, with $ff = 1.3$ (see dotted line in the σ_c, σ_I diagram in Fig. 15.13). The $ff = 1.3$ line intersects the flow function (extrapolated to the left) at about $\sigma_I = 3$ kPa. The corresponding effective angle of internal friction is $\varphi_e = 47^\circ$. Since the wall normal stress is somewhat smaller than the major principal stress (see Fig. 10.14), the wall normal stress is estimated to about 80% of the major principal stress, thus $\sigma_w = 2.4$ kPa. The corresponding wall friction angle is $\varphi_x = 26^\circ$ (determined from the wall yield locus according to Sect. 3.3.2).

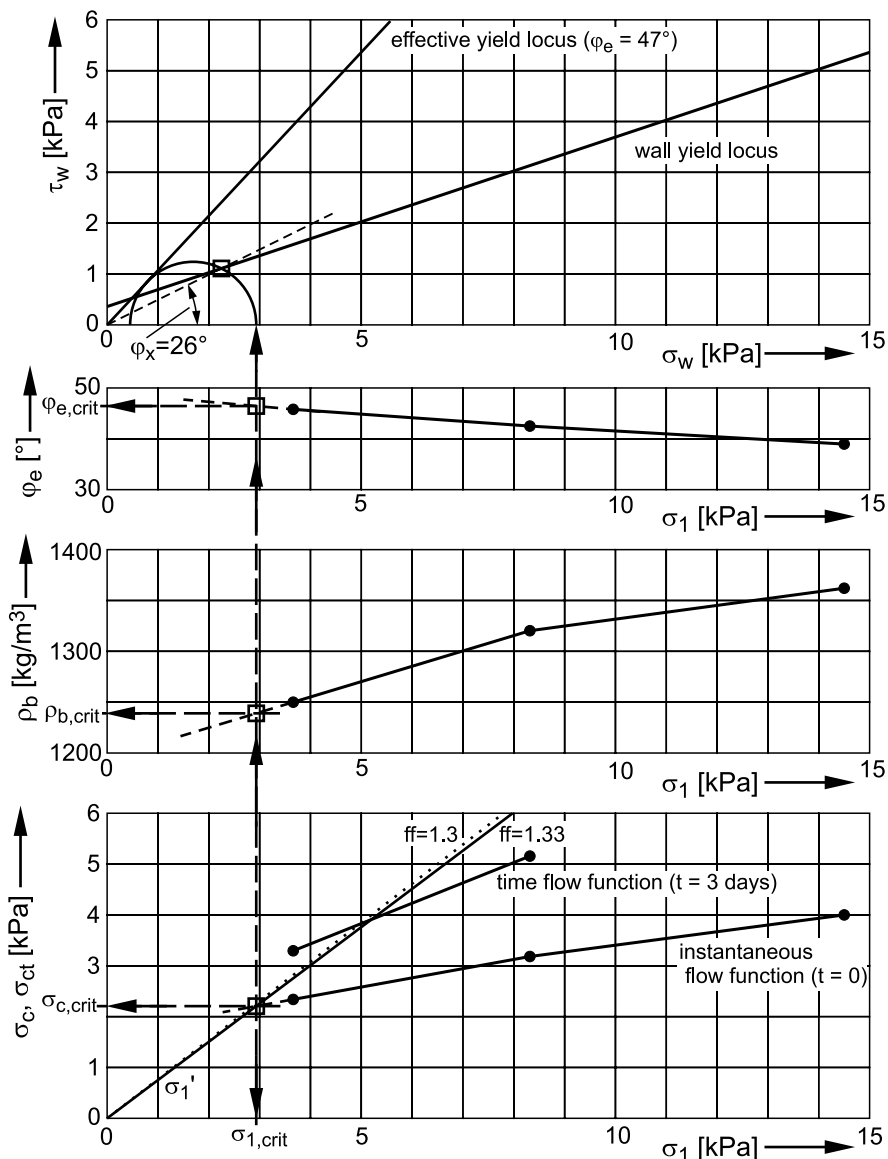


Fig. 15.13. Diagrams showing flow properties for the determination of the minimum outlet dimensions to avoid arching (measured values are plotted as circles; squares represent the finally determined critical values according to the point of intersection of the flow function with the major stress in a stable arch, σ_1')

On the basis of estimated values the maximum hopper wall slope from vertical can be determined with the diagram in Fig. 10.6: $\Theta_c = 19.5^\circ$. After

subtraction of the safety margin (assuming that the properties of the bulk solid and the wall surface are well-defined and do not change with time (Sect. 10.3.1), a safety margin of 2° to 3° may be sufficient) one obtains $\Theta_c = 17^\circ$.

The flow factor, depending on the hopper shape and the bulk solid, is determined with the flow factor diagrams for conical hoppers and effective angles of internal friction of 40° and 50° (Figs. 10.10 and 10.11):

$$ff(\varphi_x = 26^\circ, \varphi_e = 40^\circ, \Theta_c = 17^\circ) = 1.45$$

$$ff(\varphi_x = 26^\circ, \varphi_e = 50^\circ, \Theta_c = 17^\circ) = 1.28$$

Interpolation leads to a flow factor $ff = 1.33$ for $\varphi_e = 47^\circ$. The corresponding $ff = 1.33$ line according to Eq.(10.4), representing the major stress in the arch, σ_I' , intersects the flow function at $\sigma_{I,crit} = 2.9$ kPa. For this consolidation stress one obtains the critical values of unconfined yield strength, bulk density and effective angle of internal friction shown in Table 15.10.

Table 15.10. “Critical” parameters at the intersection of the flow function with the ff line

$\sigma_{I,crit}$ [Pa]	$\sigma_{c,crit}$ [Pa]	$\rho_{b,crit}$ [kg/m ³]	$\varphi_{e,crit}$ [°]	$\varphi_{x,crit}$ [°]
2900	2200	1240	47	26

For the determination of wall friction angle corresponding to the critical consolidation stress, $\sigma_{I,crit}$, it has to be considered that the direction of the wall normal stress, σ_w , is different from the direction of the major principal stress at the wall. Therefore the wall friction angle has to be determined with a procedure according to Fig. 10.14: The effective yield locus for $\varphi_{e,crit} = 47^\circ$ is drawn through the origin of the wall yield locus diagram. Then a Mohr stress circle is drawn tangential to the effective yield locus with a major principal stress equal to $\sigma_{I,crit}$ ($\sigma_{I,crit}$ is plotted on the σ_w axis). This Mohr stress circle represents steady-state flow at the outlet opening. The right point of intersection of the Mohr stress circle with the wall yield locus represents conditions at the hopper wall close to the outlet opening resulting in a wall friction angle of $\varphi_{x,crit} = 26^\circ$.

Since both $\varphi_{e,crit}$ and $\varphi_{x,crit}$ are equal to the values φ_e and φ_x , estimated at the beginning of the design procedure, further calculations are not necessary. If the latter were not the case, one would have to repeat the procedure using $\varphi_{e,crit}$ and $\varphi_{x,crit}$ as new estimates (iteration).

The minimum outlet diameter to avoid arching follows from Eq.(10.7a) with the critical values of Table 15.10 :

$$d_{crit} = H(\Theta_c) \frac{\sigma_{c,crit}}{g \cdot \rho_{b,crit}} \quad (15.30)$$

According to Fig. 10.13, the factor $H(\Theta_c = 17^\circ)$ is equal to 2.3. Therefore the minimum outlet diameter to avoid arching is $d_{crit} = 0.4$ m.

For the storage time at rest of three days a time flow function $\sigma_{ct} = \sigma_c(\sigma_l, t)$ has been measured (Fig. 15.13). It is located clearly above the (instantaneous) flow function due to the pronounced increase of unconfined yield strength with time. Thus the point of intersection with the ff line is shifted towards larger values of σ_c and σ_l . When determining the minimum outlet diameter with this point, it has to be considered that due to the larger consolidation stress the flow properties (e.g., the effective angle of internal friction and the wall friction angle) may be different from those determined for the point of intersection with the instantaneous flow function. Thus a different maximum hopper slope for mass flow can result for the larger outlet opening. Therefore, the whole design procedure as shown above for the instantaneous flow function must be repeated for the time flow function.

First the point where the time flow function intersects the ff line is estimated with $ff = 1.3$ (dotted line in the σ_c, σ_l diagram; see Fig. 15.14). This point is found at $\sigma_l = 5$ kPa. The corresponding flow properties are $\varphi_e = 45^\circ$ and $\varphi_x = 22^\circ$. These values lead to a maximum hopper slope for mass flow of $\Theta_c = 22^\circ$ (safety margin included). Then the flow factor is determined: $ff = 1.40$. The critical values found for $ff = 1.40$ (see squares in Fig. 15.14) are depicted in Table 15.11.

Table 15.11. “Critical” parameters at the intersection of the ff line and the time flow function for 3 days storage time

$\sigma_{l,crit}$ [Pa]	$\sigma_{ct,crit}$ [Pa]	$\rho_{b,crit}$ [kg/m ³]	$\varphi_{e,crit}$ [$^\circ$]	$\varphi_{x,crit}$ [$^\circ$]
5800	4200	1280	44	22

Table 15.12. Critical outlet diameters and corresponding hopper slopes

Max. storage time at rest, t [days]	Outlet diameter, d_{crit} [m]	Max. hopper slope, Θ_c [$^\circ$], according to d_{crit}
0	0.40	17
3	0.79	22

The difference between the estimated φ_e and the critical value $\varphi_{e,crit}$ amounts to only 1° . Thus a new calculation with $\varphi_{e,crit}$ would lead to nearly the same results.

With $H(\Theta_c = 22^\circ) = 2.35$ the outlet diameter to avoid arching after three days storage at rest is $d_{crit} = 0.79$ m. Table 15.12 shows all results of the silo design procedure.

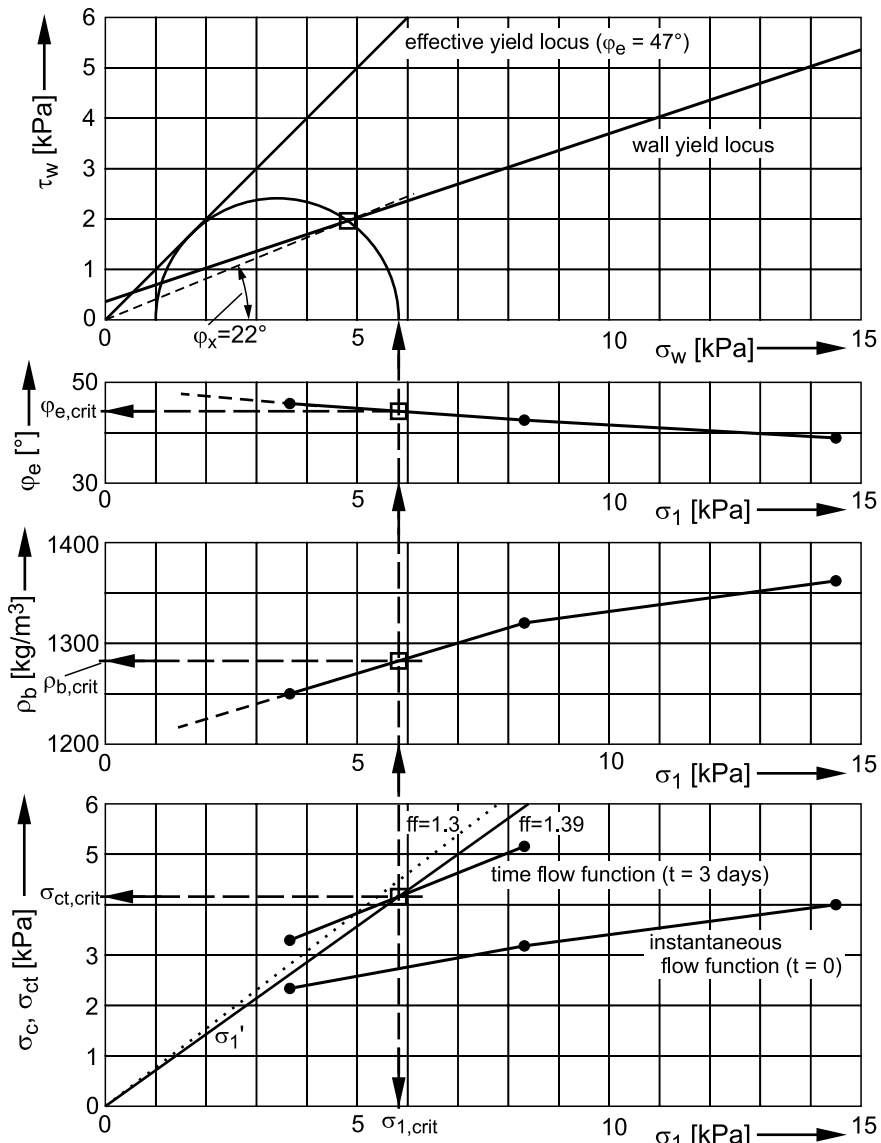


Fig. 15.14. Diagrams with flow properties for silo design; determination of the outlet size for 3 days storage at rest. The circles represent test results, the squares represent the points of intersection for the critical values determined finally.

Symbols

Please note: Units are presented as SI base units or SI derived units (SI: Système international d'unités; see ISO 1000 “SI units and recommendations for the use of their multiples and of certain other units”).

a	[m]	distance
a	[m/s ²]	acceleration
A	[m ²]	area
b	[m]	width
b_E	[m]	width of a wedge-shaped insert
b_{crit}	[m]	critical outlet width to avoid arching, i.e., the minimum width of a rectangular outlet opening to avoid arching
B	[m]	width (of the vertical section of a silo with rectangular cross-section)
c	[N/m]	spring constant
d	[m]	diameter, particle diameter
d_{crit}	[m]	critical outlet diameter to avoid arching, i.e., the minimum diameter of a circular outlet opening to avoid arching
d_f	[m]	diameter of the flow zone
D	[m]	diameter; silo diameter
D_{crit}	[m]	critical outlet diameter to avoid ratholing, i.e., the minimum diameter of a circular outlet opening or the minimum length of the diagonal of a rectangular outlet opening to avoid ratholing
f_c	[Pa]	compressive strength; unconfined yield strength (also: σ_c)
F	[N]	force
F_A	[N]	counterweight force (ring shear tester); supporting force
F_D	[N]	compressive force
F_F	[N]	centrifugal force
F_G	[N]	weight force
F_h	[N]	driving force (feeder)
F_K	[N]	contact force
F_N	[N]	normal force
F_p	[N]	drag force

F_R	[N]	resultant force; friction force
F_S	[N]	shear force
F_T	[N]	tangential force
F_v	[N]	vertical force
F_Z	[N]	tensile force
ff	[-]	flow factor (depending on flow properties and hopper geometry)
ff_c	[-]	flowability, calculated from the ratio of consolidation stress, σ_i , to compressive strength, σ_c
ff_p	[-]	density-weighted flowability
g	[m/s ²]	acceleration due to gravity, $g = 9.81 \text{ m/s}^2$
h	[m]	height; layer height; specimen height
H	[-]	Hausner ratio
h_f	[m]	filling height
hs	[m]	height of shear zone
K	[-]	(lateral) stress ratio, i.e., ratio of horizontal stress to mean vertical stress in the vertical section of a silo (λ in German code DIN 1055-6 (1987) [1.5])
K_0	[-]	(lateral) stress ratio without influence of wall friction (ratio of minor to major principal stress)
K_I	[-]	compressibility index
L	[m]	length; length of a rectangular outlet opening
m	[kg]	mass
m	[-]	parameter describing hopper geometry ($m = 0$: wedge-shaped; $m = 1$: conical)
M	[Nm]	torque, bending moment
\dot{m}	[kg/s]	discharge rate, flow rate
n	[-]	number
p	[Pa]	gas pressure
p_e	[Pa]	gas overpressure (relative to ambient pressure)
r	[m]	radius; radius of a roughness; polar coordinate
R	[m]	radius; particle radius (sphere)
R_a	[m]	arithmetic average roughness (arithmetic average of the absolute deviations from the mean surface level)
S	[-]	degree of saturation
t	[s]	time; storage time
u	[m/s]	velocity
U	[m]	circumference; perimeter
v	[m/s]	velocity
v_s	[m/s]	shear velocity
V	[m ³]	volume
w	[m/s]	superficial gas velocity

w_L	[m/s]	minimum fluidizing velocity
w_s	[m/s]	steady-state settling velocity
W	[J]	work, energy
x	[m]	coordinate; particle size; horizontal eccentricity of an insert
x_{50}	[m]	mass median of particle size distribution
y	[m]	coordinate
z	[m]	coordinate
z_a	[m]	vertical displacement (discharge device, feeder)
z_s	[m]	vertical displacement (silo)
α	[°]	angle; characteristic angle of a liquid bridge
β	[°]	angle
δ	[°]	angle
γ	[°]	angle characterizing shear deformation
$\dot{\gamma}/2$	[1/s]	shear rate
ε	[-]	porosity, void ratio
$\dot{\varepsilon}$	[1/s]	strain rate
Θ	[°]	inclination of a hopper wall to the vertical
Θ_{ap}	[°]	inclination of the inclined wall of a asymmetric wedge-shaped hopper to the vertical
Θ_c	[°]	inclination of the wall of a conical hopper to the vertical (also: hopper half-angle)
Θ_{cd}	[°]	maximum inclination of a hopper wall for complete clearance due to gravity (measured to the vertical)
Θ_p	[°]	inclination of the side walls of a wedge-shaped hopper to the vertical (also: hopper half-angle)
Θ_v	[°]	valley angle, i.e., slope of the corner of a pyramidal hopper to the vertical
λ	[-]	(lateral) stress ratio (according to DIN 1055 part 6 (1987) [1.5]; internationally known as K)
μ	[-]	friction coefficient
μ_0	[-]	coefficient of static friction
ν	[°]	angle of dilation
ρ_b	[kg/m ³]	bulk density
ρ_{bo}	[kg/m ³]	aerated density; bulk density of a loose, uncompressed bulk solid
ρ_f	[kg/m ³]	fluid density
ρ_s	[kg/m ³]	solid density
ρ_t	[kg/m ³]	tap density
σ	[Pa]	normal stress
σ_{sh}	[Pa]	normal stress at shear to failure
σ_{pre}	[Pa]	normal stress at preshear

σ_a	[Pa]	normal stress in a cutting plane inclined to the horizontal by angle α
σ_c	[Pa]	compressive strength; unconfined yield strength (also known as f_c)
σ_{ct}	[Pa]	unconfined yield strength attained after time consolidation; $\sigma_{ct} = \sigma_c(\sigma_I, t)$
σ_h	[Pa]	horizontal stress
σ_{hm}	[Pa]	mean horizontal stress
σ_t	[Pa]	tensile strength
σ_v	[Pa]	vertical stress
σ_{va}	[Pa]	vertical stress at the outlet opening
$\sigma_{vE,spec}$	[Pa]	specific insert load
$\sigma_{v\infty}$	[Pa]	final or asymptotic stress, i.e., the vertical stress in the vertical section of a silo in infinite depth
σ_w	[Pa]	wall normal stress
σ_I	[Pa]	major principal stress
σ_I'	[Pa]	major stress in an arch
σ_I''	[Pa]	circumferential stress in the wall of a rathole
σ_2	[Pa]	minor principal stress
σ_3	[Pa]	mean principal stress
τ_{ad}	[Pa]	adhesion (shear stress at the intersection of the wall yield locus with the shear stress axis)
τ_{sh}	[Pa]	maximum shear stress at shear to failure
τ_{pre}	[Pa]	shear stress at the end of preshear (steady-state flow)
τ_c	[Pa]	cohesion (shear stress at the intersection of the yield locus with the shear stress axis)
τ_{sf}	[Pa]	shear stress at steady-state flow
τ_w	[Pa]	wall shear stress
τ_{xy}	[Pa]	shear stress (parallel to y axis, perpendicular to x axis)
φ	[°]	angle of internal friction
φ	[°]	liquid portion of a liquid bridge
φ_e	[°]	effective angle of internal friction
φ_i	[°]	local slope of a yield locus
φ_{lin}	[°]	slope of a linearized yield locus
φ_{sf}	[°]	internal angle of friction at steady-state flow
φ_t	[°]	local slope of a time yield locus
φ_x	[°]	kinematic angle of wall friction
$\varphi_{x,st}$	[°]	static angle of wall friction
ω	[1/s]	angular velocity

Indices:

a	outlet opening
c	axisymmetric state of flow; conical hopper
p	plane state of flow; wedge-shaped hopper
ap	plane-asymmetric state of flow; asymmetric wedge-shaped hopper
tot	total
h	horizontal
crit	critical (representing conditions at the minimum outlet size required to avoid arching or ratholing, respectively)
max	maximum
min	minimum
rel	relative
v	vertical

References

- [1.1] Hampe E (1987) Silos, Band 1, Grundlagen. VEB Verlag für Bauwesen. Berlin
- [1.2] Roberts I (1882) On the pressure of wheat stored in elongated cells or bins. *Engineering* 34:399
- [1.3] Roberts I (1884) Determination of the vertical and lateral pressures of granular substances. *Proceed. Royal. Soc. of London* 36:225–240
- [1.4] Janssen HA (1895) Versuche über Getreidedruck in Silozellen. *Ztg. Ver. dt. Ing.* 39:1045–1049
- [1.5] DIN 1055 part 6 (1987) Loads in silos. German code.
- [1.6] EN 1991-4:2006-12 (2006) Eurocode 1: Actions on structures – Part 4: Silos and tanks.
- [1.7] Jenike & Johanson, Inc. (2003) Newsletter Fall 2003 (www.jenike.com)
- [1.8] Jenike AW (1961) Gravity flow of bulk solids. Bull. No. 108, Engng. Exp. Station, Univ. Utah, Salt Lake City
- [1.9] Jenike AW (1964) Storage and flow of solids. Bull. No. 123, Engng. Exp. Station, Univ. Utah, Salt Lake City
- [1.10] Schwedes J (1970) Fließverhalten von Schüttgütern in Bunkern. Verlag Chemie, Weinheim, Germany

- [2.1] Molerus O (1985) Schüttgutmechanik. Springer, Berlin Heidelberg New York Tokyo
- [2.2] Schulze D (1991) Untersuchungen zur gegenseitigen Beeinflussung von Silo und Austragorgan. Ph.D. thesis, Techn. Univ. Braunschweig, Germany
- [2.3] Neuber H (1971) Technische Mechanik, Zweiter Teil. Springer, Berlin Heidelberg New York
- [2.4] Kwade A, Schulze D, Schwedes J (1994) Determination of the stress ratio in uniaxial compression tests. *Powder Handling & Processing* 6:61–65 and 6:199–203
- [2.5] Schwedes J (1968) Fließverhalten von Schüttgütern in Bunkern. Verlag Chemie, Weinheim, Germany
- [2.6] Schulze D, Schwedes, J (1993) Fließverhalten von Schüttgütern. In: Weipert D et al.: *Rheologie der Lebensmittel*. Behr's Verlag, Hamburg
- [2.7] Stieß M (1995) Mechanische Verfahrenstechnik Bd. 1 und 2. Springer, Berlin Heidelberg New York, 2. Aufl.
- [2.8] Schubert H (1982) Kapillarität in porösen Feststoffsystmen. Springer, Berlin Heidelberg New York

- [2.9] Schubert H (1972) Untersuchungen zur Ermittlung von Kapillardruck und Zugfestigkeit von feuchten Haufwerken aus körnigen Stoffen. Ph.D. thesis, Univ. Karlsruhe, Germany
- [2.10] Rumpf H (1975) Mechanische Verfahrenstechnik. Carl Hanser Verlag, München und Wien
- [2.11] Schubert H, Liepe F, Schönert K (2003) Mechanische Grundvorgänge und Mikroprozesse. In: Schubert H (Ed) Handbuch der Mechanischen Verfahrenstechnik, Bd. 1. WILEY-VCH Verlag, Weinheim, Germany
- [2.12] Rumpf H (1974) Die Wissenschaft des Agglomerierens. Chem.-Ing.-Tech 46:1–11
- [2.13] Krus M (1995) Feuchtetransport- und Speicherkoefizienten poröser mineralischer Baustoffe. Theoretische Grundlagen und neue Meßtechniken. Ph.D. thesis, Univ. Stuttgart, Germany
- [2.14] Schubert H (1984) Capillary forces – Modeling and application in particulate technology. Aufbereitungstechnik 25:39–49
- [2.15] Tomas J, Schubert H (1985) Flow behaviour of moist bulk materials. Aufbereitungstechnik 7:399–404
- [2.16] Israelachvili JN (1992) Intermolecular and surface forces. Academic Press, London
- [2.17] Schubert H (1979) Grundlagen des Agglomerierens. Chem.-Ing.-Techn. 51:266–277
- [2.18] Barthlott W, Neinhuis, C. (1997) Purity of the sacred lotus. or escape from contamination in biological surfaces. Planta 202:1–8
- [2.19] Autumn K, Liang YA, Hsieh ST, Zesch W, Chan WP, Kenny WT, Fearing R, Full RJ (2000) Adhesive force of a single gecko foot-hair. Nature 405:681–685.
- [3.1] Jenike AW (1964/1980) Storage and flow of solids. Bull. No. 123, 20th Printing, revised 1980. Engng. Exp. Station, Univ. of Utah, Salt Lake City.
- [3.2] Schwedes J, Schulze D (1990) Measurement of flow properties of bulk solids. Powder Technology 61:59–68
- [3.3] Harder J (1985) Ermittlung der Fließeigenschaften kohäsiver Schüttgüter mit einer Zweiaxialbox. Ph.D. thesis, Techn. Univ. Braunschweig, Germany
- [3.4] Gerritsen AH (1982) The mechanics of cohesive powders. Ph.D. thesis, Rijksuniv. te Groningen, The Netherlands
- [3.5] Schulze D (1995) Zur Fließfähigkeit von Schüttgütern – Definition und Meßverfahren. Chem.-Ing.-Techn. 67:60–68
- [3.6] Schulze D (1998) The measurement of the flowability of bulk solids. In: Brown CJ, Nielsen J (Eds) Silos – Fundamentals of theory, behaviour and design. E & FN Spon, London and New York, pp 18–52
- [3.7] Carr JF, Walker DM (1967/68) An annular shear cell for granular materials. Powder Technology 1:369–373
- [3.8] Molerus O (1985) Schüttgutmechanik. Springer, Berlin Heidelberg New York Tokyo

- [3.9] Schwedes J (1968) Fließverhalten von Schüttgütern in Bunkern. Verlag Chemie, Weinheim, Germany
- [3.10] Schwedes J (1976) Fließverhalten von Schüttgütern in Bunkern. Chem.-Ing.-Tech. 48:294–300
- [3.11] Schwedes J (1971) Scherverhalten leicht verdichteter, kohäsiver Schüttgüter. Ph.D. thesis, Univ. Karlsruhe, Germany
- [3.12] The Institution of Chemical Engineers (Publ) (1989) Standard shear testing technique for particulate solids using the Jenike shear cell. Rugby, England, UK
- [3.13] Münz G (1976) Entwicklung eines Ringschergerätes zur Messung der Fließeigenschaften von Schüttgütern und Bestimmung des Einflusses der Teilchengrößenverteilung auf die Fließeigenschaften kohäsiver Kalksteinpulver. Ph.D. thesis, Univ. Karlsruhe, Germany
- [3.14] Gebhard H (1982) Scherversuche an leicht verdichteten Schüttgütern unter besonderer Berücksichtigung des Verformungsverhaltens. Ph.D. thesis, Univ. Karlsruhe, Germany
- [3.15] Schulze D (2000) Zur Anwendung des effektiven Reibungswinkels. Schüttgut 6:395–400
- [3.16] Jenike AW (1961) Gravity flow of bulk solids. Bull. No. 108, Engng. Exp. Station, Univ. Utah, Salt Lake City
- [3.17] Schulze D, Wittmaier A (2003) Flow properties of highly dispersed powders at very small consolidation stresses, Chem. Eng. Technol. 26: 133–137
- [4.1] Gebhard H (1982) Scherversuche an leicht verdichteten Schüttgütern unter besonderer Berücksichtigung des Verformungsverhaltens. Fortschr.-Ber. VDI-Z., Reihe 3, Nr. 68, VDI-Verlag, Düsseldorf, Germany
- [4.2] Wilms H, Schwedes J (1985) Interpretation of ring shear tests. Bulk Solids Handling 5:1017–1020
- [4.3] Hesse T, Hoffmann OH (1977) Scherverhalten körniger landwirtschaftlicher Haufwerke. Grundl. Landtechn. 27:205–213
- [4.4] Münz G (1976) Entwicklung eines Ringschergerätes zur Messung der Fließeigenschaften von Schüttgütern und Bestimmung des Einflusses der Teilchengrößenverteilung auf die Fließeigenschaften kohäsiver Kalksteinpulver. Ph.D. thesis, Univ. Karlsruhe, Germany
- [4.5] Peschl IASZ (1989) Equipment for the measurement of mechanical properties of bulk materials. Powder Handling & Processing 1:73–81
- [4.6] Peschl IASZ (1989) Measurement and evaluation of mechanical properties of powders. Powder Handling & Processing 1:135–142
- [4.7] Schmitt R, Feise H (2004) Influence of tester geometry, speed and procedure on the results from a ring shear tester. Part. Part. Syst. Charact. 21:403–410
- [4.8] Jenike AW (1964/1980) Storage and flow of solids. Bull. No. 123, 20th Printing, revised 1980. Engng. Exp. Station, Univ. of Utah, Salt Lake City.

- [4.9] Jenike AW (1961) Gravity flow of bulk solids. Bull. No. 108, Engng. Exp. Station, Univ. Utah, Salt Lake City
- [4.10] Schwedes J (1979) Vergleichende Betrachtungen zum Einsatz von Schergeräten zur Messung von Schüttguteigenschaften. Proc. PARTEC, Nürnberg, pp 278–300
- [4.11] Schwedes J, Schulze D (1990) Measurement of flow properties of bulk solids. Powder Technology 61:59–68
- [4.12] Schulze D (1985) Einfluß unterschiedlicher Scherzellengeometrien auf die Ergebnisse von Scherversuchen. Student project at the Institute for Mechanical Process Engineering, Techn. Univ. Braunschweig, Germany (not published)
- [4.13] The Institution of Chemical Engineers (Publ) (1989) Standard shear testing technique for particulate solids using the Jenike shear cell. Rugby, England, UK
- [4.14] ASTM Standard D6128: Standard test method for shear testing of bulk solids using the Jenike shear cell. ASTM International, www.astm.org
- [4.15] Schulze D (1996) Vergleich des Fließverhaltens leicht fließender Schüttgüter. Schüttgut 2:347–356
- [4.16] Hvorslev MJ (1937) Über die Festigkeitseigenschaften gestörter bindiger Böden. Ingenørvidenskabelige Skrifter A, Nr. 45, Copenhagen, Denmark
- [4.17] Carr JF, Walker DM (1967/68) An annular shear cell for granular materials. Powder Technol. 1:369–373
- [4.18] Bagster DF (1981) Tests on a very large shear cell. Bulk Solids Handling 1:743–746
- [4.19] Rippie EG, Chou CH (1978) Kinetics of mass transport in sheared particular beds: Markov chains. Powder Technol. 21:205–216
- [4.20] Bagster DF, Arnold PC, Roberts AW, Fitzgerald TF (1974) The interpretation of ring shear results. Powder Technol. 9:135–139
- [4.21] Novosad J (1964) Studies on granular materials II, apparatus for measuring the dynamic angle of internal and external friction of granular materials. Coll. Czech. Chem. Com. 29:2697–2701
- [4.22] Bishop AW, Green GE, Garga VK, Anderson A, Brown JD (1971) A new ring shear test apparatus and its application to the measurement of residual strength. Géotechnique 21:273–328
- [4.23] Scarlett B, Todd AC (1968) A split ring annular shear cell for the determination of the shear strength of powder. J. of Sci. Instruments 1:655–656
- [4.24] Schulze D (1994) Development and application of a novel ring shear tester. Aufbereitungstechnik 35:524–535
- [4.25] Schulze D (1995) Appropriate devices for the measurement of flow properties for silo design and quality control. Preprints PARTEC 95 “3rd Europ. Symp. Storage and Flow of Particulate Solids”, 21–23 March 1995, Nuremberg, Germany, pp 45–56
- [4.26] Wittmaier A (2003) Fließverhalten hochdisperser Pulver bei sehr kleinen Spannungen. Ph.D. thesis, Techn. Univ. Braunschweig, Germany

- [4.27] Schulze D, Wittmaier A (2003) Flow properties of highly dispersed powders at very small consolidation stresses, *Chem. Eng. Technol.* 26: 133–137
- [4.28] Schulze D (2004) Ein neues Prinzip zur Messung der Fließeigenschaften von Pulvern und Schüttgütern. *Schüttgut* 10:369–377
- [4.29] ASTM Standard D6773: Standard shear test method for bulk solids using the Schulze ring shear tester. ASTM International, www.astm.org
- [4.30] Behres M, Riemenschneider H, Kiesewetter W, Peterlic J (1997) Vergleichsmessungen an einem neuartigem Ringschergerät und dem Jenike-Schergerät. *Schüttgut* 3:155–160
- [4.31] Schulze D (1998) Measurement of flow properties of particulate solids in food and pharmaceutical technology using a new automated ring shear tester. Preprints PARTEC “1st Europ. Symp. Process Technology in Pharmaceutical and Nutritional Sciences”, 10–12 March 1998, Nuremberg, Germany, pp 276–285
- [4.32] Verlinden A (2000) Experimental assessment of shear testers for measuring flow properties of bulk solids. Ph.D. thesis, Univ. of Bradford, UK
- [4.33] Behres M, Klasen CJ, Schulze D (1998) Development of a shear cell for measuring the wall friction of bulk solids with a ring shear tester. *Powder Handling & Processing* 10:406–409
- [4.34] Schulze D, Schwedes J, Leonhardt C, Kossert J (1998) Design of a silo for the storage of 10.000 t sulphur granules. *Bulk Solids Handling* 18:211–217
- [4.35] Kwade A, Schulze D (1998) Proper silo design for food products – Today strategies for avoiding segregation, degradation and hang-ups. Preprints PARTEC “1st Europ. Symp. Process Technology in Pharmaceutical and Nutritional Sciences”, 10–12 March 1998, Nuremberg, pp 157–166
- [4.36] Ghadiri M, Ning Z, Kenter SJ, Puik E (2000) Attrition of granular solids in a shear cell. *Chem. Eng. Sci.* 55:5445–5456
- [4.37] Bemrose, CR, Bridgwater J (1987) A review of attrition and attrition test methods. *Powder Technol.* 49:97–126
- [4.38] Schulze D (1998) The characterization of bulk solids for silo design and flowability tests. *Aufbereitungstechnik* 39:47–57
- [4.39] Runge J, Weißgüttel U (1989) A contribution to the description of the compressibility of bulk materials at normal stresses up to 30 kPa. *Aufbereitungstechnik* 3:138–143
- [4.40] Schulze D (1999) Silo Stress Tool, Computer program for the assessment of stresses in silos. Freeware (www.dietmar-schulze.de)
- [4.41] Schulze D (2003) Towards more reliability in powder testing. Proc. “4th Intl. Conf. on Conveying and Handling of Particulate Solids (CHoPS)”, Budapest, Hungary, 27–30 May 2003, Vol. 1, 5.31–5.36
- [4.42] Schwedes J (1968) *Fließverhalten von Schüttgütern in Bunkern*, Verlag Chemie, Weinheim, Germany
- [4.43] Schwedes J (1971) *Scherverhalten leicht verdichteter, kohäsiver Schüttgüter*. Ph.D. thesis, Univ. Karlsruhe, Germany

- [4.44] Schulze D, Heinrici H, Zetzener H (2001) The ring shear tester as a valuable tool for silo design and powder characterization. *Powder Handling & Processing* 13:19–24
- [4.45] Schulze D (2007) RST-CONTROL 95 – Program for the measurement of flow properties with the ring shear testers RST-01.pc and RST-XS.
- [4.46] Schulze D (2006) Automatische Bestimmung der optimalen Normalspannungen für Fließorte während der Messung. (Oral presentation, VDI-GVC Fachausschuss “Agglomerations- und Schüttguttechnik”, Reinbek, Germany, 20–21 March 2006)
- [5.1] Schulze D (2003) Time and velocity dependent properties of powders effecting slip-stick oscillations, *Chem. Eng. Technol.* 26:1047–1051
- [5.2] Schwedes J, Schulze D (1990) Measurement of flow properties of bulk solids. *Powder Technology* 61:59–68
- [5.3] Harder J (1985) Ermittlung der Fließeigenschaften kohäsiver Schüttgüter mit einer Zweiaxialbox. Ph.D. thesis, Techn. Univ. Braunschweig, Germany
- [5.4] Van der Kraan M (1996) Techniques for the measurement of the flow properties of cohesive powders. Ph.D. thesis, Univ. Delft, The Netherlands
- [5.5] Maltby LP (1993) Investigation of the behaviour of powders under and after consolidation. Ph.D. thesis, Telemark Institute of Technology, Norway
- [5.6] Maltby LP, Enstad GG, De Silva SR (1995) Investigation of the behaviour of powders under and after consolidation. Part. Part. Syst.Charact. 12:16–27
- [5.7] Enstad GG, Feise H (1998) Flow properties testing of particulate solids by uniaxial and biaxial testers. In: Brown CJ, Nielsen J (Eds) *Silos – Fundamentals of Theory, Behaviour and Design*. E & FN Spon, London and New York, pp 53–64
- [5.8] Nowak M (1993) Spannungs-/Dehnungsverhalten von Kalkstein in der Zweiaxialbox. Ph.D. thesis, Techn. Univ. Braunschweig, Germany
- [5.9] Nowak M, Schwedes J (1993) Measuring the fundamental material properties with true biaxial tester. Proc. Reliable Flow of Particulate Solids II, Oslo, Norway, 23.–25. August 1993, EFChE Publ. Ser. No. 96, pp 285–305
- [5.10] Feise H, Schwedes J (1995) Investigation of the behaviour of a cohesive powder in the biaxial tester. Proc. PARTEC “3rd European Symp. on Storage and Flow of Particulate Solids (Janssen Centennial)”, 21–23 March 1995, Nuremberg, Germany, pp 119–128
- [5.11] Feise HJ (1996) Modellierung des mechanischen Verhaltens von Schüttgütern. Ph.D. thesis, Techn. Univ. Braunschweig, Germany
- [5.12] Allersma HGB (1987) Optical analysis of stress and strain in photoelastic particle assemblies. Ph.D. thesis, Univ. Delft, The Netherlands
- [5.13] Oda M, Iwashita K (1999) Mechanics of granular materials. A.A.Balkema, Rotterdam/Brookfield

- [5.14] Gröger T, Tüzün U, Heyes DM (2003) Modelling and measuring of cohesion in wet granular materials. *Powder Technology* 133:203–215
- [5.15] Thornton C (1997) Force transmission in granular media. *KONA* 15:81–90
- [5.16] Tykhouiu R, Lüding S, Tomas J (2004) Simulation der Scherdynamik kohäsiver Pulver. *Chem.-Ing.-Techn.* 76:59–62
- [5.17] Kaldenhoff M (1998) Simulation von grobgranularen Schüttgütern mit Hilfe zellulärer Automaten. Ph.D. thesis, Techn. Univ. Braunschweig, Germany
- [5.18] Oda M, Kazama H, Konishi J (1998) Effects of induced anisotropy on the development of shear bands in granular materials. *Mechanics of Materials* 28:103–111
- [5.19] Arthur JRF, Menzies BK (1972) Inherent anisotropy of sand. *Géotechnique* 22:115–128
- [5.20] Goldscheider M (1972) Spannung in Sand bei räumlicher, monotoner Verformung. Ph.D. thesis, Univ. Karlsruhe, Germany
- [5.21] Hambly EC (1969) A new true triaxial apparatus. *Géotechnique* 19:307–309
- [5.22] Gerritsen AH (1982) The mechanics of cohesive powders. Ph.D. thesis, Rijksuniv. te Groningen, The Netherlands
- [5.23] Haaker G, Rademacher FJC (1983) Direct measurement of the flow properties of bulk solids by a modified triaxial tester. *Aufbereitungstechnik* 11:647–655
- [5.24] Kolymbas D, Wu W (1988) Recent results of triaxial tests with grain materials. Preprints “Silos – Forschung und Praxis”, Conference of the SFB 219, Karlsruhe, Germany, pp 99–117
- [5.25] Kwade A, Schulze D, Schwedes J (1994) Die direkte Messung des Horizontallastverhältnisses. *Beton- und Stahlbetonbau* 89:58–63 and 89:117–119
- [5.26] Kwade A, Schulze D, Schwedes J (1994) Determination of the stress ratio in uniaxial compression tests. *Powder Handling & Processing* 6:61–65 and 6:199–203
- [5.27] Molerus O (1985) *Schüttgutmechanik*. Springer, Berlin Heidelberg New York Tokyo
- [5.28] Molerus O (1975) Theory of yield of cohesive powders. *Powder Technol.* 12:259–275
- [5.29] Hirota M, Oshima T (1987) Shear properties of uniaxially preconsolidated powder bed – non-uniformity of the shear stress acting on the shear plane. *Powder Technol.* 53:49–54
- [5.30] Saraber F, Enstad GG, Haaker G (1991) Investigations on the anisotropic yield behaviour of a cohesive bulk solid. *Powder Technol.* 64:183–190
- [5.31] Wittmaier A (2003) Fließverhalten hochdisperser Pulver bei sehr kleinen Spannungen. Ph.D. thesis, Techn. Univ. Braunschweig, Germany
- [5.32] Schwedes J (1971) Scherverhalten leicht verdichteter, kohäsiver Schüttgüter. Ph.D. thesis, Univ. Karlsruhe, Germany

- [5.33] Mandl G, de Jong LNJ, Maltha A (1977) Shear zones in granular material. *Rock Mechanics* 9:95–144
- [5.34] Hill R (1960) The mathematical theory of plasticity, Oxford Press
- [5.35] Lade P (1982) Localization effects in triaxial tests on sand. Proc. IUTAM Conference on Deformation and Failure of Granular Materials, Delft, The Netherlands, pp 461–471
- [5.36] Airey DW, Budhu M, Wood DM (1985) Some aspects of the behaviour of soils in simple shear. In: Banerjee PK, Butterfield R (Eds) Developments in solid mechanics and foundation engineering 2. Elsevier Applied Science, London
- [5.37] Morgan JK, Boettcher MS (1999) Numerical simulations of granular shear zones using the distinct element method: 1. Shear zone kinetics and the micromechanics of localization. *Journ. of Geophys. Res.* 104:2703–2719
- [5.38] Beeler NM, Tullis TE, Blanpied ML, Weeks JD (1996) Frictional behavior of large displacement experimental faults. *Journ. of Geophys. Res.* 101:8697–8715
- [5.39] Gebhard H (1982) Scherversuche an leicht verdichteten Schüttgütern unter besonderer Berücksichtigung des Verformungsverhaltens, Ph.D. thesis, Univ. Karlsruhe, Germany
- [5.40] Ogniwek D (1979) Die innere Reibung von Schüttgütern – Untersuchungen von Materialeigenschaften verschiedener Silo-Lagerstoffe. *Fortschr.-Ber. VDI-Z. Reihe 3, Nr. 50*
- [5.41] Roscoe KH (1970) Tenth Rankine lecture: The influence in strains in soil mechanics. *Géotechnique* 20:129–170
- [5.42] Mühlhaus HB, Vardoulakis IG (1987) The thickness of shear bands in granular materials. *Géotechnique* 37:271–283
- [5.43] Stadler R (1986) Stationäres, schnelles Fließen von dicht gepackten trockenen und feuchten Schüttgütern. Ph.D. thesis, Univ. Karlsruhe, Germany
- [5.44] Dieterich JH (1979) Modeling of rock friction: 1. Experimental results and constitutive equations. *Journ. Geophys. Res.* 84:2161–2168
- [5.45] Oda M, Kazama H (1998) Microstructure of shear bands and its relation to the mechanics of dilatancy and failure of dense granular solids. *Géotechnique* 48:465–481
- [5.46] Marone C (1998) Laboratory-derived friction laws and their application to seismic faulting. *Annual Review Earth & Planetary Science Letters* 26:643–696
- [5.47] Lohrmann J, Kukowski N, Adam J, Oncken O (2003) The impact of analogue material properties on the geometry, kinematics, and dynamics of convergent sand wedges. *Journ. of Structural Geology* 25:1691–1711
- [5.48] Riedel W (1929) Zur Mechanik geologischer Brucherscheinungen. *Zentralblatt für Mineralogie, Geologie und Paläontologie, Abt. B*, pp 354–368

- [5.49] Beeler NM, Tullis TE: (1995) Implications of Coulomb plasticity for the velocity dependence of experimental faults. *Pure and Applied Geophysics (PAGEOPH)* 144:251–276
- [5.50] Sammis CG, Steacy SJ (1994) The micromechanics of friction in a granular layer. *Pure and Applied Geophysics (PAGEOPH)* 142:777–794
- [5.51] Cleaver JAS, Nedderman RM, Thorpe RB (2000) Accounting for granular material dilation during the operation of an annular shear cell. *Advanced Powder Technology* 11:385–399
- [5.52] Münz G (1976) Entwicklung eines Ringschergerätes zur Messung der Fließeigenschaften von Schüttgütern und Bestimmung des Einflusses der Teilchengrößenverteilung auf die Fließeigenschaften kohäsiver Kalksteinpulver. Ph.D. thesis, Univ. Karlsruhe, Germany
- [5.53] Schofield A (1998) Mohr Coulomb error correction. *Ground Engng.* 31:30–32
- [5.54] Jenike AW (1964/1980) Storage and flow of solids. Bull. No. 123, 20th Printing, revised 1980. Engng. Exp. Station, Univ. of Utah, Salt Lake City.
- [5.55] The Institution of Chemical Engineers (Publ) (1989) Standard shear testing technique for particulate solids using the Jenike shear cell. Rugby, England, UK
- [5.56] Schwedes J (1968) Fließverhalten von Schüttgütern in Bunkern. Verlag Chemie, Weinheim, Germany
- [5.57] Schulze D (1994) Development and application of a novel ring shear tester. *Aufbereitungstechnik* 35:524–535
- [5.58] Schmitt R, Feise H (2004) Influence of tester geometry, speed and procedure on the results from a ring shear tester. *Part. Part. Syst. Charact.* 21:403–410
- [5.59] Jenike AW (1961) Gravity flow of bulk solids. Bull. No. 108, Engng. Exp. Station, Univ. Utah, Salt Lake City
- [5.60] Schwedes J (1976) Fließverhalten von Schüttgütern in Bunkern. *Chem.-Ing.-Tech.* 48:294–300
- [5.61] Höhne D (1985) Die Vergleichbarkeit unterschiedlicher Methoden zur Ermittlung der Scherfestigkeit feinkörniger Schüttgüter. Ph.D. thesis, Forschungsinstitut für Aufbereitung (FIA), Freiberg, Germany
- [5.62] Schulze D (1996) Vergleich des Fließverhaltens leicht fließender Schüttgüter. *Schüttgut* 2:347–356
- [5.63] Schulze D, Wittmaier A (2004) Flow properties of highly dispersed powders at very small consolidation stresses. In: Müller E, Oestreich C (Eds) *Handling of highly dispersed powders*. Schwerpunktprogramm der Deutschen Forschungsgemeinschaft, Shaker-Verlag, Aachen, Germany, pp 276–283
- [5.64] Schulze D, Wittmaier A (2003) Flow properties of highly dispersed powders at very small consolidation stresses, *Chem. Eng. Technol.* 26: 133–137
- [5.65] Tomas J (2004) Fundamentals of cohesive powder consolidation and flow. *Granular Matter* 6:75–86

- [5.66] Tomas J (2003) The mechanics of dry, cohesive powders, *Powder Handling & Processing* 15:296–314
- [6.1] Enstad GG, Pitchumani B, Sharma AK (1995) A simplified procedure for flow property testing using the Jenike shear tester. Proc. “5th Intnl. Conf. on Bulk Materials Storage, Handling and Transportation”, Newcastle, Australia, pp 371–179
- [6.2] Tsunakawa H, Aoki R (1982) Measurements of the failure properties of granular materials and cohesive powders. *Powder Technology* 33:249–256
- [6.3] Ladipo DD, Puri VM (1997) Computer controlled shear cell measurement of flow properties of particulate materials. *Powder Technology* 92:135–146
- [6.4] Schulze D (2000) Letter to the Editor. *Powder Technology* 107:186–190
- [6.5] Kirby JM (1984) Letter to the Editor. *Powder Technology* 39:291–292
- [6.6] Haaker G, Wiersma-van Schendel WJA (1993) A constant volume sheartester: development and experiences. *Bulk Solids Handling* 13:129–133
- [6.7] Haaker G, Schreuder R (1992) Development of a constant volume translational shear tester. Proc. “Int. Conf. on Bulk Materials Handling and Transportation”, Wollongong, Australia, pp 287–291
- [6.8] The Institution of Chemical Engineers (Publ) (1989) Standard shear testing technique for particulate solids using the Jenike shear cell. Rugby, England, UK
- [6.9] Umeya K, Hara R, Kikuta J (1975) On two-dimensional shear tests by model powders. *Journ. of Chem. Eng. of Japan* 8:56–62
- [6.10] Schwedes J, Schulze D (1990) Measurement of flow properties of bulk solids. *Powder Technology* 61:59–68
- [6.11] Harder J (1985) Ermittlung der Fließeigenschaften kohäsiver Schüttgüter mit einer Zweiaxialbox. Ph.D. thesis, Techn. Univ. Braunschweig, Germany
- [6.12] Gerritsen AH (1982) The mechanics of cohesive powders. Ph.D. thesis, Rijksuniv. te Groningen, The Netherlands
- [6.13] Schwedes J (1971) Scherverhalten leicht verdichteter, kohäsiver Schüttgüter. Ph.D. thesis, Univ. Karlsruhe, Germany
- [6.14] Haaker G, Rademacher FJC (1983) Direct measurement of the flow properties of bulk solids with a modified triaxial tester. *Aufbereitungstechnik* 11:647–655
- [6.15] Arthur JRF, Dunstan T, Enstad GG (1985) Determination of the flow function by means of a cubic plane strain tester. *Int. Journ. Bulk Solids Storage in Silos* 1:7–10
- [6.16] Schulze D (1996) Flowability of bulk solids – definition and measuring techniques, part I and II. *Powder and Bulk Engineering* 4:45–61 and 6:17–28

- [6.17] Schulze D (1998) The measurement of the flowability of bulk solids. In: Silos – Fundamentals of Theory, Behaviour and Design. Brown CJ, Nielsen J (Eds), E & FN Spon, London and New York, pp 18–52
- [6.18] Nowak M, Schwedes J (1993) Measuring the fundamental material properties with true biaxial tester. Proc. Reliable Flow of Particulate Solids II, Oslo, 23.–25. August 1993, EFChE Publ. Ser. No. 96, pp 285–305
- [6.19] Schwedes J (1979) Vergleichende Betrachtungen zum Einsatz von Schergeräten zur Messung von Schüttguteigenschaften. Preprints PARTEC, Nuremberg, Germany, pp 278–299
- [6.20] Schwedes J (2003) Review on testers for measuring flow properties of bulk solids. *Granular Matter* 5:1–43
- [6.21] Schulze D, Heinrici H, Zettner H (2001) The ring shear tester as a valuable tool for silo design and powder characterization. *Powder Handling & Processing* 13:19–24
- [6.22] Schmidt R, Feise H (2004) Influence of tester geometry, speed and procedure on the results from a ring shear tester. *Part. Part. Syst. Charact.* 21:403–410
- [6.23] Degussa AG (1981) AEROSIL zur Verbesserung des Fließverhaltens pulverförmiger Substanzen. Schriftenreihe Pigmente Nr.31
- [6.24] Council of Europe (COE) – European Directorate for the Quality of Medicines (2005) European Pharmacopoeia, Supplement 5.3.
- [6.25] DIN EN ISO 6186:1998 (1998) Kunststoffe – Bestimmung der Rieselfähigkeit.
- [6.26] Schwedes J (1968) Fließverhalten von Schüttgütern in Bunkern. Verlag Chemie, Weinheim, Germany
- [6.27] Wouters IMF, Geldart D (1996) Characterising semi-cohesive powders using angle of repose. *Part. Part. Syst. Charact.* 13:254–259
- [6.28] DIN ISO 4324 (1983) Tenside; Pulver und Granulat; Bestimmung des Schüttwinkels. Ausgabe 1983-12
- [6.29] Kalman H, Goder D, Rivkin M, Ben-Dor G (1993) The effect of the particle-surface friction coefficient on the angle of repose. *Bulk Solids Handling* 13:123–128
- [6.30] Brown RL, Richards JC (1970) Principles of powder mechanics. Pergamon Press, Oxford, UK
- [6.31] Liu XY, Specht E, Mellmann J (2005) Experimental study of the lower and upper angles of repose of granular materials in rotating drums. *Powder Technology* 154:125–131
- [6.32] Hobbs JW, Rhodes D (2000) The use of dynamic avalanching and fractal analysis to characterise uranium oxide powders. Atalante 2000, Int. Conf., Scientific Research on the Back End of the Fuel Cycle for the 21th Century, Avignon, France, 24–26 October 2000
- [6.33] Lavoie F, Carilier L, Thibert R (2002) New methods characterizing avalanche behavior to determine powder flow. *Pharmaceutical Res.* 19:887–893

- [6.34] Kaye BH (1997) Characterizing the flowability of a powder using the concepts of fractal geometry and chaos theory. Part. Part. Syst. Charact. 14:53–66
- [6.35] Castellanos A, Valverde JM, Quintanilla MAS (2004) The Sevilla powder tester: A tool for characterizing the physical properties of fine cohesive powders at very small consolidations. KONA 22:66–81
- [6.36] Imse W (1972) Messung der Fließfähigkeit von Zement. Zement Kalk Gips 25:147–149
- [6.37] Mayerhauser D (1989) Pulver im Test. Die Chemische Produktion, Special issue October 1989, pp 24–31
- [6.38] Hosokawa Micron Corporation: Powder Characteristics Tester, Operating Instructions.
- [6.39] ASTM Standard D6393: Standard test method for bulk solids characterization by Carr indices. ASTM International, www.astm.org
- [6.40] Carr RL (1965) Evaluating flow properties of solids. Chem. Engng. 72:163–168
- [6.41] Carr RL (1965) Classifying flow properties of solids. Chem. Engng. 72:69–72
- [6.42] Freeman R (2004) Go with the flow. LabPlus Int. Feb./March 2004, pp 8–10
- [6.43] Kammler RR (1985) Process for rapid determination of the flow properties of bulk materials. Aufbereitungstechnik 3:136–141
- [6.44] DIN 53194: Bestimmung des Stampfvolumens und der Stampfdichte.
- [6.45] DIN EN ISO 787-11 (1995) Allgemeine Prüfverfahren für Pigmente und Füllstoffe – Teil 11: Bestimmung des Stampfvolumens und der Stampfdichte. Ausgabe 1995-10
- [6.46] Abdullah EC, Geldart D (1999) The use of bulk density measurements as flowability indicators. Powder Technol. 102:151–165
- [6.47] Svarovski L (1987) Powder testing guide. Elsevier Applied Science Publishers Ltd., London and New York
- [6.48] Verlinden A (2000) Experimental assessment of shear testers for measuring flow properties of bulk solids. Ph.D. thesis, Univ. of Bradford, England
- [6.49] Orband JLR, Geldart D (1997) Direct measurement of powder cohesion using a torsional device. Powder Technol. 92:25–33
- [6.50] Brabender OHG, Duisburg (1982) Flowabilitytest. Specification sheet No. 2124
- [6.51] Knight PC, Johnson SH (1988) Measurement of powder cohesive strength with a penetration test. Powder Technology 54:279–283
- [6.52] Maltby LP, Enstad GG (1993) Uni-axial tester for quality control and flow property characterization of powders. Bulk Solids Handling 13:135–139
- [6.53] Kozler J, Novosad J (1989) A method for testing the flowability of fertilizers. Bulk Solids Handling 9:43–48

- [6.54] Williams JC, Birks AH, Bhattacharya D (1970/71) The direct measurement of the failure function of a cohesive powder. *Powder Technol.* 4:328–337
- [6.55] Beckhaus R, Felgner W, Runge J (1992) Auslegung von Silos für verklebende grobkörnige Schüttgüter. *Chem.-Ing.-Tech.* 64:292–293
- [6.56] Bell TA, Catalano EJ, Zhong Z, Ooi JY, Rotter JM (2007) Evaluation of the Edinburgh powder tester. Proc. PARTEC, 27–29 March 2007, Nuremberg, Germany, paper S30-1
- [6.57] Peschl IASZ, Colijn H (1977) New rotational shear testing technique. *Journ. of Powder & Bulk Solids Technology* 1:55–60
- [6.58] Sankyo Dengyo Co., Ltd., Tokio: Powder Bed Tester. Catalog Nr. 111018903
- [6.59] Hong GH, Watanabe K (1990) Powder bed tester. *Powder, Handling & Processing* 2:137–143
- [6.60] Ashton MD, Cheng DHC, Farley R, Valentin FHH (1965) Some investigations into the strength and flow properties of powders. *Rheologica Acta* 4:206–218
- [6.61] Ashton MD, Farley R, Valentin FHH (1964) An improved apparatus for measuring the tensile strength of powders. *Journ. Sci. Instruments* 41:763–765
- [6.62] Oshima T, Hirota M (1985) Experimental examination on the shear process of powder bed. *KONA* 3:63–68
- [6.63] Hirota M, Oshima T (1987) Shear properties of uniaxially preconsolidated powder bed – Non-uniformity of the shear stress acting on the shear plane. *Powder Technol.* 53:49–54
- [6.64] Schubert H, Wibowo IW (1970) Zur experimentellen Bestimmung der Zugfestigkeit von gering verdichteten Schüttgütern. *Chem.-Ing.-Techn.* 42: 541–545
- [6.65] Wittmaier A (2003) Fließverhalten hochdisperser Pulver bei sehr kleinen Spannungen. Ph.D. thesis, Techn. Univ. Braunschweig, Germany
- [6.66] Schweiger A, Zimmermann I (1999) A new approach for the measurement of the tensile strength of powders. *Powder Technol.* 101:7–15
- [6.67] Schmidt PC, Walter R (1994) Investigation of the cohesion behaviour of powders and their adhesion to a carrier by an electronic tensiometer. *Pharmazie* 49:183–187
- [6.68] Valverde JM, Ramos A, Castellanos A, Watson PK (1998) The tensile strength of cohesive powders and its relationship to consolidation, free volume and cohesivity. *Powder Technol.* 97:237–245
- [6.69] Watson PK, Valverde A, Castellanos A (2001) The tensile strength and free volume of cohesive powders compressed by gas flow. *Powder Technol.* 115:45–50
- [6.70] Quintanilla MAS, Castellanos A, Valverde JM (2001) Correlation between bulk stresses and interparticle contact forces in fine powders. *Phys. Rev. Lett.* E 64:031301
- [6.71] Johanson JR (1992) The Johanson Indicizer™ system vs. the Jenike shear tester. *Bulk Solids Handling* 12:237–240

- [6.72] Johanson JR (1993) Characterizing dry particulate solids for systems design. Proc. Reliable flow of particulate solids II, Oslo, 23.–25. August 1993, EFChE Publ. Ser. No. 96, pp 11–32
- [6.73] Bell TA, Ennis BJ, Grygo RJ, Scholten WJF, Schenkel MM (1990) Practical evaluation of the Johanson Hang-up Indicizer. Bulk Solids Handling 14:117–125
- [6.74] Bell TA, Grygo RJ, Duffy SM, Puri VM (1995) Simplified methods of measuring powder cohesive strength. Preprints PARTEC “3rd Europ. Symp. Storage and Flow of Particulate Solids”, 21–23 March 1995, Nuremberg, Germany, 79–88
- [6.75] Van der Kraan M (1996) Techniques for the measurement of the flow properties of cohesive powders. Ph.D. thesis, Univ. Delft, The Netherlands
- [6.76] Schwedes J, Schulze D (1992) Letter to the Editor: The Johanson Indicizer system vs. the Jenike shear tester. Bulk Solids Handling 12:454–455
- [6.77] Marjanovic P, Geldart D, Orband JLR, Mooney T (1995) A comparative analysis of two hopper design methods. Preprints PARTEC “3rd Europ. Symp. Storage and Flow of Particulate Solids”, 21–23 March 1995, Nuremberg, Germany, pp 69–78
- [6.78] Ploof DA, Carson JW (1994) Quality control tester to measure relative flowability of powders. Bulk Solids Handling 14:127–132
- [6.79] Schulze D (2004) Ein neues Prinzip zur Messung der Fließeigenschaften von Pulvern und Schüttgütern. Schüttgut 10:369–377
- [6.80] Schulze D (2003) Towards more reliability in powder testing. Proc. “4th Intl. Conf. on Conveying and Handling of Particulate Solids (CHoPS)”, Budapest, Vol. 1, pp 5.31–5.36
- [6.81] Jenike AW (1964/1980) Storage and flow of solids. Bull. No. 123, 20th Printing, revised 1980. Engng. Exp. Station, Univ. of Utah, Salt Lake City.
- [6.82] ASTM Standard D6128: Standard test method for shear testing of bulk solids using the Jenike shear cell. ASTM International, www.astm.org
- [6.83] ASTM Standard D6773: Standard shear test method for bulk solids using the Schulze ring shear tester. ASTM International, www.astm.org
- [6.84] Schulze D (1994) Development and application of a novel ring shear tester. Aufbereitungstechnik 35:524–535
- [6.85] Münz G (1976) Entwicklung eines Ringschergerätes zur Messung der Fließeigenschaften von Schüttgütern und Bestimmung des Einflusses der Teilchengrößenverteilung auf die Fließeigenschaften kohäsiver Kalksteinpulver. Ph.D. thesis, Univ. Karlsruhe, Germany
- [6.86] Peschl IASZ (1989) Equipment for the measurement of mechanical properties of bulk materials. Powder Handling & Processing 1:73–81
- [6.87] ASTM Standard D6682: Standard test method for measuring the shear stresses of powders using the Peschl rotational split level shear tester. ASTM International, www.astm.org

- [6.88] Akers RJ (1992) EUR14022 – The certification of a limestone powder for Jenike shear testing. Publ. by the Commission of the European communities, www.irmm.jrc.be
- [6.89] Institute für Reference Materials and Measurements (IRMM) (2006) Certified Reference Materials. Address: Retieseweg 111, B-2440 Geel, Belgium, Tel.: +32 (0)14 571 211, www.irmm.jrc.be
- [6.90] Markefka P, Steckel H (2005) Powder flowability analysis as predictor for delivered mass uniformity from dry powder inhalers. *Pharm. Ind.* 67:823–829
- [6.91] Schulze D (1995) Appropriate devices for the measurement of flow properties for silo design and quality control. Preprints PARTEC “3rd Europ. Symp. Storage and Flow of Particulate Solids”, 21–23 March 1995, Nuremberg, Germany, pp. 45–56
- [6.92] Wilms H, Schwedes J (1985) Interpretation of ring shear tests. *Bulk Solids Handling* 5:1017–1020
- [6.93] Bagster DF (1981) Tests on a very large shear cell. *Bulk Solids Handling* 1:145–149
- [6.94] Margreiter H (2003) Scherzellenuntersuchungen für die Präformulierung fester Arzneiformen. Ph.D. thesis, Univ. Innsbruck, Austria
- [6.95] Maltby LP (1993) Investigation of the behaviour of powders under and after consolidation. Ph.D. thesis, Telemark Institute of Technology, Norway
- [6.96] Schubert H (Ed) (2003) Handbuch der Mechanischen Verfahrenstechnik, Bd. 1 und 2. WILEY-VCH Verlag Weinheim, Germany
- [6.97] Heim LO, Ecke S, Preuss M, Butt HJ (2002) Adhesion forces between individual gold and polystyrene particles. *Journ. Adh. Sci. Technol.* 16:829–843
- [7.1] Hinrichs N (1997) Reibungsschwingungen mit Selbst- und Fremderregung: Experiment, Modellierung und Berechnung. Fortschr.-Ber. VDI Reihe 11 Nr. 240 , VDI-Verlag, Düsseldorf, Germany
- [7.2] Wensrich CM, Roberts AW (2000) The role of slip-stick motion in silo quaking. IMechE Conf. Transactions “From Powder to Bulk”, London, Nr. C566/028/2000
- [7.3] Schulze D (2003) Time and velocity dependent properties of powders effecting slip-stick oscillations, *Chem. Eng. Technol.* 26:1047–1051
- [7.4] Baumberger T, Heslot F, Perrin B (1994) Crossover from creep to inertial motion in friction dynamics. *Nature* 367:544–546
- [7.5] Rabinowicz E (1958) The intrinsic variables affecting the stick-slip process. *Proc. of the Phys. Soc., London* 71:668–675
- [7.6] Stelter P (1990) Nichtlineare Schwingung reibungserregter Strukturen. Ph.D. thesis, Technical Univ. Hannover, Germany
- [7.7] Dieterich JH (1979) Modeling of rock friction, 1: Experimental results and constitutive equations. *J. Geophys. Res.* 84:2161–2168

- [7.8] Dieterich JH, Kilgore BD (1994) Direct observation of frictional contacts: New insights for state-dependent properties. *Pure and Appl. Geophys.* 143: 283–302.
- [7.9] Lubert M, Sjølist KN, de Ryck A, Dodds JA (1999) Characterization of powders using slip-stick oscillations. Proc. “Int. Symp. Reliable Flow of Particulate Solids”, Porsgrunn, Norway, pp 169–174
- [7.10] Haaker G (1988) Measurement of wall friction and wear in bulk solids handling. Tagung „Silos – Forschung und Praxis“ des SFB 218, Karlsruhe, pp 389–403
- [7.11] Molerus O (1985) Schüttgutmechanik. Springer, Berlin Heidelberg New York Tokyo
- [7.12] Eber M (2004) Wirksamkeit und Leistungsfähigkeit von nanoskaligen Fließregulierungsmitteln. Ph.D. thesis, Univ. Würzburg, Germany
- [7.13] Zimmermann I, Eber M, Meyer K (2004) Nanomaterials as flow regulators in dry powders. *Zeitschrift für physik. Chemie* 218:52–102
- [7.14] Duenisch S (2005) Untersuchung der Wirkungsweise von Nanomaterialien. Ph.D. thesis, Univ. Würzburg, Germany
- [7.15] Meyer K (2003) Nanomaterialien als Fließregulierungsmittel. Ph.D. thesis, Univ. Würzburg, Germany
- [7.16] Schubert H (1982) Kapillarität in porösen Feststoffsystemen. Springer, Berlin Heidelberg New York
- [7.17] Stieß M (1995) Mechanische Verfahrenstechnik Bd. 1 und 2. Springer, Berlin Heidelberg New York
- [7.18] Molerus O (1982) Fluid-Feststoff-Strömungen. Springer, Berlin Heidelberg New York Tokyo
- [7.19] Klein J, Höhne D, Husemann K (2001) Entwicklung eines mathematischen Modells zur Beschreibung der Änderung der Scherspannungen in einem luftdurchströmten Ringschergerät. *Schüttgut* 7:13–20
- [7.20] Geldart D (1973) Types of gas fluidization. *Powder Technol.* 7:285–292
- [7.21] Schulze D (2002) Fließeigenschaften von Schüttgütern mit faser- und plättchenförmigen Partikeln. *Schüttgut* 8:538–546
- [8.1] Schulze D, Schwedes J (1991) Examples of Modern Silo Design. *Bulk Solids Handling* 11:47–52
- [8.2] Schulze D, Schwedes J (1991) Das Fließverhalten und die Silolagerung von REA-Gips. *Chem.-Ing.-Tech.* 63:256–257
- [8.3] Schulze D, Schwedes J, Leonhardt C, Kossert J (1998) Design of a silo for the storage of 10.000 t sulphur granules. *Bulk Solids Handling* 18:211–217
- [8.4] Kwade A, Schulze D (2001) Proper silo design for food products – Today strategies for avoiding segregation, degradation and hang-ups. *Powder Handling & Processing* 13:173–176
- [8.5] Wittmaier A (2003) Fließverhalten hochdisperser Pulver bei sehr kleinen Spannungen. Ph.D. thesis, Techn. Univ. Braunschweig, Germany
- [8.6] Schulze D (1998) The characterization of bulk solids for silo design and flowability tests. *Aufbereitungstechnik* 39:47–57

- [8.7] DIN 1055 part 6 (1987) Loads in silos. German code.
- [8.8] Fanghänel E, Höhne D, Schünemann U (1989) Characterization of wall friction processes with bulk materials and factors influencing the wall friction. *Aufbereitungstechnik* 40:130–137
- [8.9] Dau G (1983) Measurement of the wall friction angle for bulk solids on different wall materials. *Aufbereitungstechnik* 24:633–647
- [8.10] ter Borg L (1981) Erfahrungen aus Scherversuchen mit Schüttgütern der Chemie. *Chem.-Ing.-Techn.* 53:662–663
- [8.11] ter Borg L (1980) Erfahrungen aus Scherversuchen mit Schüttgütern der Chemie. Preprints “European Symp. Particle Technology”, Amsterdam, Volume B, 955–967
- [8.12] Heinrici H, Jacob T (2005) Die schüttgutmechanische Betrachtung der Siloauslegung und ihre Anwendung auf ein Silo unter Tage. *Schüttgut* 11:430–435
- [8.13] Heinrici H (2006) Wie lassen sich Siloschäden vermeiden? *VDI-Berichte* 1918, pp 117–130
- [9.1] DIN 1055 part 6 (1987) Loads in silos. German code.
- [9.2] DIN 1055-6:2005-03 (2005) Actions on structures – Part 6: Design loads for buildings and loads in silo bins. German code.
- [9.3] EN 1991-4:2006-12 (2006) Eurocode 1: Actions on structures – Part 4: Silos and tanks.
- [9.4] Kwade A, Schulze D, Schwedes J (1994) Determination of the stress ratio in uniaxial compression tests, Part 1 and 2. *Powder Handling & Processing* 6:61–65 and 6:199–203
- [9.5] Nowak M (1993) Spannungs-/Dehnungsverhalten von Kalkstein in der Zweiaxialbox. Ph.D. thesis, Techn. Univ. Braunschweig, Germany
- [9.6] Feise HJ (1996) Modellierung des mechanischen Verhaltens von Schüttgütern. Ph.D. thesis, Techn. Univ. Braunschweig, Germany (Braunschweiger Schriften zur Mechanik Nr. 23-1996)
- [9.7] Martens P (Ed) (1988) Silohandbuch. Wilhelm Ernst&Sohn Verlag, Berlin
- [9.8] Arnold PC, McLean AG (1976) Improved analytical flow factors for mass-flow hoppers. *Powder Technol.* 15:279–281
- [9.9] Stiglat K (1991) Statisch-konstruktive Bemessung von Silos. Preprints VDI-GVC Conference “Agglomerations- und Schüttguttechnik”, Baden-Baden, Germany, pp 109–138
- [9.10] Hampe E (1987) Silos, Band 1 (Grundlagen). VEB Verlag für Bauwesen, Berlin
- [9.11] Enstad GG (1981) A novel theory on the arching and doming in mass flow hoppers. Ph.D. thesis, Chr. Michelsen Inst., Bergen, Norway
- [9.12] Walters JK (1973) A theoretical analysis of stresses in silos with vertical walls. *Chem. Eng. Sci.* 28:13–21
- [9.13] Walters JK (1973) A theoretical analysis of stresses in axially-symmetric hoppers and bunkers. *Chem. Eng. Sci.* 28:779–789

- [9.14] Jenike AW, Johanson JR, Carson JW (1973) Bin loads – Part 2 and 3. Journ. of Engng. for Industry, Trans. ASME, Series B, Vol.95, No 1, pp 1–12
- [9.15] Roberts I (1882) On the pressure of wheat stored in elongated cells or bins. Engineering 34:399
- [9.16] Roberts I (1884) Determination of the vertical and lateral pressures of granular substances. Proceed. Royal. Soc. of London 36:225–240
- [9.17] Janssen HA (1895) Getreidedruck in Silozellen, Z. Ver. Dt. Ing. 39:1045–1049
- [9.18] Koenen M (1896) Berechnung des Seiten- und Bodendrucks in Silozellen. Centralblatt der Bauverwaltung 16:446–449
- [9.19] Jenike AW (1964/1980) Storage and flow of solids. Bull. No. 123, 20th Printing, revised 1980. Engng. Exp. Station, Univ. of Utah, Salt Lake City.
- [9.20] Jenike AW (1961) Gravity flow of bulk solids. Bulletin No 108, Eng. Exp. Station, Univ. of Utah, Salt Lake City
- [9.21] Walker DM (1966) An approximate theory for pressures and arching in hoppers. Chem. Eng. Sci. 21:975–997
- [9.22] Walker DM (1967) A basis for bunker design. Powder Technology 1:228–236
- [9.23] Benink EJ (1989) Flow and stress analysis of cohesionless bulk materials in silos related to codes. Ph.D. thesis, Univ. of Twente, Enschede, The Netherlands
- [9.24] Motzkus U (1974) Belastung von Siloböden und Auslauftrichtern durch körnige Schüttgüter. Ph.D. thesis, Techn. Univ. Braunschweig, Germany
- [9.25] Schulze D, Schwedes J (1994) An examination of initial stresses in hoppers. Chem. Engng. Sci. 49:2047–2058
- [9.26] Rombach G, Eibl J (1988) Consistent modelling of filling and discharging processes in silos. Preprints “Silos – Forschung und Praxis”, Karlsruhe, Germany, PP 1–15
- [9.27] Rombach G (1991) Schüttguteinwirkungen auf Silozellen – Exzentrische Entleerung. Ph.D. thesis, Univ. Karlsruhe, Germany
- [9.28] Langston PA, Tüzün U (1994) Continuous potential discrete particle simulations of stress and velocity fields in hoppers. Chem. Engng. Sci. 49:1259–1275
- [9.29] Kafui KD, Thornton C (1995) Some aspects of silo design: Computer simulations. Proc. PARTEC 95 “3rd Europ. Symp. Storage and Flow of Particulate Solids (Janssen Centennial)”, Nuremberg, Germany, pp 379–388
- [9.30] Kaldenhoff M (1998) Simulation von grobgranularen Schüttgütern mit Hilfe zellulärer Automaten. Ph.D. thesis, Techn. Univ. Braunschweig, Germany
- [9.31] AS 3774-1990 (1987) Loads on bulk solids containers. Australian Standard
- [9.32] British Material Handling Board (Publ) (1985) BMHB Draft code of practice for the design of silos, bins, bunkers and hoppers.

- [9.33] Schulze D (1991) Untersuchungen zur gegenseitigen Beeinflussung von Silo und Austragorgan. Ph.D. thesis, Techn. Univ. Braunschweig, Germany
- [9.34] Arnold PC, McLean AG, Roberts AW (1979) Bulk solids: Storage, flow and handling. TUNRA Ltd., The Univ. of Newcastle, N.S.W., Australia
- [9.35] Schulze D (1999) Silo Stress Tool, program for the assessment of stresses in silos. www.dietmar-schulze.de
- [9.36] Pieper E, Wenzel F (1964) Druckverhältnisse in Silozellen. Verlag Wilhelm Ernst & Sohn, Berlin
- [9.37] Wolf K (1984) Der Anfangsschlag und andere Belastungsgrößen im Silo. Ph.D. thesis, Techn. Univ. Braunschweig, Germany
- [9.38] Schneider HG (1987) Experimentelle Untersuchung der Schüttgutdrücke bei Kern- und Massenfluss. Ph.D. thesis, Techn. Univ. Braunschweig, Germany
- [9.39] Lohnes RA, Bokhoven WH (1985) Experimental determination of K_0 stress ratios in grain. Proc. 10th Annual Powder & Bulk Solids Conf. Rosemont, IL, USA
- [9.40] Nothdurft H (1975) Schüttgutlasten in Silozellen mit Querschnittsverengungen. Ph.D. thesis, Techn. Univ. Braunschweig, Germany
- [9.41] Kézdi A (1962) Erddrucktheorien. Springer, Berlin
- [9.42] Roberts AW (1990) Modern concepts in the design and engineering of bulk solids handling systems. TUNRA Ltd., The Univ. of Newcastle, N.S.W., Australia
- [9.43] Jenike AW (1964/1980) Storage and flow of solids. Bull. No. 123, 20th Printing, revised 1980. Engng. Exp. Station, Univ. of Utah, Salt Lake City.
- [9.44] Zachary LW, Lohnes RA (1988) A confined compression test for bulk solids. Proc. 13th Annual Powder & Bulk Solids Conf., Rosemont, IL, USA
- [9.45] Nielsen J, Kolymbas D (1988) Properties of granular media relevant for silo loads, Preprints "Silos – Forschung und Praxis", Karlsruhe, pp 119–132
- [9.46] Manjunath KS, Roberts AW (1986) Wall pressure-feeder load interactions in mass flow hopper/feeder combinations. Bulk Solids Handling 6:769–775 and 6:903–911
- [9.47] Strusch J (1996) Wandnormalspannungen in einem Silo mit Einbau und Kräfte auf Einbauten. Ph.D. thesis, Techn. Univ. Braunschweig, Germany
- [9.48] Pajer G, Kuhnt H, Kurth F (1988) Stetigförderer. VEB Verlag Technik, Berlin
- [9.49] Schulze D, Schwedes J (1990) Experimental investigation of silo stresses under consideration of the influence of hopper/feeder interface. Kona 8:134–144
- [9.50] Rademacher FJC (1982) Reclaim power and geometry of bin interfaces in belt and apron feeders. Bulk Solids Handling 2:281–294

- [9.51] Reisner W, v. Eisenhardt-Rothe M (1971) Silos und Bunker für die Schüttgutspeicherung. Trans. Tech. Publications, Clausthal-Zellerfeld, Germany
- [9.52] Schumacher W (1987) Zum Förderverhalten von Bunkerabzugsschnecken mit Vollblattwendeln. Ph.D. thesis, TH Aachen, Germany
- [9.53] Vetter G, Gericke H, Fritsch D (1984) Zur kontinuierlichen Dosierung von Schüttgütern mit Schneckendosiergeräten. Aufbereitungstechnik 25:705–717
- [9.54] Bates L (1969) Entrainment patterns of screw hopper dischargers. Journ. of Engng. for Industry 91:295–302.
- [9.55] Carroll PJ (1970) Hopper designs with vibratory feeders. Chem.. Engng.. Progr. 66:44–49
- [9.56] Jenike AW (1977) Load assumptions and distributions in silo design. Conf. on construction of concrete silos, Oslo, Norway
- [9.57] Van Zanten DC, Mooij A (1977) Bunker Design, Part 2: Wall pressures in mass flow. Journ. of Engng. for Industry, Trans. ASME, Nov. 1977, pp 814–818
- [9.58] Kahl J (1976) Grundlagenuntersuchungen über die Belastung von Siloeinbauten bei ruhenden und fließenden Schüttgütern. Ph.D. thesis, Techn. Univ. Clausthal, Germany
- [9.59] Kroll D (1974) Untersuchungen über die Belastung horizontaler Zuganker sowie vertikaler Hängependel und Gehänge durch Schüttgütern in Silozellen. Ph.D. thesis, Techn. Univ. Braunschweig, Germany
- [9.60] Frese B (1977) Druckverhältnisse in zylindrischen Silozellen. Ph.D. thesis, Techn. Univ. Braunschweig, Germany
- [9.61] Chrisp TM, Wood JGM, Blackler MJ (1988) Comparison of model and full-scale test results with simplified and finite element analyses of eccentrically discharged silos. Preprints “Silos – Forschung und Praxis”, Karlsruhe, Germany, pp 55–68
- [9.62] Rotter JM (1986) The analysis of steel bins subject to eccentric discharge. Proc. “2nd Int. Conf. on Bulk Materials Storage, Handling and Transportation”, Wollongong, Australia, pp 264–271
- [9.63] Rotter JM (1998) Cylindrical shells: Unsymmetrical solids loading and supports. In: Brown CJ, Nielsen J (Eds) Silos, fundamentals of theory, behaviour and design. E & FN Spon, London and New York, pp 367–377
- [9.64] Lippold D, Harder J (2004) Analysis and design of silo walls. World Cement 35:63–68
- [9.65] Jenike AW (1967) Denting of circular bins with eccentric drawpoints. Journal of the Structural Division, Proceedings of the American Society of Civil Engineers, 93:27–35.
- [9.66] Colijn H, Peschl IASZ (1981) Non-symmetrical bin flow problems. Bulk Solids Handling 1:81–88
- [9.67] McLean AG, Arnold PC, Bravin B (1985) Eccentric discharge silo wall loads. Proc. “Reliable Flow of Bulk Solids”, Bergen, Norway, EFCE Publ. Ser. No. 49, pp 194–209

- [9.68] Khelil A (1998) Internal structures (ties and internals). In: Brown CJ, Nielsen J (Eds) Silos, fundamentals of theory, behaviour and design. E & FN Spon, London and New York, pp 443–451
- [9.69] Kaldenhoff M, Schütte J (2004) Schäden an Silos mit großen Entleerungsexzentrizitäten. Bauingenieur 79:560–567
- [10.1] Jenike AW (1964/1980) Storage and flow of solids. Bull. No. 123, 20th Printing, revised 1980. Engng. Exp. Station, Univ. of Utah, Salt Lake City. Available at: The University of Utah, Utah Engineering Experiment Station, 1515 Mineral Square Room 138, Salt Lake City, UT 84112-1109, USA
- [10.2] Jenike AW (1964) Storage and flow of solids. Bull. No. 123, 1st printing, Engng. Exp. Station, Univ. of Utah, Salt Lake City, USA
- [10.3] EN 1991-4:2006-12 (2006) Eurocode 1: Actions on structures – Part 4: Silos and tanks.
- [10.4] Schwedes J (1968) Fließverhalten von Schüttgütern in Bunkern. Verlag Chemie, Weinheim, Germany
- [10.5] Enstad GG (1981) A novel theory on the arching and doming in mass flow hoppers. Ph.D. thesis, Chr. Michelsen Inst., Bergen, Norway
- [10.6] Molerus O (1985) Schüttgutmechanik. Springer, Berlin Heidelberg New York Tokyo
- [10.7] McLean AG (1986) Empirical critical flow factor equations. Bulk Solids Handling 6:779–782
- [10.8] Janssen HA (1895) Getreidedruck in Silozellen. Ztg. Ver. dt. Ing. 39:1045–1049
- [10.9] Schulze D, Schwedes J (1991) Examples of Modern Silo Design. Bulk Solids Handling 11:47–52
- [10.10] Schulze D, Schwedes J, Leonhardt C, Kossert J (1998) Design of a silo for the storage of 10.000 t sulphur granules. Bulk Solids Handling 18:211–217
- [10.11] Schäfer R, Schröer H, Schwedes J (1986) Auslegung einer Großsilo-Anlage für die Einlagerung eines feuchten Schüttgutes und praktische Erfahrungen. Zement Kalk Gips 75:587–592
- [10.12] Schulze D, Schwedes J (1990) Storage and flow of bulk solids in silos and information for planning new installations. VGB-Kraftwerkstechnik (English Issue) 70:665–669
- [10.13] Schulze D, Schwedes J (1991) Das Fließverhalten und die Silolagerung von REA-Gips. Chem.-Ing.-Techn. 63:256–257
- [10.14] Roberts AW (1990) Modern concepts in the design and engineering of bulk solids handling systems. TUNRA Ltd., The Univ. of Newcastle, N.S.W., Australia
- [11.1] Jenike AW (1964/1980) Storage and flow of solids. Bull. No. 123, 20th Printing, revised 1980. Engng. Exp. Station, Univ. of Utah, Salt Lake City.

- [11.2] Woodcock CR, Mason JS (1987) Bulk solids handling. Leonard Hill, Glasgow and London
- [11.3] Schulze D, Schwedes J (1990) Storage and flow of bulk solids in silos and information for planning new installations. VGB-Kraftwerkstechnik (English Issue) 70:665–669
- [11.4] Kalenborn Kalprotect – Dr. Mauritz GmbH & Co. KG (2003) Gleitfördernde Auskleidungen für Produktions- und Förderanlagen. Product brochure 12/03
- [11.5] Strusch J (1996) Wandnormalspannungen in einem Silo mit Einbau und Kräfte auf Einbauten. Ph.D. thesis, Techn. Univ. Braunschweig, Germany
- [11.6] Johanson JR, Kleysteuber WK (1966) Flow corrective inserts in bins. Chem. Engng. Progr. 62:79–83
- [11.7] Schulze D (1993) Austragorgane und Austraghilfen. Chem.-Ing.-Techn. 65:48–57
- [11.8] Schulze D (1991) Untersuchungen zur gegenseitigen Beeinflussung von Silos und Austragorgan. Ph.D. thesis, Techn. Univ. Braunschweig, Germany
- [11.9] Johanson JR (1983) Controlling flow patterns in bins by use of an insert. Bulk Solids Handling 2:495–498
- [11.10] Schwedes J, Richter W (1975) Grundlagen zur Auslegung pneumatischer Granulatmischer. VDI-Berichte Nr. 232:296–301
- [11.11] Schulze D, Schwedes J (1992) Tests on the application of discharge tubes. Bulk Solids Handling 12:33–39
- [11.12] Doeksen G (1973) Precautions in order to attain design capabilities of mass-flow systems. J. Engng. for Industry, Trans. ASME Vol. 95, Ser. B 1:93–96
- [11.13] Schwedes J, Schulze D (1991) Examples of modern silo design. Bulk Solids Handling 11:47–52
- [11.14] Schäfer R, Schröer H, Schwedes J (1986) Auslegung einer Großsiloden-Anlage für die Einlagerung eines feuchten Schüttgutes und praktische Erfahrungen. Zement Kalk Gips 75:587–592
- [11.15] McLean AG (1985) The design of silo side discharge outlets for safe and reliable operation. Bulk Solids Handling 5:185–190
- [11.16] Peter J, Lippold D (1985) Baukonstruktion eines Grossraumsilos für Flugasche. Zement Kalk Gips 1:49–51
- [11.17] Kaminski M, Zubrzycki M (1985) Reduzieren des dynamischen Horizontaldruckes in Getreidesilos. Bauingenieur 60:313–318
- [11.18] Wilms H (1992) Blending silos. Powder Handling & Processing 4:293–299
- [11.19] Wilms H (1992) Inserts in silos for blending. In: Brown CJ, Nielsen J (Eds) Silos – Fundamentals of theory, behaviour and design. E & FN Spon, London and New York, pp 131–141
- [12.1] Brown, RL, Richards JC (1970) Principles of powder mechanics. Pergamon Press, Oxford, UK

- [12.2] Schwedes J (1968) Fließverhalten von Schüttgütern in Bunkern. Verlag Chemie, Weinheim, Germany
- [12.3] Schulze D (1999) A theoretical model for the prediction of the gas pressure distribution in silos at filling and discharge, Proc. "Int. Symp. Reliable Flow of Particulate Solids", Porsgrunn, Norway, pp 331–340
- [12.4] Johanson JR, Jenike AW (1971/72) The effect of the gaseous phase on pressures in a cylindrical silo. *Powder Technology* 5:133–145
- [12.5] Murfitt PG, Bransby PL (1980) Daeaeration of powders in hoppers. *Powder Technol.* 27:149–163
- [12.6] Royal TA, Carson JW (1991) Fine powder flow phenomena in bins, hoppers and processing vessels. *Bulk 2000*, London
- [12.7] Rathbone T, Nedderman RM, Davidson JF (1987) Aeration, deaeration, and flooding of fine particles. *Chem. Eng. Sci.* 42:725–736
- [12.8] Gu ZH, Arnold PC, McLean AG (1992) Modelling of air pressure distributions in mass flow bins. *Powder Technol.* 71:121–130
- [12.9] Spink CD, Nedderman RM (1978) Gravity discharge rate of fine particles from hoppers. *Powder Technol.* 21:245–261
- [12.10] Nedderman RM, Tütün U, Savage SB, Houlby G (1982) The flow of granular materials. *Chem. Engng. Sci.* 37:1597–1609
- [12.11] Hagen E (1852) Druck und Bewegung des trockenen Sandes. In: Bericht über die zur Bekanntmachung geeigneten Verhandlungen der Königlich Preußischen Akademie der Wissenschaften zu Berlin, pp 35–42
- [12.12] Beverloo WA, Leniger HA, van der Felde J (1961) The flow of granular solids through orifices. *Chem. Engng. Sci.* 15:260–269
- [12.13] British Standards Institution (Ed) (1987) Draft design code for silos, bins, bunkers and hoppers. Published by BSI in association with the British Materials Handling Board
- [12.14] Woodcock CR, Mason JS (1987) Bulk Solids Handling. Leonard Hill, Glasgow and London
- [12.15] Schulze D, Schwedes J (1992) Tests on the application of discharge tubes. *Bulk Solids Handling* 12:35–39
- [12.16] Crewdson BJ, Ormond AL, Nedderman RM (1977) Air-impeded discharge of fine particles from a hopper. *Powder Technol.* 16:197–207.
- [12.17] Gu ZH, Arnold PC, McLean AG (1993) Simplified model for predicting the particle flowrate from mass flow bins. *Powder Technol.* 74:153–158
- [12.18] Gu ZH, Arnold PC, McLean AG (1992) Prediction of the flowrate of bulk solids from mass flow bins with conical hoppers. *Powder Technol.* 72:157–166
- [12.19] Nedderman RM, Tütün U, Thorpe RB (1983) The effect of interstitial air pressure gradients on the discharge from bins. *Powder Technol.* 35:69–81
- [12.20] Scheibe M (1997) Die Fördercharakteristik einer Zellenradschleuse unter Berücksichtigung der Wechselwirkung von Silo und Austragorgan. Ph.D. thesis, Techn. Univ. Bergakademie Freiberg, Germany
- [12.21] Bruff W, Jenike AW (1967/68) A silo for ground anthracite. *Powder Technol.* 1:252–262.

- [12.22] Sutton HM, Richmond RA (1973) Improving the storage conditions of fine powders by aeration. *Trans. Instn. Chem. Engrs.* 51:97–104
- [12.23] Johanson JR (1965) Method of calculating rate of discharge from hoppers and bins. *Trans. Min. Engrs. AIME* 232:69–80
- [12.24] Jochem K (1997) Belüftung als Austraghilfe für Silos. Ph.D. thesis, Techn. Univ. Braunschweig, Germany
- [12.25] Zimmer W (2006) Luftkanonen und Luftpumpe – Was ist der Unterschied? *Schüttgut* 12:262–268
- [12.26] Raabe T (1998) Wirkungsweise von Luftkanonen als Austragshilfe. Ph.D. thesis, Techn. Univ. Braunschweig, Germany
- [12.27] Raabe T, Schwedes J (1997) Experimentelle Untersuchungen zum Einsatz von Luftkanonen als Austragshilfe. *Schüttgut* 3:21–27
- [12.28] Raabe T, Schwedes J (1998) On the operation of air blasters as discharge-aids – experimental investigations. Proc. “6th Int. Conf. on Bulk Materials Storage, Handling and Transportation”, Wollongong, Australia, pp 507–514
- [12.29] Terziovski A, Arnold PC (1990) On the effective sizing and placement of air blasters. *Bulk Solids Handling* 10:181–185
- [12.30] SAT GmbH, Weingarten (1988) Horizontal-Zellenradschleuse ROTOSTAR. Product brochure no 2003/06.88
- [12.31] Roberts AW (1984) Vibration of fine powders and its application. In: Fayed ME, Otten L (Eds) *Handbook of Powder Science and Technology*. Van Nostrand Reinhold Company Inc., New York
- [12.32] Schumacher W (1987) Zum Förderverhalten von Bunkerabzugsschnecken mit Vollblattwendeln. Ph.D. thesis, TH Aachen, Germany
- [12.33] Jenike AW (1964/1980) Storage and flow of solids. Bull. No. 123, 20th Printing, revised 1980. Engng. Exp. Station, Univ. of Utah, Salt Lake City.
- [12.34] Reisner W, v.Eisenhardt-Rothe M (1971) Silos und Bunker für die Schüttgutspeicherung. Trans Tech Publications, Clausthal-Zellerfeld, Germany
- [12.35] Haaker G, van Poppel MP, Jongejan MP, Stokkers GJ (1993) Improvement of screw feeder geometry for better draw-down performance. Proc. Int. Symp. Reliable flow of Particulate Solids II, Oslo, Norway, pp 551–561.
- [12.36] Bates L (1969) Entrainment patterns of screw hopper dischargers. *Trans ASME, Journ. of Engng. f. Industry* 91:295–302.
- [12.37] Meyer HJ (1989) Experiences with coal bunkers and coal feeders. *Bulk Solids Handling* 9:27–31
- [12.38] Schulze D (1991) Untersuchungen zur gegenseitigen Beeinflussung von Silo und Austraggerät. Ph.D. thesis, Techn. Univ. Braunschweig, Germany
- [12.39] Rademacher FJC (1982) Reclaim power and geometry of bin interfaces in belt and apron feeders. *Bulk Solids Handling* 2:281/294
- [12.40] Marinelli J, Carson JW (1992) Use screw feeders effectively. *Chemical Engineering Progress* 88 (No. 12): 47–51

- [12.41] Krambrock W (1979) Lagern und Umschlagen von Schüttgütern in der Chemischen Industrie. *Chem.-Ing.-Tech.* 2:104–112
- [12.42] Schulze D, Schwedes J (1990) Experimental investigation of silo stresses under consideration of the influence of hopper/feeders interface. *Kona* 8:134–144
- [12.43] Bridge DT, Carson JW (1987) How to design efficient screw and belt feeders for bulk solids. *Powder and Bulk Solids* 12th Annual Conf., Rosemont, IL, USA
- [12.44] Aumund Fördertechnik GmbH, Rheinberg (2006) Hopper discharge systems. Product brochure, www.aumund.de
- [12.45] Ramos CM (1987) Design of apron feeders. *Bulk Solids Handling* 7:815/825
- [12.46] Eisele S (1978) Diskontinuierliche Wägesysteme. In: Dosieren in der Kunststofftechnik, VDI-Verlag, Düsseldorf, Germany
- [12.47] Pajer G, Kuhnt H, Kurth F (1988) Stetigförderer. VEB Verlag Technik, Berlin
- [12.48] Funke H (1978) Mechanisches Fördern mit Gurt-, Schwing- und Schneckenförderern. In: Dosieren in der Kunststofftechnik. VDI-Verlag, Düsseldorf, Germany
- [12.49] Bules WS (1989) The care and feeding of a vibratory feeder. *Bulk Solids Handling* 9:209–210
- [12.50] Carroll PJ (1970) Hopper design with vibratory feeders. *Chem. Engng. Progr.* 66:44–49
- [12.51] Brabender Technologie KG, Duisburg, Germany (2006) The Brabender SiloTray Feeder. www.brabender-technologie.com
- [12.52] FCE Group – Materials Handling, Leven, Five, UK (2006) Hogan Bin Discharger. www.fcegroup.com
- [12.53] Matcon Group Ltd., Moreton-In-Marsh, Gloucestershire, UK (2006) Matcon silo/hopper discharger valves. www.matcon-cone.com
- [12.54] Hoppe H, Heep D, Storf R (1985) Modern rotary valve technology for various pneumatic conveying systems. *Bulk Solids Handling* 4:795–799
- [12.55] Al-Din N, Gunn DJ (1983) Metering of solids by a rotary valve feeder. *Powder Technology* 36:25–31.
- [12.56] Hoppe H (1982) Discharge of finest-grained products from storage and conveying bins. *Proc. Powtech, I. Chem. E. Symp. Ser.*, Bd. Nr. 69
- [12.57] Krambrock W (1978) Pneumatisches Fördern. In: Dosieren in der Kunststofftechnik, VDI-Verlag, Düsseldorf, Germany
- [12.58] Stamer W (1975) Pneumatische Fördereinrichtungen in Zementwerken und in der chemischen Industrie. *Aufbereitungstechnik* 4:171/176
- [12.59] Peter J (1997) Großraumsilos für die Zementindustrie – Freistehende kreiszylindrische Silos mit Zentralkegel. *ZKG International* 50:657
- [12.60] Peter J (1981) Der Zentralkegelsilo aus statisch-konstruktiver Sicht. *ZKG International* 34:647–654
- [12.61] Martens P (Ed) (1988) Silohandbuch. Verlag Ernst & Sohn, Berlin
- [12.62] Duda WH (1977) Cement Data Book. Bauverlag GmbH, Wiesbaden, Berlin

- [12.63] Lippold D, Harder J (2004) Analysis and design of silo walls. *World Cement*, 35:63–68
- [12.64] Kaldenhoff M, Schütte J (2004) Schäden an Silos mit großen Entleerungsexzentritäten. *Bauingenieur* 79:560–567
- [12.65] Aumund Fördertechnik GmbH, Rheinberg, Germany (2006) Centrex product brochure. www.aumund.de
- [12.66] Maschinenfabrik Meyer & Co, Püttlingen, Germany (2006) Extromat product brochure. www.meyco.net
- [12.67] Fink R (1988) Bunker and silo reclaiming units for handling highly cohesive and difficult bulk materials. *Bulk Solids Handling* 1:27/30
- [12.68] Fink R (1987) Bunker- und Siloaustragsgeräte für schwerfließende Schüttgüter. TIZ 5
- [12.69] Fink R (1987) REA-Gipsentsorgung für das Kraftwerk Weisweiler. TIZ 9
- [12.70] NEMA Engineering GmbH, Wiefelstede, Germany (2004) Information brochure. www.nema.de
- [12.71] Geroldinger GmbH & Co. KG, Sigharting, Austria (2006) Oszillomat. www.geroldinger.com
- [12.72] Agrichema Materialflusstechnik GmbH & Co. KG, Waldlaubersheim, Germany (2006) Rotostar. www.agrichema.de
- [12.73] Hignett CIW (1981) Silo dischargers for non free-flowing bulk materials. *Bulk Solids Handling* 1:427–428
- [12.74] Kelka W (1968) Bunker mit fahrbaren Austragschnecken für schwerfließende Schüttgüter. *Fördern und Heben* 18:805–807
- [12.75] Roberts AW (2006) Performance of orbiting screw reclaimers. *Bulk Solids Handling* 26:24–31
- [12.76] Khelil A (1998) Internal structures (ties and internals). In: Brown CJ, Nielsen J (Eds) *Silos – fundamentals of theory, behaviour and design*. E & FN Spon, London and New York, pp 443–451
- [12.77] VibraScrew Inc., Totowa, NJ, USA (2006) Bin activator product brochure. www.vibrascrewinc.com
- [12.78] Monitor Technologies, LLC., Elburn, IL, USA (2007) Bulletin 943. www.monitortech.com

- [13.1] Bates L (1997) User guide to segregation. British Materials Handling Board Press, UK
- [13.2] Carson JW, Royal TA, Goodwill DJ (1986) Understanding and eliminating particle segregation problems. *Bulk Solids Handling* 6:139–144
- [13.3] Schwedes J (1968) Fließverhalten von Schüttgütern in Bunkern. Verlag Chemie, Weinheim, Germany
- [13.4] Williams JC (1976) The segregation of particulate materials. *Powder Technol.* 15:241–251
- [13.5] Johanson JR (1978) Particle segregation and what to do about it. *Chem. Engng.* 5:183–188
- [13.6] Arnold PC (1991) On the influence of segregation on the flow pattern in silos. *Bulk Solids Handling* 11:447–449

- [13.7] Williams JC (1990) Mixing and segregation of powders. In: Rhodes M (Ed) *Principles of powder technology*. Wiley, New York, pp 71–90
- [13.8] Fürll C (1992) Segregation in bins for bulk materials. *Aufbereitungstechnik* 33:394–401
- [13.9] Shinohara K (1990) General segregating mechanism of binary solids mixtures in filling two-dimensional hoppers. *Aufbereitungstechnik* 31:482–488
- [13.10] Bagster DF, Killalea C (1986) Fine particles and their effect on segregation in bins. Intern. Conf. Bulk Materials Storage, Handling and Transportation, Wollongong, Australia, pp 153–159
- [13.11] Drahun J, Bridgewater J (1983) The mechanisms of free surface segregation. *Powder Technol.* 36:39–53
- [13.12] Matthée H (1967/68) Segregation phenomena relating to bunkering of bulk materials: Theoretical Considerations and Experimental Investigations. *Powder Technol.* 1:265–271
- [13.13] Bridgewater J, Ingram ND (1971) Rate of spontaneous interparticle percolation. *Transaction of the Institution of Chemical Engineers* 49:163–169
- [13.14] Williams JC, Khan MI (1973) The mixing and segregation of particulate solids of different particle size. *Chem. Eng.* 269:19–25
- [13.15] Lawrence LR, Beddow JY (1969) Powder segregation during die filling. *Powder Technol.* 2:253–259
- [13.16] Schulze D (1999) A theoretical model for the prediction of the gas pressure distribution in silos at filling and discharge, Proc. “Reliable Flow of Particulate Solids III”, Porsgrunn, Norway, 11th – 13th August 1999, pp 331–340
- [13.17] Johanson JR (1988) Solids segregation – causes and solutions. *Powder and Bulk Engng.*, August 1988, pp 13–19
- [13.18] Fürll C, Scholz V (1981) Lagerung von Trockenmischfutter in Behältern. *Agrartechnik* 31:353–357
- [13.19] Fürll C (1994) Investigation of the segregation in big bins. *Powder Handling and Processing* 6:395–397
- [13.20] Kwade A, Ziebell O (2001) Reduzierung der Entmischungen von Putzgips durch gezielte Änderung der Silogeometrie. *ZKG International* 54:680–688
- [13.21] Jenike AW (1964/1980) Storage and flow of solids. Bull. No. 123, 20th Printing, revised 1980. Engng. Exp. Station, Univ. of Utah, Salt Lake City.
- [13.22] Roberts AW (1991) Design of bins and feeders for anti-segregation and blending. IMechE, paper C418/049, pp 257–264
- [13.23] Johanson JR (1982) Controlling flow patterns in bins by use of an insert. *Bulk Solids Handling* 2:495–498
- [13.24] Jochem K, Schwedes J, Vidal JL (1998) Entmischung binärer Schüttgutmischungen in einem Versuchssilo. *Schüttgut* 4:31–36
- [13.25] Schulze D, Schwedes J (1992) Tests on the application of discharge tubes. *Bulk Solids Handling* 12:35–39

- [13.26] Sommer K (1979) Probenahme von Pulvern und körnigen Massengütern. Springer, Berlin Heidelberg New York
- [13.27] Stiess M (1995) Mechanische Verfahrenstechnik, Bd. 1 und 2. Springer, Berlin Heidelberg New York
- [14.1] Roberts AW, Wiche SJ (1991) Silo-quaking – a pulsating load problem during discharge in bins and silos. IMechE Paper No C418/048
- [14.2] Tejchman J, Gudehus G (1993) Silo-music and silo-quake experiments and a numerical Cosserat approach. Powder Technol. 76:201–212
- [14.3] Schneider H, Wilms H (2004) Erschütterungen und Geräusche beim Entleeren von Silos – Erfahrungen und Maßnahmen. VDI-Berichte Nr. 1824, pp 113–125
- [14.4] Purutyan H, Bengtson KE, Carson JW (1993) Flow-induced silo vibrations. Powder & Bulk Solids Conference/Exhibition, Chicago
- [14.5] Pieper K (1975) Über das “Schlagen” in Silozellen. Aufbereitungstechnik 16:190–193
- [14.6] Jöhnk H (1985) Reduzierung von Erschütterungen beim Abzug aus Klinkersilos. Zement Kalk Gips 38:657–659
- [14.7] Calil C (1988) Experimental study of impact loads in silos with funnel flow. Preprints “Silos – Forschung und Praxis”, Karlsruhe, Germany, pp 179–189
- [14.8] Wensrich C (2002) Selected case studies on the silo quaking problem. Bulk Solids Handling 22:116–122
- [14.9] Schwedes J, Schulze D (1991) Examples of modern silo design. Bulk Solids Handling 11:47–52
- [14.10] Levison B, Munch-Andersen J (1994) Shocks in coal silos. Powder Handling & Processing 6:385–388
- [14.11] Wright H, Rappen A (1984) The phenomenon of silo-quaking – Strategically placed air cannons solved shock load problems in 6 x 1000 t capacity borderline mass flow coal bunkers. CHISA Conference, Prag, pp 184–185
- [14.12] Roberts AW (1993) Mechanics of self excited dynamic loads in bins and silos. Proc. Int. Symp. Reliable Flow of Particulate Solids II, Oslo, Norway, pp 983–1004
- [14.13] Wright H, Schulze D (1999) Can mass flow silos quake? Bulk Solids Handling 19:157–162
- [14.14] Wei ML, Johanson JR (1974) Elimination of vibrations in an ore unloading bin. Journ. of Eng. for Industry, Trans. of the ASME, August 1974, pp 761–765
- [14.15] Buick JM, Pankaj, Ooi JY, Chavez-Sagarnaga J, Pearce A, Houghton G (2004) Motion of granular particles on the wall of a model silo and the associated wall vibrations. J. of Physics D: Appl. Phys. 37:2751–2760
- [14.16] Tejchman J (1999) Technical concept to prevent the silo honking. Powder Technology 106:7–22

- [14.17] Buick JM, Chavez-Sagarnaga J, Zhong Z, Ooi JY, Pankaj, Campbell DM, Greated CA (2005) Investigation of silo honking: Slip-stick excitation and wall vibration. ASCE Journ of Engng. Mechanics 131:199–307
- [14.18] Schwedes + Schulze Schüttguttechnik GmbH, Braunschweig (1998–2006) Consultant reports for various customers (not published)
- [14.19] Wensrich CM, Roberts AW (2000) The role of slip-stick motion in silo quaking. IMechE Conference Transactions “From Powder To Bulk”, Paper No C566/028/2000, pp 143–152
- [14.20] Wensrich C (2002) Experimental behaviour of quaking in tall silos. Powder Technol. 127:87–94
- [14.21] Möller H (1990) Langzeitlagerung und pneumatische Entleerung von Flugasche aus Großraumsilos. VGB Kraftwerkstechnik 70:418
- [14.22] Hardow B, Schulze D, Schwedes J (1998) An experimental analysis of the silo quaking phenomenon. World Congress Chemical Engineering, Brighton, 6.–8. Juli, Text Nr. 318 (CD-ROM)
- [14.23] Tejchman J (1997) Modelling of shear localization and autogeneous dynamic effects in granular bodies. Veröffentlichungen des Instituts für Bodenmechanik der Universität Karlsruhe (Germany), Vol. 140
- [14.24] Muite BK, Quinn SF, Sundaresan S, Rao KK (2004) Silo music and silo quake: Granular flow induced vibration. Powder Technol. 145:190–202
- [14.25] Hardow B (1998) Spannungsschwankungen im Schüttgut beim Entleeren in einem Silo. Ph.D. thesis, Techn. Univ. Braunschweig, Germany
- [14.26] Schulze D (1998) Silo quaking. In: Brown CJ, Nielsen J (Eds) Silos – fundamentals of theory, behaviour and design. E & FN Spon, London and New York, pp 171–182
- [14.27] Schulze D (2003) Zeit- und geschwindigkeitsabhängiges Verhalten von Schüttgütern als Bedingung für Slip-Stick. Chem. Ing. Techn. 75:104–108
- [14.28] Schulze D (2003) Time and velocity dependent properties of powders effecting slip-stick oscillations. Chem. Eng. Technol. 26:1047–1051
- [14.29] Logan, JM, Dengo CA, Higgs NG, Wang ZZ (1992) Fabrics of experimental fault zones: Their development and relationship to mechanical behavior. In Evans B, Wong T (Eds) Fault Mechanics and Transport Properties of Rocks, Academic Press, London, pp 33–67
- [14.30] Blair-Fish PM, Bransby PL (1973) Flow patterns and wall stresses in a mass-flow bunker. Journ. of Engng. f. Industry, Trans. ASME 95:17–26
- [14.31] Cutress JO, Pulfer RF (1967) X-ray investigations of flowing powders. Powder Technol. 1:213–220
- [14.32] Michalowski RL (1987) Flow of granular media through a plane parallel/converging bunker. Chem. Eng. Sci. 42:2587–2596
- [14.33] Ostendorf M (2004) Geschwindigkeitsmessungen in Silos mit der Particelle Image Velocimetry. Ph.D. thesis, Techn. Univ. Braunschweig, Germany
- [14.34] Carson JW, Johanson JR (1977) Vibration caused by solids flow in storage bins. Preprints International Powder and Bulk Solids Handling and Processing Conf., Rosemont, IL, USA, pp 237–243

- [14.35] EP 0 883 561 B1 (2000) Verfahren und Vorrichtung zur Verminderung von geräuschverursachenden Schwingungen bei der Entleerung von Silos. European Patent
- [14.36] Bruff W, Jenike AW (1967/68) A silo for ground anthracite. Powder Technol. 1:252–262
- [14.37] Jenike AW (1964/1980) Storage and flow of solids. Bull. No. 123, 20th Printing, revised 1980. Engng. Exp. Station, Univ. of Utah, Salt Lake City.
- [14.38] Rappen A, Wright H (1984) The use of air cannons to solve coal flow problems in bunkers. Aufbereitungstechnik 25:200–208

Index

A

abrasion
 reduction 335
active state of stress 252
active stress field 252
adhesion 72, 218
adhesive force 23
 adsorption layer 28
 distance 25
 electrostatic force 24
 flow agent 211
 liquid bridge 24
 measurement 196
 particle size 26
 roughness 28
 sintering 30
 solid bridge 29
 van der Waals force 24
adsorption layer 28
aeration nozzle 347
aeration pad 347
agitator 350
air cannon 350
air injection 344, 347
air slide 368
air-assisted discharge 367
angle of dilatancy
 definition 141
 yield locus 148, 154
angle of dilation *see* angle of dilatancy
angle of internal friction
 at incipient flow 61
 at steady-state flow 62

time yield locus 68
angle of repose 172
anisotropy 113, 126
 induced 122
 inherent 125
 strength 126
antidynamic tube 336
apron feeder 361
 driving force 275
arched stress field 254
arching 3, 294
 design example 452, 461
 outlet dimensions 299
attrition
 attrition test 94
 example 240, 441, 442
avalanching test 174

B

belt feeder 359
 driving force 275
biaxial compression test 189
biaxial tester 113
bin activator 363
Binsert® 332
blending silo 336
boundary shears 138
bridging *see* arching
buckling 288
bulk density
 example 241
influence of consolidation stress
 37
influence of deformation 125

C

caking *see* time consolidation
Carr compressibility index 178
Carr flowability index 176
Carr index *see* Carr flowability index
circumferential stress (rathole) 307
coefficient of wall friction 71
cohesion
 definition 62
 yield locus 62, 151
cohesion tester 179
cohesive strength *see* unconfined yield strength
coincidence of principal stress and principal strain axes 148
compact strength tester 186
comparative test
 selection of stresses 103, 110
complete clearance
 hopper inclination 307
compressibility
 example 241
 test procedure 97
compressibility index 178
compressibility test 178
compressive strength *see* unconfined yield strength
cone-in-cone insert 332
consolidation stress
 assessment 100
 selection 99
 yield locus 55
core flow *see* funnel flow
critical outlet dimension
 arching 303
 ratholing 310
cylinder section *see* vertical section

D

dead zone *see* stagnant zone
deformation
 elastic 21
 isochoric 114, 117
 isotropic 122

plastic 21
pure shear 129
simple shear 129
steady-state flow 121
uniaxial compression 120
deformation history 116
degree of saturation 20, 216
dilatancy 139
 angle of dilatancy 141
dilation
 during shear deformation 140
 influence on shear tests 144
discharge aid 347
 application 352, 377
 mechanical 350
 placement 377
 pneumatic 347
discharge device 353
 air slide 368
 apron feeder 361
 belt feeder 359
 bin activator 363
 driving force 272
 en-masse feeder 358
 multiple screw feeder 374
 orbiting screw feeder 375
 oscillating bars 375
 rotary discharge machine 371
 rotary plow 330, 371
 rotary valve 365
 screw feeder 356, 357
 uniform discharge 356
 vibratory feeder 362
discharge rate 339
 coarse-grained bulk solids 341
 example 450
 fine-grained bulk solid 342
 gas injection 344
discharge tube 333
 antidynamic tube 336
 reduction of segregation 400
 stress (example) 442
discrete element method 132, 258
doming *see* arching
drained angle of repose 172

driving force (discharge device)

272

example 444

dynamic angle of repose 172

E

eccentric discharge 288, 356, 358,
360, 363, 366, 369, 377

eccentric flow 285

reasons 287

stress distribution 256, 286

eccentric pipe flow 256, 292

effective angle of internal friction
62

effective yield locus 62

electrostatic force 24

emptying conditions 254

emptying state of stress 254

en-masse feeder 358, 444

driving force 275

expanded flow 326

F

failure plane 41

feeder 353

application 377

apron feeder 275, 361

belt feeder 275, 359

design for mass flow 353

driving force 272

en-masse feeder 275, 358, 444

increasing capacity 357

large outlet opening 374

multiple screw feeder 374

orbiting screw feeder 289

reason for funnel flow 356

rotary valve 365

screw feeder 356, 357

uniform discharge 356

vibratory feeder 362

fibrous particles 224

filling conditions 253

filling state of stress 253

filling tube 401

flooding 3, 222, 293, 345

flow agent 211

example 231

highly dispersed powders 211

flow factor 301

diagram 302, 314

flow function 37, 64, 156

flow profile 291

flow promoting device *see*
discharge aid

flow properties

at small stresses 156

basic rules for the measurement
163

flow agent 231

influence of consolidation stress
64

influence of gas flow 219

influence of moisture 215, 233

influence of particle shape 223

influence of particle size 32, 210,
237

influence of temperature
(example) 235

influence of test method 163

influencing parameters 35

flow velocity

influence 160

silo 292

flowability

classification 42

definition 41

density-weighted flowability 47

flow agent 231

influence of consolidation stress
43

selection of consolidation stress
99

temperature (example) 235

time consolidation 44, 68

fluidization 219

air slide 367

behavior 222

force chain 120

funnel (test procedure) 171

funnel flow 2, 291

caused by the feeder 356

design (example) 456
eccentric pipe flow 256, 292
mixed flow 253, 292
pipe flow 256, 291

G

gas flow 219, 264
silo 339
gas injection 344
gas pressure in silos 340
gecko 34
Geldart's classification 222
gravity blender 336

H

Hausner ratio 178
homogenizing silo 336, 369
honking *see* silo honking
hopper (silo)
asymmetric 322
conical 321
design *see* silo design
inclination for complete clearance 307
inclination for mass flow 296
pyramidal 321
shape 296, 320
stress 252, 299
varying steepness 326
wedge-shaped 321
horizontal stress ratio *see* lateral stress ratio

I

imperfection 278
Imse test 175
incipient flow 36, 50
increasing capacity (feeder) 357
induced anisotropy 122
inherent anisotropy 125
insert 328
application 328
Binsert® 332
cone-in-cone 332

discharge tube 333, 442
enlargement of the flow zone 330
filling tube 401
influence on stresses 280
inverted cone 329, 401
loads on inserts 280
wedge 329
instantaneous flow function *see* flow function
instantaneous yield locus *see* yield locus
internal *see* insert
inverted cone insert 329, 401
inverted cone silo 330, 369

J

Janssen 4, 259
Janssen equation 5, 259
example 439, 445, 447
upward movement of a plug 263
with gas flow 264
with surcharge load 262
with surcharge load (example) 445, 447
Jenike 6
procedure for silo design 295
Jenike shear tester 76, 190
alternative procedures 165
shear cell 76
test procedure 76
time consolidation 88
twisting 79
wall friction 91
Johanson Hang-up Indicizer™ 186

K

K (stress ratio) *see* lateral stress ratio
kinematic wall yield locus 71
knocker 350

L

Lambdameter 122, 268

lateral stress ratio 12, 249, 266
 measurement 122, 268
 linearized yield locus 61
 liquid *see* moisture
 liquid bridge 24, 215
 localization of the shear zone 134
 silo 410
 Lotus effect 31

M

major principal stress 14
 dependence on deformation 116
 orientation (silo) 252, 279, 281
 steady-state flow 55
 mass flow 6, 291
 boundaries 298, 317
 design 296
 design example 451, 452, 461
 diagram 298, 317
 mass flow rate *see* discharge rate
 measuring technique
 accuracy 193
 angle of repose 172
 avalanching 174
 biaxial compression test 189
 Carr flowability index 176
 cohesion tester 179
 compact strength tester 186
 compressibility test 178
 flowability test 179
 funnel 171
 Imse test 175
 Jenike shear tester 190
 Johanson Hang-up Indicizer™
 186
 monoaxial shear test 182
 overview 169
 penetration test 180
 powder bed tester 183
 quality control tester 188
 ring shear tester 192
 stirrer 177
 tensile strength test 183, 184
 tensile strength test with gas flow
 185

torsional shear tester 191
 uniaxial compression test 181
 minimum outlet dimension
 arching 303
 ratholing 310
 mixed flow 253, 292
 mixing silo 336
 Mohr strain circle 131
 Mohr stress circle
 derivation 16
 explanation 12
 steady-state flow 55
 three-dimensional state of stress
 14
 uniaxial compression test 39
 moisture
 adhesive forces 24
 influence on flow properties 215,
 233
 influence on wall friction 217,
 234
 monoaxial shear test 182
 multiple outlets 325
 multiple screw feeder 374

N

non-uniform discharge 3, 288, 356,
 358, 360, 363, 366, 369, 377
 normal stress 10
 sign convention 11
 normal stress at preshear 50
 automatic selection 105
 selection 101
 normal stress at shear 52
 automatic selection 105, 108

O

orbiting screw feeder 375
 oscillating bars discharger 375
 outlet
 multiple outlets 325, 398
 outlet opening
 minimum dimensions 294, 299,
 307
 stress 270

overconsolidated specimen 49, 146

P

particle shape 223

particle size

influence on flow properties 32,
210, 237

Pascal (unit) 12

passive state of stress 254

passive stress field 254

penetration test 180

permeation *see* gas flow

pipe *see* ratholing

pipe flow 256, 291, 292

piping *see* ratholing

plate-like particles 224

pneumatic blending silo 333

point of incipient flow 52

porosity 20

powder bed tester 183

preshear 47

Mohr stress circle 58

normal stress 50

shear stress 51

shear stress maximum 145

stress selection 101

preshear point 52

assumptions 148

press (stress distribution) 445

principal strain direction 130

principal stress 14

principal stress direction 130

principal stress ratio

influence of deformation 116

pure shear 129

Q

quality control tester 188

R

radial stress field 296

rathole *see* ratholing

ratholing 3, 295

circumferential stress 307

design 307

design example 456

relaxation 205

Riedel shears 138

ring shear tester 84, 192

attrition test 95

shear cell 84

test procedure 84

time consolidation 88

wall friction 92

rotary discharge machine 371

rotary feeder *see* rotary valve

rotary plow 330, 371

rotary valve 364, 365

leakage air 367

vertical axis 351

rotational shear tester 75

S

saturation 20, 215

Schulze ring shear tester *see* ring

shear tester

screw feeder 356, 357

segregation 3, 294, 381

air resistance 386

influence of flow profile 396

mechanisms 381

multiple outlets 398

on inclined surfaces 382

percolation 384

reduction 390

sampling 403

trajectory 386

settling behavior 222

settling velocity 386

shear band *see* shear zone

shear cell

Jenike shear tester 76

ring shear tester 84

shear deformation 129

shear point 52

assumptions 148

shear rate *see* shear velocity

shear stress 10

influence of dilation 142

-
- influence of shear deformation 136
 influence of shear rate 136
 localization 135
 shear stress at preshear 51
 shear stress at shear to failure 52
 shear test 47
 incipient flow 50
 preshear 47
 shear to failure 47
 steady-state flow 49
 shear tester
 Jenike shear tester 76, 190
 principal stresses 164
 principle 47, 75
 ring shear tester 76, 84, 192
 test procedure 47
 torsional shear tester 76, 191
 shear to failure 47
 Mohr stress circle 58
 normal stress 52
 stress selection 101
 shear velocity
 influence 136, 160, 199, 203
 slip-stick 206
 shear zone 132
 localization 134, 144
 silo 409
 thickness 135
 shocks *see* silo quaking
 silo
 configurations 319
 hopper shape 296, 320
 imperfection 278
 insert 280, 328
 principal stresses 254
 stress distribution 252
 stress peak 255
 switch 255
 velocity distribution 292
 silo cylinder *see* vertical section
 silo design 377
 application of the results 377
 arching (example) 452, 461
 funnel flow 307
 funnel flow (example) 456
 Jenike's procedure 295
 mass flow 296
 mass flow (example) 451, 452, 461
 ratholing (example) 456
 stresses for shear tests 110
 time consolidation (example) 461
 silo honking 405, 425
 reasons 429
 reduction 335, 431
 silo music *see* silo honking
 silo noise *see* silo honking
 silo outlet
 minimum dimensions 294
 silo quaking 405
 reasons 429
 reduction 431
 slip-stick 408
 silo shocks *see* silo quaking
 silo thumps *see* silo quaking
 silo vibrations *see* silo honking
 simple shear 129
 sintering 30
 slide-hold-slide test 204
 slip-stick 199
 reasons for 199
 shear test 208
 shear velocity 206
 silo 408
 solid bridge 29
 stagnant zone 2, 291
 static wall friction 72, 74
 steady-state flow 121
 dilation 144
 direction of principal stresses 59
 in a shear tester 49
 localization 134, 144
 shear stress maximum 145
 silo 254
 tensile stress 159
 steady-state settling velocity 386
 steady-state yield locus 158
 definition 63
 stirrer (test method) 177
 strain path 115

- strength anisotropy 126
stress
 assessment (silo) 258
 discharge tube 333
 distribution (silo) 278
 feeder 272
 FIBC (example) 449
 for testing 99
 history 116
 insert 280
 outlet opening 270, 272
 outlet opening (example) 444
 sacks on a pallet (example) 449
 silo 252, 271
 small stresses 156
 transmission in bulk solids 120
 unit 12
variation of the cross-section
 (vertical section) 278
vertical channel 259
vertical section 259
vertical section (example) 439,
 447
stress chain 120, 140
stress path 115
stress peak
 imperfection 278
 insert 281
 mass flow hopper 253
 reason 256
 silo 255
 stagnant zone 253, 256
 variation of the cross-section 278
stress ratio (K) *see* lateral stress
 ratio
surface roughness 245
switch 254, 441
- T**
- tap volumeter 178
tapped density 178
temperature
 influence on flow properties
 (example) 235
tensile strength
 influence of particle size 32
 measurement 32, 183, 184, 185
 yield locus 63, 151
tensile strength test
 powder bed tester 183
 uniaxial 184
 with gas flow 185
tensile stress
 steady-state flow 159
 yield locus 152
test equipment 169
test procedure
 accuracy 193
 angle of repose 172
 avalanching 174
 biaxial compression test 189
 Carr flowability index 176
 cohesion tester 179
 compact strength tester 186
 compressibility test 178
 flowability test 179
 funnel 171
 Imse test 175
 Jenike shear tester 76, 190
 Johanson Hang-up IndicizerTM
 186
 monoaxial shear test 182
 penetration test 180
 powder bed tester 183
 quality control tester 188
 ring shear tester 84, 192
 stirrer 177
 tensile strength test 183, 184
 tensile strength test with gas flow
 185
 torsional shear tester 191
 uniaxial compression test 181
thumps *see* silo quaking
time consolidation 38
 example 236
 influence of storage time 38
 measurement (shear tester) 66,
 88
 mechanisms 29
 silo design (example) 461
time consolidation bench 88

time flow function 38

time wall yield locus

definition 72

test procedure 72

time yield locus

definition 67

selection of stresses 107

torsional shear tester 75, 191

trajectory segregation 386

translational shear tester 75, 190

twisting 79

U

unconfined yield strength

anisotropy 126

definition 36

influence of consolidation

procedure 126

influence of consolidation stress

37

yield locus 57

underconsolidated 48

uniaxial compression

force chains 120

stress distribution 262, 445

stress ratio 249

uniaxial compression test 35, 165,

181

uniaxial tensile strength *see* tensile

strength

uniform discharge 356, 359, 360

V

valley angle (pyramidal hopper)

322

van der Waals force 24, 211

vertical section

stress 252

vibrating aeration nozzle 347

vibrations *see* silo honking

vibrator 351

vibratory feeder 362

volumetric strain energy 142

W

wall friction *see* wall friction angle

wall friction angle

definition 71

example 239, 243

influence of displacement 209

influence of moisture 217, 234

influence of particle size 239

influence of surface roughness
245

influence of time 72

influence of wall normal stress
71, 243, 327

kinematic 71

measurement with shear testers
69

shear tester 91

static 72, 74, 94

wall material 245

wall material

influence on wall friction 245

roughness 245

wettability 245

wall yield locus

definition 69

kinematic 71

selection of stresses 109

static 72

test procedure 69, 91

wide residence time distribution 3

Y

yield limit

definition 40

yield locus

angle of dilatancy 154

assumptions 147

consolidation stress 55

construction 55

definition 55

end point 56, 150

selection of stresses 99

tensile stress 152

unconfined yield strength 57

Y-shears 138